GEOLOGY, MINERAL ZONING, AND LITHOCHEMISTRY OF THE EL SOLDADO MANTO TYPE COPPER DEPOSIT, CHILE

GEOLOGY, MINERAL ZONING, AND LITHOCHEMISTRY

OF THE

EL SOLDADO MANTO TYPE COPPER DEPOSIT, CHILE

by

Ricardo Boric

**Submitted in partial fulfillment of the requirements
For the degree of Master of Science**

at

**Dalhousie University
Halifax, Nova Scotia
Canada
September 2002**

DALHOUSIE UNIVERSITY

DEPARTMENT OF EARTH SCIENCES

The undersigned hereby certify that they have read and recommend to the Faculty of Graduate Studies for acceptance a thesis entitled "Geology, Mineral Zoning, and Lithochemistry of the El Soldado Manto Type Copper Deposit, Chile" by Ricardo Boric in partial fulfillment of the requirements for the degree of Master of Science.

..

DALHOUSIE UNIVERSITY

DATE: September 13th, 2002

AUTHOR: <u>Ricardo BORIC</u>

TITLE: **GEOLOGY, MINERAL ZONING, AND LITHOCHEMISTRY OF THE EL SOLDADO MANTO TYPE COPPER DEPOSIT, CHILE**

DEPARTMENT: **Earth Sciences**

DEGREE: **Master of Science   CONVOCATION: October   YEAR: 2002**

Permission is herewith granted to Dalhousie University to circulate and to have copied for non-commercial purposes, at its discretion, the above title upon the request of individuals or institutions.

Redacted

_____
Signature of Author

TABLE OF CONTENTS

Page

LIST OF TABLES

LIST OF FIGURES

ABSTRACT

El Soldado is the largest (>200 Mt @ 1.4 % Cu) of the known Cu-(Ag) manto-type deposits in central Chile. The submarine volcanic upper member of the early Cretaceous Lo Prado Formation, which also contains marine carbonaceous shales and volcaniclastic sandstones, hosts the deposit. Petrographic and lithochemical evidence indicates that the volcanic host rocks are a bimodal suite of arc-related, calc-alkaline basalts and rhyodacites, which have been regionally affected by very-low-grade metamorphism and extensive albitisation. The rocks have acquired the characteristic alteration of *spilite* and *keratophyre*, explaining the previous misidentification as alkaline andesites and trachytes. U/Pb dates on zircons (138-126 Ma) from a rhyodacitic host dyke confirm the Hauterivian age assigned to host rocks on the basis of paleontology..

Although stratigraphically restricted (strata-bound), the clustered orebodies are mostly vein-like and discordant, controlled by a system of NS to NNW faults formed within a dilational jog along a sinistral, strike-slip brittle shear system. Individual orebodies are zoned, with an external zone of barren pyrite, followed inward by concentric zones with chalcopyrite-pyrite, chalcopyrite, chalcopyrite-bornite, and a central zone of bornite-chalcocite plus fine grained hematite. At the deposit scale, the bornite-chalcocite association is more abundant along the western branch of the deposit, and toward the south. Pyrite prevails at depth and to the east away from the main controlling shear faults. Specular hematite is recognised for the first time as an important constituent of the ore in the northern part of the deposit. Gangue minerals are calcite, chlorite, albite, k-feldspar, and scarce quartz and rutile. Local hydrothermal alteration associated with orebodies is characterised by an increase in Na_2O and depletion in K_2O in host rocks, reflecting a pervasive albitisation. Yet there are localised zones of substantial K_2O gain and Na_2O loss in bornite-chalcocite ore assemblages near structures, reflecting an alteration to microcline. FeO and MgO also show relevant increments associated with chloritisation within orebody cores.

The deposit was formed in two main stages: 1) a low-temperature, diagenetic stage during which framboidal pyrite developed in association with migrated petroleum, at c.a. 130 to 120 Ma; 2) a higher-temperature (> 300°C from fluid inclusions) hydrothermal stage at ca. 103 Ma (coinciding with the main phase of batholith emplacement and shear development), which deposited chalcopyrite, bornite, chalcocite, and scarce pyrite and specularite. Copper sulphides replaced pre-existing pyrite, with the excess Fe developing fine-grained hematite. Ag was deposited during this second stage as an impurity within bornite and chalcocite. Sulphur isotope data indicate that most of the sulphur was inherited from the diagenetic pyrite. It is suggested that the Cu was extracted from oxidised subaerial lavas of the overlying Veta Negra Formation, and was precipitated when, channelled by faults and responding to hydraulic gradients, the oxidised hydrothermal brines descended into, and reacted with reducing diagenetic pyrite and pyrobitumen. The salinity of fluid inclusions (21-26% NaCl equivalent) suggests that basinal brines were responsible for Cu transport. The Cretaceous batholith probably provided heat, and a (distal) magmatic contribution to the mineralizing fluids is possible. The patterns of lithologyl, structure, alteration and ore mineralogy of at El Soldado have similarities with other large strata-bound Cu deposits such as Mantos Blancos and Punta del Cobre, suggesting a similar genesis for many of these Mesozoic Cu deposits.

ACKNOWLEDGEMENTS

CHAPTER 1. INTRODUCTION

1.1. General Statement

The El Soldado is the largest volcanic-hosted, manto-type copper deposit of Central Chile (Figure 1.1). The mine has been operative since the eighteenth century and has produced more than 100 millions of tons @ 1.6% Cu. At the time of writing it is owned and operated by Compañía Minera Disputada de las Condes Ltda. (CMD), an Exxon-Mobil-Coal and Minerals Co. (EMCMC) affiliate, at an annual rate of 6.5 million metric tons @ 1.2 % Cu. Total identified resources at El Soldado, considering production plus reserves, are well over 200 million metric tons @ 1.35 % Cu, thus making El Soldado equivalent - in terms of total metal content - to a medium size porphyry copper deposit such as El Salvador.

Manto type deposits (*mantos*) such as El Soldado are epigenetic strata-bound copper-sulphide deposits, hosted by volcanic and volcano-sedimentary sequences of mostly Upper Jurassic to Lower Cretaceous age, which are distributed along the Coastal Range of Chile between 21° to 34° latitude S. These mantos represent the second largest concentrations of copper in the Central Andes after the giant porphyry type deposits, and have been very important to the Chilean economy during the last fifty years. Whereas most Andean copper deposits, including the porphyry copper types, are understood to be hydrothermal and spatially and genetically related to calc-alkaline plutons, the origin of the copper mantos is not so evidently related to intrusives and remains controversial (e.g Sillitoe, 1992; Maksaev and Zentilli, 2002). El Soldado has not been an exception to this controversy, and genetic models, ranging from syngenetic volcanogenic through to epigenetic, either related to magmatic sources or metamorphic fluids, have been proposed to explain its origin.

The geology and mineralogy of El Soldado were described in detail by the staff of geologists of CMD, more than a decade ago (Holmgren, 1987; Klohn et al., 1990). This team created a descriptive geological model, which was applied successfully to enlarge the ore reserves in the 1980s and early 1990s. These authors explained the origin of El Soldado to be hydrothermal-epigenetic, related to the waning phases of "particularly

1
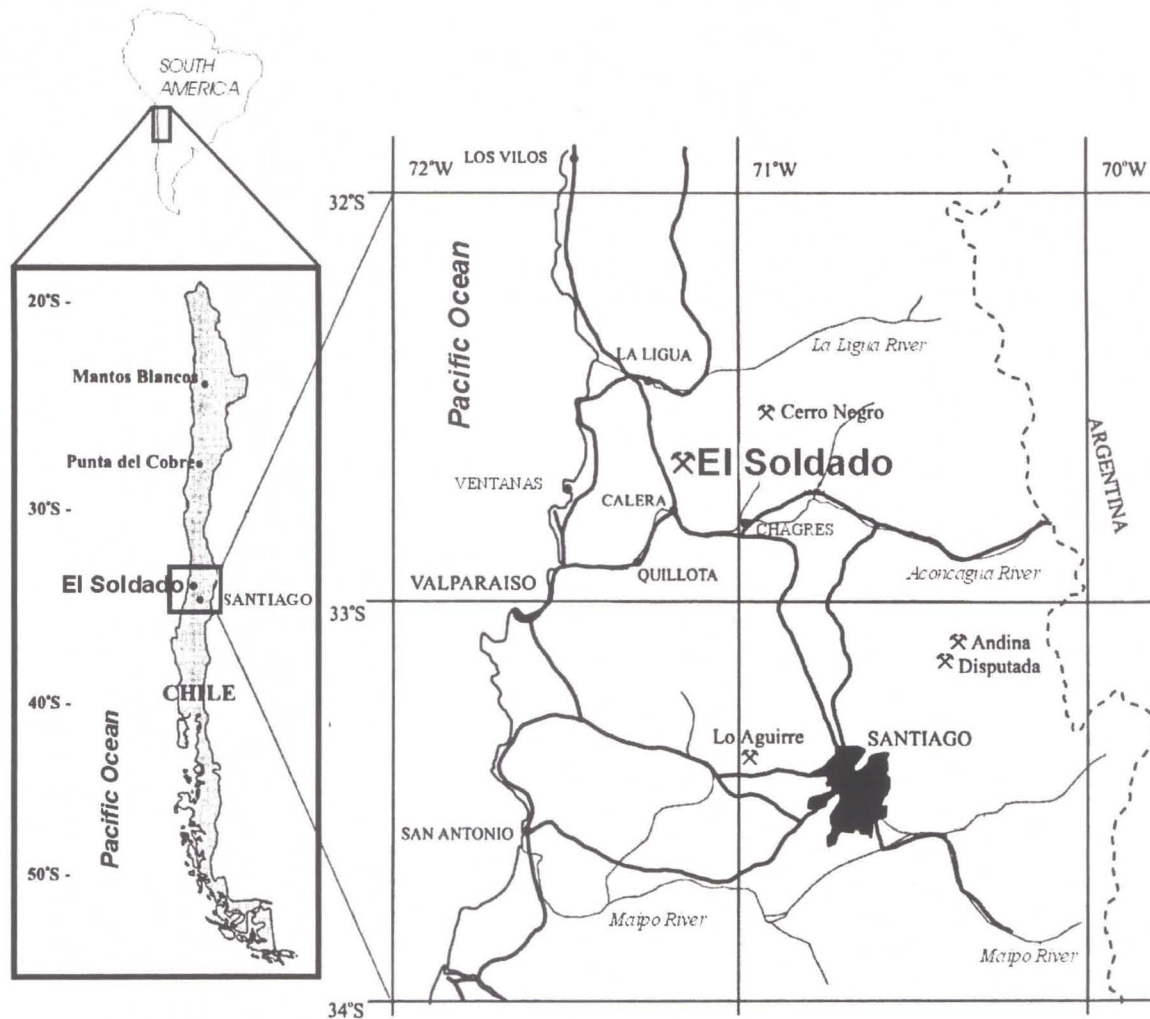
Figure 1.1 Location map of El Soldado deposit in Central Chile.
The Chagres Smelter by the Aconcagua River, and the Disputada (Los Bronces) porphyry Cu deposit and mine in the high Andes, as well as El Soldado, are owned and operated by Compañía Minera Disputada de las Condes. Also shown are manto type Cu deposits Mantos Blancos, Punta del Cobre, Cerro Negro and Lo Aguirre, which are referred to in future chapters.

alkaline" Early Cretaceous volcanism (e.g. Holmgren, 1987; Klohn et al., 1990). However, the knowledge acquired in the last decade in the course of the development of new blocks at the mine, is not consistent with the above genetic hypothesis, and has demonstrated that their descriptive model was incomplete. An alternative hypothesis postulated by Westra (1988a) suggested that the origin of El Soldado was related to fluids liberated during low-grade metamorphism of the volcanic pile within the Cretaceous basin. The recognition of widely distributed bitumen (solidified petroleum) associated with the copper ores (Zentilli et al., 1994; 1997) also argued into favour of basinal processes rather than a local igneous source.

A critical need in predicting sufficient reserves to extend the mine operation for a decade or more was an updated geological model that would properly describe mineralogical and metallurgical units, and at the same time would highlight empirical tools useful in logging and exploration. Such a model cannot have predictive capabilities unless based on a real understanding of the processes that lead to the deposit's genesis. Unfortunately, although desirable, this goal was difficult to achieve in parallel with routine work, due to the day-to-day pressures of the mining operation, and to the reluctance of management to deploy qualified personnel to perform duties that they perceived as not having immediate and guaranteed business benefit. This situation led to the development of this thesis in part during consecutive leaves of absence from the mine by the author.

At the beginning of the research, essential parameters, such as the spatial distribution and zoning of sulphide and alteration minerals, the geochemistry of fresh and altered host volcanic rocks, and the absolute age of host rocks and mineralisation events were poorly constrained, and required re-definition. After a review and evaluation of existing data, mapping, core logging and sampling were followed by a mineralogical and geochemical study of rocks and ores. A set of cross-sections and level plans of the deposit were constructed and helped to visualise the geometry and explain mineral and geochemical zoning. Various analytical techniques (ore and alteration petrology, lithochemistry, and geochronology) were used to pose constraints and to test genetic hypotheses. The ultimate goal was to develop and refine a general genetic model with

predictive capabilities, useful in exploration for new reserves at El Soldado district and for new manto type deposits in the Andean region.

The thesis was carried out to complement a Ph.D. thesis study by N.S.F.Wilson (1995-1998), which focussed on the role of organic matter in the formation of El Soldado. Both research projects were supervised by Dr. Marcos Zentilli and were part of an informal collaborative effort between the company (CMD) and Dalhousie University.

1.2. Location and Geography

The El Soldado copper deposit (Lat. 32° 38' S; Long. 71° 04' W) is located in the Coastal Range of Central Chile, 120 km north-west of Santiago, the capital city of Chile, and 30 km away from the Pacific coast, at about 500 to 1100 m above sea level (Figure 1.1). The mine is within 8 km of the Pan American Highway, railway links and major power grids. The mine lies on the very steep west flank (Figure 1.2) of a 1500-m high range. The slope is heavily vegetated, with brush and deciduous trees, especially up to an altitude of 800 m. Outcrops cover less than 30 % of the surface at lower altitudes but they are almost continuous at the top of the range (Figure 1.2). The zone has a temperate climate, with abundant winter fog, irregular precipitation in the form of rain (>40 cm/year), and occasional snow during April to September. Minimum temperatures range from -2° C in winter to 15° C in summer, and maximum temperature range between 10° C in winter to 30° C in summer (adapted from Fuenzalida, 1965). North, northeast and northwest trending faults control the drainage.

1.3. Production and History

At the time of writing of this thesis, the mine was owned and operated by Cia. Minera Disputada de las Condes Ltda. (CMD), an Exxon-Mobil Coal and Minerals Co. (EMCM) affiliate. El Soldado's primary operations comprise an open pit mine (the Morro pit), an underground mine, using a sublevel stoping method, a sulphide flotation concentrator plant (El Cobre plant), and a leaching plant with Solvent Extraction Electro Wining (SXEW) technology (Figures 1.2, 1.3, and 1.4). Concentrates are sent by road to
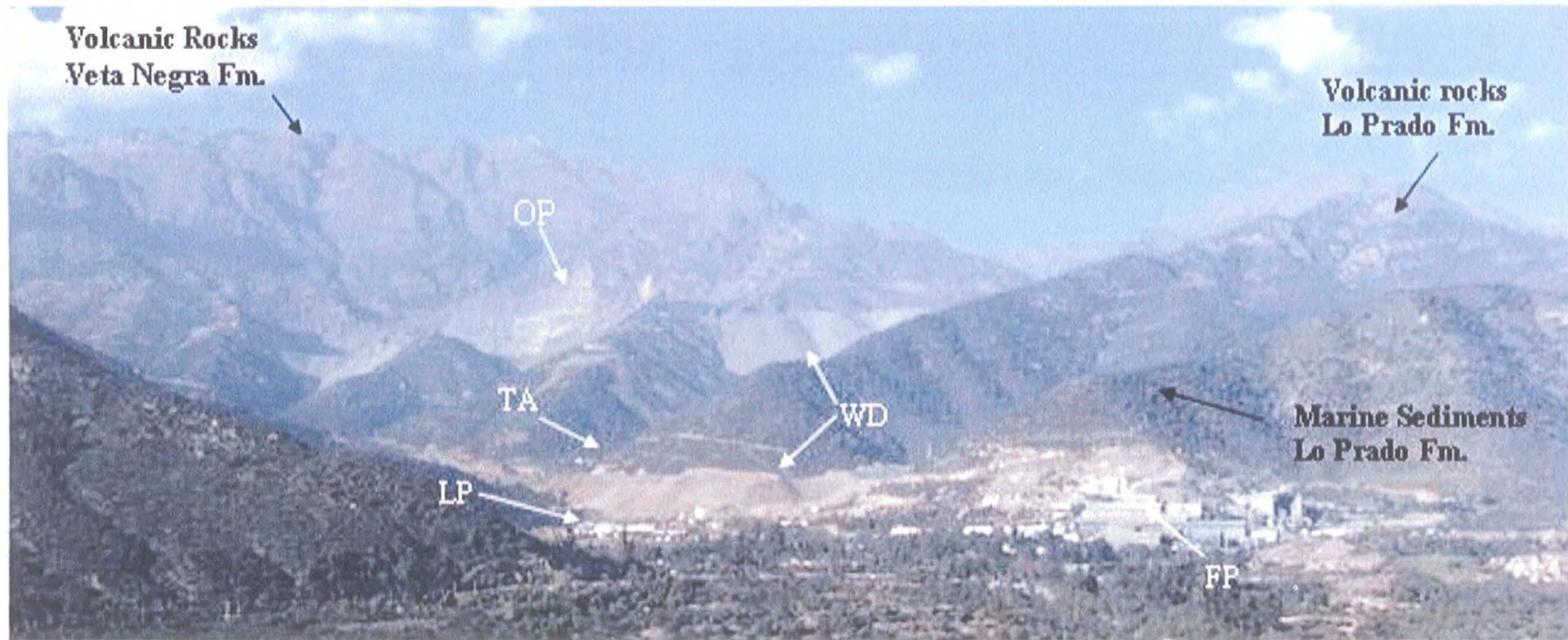
Figure 1.2. Field photograph showing a general view of the El Soldado mine and facilities, looking north east.
The open pit (OP), the floatation plant (FP), the leaching plant (LP), the transport level of the underground mine, and some waste dumps (WD) can be appreciated. The top of the open pit marks approximately the boundary between the Lo Prado Formation and the Veta Negra Formation
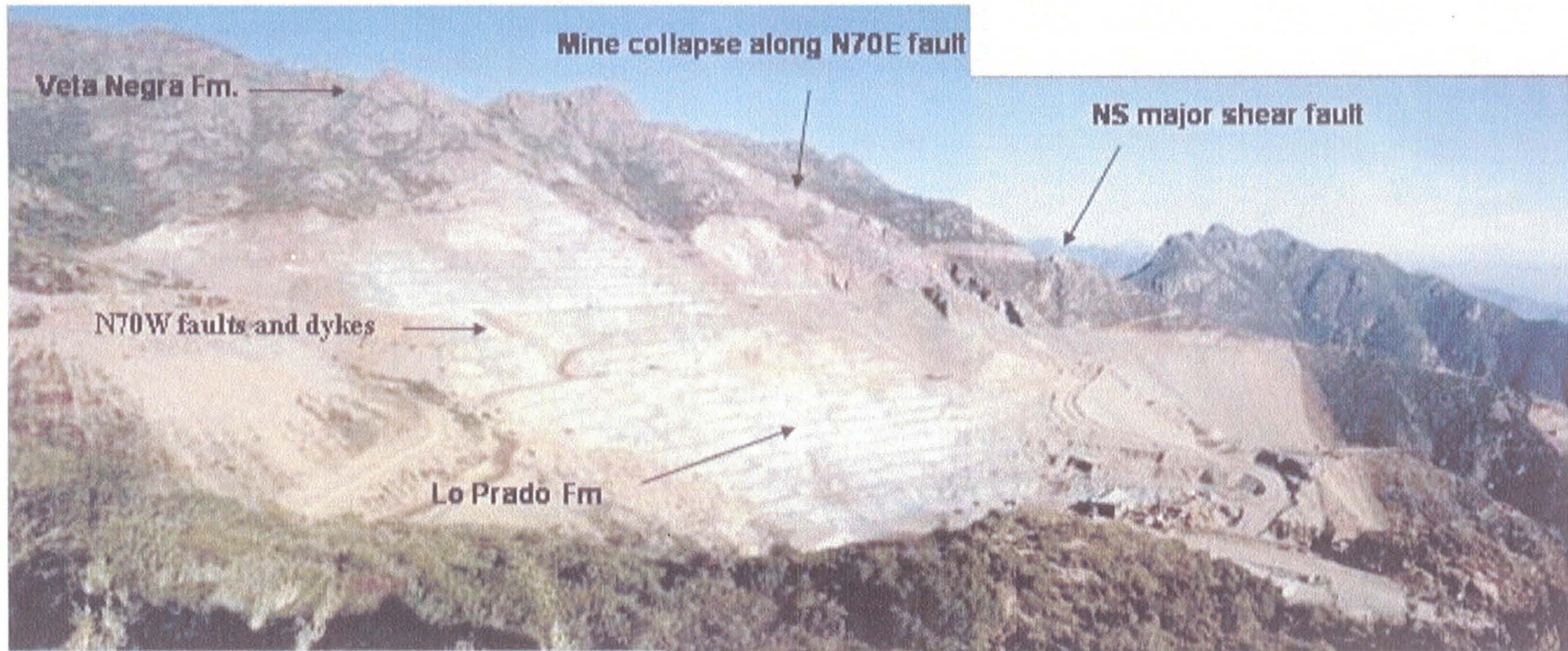
Figure 1.3. Field photograph of the Morro open pit, in the northern part of El Soldado mine (1995) looking south.
Benches are 12.5 m high and the total height of the face is around 375m. The mine stopes are all underground, but the present day open pit has exposed underground workings. The boundary between the Lo Prado Formation and the Veta Negra Formation is identified by the presence of red oxidised rocks in the upper benches of the pit. Some major faults are visible.
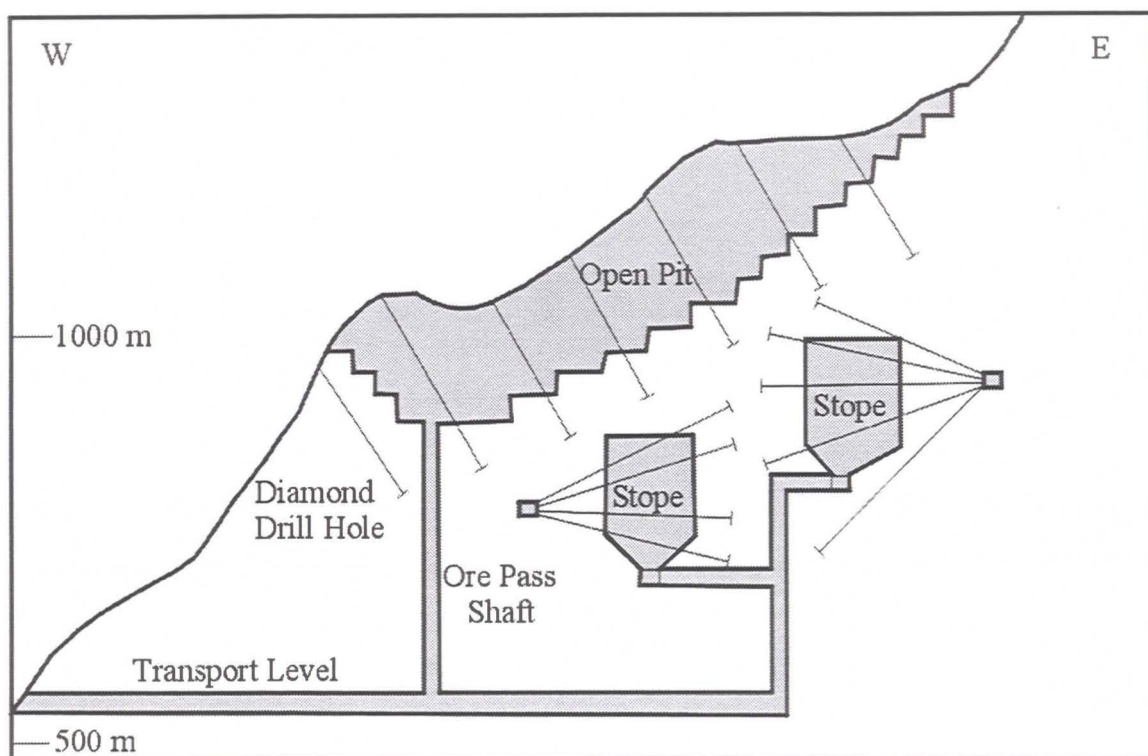
Figure 1.4. Schematic cross section showing the mining methods at El Soldado.
The drilling pattern used to prospect new reserves is also shown. Mapping and sampling drill core were essential to developing this research.

the CMD Chagres smelter, or to the Ventanas port on the Pacific Coast (Figure 1.1).

At El Soldado, mining of exposed high-grade pods began in the eighteenth century, but the first modern exploitation began in 1919, when ore grading between 7 and 15 % Cu was extracted from underground workings. Since then, under a number of subsequent owners, production was almost continuous, but limited to less than 600 tonne/day until the late 1960s, when it was increased to 3,300 tonne/day. Exxon Minerals (EMCMC) assumed control of El Soldado in 1978 and developed an intensive drilling campaign, which led to the discovery of many unexposed sulphide orebodies, significantly increasing the ore reserves. These discoveries and the change in underground mining method to sublevel open stoping, allowed stepwise expansions in sulphide ore treatment to 5,500 and 11,500 tonne/day. In 1989 the Morro open pit

(Figures 1.2, 1.3 and 1.4) began operating, to support an increase in the production rate up to the current 17,500 tonne/day. In 1990, the SXEW plant was added to treat the oxide ore from the Morro pit. In 2001 the production was 6,400,000 tonnes @1.2% Cu, 70 % of which was provided by the open pit.

Total identified resources at El Soldado, considering production to date plus reserves, are well over 200 million tonnes @ 1.35 % Cu, including 70 million tonnes @ 1.8 % Cu mined out from rich zones (Contador and Glavic, 2001).

1.4. Aims of the Thesis

The ultimate goal of the thesis was to contribute to the development and refinement of a general genetic model with predictive capability for El Soldado deposit, to be useful in exploring new reserves at the district scale, and new manto type deposits in the Andean region. The short-term objectives were:

1. To define the original pre-alteration protolith, geochemical character, and absolute age of the volcanic/sub volcanic host rocks.
2. To better define the spatial distribution (zoning) of ore and alteration minerals at the global mine scale, and to explain the probable processes that led to their existence.
3. To identify the geochemical changes in both major and trace elements, related to ore.

1.5. Methodology

The following methodologies were used during the development of this thesis:

1.5.1. Compilation and Evaluation of Previous Data.

The first step in this research was the compilation and evaluation of available data (maps, sections, petrography, rock geochemistry, stable and radiogenic isotopes, geochronology) generated during different stages of mine development, but particularly in the last decade. This reviewed database was compiled under the direction of the author in September 1997, and has served as a baseline to develop the present study.

1.5.2. Fieldwork and Sampling.

Fieldwork was carried out in 3 different stages: September-December 1997, June-

August 1998, and January-March 1999. During these periods, detailed geological/mineralogical logging and sampling of selected drill cores were performed. Sampling was completed for a variety of areas, including main orebodies, alteration zones as well as barren rocks away from mineralisation and alteration. As a complement, mapping on the surface and underground levels was performed focussed on the possible spatial relationship between ore and sub-volcanic bodies (dikes, stocks). A more detailed logging and sampling were carried out along a specific transversal east - west profile in the central-south part of the mine (cross sections -750N and -900N according to mine terminology). Along this profile, the principal rhyodacite and basalt flows hosting the ore were systematically sampled, including the peripheral barren areas, distal to mineralisation, the different ore zones intercepted in the orebodies, and the "intra-orebody" barren zones. Samples of this profile were used to study the geochemical pattern associated with copper mineralisation.

The Na-cobaltinitrite (yellow stain for K minerals) staining procedure (e.g. Reid, 1969) was performed regularly on drill cores during logging at the mine, in order to both locate and map the distribution of K-feldspar at the orebody scale. The staining was performed especially on rocks along the representative profile mentioned above.

As a result of this fieldwork, a representative set of un-mineralized "background" samples from all different volcanic and subvolcanic rock units was selected. Also the different ore zones of main orebodies and the most important gangue and alteration assemblages were sampled.

1.5.3. Mineral Zoning

Using the compiled database plus the information recorded from drillcore, a set of 32 cross sections was plotted (every 50 m in the N-S direction), which displayed the deposit's geometry and variations of mineralogy and their relationships with the various host rocks and structures. Geological sections were available at the mine but the mineralogy was only partially defined and required completion during this study. The orebodies were subdivided into 6 zones representing the predominant (and mappable) mineral assemblages from outside to their core: 1) pyrite, 2) pyrite-chalcopyrite, 3)

chalcopyrite, 4) chalcopyrite-bornite, 5) bornite and 6) bornite-chalcocite zones. Specular hematite was also recorded where it was relatively abundant. Using the generated cross-sections as a base, three different level plans were produced.

1.5.4. Mineralogy and Petrography

Standard mineralogical techniques available with the Fission Track Research Laboratory at Dalhousie University (FTRL) were utilised to identify mineral species on grains, powders, slabs and thin sections. A new automated Philips X-ray diffractometer was used to identify mineral species, mainly gangue minerals (67 analyses from 39 rock samples). Sodium-cobaltinitrite staining was used to map the distribution of K-feldspar in the rocks at the hand-specimen scale.

Petrography was carried out using transmitted (conventional and polished-thin sections) and reflected light (polished thin sections) using research microscopes. Detailed microprobe analyses were done on ore and gangue minerals utilising the Jeol Microprobe of the Dept. of Earth Sciences, Dalhousie University. The microprobe study included spot analyses (425 from 27 sulphide and silicate samples) and backscatter and X-Ray images (19) for Al, Na, K, Si, Mg, Ca, P, S, Mn, Fe, And Ti. A set of another 271 spot analyses, performed in 1995-1996 by Milton C. Graves, at the same laboratory, in 44 polished thin sections of samples collected by the author, was also included in the research.

1.5.5. Geochemistry

Whole rock, $-H_2O$, $+ H_2O$, FeO, total S, and trace elements including REE analyses were carried out in 36 selected samples, utilising a combination of XRF, ICP-MS and wet-chemical methods. Most of the geochemical samples were collected in a single cross section (traverse) along the south-central portion of the mine (Valdivia Sur - Osorno cross section), and are considered to be representative of the El Soldado. For the sake of consistency with previous work at the mine, the analyses were carried out at the laboratories of the Chemex Laboratories, Vancouver. A previous set of 56 geochemical analyses, analysed in the same laboratory, and collected by the author, was also included in the study.

1.5.6. ^{40}Ar/^{39}Ar Geochronology

The author helped in the selection of a number of samples for dating by the ^{40}Ar/^{39}Ar method at the Geochronological Facility of Dalhousie University (Dr. P.H.Reynolds). These samples were incorporated in the Ph.D. thesis by Wilson (1998a), and have been mostly discussed in a publication submitted to Chemical Geology (Wilson et al., in press a) in which the writer is a co-author. In addition, one new ^{40}Ar/^{39}Ar age of a sample of K-feldspar associated with chalcopyrite-pyrite and collected 1 km south of the mine was added in this study. Therefore the argon dating part of the study is only referred to in passing in this thesis.

1.5.7. U/Pb Geochronology

Three samples from the main rhyodacite flow, the main rhyodacite feeder dyke, and the gabbro stock, were collected to date zircons using the U/Pb methodology. Samples were obtained from drillcores and, as much as possible removed from the orebodies. Samples were sent to Geospec Labs. in Edmonton, where they were dated using conventional thermal ionisation mass spectrometry (TIMS) methodology (Heaman and Parrish *in* Heaman and Luben, 1991).

1.6. Organisation of the Thesis

The thesis is divided into 8 chapters. Chapter 2 is a summary of the general characteristics and geological setting of Chilean strata-bound volcanic-hosted Mesozoic copper deposits, taking in account El Soldado is a prominent member of this group.

Chapter 3 introduces the geology of the El Soldado deposit. The basic geology, including stratigraphy, lithology, structural pattern, mineralogy, geochronology, isotopic and fluid inclusion data, as well as the proposed genetic models are presented and briefly discussed.

Chapter 4 is divided in three parts: part 1 shows a detailed petrographic description of the background or "less altered" volcanic and subvolcanic host rocks.

Optical and microprobe data are presented and discussed. Part two deals with the geochemistry and petrology of these rocks. Rocks are classified according their immobile trace elements lithochemistry. Previous regional data are used as a comparison. Part three gives the results of U/Pb dating.

Chapter 5 is divided in two parts. Part 1 describes the hypogene ore minerals in order of abundance. Part 2 shows the spatial distribution (zoning) of the main ore minerals throughout the deposit. Schematic cross sections and level plans showing the zoning are represented. Optical, microprobe, and XRD data of ore minerals are presented.

Chapter 6 has three parts. Part 1 presents the description of gangue-alteration minerals and their distribution in the different ore zones. In part 2 the changes in chemical composition (major and selected trace elements) of host rocks associated with the hydrothermal alteration-copper mineralisation are estimated normalising the average composition of ore zones versus what are considered the "background" or least-altered rocks. Part 3 shows a comparison among the patterns of alteration of El Soldado and other large Chilean strata-bound Mesozoic copper deposits.

Chapter 7 presents a synthesis of the genetic evolution of the El Soldado deposit, based on the integration of all available data.

Chapter 8 gives the conclusions of the thesis.

The thesis includes also the following eight Appendices: 1) the list of studied samples, 2) the geochemical data, 3), the microprobe data, 4) the X-ray diffractometry data, 5) the magnetic susceptibility and specific gravity data, 6) the photographs of Na-cobaltinitrite stained samples, and 7) the compilation of relevant analytical data from previous studies. Appendix 8) is a professional resumé of the writer.

CHAPTER 2. REVIEW OF CHILEAN VOLCANIC-HOSTED STRATA-BOUND COPPER DEPOSITS

2.1. Introduction

Chile represents one of the largest copper concentrations on Earth and produces annually about 37% of the world's copper (Camus and Dilles, 2001). Most of that production comes from the giant Tertiary porphyry copper deposits, but a relevant proportion comes from Mesozoic strata-bound copper- (silver) and copper- (gold-iron) deposits (Figure 2.1). These strata-bound deposits are distributed in the Coastal range of Chile between 21° to 34° latitude S and are hosted by volcanic and volcano-sedimentary sequences of Jurassic to Lower Cretaceous age which were accumulated in intra-arc basins, and are coeval with copper vein bearing granitoids. A number of smaller strata-bound deposits of Cenozoic age also found in the Chilean Andes (e.g. Fontboté, 1990) are purposely excluded from this discussion.

This chapter introduces the strata-bound volcanic-hosted copper deposits of Chile taking into account that El Soldado is a prominent member of this group of deposits. In the first place the strata-bound Cu-(Ag) group, also known as "*mantos*" or "*manto-type*" deposits, is described. Then the strata-bound Cu-(Au-Fe) deposits, also referred as "*Candelaria-type*", are described. Later a synthesis of the tectonic setting of these deposits is attempted.

The term "strata-bound" applied to the Chilean deposits is used in the sense of Evans (1993), and refers to an ore deposit restricted to a stratigraphic unit, but which can be concordant or discordant with strata. In this sense, stratiform deposits are strata-bound but strata-bound deposits are not necessarily stratiform. The strata-bound Cu-(Ag) deposits are known as manto-type deposits, because initial exploitations were performed on low-angle stratiform sections of the deposits referred as "*manto*" by miners, after the Spanish word for blanket, mantle or cloak.

In the literature, the Chilean Cu-(Ag) mantos have been grouped within the "volcanic redbed" category (e.g. Kirkham, 1989,1996; Sillitoe, 1992), which includes the

13

14
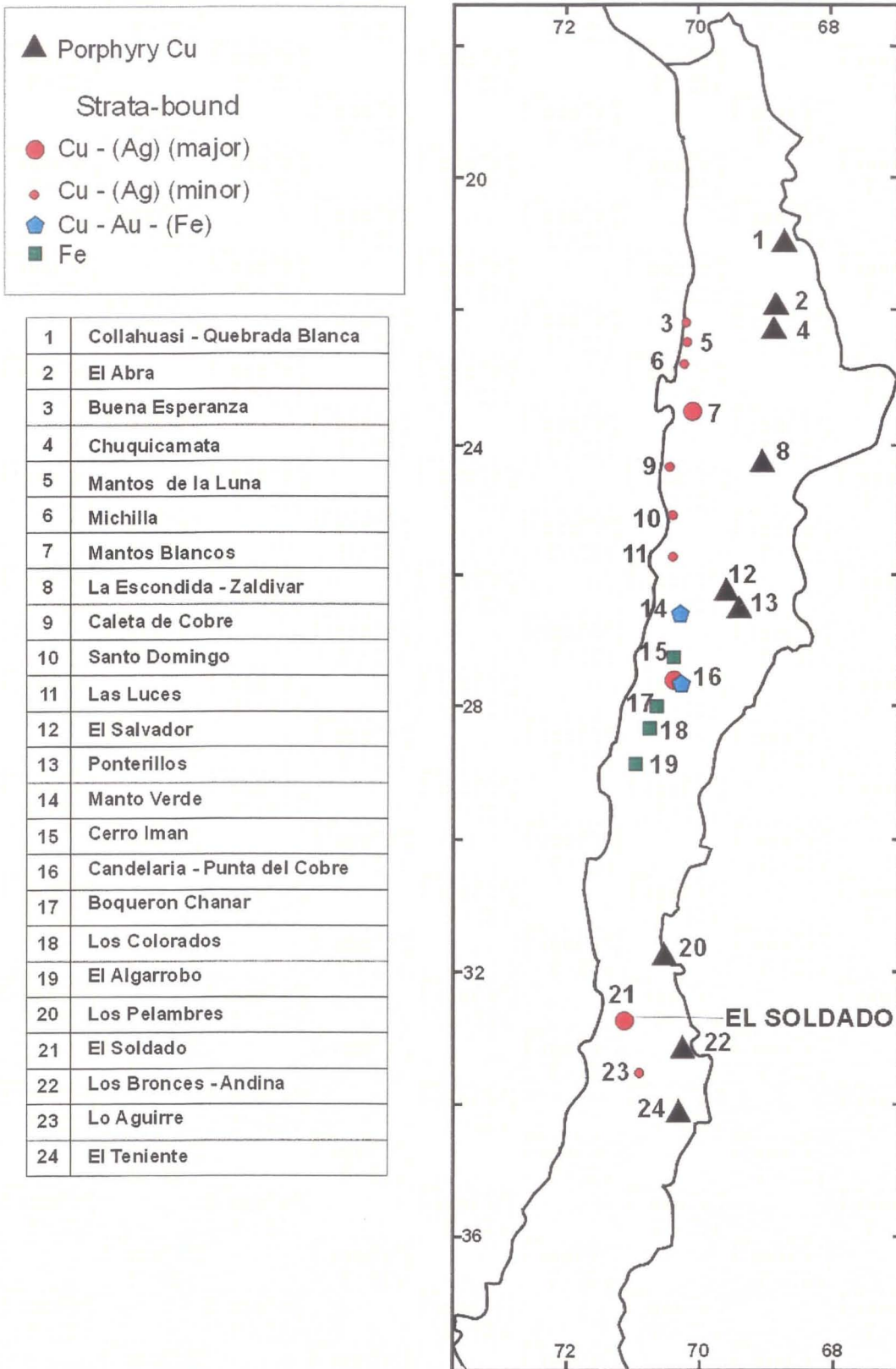
Figure 2.1. Location of El Soldado and distribution of major stratabound (Mesozoic) and porphyry copper (Cenozoic) deposits of Chile.

Legend:
- ▲ Porphyry Cu
- Strata-bound
- ● Cu - (Ag) (major)
- • Cu - (Ag) (minor)
- ⬟ Cu - Au - (Fe)
- ■ Fe

1	Collahuasi - Quebrada Blanca
2	El Abra
3	Buena Esperanza
4	Chuquicamata
5	Mantos de la Luna
6	Michilla
7	Mantos Blancos
8	La Escondida - Zaldivar
9	Caleta de Cobre
10	Santo Domingo
11	Las Luces
12	El Salvador
13	Ponterillos
14	Manto Verde
15	Cerro Iman
16	Candelaria - Punta del Cobre
17	Boqueron Chanar
18	Los Colorados
19	El Algarrobo
20	Los Pelambres
21	El Soldado
22	Los Bronces - Andina
23	Lo Aguirre
24	El Teniente

famous native copper deposits of White Pine district in the Keeweenaw peninsula (Michigan) (e.g. Calumet and Kearsarge mines) and other minor deposits such as Sustut (British Columbia), Kennecott (Alaska), and the 47 Zone in Coppermine River area (NWT). However, the Chilean deposits are richer in sulphur and display a stronger structural control than the North American deposits, and deserve a class of their own, being considerably larger than the above.

A separate, but equally controversial association, the strata-bound Cu-(Au–Fe) deposits, also referred as Candelaria-type, have been discussed together with the Olympic Dam (Cu-U-Au-REE) type deposits (e.g. Porter, 2000). These deposits, which have clear associations with intrusions, have some similarities with the anphibole-magnetite-chalcopyrite Lower Cretaceous Raúl-Condestable deposit in Perú, considered hydrothermal (Atkin et al., 1985), skarn (Vidal et al., 1990) or belonging to the massive sulphide category (e.g. Cardoso, 1990; Steinmüller et al., 2000). Some authors, such as Sillitoe (1992) and Marschik and Fontboté (1996) suggest these strata-bound Cu-(Au–Fe) deposits may be intermediate members between metasomatic magnetite-apatite deposits and porphyry Cu-Au deposits.

2.2. Chilean Strata-bound Cu-(Ag) Deposits ("Manto Type" Cu-(Ag) Deposits)

Among the Chilean strata-bound deposits, the Cu-(Ag) family, also known as "mantos"or "manto-type" copper deposits in the literature, are the more abundant and better studied (see overviews in Sato, 1984; Camus, 1985; Fontboté, 1990; and Sillitoe, 1992). This family of deposits usually has a high copper grade (1.5-2 % Cu), relatively low contents of silver (5-20 g/t) and are practically devoid of gold. They are hosted by Upper Jurassic volcanic rocks in northern Chile (21°- 26° latitude S; e.g. Mantos Blancos, Michilla, Buena Esperanza) and by Lower Cretaceous volcano sedimentary sequences (27°-34° latitude S; e.g. Punta del Cobre, El Soldado). The most important mines of this subtype are Mantos Blancos in northernmost Chile, and El Soldado (the subject of this thesis) in central Chile (Figures 2.1, 2.2, 2.3, and 2.4). For these two deposits the total identified resources, including production plus reserves are over 200
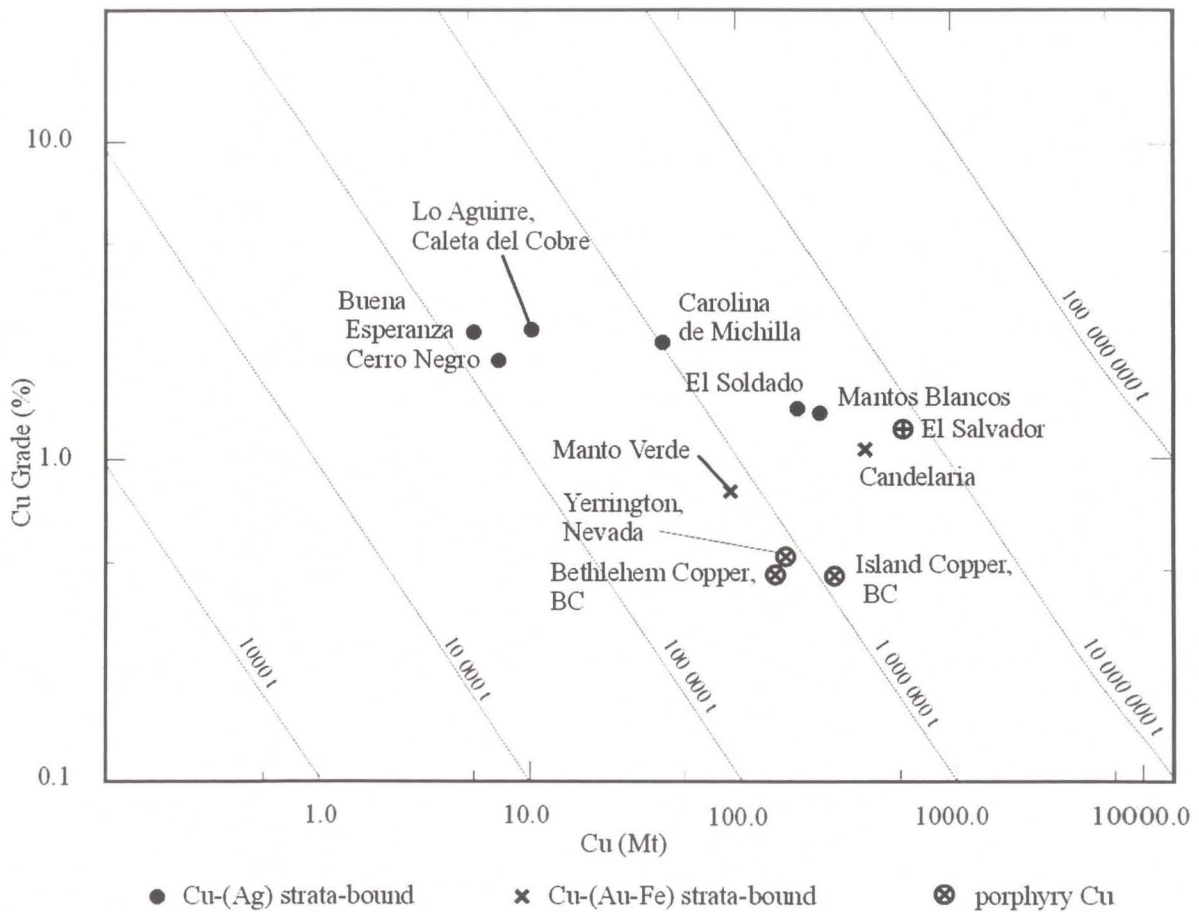
Figure 2.2. Grade tonnage plot for major Chilean strata-bound Cu (Ag) and Cu (Au-Fe) deposits.
It shows that El Soldado is larger, in terms of contained Cu metal, than some well known North American deposits. Modified from Kirkham (1996) and Clark (1993).
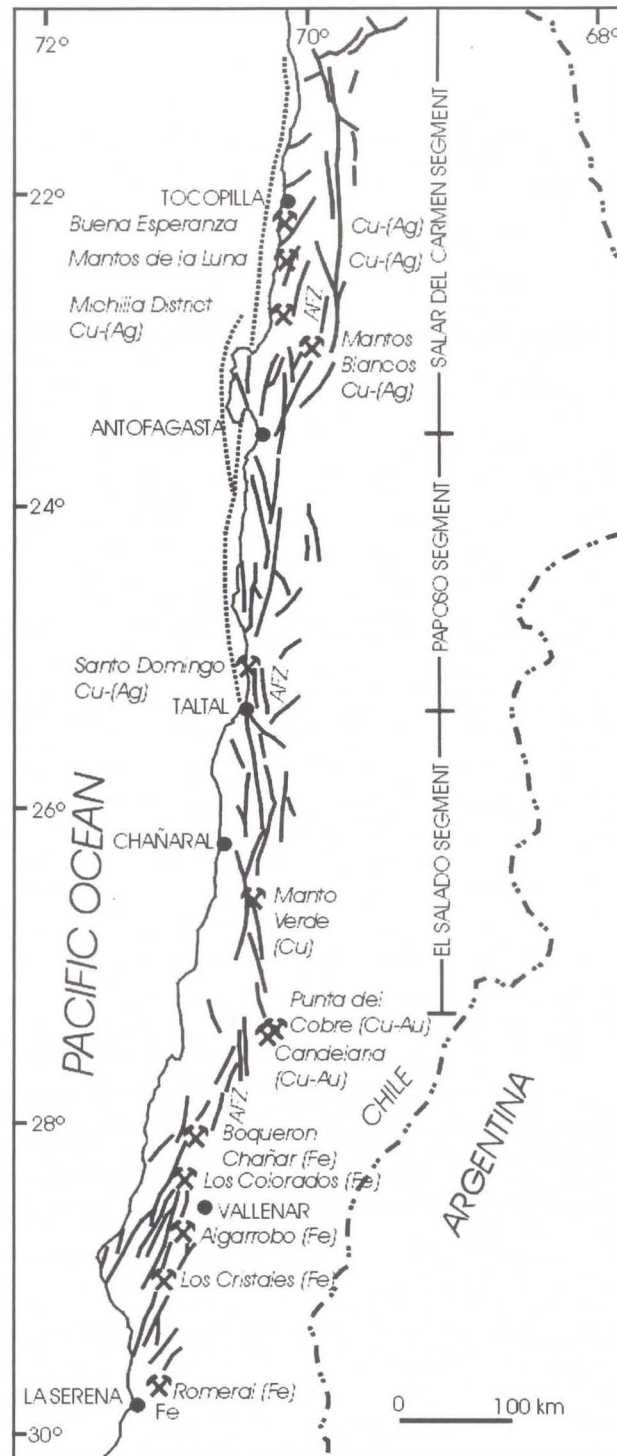
Figure 2.3. Major faults of the sinistral Atacama Fault Zone (AFZ) along the coastal cordillera of northern Chile.
Main Cu (Ag), Cu (Au-Fe) and Fe strata-bound deposits within the domain of the fault zone are shown (after Maksaev and Zentilli, 2002).
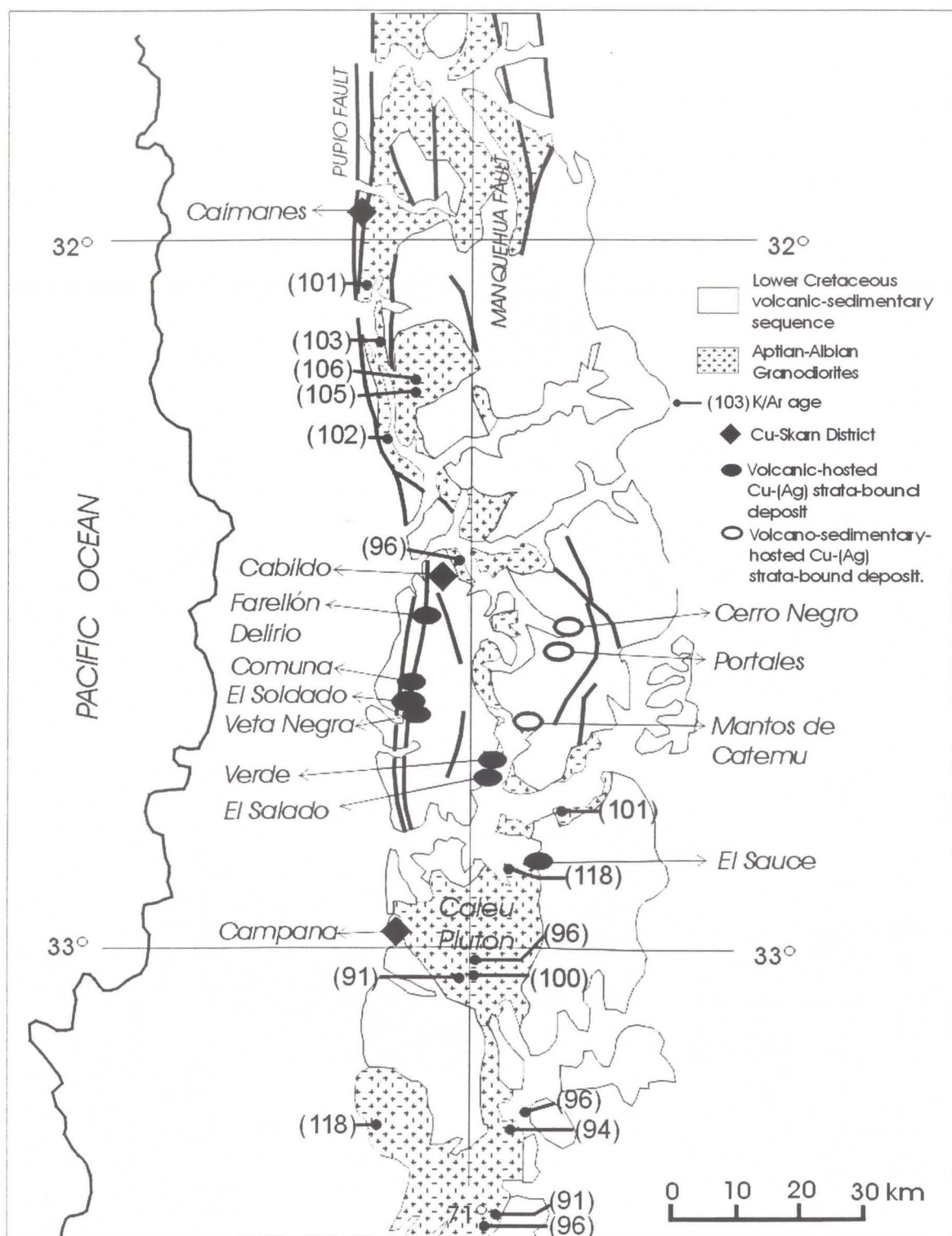
Figure 2.4. Volcanic-hosted and volcano-sedimentary hosted Cu-(Ag) strata-bound depostis in the coastal cordillera of central Chile between 32° and 33°S. K/Ar ages of the batholith are also shown (modified from Maksaev and Zentilli, 2002)

million tonnes @ 1.3-1.4% Cu (Figure 2.2).

The mineralisation in these epigenetic deposits is strata-bound only in a regional sense, meaning that it is restricted to particular stratigraphic units, but in detail it is discordant; orebodies are structurally controlled or follow relatively permeable horizons in the strata (vesicular flow tops, and volcaniclastic breccias). The deposits are usually composed of a number of orebodies, which include stratiform, lenticular, pipe, veins and irregular bodies.

Most of the strata-bound Cu-(Ag) deposits are hosted by mafic basaltic to andesitic host rocks, but notably the largest ones (Mantos Blancos, El Soldado, Punta del Cobre) are hosted by bimodal suites of felsic (rhyolite-rhyodacite) and mafic (basaltic-andesitic) rocks (Chavez, 1985; Boric, 1997; Marschik and Fontboté, 1996). These deposits often occur near subvolcanic intrusives (sills, dykes, stocks, volcanic necks) of gabbroic, dioritic, andesitic, or rhyodacitic composition. These subvolcanic intrusives can be mineralized or not, and some of them clearly pre-date, whereas others post-date copper mineralisation. The intrusives have been interpreted as feeder conduits of the host volcanic flows (Ahumada, 1985a; Palacios and Definis, 1981; Espinoza et al., 1996). The nature of the hosted volcanic sequences has been greatly debated and, they have been considered tholeiitic, low and high K cal-alkaline, shoshonitic (Levi et al., 1988; Pichowiak et al., 1990; Vergara et al., 1995) and even alkaline (Klohn et al., 1990). Nevertheless, geochemistry of immobile trace elements, at the main mine districts, shows that these host rocks are arc-related and have a calc-alkaline signature (Chavez, 1985; Marschik and Fontboté, 1996; Boric, 1997).

A sub-group of these deposits is hosted by sedimentary or volcano-clastic rocks of Lower Cretaceous age (Talcuna, Uchumí, Cerro Negro, Portales, Mantos de Catemu Figure 2.4). These are relatively small deposits formed by roughly tabular conformable orebodies restricted to specific strata. Copper mineralisation concentrates in the upper metres (1 to 10 m in thickness) of specific sedimentary or pyroclastic units that normally underlie impervious rock units. Nevertheless, even in this simpler sub-group of deposits, copper mineralisation shows a structural control, being consistently richer in the proximity of fault zones (Boric, 1985; Camus, 1990).

Despite the difference in host rocks and shapes, the hypogene mineralogy of all these strata-bound Cu-(Ag) deposits is remarkably constant and relatively simple. The common hypogene minerals are bornite, chalcocite (chalcocite, digenite, covellite), chalcopyrite, pyrite, hematite, and minor magnetite. Typical deposit features include a lateral zoning with rich cores (>2 % Cu) dominated by chalcocite-bornite-hematite, surrounded by zones of bornite-chalcopyrite or chalcopyrite and restricted external halos (usually uneconomic) of pyrite-chalcopyrite (Chavez, 1985; Ruge, 1985; Definis, 1985; Boric, 1997). The sulphide ores occur in reduced (probably sub-marine) strata rather than in oxidized (sub-aerial) strata, suggesting that redox reactions were important in their genesis.

Supergene metal enrichment related to surficial weathering, which is significant in porphyry copper deposits, is not a major factor in the ore grade of the mantos. However, oxidized ores are exploited in many mantos. Paragenetic studies of these strata-bound Cu-(Ag) deposits have shown that pyrite was deposited first, followed by chalcopyrite, then by bornite and later by hypogene chalcocite accompanied by hematite. This sequence indicates a gradual increase of the proportion of copper in the sulphides, and probably a decrease of sulphur activity in the mineralising fluids with time (Losert, 1974; Martin, 1981; Camus, 1985; Chavez, 1985). The paragenetic sequence is characterized by the successive hypogene replacement of iron rich sulphides (pyrite, chalcopyrite) by copper-rich sulphides (bornite, chalcocite) this may account for iron release and formation of hypogene hematite associated with the copper sulphides (Chavez, 1985; Holmgren, 1987). The hydrothermal alteration assemblage of albite, chlorite, hematite, quartz, calcite, epidote, K-feldspar, sphene-rutile, and minor sericite and clays is associated with ore minerals in these strata-bound Cu-(Ag) deposits, but the primary textures of the volcanic rocks are preserved (Losert, 1973; Chavez, 1985). Alteration assemblages are broadly similar to low grade metamorphic facies developed in the barren volcanic country rocks (e.g. Sato, 1984; Sillitoe, 1992). Nevertheless, the hydrothermal alteration is particularly pervasive in Mantos Blancos, where litho-geochemistry shows significant metasomatism of the host rocks with addition of Na, Fe and Mg (Chavez, 1984, 1985).

An exception is the Punta del Cobre deposit (Figures 2.1 and 2.3) where the hypogene mineralisation is composed of hematite, magnetite, pyrite, and chalcopyrite, deposited in the same paragenetic sequence (Hopf, 1990; Marschik and Fontboté, 1996). In this district a strong alkali metasomatism (including rich sodium and potassic zones) has been documented (Marschik and Fontboté, 1996). Punta del Cobre has been traditionally included as a member of the manto-type Cu-(Ag) group, but it has minor gold content and it is located in the same district than the La Candelaria Cu-(Au-Fe) deposit, proximal to a Lower Cretaceous batholith. Consequently it may be considered as a transitional deposit between the Cu-(Ag) and the Cu-(Au-Fe) deposits discussed below.

Organic matter in the form of solid bitumen has been recognised as an important mineral facies (gangue) associated with copper sulphides in many manto type Cu-(Ag) deposits hosted by Lower Cretaceous rocks (Zentilli et al., 1994; 1997; Wilson, 1998a). Bitumen has been recognised in sedimentary-hosted deposits such as Talcuna, Cerro Negro and Uchumi, but also in the El Soldado volcanic-hosted deposit. Detailed studies carried out by Wilson (1998a), indicate that at El Soldado bitumen was generated in an earlier, and low temperature (<120 °C), diagenetic stage associated with framboidal pyrite. Copper mineralisation was produced in a second hydrothermal stage of higher temperature (200 to >300 °C), when copper sulphides replaced the previous diagenetic pyrite. According to Wilson and Zentilli (1999) the presence of bitumen within other strata-bound Cu-(Ag) deposits hosted by Lower Cretaceous strata (e.g. Uchumi, Talcuna, Cerro Negro) suggests that degraded petroleum reservoirs were suitable sites for mineralisation by Cu-bearing solutions of different origins in north-central Chile.

2.2.1. Genetic Affinities

The genesis of these strata-bound Cu-(Ag) deposits has been the subject of much controversy (e.g. Fontboté, 1990). Stratiform orebodies were first thought to be syngenetic exhalative (Ruiz et al., 1965; 1971). However, their epigenetic origin is now widely accepted, due to the subsequent discovery of unconformable orebodies, evident structural control by brittle faults, and significant hydrothermal alteration associated with the deposits. The paucity of effectively datable minerals makes problematic the dating of

mineralisation events, and the regional low-grade metamorphism or alkali metasomatism of host rocks complicated the interpretation. Available geochronological data suggest that mineralisation in these deposits took place 15-30 My after the deposition of the host strata, mainly during two metallogenic pulses, in the Upper Jurassic (~160-145 Ma) and in the uppermost Lower Cretaceous (~115-100 Ma) (Boric et al., 1990; Tassinari et al., 1993; Munizaga et al., 1995; Vivallo and Henríquez, 1998; Maksaev and Zentilli, 2002 Wilson et al., in press a).

Nevertheless, the origin of the hydrothermal fluids and the source of metals and sulphur are still poorly constrained. The proposed genetic models ranging from hypotheses that call for fluids liberated during low-grade metamorphism of the volcanic piles (e.g. Sato, 1984; Westra, 1988a; Sillitoe, 1992); magmatic fluids directly derived from the subvolcanic associated bodies (Espinoza, 1981; Palacios, 1986; Klohn et al., 1990; Espinoza et al., 1996), or magmatic fluids derived from distal batholiths (Carter, 1961, Vivallo and Henríquez, 1998). A combination of magmatic and metamorphic fluids has also been considered (e.g. Fontboté, 1990).

Fluid inclusion data from quartz and calcite veins related to ore in this family of deposits show no evidence of boiling, and indicate high salinities, in the range of 5-40 % NaCl-equivalent (mostly clustereded between 15-35 %) and homogenisation temperatures in the range of 70-400 °C (mostly concentrated at 220-350 °C; Nisterenko et al., 1973; Holmgren, 1987; Collao, 1993; Oyarzún et al., 1998; Trista, 2001). The highest homogenisation temperatures have been obtained from the volcanic hosted deposits (El Soldado, Mantos Blancos) and the lowest in the sedimentary-hosted, Talcuna deposit, where evidence of boiling has been noted (Oyarzún et al., 1998). These data suggest that saline fluids, at moderate temperatures and at relatively deep emplacements (1000-3000 m assuming hydrostatic conditions) formed most of deposits. Sedimentary-hosted deposits could have formed at shallow depths as suggested for lower temperatures and evidence of boiling. Based on few and preliminary isotopic studies of sulphides, a magmatic source for S in the volcanic-hosted deposits ($\delta^{34}S$ -10 to +10 ‰) and a biodegraded origin for S in sedimentary hosted deposits ($\delta^{34}S$ -10 to -40 ‰), was suggested (Holmgren, 1987; Munizaga and Zentilli, 1994). But new data by Wilson

(1998a) at El Soldado show a wide spectrum for copper sulphides ($\delta^{34}S$ -13 to +19 ‰) and indicate that sulphur may be not magmatic in origin even for the volcanic hosted deposits. Instead it could be inherited from pre-existing pyrite ($\delta^{34}S$ -11 to 28 ‰) formed in a low-temperature diagenetic stage (Wilson 1998a; Wilson and Zentilli, 1999).

In short, these strata-bound Cu-(Ag) deposits are envisaged as epigenetic hydrothermal deposits formed in two metallogenetic episodes by saline fluids, (metamorphic, magmatic?) at low to moderate temperatures which reacted with the reduced host rocks and or the diagenetic pyrite and deposited the copper sulphide ores in permeable and structural favourable places.

2.3. Chilean Strata-bound Cu-(Au-Fe) Metasomatic Deposits

The strata-bound Cu-(Au- Fe) subtype has gained relevance and interest in the last decade with the discovery and development of the large Candelaria and Manto Verde deposits, both located in the Copiapó region of northern Chile (Figures 2.1 and 2.3). Lower Cretaceous volcanic rocks host these deposits; they have relatively low copper grades (0.8 - 1.1 %) but important gold contents (0.2 - 0.4 g/tonne). Mineable reserves in Candelaria are estimated at 366 million tonnes @ 1.08 % Cu and 0.26 g/tonne Au (Ryan et al., 1995), and in Manto Verde at 85 million tonnes @ 0.82% Cu with gold ranging between 0.1 and 0.5 g/tonne (Vila et al., 1996; Figure 2.2).

These Cu-(Au-Fe) deposits are composed of stockworks, breccias, mantos and veins and are strongly structurally controlled by faults, which are branches of the Atacama Fault Zone, a major sinistral strike-slip fault system that extends more than 1,000 Km along the Coastal Cordillera of northern Chile from latitude 20° to 30° S, and which was active in the Jurassic-Early Cretaceous interval (Maksaev, 1990; Scheuber and Reutter, 1992; Figure 2.3). Both deposits are proximal (<2 km) to an Aptian-Albian batholith and in Manto Verde NNW-trending dikes intrude the host rocks. The hypogene ore assemblage is composed of chalcopyrite and pyrite (in the proportion of cp:py = 5:1) and is rich in magnetite (Candelaria) or specularite (Manto Verde) and is accompanied by strong K-silicate alteration. At Candelaria multiple hydrothermal stages have been recognized (Ryan et al., 1995). A first stage produced a potassic alteration (biotite, minor

K-feldspar) and magnetite plus minor apatite. A second stage formed a sodic-calcic assemblage (actinolite, scapolite, albite) plus chalcopyrite and minor pyrite and magnetite. Later stages include a retrograde pulse (amphibole, chlorite, epidote, minor sericite) and a later introduction of K-feldspar (Ryan et al., 1995). K-feldspar, chlorite, and minor quartz and tourmaline characterize potassic alteration at Manto Verde. Late veins of calcite have also been reported (Vila et al., 1996). The ore and alteration mineral in these Cu-(Au-Fe) deposits clearly represent a higher temperature association than the Cu-(Ag) strata-bound deposit discussed above. At Candelaria the temperature of mineralising fluids may have been 500-600 °C (Marschick and Fontboté, 2001). At Manto Verde fluid inclusions yield relatively low homogenisation temperatures (180–250 °C) but very high salinities (30-50 % NaCl equivalent) interpreted by Vila et al. (1996) to indicate a magmatic source.

Candelaria is located close to Punta del Cobre (Figures 2.1, 2.3), the only important manto-type deposit with minor gold content (see above), and a genetic link between both deposits has been suggested (e.g. Pop et al., 2000). Although there is some debate about the genesis of these deposits, most authors consider them as metasomatic and related to the emplacement of the proximal Aptian-Albian batholith (e.g. Ryan et al., 1995; Vila et al., 1996). The age of mineralisation has been set at 117-121 Ma for Manto Verde, according to K/Ar sericite ages of altered host rocks (Vila et al., 1996). At Candelaria, two pulses of mineralisation have been recognised, one at 117-114 Ma and other at 112-110 Ma, according to $^{40}Ar/^{39}Ar$, Rb/Sr, U/Pb and Re/Os dating (Ulrich and Clark, 1999; Arévalo et al., 2000; Marschik and Fontboté, 2001).

It is interesting to note that these Cu-(Au-Fe) deposits occur in the vicinity of a group of metasomatic Fe deposits (the "Chilean Iron Belt" of Ruiz et al., 1965; Figures 2.1 and 2.3) composed of massive magnetite and minor actinolite-apatite, exposed between 27° to 30° latitude S and also Early Cretaceous in age (128-111 Ma; Zentilli, 1974; Vivallo and Henríquez, 1998). A more global genetic connection has been proposed for these two families of deposits taking in account the similarity in location, mineralogy, lithology and age (Vivallo and Henríquez, 1998).

2.4. Tectonic Setting for Chilean Volcanic-Hosted Strata-bound Copper Deposits

In terms of tectonics, the Jurassic-Early Cretaceous interval in Central-Northern Chile was a critical period in the Andean evolution, characterised by the development of a magmatic (plutono-volcanic) arc along the present Coastal Cordillera, and extensional back arc basins filled with marine sediments further east (Figure 2.5). Along the magmatic arc, major (regional scale) strike slip faults, such as the Atacama Fault Zone (Figure 2.3) were developed. These features are explained by an oblique and low stress, Marianas type (extensional) subduction during the interval (e.g. Boric et al., 1990; Scheuber et al., 1994). The emplacement of batholiths and volcanism were controlled by transtensional and tensional regimes within these fault systems as postulated by Dallmeyer et al. (1996).

Tectonic inversion, including the emergence of the back-arc basin system, took place during the Cenomanian to Santonian as a result of compressive deformation pulses that affected the whole Central Andes (Figure 2.5; Maksaev, 1990; Scheuber et al., 1990; Ramos and Alemán, 2000). The subsequent Late Cretaceous-Cenozoic period, in North Central Chile, was characterized by the development of new magmatic arcs 50 to 100 km eastward from the previous ones. These new arc-systems developed on a continental environment within an overall compressive tectonic setting. These paleogeographic and geotectonic changes have been interpreted as an adjustment of the active continental margin of South America from a Marianas (extensional) to a Chilean (compressive) type of subduction (Davidson and Mpodozis, 1991; Ramos and Alemán, 2000). During this Late Cretaceous - Cenozoic interval, giant mesothermal porphyry copper deposits (e.g., Chuquicamata; El Teniente) and world-class epithermal gold and silver deposits (e.g. El Indio, La Coipa) were formed along the magmatic arcs. (e.g. Maksaev, 1990; Sillitoe, 1990, 1992).

In summary, El Soldado, the subject of this thesis, is one of the largest representative copper deposits generated in a critical period of Andean evolution, (Jurassic-Early Cretaceous), which was characterised by the generation of Cu-(Ag), Cu-(Au-Fe), and Fe volcanic-hosted deposits under an extensional (Marianas type) geotectonic regime. These deposits originated in two discrete pulses in the Late Jurassic
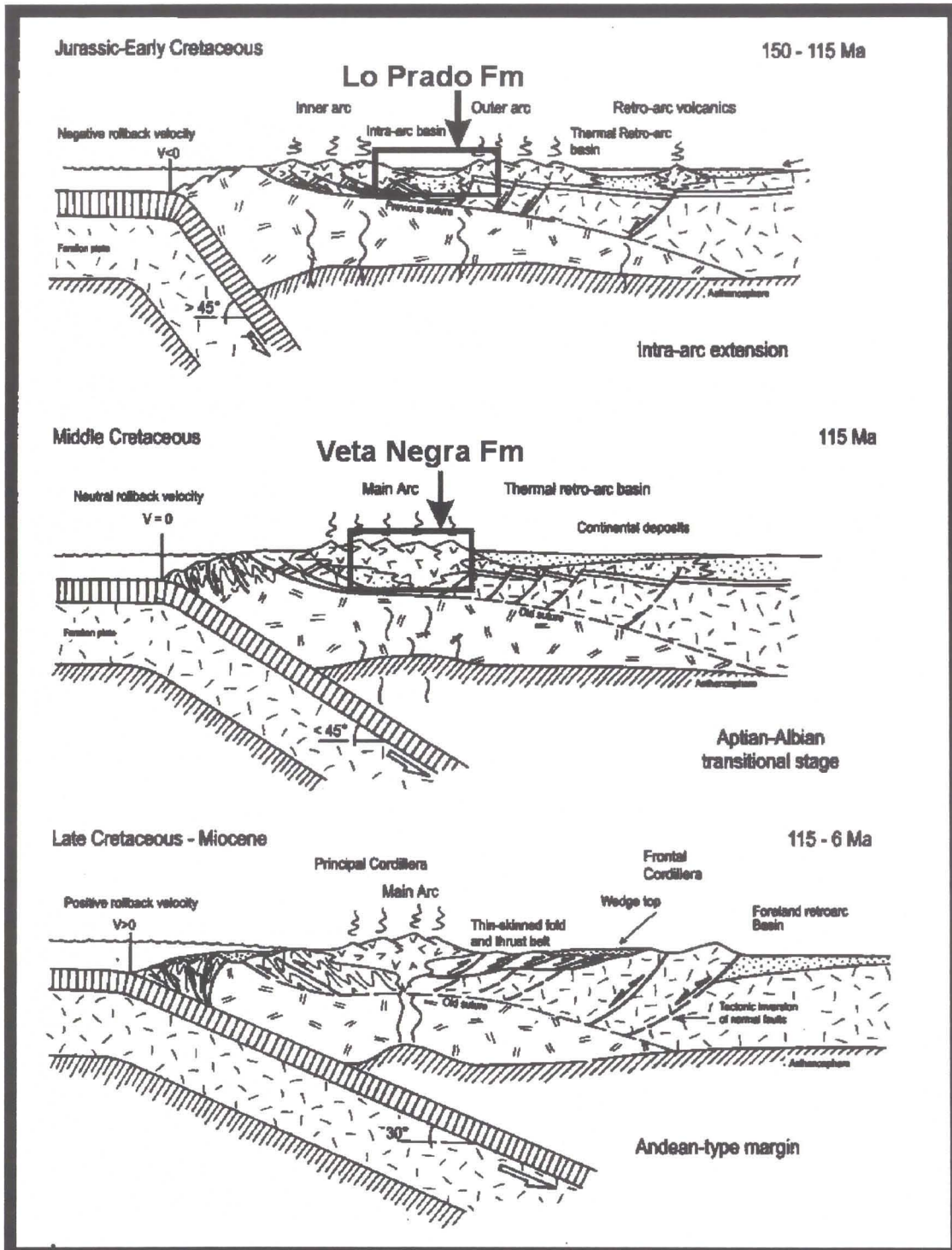
Figure 2.5. Different tectonic regimes in the southern Central Andes.

Illustration shows the change between an extensional and compressional tectonic regime about 115Ma (Ramos and Aleman, 2000).

and in the latest Early Cretaceous, at the time of emplacement of dioritic to granodioritic batholiths probably controlled by trans-tensional sinistral regional faults. The Cu-(Ag) manto-type deposits (such as El Soldado) are distal to these batholiths and no direct relation with them is recognised. The Cu-(Au-Fe) and the Fe deposits are proximal to the Lower Cretaceous batholiths, and a genetic relationship with the intrusives is evident. This Jurassic-Early Cretaceous interval predated the emplacement of the giant porphyry copper deposits and the world-class epithermal gold-silver deposits during the Late Cretaceous - Tertiary, which were emplaced under compressive geotectonic conditions (Chilean subduction type) and typically related to calc-alkaline ("Andean") magmatic rocks (e.g. Maksaev, 1990; Sillitoe, 1990; 1992).

CHAPTER 3. GEOLOGY OF EL SOLDADO COPPER DEPOSIT: A GENERAL SYNTHESIS AND UPDATE

3.1. Introduction

As indicated above, El Soldado is a strata-bound copper-(silver) deposit hosted by volcanic rocks of the upper member of Lo Prado Formation of Early Cretaceous age. The deposit is made up of a number of discordant and irregular orebodies composed of hypogene sulphides and minor supergene copper oxides, controlled by structures and lithology. An overview and a new interpretation of the geology are offered, based on the work for this study.

A listing of the previous publications, theses and abstract published on El Soldado is given in Tables 3.1, 3.2, and 3.3. The following description is here compiled from Ruge (1985), Holmgren (1987), Klohn et al. (1990), Zentilli et al. (1997), Boric (1997), Wilson (1998a) plus additional observations by the author.

3.2. Geological Setting

The El Soldado deposit is hosted by the upper member of the Lower Cretaceous Lo Prado Formation, a volcaniclastic arc suite, which represents an important regional metallotect, hosting more than 20 copper mines between the Aconcagua and the La Ligua rivers (Figure 3.1). At El Soldado, this unit is composed of bimodal rhyodacite (felsic) and basaltic (mafic) flows and with sedimentary volcaniclastic (epiclastic) and marine sedimentary intercalations. The lower member of Lo Prado Formation, which underlies these strata, is a marine, shaly, organic-rich sequence, 1200 m in thickness. The Lo Prado Formation conformably overlies the volcanic Upper Jurassic Horqueta Formation, and is conformably overlain by 5-7 km of basaltic andesites, tuffs and redbeds of the continental Lower Cretaceous (Barremian-Albian) Veta Negra Formation, which in turn is overlain by the Cretaceous (Aptian - Turonian) Las Chilcas Formation (Figure 3.1; Rivano et al., 1993; Wall et al., 1996; Wall et al., 1999).

Deposition of the sedimentary-volcanic sequence took place in a transitional marine-terrestrial environment during the Early Cretaceous. The Lo Prado Formation

Table 3.1. Unpublished Theses on the El Soldado Deposit

Date	Title	Data Presented	Author
1977	Translated Title:"Petrography, hydrothermal alteration, and mineralization of the El Soldado copper deposit, Valparaiso Province, Chile"	Rock petrography; major element geochemistry; description of hydrothermal alteration	Terrazas, R.
1981	Translated Title: "Distribution of mineralization in the El Soldado copper deposit, V region"	Rock and ore petrography; paragenetic study; mineral zoning	Martin, W.
1985	Translated Title: "Intrusive events in the El Soldado copper deposit, V region"	Description of lithological units including subvolcanic bodies; rock petrography; major element geochemistry	Ahumada, R.
1988	Translated Title: "Relationships among fractures, stresses, and mineralization in the El Soldado deposit, V region"	Structural study; fracture classification; crhonology of fracturing; structural modeling	Chavez, A.
1995	Translated Title: "Evidences for the genetic model of the Veta Negra deposit and its relation to the El Soldado deposit"	Geology of the Veta Negra deposit and its relation with El Soldado mine; S, C, and O isotope data; organic matter reflectance analyses	Villalobos, H.
1998	"The role of petroleum in the formation of the El Soldado copper deposit, Chile: hydrothermal replacement of a biodegraded petroleum reservoir"	Study of organic matter (bitumen) and its relation with ore; ore petrography; mineral geochemistry; S, O, and C isotope data; Ar/Ar geocrhonology; genetic model proposition	Wilson, N.
2000	Translated title:"Geology, mineralization, and distribution of trace elements in Filo area, El Soldado mine, V region"	Geology of Filo area; ore petrography; mineral zoning; microprobe data; chemical characterization (major and trace elements) of ore zones	Ponce, R.

Table 3.2. Published Papers on The El Soldado Deposit

Date	Author(s)	Data Presented	Title
1975	Olcay, L., and Alarcón B.	Petrography; hydrothermal alteration description	Translated title:"Sodic hydrothermal alteration in the El Soldado mine, Valparaiso Province, Chile"
1984	Bassi, H.	Structural data	"El Soldado, a Chilean, apparently stratiform disseminated ore deposit, with tectonic and lithological controls"
1984	Sato, T.	Review of manto-type deposits	Manto -Type copper deposits of Chile
1985	Ahumada, R.	Petrography; description of volcanic and subvolcanic rock units; major element geochemistry	Translated Title:"Intrusive events in the El Soldado copper deposit"
1985	Bassi, H.	Exploration geochemistry	"Results of extrapolating metallogenic controls of the El Soldado Mine to strategic prospecting in the Aconcagua Region, central Chile"
1985	Holmgren, C.	Petrography; fluid inclusion and S isotope data; proposal of a genetic model	Translated title: "Constraints for the genetic model of the El Soldado deposit"
1985	Ruge, H.,	Description of geology and mineralization; major element geochemistry	Translated title: "Geology and Mineralizarion of the El Soldado copper deposit"
1986	Klohn, E., Holmgren, C.,and Ruge, H.	Description of deposit; petrography; major element geochemistry; fluid inclusion and S isotope data	El Soldado, a peculiar copper deposit associated with anomalous alkaline volcanism in the Central Chilean Coastal Range
1987	Holmgren, C.	Petrography; description of hydrothermal alteration; fluid inclusion and S isotope data; genetic model discussion	Translated title:"Evidences for a genetic model of the El Soldado deposit, region V, Valparaiso, Chile"
1988	Bassi, H.	Geological model discussion	"Evolution in the geological knowledge of the El Soldado disseminated copper deposit, region 5, Chile"
1988	Holmgren, C. and Gonzalez, F.	Ore description; ore zoning; metallurgical zoning	Translated title:"Mineralogical-Metallurgical zoning of El Soldado deposit, region V"
1988	Munizaga, F., Holmgren, C., Huete, C., and Kawashita, K.	K-Ar and Rb-Sr data	Translated title: "Geocrhonology of El Soldado and Lo Aguirre copper deposits, Central Chile"
1988	Westra, G.	Proposition of a metamorphic model for manto type copper deposits	Translated title: Importance of metamorphism in the formation of manto type copper deposits
1990	Klohn, E., Holmgren, C., and Ruge, H.	Description of deposit; petrography; major element geochemistry; fluid inclusion and S isotope data; genetic model discussion	El Soldado, a strata-bound copper deposit associated with alkaline volcanism in the Central Chilean Coastal Range
1992	Ruge, H., and Vera, I.	Ore sampling and ore grade control methodologies	"Evaluation of sampling and grade control methods at the El Soldado underground copper mine, Chile"
1993	González, F. and Holmgren, C.	Description of oxide ore minerals; metallurgical study	Translated title:"Mineralogical characteristics of the oxidation zone and its implication in the recovery of sulfides in the El Soldado deposit"
1994	Boric, R., and Munizaga, F.	Ar-Ar and Rb-Sr data	Translated title: "Ar-Ar and Rb-Sr geocrhonology of the strata-bound El Soldado copper deposit, Central Chile"
1994	Munizaga, F. and Zentilli, M.	S isotope data	Translated title: "Sulphur isotopic characterization of manto-type deposits of Chile"
1997	Zentilli, M., Munizaga, F., Graves, M. C., Boric. R., Wilson. N., Mukhop-adhyay, P. K., and Snow-don, L.R.	C and O isotopes data; reflectance data for bitumen; discussion of the role of bitumen within the manto-type Cu deposits	"Hydrocarbon Involvement in the genesis of Ore Deposits: an example in Cretaceous strata-bound (Manto Type) Copper Deposits of Central Chile"
1997	Ruiz, J., Freydier, C., McCandless, T., Chesley, J., and Munizaga, F.	Re/Os isotopic data for pyrite samples	Re-Os -Isotope Systematics of sulfides from base- metal porphyry and manto-type mineralization in Chile
1999	Wilson, N. and Zentilli, M.	Sulfide and organic petrology; compositional data for bitumen; paragenesis; genetic model discussion	The role of organic matter in the genesis of the El Soldado volcanic- hosted manto-type Cu deposit, Chile
2000	Wilson, N.	Petrography and reflectance data for bitumen; compositional data for bitumen (microprobe and LA-ICPMS analyses)	Organic petrology, chemical composition, and reflectance of pyrobitumen from the El Soldado Cu deposit, Chile

Table 3.3. Published Abstracts on the El Soldado Deposit

Date	Author(s)	Thopic	Title
1994	Zentilli, M., Boric, R., Munizaga, F., and Graves, M.C.	Role of organic matter in mineralization	Petroleum involvement in the genesis of some strata-bound copper deposits of Chile
1994	Munizaga, F. and Zentilli, M.	S isotope data	Translated title: "Sulphur isotopic characterization of manto-type deposits of Chile"
1994	Zentilli, M., Munizaga, F., Mukhopadhyay, P.K., Graves, M., and Boric, R.	Role of organic matter in mineralization	Organic matter involvement in the genesis of epigenetic, predominantly volcanic-hosted, strata-bound copper deposits in Chile
1995	Ahumada, R. and Gonzalez, F.	Ore reserve estimation	translated title: "Use of geological restrictions in the geostatistical estimation of ore reserves, in the El Soldado deposit"
1995	Boric, R.	Mineral zoning	Mineral zoning at El Soldado copper deposit, Central Chile
1996	Wilson, N.	Mineral paragenesis and petrography	Framboidal copper sulphides associated with bitumen:implications to genesis of the El Soldado copper deposit
1997	Boric, R.	Summary of geology	Translated title: "New evidences about the genetic model of El Soldado copper deposit, central Chile"
1997	Wilson, N. and Zentilli, M.	Bitumen-copper sulphides textures; paragenetic study	Copper sulphides formed in a degraded petroleum reservoir of the Cretaceous Andean arc basin, central Chile
1997	Wilson, N. and Zentilli, M.	Role of organic matter in mineralization	The role of petroleum in the formation of strata-bound copper deposits in Central Chile
1997	Wilson, N.	Role of organic matter in mineralization	The role of petroleum in the genesis of central Chilean strata-bound copper deposits
1998	Wilson, N.	Bitumen description	Organic petrology of pyro-bitumen from the El Soldado copper deposit, Chile
1998	Wilson, N. and Zentilli, M.	Stages of evolution in the genesis of El Soldado deposit	The formation of stratabound copper deposits in degraded petroleum reservoirs, Central Chile
2001	Boric, R. and Zentilli, M.	Mineral zoning and lithochemistry	Geology, mineral zoning, and lithogeochemistry of hydrothermal alteration at the El Soldado manto type copper deposit, Chile

Figure 3.1 El Soldado in its regional stratigraphic setting.
Note the large number of Cu deposits, mines, and occurrences hosted by the Lower Cretaceous Lo Prado Formation and the distal location of El Soldado with respect to outcrops of the Cretaceous batholith. Cross-section A-A' shows the relative position of the small Veta Negra Cu deposit in the Purehue member of the Veta Negra Formation. Modified from Boric et al. (2002).
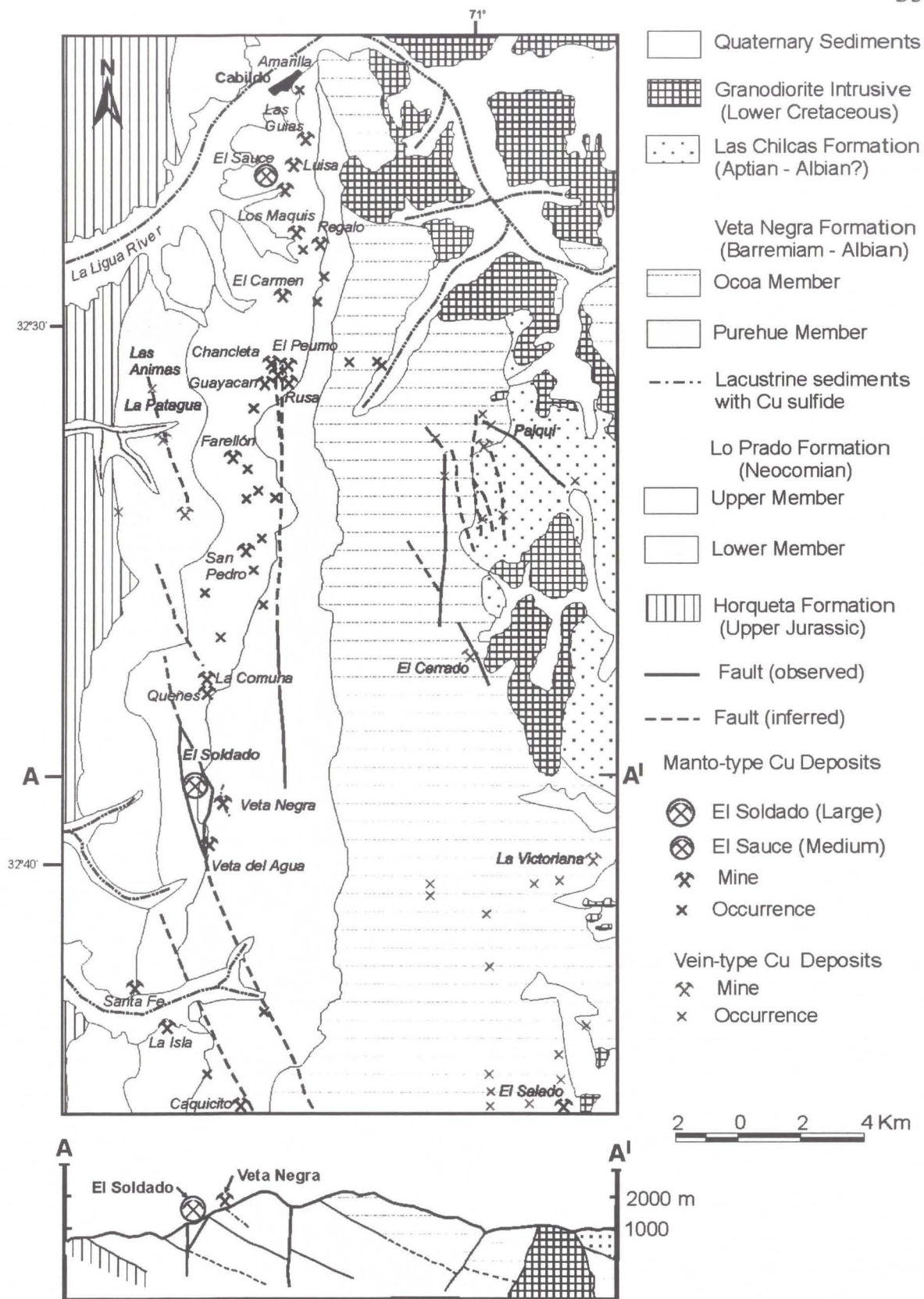
Figure 3.1 El Soldado in its regional stratigraphic setting

contains both marine (ammonites, pelecypods, algae, corals, rudists, crinoids, echinoids of Berriasian to Hauterivian age; Vergara et al., 1995; Wall et al., 1999) and plant remains, indicating proximity to a coast. Pillow basalts are locally developed in the upper member of Lo Prado Formation (Vergara et al., 1995), but none have been found in the mine area. The overlying Veta Negra Formation marks a transition to a terrestrial environment, and is characterised by oxidised lavas and intercalated volcaniclastic redbeds and lacustrine sediments. However, the presence of Lower Cretaceous marine fossils in the overlying Las Chilcas Formation (Rivano, 1996; Wall et al., 1999) indicates that brief marine transgressions occurred after deposition of the Veta Negra Formation in the subsiding basin.

Lower Cretaceous, calc-alkaline, I type granitoids intrude both Lo Prado and Veta Negra Formations, and are responsible for relatively small skarnoid copper deposits at Cabildo (Figure 3.1) and La Campana districts (Ruiz and Peebles, 1988). Geochronological K/Ar and $^{40}Ar/^{39}Ar$ data for this batholith yield a range between 118 to 94 Ma, but most of the ages are clustered in the range 106-96 Ma (Rivano et al., 1993; Wall et al., 1999; Parada and Larrondo, 1999). This suggests that the main pulse of intrusion occurred during the Albian. Despite the great extent of the granitoids, they do not outcrop close to El Soldado where the only recognised intrusive rocks are subvolcanic dykes and stocks (Figures 3.1, 3.2, and 3.3).

Major structures recognised at the district scale are NS to NNW left lateral strike-slip faults and reactivated normal faults; the latter dipping 60° to west (Figures 3.1, 3.2, and 3.3). At El Soldado, the strata have been tilted into a 30° east-dipping homocline, but the dip of the strata decreases progressively to the east. The predominantly volcanic sequence has been metamorphosed to zeolite facies and prhenite-pumpellyte facies (e.g. chlorite, epidote, and albite; Levi, 1969; Holmgren, 1987). Superimposed contact metamorphic effects and hydrothermal alteration have locally overprinted the effects of very low-grade metamorphism.

In terms of tectonics, these Lower Cretaceous volcano-sedimentary sequences and granitoids, are inferred to represent a volcano-plutonic arc developed at a continental margin (e.g. Charrier and Muñoz, 1994; Vergara et al, 1995). The great thickness of the
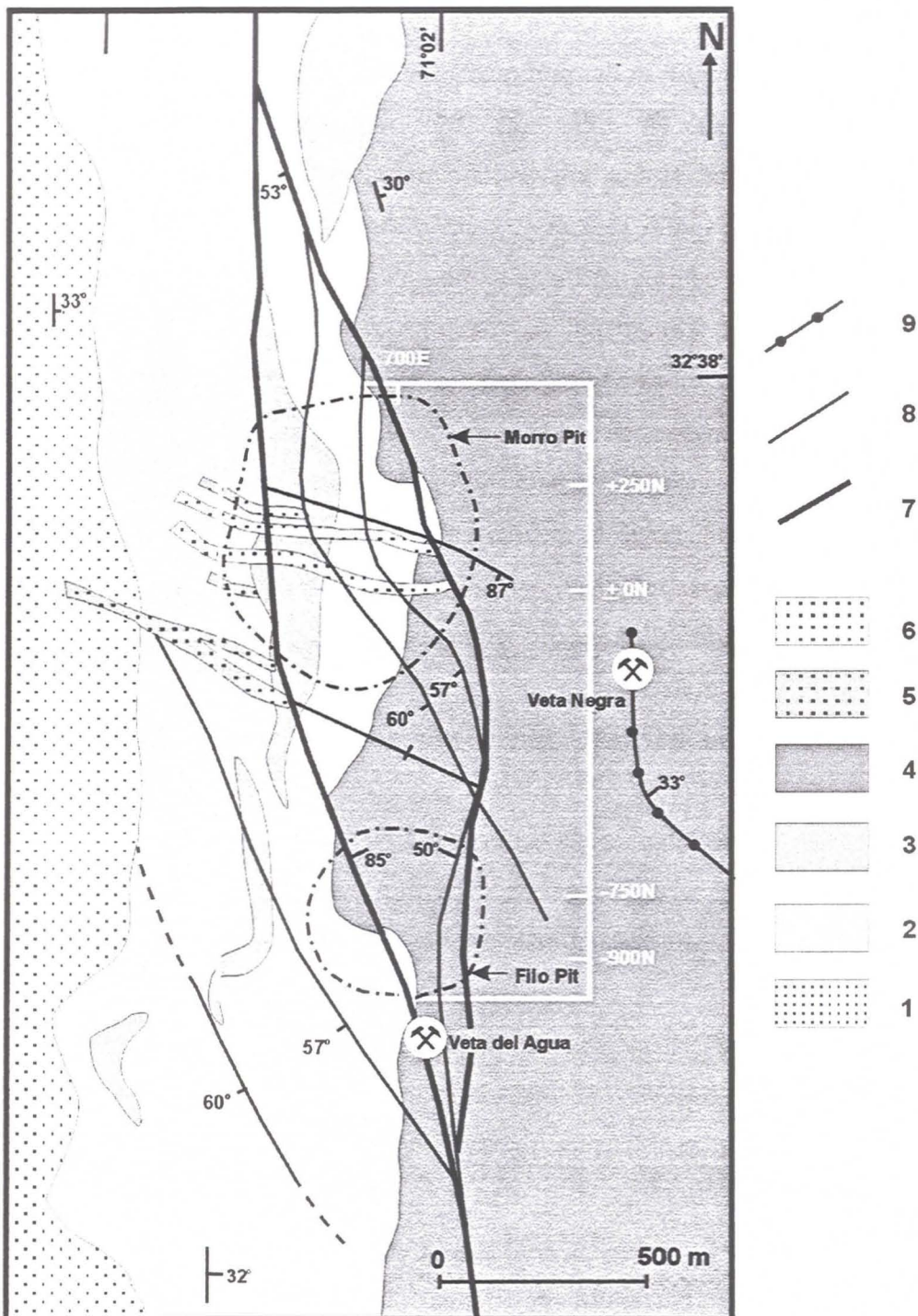
Figure 3.2. Simplified geological map of El Soldado.
Note dash-dot outline of open pits. **1**: Lower sedimentary member of Lo Prado
Formation; **2**: Upper volcanic member of Lo Prado Formation; **3**: Rhyodacite flows and
domes; **4**: Veta Negra Formation; **5**: Rhyodacitic feeder dykes; **6**: Feeder dykes for
Veta Negra Formation; **7**: Main strike slip fault; **8**: Fault; **9**: Mineralised (Cu) lacustrine
shale at Veta Negra mine (see **Fig. 3.1**), showing dip of strata. Due to generalisation,
dyke displacements are not shown (modified from Boric, 1997 and Boric et al., 2002).
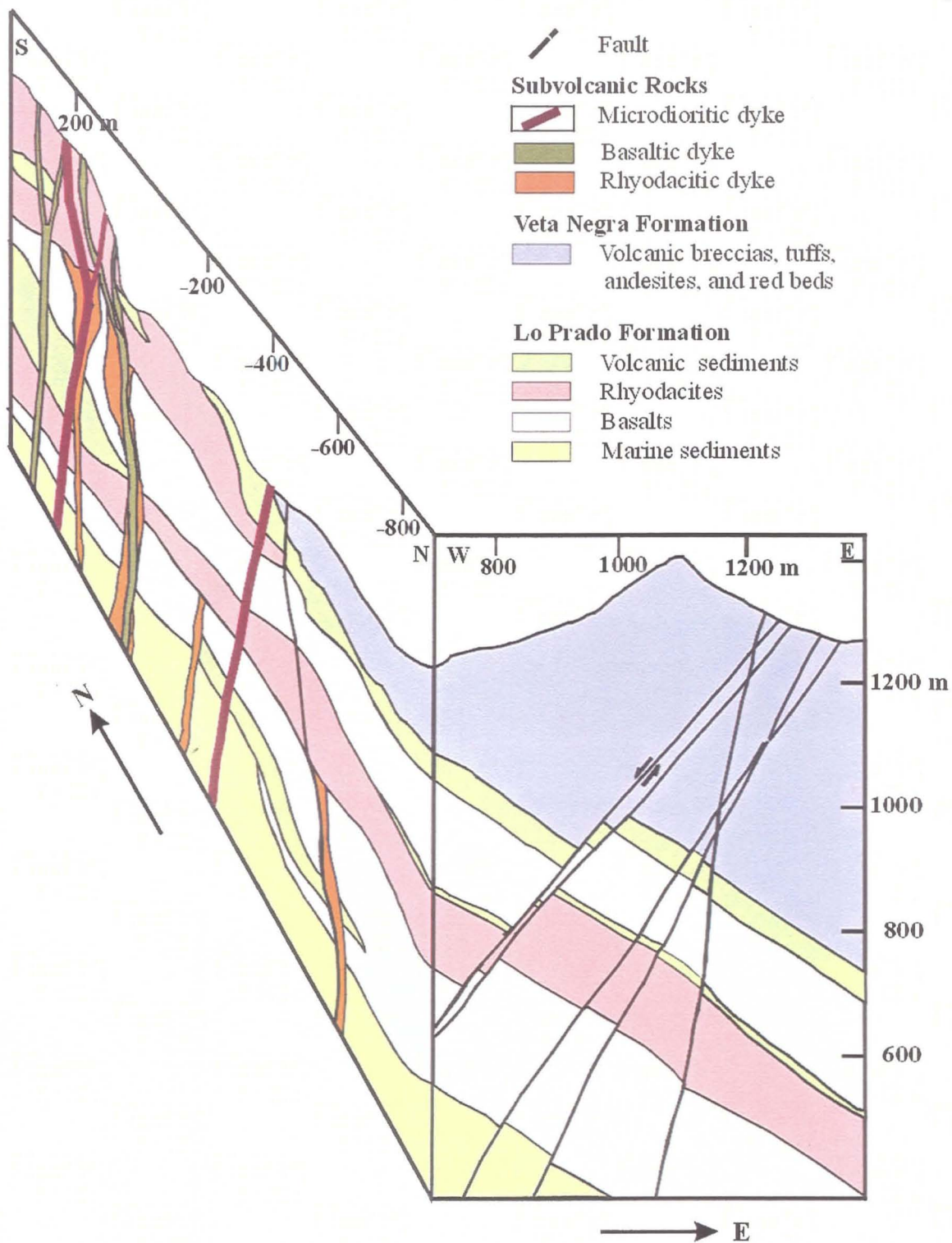
Figure 3.3. Simplified geological block diagram along the NS (700 E mine coordinate) and EW (-900 N mine coordinate), showing the main rock units at the mine scale.

formations and the recurrence of marine facies are indicative of subsidence and the deposition under extensional conditions, which had prevailed at the arc and back arc domains (Mpodozis and Ramos, 1989; Vergara et al., 1995). This environment is consistent with conditions of a steep and relatively low-stress subduction regime ("Marianas" Type) in the Andes during the Early Cretaceous (e.g. Åberg et al., 1984; Sillitoe, 1992; see also chapter 2.1).

3.3. Geology of El Soldado Copper Deposit
3.3.1. Lithology

At El Soldado mine three main stratigraphic units, with a general north-south trend and dipping 30°-33° east, are recognised. The sequence is intruded by a set of subvertical dykes mostly trending WNW and by a gabbro stock. The main rock units are (see Figures 3.2, 3.3, 3.4, and 3.10 below)

3.3.1.1. Lower Member of Lo Prado Formation

The lower member of Lo Prado Formation is composed of planar, bedded calcareous sandstones, organic rich silstones, and calcareous shales (Figure 3.4, 3.5). These rocks locally show soft-sediment (intraformational; possibly seismites, M.Zentilli, personal communication) deformation (Wilson, 1998a), are organic-rich, and contain calcite and bitumen veinlets. The best outcrops of this member occur along the access road to the mine, where only the upper 600 m of the unit are exposed. This lower member is also intersected by the bottom levels of the underground mine. This member does not host any copper ore, although finely disseminated pyrite occurs along bedding planes. Only traces of sphalerite, galena, chalcopyrite, pyrrhotite and framboidal pyrite have been identified in shale samples of this unit (sample MP761, appendix 1).

This member contains marine fossils (e.g. pelecypods and ammonites) some of them found in the mine camp. The fossil record and lithology suggest a bathial to sublittoral environment of deposition (Vergara et al., 1995; Rivano, 1996). The thickness of this unit varies along strike, but at the El Soldado it is over 1.2 km (Figure 3.1).
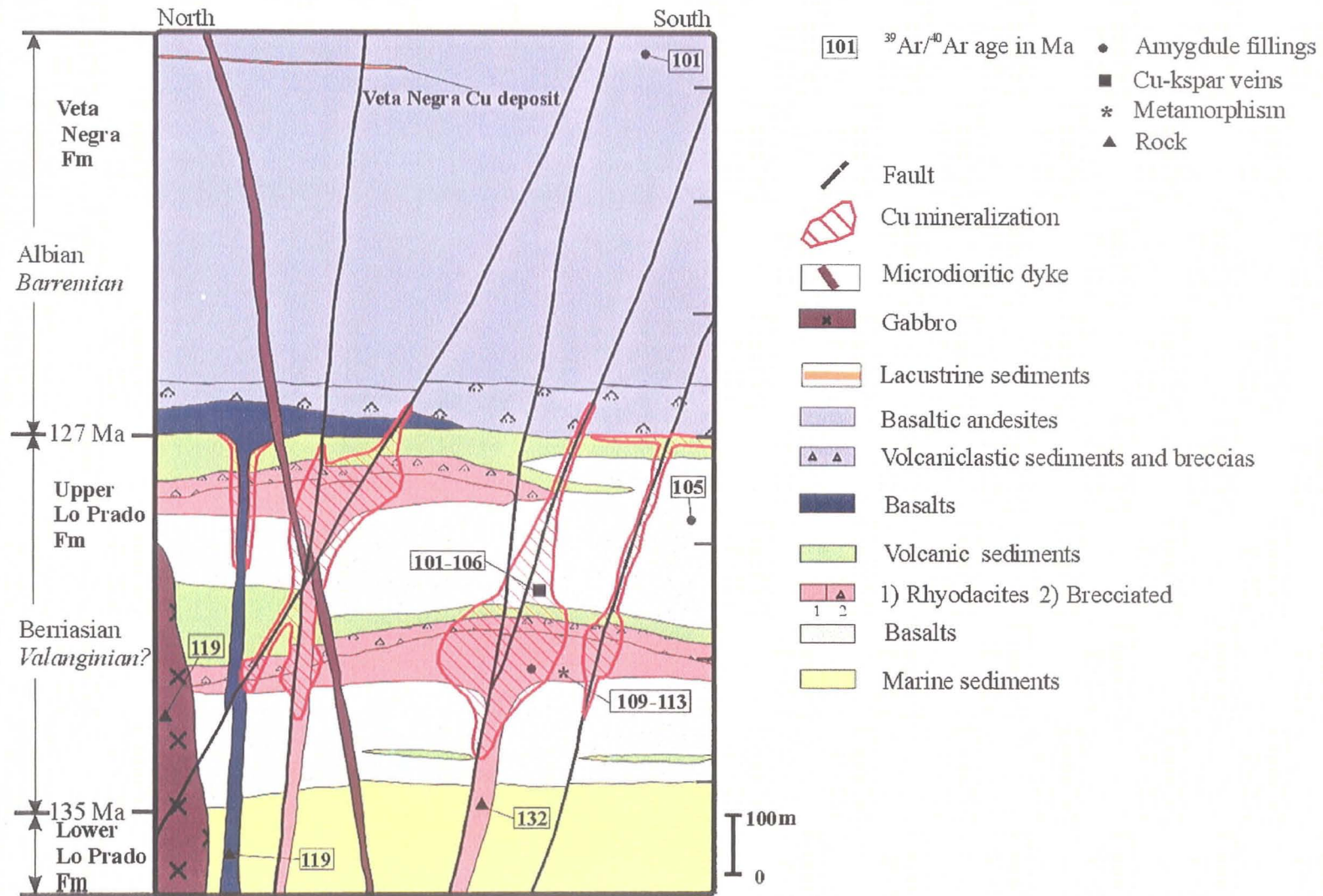
Figure 3.4. Schematic cross section of El Soldado showing rocks, faults and Cu mineralisation.
Selected ^{39}Ar/^{40}Ar ages are shown. See text.
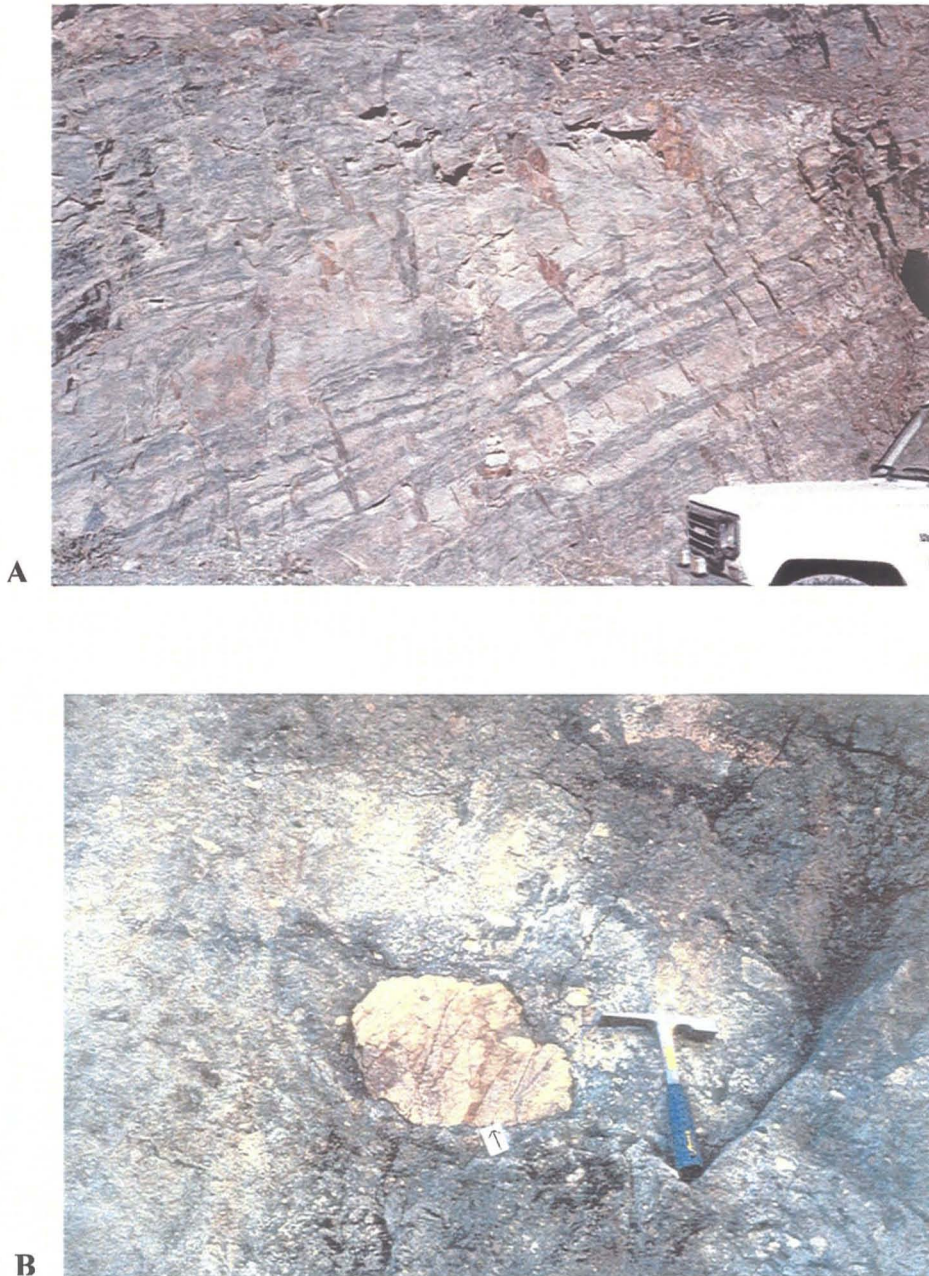
Figure 3.5. Photographs of sedimentary rocks of Lo Prado Formation.
A) Outcrop of well-stratified calcareous sandstones (light grey) and organic- rich
siltstones (black) of the lower member of Lo Prado Formation.

B) Sedimentary volcanic-clastic rock of the upper-most strata of the upper member of Lo
Prado Formation. The rock contains large angular blocks of rhyodacite (arrow) within an
angular, unsorted, fine-grained matrix, composed of volcanic rocks. The presence of
rhyodacitic clasts identical to underlying rocks, indicates active, high-energy erosion and
reworking of the underlying volcanic sequence during deposition of this unit, confirming
the rhyodacite unit is a dome (from Wilson, 1998).

3.3.1.2. Upper Member of Lo Prado Formation

The upper member of Lo Prado Formation is made up of 500 to 650 m of interlayered rhyodacite and basalt flows with intercalations of volcanic clastic (epiclastic) rocks, and minor calcareous sandstones, siltstones, and shales. The stratified volcanic rocks show both compositional and textural lateral variations, but the main flows have continuity at the mine scale (Figure 3.2).

Basalts: these rocks (previously denominated "*andesites*" represent about 45 % of the entire volcanic sequence being more abundant at the southern part of the mine (Figure 3.3). They are concentrated in two main units, which can be recognised, with some textural variations, throughout the deposit. The lower unit rests conformably over the lower marine sediments, and its thickness ranges from 250 m in the south to 30 m in the northern of the mine (Figure 3.3). This unit does not host any important ore, and usually its upper contact acts as a lower boundary for economic mineralisation at El Soldado (Figures 3.4 and 3.10 below). The upper unit is 40 to 150 m thick and is located close to the top of Lo Prado Formation, and it hosts important orebodies (e.g. Morro, Arauco, Valdivia Sur, and Filo areas; see Figures 3.4 and 3.10 and 5.3 through 5.6 below). Other minor basaltic units are locally recognised and minor volcaniclastic (sandstone, breccia) beds are intercalated within the two major basaltic units.

These basalts have a distinctive dark grey to green colour, and are typically massive and porphyritic (see below, Figure 4.2.1a), commonly amygdaloidal, blocky and brecciated; no pillow basalts have been recognised at the mine (yet are known regionally, see above). Most common alteration (visible with the naked eye) consists of calcite, chlorite and epidote (see below, Figure 4.2.1b). The lower basaltic level is more brecciated and is more altered to epidote than the upper one. Common secondary minerals filling pores, amygdules, and veinlets are calcite, chlorite, K-feldspar (microcline), albite, bitumen and sulphides. Disseminated (in part framboidal) pyrite is a common secondary component (usually < 1% volume).

Rhyodacites: these rocks (previously denominated "*trachytes*") represent about 40% of the total upper member and are relatively more abundant at the northern part of the El Soldado camp. They are concentrated in two main flows each one fed by a

different rhyodacite dyke (Figures 3.3 and 3.4). The lower unit has a maximum thickness of 140 m and hosts many large orebodies in the central-south part of the mine (e.g. Santa Clara, Valdivia Sur, Osorno, Filo). The upper rhyodacite unit is exposed at the north side of the mine where has more than 200 m of thickness. This unit hosts most of the ore mined at the Morro open pit. The rhyodacite flows are thicker above the feeder dykes and constitute domes (Figures 3.2, and 3.3). Away from such structures the rhyodacites grade into volcaniclastic rocks. The most evident dome could be observed at the Morro pit, where, previous to mining, it constituted a topographic high (Figures 3.2 and 5.8 below).

Rhyodacites are light colored (pink, gray, green) and typically porphyritic, flow banded, and brecciated. Other textural varieties are spherulitic and amygdaloidal (Wilson, 1998a). Scarce amygdules and veinlets are filled with calcite, quartz, bitumen and sulphides. Columnar jointing is well-developed perpendicular to cooling surfaces (Figure 3.6a). Brecciated varieties occur typically at the top of the flows and are relatively more abundant away from the feeder dykes (Figure 3.4). Most of the breccias are interpreted to represent autobrecciation of the rhyodacite during extrusion, and some of them are no doubt *in situ* rhyolitic hyaloclastites (e.g. p. 74, McPhie et al., 1993). Another type of breccias are clast-supported angular breccias formed by the accumulation of blocks at boundaries between flows (Wilson, 1998a). The rhyodacite were extrusive flows and domes, as evidenced by irregular, brecciated tops filled with sediment, local erosional unconformities, and angular clasts of rhyodacite in epiclastic strata overlying these felsic bodies (Figure 3.5b). The shape and texture of these rhyodacites resemble the rhyolitic domes formed by subaqueous extrusions (e.g. Pichler, 1965, in Cas and Wright, 1987; Allen, 1988), which is consistent with the depositional environment suggested for Lo Prado Formation (e.g. Vergara et al., 1995; Rivano, 1996).

Volcaniclastic Sediments: these rocks (mapped as "*tuffs*" at the mine) represent about 15 % of the upper member of Lo Prado Formation, and are more abundant at the northern section of the mine (Figure 3.3). Field and petrographic observations support that these rocks are volcaniclastic (epiclastic) sediments and not tuffs because they are not derived directly from a volcanic eruption (Wilson, 1998a). These sediments occur typically above the main volcanic flows and the most conspicuous horizon (40 m thick)

Figure 3.6. Photographs of rhyodacite flows and basaltic dykes at Morro open pit.
A) Strongly developed columnar jointing in mineralised rhyodacite unit. Primary porosity
and the competent nature of the rhyodacite make it the most favourable host rock.
Note the different style of fracturing in basaltic dyke (D), and steep fault plane (F).
Height of the bench is 12.5 m.
B) Vertical basaltic dyke intruding rhyodacite. Most of these dykes are barren even
though hydrothermal alteration and Cu mineralisation are usually strong within the
volcanic country rocks adjacent to their contacts.

constitutes the upper most level of the Lo Prado Formation (Figures 3.4 and 3.10 below). Other important concentration of volcaniclastic sediments occurs in the Morro area, where they laterally interfinger with the upper basaltic unit (Figure 3.3). These rocks are grey to green, well stratified and locally show graded bedding. Angular to sub-rounded volcanic fragments of rhyodacite and basalt within a fine-grained matrix and cemented by calcite, chlorite, and clays (montmorillonite) are the main components of this unit. Bitumen is also a common pore filling in coarse-grained sediments. The composition of clasts varies considerably, even at a hand-specimen scale (polymictic). These rocks vary from fine-grained siltstones (mm-scale) to breccias, which contain large angular blocks. As indicated above, the presence of angular boulders of rhyodacite in the uppermost level of sedimentary breccias (Figure 3.5b) is evidence for high-energy erosion. In the Morro area, at the middle portion of the upper member of Lo Prado Formation, some thin lenses (<5 m thick) of calcareous breccias contain marine fossils (Ahumada, 1985a). The fossils are pelecypods and gastropods and are poorly preserved but confirm the marine environment of deposition.

These volcaniclastic rocks host discordant Cu mineralisation, although they are less relevant than the rhyodacites and basalts as host rocks at El Soldado deposit. The upper level of breccias hosts minor lenses of concordant-stratiform Cu ore that have been mined at a small scale in the past.

Regional studies indicate that the upper member of Lo Prado was deposited in a shallow marine (sublittoral to littoral) environment (e.g. Vergara, et al., 1995; Rivano, 1996), an interpretation supported by the lithology and fossils recognised at the mine.

3.3.1.3. Purehue Member of the Veta Negra Formation

The basal member of the Veta Negra Formation (Purehue Member) is composed of red, oxidised, subaerial basaltic to basaltic-andesitic flows (mostly brecciated), intercalated red sandstones and tuffaceous-breccias and a few lenses of lacustrine siltstones (Rivano, 1996). This unit outcrops at the East of the mine camp along the crest of the hill (Figures 1.2, 1.3, and 3.10 below). The base of this unit is defined by red volcanic sandstones and breccias (~200 m thick) or by a reddish basalt flow, which

overlies the green fine sediments of the upper part of Lo Prado Formation. Basaltic andesitic flows predominate above (Figure 3.7).

Minor copper sulphide orebodies (veins, "pockets") are recognised at the lower levels of this unit, mostly in basalts (e.g. Veta Lena, 200 m above the Morro open pit). They do not have economic significance and represent extensions of the mineralisation of El Soldado (Figure 3.4).

About 700 m above the Lo Prado Formation a thin (2-10 m thick) intercalation of lacustrine siltstones with abundant carbonised plant remains, and disseminated Cu sulphide is exposed. This Cu-rich level was mined at the Veta Negra Mine (the type location for the Veta Negra formation) and represents a diagenetic low-temperature Cu deposit not directly related with El Soldado deposit (Villalobos, 1995).

This Purehue Member of the Veta Negra Formation was deposited in a terrestrial, mostly subaerial environment (Rivano, 1996), and its thickness at the latitude of El Soldado is about 1.9 km (Figure 3.1).

3.3.1.4. Subvolcanic Dykes and Stocks

Three different types of subvertical dykes, which crosscut the Lo Prado Formation, are observed: felsic (rhyodacite) dykes, 10 to 30 m thick, have a N60°-70°W trend and some of them are the feeders of the host rhyodacite flows and domes. There are two main rhyodacite dykes; one outcrops in the north (Morro pit area) and the other in the south (Santa Clara-Valdivia Sur area); each one feeds major rhyodacite flows (Figures 3.3 and 3.4). These rhyodacite dykes host some of the major orebodies of the El Soldado deposit.

Mafic to intermediate (basaltic to andesitic) dykes cut the older ones, have a N70°-80°W trend, and some of them intrude, and represent feeders for, the lowermost strata of Veta Negra Formation. This relationship was observed at the upper benches of the Morro open pit. Major mafic dykes (up to 20 m thick) are concentrated in the northern part of the mine, where they intrude along the same fault system than the rhyodacite dykes (Figures 3.3 and 3.4). Microdiorite dykes (usually < 2 m thick) cut all the above units and have NW and NE trends (Figures 3.3 and 3.4). For the mining operation, these basaltic and

Figure 3.7. Photographs of volcanic rocks of Veta Negra Formation.
A) Field photograph at Filo area, showing grey-reddish basalts (above) and red volcanic-
   clastic sediments of the base of the Purehue Member of Veta Negra Formation. The
   hill behind is made of coarse porphyritic andesitic-basaltic flows of upper levels of
   Purehue Member.
B) Typical porphyritic, amygdaloidal, reddish basalt of the lower strata of Veta Negra
   Formation. Amygdales are filled with calcite, epidote and chlorite. Hematite is
   abundant in the groundmass and rimming ferromagnesian crystals.

microdioritic dykes are considered barren although they can present a weak Cu mineralisation, mostly in their borders (Figure 3.6).

The only faneritic intrusive recognised in the camp is a gabbro stock, intercepted by deep drill holes in the northern part of the mine (see Figure 5.8 below). It does not outcrop and it is interpreted coeval with the major basaltic dykes and possible with the lower levels of the Veta Negra Formation. This gabbro is barren although it has a weak mineralisation of pyrite and traces of chalcopyrite in the contact zone (~10 m of thickness).

3.3.2. Structural Geology

El Soldado is located at the centre of a NS-NNW structural left-lateral (sinistral) strike-slip fault system. Major faults of this system (Figures 3.2, 3.8, and 3.9) form a cymoid loop (e.g. McKinstry, 1948), which closes south and north of the mine, and represents a locally dilatant zone or dilational jog (e.g. Cox et al., 2001; Sibson, 2001). When this kind of brittle structure is formed in a strike-slip system, the zone of high fracture density, aperture and connectivity is vertical, and favours fluid circulation and mineral deposition, forming chimney-like orebodies, which is the case in El Soldado. Other faults are N60°-70° W trending, right-lateral faults, along which the main dykes were intruded, and N20°-30° W extensional faults. Also minor N60°-70° E trending faults, interpreted as release fractures, are common at the mine. This structural pattern is also reproduced at more detailed scales at the mine (subordinate faults, veins, joints) and exerted a strong control on the copper mineralisation (e.g. Chávez, 1988).

Crosscutting relationships indicate that most faults are pre- and syn-mineralisation (Chávez, 1988) although post-mineralisation offsets are evident in the major faults (Figure 3.10 below). This structural pattern can be explained by a single compressive (transpressive) tectonic event, occurred at the end of the Early Cretaceous under brittle plain strain conditions. Main stress ($\sigma 1$) is inferred to have been oriented NNW-SSE

Stuctural Map, ± 0 Level

Theoretical Structural Development

Release fracture
Extensional fault
Shear fault

>1.2% Cu
>0.5% Cu

Structural dilated zone (see Fig. 3.2)
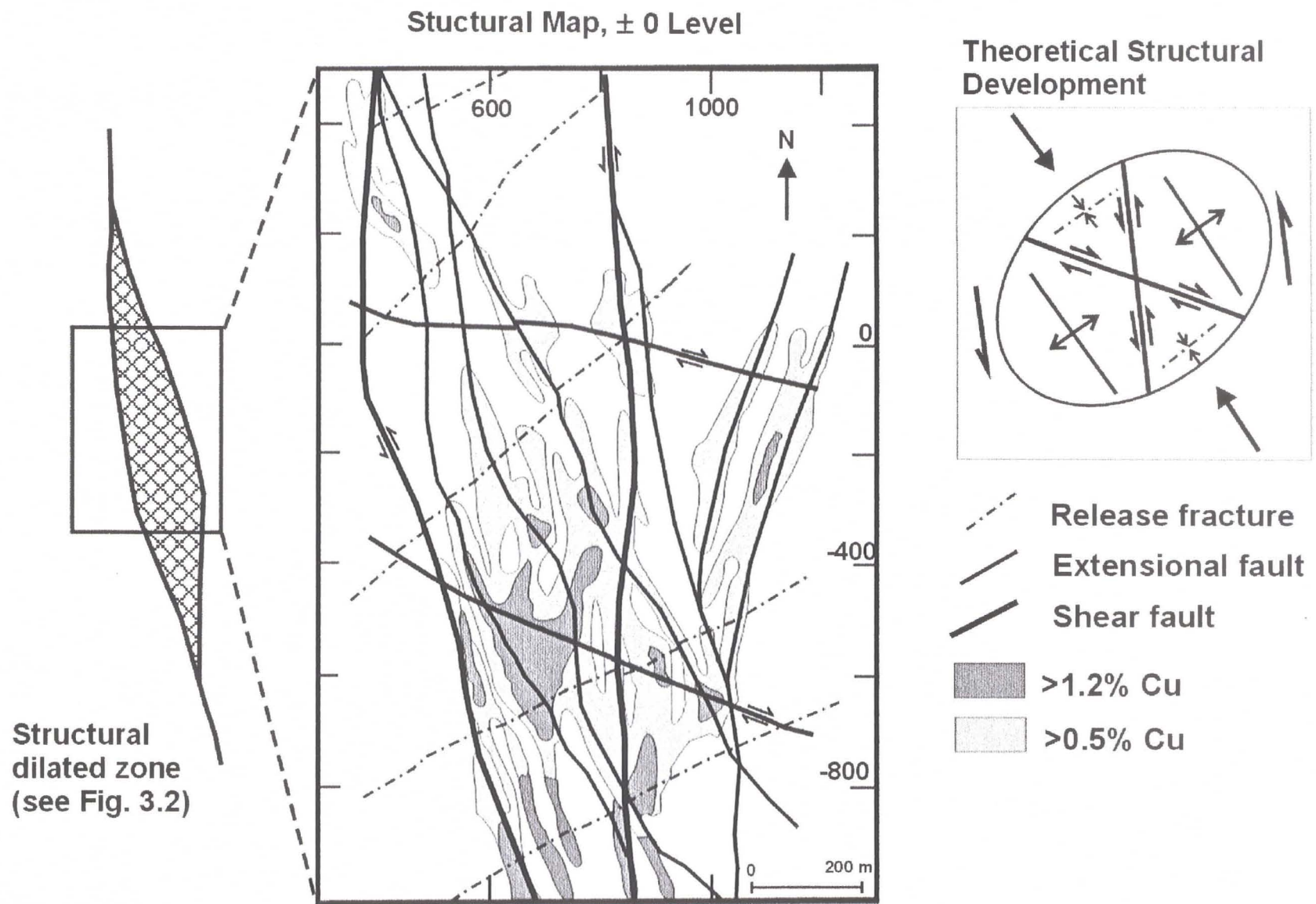
Figure 3.8. Generalised structural map and Cu mineralisation of zero mine level.
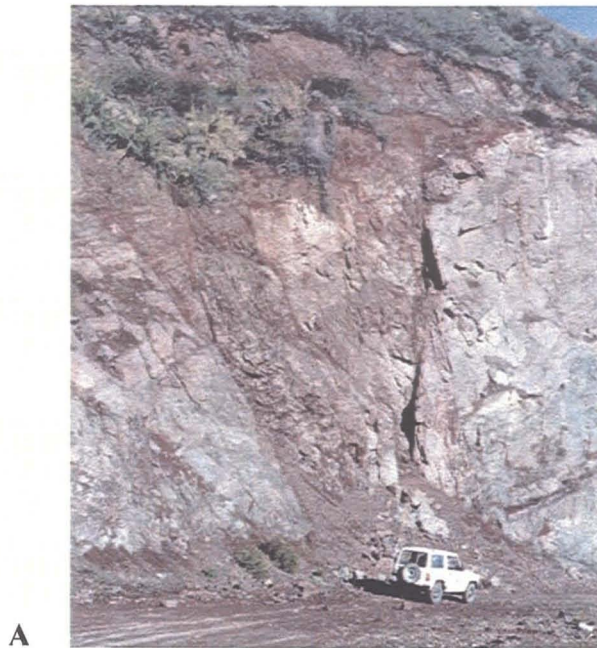
Figure 3.9. Photographs of main faults.

A) Field photograph of Adelita fault, looking south at Filo area, cutting volcanic strata of the Veta Negra Formation. Adelita is one of the master (major) left-lateral strike-slip faults, which form the cymoid loop at El Soldado. This fault is one of the main ore controls of the El Soldado deposit.

B) Field photograph of Arauco 105 fault at the Morro open pit. Arauco 105 is a north-south trending fault, which hosts vein ore bodies at the Arauco mine-block. Note horizontal slickensides and red stain by hematite-bornite-chalcopyrite ore.

(e.g. Boric, 1997; Caddey, 2001). This inferred local tectonic stress is similar to the regional stress field active during the Early Cretaceous and responsible of the left lateral motion along the Atacama fault system active along the Andean margin during the Early Cretaceous in northern Chile (e.g. Maksaev, 1990; see chapter 2). Considering such a simplified scheme, north-south faults represent the main shear; N60°-70° W faults are the conjugate shear; the N20°-30° W faults are the extension faults and the N60°-70°E faults are release fractures formed subsequent to compression (Figure 3.8). Detailed studies of the geological structures (bedding, fracture, joints, etc) recently completed at the mine, suggest that the same structural conditions may have prevailed earlier, during deposition of the sequence and intrusion of dykes (Caddey, 2001).

Wilson (1998a) in his study of the bitumen present at El Soldado concluded that oil (now solid bitumen) generated in the lower sediments of Lo Prado Formation migrated upwards along early-formed extensional "basinal" faults. Migration had occurred prior to tilting of the strata, according to geopetal structures in the bitumen that give the paleo-horizontal at the time of degassing (Wilson and Zentilli, 1999). These faults should be identifiable by anomalous accumulations of bitumen (bitumen veins), but they have not been specifically mapped for this purpose at the mine scale. Some relatively flat (low dip) faults (such as the *California* fault) may represent these early faults, which were reactivated during the major shear deformation (e.g. Caddey, 2001).

Thus, El Soldado deposit was formed in a structurally dilatant zone probably developed in an inflexion of the general trend of regional faults (Figures. 3.1 and 3.2). This localisation of this inflexion may be explained by a change in the competence of the rocks of Lo Prado Formation at El Soldado area, such as the presence of a local concentration of brittle rhyodacite flows and domes related to an active volcanic centre.

3.4. Description of El Soldado Copper Mineralisation

3.4.1. General Description

The deposit consists of numerous isolated irregular orebodies with intervening barren zones grouped in clusters (known as mining *blocks* at the mine). These blocks are spatially distributed within a volume of 2,000 m (NS) length, 800 m (EW) width and 600

m in vertical extension (Figures 3.10 and 3.11). Nevertheless, copper mineralisation continues to the south into the Veta del Agua property, where minor copper-rich vein–ore (approximately 2 million tonnes @ >2% Cu) were extracted along a fault zone (vein) about 1,000 m in strike length (Figure 3.2). Also new prospective drillholes have shown that copper mineralisation extends to the north of the current mine workings for at least 500 m. Thus the NS strike extension of copper mineralisation is greater than 3.5 Km.

Single orebodies are extremely variable in size from very small to 450 m long, 150 m wide and 450 m in vertical extension. Although described as strata-bound in a regional scale, the orebodies at El Soldado are clearly discordant and have a strong structural control. Orebodies are irregular in shape, but most of them are orientated parallel to NS and NW faults (Figure 3.8). Copper mineralisation is clearly controlled by the structural dilatant zone related to the NS-NNW sinistral shear system previously described. Larger and rich orebodies are emplaced within this zone, particularly at the intersections of NS and NNW faults with N60°-70°W conjugate faults. The best example is the Valdivia Sur chimney (Figure 3.10) which contains 14 Million tonnes @ >2 % Cu including core zones grading 5 % Cu and 20-30 g/tonne Ag. North and south of this structurally dilated zone, orebodies are narrow and can be best described as veins (e.g. Veta del Agua, Figure 3.2).

Orebodies are also controlled by lithology, being better developed in rhyodacite than in basalt and volcaniclastic sediments. About 60-65% of copper production has come from the rhyodacite host rocks, 25-30 % from basalt host rocks and 5-10 % from volcaniclastic sediments. This is related to a more pervasive fracturing, in part due to primary columnar jointing, but also because the rhyodacite is extremely competent (brittle). Accordingly, rhyodacite dykes also host copper mineralisation, whereas the mafic (basaltic, andesitic) dykes are poorly mineralized. Narrow (1-5 meters) copper-rich veins are usually observed at the borders of mafic dykes suggesting that these impervious rocks acted as barriers for copper bearing fluids but that permeability had developed on the dyke contacts (Figure 3.12a), as is the case in many basaltic dyke swarms in Iceland (M. Zentilli, pers. comm.). Finally, few and relatively unimportant stratiform orebodies
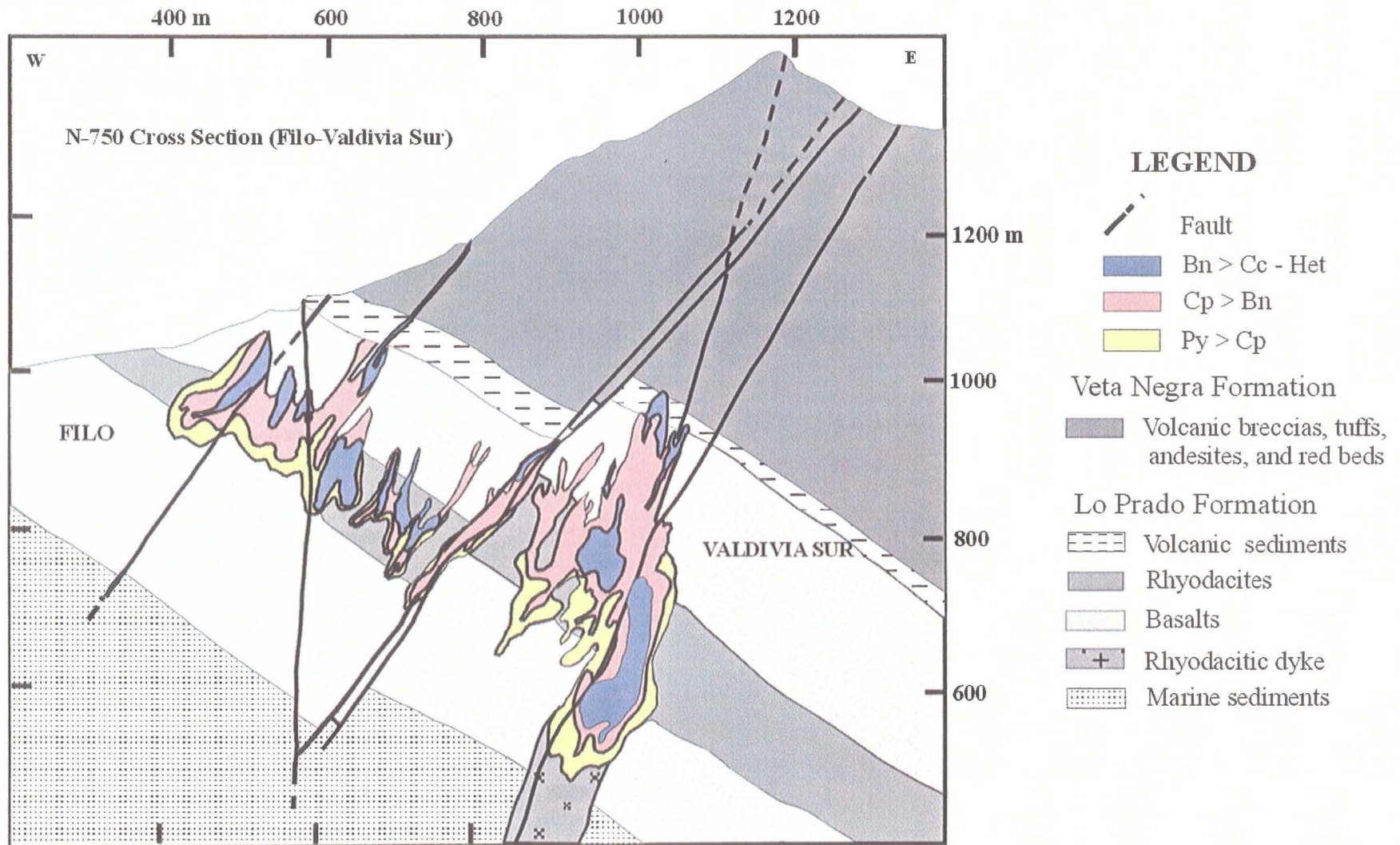
Figure 3.10. Simplified cross-section showing main rock units, faults and Cu ore bodies.
Note the strata-bound, yet discordant nature of Cu mineralization.
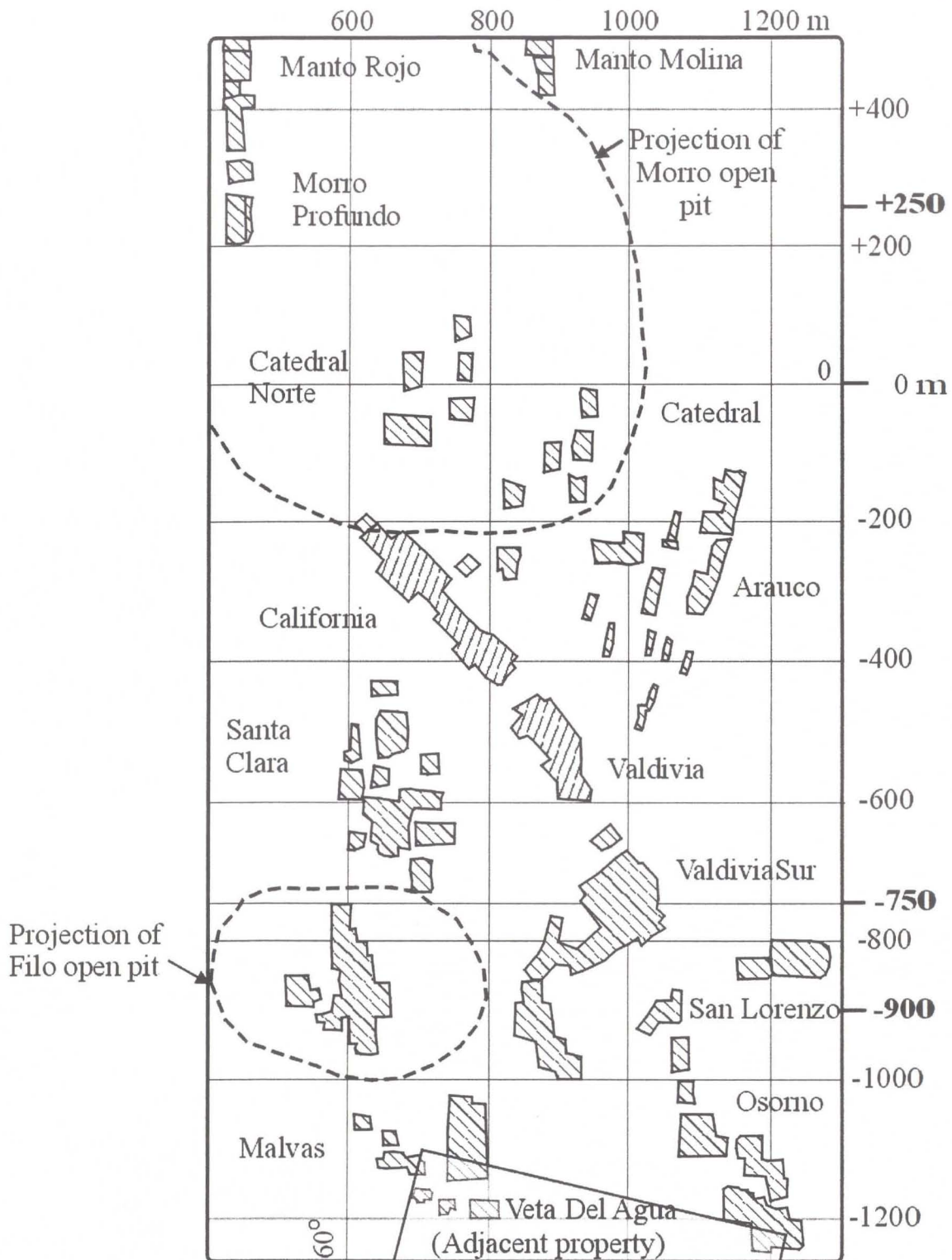
Figure 3.11. Level 0 of the underground mine showing main stopes grouped into "mine blocks".
Projection of Morro and Filo (under development) open pits are also shown.
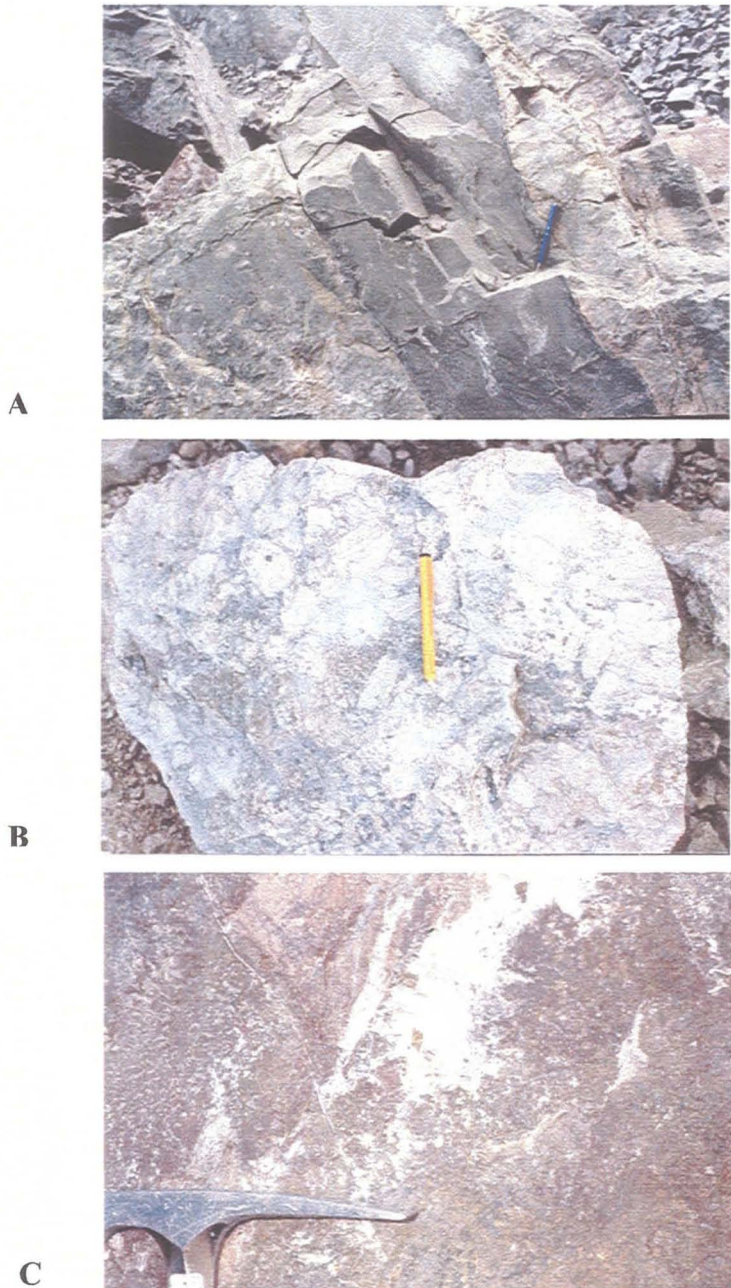
Figure 3.12. Hydrothermal alteration related to copper ore.
A) Microdioritic dyke at Morro open pit showing strong hydrothermal alteration (microcline > epidote, calcite, chlorite) on its contacts. These altered haloes host narrow Cu-rich veins
B) Hydrothermally brecciated rhyodacite, cemented by bornite-chalcopyrite-hematite and calcite. These breccias (although not very common) are found in the Morro open pit, close to the main rhyodacitic feeder dyke.
C) Calcite veins with chalcopyrite crystals in a rhyodacite flow. Note the albitised halo (pink) and chalcopyrite along the main face. (Osorno area, underground mine). These textures demonstrate the epigenetic nature of Cu mineralisation at El Soldado.

are hosted by volcaniclastic rocks at the uppermost levels of Lo Prado Formation. They were developed in permeable and organic-rich clastic beds. Figure 3.4 shows a diagram summarising the different styles of mineralisation observed at El Soldado.

Economic copper mineralisation is restricted to the upper member of Lo Prado Formation, but narrow veins (fault or dyke-related) continue upwards into the basal units of Veta Negra Formation, clearly indicating that copper mineralisation occurred later than the deposition of the base of that unit. It is also interesting to note that the roots of orebodies are usually located well above (100-150 m) the lower sedimentary member of Lo Prado Formation (Figure 3.9). Lowermost strata of the upper member of the Lo Prado Formation, which is composed of brecciated basalt flows with minor volcaniclastic, are mostly barren, containing only minor pyrite.

Copper ore is mostly hypogene (primary) although minor supergene-oxidised (secondary) zones were developed close to the present-day surface. Hypogene ore minerals are chalcopyrite, bornite, chalcocite, and minor amounts of covellite. These ore minerals occur as dissemination and veinlets, largely filling primary (columnar joints, vesicles, inter-clast pores) and secondary (shear-related) porosity of the volcanic host rocks (Figures 3.12 and 3.13). Common waste or gangue minerals are pyrite, hematite, calcite, chlorite, albite, microcline, bitumen (solid organic matter), quartz, opaline silica, titanite, rutile, and minor amounts of magnetite, sphalerite, galena, and rare arsenopyrite.

Individual orebodies are mineralogically zoned. An ideal zoning consists of: a core of chalcocite-hematite or bornite-chalcocite-hematite, followed outward by approximately concentric zones of bornite-chalcopyrite, chalcopyrite, chalcopyrite-pyrite and pyrite in the most external zone (Figure 3.10; Ruge, 1985; Boric, 1997). The deeper roots of the orebodies contain relatively more pyrite than their upward terminations, which are richer in bornite, chalcocite and hematite. A more global zoning at district scale has also been noted; the southern orebodies have relatively more chalcocite and bornite, whereas chalcopyrite predominates in the northern orebodies (Martin, 1981; Holmgren and González, 1988; Boric, 1997). Nevertheless this global tendency is still poorly described and understood.

Figure 3.13. Ore textures.
A) DDH of rhyodacite with chalcopyrite-hematite mineralization in calcite veins.
B) Typical Cu sulphide veins in DDH samples of rhyodacite.
  i.bornite > chalcopyrite;
 ii.chalcopyrite > bornite.
   Pink coloration of rhyodacite is related with strong albitization.
C) Brecciated rhyodacite cemented by chalcopyrite, pyrite, specularite (specular
   hematite), calcite, and quartz (Manto Rojo area).
D) Pyrite and chalcopyrite, finely disseminated in the groundmass and replacing
   titanomagnetite in rhyodacite, Valdivia Sur area. Cu ore can be extremely fine at El
   Soldado.

In conformity with their mineralogical zoning, the orebodies have a very variable copper grade, especially in the lateral direction. Lateral limits are characterised by abrupt variations in the copper content. The transition from core high-grade zones (~1.2- 2.0 % Cu) to lateral medium-grade zones (0.5-1.2% Cu), and external low-grade zones (0.2-0.5 % Cu) takes place within few metres. Least altered (background) country rocks between the orebodies are barren (usually below 0.1% Cu). Variations in copper grade are lower along the strike and (subvertical) plunge of the orebodies. The cut-off grade is generally 0.8 % Cu for the underground mine, and 0.5 % Cu for the open pit.

Orebodies exposed to the present surface contain an uppermost oxide zone produced by supergene processes. Malachite (70%), chrysocolla (10%), minor copper pitch (10%), and traces of brochantite, chalcantite, azurite and chrysocolla (González and Holmgren, 1993) make up this oxide zone. The average thickness of the oxide zone is between 10 to 30 m, although it can reach downwards of 60 m along open fault systems. Gangue minerals observed in this zone are goethite, jarosite, hematite and clays (kaolinite, montmorillonite). Copper has been detected in goethite and kaolinite. The abundance of oxidized copper minerals diminishes gradually from surface to depth, and below 5-10 metres usually copper oxides are mixed with copper sulphides. Traces of supergene sulphides (chalcocite, digenite) are observed at the bottom of the oxide zone, but they do not constitute a supergene-enriched blanket (González and Holmgren, 1993). The absence of supergene copper enrichment has been explained by the relatively active erosion in the steep topography, the relative scarcity of pyrite in the upper levels of orebodies, and the abundance of calcite, which would neutralize the acidic, oxidising solutions necessary to produce enrichment (González and Holmgren, 1993).

Ore grade in this zone is usually lower than the original hypogene copper grade, meaning that during the oxidation process part of copper has been leached. Total oxide reserves were assessed at ca. 8 M tonnes @ 1.2 % total copper and 1.0 % soluble copper.

3.4.2. Hydrothermal Alteration

Volcanic host rocks show hydrothermal alteration characterised by the assemblage: calcite, chlorite, albite, quartz, K-feldspar, epidote, titanite, and minor

muscovite and clays (montmorillonite). The significance of this alteration and its relationship with the copper mineralisation remains enigmatic. Calcite, chlorite and quartz have been ascribed to the hydrothermal copper mineralisation process (Terrazas, 1977; Holmgren, 1987), and also K-feldspar (Boric, 1997; Wilson, 1998a). Terrazas (1977) considered the albite to be related to ore, but Klohn et al. (1990) argued against this hypothesis. Some staff geologists have concluded that the spatial distribution of hydrothermal minerals does not show any relationship with orebodies and could be merely a result of regional low-grade metamorphism (e.g. Martin, 1981). However others postulate that there is a local hydrothermal alteration related to ore overprinting the effects of regional metamorphism (e.g. Terrazas, 1977; Holmgren, 1987).

Despite the enigmatic nature of this alteration, according to the observations of the author, it is clear that host rocks at El Soldado have a hydrothermal alteration related to copper mineralisation. It is evidenced by changes in colour, mineralogy, and textures of rocks (Figures 3.12 and 3.13). Alteration is more intense within the core of larger orebodies and follows narrow zones along the contact with mafic impervious dykes. Within these areas, alteration has been strong and the original composition and texture of rocks are often difficult to discern. Away from these areas, hydrothermal alteration grades into, and it is difficult to distinguish from, the background or regional pattern, which is probably owed to regional basinal diagenesis and very-low-grade metamorphism (e.g. Levi, 1969; Levi et al., 1982, 1989; Holmgren, 1987).

3.4.3. Organic Matter (Bitumen)

Bitumen (solid organic matter) has been observed associated with copper ores in all orebodies and most lithologies present at El Soldado (including basalts, rhyodacites lavas and dykes). Bitumen filled in pores and veinlets and it is associated with pyrite and copper sulphides (Figures 3.14a,b; Zentilli et al., 1997; Wilson, 1998a). Textures show that copper sulphides were introduced after bitumen (Figure 3.14d). Carbon isotopes in bitumen suggest that bitumen represents petroleum generated in the Lower Member of Lo Prado Formation (Figure 3.14b), and that the carbonate coexisting with bitumen could have formed by oxidation of petroleum (Zentilli et al., 1994; 1997). R_o (reflectance), and
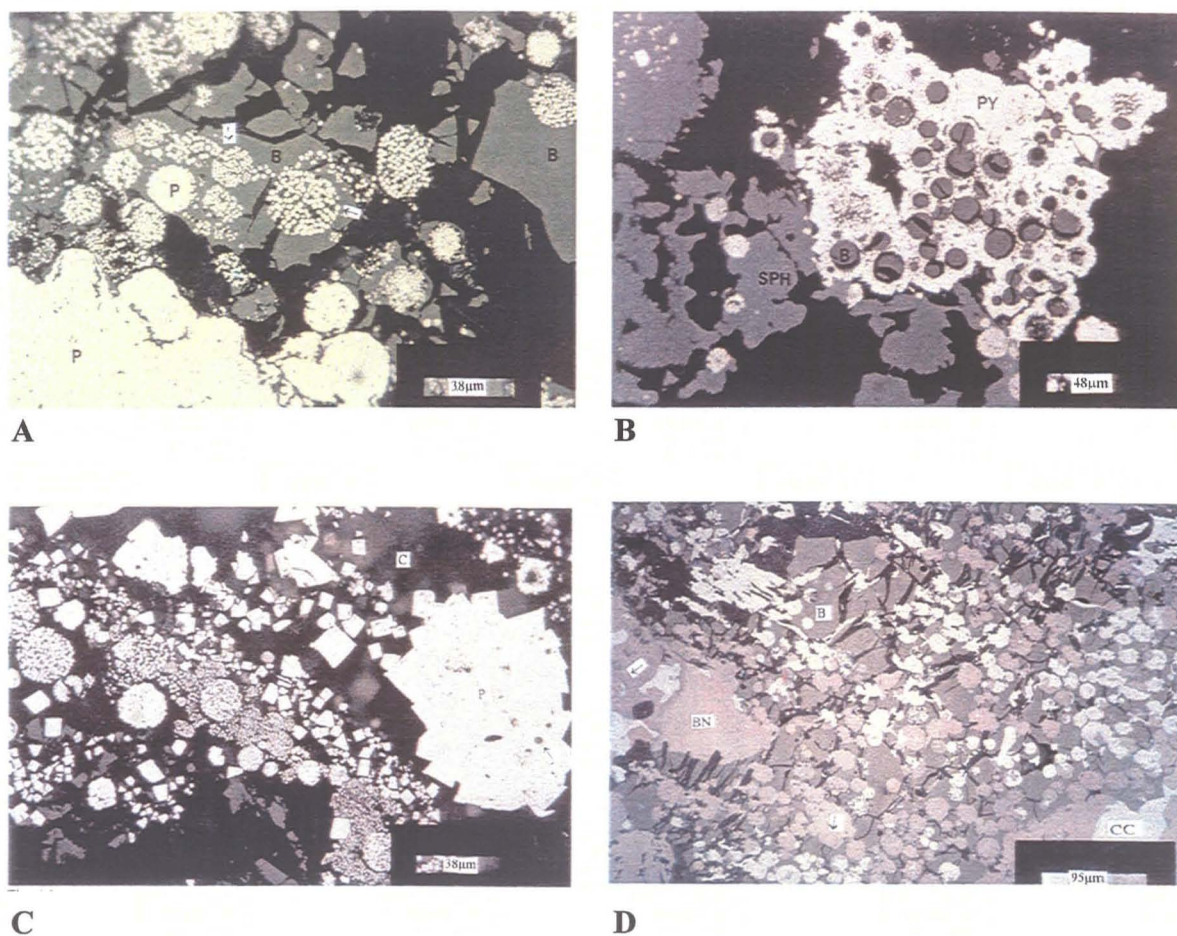
Figure 3.14. Reflected light photomicrographs of framboidal textures.
(After Wilson, 1998).

A) Pyrite (P) framboids and spherules in bitumen (B) surrounded by calcite (C).

B) Bitumen (B) globules surrounded by framboidal pyrite (PY) with adjacent sphalerite (SPH) in calcite (C). The globules are interpreted to represent original droplets of semi-liquid petroleum.

C) Pyrite (P) grains in bitumen (B) with different morphologies (framboidal, spheroidal, euhedral), and composite pyrite aggregates.

D) Bornite (BN) and chalcocite (CC) framboids and spherules after pyrite, surrounded by bitumen (B). Cu sulphide replaced pre-existing framboidal pyrite.

microprobe analyses of bitumen samples associated with copper ores indicate that bitumen was both chemically and thermally altered by the action of later Cu-bearing hydrothermal fluids (Wilson, 1998a; Wilson and Zentilli, 1999).

3.4.4. Paragenesis

Recent petrographic studies carried out in parallel with the development of this thesis have shown that the mineralisation at El Soldado took place in two different stages, separated in time (Wilson, 1998a; Wilson and Zentilli, 1999; Ponce, 2001). During the first or diagenetic stage, framboidal pyrite and traces of chalcopyrite, sphalerite, rare galena, pyrrhotite and arsenopyrite were formed at low temperatures (60-120 °C) and coincided with the migration of liquid petroleum into the Upper Member of Lo Prado Formation. Sulphate reduction and biodegradation of petroleum (Wilson, 1998a; Wilson and Zentilli, 1999) led to the formation of framboidal pyrite. The second stage was hydrothermal and occurred at higher temperatures according fluid inclusion data (200-400 °C; Holmgren, 1987; Table 3.4). During this second stage chalcopyrite, bornite and chalcocite were generated, mostly replacing the framboidal pyrite. Other minerals formed during this hydrothermal stage were hematite, covellite and traces of magnetite, anilite, and cobaltite. Pyrite and bitumen acted as reductant at the place of precipitation of copper sulphides. Gangue minerals related to this second stage were calcite, chlorite, albite, microcline, epidote, quartz, and rutile.

3.4.5. Age of Copper Mineralisation

The first diagenetic stage probably occurred a few million years after deposition of the host sequence (Wilson, 1998a), but its age remains poorly constrained. The age of the second hydrothermal stage has been constrained using geochronology. A set of $^{40}Ar/^{39}Ar$ ages in K-feldspar veinlets-vugs associated with copper ore has yielded ages between 101 and 112 Ma (Table 3.4; Appendix 7.1). The most obvious samples related to ore (mostly from mineralized basalts) range from 101 to 106 Ma (average 103 ± 2 Ma; Wilson, 1998a; Wilson et al., in press a). This average was considered to be representative of the age of copper mineralisation (Wilson, 1998a). The older ages (109-

Table 3.4.- Summary of Relevant Analytical Data for El Soldado Deposit

1.- Range of Geochronological Ages

Geological Unit/Event	Method	Mineral	Age (Ma)	References
Host rhyodacitic dyke, Upper Lo Prado Fm.	$^{40}Ar/^{39}Ar$	plagioclase	131.8 ± 3.1	1
Mafic dykes, intruding Upper Lo Prado Fm.	$^{40}Ar/^{39}Ar$	plagioclase	123 to 119	1
Andesites extrusion, Veta Negra Fm.	$^{40}Ar/^{39}Ar$, K/Ar	plagioclase	119 to 115	1, 2
Alkali metasomatism in Upper Lo Prado Fm.?	$^{40}Ar/^{39}Ar$	K-fd	112 to 109	1, 3
Copper mineralization in Upper Lo Prado Fm.	$^{40}Ar/^{39}Ar$	K-fd	106 to 101	3
Regional metamorphism in Veta Negra Fm.	$^{40}Ar/^{39}Ar$	K-fd, muscovite	104 to 97	1, 2
Regional batholith	$^{40}Ar/^{39}Ar$, K/Ar	biotite, hornblende	118 to 94	4, 5
Uplift and exhumation	Fission track	apatite	88 ± 18	6

2.- Range of Isotopic Values of S, C, and O

	Delta	Mineral	‰	References
Sulphur stage I	$\delta^{34}S$	pyrite	-11.9 to 28.0	3, 7
Sulphur stage II	$\delta^{34}S$	Cu sulfides	-12.7 to 19.0	3, 7
Organic matter Stage I	$\delta^{13}C$	bitumen associated to ore	-22.0 to -30.8	3, 8
Hydrothermal fluids	$\delta^{13}C$	calcite associated to ore	-4.2 to -20.2	3, 8, 9
Hydrothermal fluids	$\delta^{18}O$	calcite associated to ore	12.0 to 15.0	3, 8, 9
Hydrothermal fluids	$\delta^{18}O$	k-feldspar associated to ore	12.0 to 12.6	3, 9

3.- Range of Homogenization Temperatures (T_H) and Salinities of Fluid Inclusions

Mineral and Ore Zone	T_H min. °C	T_H max. °C	Salinity %	References
calcite and quartz in py-cp	118 to 240	155 to 296	10 to 31	7, 10, 11, 12
calcite and quartz in cp-bn	102 to 239	119 to 303	3 to 31	7, 10, 11, 12
calcite and quartz in bn-cc	93 to 244	137 to 204	3 to 31	7, 10, 11, 12
calcite in late barren veins	82 to 122	104 to 170	22 to 29	7, 10, 11, 12

4.- Range Reflectance (BR_0) and Total Organic (TOC) for Bitumen Associated to Copper Ore

Rock Unit	Mineral	TOC wt %	BR_0	References
In Upper Lo Prado Fm. (El Soldado deposit)	bitumen	0.1 to 5.4	2.4 to 5.7	3, 8
In Veta Negra Fm. (Veta Negra deposit)	bitumen	0.1 to 5.7	1.3 to 3.3	3, 8

References: (1) Boric & Munizaga, 1994; (2) Morata et al., 2001; (3) Wilson, 1998a; (4) Rivano et al., 1993;

(5) Parada & Larrondo, 1999; (6) Wilson et al submitted a; (7) Holmgren, 1987; (8) Zentilli et al., 1997; (9) Munizaga, 1992;

(10) Skewes, 1987a; (11) Skewes 1987b; (12) Skewes 1988. See also Appendix 7

-112 Ma), mostly from mineralized rhyodacites, have been interpreted to reflect the age of the early alkali metasomatism that affected the volcanic sequence (Boric et al., 2002 Wilson et al., in press a).

A similar range of ages (101-113 Ma) had been obtained in previous work for altered and mineralized rocks using K/Ar, and Rb/Sr methodologies (Table 3.4; Appendix 7.1).

In this thesis a new $^{40}Ar/^{39}Ar$ age was obtained from mineralised basalt collected at Tardones hill (1.3 km south of Filo mine block) from the uppermost levels of Lo Prado Formation. The sample (RB200-2) is a K-feldspar concentrate from veinlets composed of K-feldspar, calcite, and minor chalcopyrite, chlorite and epidote within a low-grade (0.2-0.4 % Cu) orebody. This sample yields a plateau age of 103.0 ± 1.2 Ma (Table 3.5; Figure 3.15), confirming the age assigned to copper mineralisation by Wilson (1998a).

In summary the available geochronological data indicate that copper mineralisation at El Soldado occurred during the Albian, 25-30 Ma after deposition of the host rocks.

A similar $^{40}Ar/^{39}Ar$ age of 104.3 + 1.7 Ma has been obtained 10 Km south of El Soldado for a altered and mineralized dacite porphyry at La Isla Cu mine (Figure 3.1), suggesting that the copper mineralisation event had a regional extent. In addition comparable $^{40}Ar/^{39}Ar$ (97-104Ma) age have been obtained from K-feldspar fillings and secondary sericite in volcanic rocks of the Veta Negra Formation several kilometres away from the El Soldado mine (e.g. Boric and Munizaga, 1994; Fuentes et al., 2001; Morata et al., 2001). K/Ar Ages obtained in the batholith east of El Soldado also overlap with these ages. This coincidence suggests that the mineralisation is coeval with the peak of regional metamorphism and batholith intrusion and that the mineralisation is part of the same process.

TABLE 3.5.- K-Feldspar Argon Summary of Sample RB2000-2

T°C	mV 39	39%	AGE (Ma)±1sigma	% ATM	37/39	36/40	39/40	% IIC
550	104.4	2.7	87.6 ± 1.6	15.3	0	0.000518	0.036558	0
600	227.6	6	96.9 ± .8	5.3	0.02	0.000182	0.036817	0
650	226.3	5.9	104.4 ± .8	3.5	0.13	0.000119	0.03477	0.04
700	144	3.8	103.2 ± 1.2	10.3	0.21	0.00035	0.032682	0.07
750	88	2.3	105.3 ± 1.7	4.9	0.05	0.000169	0.033934	0.01
800	81.7	2.1	105.1 ± 1.9	7.9	0	0.000268	0.032946	0
850	86.3	2.2	105.4 ± 1.8	8.1	0	0.000277	0.03278	0
900	124.1	3.2	105.3 ± 1.4	11.7	0	0.000397	0.031533	0
950	188.6	4.9	104.4 ± 1.1	17.1	0	0.000581	0.029848	0
1000	271.3	7.1	104 ± 1	22.8	0	0.000773	0.027904	0
1025	294.7	7.7	101.5 ± 1	24.7	0	0.000838	0.027904	0
1050	193.4	5.1	101 ± 1.2	25.7	0	0.000872	0.027675	0
1075	195	5.1	103.7 ± 1.1	20.9	0	0.00071	0.028678	0
1100	97.8	2.5	103.9 ± 1.8	19.5	0	0.000662	0.029125	0
1125	209.3	5.5	103.5 ± 1.2	27.5	0	0.000933	0.026325	0
1150	84.3	2.2	104.5 ± 2	16.1	0	0.000545	0.030196	0
1175	136.9	3.6	103.1 ± 1.4	19.6	0	0.000664	0.029346	0
1200	202	5.3	103.4 ± 1.2	20.9	0	0.000707	0.02878	0
1225	355.2	9.3	102.1 ± 1	25	0	0.000846	0.027645	0
1250	317.2	8.3	103.1 ± 1.1	29.1	0	0.000986	0.025854	0
1300	104	2.7	102.4 ± 1.8	30.1	0	0.001019	0.02568	0
1350	29.1	0.7	101.7 ± 5.4	31.8	0	0.001079	0.025241	0
1450	21.7	0.5	102.9 ± 7.3	47.4	0	0.001605	0.019242	0

Mean age (900°C-1450°C)= 103 ± 1.2 Ma (2 Uncertainty, including error in J)

J = .002148 ± .0000215 (1 %)

37/39, 36/40 and 39/40 Ar ratios are corrected for mass spectrometer

Discrimination, interfering isotopes and system blanks

% IIC - interfering isotopes and system blanks
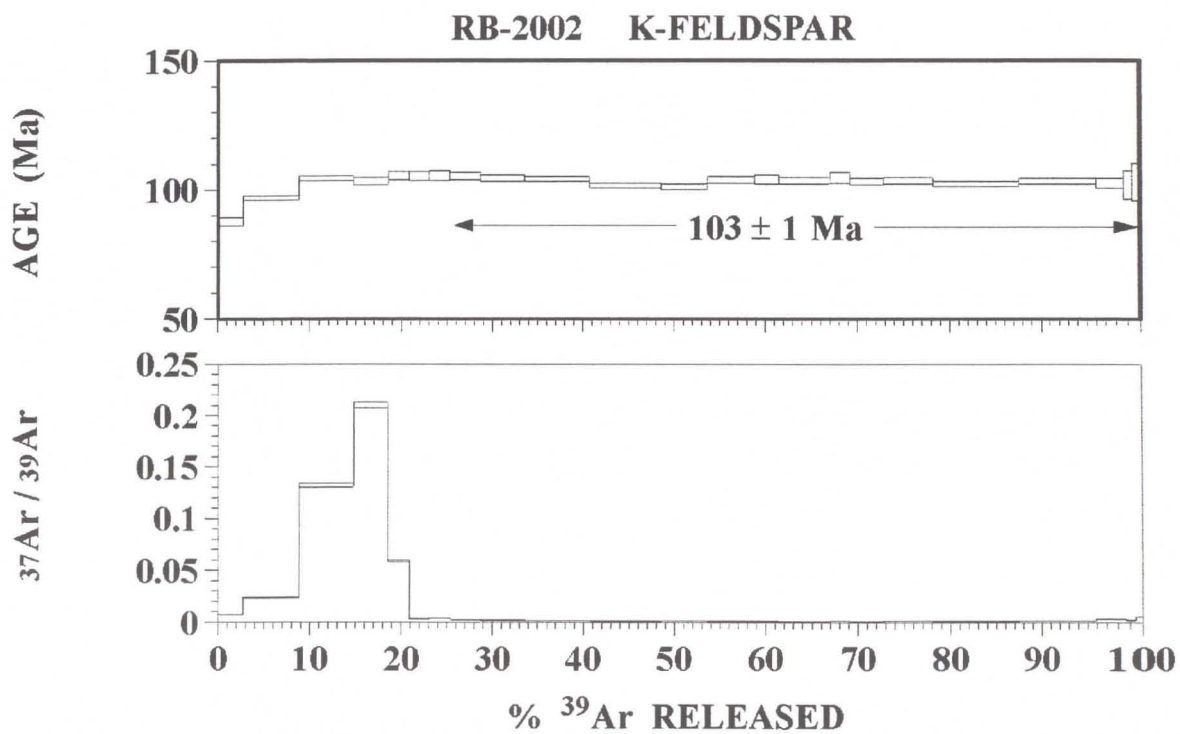
Figure 3.15. ^{40}Ar/^{39}Ar **Age of ore phase K-feldspar.**
Dated mineral is K-feldspar filling in pores associated with calcite, chlorite, epidote and chalcopyrite, from a mineralised basalt of the Upper Member of Lo Prado Formation from Tardones hill (sample RB-2000-02).

3.4.6. Fluid Inclusion Data

Fluid inclusion data from previous studies, including over 400 homogenisation temperatures (T_H) measurements, ice-melting and NaCl-dissolution measurements made in veinlets of calcite and quartz, are summarised in Table 3.4 and complete data are shown in Appendix 7.2. The work was carried out by Holmgren (1985; 1987) and M. Skewes (CMD internal reports, 1987a, b, 1988), and only partially reported in Klohn et al. (1990).

Data in Table 3.4 are grouped in four mineralogical zones. The averages minimum and maximum T_H for the 4 groups overlap somewhat as follows: pyrite-chalcopyrite (172-249 °C); chalcopyrite-bornite (153-178 °C); bornite-chalcocite (138-181 °C); late barren veins (102-137 °C), suggesting a cooling trend from a maximum of ca. 250 °C; all these temperatures are uncorrected for pressure. No evidence of boiling of the fluids was observed in the fluid inclusions.

Klohn et al. (1990) applied pressure corrections to the data assuming a rock column of 7 km, representing the total thickness of the overlying Veta Negra Formation (Levi, 1969). They suggested temperatures of Cu-rich hydrothermal fluids to have been ca. 300 °C (hydrostatic, 680 bar) or ca. 400 °C (lithostatic, 1800 bar), and for the late barren veins 175 °C (hydrostatic) and 250 °C (lithostatic). The maximum burial of the deposit by Lower Cretaceous strata is poorly constrained, and new regional studies indicate a maximum thickness of only 5 km for the Veta Negra Formation (Rivano, 1996), thus the fluid temperatures may have been lower than what Klohn et al. (1990) estimated. Taking in account the absence of high-temperature alteration minerals such as biotite or actinolite, which in the Salton Sea basin appear at temperatures slightly higher than 300 °C (e.g. Elders et al., 1979) it is unlikely that maximum fluid temperatures at El Soldado were much higher than 300 °C during mineralisation.

Salinities are consistently high (21-26 % NaCl equivalent) with some analyses as high as 34 %, suggesting $CaCl_2$ in addition to NaCl in the fluids. A few samples indicated salinities as low as 3% NaCl equivalent. Although no evaporites are known in the Lo Prado and Veta Negra, the consistently high salinities suggest their presence in what may represent basinal fluids. Klohn et al. (1990) interpreted these high salinities as evidence

for magmatic fluids. The present author prefers to interpret these salinities as representing deeply circulating basinal brines analogous to those in the Salton Sea geothermal system of southern California (23-30 wt % NaCl equivalent), with maximum temperatures of ca. 300°C (e.g. Elders et al., 1979). Westra (1988a) using the analogy of other metamorphosed mafic volcanic piles hosting copper ores in Chile and North America, strongly favoured the participation of regional metamorphic, rather than magmatic fluids. Fluid inclusions in ore deposits that are interpreted to be formed by intervention of basinal fluids commonly have salinities in the range found at El Soldado (e.g. Roedder, 1979; Westra, 1988a).

3.4.7. Isotopic Data

A handful of sulphur isotope data on pyrite and Cu sulphides were obtained by Holmgren (1987), Westra (1988b) and Villalobos (1995) (see Appendix 7.3), and recently a detailed study was carried out by Wilson (1998a) as a fundamental part of his thesis. A synthesis of his results follows. Sulphur isotope data on the pyrite have a wide range in $\delta^{34}S$ values (-11.1 ‰ to 28.0 ‰), consistent with strong fractionation in compartmentalised pore domains where variable proportions of sulphate are incompletely reduced. The fractionation is probably biogenic, such as with the intervention of sulphur-reducing bacteria (e.g. Love, 1967), most likely at temperatures below 100°C (Wilson, 1998a, Wilson et al., in press b). Sulphur isotope data on copper sulphides, which pseudomorphically replace framboidal pyrite, also have a wide range in $\delta^{34}S$ ratios (-12.7 ‰ to 19 ‰), indicating that sulphur was inherited piecemeal from the pyrite during replacement of pyrite by Cu sulphides (Wilson, 1998a). A few Cu sulphide samples (with no evidence of replacing pre-existing pyrite) have $\delta^{34}S$ ratios near zero, and could possibly indicate an igneous origin for S (Wilson, 1998a). The same interpretation was forwarded by Klohn et al. (1990) with the scarce data at that time. Nevertheless, the wide range observed in many new analyses suggests that a "magmatic" signature is volumetrically insignificant. Also this "magmatic" sulphur ($\delta^{34}S$ ratios near zero) could be the result of leaching and homogenisation from primary sulphides dispersed in volcanic rocks into the mineralising fluid, or represent the effects of leaching and

homogenisation of pre-existing pyrite, therefore not necessarily coming from a direct igneous (batholithic) origin (Wilson, 1998a).

Bitumen associated with gangue calcite has $\delta^{13}C$ values of -30 to -22 ‰, indicative of solidified petroleum (Wilson, 1998a). The $\delta^{13}C$ values of gangue calcite at El Soldado vary between -4 to -20 ‰ (Zentilli et al., 1997; Wilson, 1998a). The lightest values ($\delta^{13}C$ between -10 to -20 ‰) can be interpreted as the calcite having grown at the expense of bitumen (by oxidation). The heavier values of $\delta^{13}C$ may represent the general composition of the incoming fluids.

The $\delta^{18}O$ ratios of K-feldspar (microcline) range between 12.0 and 12.7 ‰, and are compatible with the fluids being of metamorphic/basinal origin (Wilson et al., in press a). $\delta^{18}O$ values of calcite vary between 12.0 and 14.7 ‰, a range of less than 3 ‰. The relatively small range in $\delta^{18}O$ values in calcite and K-feldspar suggest that the external fluid was relatively homogeneous and there was no great variation in temperature during crystallisation. Recalculation of $\delta^{18}O$ values for water in equilibrium with calcite and k-feldspar is difficult because of the uncertainty regarding the temperature of the hydrothermal fluids; values obtained are compatible with either a metamorphic or a magmatic fluid (Wilson et al., in press a).

The $^{87}Sr/^{86}Sr$ ratios in calcite (which contains less than 60 ppm Rb) of 0.7041 to 0.7051 are similar to those of the host basaltic rocks at the time of mineralisation (e.g. Munizaga et al., 1995), and lower than values obtained from marine carbonates in the Lo Prado Formation (0.7051-0.7071; F. Munizaga, CMD internal report, 1992). These results are consistent with a basinal or metamorphic fluid having inherited the low $^{87}Sr/^{86}Sr$ ratios during water-rock reaction for several million years. Furthermore, during the geochronological study (Wilson, 1998a; Wilson et al., in press a), it was noted that all $^{40}Ar/^{39}Ar$ dated samples of K-feldspar contain high proportions of atmospheric argon; this anomaly is interpreted to indicate a high proportion of meteoric water in the basinal mineralising fluids, lessening the probable importance of any magmatic component.

Re-Os-isotope data for El Soldado (Ruiz et al., 1997) are significantly more radiogenic than those of the porphyry copper type deposits of Chile. Whereas the initial

$^{187}Os/^{188}Os$ ratios in pyrite from El Soldado is 3.95, in the Los Bronces (Disputada) porphyry copper south-east of El Soldado the pyrite has $(^{187}Os/^{188}Os)_i$ of 0.18 (mantle ~0.12). Ruiz et al. (1997) suggested that black shales are the one crustal reservoir (continental crust ~ 1.0) that could possibly account for the anomalously high $(^{187}Os/^{188}Os)_i$ of El Soldado sulphides. These results are consistent with the present interpretation that the diagenetic pyrite in El Soldado is related to petroleum (Wilson and Zentilli, 1999); however they say little about the source of the Cu deposited during the hydrothermal stage.

3.4.8. Proposed Genetic Models

The El Soldado is clearly an epigenetic deposit whose genesis was controlled by the conjunction of chemically (highly reducing) and physically (extremely brittle) favourable host rocks, and a dilatant structural zone produced within a left-lateral shear system of regional scale. Plausible hydrothermal-magmatic (e.g. Klohn et al., 1990) and metamorphic (e.g. Westra, 1988a) models have been postulated to explain the origin of El Soldado. Klohn et al. (1990) on the basis of: a) the high salinity of fluid inclusions, b) the absence of evidence for boiling of fluids, and c) the $\delta^{34}S$ values close to 0 per mil, concluded that the hydrothermal fluids had a "deep magmatic source". They proposed that the mineralising fluids *ascended* during the waning phases of the same alkaline (*trachytic*) magmatism that had generated the Lo Prado Formation lavas. They also suggested that the most probable ore precipitation mechanism was fluid reaction with wall rocks. Differing from this hypothesis, Westra (1988a) proposed a redox-model that involves circulating, but *descending* waters, flowing through the El Soldado system during low-grade (burial) metamorphism of the Lower Cretaceous volcanic pile. Copper would have been leached from the overlying oxidised Veta Negra basaltic flows and precipitated in the chemically reduced and reducing Lo Prado Formation, by a decrease in oxygen fugacity (Westra, 1988a).

More recently Zentilli et al. (1994; 1997) proposed that petroleum was involved in El Soldado genesis. Wilson (1998a) and Wilson and Zentilli (1999) upheld the model put forward by Westra (1988a), although recognising for the first time that the deposit

formed in two separate stages: a first stage when biogenic (framboidal) pyrite grew during diagenetic degradation of (migrated) petroleum (now bitumen), and a second stage, some 15-25 Ma later, during which hot hydrothermal fluids poor in sulphur brought in copper transported as copper chloride complexes, to form the copper deposit. This genetic model is further discussed in Chapter 7 below.

3.5. Summary

At the beginning of this study it was clear that El Soldado is an epigenetic and strata-bound manto-type copper deposit, formed by a combination of structural and lithological controls. Concurrent research by this lab (e.g. Wilson, 1998a) has shown that two very distinct stages in its evolution must be considered: a diagenetic stage that formed pyrite, related to petroleum degradation, and a hydrothermal stage that brought the copper, which replaced the original pyrite and formed copper sulphides. However, many questions remained about the absolute age of the mineralisation event, the nature and role of the host rocks, the mineralogy, chemistry and distribution of hydrothermal alteration, the spatial distribution of sulphides and their paragenesis. These aspects are discussed in the following chapters.

CHAPTER 4. PETROGRAPHY, GEOCHEMISTRY, AND U/PB DATING OF THE VOLCANIC AND SUBVOLCANIC HOST ROCKS

4.1. General Statement

In most previous publications such as the company reviews by Klohn et al. (1986, 1990), the host rocks to ore in El Soldado were referred to as "anomalous alkaline andesites" and "trachytes", and the titles of the papers (if not their conclusions) implied that the ores are related to *alkaline* magmatism. The mafic rocks were designated "alkaline andesites", despite their low silica content (< 52 %), and the felsic rocks were described as "alkaline trachytes" on the basis of their trachytic texture, major-element chemistry and mineralogy (e.g. Ahumada, 1985a, b; Klohn et al., 1986, 1990; Holmgren, 1987). Other workers suggested that the felsic rocks are either albitised (Na metasomatised) andesites (e.g. Olcay and Alarcón, 1975), or rhyolitic ignimbrites (Terrazas, 1977).

In this chapter the author presents new petrographic and geochemical evidence that clearly indicate that, before alteration, the rock suite was not alkaline, nor were the rocks trachytes and andesites, but an alkali-metasomatised, bimodal calc-alkaline suite of basalts and rhyodacites. It is also evident that the rocks were affected by superimposed processes of diagenesis, regional very-low grade metamorphism and locally by hydrothermal alteration related to Cu mineralisation. The volcanic rocks exposed at El Soldado have the characteristics of altered and metasomatised rocks referred to in the past as "spilites" and "keratophyres" (Levi et al., 1982). The same rock types have been recognised in other important Chilean strata-bound Cu districts, such as Mantos Blancos (Chavez, 1985) and Punta del Cobre (Marschik and Fontboté, 1996).

4.2. Petrography of Volcanic and Subvolcanic Host Rocks

4.2.1. Methodology

In order to determine the original petrographic composition (protolith) of the rocks, detailed geological - petrographic logging and sampling of selected drill-cores was carried out during fieldwork. To avoid the effects of hydrothermal alteration related to Cu

mineralisation, mapping and sampling was focussed, as much as possible, on the barren areas, away from orebodies. The study of volcanic rocks was concentrated along a representative vertical cross-sections in the central-south part of the mine (cross sections -750 N, Filo-Valdivia Sur; and -900 N, Filo-Osorno) where the main volcanic units are well exposed and therefore accessible (Figures 3.3, 3.10 above, and 5.5, and 5.6 below). As a complement, samples from other areas were also collected. However, in order to study the mafic dykes and subvolcanic intrusive bodies, it was necessary to sample the northern part of the deposit; therefore these samples were collected in sections +250 N (Morro-Arauco Norte) and 0 N (Morro- Arauco) or at the surface in the Morro open pit (see Figures 3.3, 5.7 and 5.8 below).

As a result, and after pre-screening of samples, a representative suite of 56 unmineralised "background" (prime) samples from all different volcanic and subvolcanic rock units was selected. These samples were studied as cut and polished (to remove saw marks) slabs under the binocular microscope; they were stained with Na-cobaltinitrite to identify and locate K-feldspar, and their magnetic susceptibility was measured with a hand-held EDA K-2 Magnetic Susceptibility Meter. A selected subgroup of 26 samples was studied as thin and polished thin sections, under reflected light and transmitted light microscopy using a Zeiss Axioplan microscope in the Fission Track Research Laboratory (FTRL), Dalhousie University. Mineral (spot) analyses (6 samples) and X-ray maps (6 samples) of polished thin sections were carried out at Dalhousie University using a Link eXL system with a JEOL 733 electron microprobe, 15kV accelerating voltage, 15nA probe current, and 1 μm bean diameter. The counting time was 40 seconds for individual probe analysis and 25 milliseconds for X-ray mapping, at approximately 7600 total counts per second. Calibration used geological silicate standards (feldspar) and a ZAF matrix correction program was employed in the reduction of raw data. Microprobe analyses were done under the supervision and with the instrument calibration of Robert MacKay, Analyst. Previous microprobe analyses (11 samples), performed with the same instrument, were also integrated to this study (M.C. Graves, Cuesta Research Ltd. internal report CMD, 1995c). Finally, X-ray difractograms (XRD) analyses were done using the automated Philips X-ray diffractometer of FTRL, to identify secondary

minerals (7 samples). XRD analysis were done under the guidance of Keith Taylor, analyst. Data for this chapter are displayed in Tables 4.1 to 4.9 and Figures 4.1 to 4.18.

4.2.2. Basalt Flows

The microscopic study of samples from massive parts of the flows shows that they have a porphyritic to glomerophyric texture, with plagioclase, scarce clinopyroxene, and rare olivine phenocrysts in a hyalophitic to subophitic groundmass composed of microlites of plagioclase with interstitial pyroxene, opaques (titano-magnetite), devitrified glass, and secondary minerals (Figures 4.1, 4.2, and 4.3; Table 4.1).

Plagioclase phenocrysts (20-25% by volume) are euhedral to subhedral, they occur in clusters and are altered to muscovite and minor chlorite, calcite, and scarce K-feldspar, making it difficult to recognise their original nature. Muscovite is more abundant in the cores of crystals. They also have inclusions of opaque minerals (titano-magnetite), and minor apatite. Microprobe analyses in the less-altered samples indicate that the phenocrysts are compositionally zoned, ranging in composition between bytownite (inner parts) to labradorite (rims) (An_{84-63}, Figure 4.4, Table 4.4, below). The majority of the microprobe spots, however, yield an albite to oligoclase composition (An_{1-12}) even in crystals without clear secondary evidence of replacement (Table 4.4, below, Appendix 3.1). This implies that the basalts were affected by a pervasive and widespread Na alteration, which changed the composition of their plagioclase phenocrysts to albite - (oligoclase). This phenomenon has been noted previously by other workers in the Lo Prado Formation in the region (e.g. Levi, 1969; Levi et al., 1982, 1989; Vergara et al., 1995). These authors indicate that the calcic plagioclase (labradorite) is commonly altered to albite and it is preserved just in the most massive (impervious) part of the mafic flows; they ascribe this alteration to regional very low-grade (prehnite-pumpellyite facies), which affected the rocks. This is in agreement with the fact that albite is the common stable feldspar in metamorphic mafic volcanic sequences affected by very low-grade metamorphism or prehnite-pumpellyite facies (e.g. Winkler, 1974).

Clinopyroxene subhedral phenocrysts (7-10%) (Figure 4.2a, b, c, d) also occur in clusters and are zoned and normally less altered than plagioclase. Microprobe indicates

Table 4.1.- Petrographic Characteristics of Basalts (less altered background samples)

I. Basalts from Lo Prado Formation

Samples	Rock Unit	Texture	Phenocrysts			Ground mass	Iron Oxides	Amygdule and Veinlets Fillings	Na-cobalti nitrite
			Plagioclase	Pyroxene	Ferromagnesian				tintion
RB98-29 RB98-40 RB98-42 MP844 RB99-30	upper unit back-ground with magnetite	glomero-porphorityc	22-30%; 0.1-3.0 mm; bytownite-labradorite (An_{84-63}) relicts (rare), mostly albitised (An_{12-5}). Altered to sericite, chlorite, epidote, calcite, K-feldspar	5-10%; 0.2-3.0 mm; augite, weakly altered to chlorite, calcite, epidote, hematite	2-4%; 0.1-0.5 mm; Olivine? altered to chlorite, calcite, epidote, hematite, titanite	hyalo-ophitic to intersertal	Ti- magnetite; weakly repla ced by hematite	scarse, chlorite, quartz, calcite, hematite	traces in plagioclase and in groundmass
Z634-95	lower unit, back ground with magnetite	glomero-porphorityc	25%; 0.1-1.5 mm; labradorite?, albitised; altered to chlorite, epidote, sericite, K-feldspar;	5%; 0.3-3.0 mm; augite?; weakly altered to calcite, chlorite, epidote, hematite	10%; 0.1-2.0 mm; pyroxene?, olivine? altered to chlorite, epidote, hematite	hyalo-ophityc	Ti-magnetite, weakly replaced by hematite	common, chlorite, epidote, quartz, calcite	traces in plagioclase and in groundmass
RB98-06 RB98-49 RB98-50 Z632-95	upper unit, back-ground with pyrite	glomero-porphorityc amygdaloidal	22-25%; 0.2-3.0 mm; albitised (An_{2-4}); altered to sericite, chlorite, K-feldspar	5-10%; 0.3-3.5 mm; augite; weakly altered to calcite, chlorite, epidote, hematite, pyrite, titanite	3-5%; 0.1-0.5 mm; olivine? altetred to chlorite> epidote, calcite, hematite	hyalo-ophityc	Ti- magnetite, mostly replaced by pyrite, titanite, rutile, pyrite	common (5-10%) calcite, chlorite, epidote, albite, pyrite, hematite, titanite, rutile	weak in plagioclase and in groundmass

II. Basalts from Veta Negra Formation

Samples	Rock Unit	Texture	Plagioclase	Pyroxene	Ferromagnesian	Ground mass	Iron Oxides	Amygdule and Veinlets Fillings	Na-cobalti nitrite
Z603-95 Z627-95	lower level, back-ground with hematite	coarse porphyritic	20-25%; 0.3-3.0 mm; albitised (An_8), altered to sericite, calcite, chlorite, epidote, K-feldspar	7-10%; 0.2-4mm; augite, weakly altered to calcite, chlorite, epidote	3-5%; 0.1-0.5 mm; olivine?altered to chlorite, hematite> epidote, calcite, white mica	hyalo-ophitic; abundant hematite	Ti-magnetite mostly replaced by hematite and minor rutile-titanite	rare; hematite, calcite, chlorite, epidote, microcline, quartz	moderate in plagioclase and in groundmass

73

A

1 cm

B

1 cm
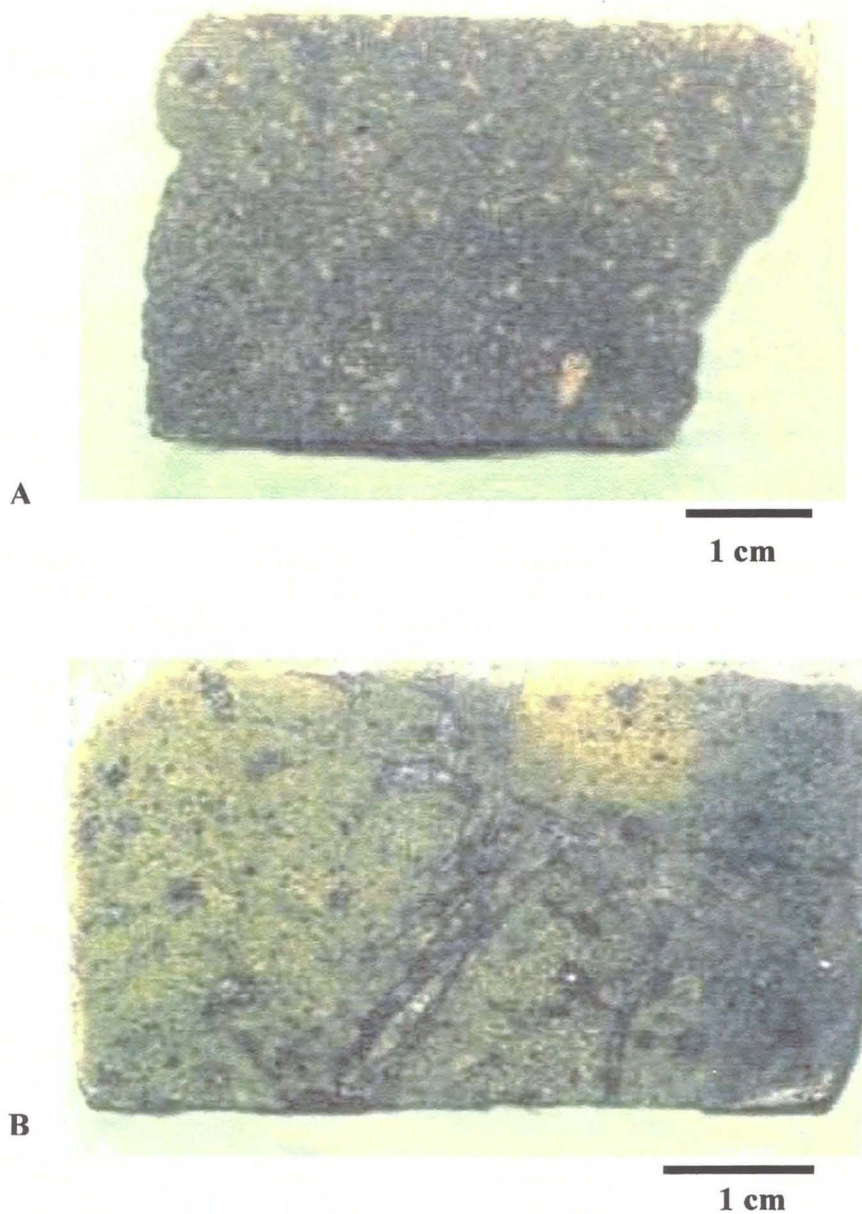
Figure 4.1. Photographs of DDH.

Sample of basalts of the upper member of Lo Prado Formation.

A) Coarse porphyritic basalt from less altered zone (background) – sample RB98-29.

B) Porphyritic basalt with veinlets of chlorite-calcite. The light-yellow tint in groundmass is after cobaltinitrite staining, indicating that some K-feldspar is present in the groundmass (sample RB98-49).
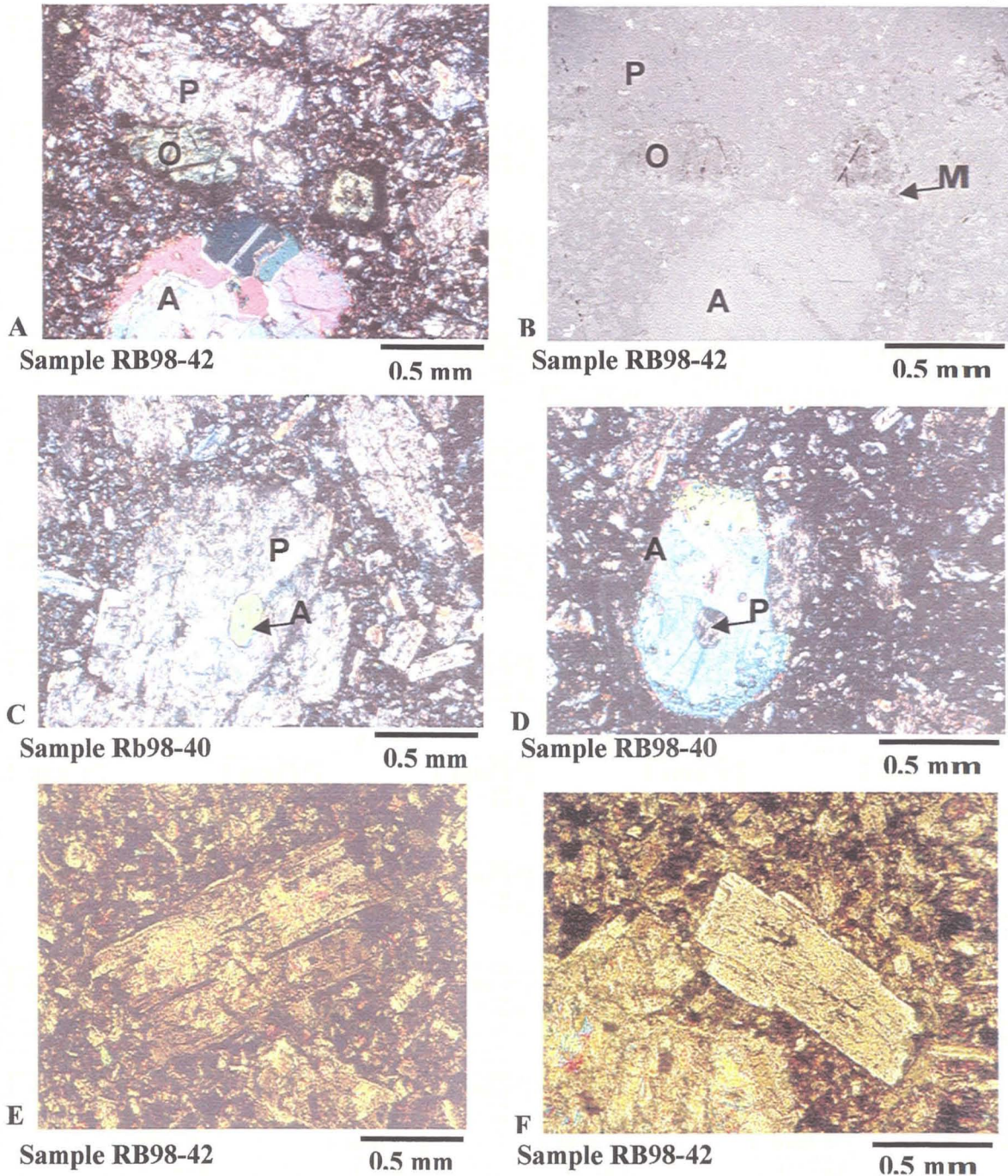
Figure 4.2. Microphotograph of "least altered" basalts.
A) Transmitted, parallel light; altered plagioclase (P), augite (A), and altered olivine (O).
B) Reflected light of A; white spots are magnetite (M).
C) Augite in plagioclase.
D) Plagioclase in augite.
E) & F) Sericitised labradorite.
Note K-feldspar external zone in labradorite in F).
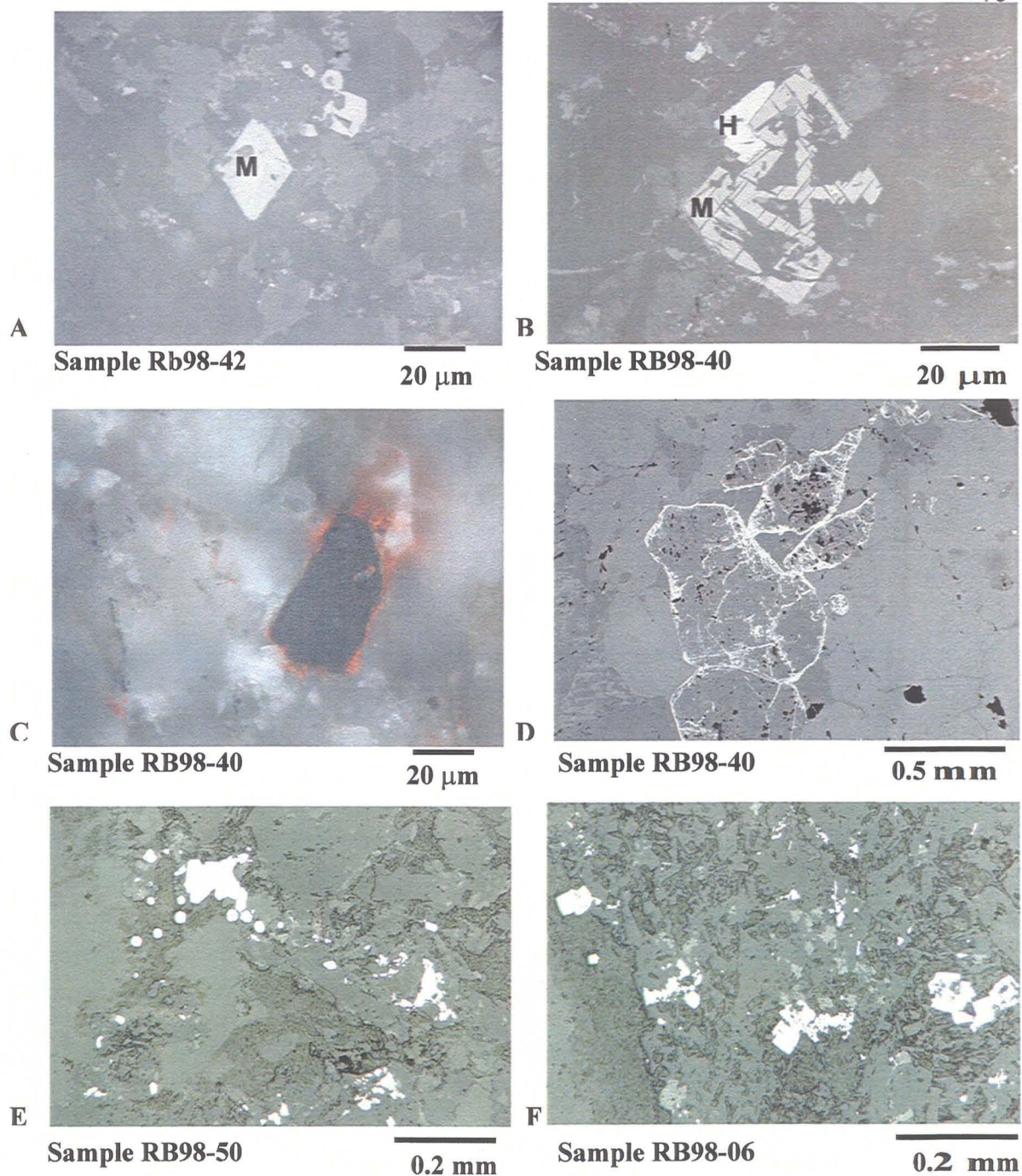
Figure 4.3. Reflected light micrograph of "least altered" basalt.
A) Magnetite (**M**)
B) Skeletal magnetite (**M**) replaced by hematite (**H**)
C) Crossed Nichols; magnetite rimmed by hematite
D) Hematite rimming olivine phenocrysts
E) Framboidal pyrite
F) Pyrite replacing magnetite
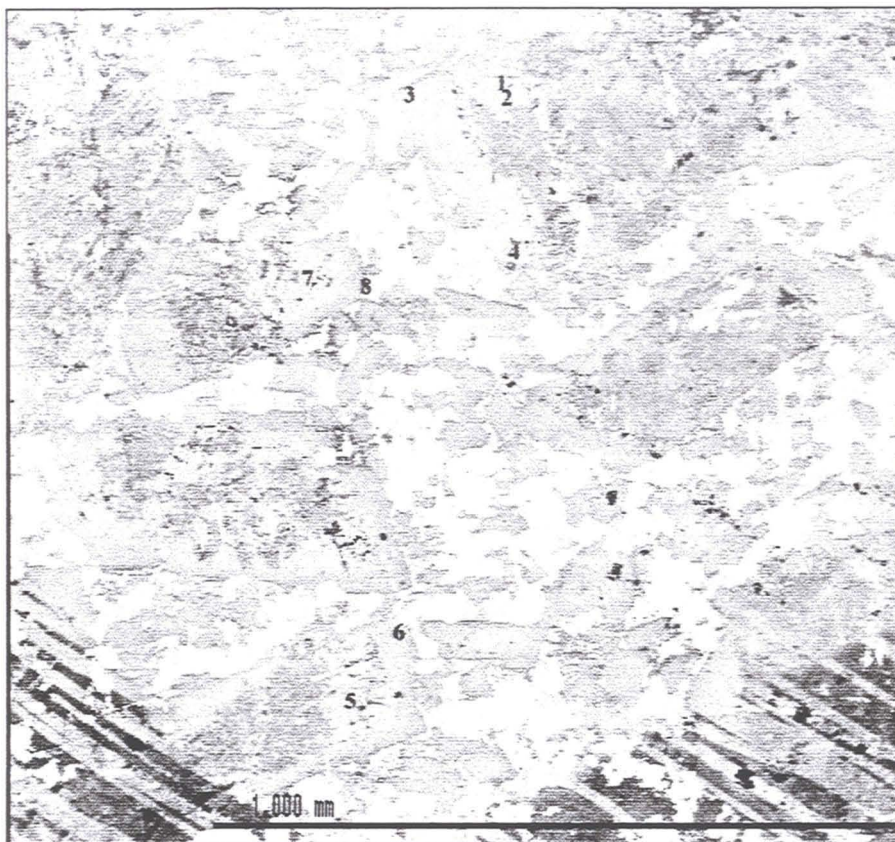
Figure 4.4. Back-scatter image of a basalt of upper Lo Prado Fm from less altered (background) zone (sample RB9842), showing plagioclase phenocrysts (gray) analysed by microprobe.

Note the zoning nature of plagioclase phenocrysts. More calcic plagioclase (bytownite) is recognised in inner parts (points 1, 2, and 7; medium gray), and more sodic (labradorite) at borders (points 3, 4, 5, 6, and 8; light gray) of phenocrysts. Darker zones at cores are altered to muscovite, and calcite and were not probed. Dark stripes are permanent marker stains.

Point	Mineral	Remarks
1	bytownite (An 82)	inner
7	bytownite (An 83)	inner
2	bytownite (An 84)	inner
3	labradorite (An 65)	border
4	labradorite (An 66)	border
5	labradorite (An 67)	border
6	labradorite (An 52)	border
8	labradorite (An 63)	border

they are augite and rarely diopside (Wo_{42-46} En_{46-48} Fs_{8-11}, Table 4.5). They are weakly altered to calcite, chlorite, and epidote and have a semi-opaque rim formed by epidote, iron oxides and titanite (rare).

Possible olivine phenocrysts (2-4%) (Figures 4.2a and 4.3d) are totally altered to calcite, chlorite, and iron oxides. Previous workers have considered these phenocrysts to be remnants of pyroxenes, but they have a clear different size, habit and grade of alteration than pyroxenes, suggesting that they are a different mineral species (Table 4.1; see also Appendix 3.3, samples RB9842 and RB9806)

Titano-magnetite crystals (2-4 %) in groundmass (Figures 4.2.b, c; 4.3a, b, c) have TiO_2 values between 7.3 to 11.2 wt % (Table 4.6, below) and are partially replaced by hematite, titanite-rutile and pyrite (Figures 4.3e, f). Pyrite replacement is very conspicuous, and few of the background basalts contain any remnant magnetite (only those samples that preserve calcic plagioclase). Sulphide replacement of magnetite is more intense close to the orebodies. Consequently, magnetic susceptibility values are high (1.2 to 3.0), only in the less altered and unmineralised basalts, but magnetic susceptibility decreases drastically to almost negligible values close to and within the orebodies (see details in Table 5.1 in Chapter 5, and in Appendix 5).

Other secondary minerals identified by microprobe and XRD analyses are chlorite, muscovite, epidote, calcite, microcline, albite, titanite, hematite and apatite. Detailed microprobe results are shown in Appendix 3.1.

The designation of these mafic rocks as basalts is based on their immobile trace-element geochemistry (see section 4.3). Yet their mineralogy, major-element chemistry (e.g. SiO_2 < 52 %, see section 4.3), and normative mineralogical composition (Table 4.7, below) are all typical elements for basalts, not for andesites as previously described (e.g. Ahumada, 1985a; Klohn et al., 1990). Vergara et al. (1995) described basalts with very similar compositions in the upper member of Lo Prado Formation, in the Chacana area, merely 10 km south of El Soldado. These basalts also have the characteristics of altered and Na-metasomatised basalts referred to in the past as *spilites* (e.g. Levi et al., 1982; Hughes, 1982; see discussion in section 4.3.2.2).

4.2.3. Rhyodacite Flows and Dykes

A study of selected samples of the massive porphyritic portion of "background" unmineralised, rhyodacites, distal from orebodies (Table 4.2), shows that they have a glomerophyritic texture, formed by phenocrysts (20-25 %) of albite (An_{0-2}) in a pilotaxitic to trachytic groundmass (Figures 4.5 and 4.6). Groundmass is composed of albite microlites, fine-grained K-feldspar, quartz, devitrified glass, and minor opaque minerals (pyrite, titanite-leucoxene, and rutile, Figure. 4.7). X-ray microprobe maps of Na, K, Si, and Al show that K-feldspar is a major component of the groundmass (Figure 4.8; see also Holmgren, 1987). Other secondary minerals identified by microprobe spot analyses in the groundmass, or filling pores and veinlets are muscovite, K-feldspar, albite, epidote, and titanite (see Appendix 3.1). Small zircon grains are rare, are visibly resorbed, an U/Pb dating (see section 4.4) indicates that part of the visible resorbed zircon is xenocrystic with apparent ages much older than their Cretaceous extrusion (Zentilli et al., 2001).

Albite phenocrysts in the rhyodacites are not optically zoned (Holmgren, 1987), an observation confirmed by microprobe analyses (Table 4.4, below) and microprobe X-ray maps (Figure 4.8); many previous workers considered albite to be a primary magmatic phase. Albite crystals are altered to calcite, chlorite, microcline (Figure 4.8), and minor muscovite and epidote. Small inclusions of titanite, pyrite and apatite are present (see Appendix 3.3).

Rhyodacites also have minor ferromagnesian phenocrysts, fully altered to calcite, chlorite, epidote, and minor hematite and pyrite and scarce magnetite, replaced by titanite-leucoxene-rutile and pyrite (Figure 4.7).

Although less abundant than in the basalts, pyrite is a very common secondary mineral in the least altered, "background" rhyodacites. Pyrite occurs as small crystals (1 to 100 μm), disseminated in the groundmass, included in albite phenocrysts and very commonly replacing ferromagnesian minerals or magnetite (Figure 4.7b, c, d). In the

Table 4.2.- Petrographic Characteristics of Rhyodacites and Rhyodacitic Dykes (less altered "background" samples)

Samples	Rock Unit	Texture	Phenocrysts		Groundmass	Xenolits	Opaques	Amygdule and Veinlets Fillings	Na-Cobaltinitrite tintion
			Plagioclase	Ferromagnesian?					
RB98-05 RB98-21 RB98-22 MP-848	upper flow	glomero-porphirityc	20-25%; 0.2-2.5 mm; albitised (An0-2); altered to calcite, chlorite, calcite, epidote, K-feldspar, sericite	2-4%, <0.3mm, altered to chlorite> calcite, epidote, titanite-rutile	hyalopilitic to pilotaxitic	1-3%, <3 cm; micro-crystaline porphyritic	pyrite, rutile, titanite; rare magnetite, more abundant in xenolits	rare, <3% calcite, quartz, K-feldspar, albite, chlorite, epidote, titanite-rutile, pyrite	strong, mostly in ground mass also in veintlets
RB98-73 MP-846 MP-754 MP-757	rhyodacityc dykes	glomero-porphirityc	15-20%; 0.2-2.5 mm; albitised (An0-3); altered to calcite, chlorite, epidote, K-feldspar, calcite, sericite	2-5%, <0.3mm, altered to chlorite> calcite, epidote, titanite-rutile	hyalopilitic to microcrystaline, partialy recrystalised	rare, < 3 cm, micro-crystaline	pyrite, rutile, titanite, traces of chalcopyrite, galena, chalcopyrite	3-10%; calcite, quartz, K-feldspar, chlorite, epidote, titanite-rutile, pyrite	strong, mostly in ground mass also in veintlets
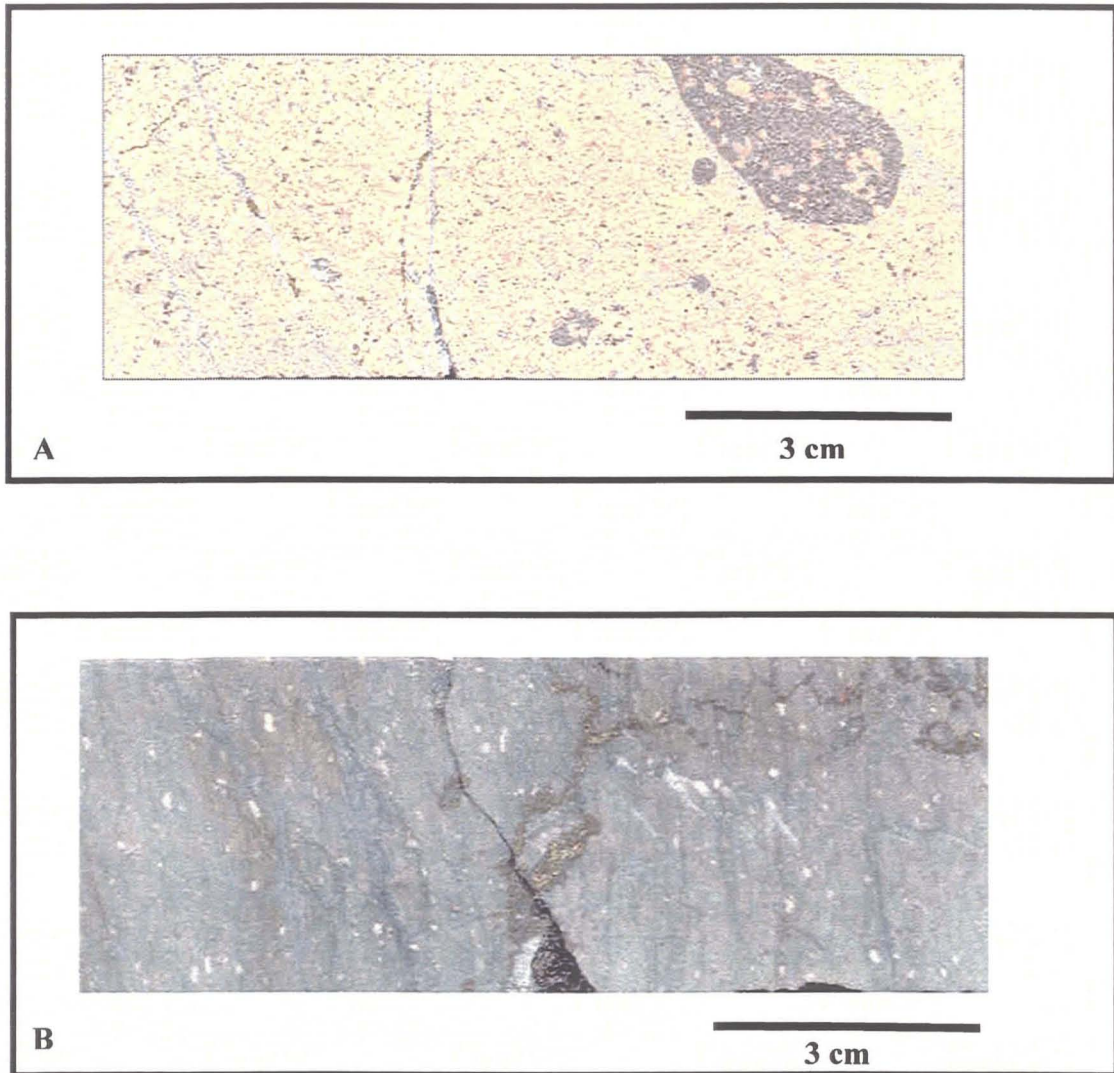
Figure 4.5. Photographs of DDH samples of rhyodacites of the upper member of the Lo Prado Formation.

A) DDH sample of rhyodacite from pyrite background zone. Note xenoliths and veinlets with calcite-quartz and pyrite.

B) DDH sample of banded rhyodacite from pyrite-chalcopyrite zone. Note phenocrysts of albite (white) and discordant veinlets of pyrite-chalcopyrite.
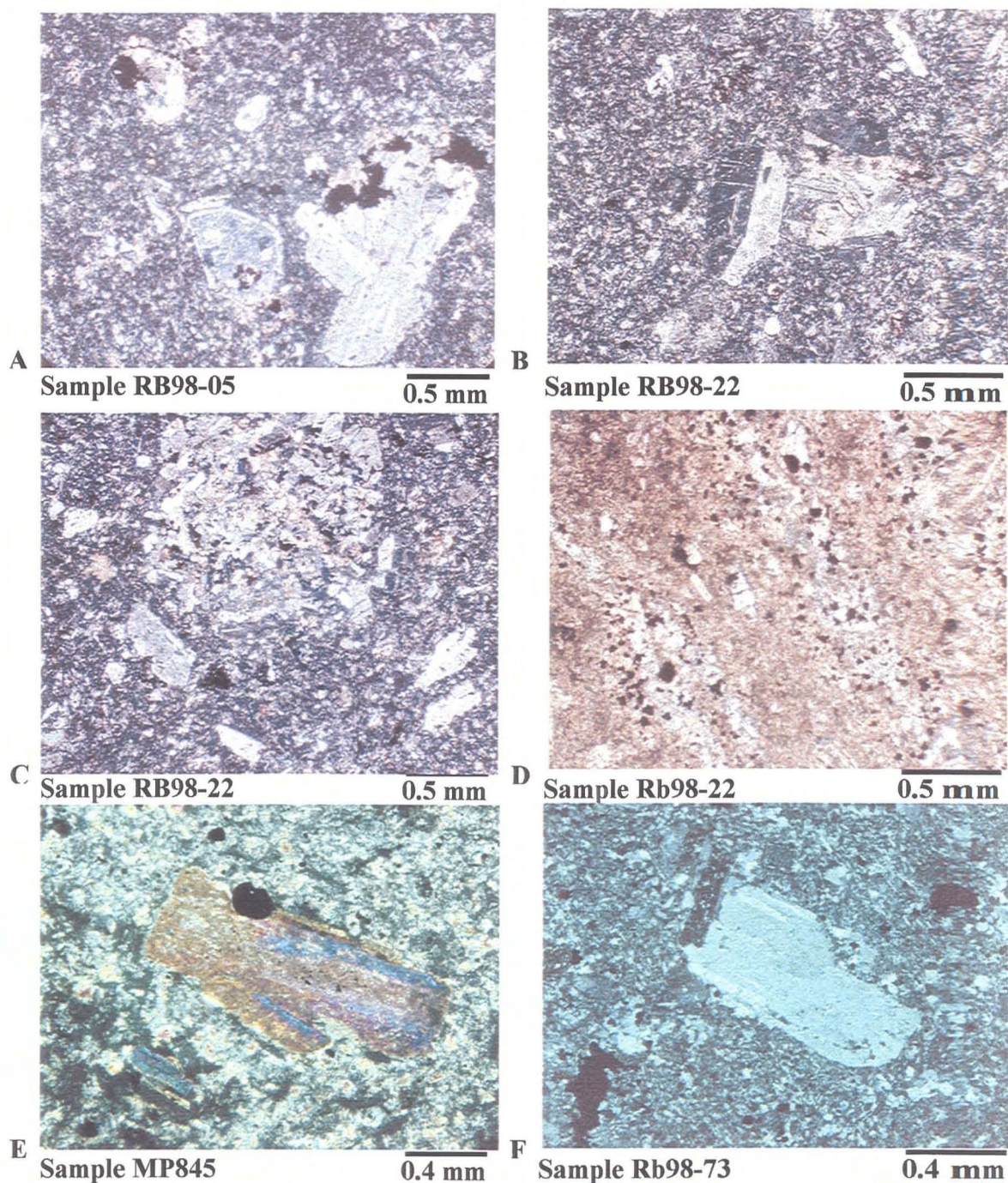
Figure 4.6. Transmitted light photomicrographs of rhyodacites and rhyodacitic dykes of the upper member of the Lo Prado Fm from less altered zone.

Rhyodacites in figures **A**, **B**, **C**, **D**; and rhyodacitic dykes in **E**, **F** from less altered zone (background). Note: glomero-porphyritic texture (**A**, **B**) with albite phenocrysts in intersertal mesostasis; xenolith (**C**); banded groundmass (**D**), and recrystallised groundmass (**E**, **F**). Also note fine opaque crystals in groundmass and albite phenocrysts.
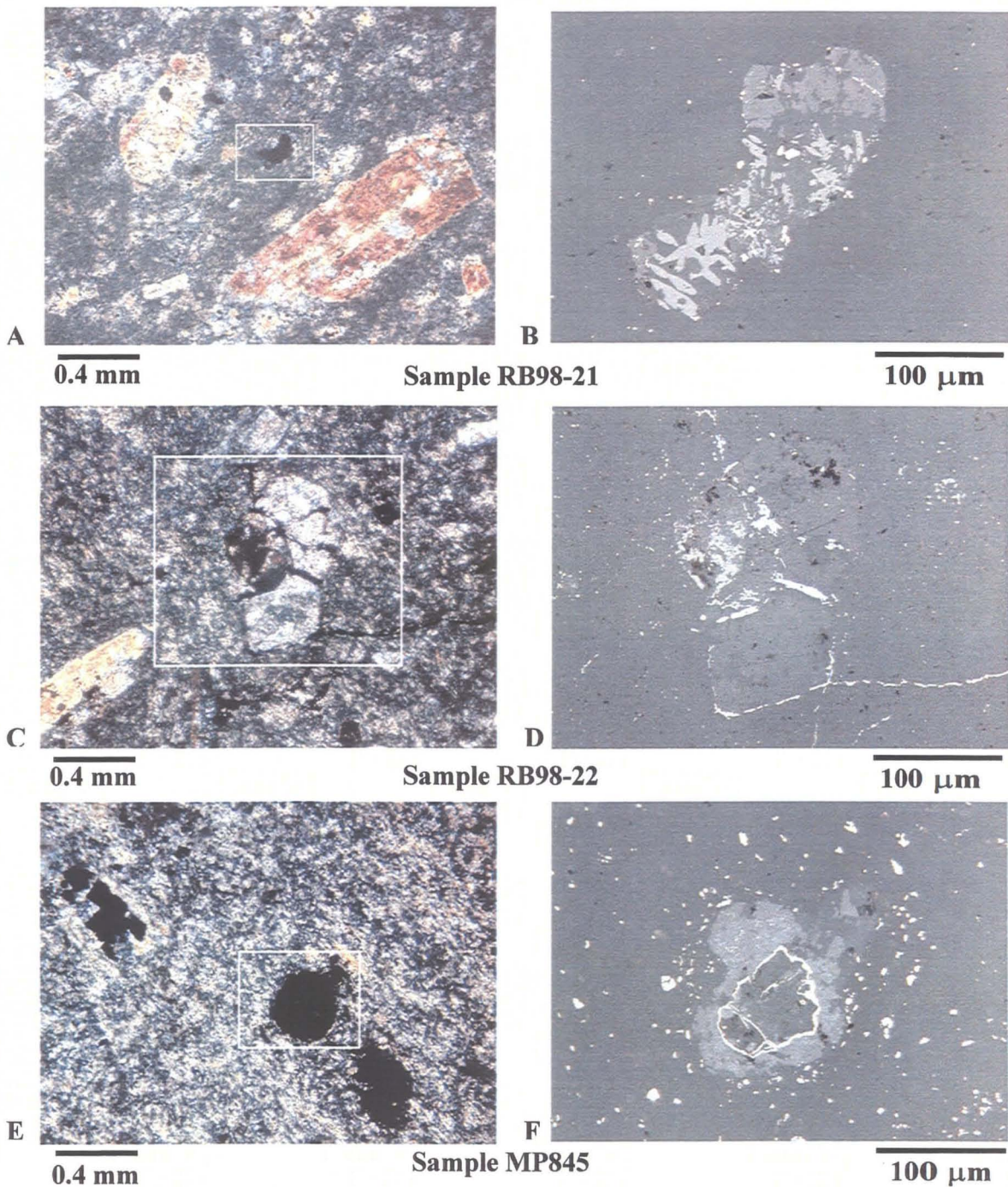
Figure 4.7. Transmitted and reflected photomicrographs of rhyodacites showing the opaque mineralogy.

Transmitted (left) and reflected (right) photomicrographs of rhyodacites of the upper member of Lo Prado Formation from less altered (background) zone, showing the opaque mineralogy. Rutile, titanite-leucoxene, and pyrite replaced early ferromagnesian or magnetite. Note also fine pyrite disseminated in groundmass and in veinlets. Insets (left) show enlarged areas (right).
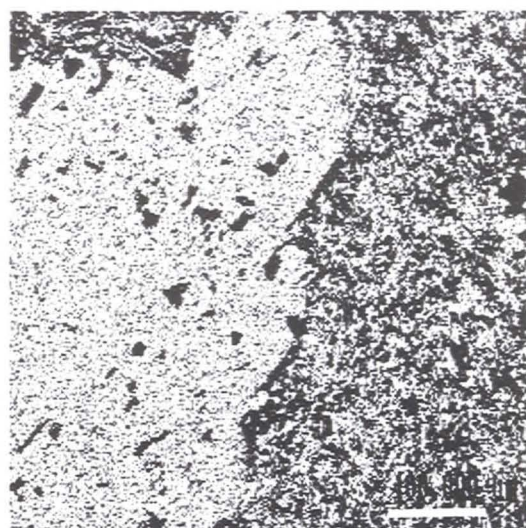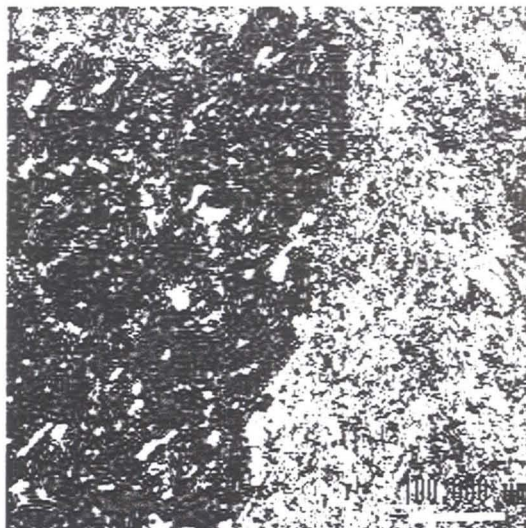
Na   X-ray microprobe image   K   X-ray microprobe image

Sample Rb98-05
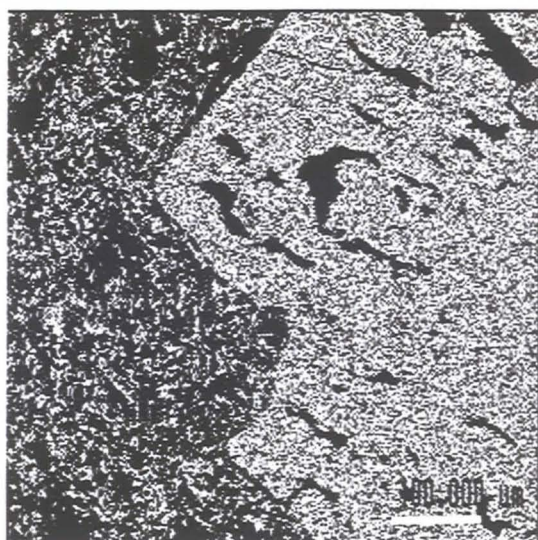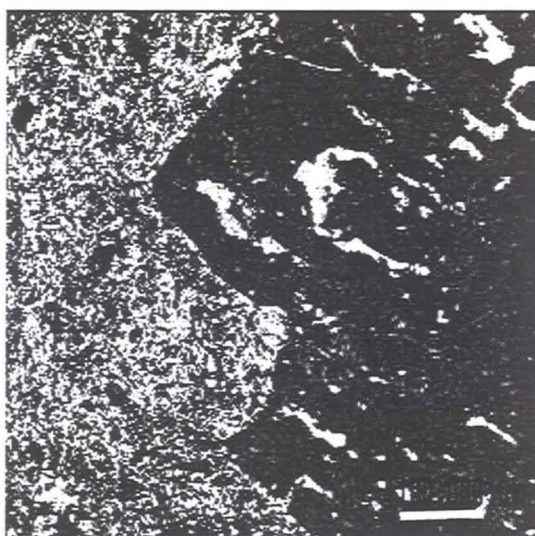
Na   X-ray microprobe image   K   X-ray microprobe image

Sample Rb98-22

Figure 4.8. Na and K X-ray images in rhyodacites from background zone.

Note the sodic composition of phenocrysts (An$_{0-2}$), and the abundance of K-feldspar in the groundmass. The albite phenocrysts and the K-feldspar in groundmass are considered products of the regional very-low-grade metamorphism. Note also veinlets and patches of K-feldspar in albite, which might represent a late phase related to hydrothermal alteration and Cu-mineralization.

same samples (e.g. RB98-21, Table 4.2) there are also larger pyrite crystals (0.3 mm) and/or pyrite is present in veinlets associated with titanite, chlorite, calcite and epidote.

Xenoliths of dark, fine-grained to porphyritic rocks (Figures. 4.5a and 4.6c) are also common (2-4%). They are usually composed of an aggregate of albite, opaque minerals (pyrite-titanite), calcite, chlorite and white mica.

It is interesting to note that the less altered "background" rhyodacite samples were found in the eastern side of the deposit (east to Valdivia Sur, Figures 5.5 and 5.6 below). Conversely, "background" samples collected from barren areas but in the western side of the deposit (Filo area, Figures 5.5 and 5.6 below) do show weak sulphide (Fe-Cu) - hematite mineralisation.

Rhyodacite dykes have been mapped underground to be continuous with flows or domes (Ahumada, 1985a) and have the same textural and mineralogical composition (Table 4.2, Figure 4.6). The only difference noted is that some samples of dykes have a coarser-grained groundmass (Figure 4.6e, f), yet this may be a secondary effect of alteration rather than a primary feature. In fact, background samples of rhyodacite dykes are relatively more altered than flows because they are more intensely fractured and seem to be more affected by faults, and the margins (contact zones) of rhyodacite dykes are often marked by zones of shattering. All studied dyke samples from barren zones (mostly sampled at lower levels of the mine) have minor contents of pyrite, and many have traces of chalcopyrite, sphalerite, and galena, indicating that they are not really "unmineralised" rocks.

In the past, these volcanic and subvolcanic rocks were referred to as *trachytes* (Ahumada, 1985a; Holmgren, 1987) because of their trachytic texture and because the albite phenocrysts were interpreted to be primary. Nevertheless, regional studies (e.g. Levi, 1969; Levi et al., 1982; 1989; Vergara et al., 1995) have demonstrated that felsic rocks in Lo Prado Formation and other Lower Cretaceous and Jurassic units exposed in the Coastal Range of Central Chile, do not preserve their calcic volcanic plagioclase, which in most cases has been replaced by albite. These authors indicate that the rocks have been affected by very low-grade metamorphism (mostly prehnite-pumpellyite facies) and designated these felsic rocks *keratophyres*. They also indicated that the

alteration is relatively less pervasive in mafic rocks, in which the volcanic calcic plagioclase is partially preserved in the more massive parts of the flows. Similar observations haven been made in many other bimodal felsic-mafic sequences affected by low-grade metamorphism (e.g Battey, 1955; Hughes, 1973; 1982). Those observations are in agreement with the patterns observed at El Soldado, consequently, even though there is no textural evidence for Na alteration, the albite phenocrysts are here interpreted to be the result of an event of regional metasomatism/metamorphism rather than a primary factor or a product of hydrothermal alteration *per se*. This is also in agreement with the immobile trace-element geochemistry of the rock (see Section 4.3) and the sodic alteration recognised in the basalts (*spilitisation*).

4.2.4. Basalts of the Lower Part of Veta Negra Formation

These rocks present a grey to green colour with a typical reddish shade associated with their hematite contents. The studied samples (Table 4.1), representing the lowermost strata of Veta Negra Formation, have a porphyritic texture, and are composed of plagioclase, augite ($Wo_{38}En_{46}Fs_{16}$, Table 4.5, below) and altered (chloritised) ferromagnesian minerals in a hyalo-ophytic groundmass with abundant titano-magnetite (Figure 4.9a, b). Plagioclase is albitised (An_8 by microprobe) and altered to sericite, chlorite, calcite and epidote. These rocks are comparable to the basalts of Lo Prado Formation, the main difference being the abundance of hematite (Table 4.1, Figure 4.9a, b), which alters ferromagnesian minerals, and in the groundmass. These features have been explained elsewhere as being the results of "deuteric" oxidation immediately after extrusion of the lavas in a subaerial environment (e.g. Lincoln, 1981; Westra, 1988a). Only one sample was analysed chemically and it plots as basalt in the discriminant diagrams (see section 4.3).

This study suggests that, at least at El Soldado mine, the contact between the two formations (Lo Prado and Veta Negra Formations) represents a change in the environment of deposition (subaquatic to subaerial extrusion) rather than in the composition of their parent magmas (see section 4.3).

0.4 mm   Basalt from lower strata of Veta Negra Fm. (sample Z603-95)   100 μm

0.4 mm   Basaltic dyke (sample Z626-95)   100 μm

0.4 mm   Gabbro (Sample Z622-95)   100 μm
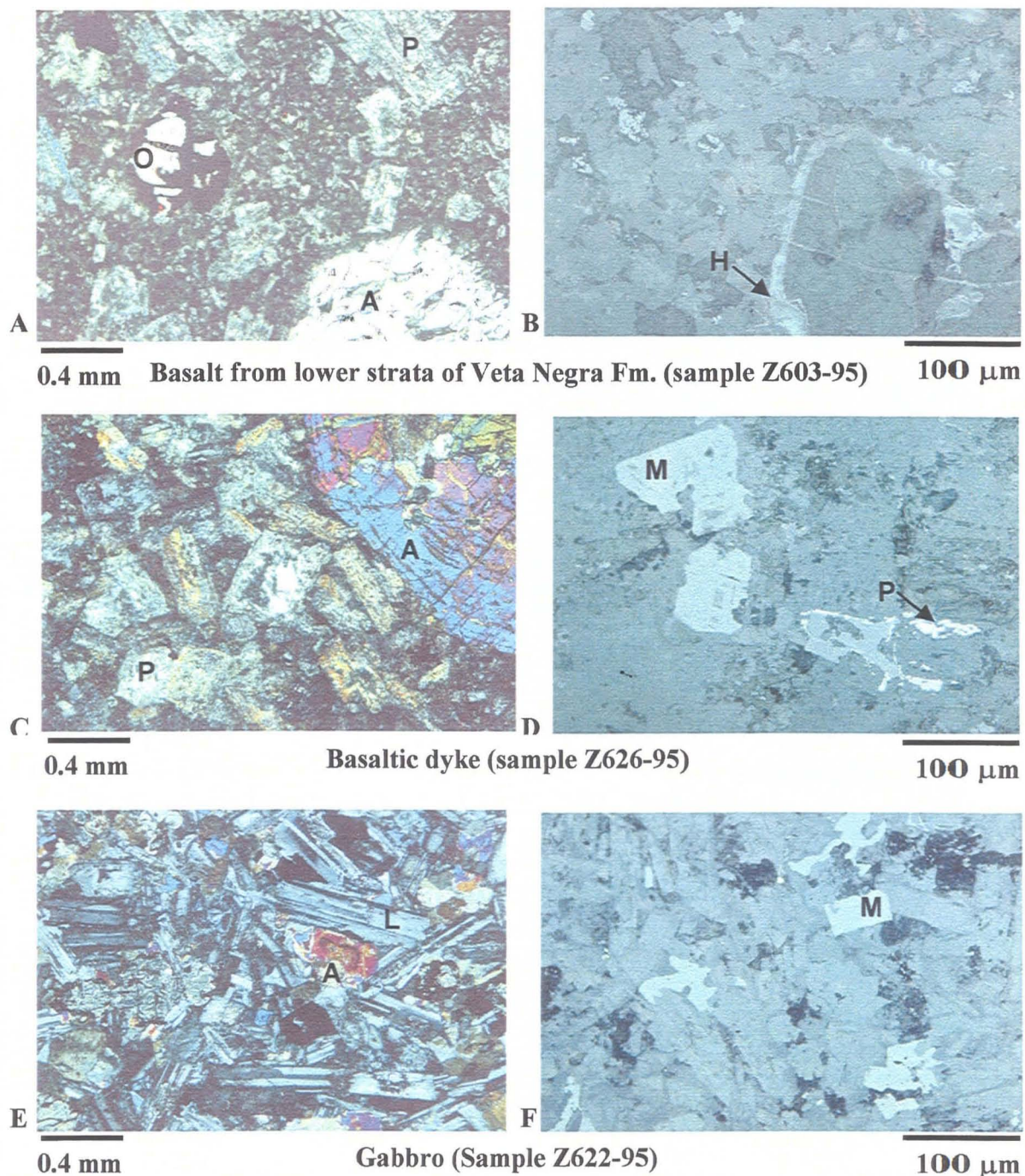
Figure 4.9. Transmitted (left) and reflected (right) microphotographs.
A) Basalt of Veta Negra Fm composed of albitised plagioclase (**P**), augite (**A**), and altered olivine (**O**).
B) Hematite (**H**) altering ferromagnesian and replacing magnetite in groundmass.
C) Basaltic dyke composed of albitised plagioclase (**P**), augite (**A**), and Ti-magnetite crystals in a sub-ophitic groundmass.
D) Ti-magnetite (**M**) partly replaced by pyrite.
E) & F) Gabbro composed of labradorite (**L**), augite (**A**), and Ti-magnetite (**M**).

4.2.5. Subvolcanic Mafic Dykes and Stocks

Included in this category are basaltic dykes, "microdioritic" (andesitic) dykes, and a gabbro body, the only phaneritic intrusive rock recognised at the mine. All these rocks are barren or very poorly mineralised with Cu and do not host any important orebody at El Soldado; consequently their detailed study was not justified.

4.2.5.1. Basaltic Dykes

These rocks (previously designated *andesitic*; Ahumada, 1985a) are recognised throughout the mine camp, but they are concentrated in the northern portion where they intrude along WNW-ESE trending faults. They feed the lower basaltic lava flows of the Veta Negra Formation. Studied samples (Table 4.3) have a coarse porphyritic texture with phenocrysts of albitised plagioclase (An_{2-8}), augite ($Wo_{40-42}En_{42-44}Fs_{14-18}$, Table 4.5, below) and altered ferromagnesian (olivine?) in a hyalo-ophytic groundmass with abundant titano-magnetite (Figure 4.9c). Titano-magnetite is partially altered (exsolved) to hematite-titanite-rutile, and pyrite (Figure 4.9d). Veinlets and vugs with chlorite, sericite, epidote and quartz are common. The rocks are comparable with the basaltic flows of Lo Prado Formation and the lower strata of Veta Negra Formation. According to their geochemistry they are basalts (see section 4.3).

4.2.5.2. "Microdioritic" (Andesitic) Dykes

These dykes cut the previously described basaltic dykes and are considered to be the youngest rocks exposed in the El Soldado camp. They extend to the east and have been mapped as high in the stratigraphy as at the elevation of the Veta Negra mine (Figures 3.2 and 3.4), where they intrude the organic- and Cu-rich, lacustrine sediments intercalated in red beds and oxidised lava flows (Villalobos, 1995).

These are green-grey, microcrystalline (saccaroidal) rocks characterised by their high magnetic susceptibility (see Appendix 5). Studied samples (Table 4.3) show a micro-porphyritic texture and are composed by laths of albitised plagioclase (An_3) and altered (chlorite>epidote-calcite) ferromagnesians in an intersertal to microcrystalline groundmass with abundant magnetite (hence their high magnetic susceptibility), chlorite

Table 4.3.- Petrographic Characteristics of Mafic Dykes and Gabbro (less altered "background" samples)

Samples	Rock Unit	Texture	Phenocrysts			Ground-mass	Opaques	Amygdule and Veinlets	Na-Co-baltini-trite
			Plagioclase	Pyroxene	Ferromagnesian			Fillings	tintion
Z626-95 MP-839 MP840	Basaltic dyke	coarse porphyritic	25-30%; 0.2-3.0mm; albitised (An$_{2-8}$); altered to sericite>	10-15%; 0.2-4.0mm; augite; weakly-moderately altered to chlorite, calcite, epidote, hematite	5-10%; 0.1-1.5mm; olivine? pyroxene; altered to chlorite, hematite> calcite, epidote	hyalo-ophytic	3-5%; Ti-magnetite; partyally replaced by titanite-rutile; pyrite; traces of chalcopyrite	common; sericite, epidote, chlorite, opaques, quartz	traces in ground-mass
Z614-95 MP-866 MP-840	Microdioritic dyke and fine andesitic dyke (MP866)	micro porphyritic	25-35%; <1.5mm; albitised (An$_3$); rimmed by K-feldpar		10-20%; <1.0 mm; altered to chlorite> epidote, calcite, opaques	intersertal to microcrys-taline	7-8% Ti-magnetite, traces of pyrite and or chalcopyite-bornite	rare, calcite, chlorite, epidote, quartz	weak; plagioclase rims
Z622-95 Z623-95 RB98-74	Gabbro	Hypidio-morphic granular	60-65%; 0.1-2.0mm; labradorite (An$_{58}$), partialy albitised; altered to sericite> epidote, K-feldspar	20-25%; 0.1-2.0mm; augite; weakly altered to chlorite, calcite, epidote	olivine? pyroxene? altered to chlorite, calcite, hematite > epidote		3-5%, Ti-magnetite, weakly replaced by hematite, rutile, titanite; traces of pyrite	rare; epidote, chlorite, K- feldspar	traces

and epidote (Figure 4.10a, b). Albite crystals are usually rimmed by K-feldspar (Figure 4.10a), which gives them a characteristically pink tint. Magnetite has high values of Ti (Table 4.6, below) and is weakly replaced by hematite and/or titanite-rutile. Some of the dykes have a fine porphyritic texture (phenocrysts < 1.5 mm) and were mapped at the mine as "*fine grained andesite*". Because they have a similar composition (e.g. sample MP866) they should be included in the same group (Table 4.3; Figure 4.10c, d). These rocks plot as andesites in discriminant diagrams (Section 4.3) thus the "microdioritic" name can be kept.

4.2.5.3. Gabbro Stock

This body has been recognised at deep levels in the northern part of the camp (Figure 5.8 below). Its shape and dimensions are unknown and it considered to represent a stock, although it could well be a coarser-grained and larger dyke emplaced in the same fault system than the major basaltic dykes. The composition of the gabbro is also similar to these basaltic dykes.

The gabbro shows a hypiodomorphic granular texture, and is composed of labradorite (An_{58}), augite (Wo_{35-44}, En_{37-46}, Fs_{13-23}) altered ferromagnesians (olivine? pyroxene?) and fine titano-magnetite (Figure 4.9a, b; Table 4.3). Secondary minerals are chlorite, sericite, epidote, quartz, hematite, rutile-titanite and rare pyrite. Alteration is stronger in a narrow zone (~10m) adjacent to the contact with the volcanic sequence where the gabbro has more pyrite (< 1% by volume) and also traces of chalcopyrite.

4.3. Geochemistry of the Volcanic and Subvolcanic Rocks of El Soldado
4.3.1. Methodology

Whole rock, $-H_2O$, $+H_2O$, FeO, total S, and trace elements including REE analyses were carried out in 35 selected samples, utilising a combination of XRF, ICP-MS and wet chemical methods. Analysed samples were selected from the set described in previous section (4.2), most of them collected along the Filo-Valdivia Sur and Filo-Osorno cross sections (lavas) or from Morro area (subvolcanic bodies). For the sake of consistency with previous work by the mine, the analyses were carried out at the
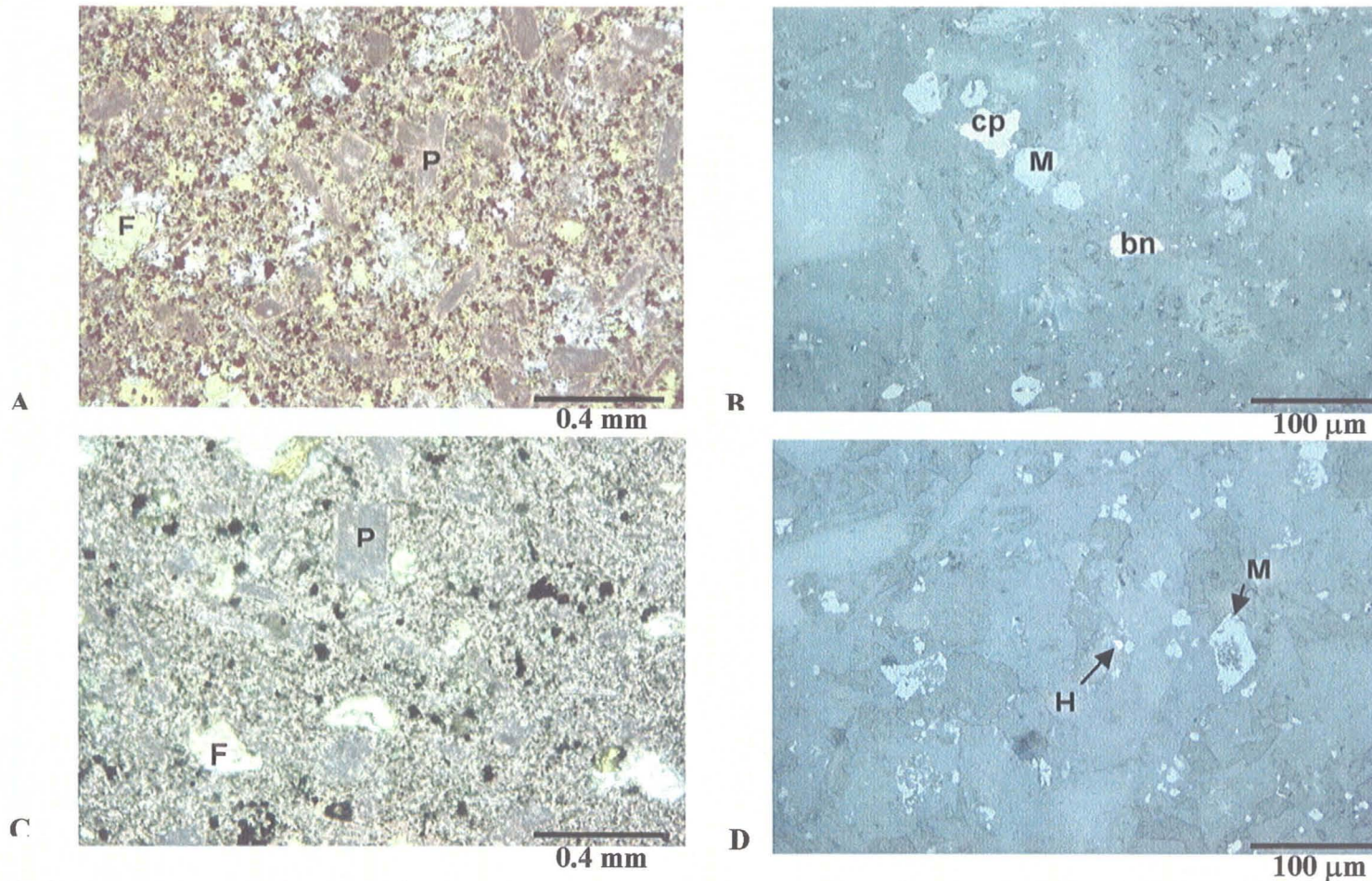
Figure 4.10. Transmitted (left) and reflected (right) light microphotographs of microdioritic and "fine andesitic" dykes.
A) & **B)** Microdioritic dyke (sample Z614-95).
C) & **D)** "Fine andesitic" dyke (sample MP866).
Albitised plagioclase (**P**) laths rimmed by K-feldspar (pink); chloritised and epidotised ferromagnesian crystals (**F**). Abundant magnetite (**M**) and minor hematite (**H**) in groundmass. Chalcopyrite (**cp**) and bornite (**bn**) also in **B**. Calcite, chlorite and epidote in groundmass.

Table 4.4.- Microprobe Spot Analyses of Plagioclase Phenocrysts of Background Rocks

Rock Type	Sample	Spot	SiO₂ %	Al₂O₃ %	Na₂O %	CaO %	K₂O %	FeO %	MnO %	MgO %	TiO₂ %	BaO %	Cl %	Total %	Mineral	Ab	An	Or	Remarks
Basalt	RB9842	5	46.61	31.10	2.31	15.22		0.65		0.22				96.11	bytownite	0.22	0.78	0.00	core
Basalt	RB9842	21	47.20	32.80	2.06	17.08	0.00	0.69	0.10	0.24	0.00	0.00		100.17	bytownite	0.18	0.82	0.00	core
Basalt	RB9842	22	46.86	33.28	1.82	17.75	0.05	0.77	0.00	0.11	0.09	0.08		100.81	bytownite	0.16	0.84	0.00	core
Basalt	RB9842	23	51.81	29.19	3.93	13.01	0.16	1.08	0.07	0.23	0.00	0.10		99.59	labradorite	0.35	0.64	0.01	border
Basalt	RB9842	24	51.10	29.76	3.93	13.61	0.12	1.29	0.00	0.20	0.03	0.19		100.22	labradorite	0.34	0.65	0.01	border
Basalt	RB9842	25	50.80	30.40	3.90	14.18	0.10	0.86	0.00	0.22	0.00	0.12		100.59	labradorite	0.33	0.67	0.00	border
Basalt	RB9842	26	55.63	26.35	4.84	9.53	0.22	1.48	0.04	0.58	0.06	0.13		98.86	labradorite	0.47	0.51	0.01	border
Basalt	RB9842	27	47.06	32.95	1.96	17.16	0.02	0.75	0.00	0.10	0.08	0.00		100.08	bytownite	0.17	0.83	0.00	core
Basalt	RB9842	28	52.19	29.74	4.37	13.63	0.09	1.00	0.00	0.31	0.06	0.05		101.44	labradorite	0.37	0.63	0.00	border
Basalt	Rb9829	4	65.00	22.33	9.09	2.31	0.49							99.21	oligoclase	0.85	0.12	0.03	
Basalt	Z63295	8	68.31	20.41	11.17	0.45								100.33	albite	0.98	0.02	0.00	rim
Basalt	MP844	1	67.63	20.95	9.71	1.04	0.07						0.10	99.51	albite	0.94	0.06	0.00	rim
Basalt	RB9930	5	67.52	20.52	9.50		0.13	0.95					0.11	98.72	albite	0.94	0.05	0.01	core
Basalt	RB9806	1	68.07	20.20	10.80	0.60							0.16	99.82	albite	0.97	0.03	0.00	rim
Basalt	RB9806	2	68.11	19.98	9.91	0.38	0.11							98.49	albite	0.97	0.02	0.01	core
Basalt	RB9806	4	68.40	20.38	10.67	0.39								99.83	albite	0.98	0.02	0.00	rim
Basalt	RB9806	5	67.30	19.90	10.75	0.44	0.18						0.10	98.67	albite	0.97	0.02	0.01	rim
Basalt	RB9806	6	64.80	21.07	9.57	0.39	1.02							96.84	albite	0.92	0.02	0.06	core
Basalt	RB9806	17	68.75	20.00	11.26	0.27								100.28	albite	0.99	0.01	0.00	cloudy cryst
Badk	Z62695	22	66.79	21.22	9.31	1.46		0.44		0.18				99.40	albite	0.92	0.08	0.00	small cryst
VNBasalt	Z60395	56	66.83	21.02	9.62	1.22	0.13							98.82	albite	0.93	0.06	0.01	core
Gabbro	Z62295	36	53.78	29.15	4.84	11.99	0.29	0.54						100.60	labradorite	0.42	0.57	0.02	core
Rhyodacite	RB9805	1	68.75	20.01	11.34								0.10	100.20	albite	1.00	0.00	0.00	core
Rhyodacite	RB9805	2	68.61	19.84	10.59	0.14								99.18	albite	0.99	0.01	0.00	rim
Rhyodacite	RB9805	6	68.54	20.16	10.72	0.42							0.12	99.96	albite	0.98	0.02	0.00	rim
Rhyodacite	RB9805	7	68.90	20.11	10.44	0.40								99.86	albite	0.98	0.02	0.00	rim
Rhyodacite	RB9805	10	68.94	20.21	11.37	0.26								100.79	albite	0.99	0.01	0.00	microlite
Rhyodacite	RB9805	14	68.98	20.09	9.99									99.06	albite	1.00	0.00	0.00	core
Rhyodacite	RB9805	17	69.74	20.06	9.71	0.15								99.66	albite	0.99	0.00	0.00	core
Rhyodacite	RB9805	18	69.51	19.86	10.60									99.97	albite	1.00	0.00	0.00	core
Rhyodacite	RB9805	27	68.54	20.02	9.40	0.44								98.40	albite	0.97	0.03	0.00	clear zone
Rhyodacite	RB9805	33	68.89	20.00	10.24	0.27								99.40	albite	0.99	0.01	0.00	core
Rhyodacite	RB9822	1	69.10	20.21	9.92	0.26							0.10	99.60	albite	0.99	0.01	0.00	clear zone
Rhyodacite	RB9822	7	69.46	20.11	9.93	0.16								99.65		0.99	0.01	0.00	rim
Rhyodacite	RB9822	16	68.68	20.06	9.39	0.55								98.69	albite	0.97	0.03	0.00	rim
Rhyodacite	MP848	14	66.72	19.85	10.94			1.00		0.38				98.88	albite	1.00	0.00	0.00	rim
Rhyodacite	MP839	13	68.72	19.96	10.79					0.16				99.62	albite	1.00	0.00	0.00	
Rhyodacite	MP845	61	68.17	20.08	9.84	0.19		0.37						98.65	albite	0.99	0.01	0.00	rim
Rhyoddk	MP846	46	67.98	20.24	10.89	0.33								99.44	albite	0.98	0.02	0.00	rim
Rhyoddk	MP846	47	67.39	19.91	10.11	0.42							0.69	98.52	albite	0.98	0.02	0.00	rim
Rhyoddk	MP846	49	66.37	19.46	9.51	0.29								95.63	albite	0.98	0.02	0.00	rim

Abbreviations: Vnbasalt: basalt of Veta Negra Formation; badk: basaltic dyke; rhyoddk: rhyodacitic dyke

Table 4.5.- Microprobe Spot Analyses of Pyroxene of Background Rocks

Rock Type	Sample	Spot	SiO$_2$ %	Al2O$_3$ %	FeO %	MnO %	MgO %	CaO %	Na$_2$O %	TiO$_2$ %	Cr$_2$O$_3$ %	NiO %	Total %	Mineral	Wo %	En %	Fs %	Remarks
Basalt	RB9829	1	52.44	2.63	6.31		17.01	21.62					100.01	diopside	43.1	47.1	9.8	
Basalt	RB9829	7	52.11	2.83	6.28	0.54	16.42	21.84	0.27		0.30		100.59	diopside	44.1	46.1	9.9	rim
Basalt	RB9829	8	51.86	2.91	6.58		16.76	21.57		0.39	0.28		100.34	augite	43.1	46.6	10.3	core
Basalt	RB9829	9	52.72	2.31	6.94		17.08	20.78	0.34	0.30			100.46	augite	41.6	47.6	10.8	rim
Basalt	RB9829	11	51.71	3.16	6.43		16.65	21.47	0.40	0.43	0.27		100.52	augite	43.2	46.7	10.1	core
Basalt	RB9829	15	51.65	2.87	7.30		16.60	20.85	0.36	0.49	0.27		100.38	augite	42.0	46.5	11.5	
Basalt	RB9842	4	51.17	3.81	4.79		16.63	22.62	0.33	0.35	0.66		100.36	diopside	45.7	46.8	7.6	
Basalt	RB9842	14	52.17	2.90	5.31		16.91	22.73	0.29	0.44			100.74	augite	45.1	46.7	8.2	
Basalt	MP844	4	48.86	4.31	10.75	0.21	14.48	20.34	0.49	1.24			100.68	augite	41.6	41.2	17.2	groundmass
VNBasalt	Z60395	53	51.09	2.72	10.63	0.23	16.54	19.24	0.46	0.58			101.49	augite	38.1	45.5	16.4	core
Badk	Z62695	18	51.27	2.85	9.06	0.27	15.75	20.89	0.33	0.50			100.92	augite	41.9	43.9	14.2	
Badk	Z62695	23	49.36	4.05	11.34	0.35	14.45	19.52	0.59	0.81			100.46	augite	40.3	41.5	18.3	
Badk	Z62695	25	50.44	2.69	10.28	0.21	15.65	20.11	0.48	0.57			100.45	augite	40.3	43.6	16.1	
Gabbro	Z62295	1	52.02	1.42	8.46	0.00	15.54	21.72	0.23	0.29	0.04	0.02	99.74	augite	43.5	43.3	13.2	core
Gabbro	Z62295	2	51.13	1.15	14.06	0.09	13.47	18.38	0.34	0.55	0.03	0.02	99.21	augite	38.2	39.0	22.8	rim
Gabbro	Z62295	3	50.89	2.54	10.08	0.03	15.23	19.45	0.26	0.59	0.07	0.01	99.15	augite	40.1	43.7	16.2	core
Gabbro	Z62295	4	51.62	0.61	0.02	0.09	12.95	19.74	0.34	0.35	0.02	0.02	99.59	augite	40.7	37.1	22.2	rim
Gabbro	Z62295	5	51.67	1.76	11.83	0.01	16.22	17.42	0.25	0.51	0.03	0.03	99.74	augite	35.4	45.9	18.7	core
Gabbro	Z62295	6	50.84	1.92	12.47	0.04	15.08	18.08	0.27	0.60	0.02	0.00	99.33	augite	37.1	43.0	20.0	rim

Abbreviations: VNbasalt: basalt of Veta Negra Formation, Badk: basaltic dyke

Table 4.6.- Microprobe Spot Analyses of Titano-Magnetite of Background Rocks

Rock Type	Sample	Spot	SiO$_2$ %	Al$_2$O$_3$ %	FeO %	MnO %	MgO %	CaO %	K$_2$O %	Na$_2$O %	TiO$_2$ %	Cr$_2$O$_3$ %	Cl %	Total %	Mineral	Remarks
Basalt	RB9842	9	8.03	1.02	66.67	0.56	0.58	6.14			8.61			91.61	magnetite / titanite	in groundmass
Basalt	RB9842	10	7.66	1.23	64.63		0.54	6.16			10.64		0.14	91.00	magnetite / titanite	in groundmass
Basalt	Mp844	5	0.31	1.33	77.53	0.35		0.14		0.79	11.20			91.64	Ti magnetite	in groundmass
Basalt	Mp844	6	0.68	0.37	82.81		0.19	0.27	0.19	0.46	7.31			92.27	Ti magnetite	in groundmass
VNbasalt	Z60395	54	1.72	0.64	85.11	0.24		0.23	0.09	0.42	0.62		0.15	89.21	magnetite?	in pyroxene
Anddk	MP866	30	0.24	6.53	75.14	0.29				0.40	5.69			88.29	Ti magnetite	in groundmass
Anddk	MP866	31	0.87	4.24	79.75	0.26	0.16	0.74		0.40	3.68		0.13	90.23	Ti magnetite	in groundmass
Anddk	MP866	32	0.32	4.26	75.79	0.97	0.23	0.43		1.85	7.51			91.35	Ti magnetite	in groundmass
Anddk	MP866	29	0.21	15.89	48.96	0.34	7.38			0.40	1.32	21.84		96.34	Cr-magnetite	in groundmass
diordk	Z61495	44	1.09	1.54	82.81	0.71	0.39	0.59		0.71	1.28		0.51	89.61	magnetite?	in groundmass
diordk	Z61495	45	0.96	1.22	84.55	0.59	0.18	0.54		0.59	1.10		0.54	90.25	magnetite?	in groundmass
Gabbro	Z62295	34	0.26	0.14	89.63					0.41	1.36	0.19		92.00	magnetite?	crystal
Gabbro	Z62295	40	2.48		88.04		0.18			0.44				91.14	magnetite?	crystal
Gabbro	Z62295	33	0.18	1.68	84.72					0.55	4.37	0.30		91.81	Ti magnetite	crystal

Abbreviations: VNBasalt: basalt of Veta Negra Formation, Anddk: andesitic dyke, diordk: microdioritic dyke

Table 4.7.- Normative Minerals for Background (less altered) Basalts

Sample		RB9842	RB9840	RB9829
Normative Minerals				
Apatite		0.27	0.30	0.27
Ilmenite		1.15	1.23	1.18
Orthoclase		13.67	9.54	11.64
Albite		22.68	25.37	21.67
Anortite		36.28	30.51	37.77
Magnetite		3.42	3.63	2.61
Diopside				
	Wollastonite	5.19	6.74	5.76
	Enstatite	3.08	4.14	3.20
	Ferrosilite	1.85	2.21	2.34
Hyperstene				
	Enstatite	5.68	6.38	4.16
	Ferrosilite	3.41	3.41	3.03
Olivine				
	Forsterite	2.09	4.25	3.53
	Fayalite	1.38	2.50	2.84
Wt % of normative minerals		**100.15**	**100.21**	**100.01**
Color Index		**27.5**	**34.8**	**28.9**
Normative plagioclase		**62**	**55**	**64**

Calculations according Philpotts (1990); entire calculations in appendix 2.3

laboratories of Chemex Laboratories, Vancouver. A previous set of 57 samples (Cuesta Research a, b, and c, 1995; CMD internal reports) analysed in the same laboratory, and collected by the author, was also included in the study. Other previous data of rocks from El Soldado mine (Ahumada, 1985a), from surroundings of El Soldado district (B. Levi, 1985, CMD internal report) and from regional studies (Vergara et al., 1995) were also reviewed and used to compare and complement the new results. Data are summarised on Table 4.8 and presented in detail in Appendices 2.1 and 7.4.

Geochemical analyses were obtained for two purposes: to study the original composition of the volcanic-subvolcanic rocks (samples from less altered-unmineralised background areas) discussed in this section, and to investigate the chemical changes (gain-losses) associated with the alteration-mineralisation processes (altered-mineralised samples). This last matter is discussed in chapter 6.

4.3.2. Rock Classification

We established above that the volcanic and subvolcanic rocks exposed at El Soldado show the effects of a regional very-low grade metamorphism and a local strong hydrothermal alteration (metasomatism) related with Cu mineralisation. Both processes caused similar effects and were probably inter-related. The local alteration was probably a more intense pulse (peak) of the regional "metasomatism" event focussed at El Soldado due to the local presence of favourable structures and permeable receptive rocks (see chapter 3). The metamorphism-alteration processes have preferentially changed the alkali contents of the rocks and consequently common major element lithochemistry cannot be used to identify or classify the rocks. This can be clearly appreciated by plotting the data on total alkalis versus silica diagrams (TAS) after Irvine and Baragar (1971, Figure 4.11a) and Cox et al. (1979, Figure 4.11b). In those diagrams it is evident that there is a wide variation in Na_2O-K_2O contents of the rocks, making them plot within sub-alkaline and alkaline fields (Figure 4.11a). Nevertheless, those samples clearly define two populations (felsic and mafic) in terms of silica, and more importantly, the relatively *less altered* samples (according to petrography) plot in the sub-alkaline field (Figure 4.11a) and in the rhyolite and basalt fields (Figure 4.11b). Using another TAS diagram (e.g. Le

Table 4.8.- Compilation of Lithochemistry of Representative Volcanic and Subvolcanic Less Altered (background) Rocks (Sumary).

I.- Rocks of El Soldado Mine

Reference (*)	Rock (**)	SiO_2 %	TiO_2 %	AL_2O_3 %	FeOT %	MnO %	MgO %	CaO %	Na_2O %	K_2O %	P_2O_5 %	LOI %	Ba ppm	Co ppm	Cs ppm	Cu ppm	Hf ppm	Nb ppm	Ni ppm	Rb ppm	Sr ppm	Ta ppm	Th ppm	U ppm	V ppm	Y ppm	Zr ppm
1	BaLP (3)	51.57	0.63	19.46	7.54	0.45	5.46	10.05	2.75	1.97	0.12	2.71	452	30	2	72	<1	<1	32	72	352	<0.5	<1	<0.5	243	12.8	32
2	BanLP (4)	54.98	0.63	16.59	8.27	0.53	4.45	6.68	5.62	2.08	0.17					879											112
3	BanLP (3)	56.64	0.69	16.39	9.00	0.32	4.93	5.18	4.50	2.22	0.14	4.40															
1	RdLP (4)	69.86	0.42	14.20	2.07	0.13	0.28	4.48	4.76	3.65	0.15	3.96	512	8	1	131	5	6	23	94	65	<0.5	9.3	2.5	53	23.0	179
2	RdLP (5)	67.47	0.44	15.47	3.39	0.12	0.69	3.32	5.95	3.03	0.11					1630											145
3	RdLP (7)	65.70	0.41	16.14	2.93	0.15	0.91	3.40	4.99	5.24	0.13	3.32															
1	Rddk (3)	69.32	0.47	13.70	3.13	0.11	1.93	2.89	3.98	4.35	0.10	2.95	555			75		5		77	49					26	216
2	Rddk (3)	66.56	0.43	15.58	2.18	0.09	0.38	5.52	6.11	3.05	0.10					666											136
3	Rddk (5)	71.95	0.38	14.79	0.53	0.04	0.14	2.59	3.61	5.88	0.09	4.42															
1	Badk (1)	51.18	0.81	19.93	9.79	1.00	6.14	4.15	5.05	1.78	0.17	4.37	543	27	1	725	1	2	30	47	322	<0.5	2.0	0.5	225	13	47
2	Badk (3)	49.06	0.74	19.49	9.63	0.43	7.33	8.06	3.45	1.69	0.12					320											136
1	Anddk (1)	62.89	0.73	16.55	3.78	0.14	2.24	4.24	4.62	4.66	0.15	4.69	405			<100		6		100	48						180
2	Bandk (5)	55.79	0.73	18.68	7.42	0.32	3.67	6.46	3.99	2.77	0.19					383											68
1	Diodk (1)	54.63	0.65	18.93	9.45	0.56	3.58	3.02	6.51	2.40	0.26	3.08	658	22	0	120	1	2	15	75	278	<0.5	1.0	0.5	95	20	89
2	Diodk (2)	56.50	0.63	17.08	7.59	0.74	3.85	4.31	6.67	2.37	0.25					719											64
1	Gabb (1)	52.15	0.92	18.06	9.31	0.17	5.36	10.28	2.85	0.74	0.15	1.30	223	32	1	95	1	1	35	19	385	<0.5	1.0	0.5	255	16.5	52
1	BaVN (1)	48.80	0.79	21.08	8.33	1.92	7.02	4.47	2.63	4.85	0.12	4.41	4420	35	2	50	1	1	35	139	445	<0.5	1.0	0.5	210	18	54

II.- Rocks of El Soldado Surroundings

Reference (*)	Rock (**)	SiO_2 %	TiO_2 %	AL_2O_3 %	FeOT %	MnO %	MgO %	CaO %	Na_2O %	K_2O %	P_2O_5 %	LOI %	Ba ppm	Co ppm	Cs ppm	Cu ppm	Hf ppm	Nb ppm	Ni ppm	Rb ppm	Sr ppm	Ta ppm	Th ppm	U ppm	V ppm	Y ppm	Zr ppm
(4)	BaLP (3)	50.02	0.96	19.01	9.20	0.24	6.03	10.16	3.08	1.16	0.14	2.55	315	48	75	213			49	35	473				287	21	59
(5)	BaLP (1)	49.43	0.97	20.66	8.83	0.28	5.59	9.66	3.25	1.18	0.15	6.09	386	86			2	1	32	44	528	0.1	1.6	0	364	16	43
(4)	BanLP (1)	55.64	0.83	16.73	8.32	0.31	4.63	8.58	3.27	1.49	0.20	1.72	385	62	48	140			46	42	428				181	34	147
(4)	AnLP (1)	59.81	0.61	16.76	6.69	0.22	3.82	6.78	3.27	2.04	0.01	2.23	509	50	32	43			40	51	267				140	25	131
(4)	RdLP (2)	73.17	0.45	13.83	2.10	0.09	0.29	4.44	2.06	3.57	0.01	5.25	455	42	<10	<10			19	139	42				10	35	208
(5)	RdLP (1)	74.71	0.34	12.86	1.30	0.11	0.34	4.89	1.29	4.07	0.07	0.53	748	1			5	5	3	92	58	0.4	9.2	2	17	26	186
(4)	Bandk (2)	53.90	0.85	20.05	8.49	0.25	3.59	6.66	4.31	1.72	0.17	3.71	445	37	14	114			45	43	498				168	26	74
(4)	BanVNp (3)	54.73	0.93	18.41	8.56	0.28	3.85	6.21	4.28	2.55	0.19	2.78	525	21	32	91			34	79	418				222	27	88
(4)	BanVNo (6)	56.81	0.92	16.81	8.21	0.23	3.75	6.73	3.44	2.87	0.24	1.65	411	42	42	65			24	104	333				201	33	138
(5)	BaVN (1)	51.91	0.88	19.99	9.25	0.18	3.38	8.08	3.77	2.35	0.21	3.81	434	22			2	1	7	34	621	0.1	2.0	1	313	19	58
(5)	BanVN (2)	55.63	1.09	16.75	9.03	0.28	3.28	7.57	2.81	3.18	0.37	5.17	562	19			5	4	29	70	562	0.3	5.8	2	267	32	160

(*) 1:this thesis; 2: Ahumada 1985a; 3: Klohn et al., 1990; 4: Levi 1985; 5: Vergara et al., 1995

(**) BaLP: basalt Lo prado Fm; BanLP: basaltic andesite Lo Prado Fm; AnLP: andesite Lo Prado Fm; RdLP: rhyodacite Lo Prado Fm; Rddk: rhyodacitic dyke; Badk: basaltic dyke; Bandk: basaltic andesitic dyke; Andk: andesitic dyke; Diodk: microdioritic dyke; Gabb: gabbro; BaVN: basalt Veta Negra; BanVN: Basaltic andesite and andesite Veta Negra, (p: Purehue member; o: Ocoa member); (#): number of samples.

Complete data in Appendix 7.4
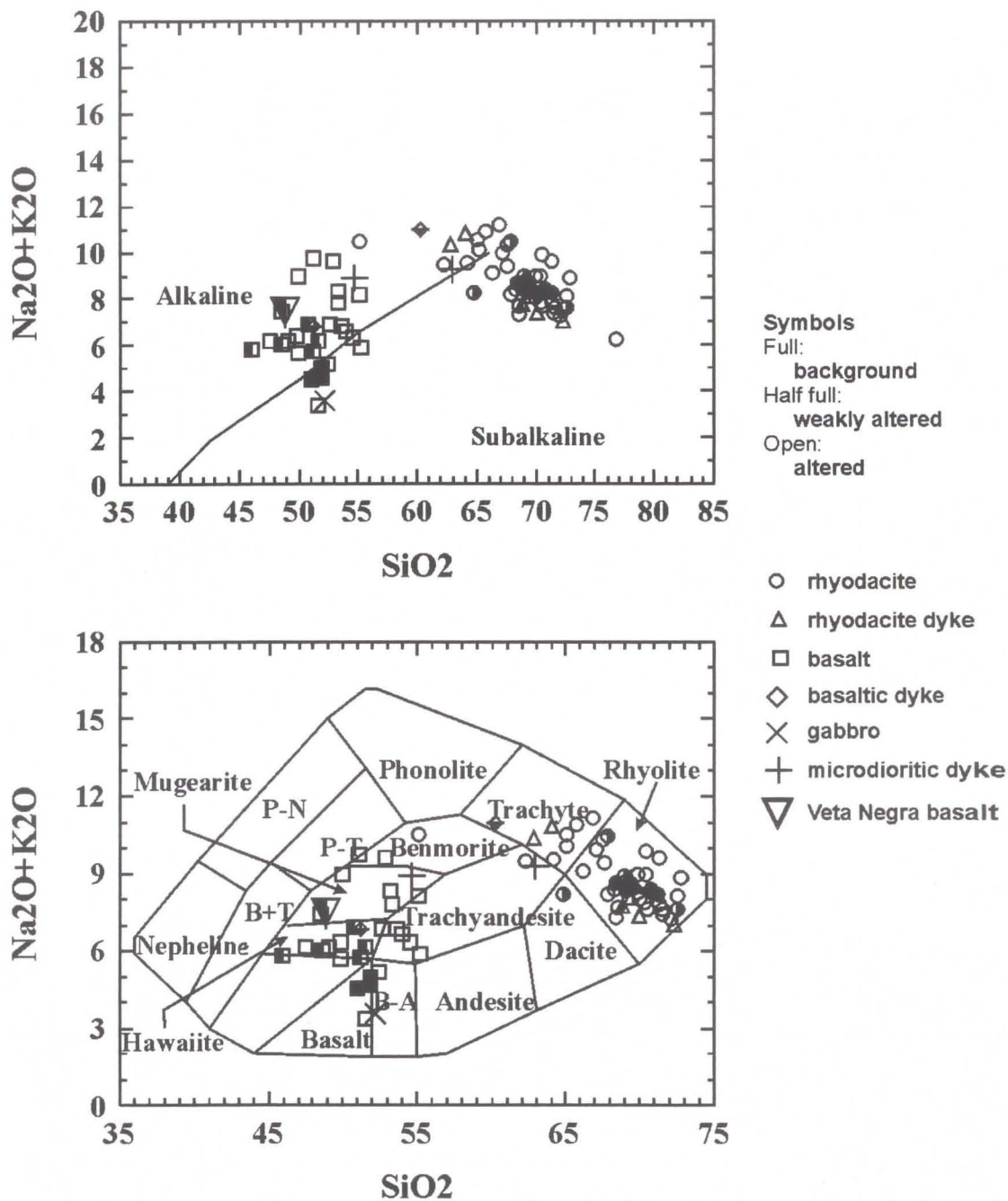
Figure 4.11. Total alkalies versus silica discriminant diagrams for El Soldado rocks.
A) Alkaline/subalkaline fields (after Irvine and Baragar, 1971).
B) Rock classification (after Cox et al., 1979).
Note the large dispersion of the data due to alkali metasomatism. Yet the "least altered" or "background" rocks plot in the basalt and rhyodacite fields.

Maitre et al., 1989) some of the petrographically <u>least altered</u> felsic rocks plot in the trachyte field. This fact, and the belief that albite is a primary mineral, led previous authors to erroneously classify these rocks as *alkaline* (e.g. Ahumada, 1985a, b; Klohn et al., 1990).

To classify the rocks, the author used the discriminant diagrams with immobile trace elements after Winchester and Floyd (1977; Figures 4.12a, b). On those diagrams the felsic lavas plot on the rhyodacite-dacite field, and the mafic lavas on the sub-alkaline basalt to andesite fields, away from the alkaline fields, clearly indicating that they represent sub-alkaline rocks, not alkaline ones. Lava samples show some scattering; especially in SiO_2 (Figure 4.12a) and in Nb/Y ratio (Figure 4.12b), but the less altered rocks have consistently less scatter than the altered rocks, and plot in a more restricted area. Silica variations could in part be related to alteration, but the Nb/Y value could be in part due to the uncertainty in the Nb analyses that are very close to the detection limit. In conclusion, by using the Zr/TiO_2 vs. Nb/Y plots as suggested by Pearce (1996), the El Soldado lavas are classified as sub-alkaline rhyodacite and basalt. The classification of the mafic rocks as basalts is consistent with their low silica content (<52 wt %) and the normative mineralogy calculated for the less altered samples (Table 4.7, Appendix 2.3).

The felsic dykes plot on the same rhyodacite-dacite field (as expected) and the mafic dykes have a more ambiguous behaviour. The less altered dyke plots on sub-alkali basalt field (as expected) but other more altered samples plot on andesite (Figure 4.12a) or andesite-basalt (Figure 4.12b) fields. Microdioritic dykes plot on andesite fields confirming that they are more evolved rocks. The gabbro, and the lava from the lowermost member of Veta Negra Formation both plot in the sub-alkaline basalt field, confirming that there was little to nor change in the magmatism in the transition from subaquatic to subaerial flows. Nevertheless, the upper levels of Veta Negra Formation are composed mostly of relatively more andesitic flows (basaltic-andesite; see next section; Levi, 1985; Vergara et al., 1995).

In conclusion, the felsic dykes have similar composition than the rhyodacitic lavas/domes and the mafic subvolcanic intrusive bodies range from basaltic to andesitic. The "microdioritic"(andesitic) dykes are the youngest igneous rocks within the camp,
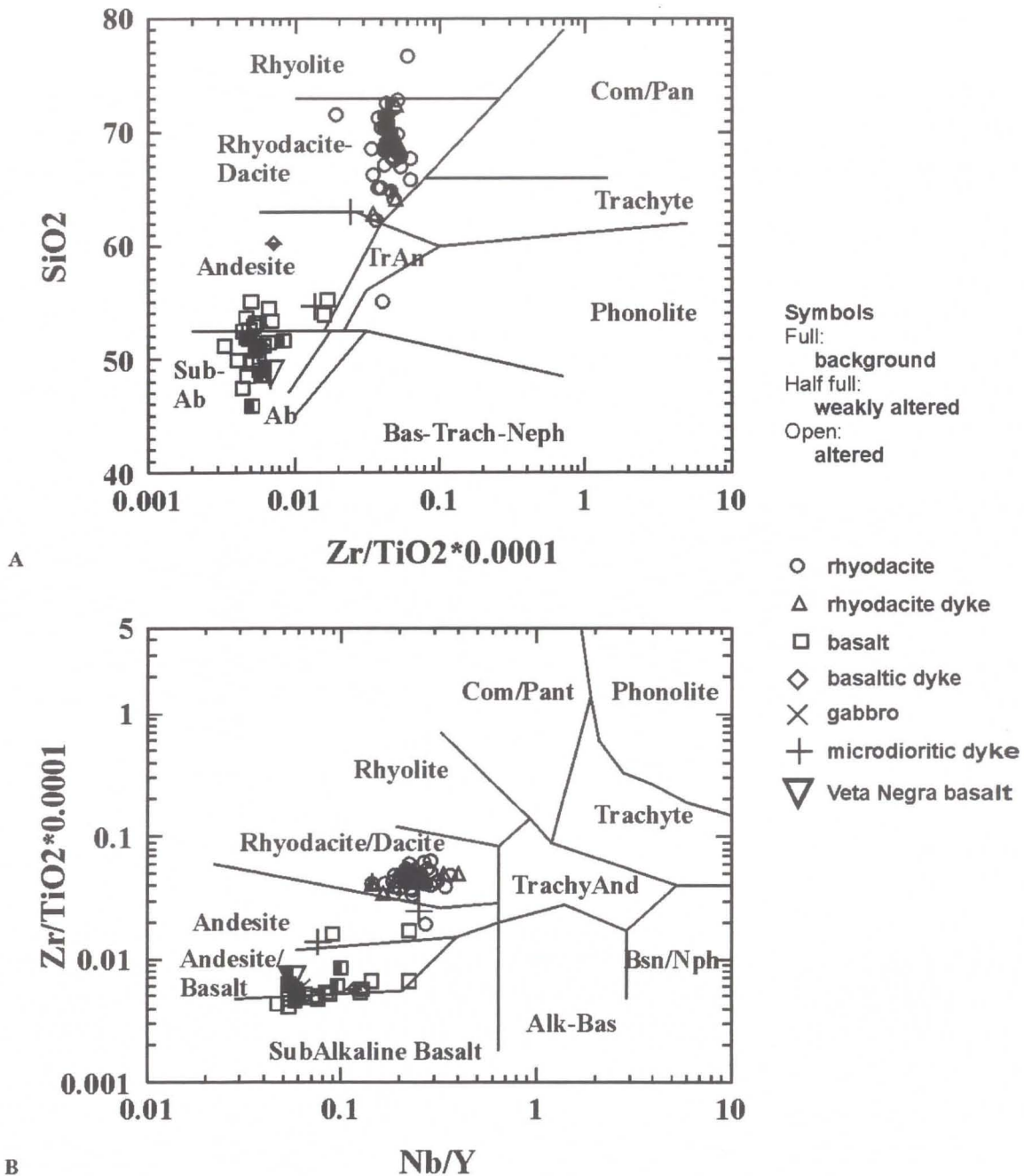
Figure 4.12. SiO₂ versus Zr/Ti and Zr/Ti versus Nb/Y discriminant diagrams for El
Soldado rocks.
(After Winchester and Floyd, 1977).

Rocks plot on andesite basalt or subalkaline basalt fields, and rhyodacite-dacite fields.
Some dykes plot as andesites. None of the rocks plots in the alkaline field.

probably reflecting an evolution of the magmatism with time (see next section).

4.3.2.1. Comparison with Previous Studies

The present results are comparable with previous studies at the mine (Ahumada, 1985a, b; Table 4.8, Appendix 7.4), which also showed a bimodal volcanism. Nevertheless the mafic rocks of Ahumada (sampled in the northern part of the mine) have more silica and plot on andesitic field (Figure 4.13a, b). Although some variation in the composition of lavas and basaltic-andesites can be expected at the mine camp; the difference can be also reflect some silica mobilisation or perhaps a different analytical method (compare Figures 4.13b and 4.12a).

Previous regional studies more distal from El Soldado mine (Levi, 1985; Vergara et al., 1995) confirm the rhyodacite-basalt (bimodal) nature of Lo Prado Formation volcanism, although Levi (1985) also reports basaltic-andesitic (SiO_2: 55.6%) and andesitic lavas (SiO_2: 59.8%). These reports also indicate that the Veta Negra Formation is composed mostly of basaltic-andesite to andesite flows (SiO_2: 54.7-59.0%). The upper levels tend to be more andesitic (including extremely coarsely porphyritic rocks colloquially called "*ocoitas*" (for the locality of Ocoa, near the Aconcagua River), indicating a change in composition of volcanism (differentiation, and more intermediate compositions rather than bimodality) with time (Table 4.8; Figures 4.12 and 4.14).

4.3.2.2. The Spilite and Keratophyre Question

The terms *spilite* and *keratophyre* have been used in the context of manto type deposits of Chile for half a century, mainly because of the association of the copper ores with high-sodium, albite-bearing mafic and felsic lavas and subvolcanic intrusives. At Punta del Cobre, a Manto Type deposit in northern Chile (#16 in Figure 2.1) the host rhyodacite was denominated *albitophyre* (Ruiz et al., 1965; Ortiz et al., 1966) and *trachyte* at El Soldado (Klohn et al., 1990). At Mantos Blancos, Chavez (1985) indicated that the albitised volcanic host rocks have characteristics of keratophyres.

Most authors agree that a **spilite** is a basaltic rock lacking penetrative deformation, with the original texture preserved and a mineralogical composition of
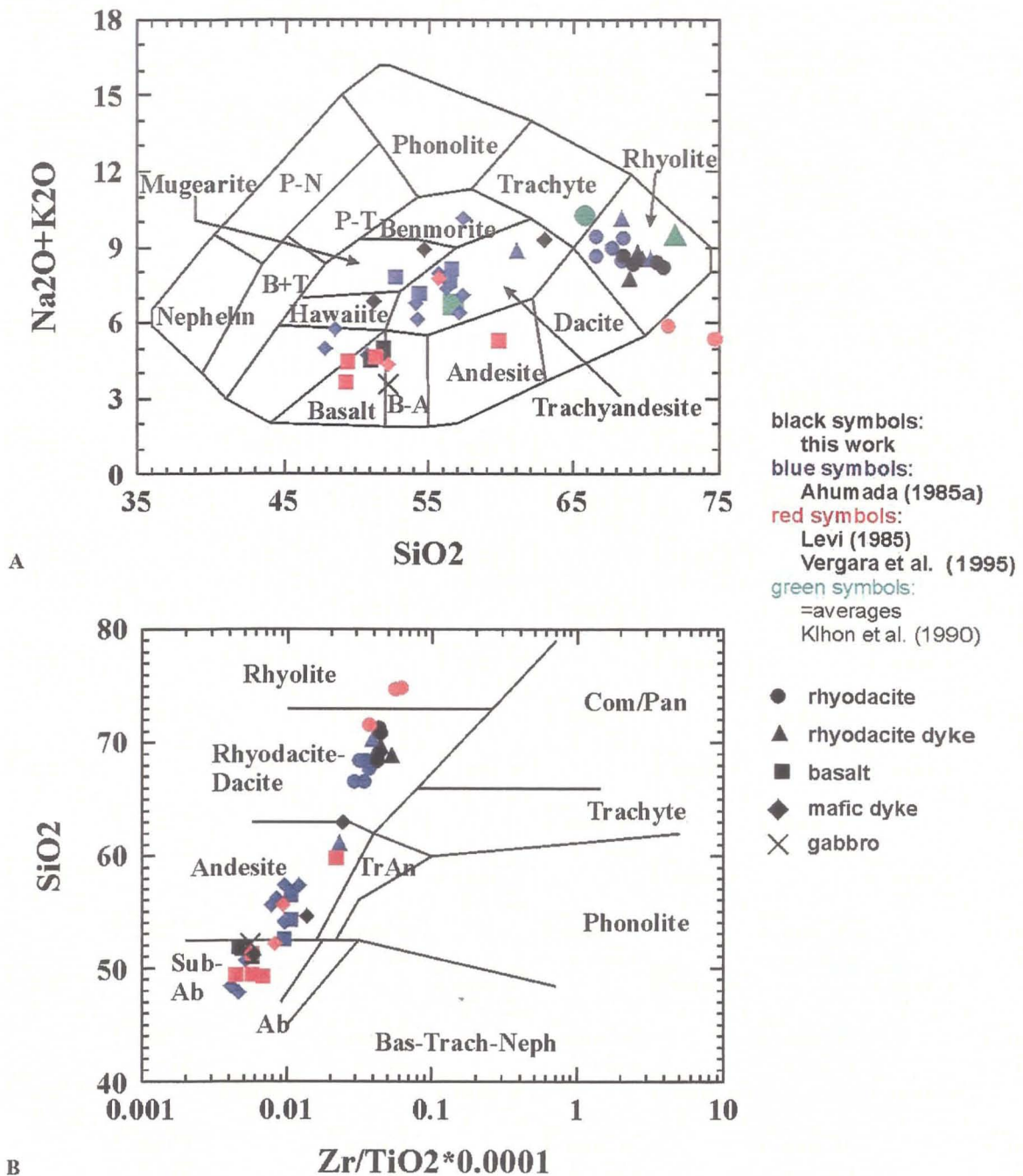
Figure 4.13. Geochemical comparison between this study and data from previous
work on El Soldado and surroundings.

A) Rock classifications (after Cox et al., 1979).
B) SiO$_2$ – Zr/TiO$_2$ (after Winchester and Floyd, 1977).
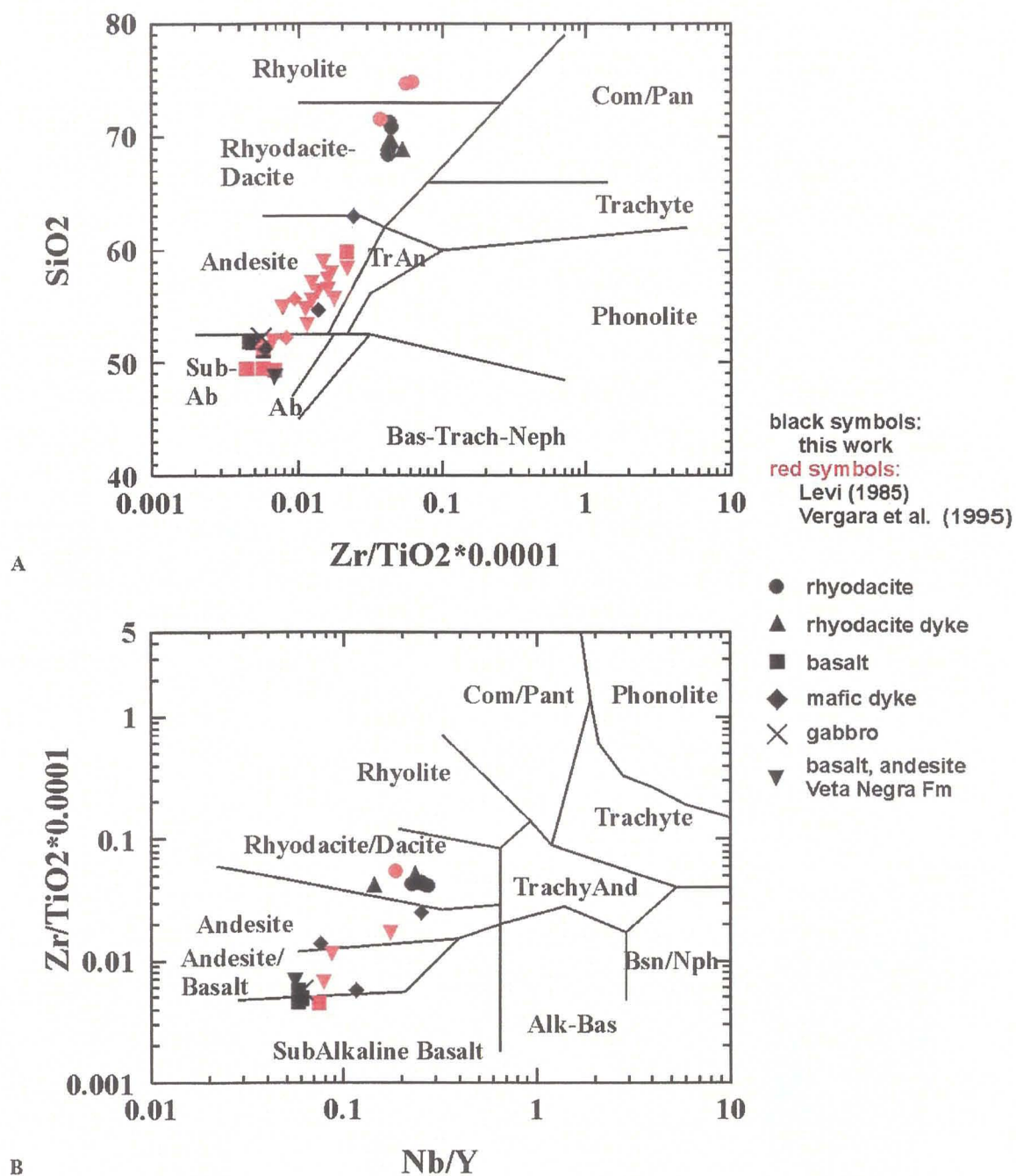
Figure 4.14. Geochemical comparison between this study and data from previous work on El Soldado and surroundings.

A) SiO_2 – Zr/TiO_2 discriminant disgram (Winchester and Floyd, 1977).
B) Zr/Ti vs. Nb/Y discriminant diagram (Winchester and Floyd, 1977).

greenschist or sub-greenschist facies (e.g. Cann, 1969; Hughes, 1973, 1982; Vallance, 1999). A typical spilite is composed of phenocrysts of albite and augite pyroxene (partially altered to chlorite or actinolite), within a groundmass composed of microlites of albite-oligoclase and abundant chlorite and epidote. Titanite and leucoxene are common, replacing titanomagnetite. Olivine relicts are altered to chlorite. Spilites frequently occur as submarine lava flows featuring pillow structures although they also occur in continental environments. Amygdules and veinlets are filling in with calcite, epidote, K-feldspar, chlorite, quartz, pumpellyte, and or prehnite (e.g. Williams et al., 1968; Cann, 1969). This composition is quite similar to the basalts present at El Soldado.

A **keratophyre** is a fine-grained igneous rock (lava or dyke) of intermediate to acid composition, showing little or no penetrative deformation, in which a primary igneous mineralogy is mimetically replaced by an assemblage appropriate to greenschist or lower facies mineralogy (Hughes, 1975). A typical keratophyre (e.g. Battey, 1955; Williams et al., 1968) is composed of "phenocrysts" of albite or albite-oligoclase, within a trachytic to microcrystalline groundmass formed of albite-oligoclase microlites, chlorite, and epidote. More felsic varieties have quartz and K-feldspar and have been called quartz-keratophyres (e.g. Battey, 1955). Titanite-leucoxene is a common accessory. Relict crystals of ferromagnesian minerals are scarce and usually altered to chlorite. This description is applicable to the rhyodacites exposed at El Soldado.

Spilites and keratophyres have been described in many geological environments but they are particularly common at active convergent plate boundaries (the "*geosynclinal*" environment, e.g. New Zeland, west North America, Central Andes; Hughes, 1973). The fact that in spilites and keratophyres, the albite "phenocrysts" show no textural evidence of alteration or replacement, has led to much confusion and the idea that these rocks could represent a different magmatic series.

As indicated by Hughes (1973): "the most deceiving features of these rocks is the presence of both primary structures and mimicked primary structures".

There have been two main hypotheses to explain the origin of spilites and keratophyres: A) states that the peculiar mineralogy and composition of spilite and keratophyre are "primary'" in the broad sense meaning that they arose during the

extrusion and cooling of a lava (e.g. Amstutz, 1968); whereas B) states that they are "secondary" in that they arose by metamorphism post-dating the period of extrusion and cooling of a lava (e.g. Battey, 1955; Hughes, 1973). Today, the first hypothesis has been left behind, and spilites and keratophyres are considered to be the product of low-grade metamorphism (e.g. Hughes, 1982; Vallance, 1999; Subarao, 2000).

The main factors that lead to the above conclusion are:

- Similar textures of spilites and keratophyres and fresh rocks (basalts-spilites; rhyolites-keratophyres; e.g. Gilluly, 1935; Cann, 1969)

- Presence of partially-albitised relicts of calcic plagioclase. Common in spilites, very rare in keratophyres (eg. Gilluly, 1935; Battey, 1955)

- Recognition of gradation from fresh basalt to altered spilitic rock, in a single flow (e.g. Levi et al., 1982; Vallance, 1999).

- Similar composition of pyroxenes (augite) in fresh basalts and spilites (e.g. Vallance, 1999).

- Improbability of simultaneously crystallisation of albite and calcic pyroxene in spilites (e.g. Gilluly, 1935; Hughes, 1973)

- Incompatibility of high temperature igneous textures with low temperature mineralogy such as albite (e.g. Battey, 1955).

- Large variations in contents of alkalis, for many keratophyres units. Usually soda rich and potash rich facies are found in the same rock unit. The range is considered to be out of the "igneous observed spectrum" (Hughes, 1973).

The mineralogical assemblage of spilites and keratophyres indicates low-grade (greenschist facies) or very low-grade (prehnite-pumpellyte facies) and their textures denote a non-deformational process (very low shear stress). For this reason they are thought to be a result of burial metamorphism (e.g. Hughes, 1982) rather than dynamothermal metamorphism. They could be ascribed to *diastathermal* metamorphism (Robinson, 1987) a kind of metamorphism developed in extensional tectonic setting (rift, back arc) with anomalously high thermal flux. The only stable plagioclase mineral, in the presence of water, under such low-grade conditions is albite (e.g Winkler, 1974); which

in both spilites and keratophyres occurs as phenocrysts and microlites mimetically replacing the originally more calcic plagioclase. The mimetic textures of albite crystals are explained by the observation that at relatively low temperatures (~300°C) and in the absence of shear stress, in which the mineralogy of these rocks may develop, there may not be sufficient energy (e.g. Cann, 1969; Hughes, 1973) to nucleate new minerals. Thus the mineralogical changes that occur in the production of spilites and keratophyres are led by diffusion and result in replacement of primary phases.

Furthermore, there is clear evidence that during the rock transformation leading to the formation of spilites and keratophyres, the rocks might not have behaved as a closed system, thus the process was metasomatic rather than metamorphic (Cann, 1969; Hughes, 1973; 1975). The metasomatism affected the content of major elements such as alkalis and calcium, making unreliable the use of many common variations diagrams (such as total alkalis vs silica) to classify these rocks. Major and more constant changes seems to be the introduction (gain) of water and sodium and the lost of calcium and potassium (Cann, 1969; Hughes, 1975). Also it is interesting to note that the rocks may not have been a closed system for Rb and Sr (e.g. Subarao, 2000), leading to misleading Rb/Sr isochrons and anomalous ages. This seems to be the case at El Soldado where a Rb/Sr age of background unmineralised rocks yield 105.9 $\pm$ 1.6 Ma (Appendix 7.1) a clearly younger age than the extrusion of the rocks (see section 4.4).

Levi et al. (1982) studied the Lower Cretaceous volcanic rocks (including the Lo Prado and Veta Negra Formations) exposed in the Coastal Cordillera of central Chile, ca. 100 km south of El Soldado. They indicated that the felsic lavas are completely altered to keratophyres and quartz keratophyres, and the basic lavas are partly altered to spilites. Spilitisation is strong and pervasive in the upper amygdaloidal parts of the flows and weak to incipient in the massive lower parts. These authors explain these alteration as a result of burial (very low-grade) metamorphism. These observations are in agreement with those presented in this thesis.

In summary, the background (relatively less altered) and "unmineralised" albite-bearing basalts and rhyodacites at El Soldado correspond to *spilites* and *keratophyres* of the literature, and their present chemistry and mineralogy represent the effects of very-

low prograde metamorphism (prehnite-pumpellyte facies). The limited Sr isotope data for El Soldado rocks (Boric and Munizaga, 1994) suggest that this spilitisation was not an early sub-seafloor process involving convecting Cretaceous seawater, but rather hydrous metamorphism at temperatures between 200 and 350 °C.

4.3.3. Volcanic Affinity and Tectonic Setting for the Volcanic Rocks at El Soldado

This aspect was not a main goal of this thesis, yet a comparison of the new El Soldado results with those from more regional studies (e.g. Levi, 1985; Vergara et al., 1995; Table 4.8; Appendix 7.4) is in order.

The studied basalts have a high Al_2O_3 content (17-21%, average 18.8%), which was almost not affected by alteration (see Chapter 6), typical of high-alumina or calc-alkaline basalts. The abundance of magnetite is also consistent with this interpretation. The calc-alkaline nature is also shown on the alkali index versus Al_2O_3 diagram and on the AFM triangle (Figure 4.15a, b). Nevertheless, the studied rocks of the Lo Prado Formation at El Soldado district do not represent a real trend, since the suite is bimodal and there are so few samples. The calc-alkaline trend is more evident integrating the data from the Veta Negra Formation (Figure 4.15b). The high values of K, Rb, Ba could be considered indicative of High K trend, but all these elements, as is the case with the alkalis, have been extensively remobilised during metamorphism-alteration, thus they cannot be used safely in this manner.

The chondrite normalised REE patterns for basalts and rhyodacites in the Lo Prado Formation are shown in Figure 4.16a and b. They both show a typical slope for calc-alkaline arc-related rocks. A negative Eu anomaly (consistent with feldspar fractionation) is clear for rhyodacites but is absent in basalts. The basaltic-andesitic rocks of Veta Negra (Figure 4.16a) are more evolved rocks and show some degree of Eu anomaly.

Immobile element contents, such as Zr, Y are also typical of calc-alkaline basalts; Zr and Nb allow classifying the rocks as belonging to calc-alkaline low-K series (e.g. Wilson 1989, petrology textbook). The "less-altered" basaltic samples were plotted on incompatible element discriminant diagrams for tectonic settings (Figure 4.17). On the
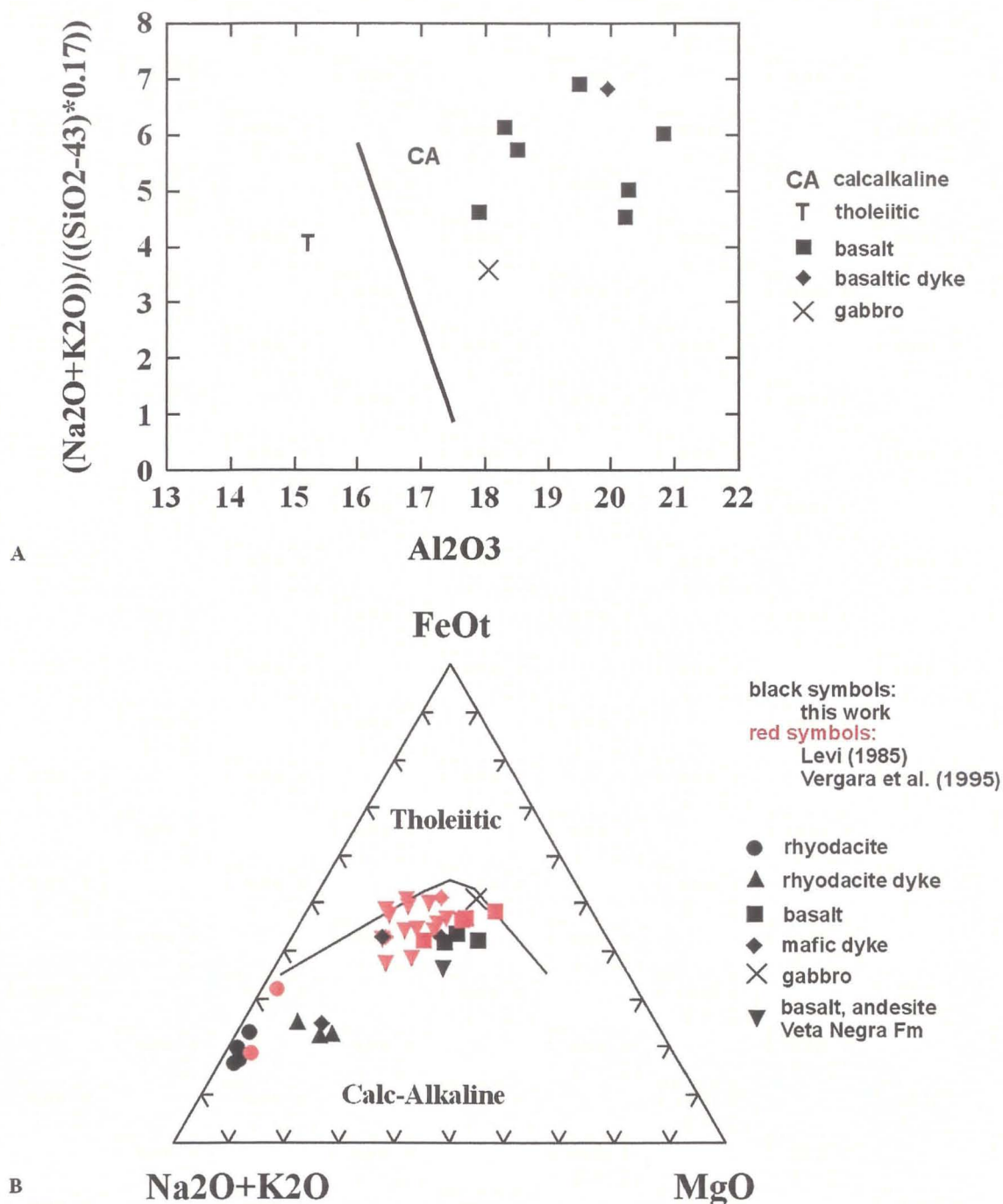
Figure 4.15. Calc-alkaline trend for rocks of Lo Prado and Veta Negra Formations.
A) Alkali index vs. alumina (after Middlemost, 1975) for less altered basalts and dykes
of Lo Prado Formation.
B) Calc-alkaline trend for rocks of the Lo Prado and Veta Negra Formations (after Irvine
and Baragar, 1971).
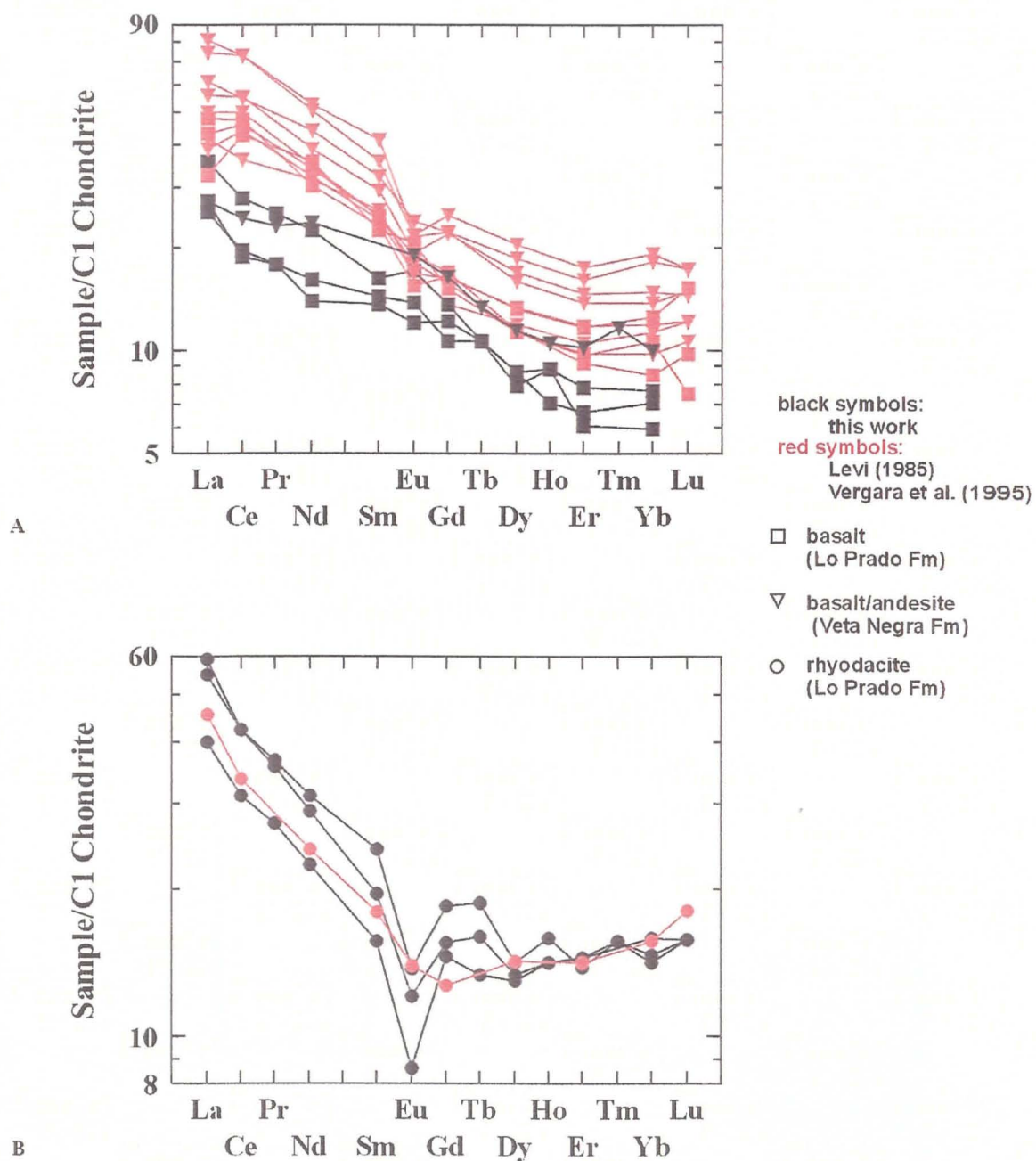
Figure 4.16. Chrondrite normalised REE plots for Lo Prado and Veta Negra Formations.

A) Basalts of Lo Prado Fm and basaltic andesites and basalts of Veta Negra Fm.
B) Rhyodacites of Lo Prado Formation. Note negative Eu anomaly.
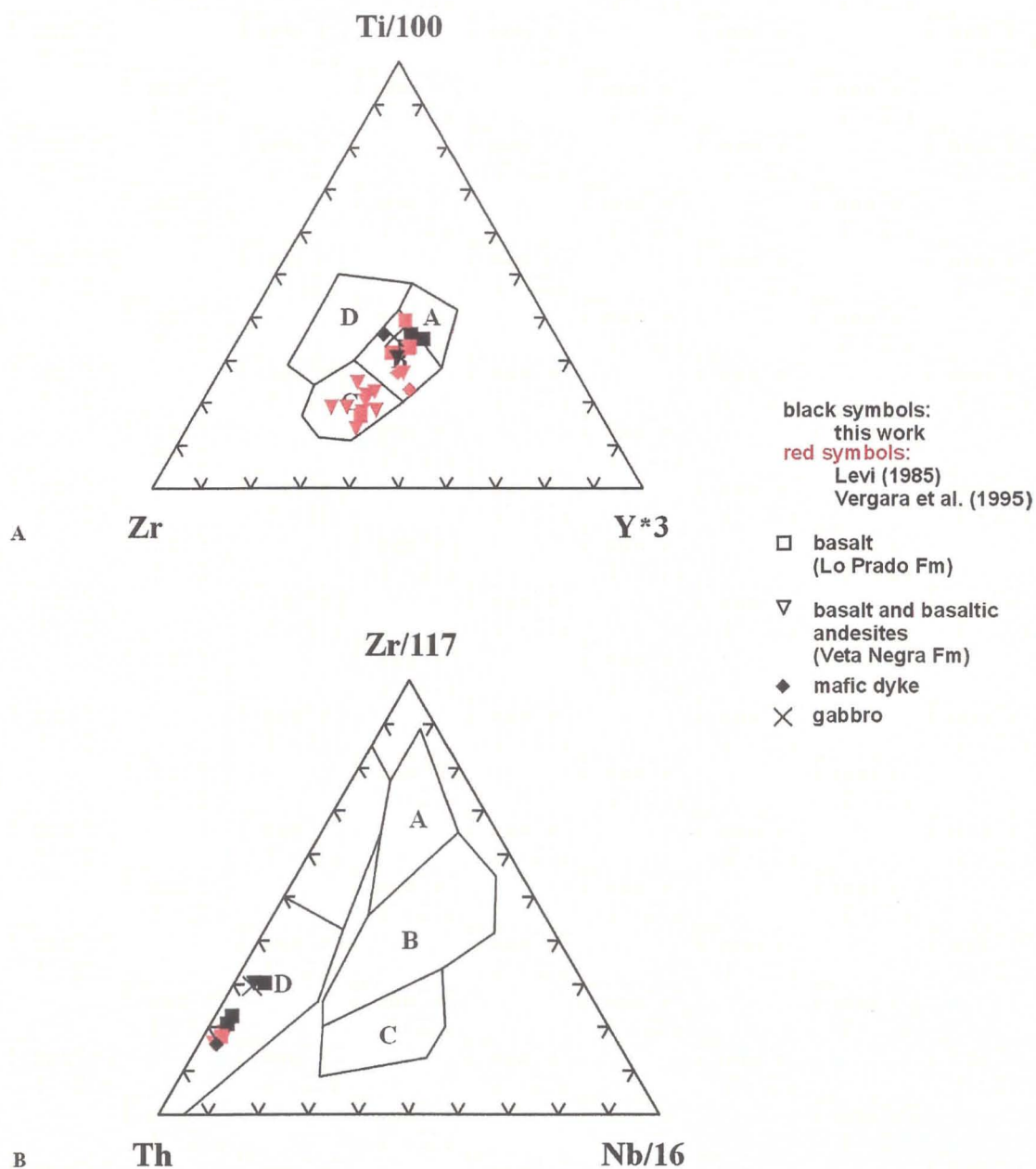
Figure 4.17. Tectonic setting discriminant diagrams for volcanic rocks of the Lo Prado and Veta Negra Formations.

A) Zr – Ti –Y (after Pearce and Cann, 1973).
B) Th – Zr – Nb (after Wood et al., 1979).

Ti-Zr-Y diagram (after Pearce and Cann, 1973) samples from Lo Prado Formation plot in field B (volcanic-arc or MORB basalts; Cann, 1996), and samples from Veta Negra plot in field C (volcanic-arc basalts; Cann, 1996). On the Zr-Th-Nb diagram (after Wood et al., 1979), rocks from both formations plot in the lower half of field D (calc-alkaline volcanic-arc basalts). These diagrams confirm that the volcanic rocks of both sequences represent a volcanic-arc, from field geology most likely a continental arc. The low values of Nb and Ta are typical of arc-related suites (Table 4.8; Appendices 2.1, and 7.4). To study this aspect in more detail a more specific work must be done using analyses with (research quality) lower detection limits.

It is interesting to note that Vergara et al. (1995) in a study of Lower Cretaceous volcanic rocks north of El Soldado ascribed the rocks to a high potassium (shoshonitic) series. Nevertheless, in their diagrams, their samples that are equivalent in age to the Lo Prado Formation clearly show a (sub-alkaline) calc-alkaline pattern. It is possible that the overlying Veta Negra Formation might represent a more evolved potassic suite (see also Cisternas et al., 1999; Morata et al., 2001). The REE values for the Veta Negra Formation equivalents do suggest similarities with high-K suites in the tables of the Wilson (1989) textbook. However, this problem, although interesting, was beyond of the scope of this thesis.

Finally the plutonic rocks of Lower Cretaceous age, which are essentially coeval with the Veta Negra Formation on the basis of geochronology, also have a calc-alkaline (intermediate K) character, based on the major element lithochemistry (e.g. Rivano, 1996; Gana et al., 1996; Wall et al., 1999).

4.4. U/Pb Geochronology of Host Rocks

After detailed regional studies carried out by the Chilean Geological Survey, the age of Lo Prado Formation is assigned to the Berriasian - Hauterivian interval, according its fossiliferous record which includes ammonites and pelecypods, which are chronologically restricted (Piracés and Maksaev, 1977; Rivano, 1996; Gana et al., 1996; Wall et al., 1996; 1999). In the proximity of the mine, the fossil record indicates a Berriasian to Valanginian age for the lower member, but fossils with limited

chronostratigraphic value have been found in the upper member. Nevertheless, about 50 km south of El Soldado the Upper Member of Lo Prado Formation has been assigned a Berriasian-Hauterivian age based on abundant marine (ammonites, etc.) fauna (Gana et al., 1996). The above paleontology constrains the age of Lo Prado Formation to the interval 145-127 Ma according the time scale of Okulitch (1999). Therefore the age of the bimodal volcanic rocks hosting the ore at El Soldado should be restricted to the end of this range (possibly Hauterivian?) or 132-127 Ma.

Previous geochronological dating of volcanic rocks at El Soldado mine by K/Ar; Ar/Ar and Rb/Sr methods have yielded ages in the range of 113-96 Ma (Table 3.4; Appendix 7.1). These ages have been interpreted to represent metamorphic or alteration events, rather than the age of the rocks (Munizaga et al., 1988; Boric and Munizaga, 1994; Wilson, 1998a). A compilation of published or unpublished ages (Boric et al., 2002; Wilson et al., in press a; Appendix 7.1), indicates that some older (K/Ar, Ar/Ar) apparent ages have been obtained in mafic dykes that intrude the Lo Prado Upper Member, and are most probably feeders to the overlying Veta Negra Formation, indicating 122.7 ± 1.1 Ma (Cerro Chacana) and 118.7 ± 2.2 Ma (El Soldado). One single Ar/Ar date of a rhyodacitic dyke sampled underground in the mine, yielded 131.8 ± 3.1 Ma. The latter is compatible with the expected age of the rock, but in view of the wholesale mobility of the alkalis documented in this study, that age cannot be taken too seriously. In summary, with a combination of regional correlation of paleontological data and dubious geochronological data the age of the El Soldado host rocks is probably older than ca. 120 Ma.

In order to obtain a more reliable absolute age of the host rocks, 3 large samples from the main rhyodacite flow, the main rhyodacite feeder dyke, and the gabbro stock, were collected to date zircons using the U/Pb methodology. The location of samples is shown in Figures 5.6 and 5.8 (see Chapter 5) and Appendix 1. Samples were obtained from drillcores and, as much as possible, distal from the orebodies. Samples were sent to Geospec Labs. in Edmonton, where they were dated using conventional thermal ionisation mass spectrometry (TIMS) methodology (Heaman and Parrish *in* Heaman and Luben, 1991).

The results were interesting but disappointing. Preliminary results for the 3 samples (Table 4.9) indicated the presence of abundant inherited and partially resorbed zircons (L.Heaman, written communication, 2001), with Paleozoic and Proterozoic ages (472-481 Ma; 532-580 Ma; and 990-1001 Ma (Figure 4.18, Table 4.9). However, one sample of rhyodacitic dyke (RB9873) yielded two high-error $^{206}Pb/^{238}$ ages of 118 ± 3 Ma and one $^{207}Pb/^{235}U$ age of 112 ± 14, which represent values somewhat closer to, yet slightly younger than, the expected age. Zircons from this sample (RB9873) were re-analysed at our request, and the new results, based on a larger number of zircon grains, yielded ages of 138 ± 3 Ma ($^{206}Pb/^{238}U$) y 126 ± 28 Ma ($^{207}Pb/^{206}Pb$), which are quite compatible with the assumed (Hauterivian) paleontological age (132 ± 1.9 to 127 ± 1.6 Ma; Okulitch, 1999; and A.V.Okulitch, written communication, March 2002).

In conclusion, the analysed samples are problematic, in that they include inherited zircon cores and grains of Paleozoic and Proterozoic age. However, at least some U/Pb analyses are consistent with the age of the El Soldado host rhyodacite being Hauterivian, the age suggested by marine fossils.

In the central Andes, Proterozoic basement rocks outcrop in isolated areas from beneath a Mesozoic and Cenozoic cover in southern Peru, northernmost Chile, Bolivia, and in northwestern Argentina (e.g. Ramos and Alemán, 2000). Many authors have discussed their possible role of basement rocks in Andean magmatism and ore genesis (e.g. Tosdal, 1996; Cornejo et al., 1997). In the southern Central Andes, Proterozoic rocks outcrop in Argentina, east of the continental divide. The new data presented here suggest that the Early Cretaceous calc-alkaline magmas that generated the Lo Prado Formation, picked-up zircons in the Proterozoic and Paleozoic crystalline basement of the Coastal Cordillera during their generation and ascent (Zentilli et al., 2001). Crustal contamination for this magmatism was already envisaged taking in account the abundance of rhyodacites in the bimodal suite at El Soldado.

As indicated by Zentilli et al (2001), the presence of Proterozoic basement underlying localities as close as 30 km from the Pacific coast has implications for the extent and age of the Chilenia Terrane (Ramos and Alemán, 2000) and gives further

Table 4.9.- U/Pb Dating Results

Rock Type (Sample)**	Mineral Description*	Weight (mg)	U (ppm)	Th (ppm)	Pb (ppm)	Th/U	TCPb (pg)	^{206}Pb/^{204}Pb	^{206}Pb/^{238}U	^{207}Pb/^{235}U	^{207}Pb/^{206}Pb	Model Ages (Ma) ^{206}Pb/^{238}U	^{207}Pb/^{235}U	^{207}Pb/^{206}Pb	% Disc
Rhyodacitic	2 z?, col, nabr (38)	143	3.5	1.2	0.6	0.33	70	28	0.0216±4	0.132±31	0.0441±102	138±3	126±28	–	–
dyke	1 z, col, nabr (1)	2	109.4	81.3	5.9	0.74	11	45	0.0184±5	0.072±32	0.0282±122	118±3	70±30	–	–
(RB98-73)	3 z?, col, nabr (22)	77	3.9	4.3	0.4	1.09	25	32	0.0184±5	0.116±16	0.0457±63	118±3	112±14	–	–
Rhyodacite	1 z, lt yellow, nabr (1)	2	179.7	94.1	20.7	0.52	14	142	0.0775±4	0.604±10	0.0565±9	481±2	480±6	472±33	-2.0
flow	2 z, col, nabr (36)	110	228.5	65.9	20.2	0.29	33	4130	0.0870±2	0.775±19	0.0646±1	538±1	582±1	760±2	30.5
(RB98-72)	3 z, col, nabr (24)	77	187.5	69.2	30.5	0.37	42	3306	0.1555±2	1.635±4	0.0763±1	932±2	984±1	1102±1	16.6
Gabbro	1 z, col, nabr (1)	1	845.6	234.3	12469.1	0.28	12265	19	0.1389	-0.170	-0.0089	839	-190	–	–
(RB98-74)	2 z, col, nabr (8)	27	227.7	45.6	44.1	0.20	22	3215	0.1835±3	2.696±6	0.1066±1	1086±2	1327±2	1742±1	40.9
	3 z, col, nabr (10)	21	107.5	46.2	20.6	0.43	44	556	0.1673±3	1.692±5	0.0734±2	997±2	1006±2	1024±5	2.8

(*) z=zircon, col=colourless, nabr=non-abraded, (#)=number of grains analyzed

(**) See figures 5.6 and 5.8 and appendix 1.1 for location
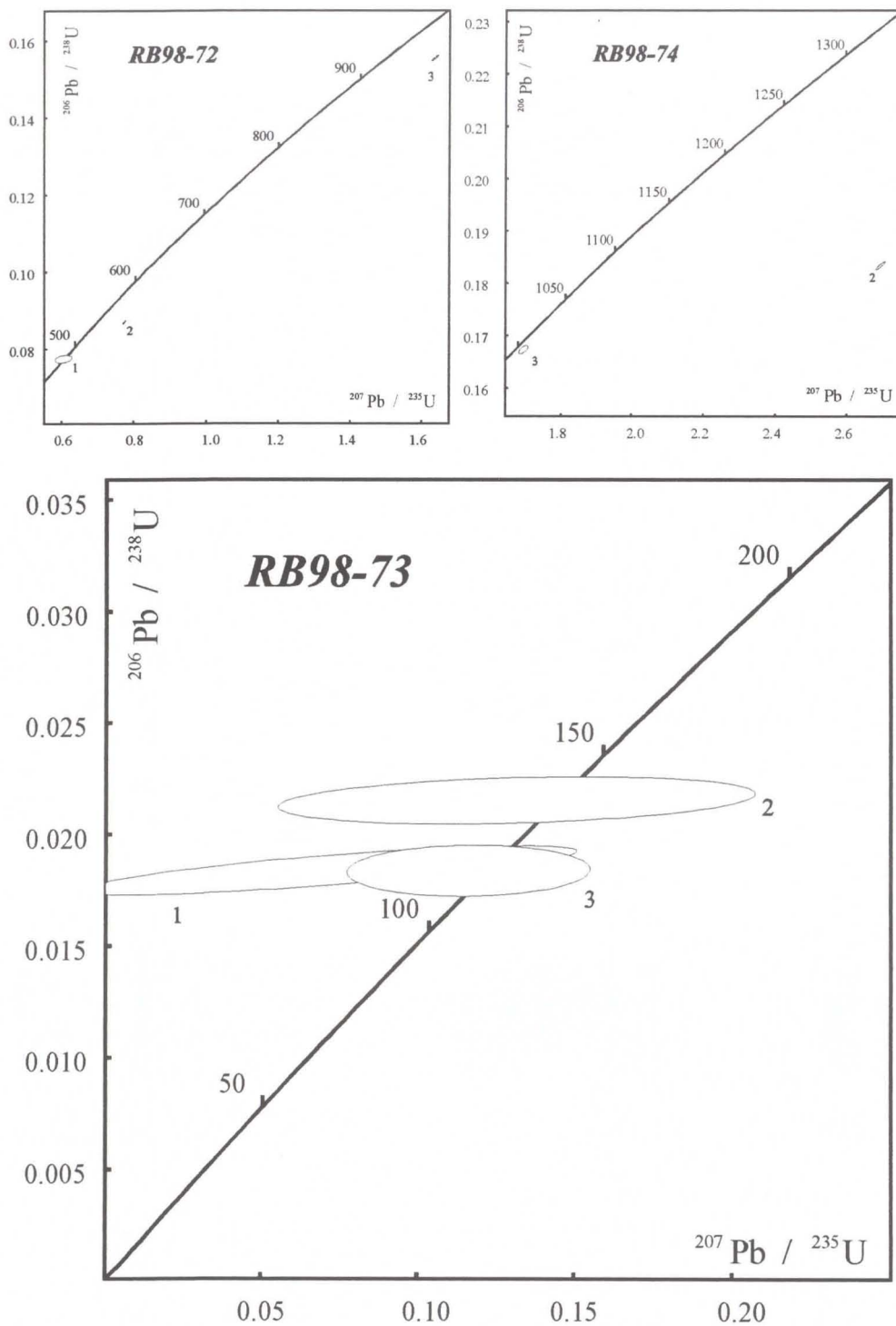
Figure 4.18. Results of U/Pb analyses of zircons from El Soldado (Lower Cretaceous age volcanic rocks).
Upper diagrams: note Paleozoic and Proterozoic ages from inherited zircons. See text for discussion.

credence to correlation models that juxtapose eastern North America (Laurentia) and south-western South America (Gondwana) during the Late Proterozoic (Tosdal, 1996). Similar results (c.a 1Ga ages) have been reported by Pop et al., (2000) in the Punta del Cobre Cu-(Ag-Au) district (27°30' S - 70°15' W), a manto-type Cu deposit hosted by a similar Lower Cretaceous bimodal suite of basalt and rhyodacite (see Chapter 2).

4.5. Summary

This study puts to rest the concept that El Soldado is hosted by "peculiar" alkaline rocks and that in some way this alkaline magmatism was responsible for the Cu mineralisation. The bimodal suite of the submarine upper member of the Lo Prado Formation consists of calc-alkaline basalt and rhyodacite, not *trachyte* and alkaline *andesite*, as previously suggested. The overlying Veta Negra Formation is a more evolved suite with andesite and basaltic-andesites, and its high-potassium character remains to be proven.

The age of the Lo Prado Formation volcanic host rocks is probably Hauterivian (ca. 132-127 Ma) on the basis of regional correlations and paleontological dating. That age is compatible with the U/Pb dates on zircon (roughly 138-126 Ma).

The host rocks, even those distal from any Cu mineralisation, show the effects of sodic alteration and are similar to *spilites* and *keratophyres* described in the literature; this widespread alteration is considered to be the result of very low-grade regional metamorphism.

Bimodal suites, with similar alteration, mineralogy and lithochemistry, are known from large manto type Cu deposits in northern Chile, such as Mantos Blancos and Punta del Cobre. Punta del Cobre's host rhyodacites are equivalent in age and also contain xenocrystic zircons of Proterozoic age.

CHAPTER 5. MINERALOGICAL ZONING OF THE DEPOSIT

5.1. General Statement

As indicated in Chapter 3, at the beginning of the present study it had been recognised that single orebodies at El Soldado have a consistent sulphide zoning and that the deposit as a whole also shows an overall zoning. Yet no rigorous analysis of this global zoning had been undertaken. Furthermore, no clear spatial pattern in the distribution of gangue or alteration minerals had been recognised, and previous work had emphatically concluded that there is "no relationship whatsoever" between high-grade ores and any particular alteration, and that alteration and metamorphic effects are indistinguishable (e.g. Martin, 1981). This study comes to a very different conclusion.

The vertical expansion in the mining operations (e.g. Morro open pit and deeper underground levels) and extensive exploration drilling in the periphery of the deposit (Figures 1.4 and 5.1) provided the opportunity for the author to study the ore and gangue-alteration mineralogy in great detail and at an overall mine scale. Since 1997, and in the context of this thesis, over one hundred exploration drill hole cores were remapped and sampled (Figure 5.2a) specifically looking for documentation of sulphide and alteration mineralogy and zoning. The aim was to try to recognize any patterns of mineralogy or geochemistry that may be associated with the richest ore, and therefore develop some criteria useful for future exploration. The orebodies (arbitrarily defined for mining operations as Cu >0.3% or ca.10 times background) were subdivided, during the drill core logging, into 6 ore zones representing the following predominant and mappable assemblages from periphery to core: 1) pyrite, 2) pyrite-chalcopyrite, 3) chalcopyrite, 4) chalcopyrite-bornite, 5) bornite, and 6) bornite-chalcocite. The ore zones were defined according to the proportions of the total sulphides in volume percent (Table 5.1). During the course of the study it became evident that specular hematite is a very relevant mineral phase, therefore its relative abundance was also carefully recorded, and zones where specularite is more abundant than 10 % of total opaque minerals were individualised. The
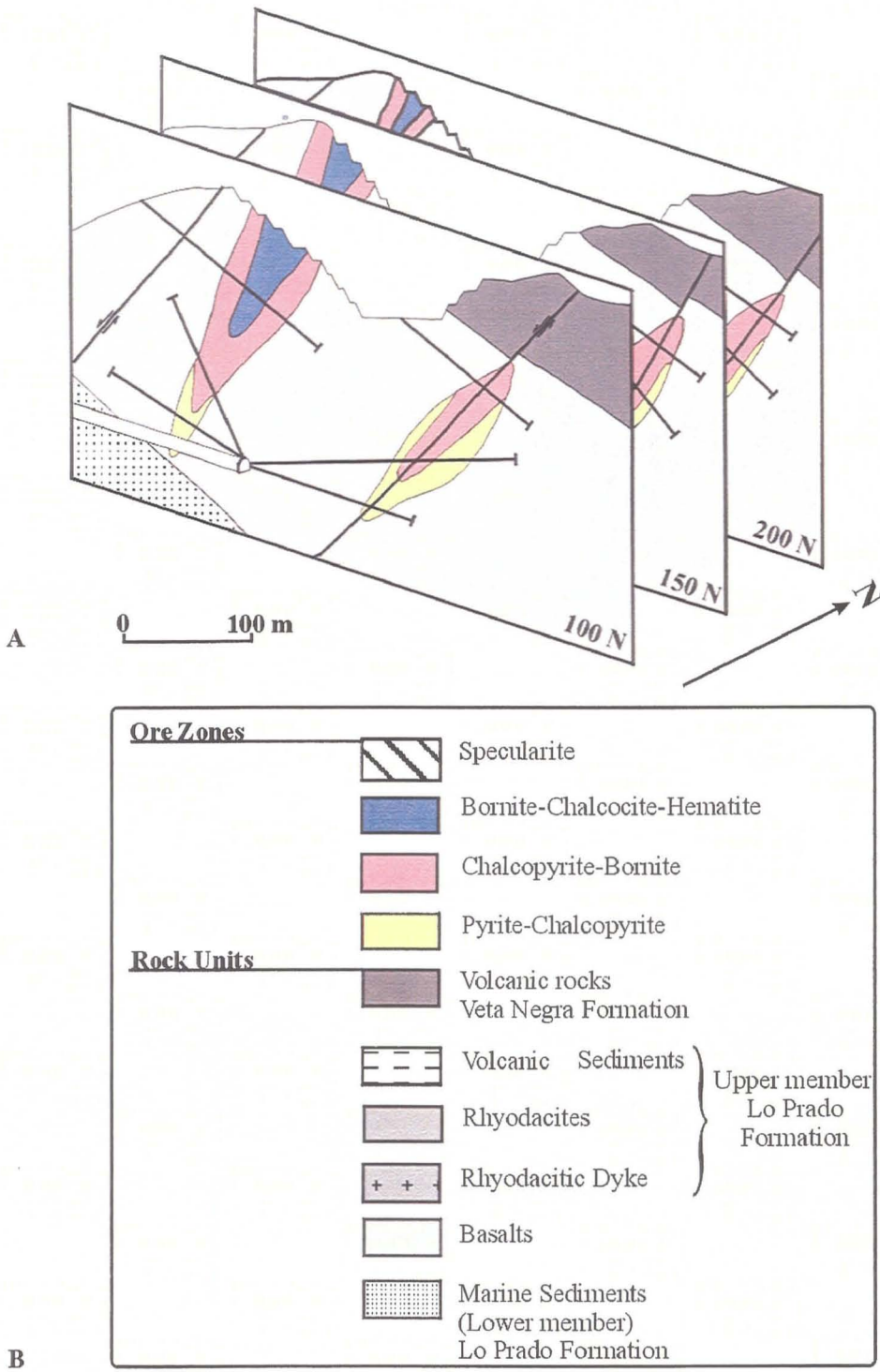
Figure 5.1. Construction of mineral zoning 3D model.
A) Construction of sections with mineralisation zoning.
B) Legend for figures 5.3 through 5.8.
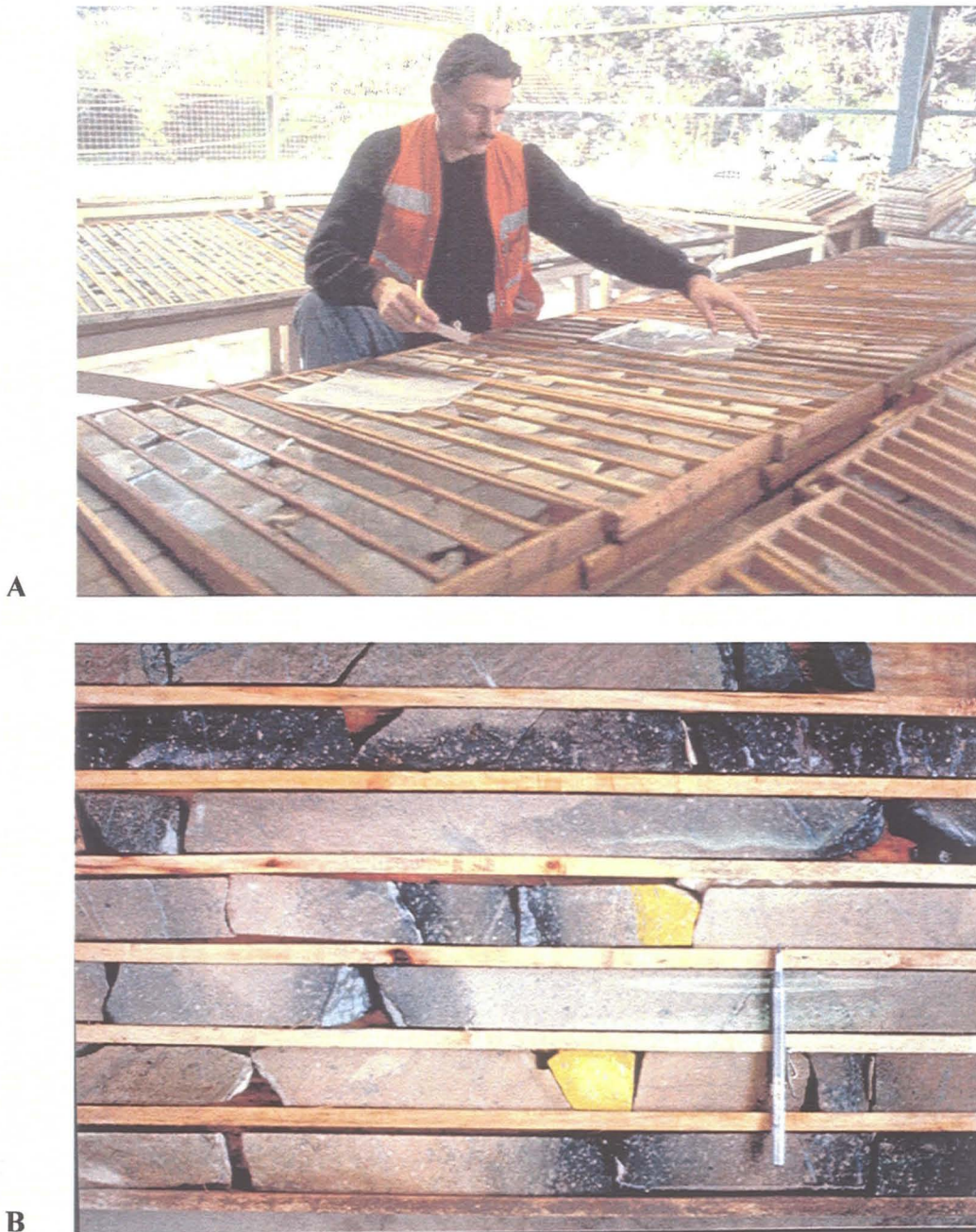
Figure 5.2. Logging and cobaltinitrite stain of drillcores.

A) Logging and sampling for the mineralogical zoning of the deposit.

B) Mineralized rhyodacite drill core showing segments stained with sodium cobaltinitrite (yellow) denoting high K-feldspar content. This technique was extremely useful during the study.

Table 5.1.- Definition of Ore Zones

Ore Zone	Minerals
Pyrite	Pyrite > 70 % of total sulphides
Pyrite - chalcopyrite	Pyrite + Chalcopyrite > 70 % total sulphides
Chalcopyrite	Chalcopyrite > 70 % total sulphides
Chalcopyrite - Bornite	Chalcopyrite + Bornite > 70 % of total sulphides
Bornite	Bornite > 70 % total sulphides
Bornite - Chalcocite	
Specularite*	Specularite > 10 % of total opaque minerals (sulphides + oxides)

* Specularite zone is superposed on sulphide ore zones

mineralogical information recorded from drill-cores was plotted on the E-W geological cross sections available at the mine and a new set of 34 mineralogical-geological cross sections was created (Figure 5.1a). These sections show the variations of mineralogy and their relationships with the various host rocks and structures. Using the generated cross-sections as a base, three different level plans were created.

In this Chapter, and due to space restrictions, the results of mineral zoning study are summarised in two representative plan views and four E-W cross sections. The plans are the Level 0 (830 m.a.s.l.; Figure 5.3) and the Level +100 (930 m.a.s.l.; Figure 5.4). The cross sections are, from south to north at coordinates -900N, -750N, 0N, and +250N (Figures. 5.5, 5.6, 5.7, 5.8 respectively). These specific cross-sections were chosen because they intersect the main orebodies and because the majority of the lithochemical samples selected for analysis could be projected into them. The northernmost section (Figure 5.8) was selected because it contains the unexposed gabbro intrusive and important deep pyritic bodies.

As a result of logging and sampling a suite of 144 samples from different orebodies and representing different ore-zones was obtained. These samples were studied as cut and polished slabs under the binocular microscope and they were stained with Na-cobaltinitrite to identify K-feldspar (see details of procedures in section 4.2.1). A selected sub-group of 76 samples was studied as thin and polished thin sections under reflected and transmitted light microscopy and their magnetic susceptibility was measured. Mineral (spots) analyses of sulphide and gangue minerals (292 from 21 samples) and X-ray maps (13 samples) of polished-thin sections were performed to study the composition of mineral species. Previous microprobe analyses (210 from 33 samples) mostly of sulphide species (M.C. Graves, Cuesta Research Ltd. internal reports CMD, 1995a, b) were also incorporated to the study. Finally X-ray diffractograms (XRD) were performed to identify secondary minerals (48 analyses from 32 altered rock samples). The analytical procedures for all these analyses were the same used to study background rocks, and were explained in detail in Chapter 4 (section 4.2.1).

This chapter briefly describes the hypogene ore mineralogy followed by a description of the different mineralogical ore zones, grouped in pairs to match the legend
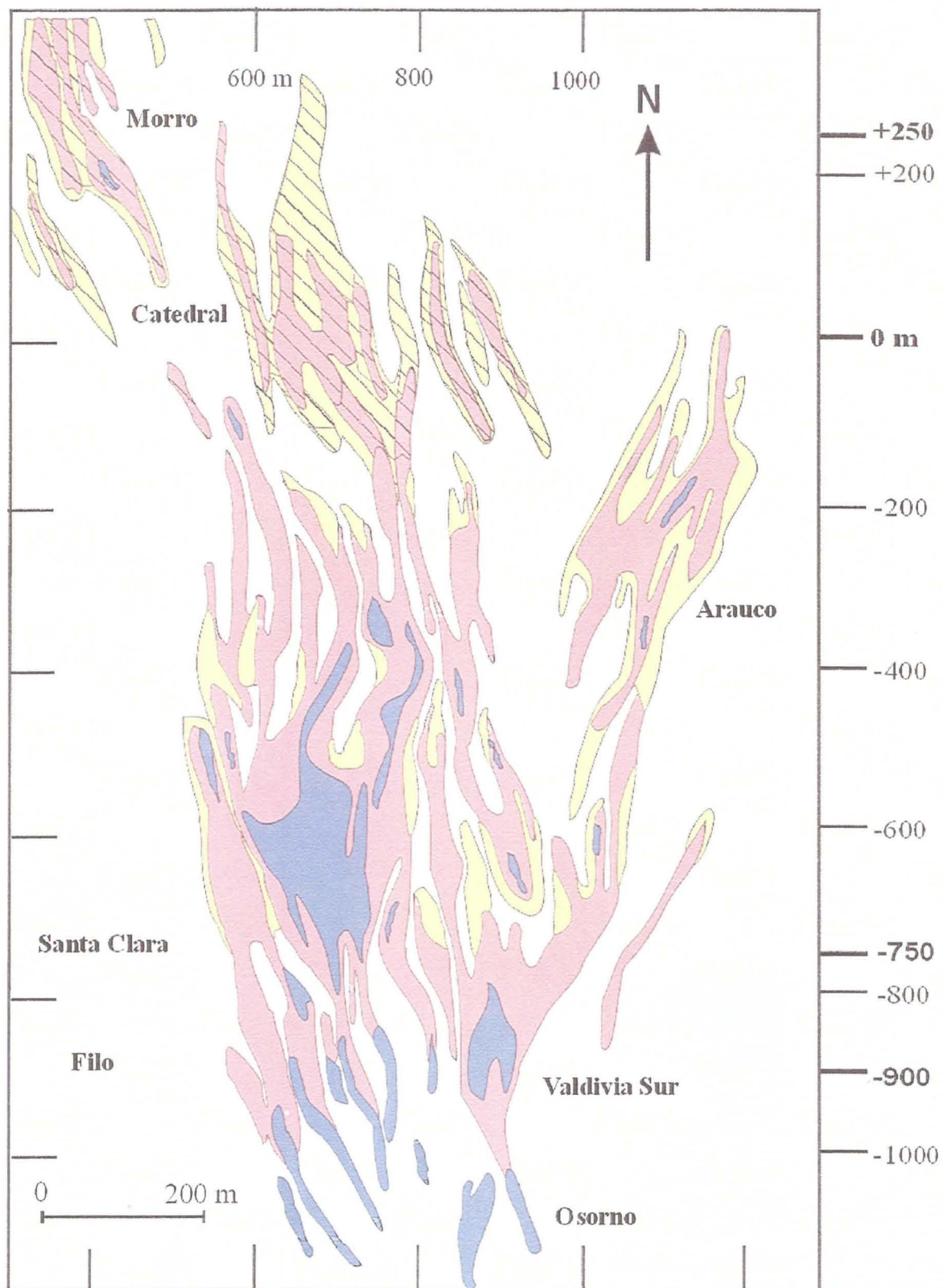
Figure 5.3. Generalised mineral zoning of level ± 0 (830 m elevation).
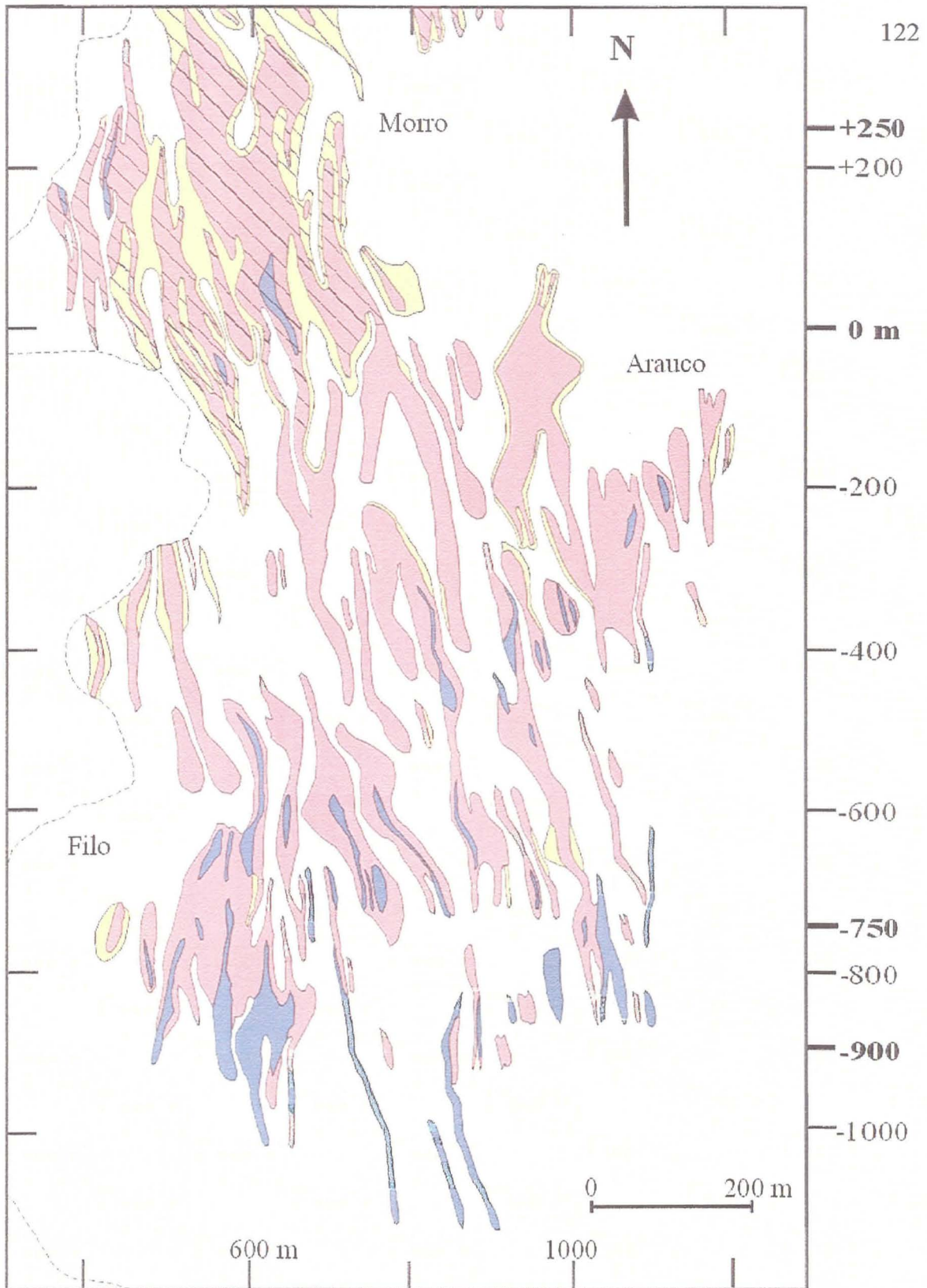
Figure 5.4. Generalised mineral zoning of Level ± 100 (930 m elevation).
For legend see **Figure 5.1.**
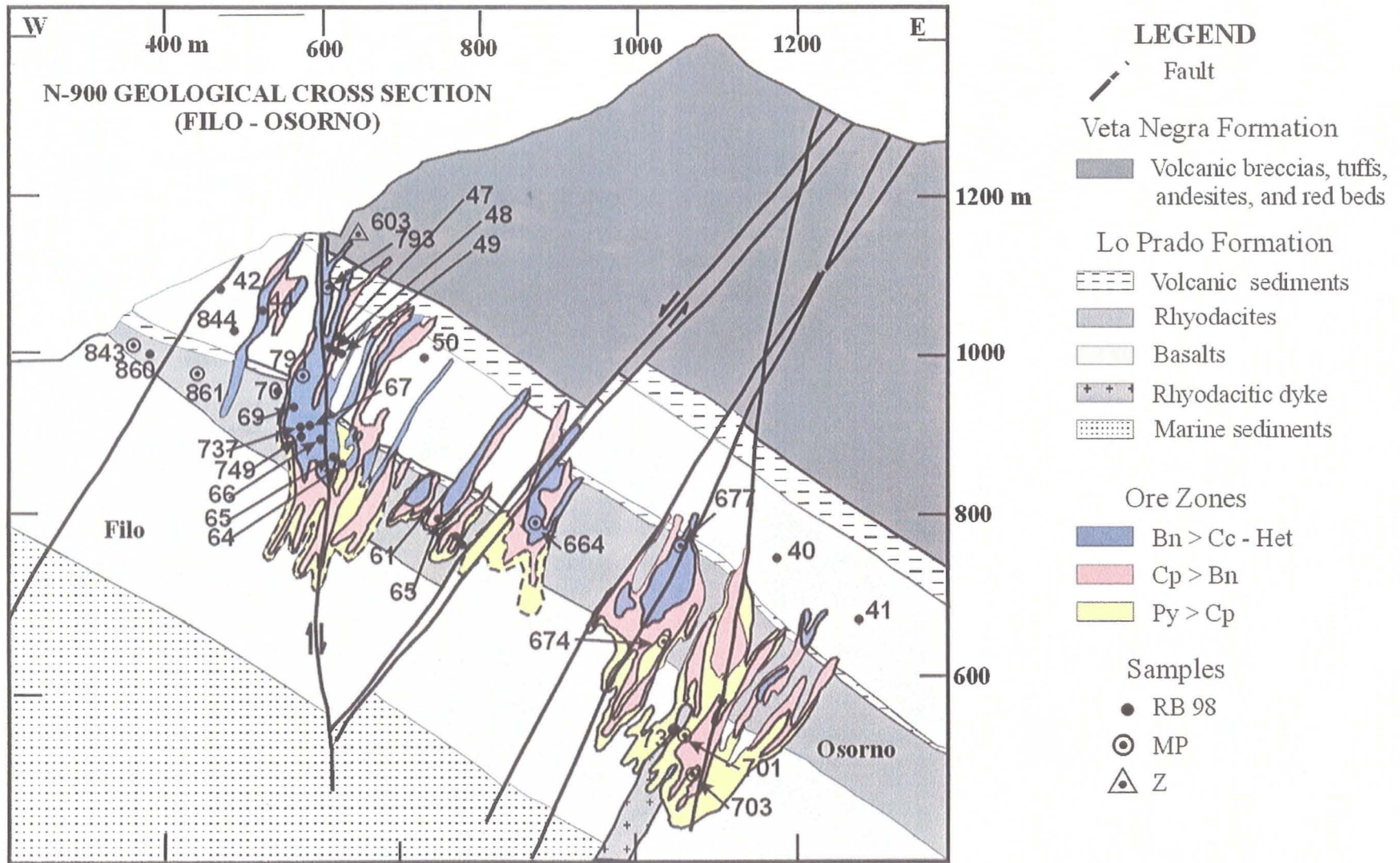
Figure 5.5. Geology and mineral zoning, N-900 cross-section.
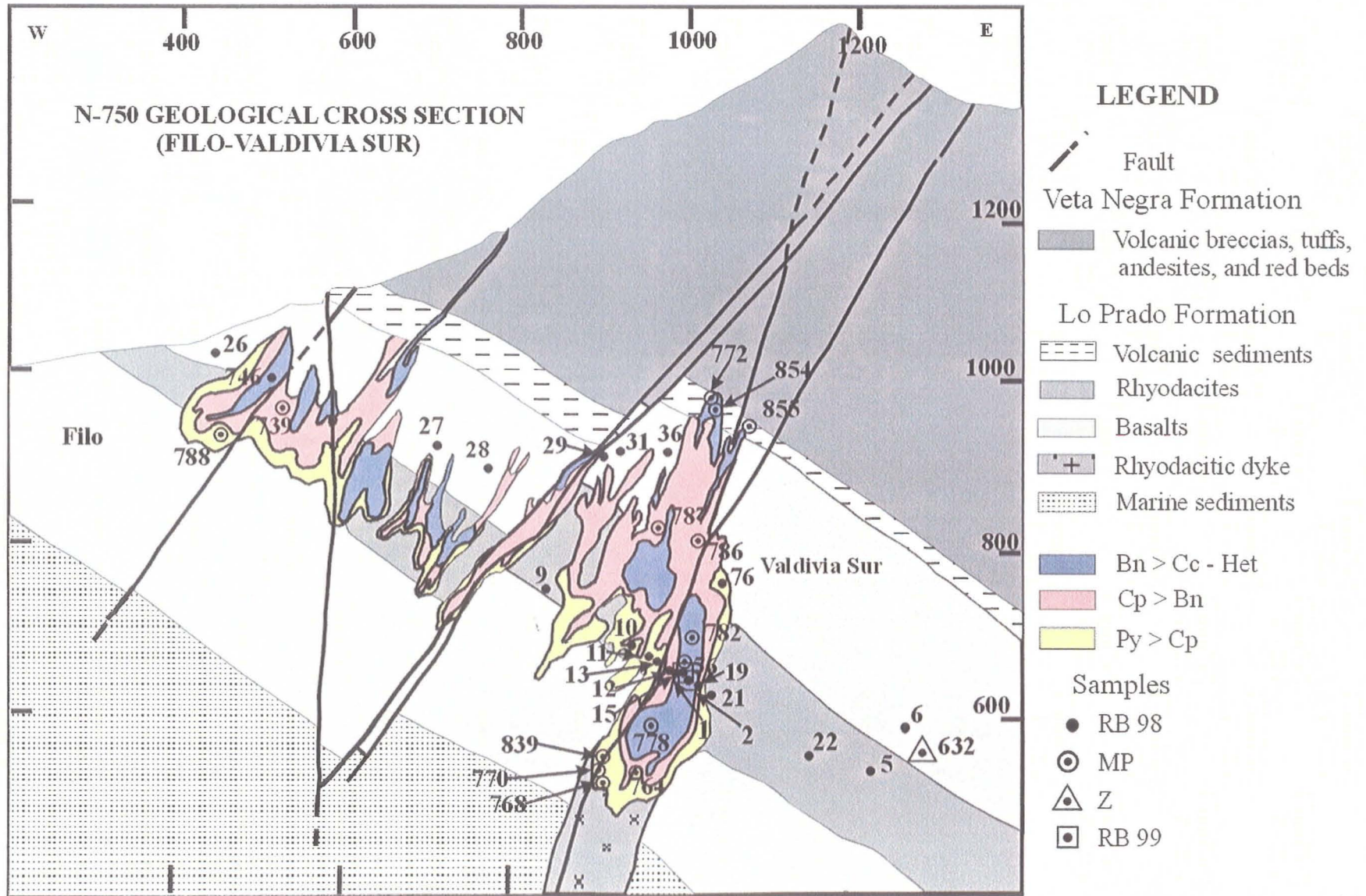
Figure 5.6. Geology and mineral zoning, N-750 cross-section.

Figure 5.7. Geology and mineral zoning, N ± 0 cross-section.

Legend:
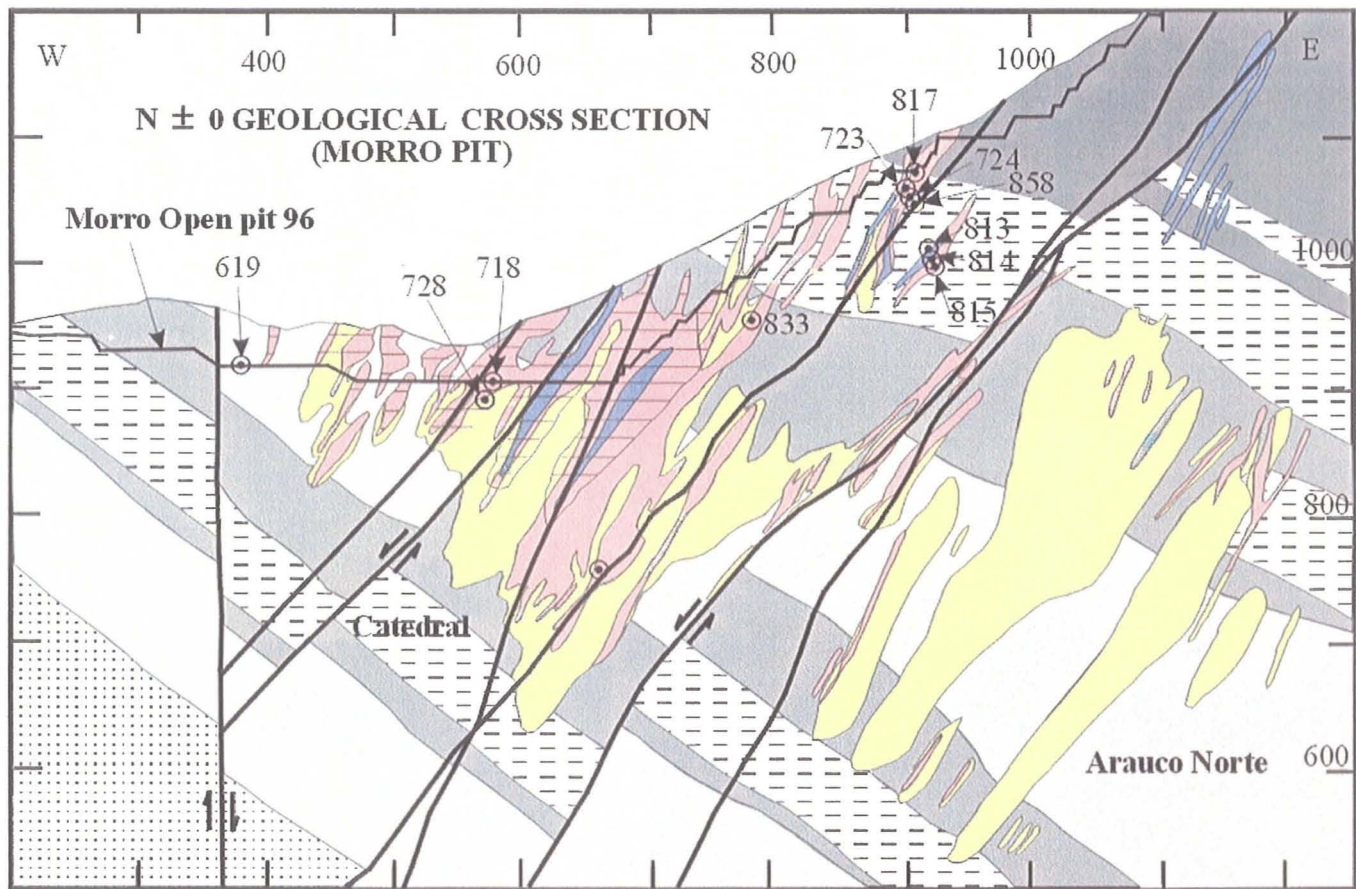
Lo Prado Formation
- Volcanic sediments
- Rhyodacites
- Basalts
- Marine sediments

Veta Negra Formation
- Volcanic breccias, tuffs, andesites, and red beds
- Fault

Ore Zones
- Bn > Cc
- Cp >
- Py > Cp
- Spec

Samples
- ⊙ MP

Figure 5.8. Geology and mineral zoning, cross-section N +250.

of the figures. The alteration-gangue mineralogy and the lithochemical aspects of the different ore zones are discussed in Chapter 6.

5.2. Hypogene (Primary) Mineralogy

The hypogene sulphide-oxide mineral assemblage at El Soldado is relatively simple and composed of pyrite, chalcopyrite, bornite, chalcocite and hematite as major phases. Accessory minerals are covellite, sphalerite, galena, and magnetite. Rare occurrences are arsenopyrite, pyrrhotite, cobaltite, and anilite. Non-metallic gangue minerals associated with Cu mineralisation are calcite, quartz, chlorite, albite, K-feldspar (microcline), epidote, bitumen, rutile and titanite.

Sulphide minerals occur as dissemination and veinlets, largely filling primary (columnar joints, vesicles, inter-clast pores) and secondary (brittle shear related) porosity of the volcanic host rocks. Disseminated grains are usually very fine-grained, ranging from less than 1 μm to few mm in size. Veinlets range from hundreds of μm to few cm in thickness, and are relatively more abundant close to faults.

Detailed microscopic studies carried out in parallel with this thesis have established that mineralisation at El Soldado formed in two different and time separated episodes: an early diagenetic stage (Stage I) and a late and superimposed hydrothermal stage (Stage II) (e.g. Wilson, 1998a; Ponce, 2001; Collins, 2002; see also Chapter 3). The mineral assemblage of Stage I is composed of pyrite plus bitumen accompanied by minor chalcopyrite, sphalerite, galena, and traces of pyrrhotite, and arsenopyrite. Stage II assemblage is composed of chalcopyrite, bornite, chalcocite, and hematite, plus minor covellite and traces of magnetite. Non-metallic gangue minerals deposited during this stage are calcite, chlorite, quartz, K-feldspar (microcline), albite, epidote, and rutile.

Observations made during this thesis are in agreement with the recent previous studies and confirm this two-stage paragenetic sequence. Consequently the paragenetic sequence is not considered in detail in this chapter, and the reader should refer to Wilson (1998a), Wilson and Zentilli (1999), Wilson (2000), Ponce (2001), and Collins (2002) to review this aspect more carefully.

A description of major and minor identified minerals in this thesis is given below.

5.2.1. Major Sulphide and Oxide Minerals

These minerals are abundant throughout the overall deposit and they are easily recognised in hand samples. Their relative abundance was mapped and used to construct the mineralogical zoning discussed in the following section.

Pyrite - FeS$_2$

Pyrite is the major non-copper sulphide in the El Soldado deposit. Pyrite is a common component in the "background" (non-mineralised, least altered) sedimentary and volcanic rocks (see Chapter 4) but it has been also documented from all studied orebodies, usually as an external halo or constituting their roots. Pyrite was not considered to be an important mineral species (eg. Martin, 1981), especially before the development of the Morro open pit and the deeper levels of the underground mine, when it became evident that its abundance had been underestimated.

In background rocks, pyrite occurs as individual and clusters of *framboids* (2-50 µm), euhedral to irregular fine grains (<1-200 µm) and replacing ferro-magnesian or titano-magnetite crystals. Pyrite framboids are spherical aggregates of individual euhedral pyrite microcrysts, which have the appearance of raspberries (French for raspberry: *framboise*). When the individual mycrocrists are not distinguished because they are densely packed, the texture is referred to as *spherules* (Wilson, 1998a). Framboidal pyrite is associated with sphalerite and rare galena, chalcopyrite, and pyrrhotite. Gangue phases related to framboidal pyrite are bitumen, calcite, and minor opaline silica. Pyrite replacing titano-magnetite and ferromagnesian minerals is described as an important occurrence in background rocks for the first time in this thesis. This background pyrite usually rims the replaced crystals and is associated with titanite-leucoxene-rutile.

Within orebodies pyrite occurs as fine disseminations, framboids, spherules and massive veinlets and veins, usually associated with chalcopyrite, calcite, quartz, opaline silica, and rare chlorite. Massive veins are composed of dense aggregates of irregular, euhedral (cubes, pyritohedra), framboidal, and colloform pyrite. At least in part, pyrite occurs as pseudomorphs after melnikovite, marcasite and/or pyrrhotite (Ponce, 2001; Collins, 2002). Chemical and textural zoning of pyrite crystals, are indicative of multiple

phases of pyrite growth (Collins, 2002). All Cu-bearing sulphides replace pyrite.

Textural, chemical, and isotopic evidence support that framboidal pyrite formed with liquid petroleum (now solid bitumen) at lower temperatures (below 120° C) during the early diagenetic stage (Wilson, 1998a; Wilson and Zentilli, 1999). Pyrite replacing ferromagnesians and titano-magnetite is probably diagenetic although it has not been observed associated with bitumen. By extension, a similar origin is postulated for very fine pyrite disseminated in background volcanic rocks, particularly because it is not found in the less altered volcanic rocks, excluding a primary origin. Euhedral pyrite associated with calcite and chalcopyrite and overgrowing pyrite framboids in massive veins may have been generated, at least in part, later during Stage II (see discussion in Section 5.3.1).

Microprobe spot analyses (55 samples) show that the main impurity in pyrite is arsenic (50 % analysed pyrites has noticeable As up to 7.5 wt %, Appendix 3.4). Wilson (1998a) based on microprobe data, established that As is more abundant in framboidal pyrite, thus arsenic is though to have been incorporated in pyrite during diagenesis and is not related to late (Phase II) copper mineralisation (see also Chapter 6). Other impurities are copper and minor cobalt (Appendix 3.4).

Chalcopyrite - CuFeS

Chalcopyrite is one of the main ore minerals at El Soldado. It is found in all orebodies and all different host rocks occurring finely disseminated and in veinlets infilling porosity. Chalcopyrite is observed as single anhedral crystals but more often replaces (to different degrees) pyrite grains or framboids or occurs intergrown with bornite. Spherules of chalcopyrite (pseudomorphed after pyrite framboids) are rare. The replacement of framboidal pyrite and the intergrowths with bornite clearly indicate that most of chalcopyrite was generated during Stage II. Nevertheless, small inclusions of chalcopyrite have been observed within sphalerite associated with bitumen, indicating that at least some chalcopyrite was also formed during Stage I.

Microprobe analyses (53 grains) of chalcopyrite show a composition very close to stoichiometric, almost without impurities (Appendix 7.4). Only 4 analyses detected As

(0.15-0.24 wt %) and 1 detected Ag (0.18 wt %) in chalcopyrite.

Bornite - Cu_4FeS_5

Bornite is a major ore mineral at El Soldado, found in all rock types throughout the camp, but being more abundant in the southern orebodies and in the upper levels of the mine. Bornite occurs infilling amygdules, in veinlets or as finely disseminated. Bornite can occur alone but usually is accompanied by chalcopyrite or/and chalcocite forming intergrowth textures. Bornite clearly replaces pyrite and framboidal bornite (after pyrite) is found in the Filo block (Wilson, 1998a). Bornite is usually associated with calcite and fine hematite, and to a lesser degree with specularite, bitumen, quartz, chlorite, K-feldspar, albite, and epidote.

Microprobe spot analyses (72 samples) indicate that bornite grains are very close to atomic ideal (stoichiometric) composition, with very scarce impurities. Silver (0.10-0.32 wt %) was recognised in 6 analyses and arsenic in 4 (0.20-0.32 wt %). According to Wilson (1998a) As is more abundant in bornite formed by replacement of pyrite framboids (0.5-1.0 wt %), implying As is inherited from this early phase.

Chalcocite - Cu_2S

Chalcocite is an important ore mineral at El Soldado, present mostly in the southern orebodies and in the upper levels of the mine. Chalcocite generally occurs intimately associated with bornite and minor fine-grained hematite. Locally it is associated with chalcopyrite or occurs as a single sulphide. Chalcocite is found infilling pores and as veinlets associated with calcite and chlorite, and to a lesser extent with K-feldspar, quartz, albite, epidote and bitumen. Chalcocite and chalcocite-bornite framboids (after pyrite) are common in the Filo block.

Microprobe spot analyses (58 samples) show a variation in composition from chalcocite to digenite ($Cu_{2.07}S$ to $Cu_{1.67}S$), the average being $Cu_{1.92}S$. Iron (wt % up to 2 %) is the most common impurity detected in more than a half of the samples. Silver (0.10-0.71 wt %) was recognised in 9 samples and arsenic (0.19-0.47 wt %) in 19. Wilson (1998a) indicated that As is more abundant where chalcocite replaces pyrite framboids.

Hematite (Fe$_2$O$_3$)

Hematite is a common gangue mineral associated with chalcocite and bornite although it also occurs accompanying chalcopyrite and pyrite. Two types of hematite associated with Cu-ore are distinguished:

1) **Fine-grained hematite**: this kind of hematite typically occurs as small needles (10-200 μm length) intergrown or rimming bornite or bornite-chalcocite crystals. This texture has been explained by crystallisation of an excess of iron during the hypogene replacement of pyrite or chalcopyrite by bornite and chalcocite (e.g. Holmgren, 1987).

2) **Specular hematite**: this habit of hematite is identified as an important component at El Soldado for the first time, particularly in the northern part of the camp (see Section 5.3). Specular hematite occurs in well-developed crystals (0.1 mm to few cm in size) associated with chalcopyrite, pyrite, calcite, and rarely with bornite. Crosscutting relationships shown that specularite was deposited later than pyrite-chalcopyrite.

Hematite also occurs in the background (non-mineralised) rocks, mostly in basalts replacing titano-magnetite or ferromagnesian (pyroxene-olivine) crystals, but this type of occurrence, generated during diagenesis-metamorphism of the volcanic pile, is not related to Cu-ore. Hematite is also very abundant in the rocks of Veta Negra Formation (see Chapter 4), probably as result of an early deuteric alteration in an oxidised environment (Westra, 1988a).

5.2.2. Minor Sulphide or Oxide Minerals

These minerals occur as accessories or curiosities and usually represent less than 1% of total sulphides in rock samples. Most of them were recognised under the microscope or by microprobe analyses because they are too fine-grained to be identified in hand samples. In order of abundance these minerals are:

Covellite - CuS

Covellite is the most frequent minor phase associated with bornite, chalcocite

and/or chalcopyrite. It is more common in the southern part of the camp although it has been also identified in Morro mine block. Covellite is easily recognized using microscope by its colour, and pleocroism. Covellite occurs filling in fractures or as overgrowths within chalcopyrite or bornite grains, sometimes associated with chalcocite. Microprobe data indicate that covellite is Cu-rich ($Cu_{1.6}S$ to $Cu_{1.3}S$) and contains Fe, As, and Ag as impurities (Appendix 3.4). A few grains yield a composition close to **anilite** ($Cu_{1.54}S$ to $Cu_{1.40}S$) but this species was not differentiated optically. Textures and chemistry indicate that this covellite is hypogene (see also Wilson, 1998a and Ponce 2001).

Sphalerite - (Zn,Fe) S

Sphalerite has been identified in few mine blocks (Paso Riel, Filo, Morro, Arauco Norte). Sphalerite occurs as veinlets and irregular fine grains disseminated within basalts, rhyodacites and volcanic sediments, associated with abundant pyrite, galena, chalcopyrite, calcite, and bitumen. Sphalerite occurs intergrown with galena usually surrounding pyrite grains. Minute inclusions of chalcopyrite and pyrite are common in sphalerite grains. In the Filo mine block, sphalerite has been observed as fine inclusions within bitumen and cut by bornite-chalcocite veins indicating that sphalerite is part of the Stage I assemblage (Wilson, 1998a). Microprobe analyses indicate that sphalerite has a variable Fe content (0.7 to 8.0 Wt %) and minor Cu (up to 2.8 wt %) and As (up to 0.4 wt %) as impurities.

Galena - PbS

Galena is a rare phase recognised in few mine blocks within background rocks or in the pyritic ore zones in basalts (Filo, Morro, Santa Clara), rhyodacitic dykes, and sedimentary rocks (Paso Riel), associated with sphalerite, pyrite, chalcopyrite, calcite and bitumen. Galena occurs in veinlets or as fine disseminated grains as well. Galena may occur as a single mineral phase but most of galena is intergrown with spahlerite or sphalerite-chalcopyrite. Galena overgrows pyrite grains and has minor inclusions of chalcopyrite. Textural relationships indicate that galena was generated late during the Stage I. Chemical composition is close to stoichiometric. Minor impurities are Fe, Cu, As

and rare Sb (Appendix 3.4).

Cobaltite - (Co,Fe)AsS

Cobaltite was identified by microprobe analyses in two samples from Filo mine block: a basalt (MP791) and a volcanic sediment (MP793). In both samples cobaltite occurs as minute inclusions (less than 30 μm in size) within bornite-chalcocite grains. Wilson (1998a) found similar cobaltite inclusions within chalcopyrite, bornite, and chalcocite grains in several samples of Filo area. All samples where cobaltite has been identified contain bitumen and pyrite replaced by Cu sulphides. Microprobe analyses indicate that Cu, Fe, Ni, and Mg are minor components of cobaltite (Appendix 3.4). Cobaltite is a very rare phase that precipitated during Stage II; cobalt (and other components) was probably inherited from diagenetic pyrite.

Pyrrhotite ($Fe_{1-x}S$), Arsenopyrite (FeAsS), Magnetite (Fe_3O_4),

These minerals were not identified in the samples studied during this thesis, but they have been reported in previous studies as rare phases at El Soldado.

Pyrrhotite is found as fine disseminated grains in calcareous sediments of the Lower Lo Prado Formation, without relationship with copper ore (Carmen Holmgren, *personal communication*). The author has mapped pyrrhotite in these sediments associated with pyrite-sphalerite, and galena in DDH core samples drilled in the Paso Riel area, but pyrrhotite was not identified in the single polished section available from these rocks (sample MP761). Wilson (1998a) recognised traces of pyrrhotite in basalts of the Filo mine block as irregular grains (about 400 μm in size) that contain inclusions of pyrite and spahlerite. Ponce (2001) found in the same rocks, relicts of pyrrhothite replaced by pyrite. Pyrrhotite formed probably late during Stage I (Wilson, 1998a).

Arsenopyrite is a very minor phase at El Soldado that has been documented in basalt rocks from the Filo mine block (Zentilli, et al., 1997; Wilson, 1998a). Arsenopyrite occurs as rhombohedric grains, associated with bitumen and quartz and partially or totally replaced by bornite-chalcocite. Arsenopyrite probably formed during Stage I although its paragenetic position is uncertain (Wilson, 1998a).

Magnetite associated with copper ore has also been reported in basalt samples from the Filo mine block (Wilson, 1998a). It occurs as fine (<40 μm) euhedral inclusions within bornite-chalcocite grains and as massive aggregates (cm scale) accompanied by bornite, chalcocite, bitumen, and calcite. This magnetite does not contain Ti and formed during Stage II. Minor magnetite associated with specular hematite and pyrite has been identified in drill holes drilled in the northern part of the camp during last year. This occurrence has not been studied in detail.

5.3. Mineral Zoning

5.3.1. Pyrite and Pyrite-Chalcopyrite Zones

The pyrite and pyrite-chalcopyrite zones are recognised as forming the external haloes and the roots of the orebodies. Good examples are exposed at Valdivia Sur and Osorno blocks (Figures 5.5 and 5.6). All orebodies have these external haloes although in the high-grade bodies they can be very thin (<1 m) and thus not representable at the map scale of this thesis. Clearly these ore zones are more prevalent in the northern part of the camp (Morro pit; Catedral Norte block), and in the eastern flank, particularly at Arauco and Arauco Norte mine blocks (Figures 5.7 and 5.8). New diamond drill-holes, drilled farther north than the present day operations (not shown on maps) confirm that towards the north pyrite and chalcopyrite (but associated with specular hematite) are the predominant metallic minerals (see Section 5.3.4).

Pyrite and pyrite-chalcopyrite ore zones are considered barren for mining purposes. Cu values are lower than 0.1% (pyrite) or between 0.1-0.5% (pyrite-chalcopyrite). Yet at Morro pit the chalcopyrite-pyrite zone has been occasionally mined and or stockpiled as "low-grade" ore. Nevertheless the zones are clearly anomalous with respect to the background rocks in their S, Cu, and pyrite contents (>1.5 %, > 0.07 %, and > 1.5 % respectively; Table 5.2).

Within these zones, pyrite occurs finely disseminated, as framboids, spherules, or replacing ferromagnesian crystals. Pyrite is also very common as massive veins, and veinlets, which are composed of dense aggregates of irregular, euhedral and framboidal pyrite grains, usually associated with calcite and minor chalcopyrite. More massive

Table 5.2.- Mineralogical and Chemical Characteristics of Ore Zones

Ore Zone	Ratio between sulphides	Other opaques	Gangue (open spaces fillings)	Pervasive Alteration	Rock Type	100* (Na$_2$O) / (Na$_2$O+K$_2$O)	Cu (%)	S (%)	# Samples
background	py > 98%, traces of (cp), (sph), (gal) (asp)	tit > rut; mt, het in basalts	cal, chl,> Kfd, ep, sil, bit	absent	Basalt	57	0.01	0.01	4
					Rhyodacite	55	0.05	0.80	5
py	py > 70%, traces of (cp), (esf), (gal) (asp)	tit >rut	cal, chl, > Kfd, ep, sil, bit	weak to very weak	Basalt	79	0.11	1.57	2
					Rhyodacite	64	0.07	1.74	5
py-cp	(py-cp) > 70%	tit > rut	cal, chl, > Kfd, ab, ep, sil	weak to very weak	Basalt	77	0.25	0.32	3
					Rhyodacite	70	0.48	1.20	4
cp	cp > 70 % (py), (bn)	tit, rut, > het	cal, chl, > ab, Kfd, qz, ep, sil, bit	moderate	Basalt	78	2.86	1.07	3
					Rhyodacite	77	2.82	2.16	4
cp-bn	(cp-bn) > 70 % (py), (cc rare)	tit, rut, het, > sp	cal, chl, > ab, qz, Kfd, ep, bit	weak to moderate	Basalt	69	0.90	0.99	3
					Rhyodacite	67	2.77	1.16	2
bn	bn > 70% (cc), (cp) > (py)	het > rut, tit, sp	cal, chl, > ab, qz, ep, Kfd, bit	moderate to strong	Basalt	75	1.49	0.45	1
					Rhyodacite	84	2.64	0.91	6
bn-cc (sodic)	(bn-cc) > 70 %	het > rut, tit, sp	cal, chl, ab > qz, ep, Kfd, bit	strong	Basalt	86	2.21	0.49	5
					Rhyodacite	80	2.95	0.78	7
bn-cc (potassic)	(bn-cc) > 70 % (cc), (cp) > (py)	het > rut, tit, sp	Kfd, chl > cal, qz, ep, qz, bit	strong	Rhyodacite	36	3.03	1.66	4

Abbreviations

asp: arsenopyrite, rut: rutile, tit: titanite, cal:calcite, chl:chlorite, ab:albite, ep:epidote, qz:quartz, sil: silica, Kfd:microcline, bit: bitumen

texture predominates at veins cores and framboids aggregates at the edges (Figure 5.9). The massive texture is interpreted as formed by recrystallisation of framboidal pyrite (Wilson, 1998a; Ponce, 2001). While framboidal pyrite and pyrite replacing ferromagnesian crystals are considered diagenetic (see Chapter 3 and section 5.1), the origin of massive pyrite veins is problematic. Wilson (1998a), although not explicitly, considered it to be diagenetic, but Ponce (2001) suggested a late hydrothermal origin. Collins (2002) recently studied this problem as a complement of this thesis using a selected set of samples provided for the author. Collins (*op cit*) using electron microprobe images, found framboidal and concentric colloform textures in most of the massive pyrite vein samples, which indicate a prolonged period of formation under consistently low temperatures. He also mentions that pyrite probably replaced (pseudomorphed) unstable early-formed low-temperature melnikovite or marcasite. In consequence this author concluded that most of pyrite in massive veins must be generated during diagenesis (Stage I). δ^{34}S values from these massive pyrite veins yield values from -7.4 to +17.1 ‰ (Collins, 2002) a similar wide range as these of framboidal pyrite (-11.1 to +28.0 ‰; Wilson, 1998a) supporting the previous conclusion. However Collins (2002) considered that some crystalline pyrite found at the edges of deep pyrite veins could have formed during stage II. This suggestion is based on the fact that this pyrite is included within a calcite matrix (considered late in the paragenesis because crosscuts pyrite framboids) and because many crystals are compositionally zoned indicating multiple-stage growth. They have a rim of massive (inclusion -free) pyrite, which could have formed during Stage II, overgrowing previous "cloudy" (inclusion-rich) diagenetic pyrite.

A similar (hydrothermal) origin is envisaged for a body in deep Arauco Norte, composed of disseminated euhedral pyrite (>3 % in volume) and hosted by rhyodacites and sediments with strong albitisation, alteration that is not related to diagenesis (Sample RB99-03; Figure 5.7). Fluid inclusions in calcite from this body yield maximum homogenisation temperatures (without pressure corrections) between 200 and 296°C (average 253 °C; Table 3.4; Appendix 7.2) well above the diagenetic range assumed by Wilson (1998a), but similar to the other Cu sulphide ore zones. This suggests that this pyrite deposited during Stage II. This is confirmed by three δ^{34}S analyses of pyrite
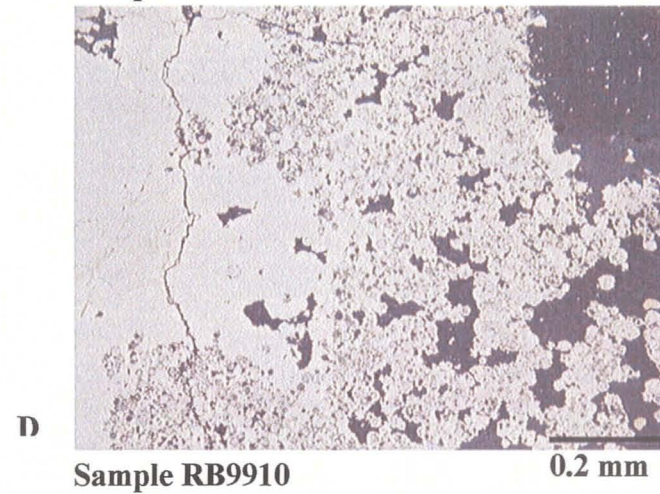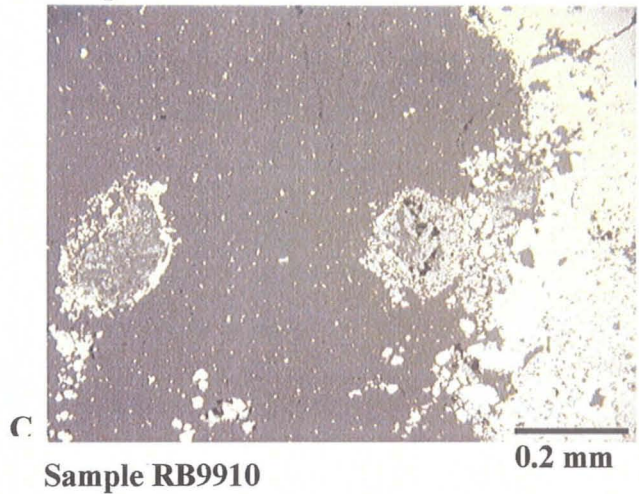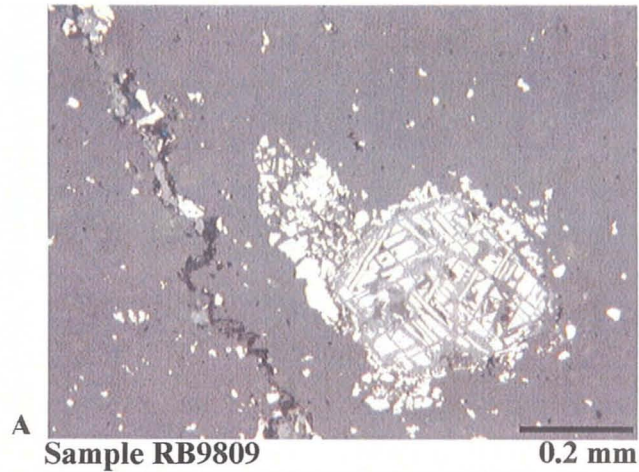
Figure 5.9. Photomicrographs of samples from the pyrite zone. See text.

A) Altered (exsolved) titanomagnetite with pyrite rim.

B) Euhedral pyrite and rutile, remnant of a Ti-bearing mineral.

C) Pyrite rimming altered titanomagnetite, and framboidal and recrystallised pyrite (right)

D) Detail of pyrite vein margin.

samples from this body that yield values from -3.3 to -02 ‰ (Collins, 2002), a restricted range similar as these obtained for Cu-sulphides precipitated during Stage II without replacement of pyrite ($\delta^{34}S$ -2 to +2 ‰, Wilson, 1998a). Yet one sample from this body has a $\delta^{34}S$ composition of +7.4 ‰ suggesting that al least part of S was inherited from early diagenetic framboids.

In conclusion, most of the pyrite is though to be formed during diagenetic Stage I, but at least some proportion of the euhedral pyrite may have crystallised during hydrothermal Stage II.

Chalcopyrite within the pyrite-chalcopyrite zone replaces (to varying degrees) pyrite grains and framboids. Replacement is more intense on borders (Figure 5.10). Resulting "atoll" textures are common (Figure 5.10c; see also Figure 5.15a below). Chalcopyrite also occurs as single anhedral grains (rare).

Minor species identified in these zones (particularly in the Filo Block) are sphalerite, galena, and rare arsenopyrite and pyrrhotite. Most common gangue mineral (open-space filling) in these zones is calcite. Other gangue minerals are quartz, opaline silica, chlorite, albite, epidote and bitumen; K-feldspar is rare. Titanite (in part leucoxene) is more abundant than rutile. Pervasive hydrothermal alteration (phenocrysts, groundmass, matrix) associated with these zones results in weak albitisation, represented by an increase in sodium and decrease in potassium respect to background (Table 5.2; see also Chapter 6). Yet in the Arauco Norte deep body, albitisation (and some silicification) are relatively strong (K was partially removed, as evidenced by staining).

5.3.2. Chalcopyrite and Chalcopyrite-Bornite Zones

These two zones are located above or interior to the external pyritic zones described above, and they constitute the bulk of the Cu ore exploited at the El Soldado mine (see Figures 5.3 trough 5. 8). They are relatively more abundant in the northern half of the mine, where they grade to an assemblage of chalcopyrite-specular hematite (Figures 5.3 and 5.4). In the northern parts of the camp and in many minor bodies they constitute the orebody core. These ore zones have Cu grades usually ranging between 0.5 to 1.3 % Cu, although some massive chalcopyrite veins (e.g Arauco block) have very rich
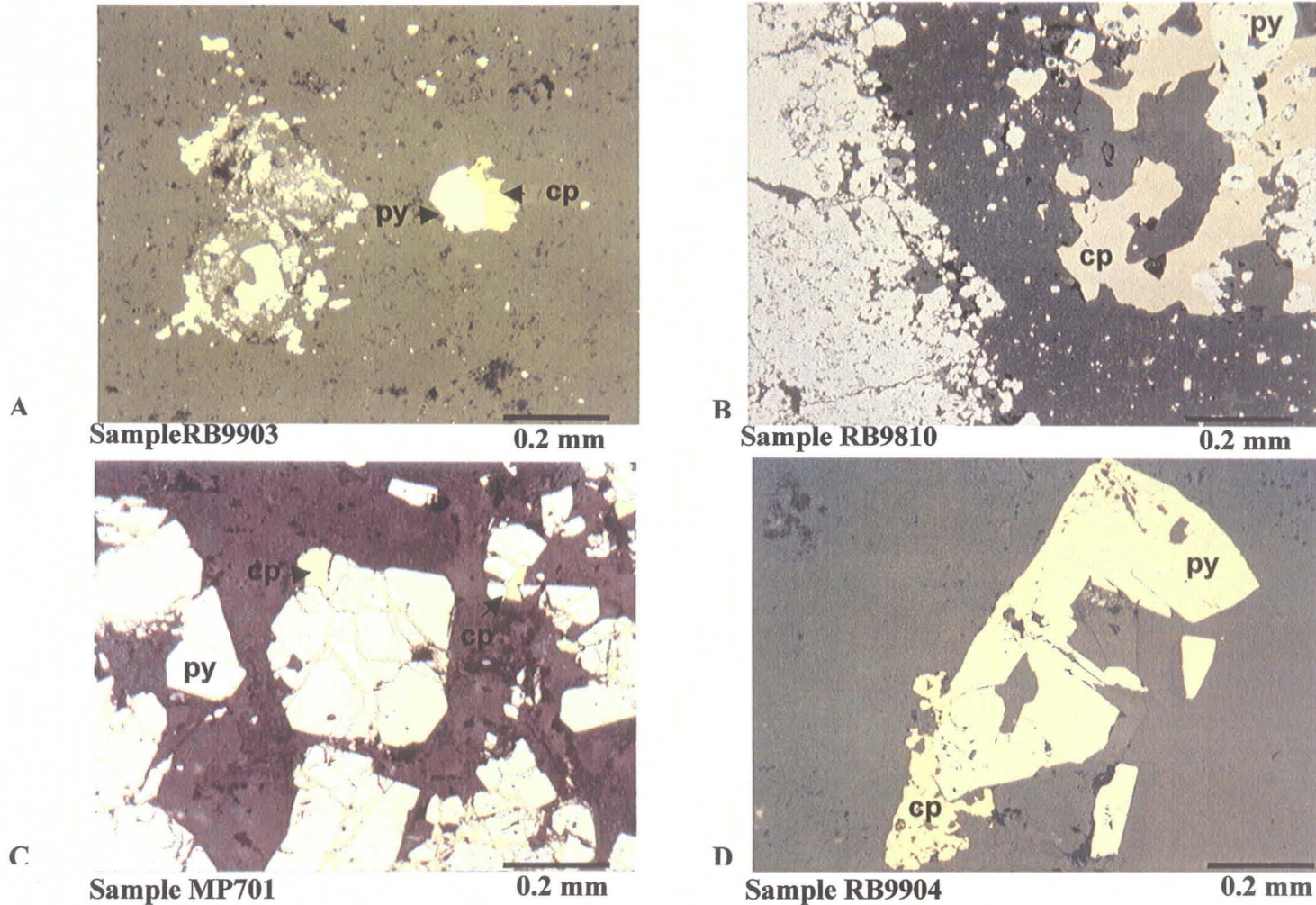
Figure 5.10. Photomicrographs of samples from the Pyrite-Chalcopyrite zone. See text.

A) Fine pyrite replacing ferromagnesian minerals. Euhedral pyrite (**py**) intergrown with chalcopyrite (**cp**).

B) Massive veilets with pyrite (**py**) in part framboidal and replacement by chalcopyrite (**cp**).

C) & D) Euhedral pyrite (**py**) with chalcopyrite (**cp**) veinlets.

grades (>3 % Cu). Silver contents are low, except when bornite is predominant (Ag up to 5 grams per tonne: [g/t] or p.p.m.).

Chalcopyrite occurs as isolated fine disseminated irregular grains (2-200 μm) along veinlets and or replacing pyrite. Replacements of previous pyrite framboids are evident (Figures 5.11b and c). Chalcopyrite also occurs inter-grown with bornite and textures show replacement of chalcopyrite by bornite (Figure 5. 11c) and vice versa (Figure 5.12 a). Relicts of pyrite, surrounded by either chalcopyrite or bornite, are minor in volume but commonly found (Figures 5.11d and 5.12 c). Fine hematite, particularly in the bornite-chalcopyrite zone, is also present (iron oxide/total opaques < 0.1) and it commonly imparts a red coloration to the rocks. A more abundant gangue mineral (as open-space fillings) is calcite, although chlorite, quartz, and albite are also common. Rutile (Figures 5.12, b, c) and titanite (Appendix 3) are both equally present. Specular hematite, associated with bornite or chalcopyrite, is rare (Figure 5.12a), but it becomes more abundant towards the north (e.g Catedral block, Morro pit), instead of bornite.

Within these ore zones, rocks show a moderate to strong alteration, mainly albitisation. Sodium contents are enhanced and potassium contents are reduced (Table 5.2; Chapter 6). Also chlorite is an important mineral, particularly associated with bornite. A pink to reddish coloration distinguishes rocks (especially rhyodacites) in these zones.

5.3.3. Bornite and Bornite-Chalcocite Zones

These zones are located in the inner part of the orebodies and represent their cores. They are better developed at the south end of the camp (Santa Clara, Valdivia Sur, Osorno blocks) and continue to the south in the Veta del Agua property (Figures 5.3, 5.4 and 3.11). They are relatively more abundant at the upper (higher elevation) levels. In the northern half of the mine they are reduced to narrow (usually less than 10 m thick) veins or are absent.

These zones constitute the richest ore grading usually between 1.5 to 2.5 % Cu. They also have important concentrations of silver (5-30 g/t). Some large orebodies have very high grades (e,g Valdivia Sur: core zones with 3-5 % Cu and 30-50 g/t Ag).
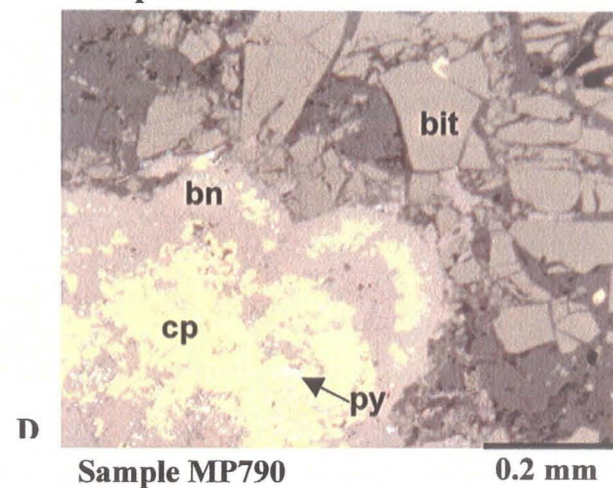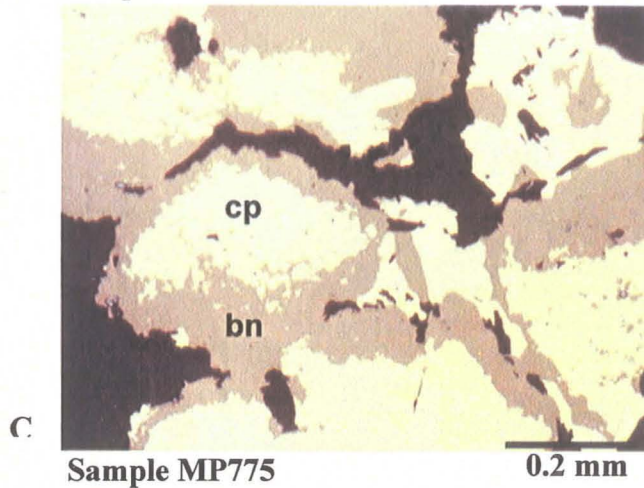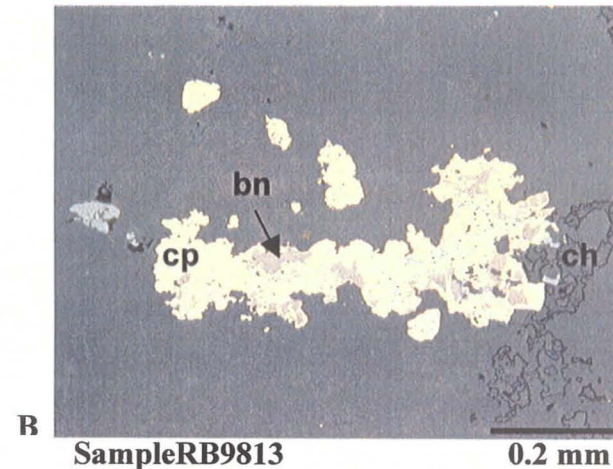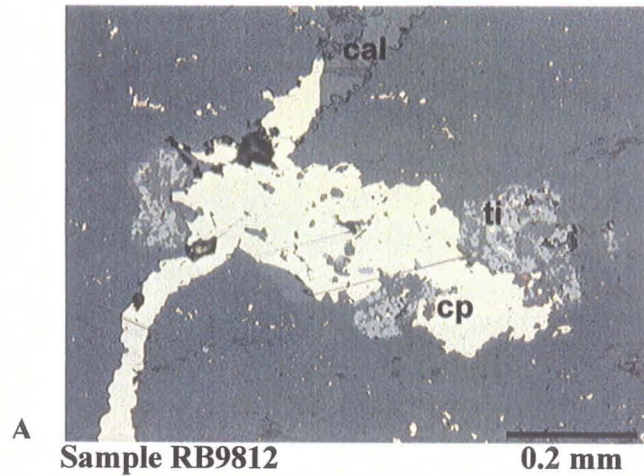
Figure 5.11. Photomicrographs of samples from the Chalcopyrite-Bornite zone. See text.

A) Chalcopyrite (**cp**) veinlet and after pyrite developed around titanite (**ti**).

B) Framboidal chalcopyrite (**cp**) (replacement of framboidal pyrite), and bornite (**bn**).

C) Chalcopyrite (**cp**) rimmed by bornite (**bn**).

D) Radial aggregates of pyrite (**py**) in fractured pyrobitumen (**bit**), replaced by chalcopyrite (**cp**) and bornite (**bn**).
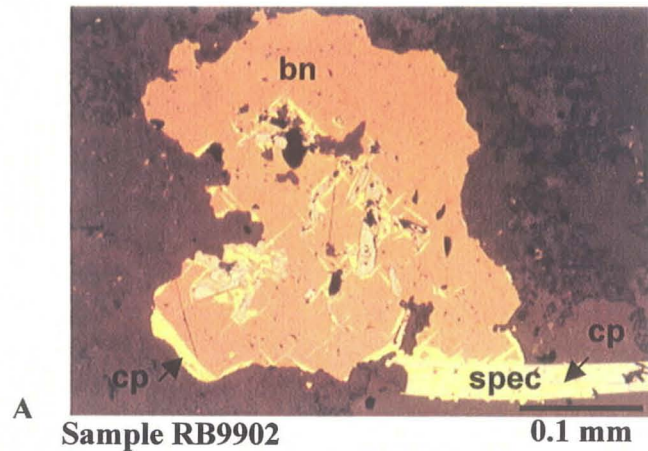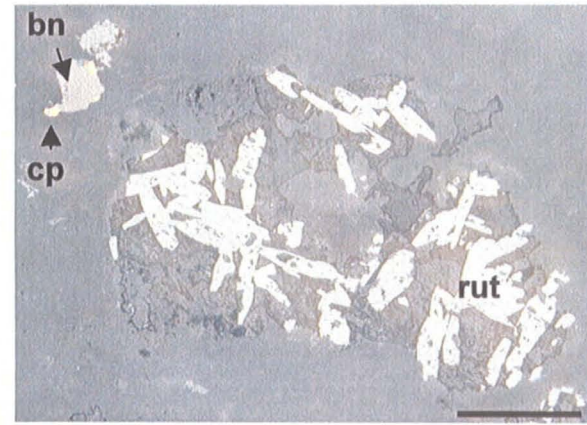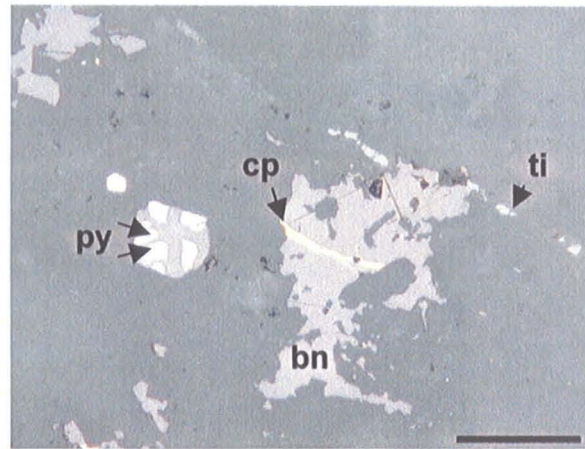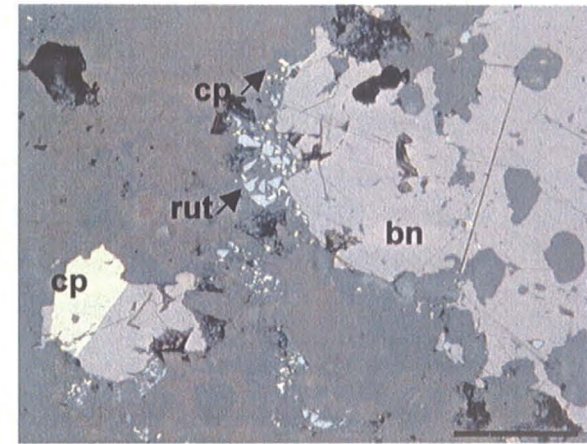
Figure 5.12. Photomicrographs of samples from the Chalcopyrite-Bornite zone. See text.

A) Bornite (**bn**), chalcopyrite (**cp**), and hematite (**he**) needles, attached to a crystal of specular hematite (**spec**), partially replaced by chalcopyrite.

B) Rutile (**rut**) needles in remnant of titanite.

C) Pyrite (**py**) replaced by bornite (**bn**), chalcopyrite (**cp**), veining bornite; titanite (**ti**) vein.

D) Bornite (**bn**) alone or with chalcopyrite (**cp**); rutile (**rut**) crystal are remnants of titanite or titanomagnetite.

The bornite zone is composed mainly of bornite (bornite >70% total sulphides) with minor chalcocite, chalcopyrite and rare pyrite. Bornite occurs finely disseminated, or filling veinlets, vugs and amygdules, usually associated with chalcocite. Isolated aggregates of bornite are rare. Bornite replaces chalcopyrite and or pyrite (Figures 5.13a, c) and framboids of bornite (after pyrite) are common at Filo block (Wilson, 1998a; Figures 3.14 and 5.13a). Most commonly, bornite occurs intergrown with chalcocite, forming sub-graphic textures that indicate simultaneous deposition (Ponce, 2001).

Within the bornite-chalcocite zone both sulphides represent more than 70 % of total sulphides by volume. Both sulphides occur mainly as intergrowths, although monomineralic aggregates are also present (Figure 5.14). Textures and occurrences are similar as those in the previous zone.

In both mineralogical zones, fine hematite, intergrown or rimming bornite or bornite-chalcocite crystals, is abundant (Figure 5.13d). This occurrence has been explained by deposition of an excess of iron after the replacement of pyrite-chalcopyrite by bornite-chalcocite (Holmgren, 1987). In the Filo block it is possible to recognise narrow bodies close to the Adelita fault, composed almost exclusively of chalcocite (Ponce, 2001); due to scale limitations they were not individualised on the figures of this thesis.

Common gangue minerals (open-space filling) are calcite, K-feldspar (microcline according to XRD), chlorite, albite and minor quartz and epidote. Rutile is much more abundant than titanite (Figure 5.14b). Pervasive albitisation of the host rocks is the rule. Na replacement can be so intense than no potassium is preserved (Na_2O/Na_2+K_2O: 0.7 to 1.0; average: 0.84 in basalts and 0.82 in rhyodacites; Table 5.2; see also Chapter 6). Nevertheless, narrow and structurally controlled potassium-rich zones are also mappable (e.g. Core of Valdivia Sur). In these subzones, the K values have increased (by deposition of K-feldspar) and sodium values have decreased (Na_2O/Na_2+K_2O: 0.1 to 0.5; average in rhyodacites: 0.36; Table 5.2, see details in Chapter 6). Host rocks within these zones present a characteristic pink-green to purple-reddish colour, reflecting their alteration. Locally the original textures of the rocks are difficult to recognise, even under the microscope.
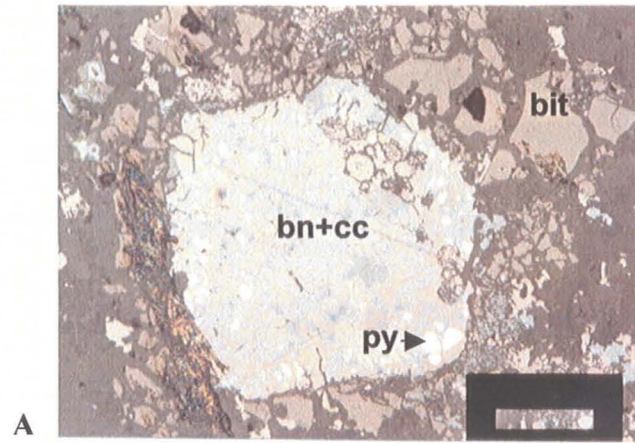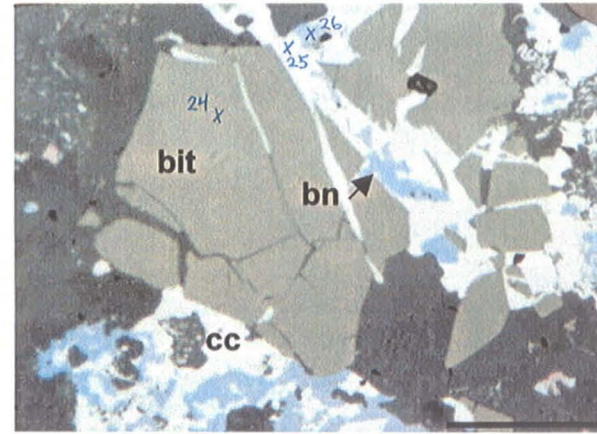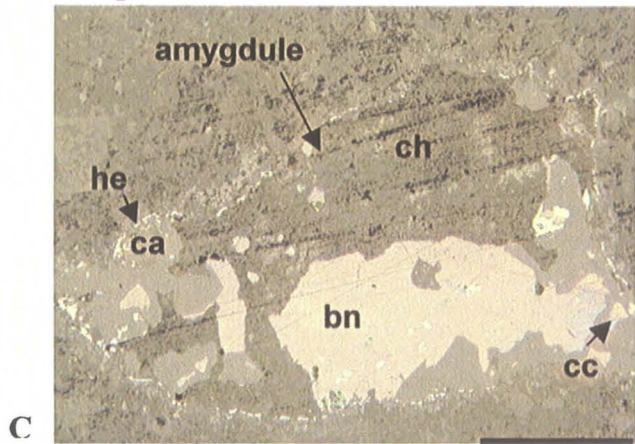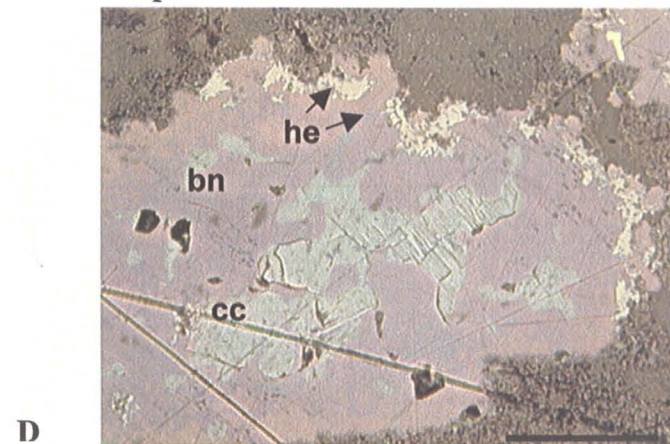
Figure 5.13. Photomicrographs of samples from the Bornite and Bornite-Chalcocite zones. See text.

A) Bornite-Chalcocite (**bn+cc**) replacing (**py**); note framboidal textures. Fragments of pyrobitumen (**bit**).

B) Pyrobitumen (**bit**) veined by chalcocite (**cc**) and bornite (**bn**).

C) Amygdule rimmed by hematite (**he**) filled with calcite (**cal**), chlorite (**ch**), and bornite (**bn**).

D) Bornite (**bn**) - Chalcocite (**cc**) and hematite (**he**) exsolved during replacement.
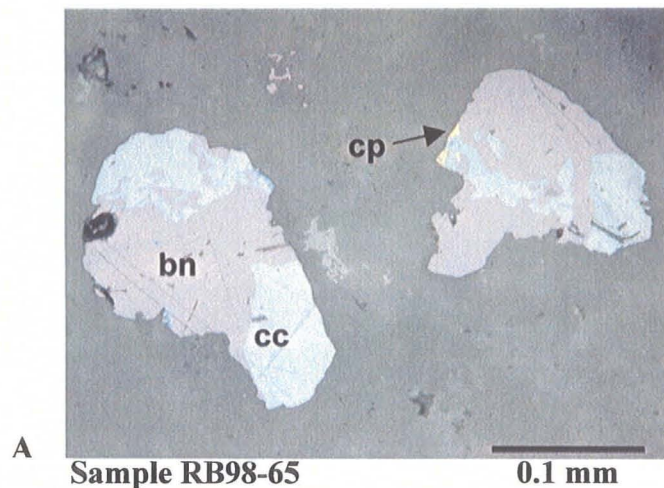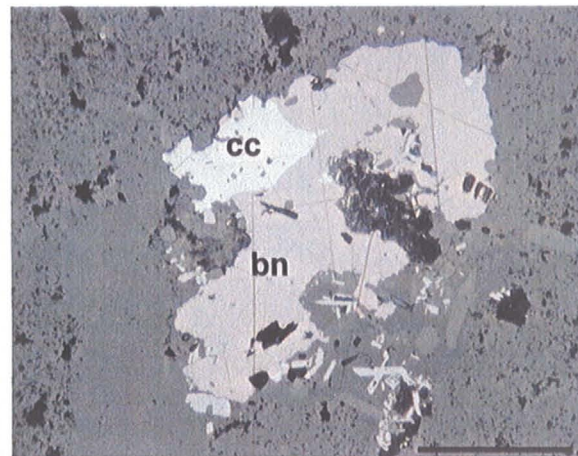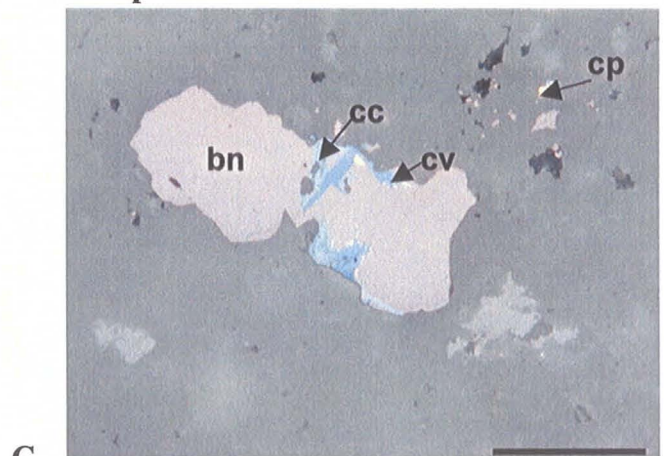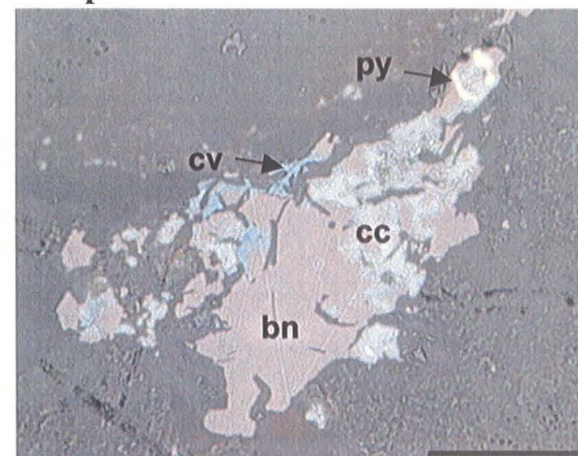
Figure 5.14. Photomicrographs of samples from the Bornite-Chalcocite zones. See text.
A) Bornite (**bn**) – Chalcocite (**cc**), chalcopyrite (**cp**).
B) Bornite (**bn**) – Chalcocite (**cc**), rutile (**rut**) and chlorite (**ch**).
C) Bornite (**bn**), chalcocite (**cc**), covellite (**cv**), specks of chalcopyrite (**cp**).
D) Bornite (**bn**), chalcocite (**cc**), covellite (**cv**), and pyrite (**py**).

5.3.4. Specular Hematite Zone

Specular hematite is relatively important only in the northern part of the mine (north of zero north coordinate) where it occurs associated with chalcopyrite, pyrite and minor bornite. The specularite zone was mapped overprinting the sulphide zones, when specularite represents more than 10 % of the total opaque minerals. This ratio is much higher in the northern portion (e.g, cross section +1000 N), where veins with 30 to 50 % of specularite have been intercepted in new (2001) drillholes.

Specular hematite occurs in well-developed crystals (0.1 mm to few cm in size) associated with chalcopyrite, pyrite, calcite, and rarely with bornite. Most of specularite infills the cores of veinlets intergrown with calcite and specularite is clearly paragenetically later than chalcopyrite-pyrite crystals (Figures 5.15, 5.16). It also may be intergrown with chalcopyrite. In one sample pyrite and magnetite pseudomorhs after specularite were observed.

The author's most current data indicate that specular hematite is present in the northern areas instead of (and occupying a similar spatial location than) bornite-chalcocite. Gangue and alteration minerals observed are similar to those found in the bornite zones, although no chemical analyses have been done to characterise the alteration.

Specular hematite had been considered a mere curiosity in previous studies of El Soldado. The present research shows that it is an important component of the overall deposit. This fact may establish a link with other important strata-bound Cu deposits in northern Chile, such as Punta del Cobre and Candelaria, where hematite and magnetite are important early phases of the hydrothermal mineral paragenesis (e.g. Ryan et al., 1995; Marschick and Fontboté, 1996).

5.3.5. Summary

The mineralogical zoning explained above has been summarized in Figure 5.17. The following important generalisations can been established:

1. Bornite and bornite chalcocite zones (Cu sulphides) are more abundant to the south and along the west flank of the mine, mostly along the Adelita shear fault, which
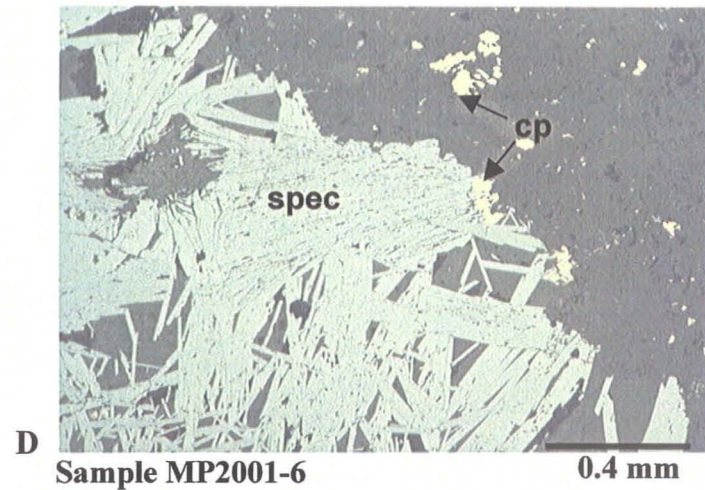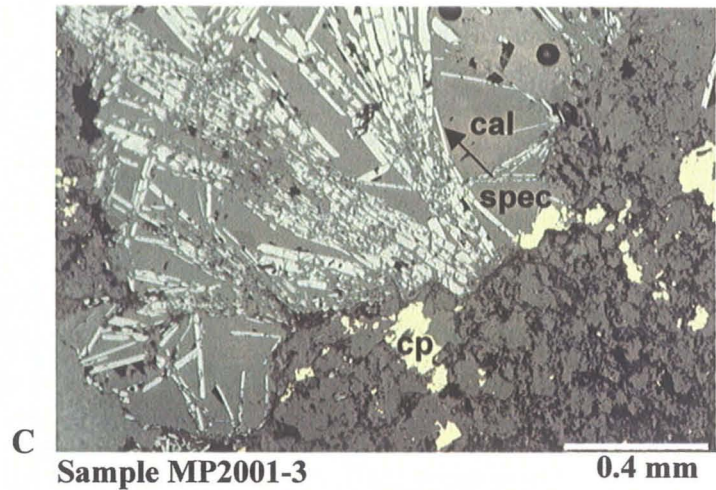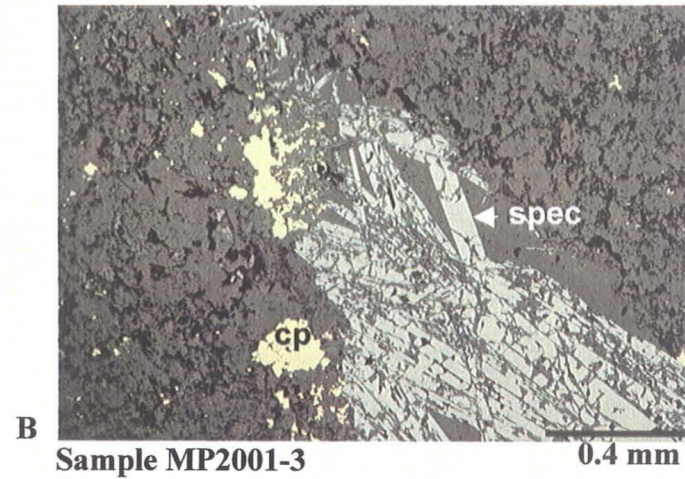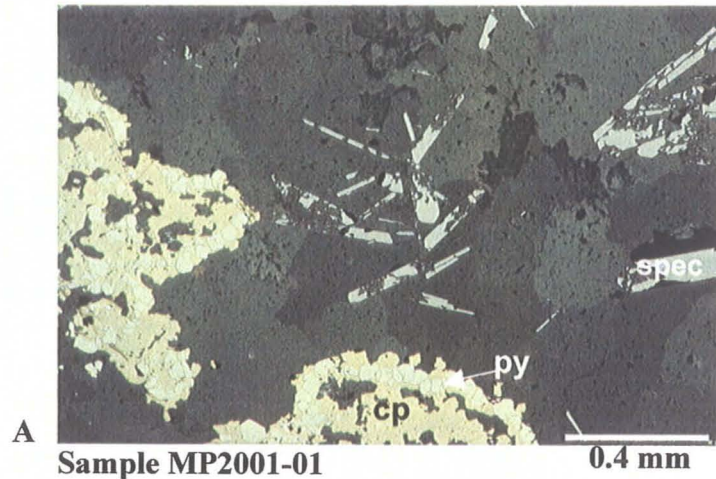
Figure 5.15. Photomicrographs of samples from the specular hematite zone, northern El Soldado. See text.

A) Atoll textures of chalcopyrite (**cp**) replacing pyrite (**py**) and specular hematite (**spec**) laths in calcite.

B) Chalcopyrite in rims of veins. Specularite (**spec**) and calcite (**cal**).

C) & D) Same as above.

Note specularite is later than pyrite-chalcopyrite.
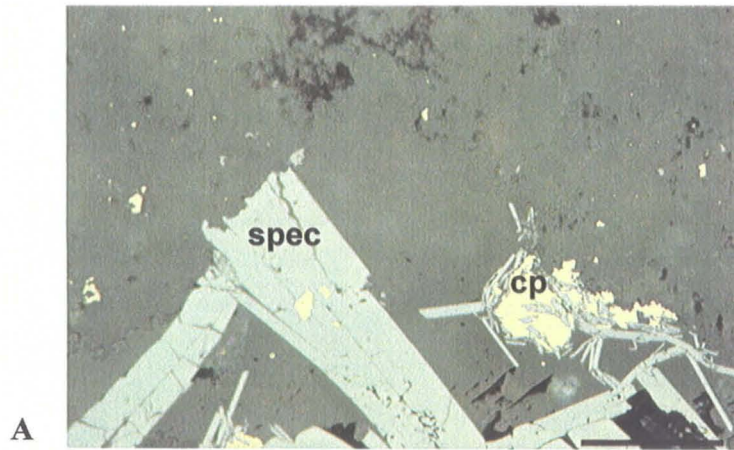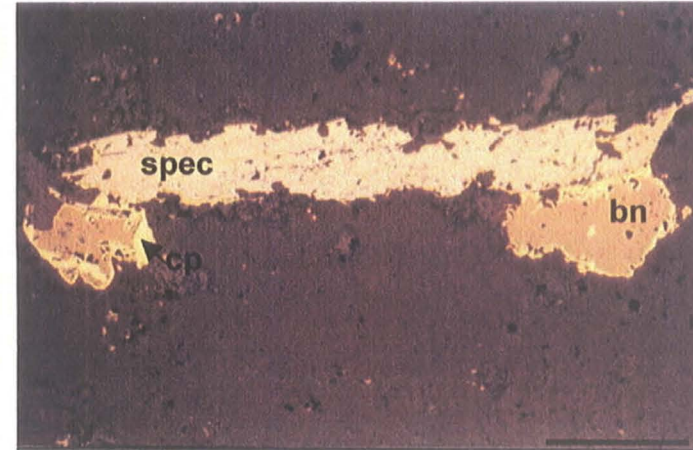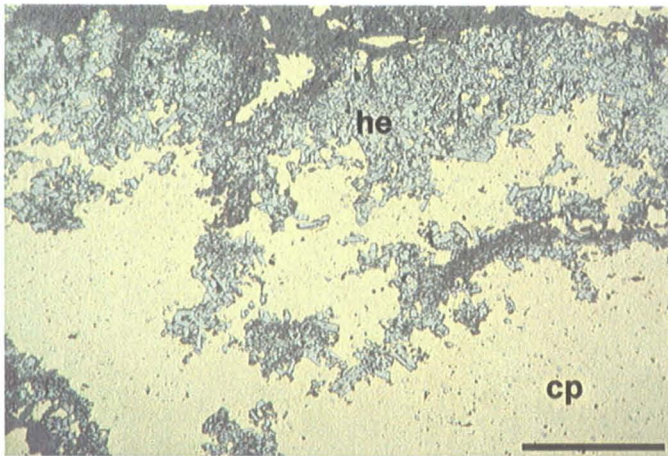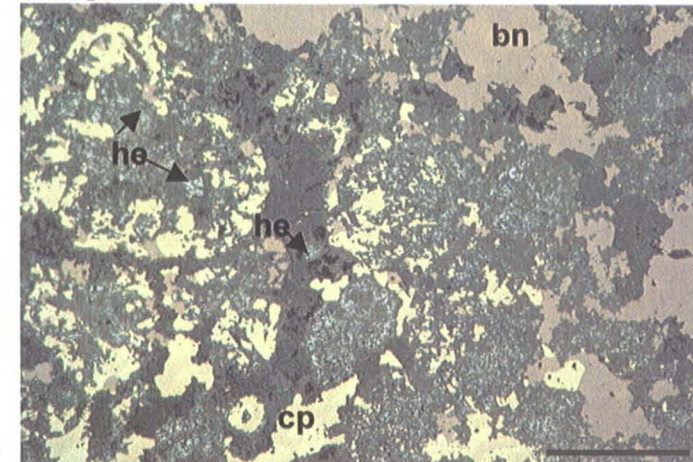
Figure 5.16. Photomicrographs of samples from the specular hematite zone, northern El Soldado. See text.
A) Specular hematite (**spec**), chalcopyrite (**cp**) intergrowths.
B) Specular hematite (**spec**) with bornite (**bn**), and chalcopyrite (**cp**).
C) Chalcopyrite (**cp**) with granular hematite (**he**); metastable or supergene assemblage.
D) Bornite (**bn**) – chalcopyrite (**cp**) with hematite (**he**) grains; metastable or supergene assemblage.
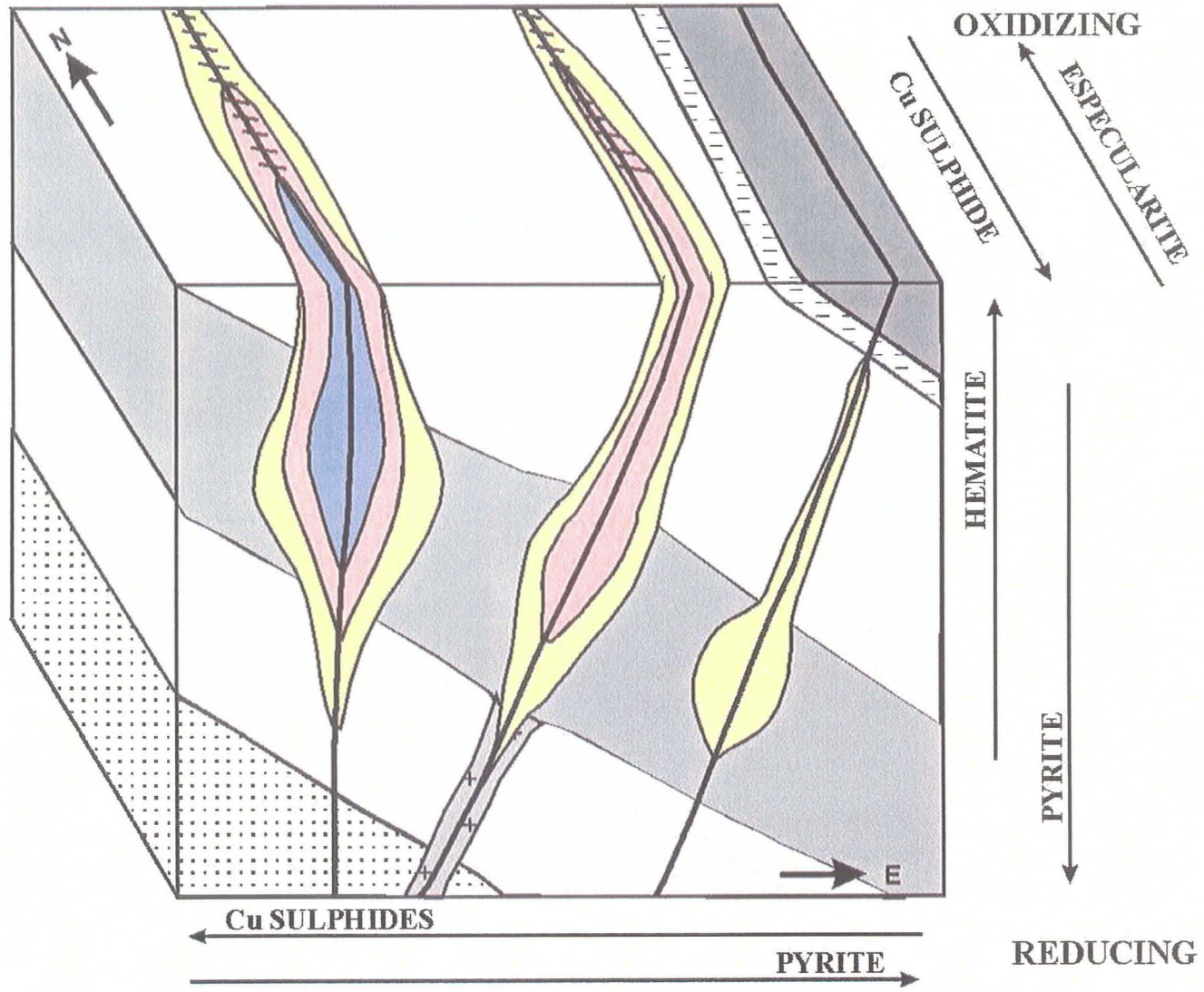
Figure 5.17. Schematic block diagram of the mine-scale mineral zoning (not to scale).
Legend shown in **Figure 5.1B**

constitutes a main control to Cu mineralisation.

2. In contrast, pyrite and chalcopyrite are more abundant to the north and to the east, away to the main shear faults. The Arauco veins, which branch off the main structural zone (See section 3. 3; Figure 3.8), are composed mainly of chalcopyrite- pyrite.

3. Sulphides in general are more abundant in the south whereas hematite (specularite) is more abundant in the north of the camp, probably reflecting a change in the oxidation-reduction conditions of the system (see discussion in Chapter 7).

4. Pyrite is also more abundant in the lower levels (roots) of orebodies, and conversely, hematite (fine crystalline and as specularite) is relatively more abundant in the upper levels, also reflecting a change in the redox conditions with depth (oxidation at upper levels, reduction at lower levels).

5. This overall pattern can be explained by generation of Cu orebodies by *descending* Cu-rich fluids channelled along the main fault shear zone (mostly along the Adelita fault), probably coming from the south. Consequently, the expectation of finding new economic reserves to the north of the property and at deeper levels is considered low.

CHAPTER 6. HYDROTHERMAL ALTERATION AND LITHOCHEMICAL CHARACTERISATION OF ORE ZONES OF THE DEPOSIT

6.1. General Statement

The volcanic host rocks at El Soldado have been affected by successive events, which have modified their original mineralogical composition. The Lo Prado Formation was affected by regional very-low-grade metamorphism (prehnite-pumpellyte facies) (Levi, 1969; Vergara et al., 1995), which among other changes produced an extensive albitisation of volcanic rocks, which acquired characteristics of *spilites* and *keratophyres* (Chapter 4). At El Soldado, the effects of such metamorphism are recognised in both barren "background" (least altered) rocks and in mineralised ones, so no such thing as "fresh" rocks can be identified in the camp. In addition, the sulphide metallic mineral assemblage identified at El Soldado was deposited in two separated episodes: an early diagenetic Stage I, and a late hydrothermal Stage II (Wilson, 1998a, see also Chapter 5). Bitumen, quartz, silica, calcite and chlorite were deposited as gangue minerals during Stage I (Wilson, 1998a) and calcite, chlorite, albite, K-feldspar (microcline), quartz, epidote, and rutile formed as alteration-gangue products during Stage II.

Previous studies have satisfactorily described most of the secondary mineralogy but they have failed to identify an overall spatial pattern in distribution of gangue-alteration minerals in relationship to copper ore. Terrazas (1977) identified carbonatisation (calcite) and albitisation as the most important alteration related to copper ore, yet Holmgren (1987) and Klohn et al. (1990) suggested that the main alteration phases were calcite, chlorite and quartz and that albite was not relevant in association with copper ore. Moreover other authors have indicated that there is no connection whatsoever between the distribution of copper ore and secondary minerals, assuming that all rock alteration in El Soldado is a product of regional metamorphism (e.g. Martin, 1981). On contrast, the present study presents mineralogical and lithochemical evidence of strong hydrothermal alteration directly related with copper ore. This alteration is characterised by pervasive albitisation and local K-feldspar alteration, and the deposition of calcite, chlorite, and minor quartz, epidote and rutile as gangue minerals. The

hydrothermal alteration is stronger at the core of orebodies where the textures and original components of rocks are difficult to identify. It is weaker in the external ore zones and laterally grades into, and is thus difficult to separate from, the effects of regional metamorphism in background barren rocks. This hydrothermal alteration was controlled by structural (secondary) permeability, and its spatial distribution matching orebody shapes is discordant with respect to stratification, implying sub-vertical fluid flow during its generation. On the contrary, the pattern of regional metamorphism traditionally has been ascribed as concordant with stratification, its grade being characteristically higher in the most permeable zones of volcanic sequences, and probably formed by lateral, sub-horizontal fluid flow (e.g. Levi, 1969; Levi et al, 1982; Westra, 1988a).

The study of gangue-alteration minerals was performed as a complement to the research on the sulphide mineralogy and zoning previously described in Chapter 5. The aim was to try to recognise any patterns of mineralogy or geochemistry that may be associated with the richest ore, and therefore develop some criteria useful to future exploration. The same set of sampling criteria and similar methodology as that explained in Chapter 5 was used to identify the gangue-alteration minerals (see details in Section 5.1).

The first part of this chapter gives a description of the gangue-alteration minerals, their mode of occurrence, their distribution in relation to sulphide ore zones, and their possible origin. Minerals are listed according to their relative abundance. In the second part a lithochemical analysis of the alteration is given, making a comparison between the chemical behaviour of the different ore zones and the "background" barren rocks. To this effect, the geochemistry of representative samples of rocks from the different mineralogical zones have been analysed for major and trace elements and compared with the "freshest", "least altered", or "background" rocks distal from ore. Specific gravity (S.G.) was measured with a beam balance, and magnetic susceptibility (M.S.) systematically with a hand-held EDA K-2 Magnetic Susceptibility Meter. The third part of this chapter is a comparison among the patterns of alteration at El Soldado and those at two other large strata-bound Mesozoic Cu-(Ag) deposits of Chile: Mantos Blancos and

Punta del Cobre.

6.2. Gangue and Alteration minerals

Calcite - CaCO$_3$

Calcite is the most abundant gangue and alteration mineral at El Soldado. Calcite occurs filling the porosity of host rocks associated with copper sulphides and pyrite and it is also common replacing primary minerals in both mineralised and barren (background) rocks. It has been observed in all samples studied from all orebodies, and in all lithologies.

Calcite is clearly more abundant within orebodies where it occurs preferentially in veinlets or veins associated with copper sulphides and, in to a lesser extent infilling pores and replacing primary components. Veins are more abundant close to main faults, where rocks are relatively more intensely fractured. Veins are usually thinner than 2 cm but massive calcite veins (up to 5 m of thickness) within faults (Figure 6.1a) are also observed. Calcite in veins occurs locally as large, well-developed clean crystals (*sparry* calcite) indicative of deposition by open-space filling, although minor fibrous aggregates of calcite rimming the borders of veins are also observed. Crosscutting relationships show evidence for several episodes of calcite deposition in veins (Figure 6.1b; Holmgren, 1987; Wilson, 1998a). Calcite also occurs associated with copper ore filling pores (amygdules) in basalts and rhyodacites and, less frequently, as the cement-matrix of volcaniclastic rocks. Calcite filling open spaces is associated with all sulphides, quartz, chlorite, K-feldspar, bitumen, and minor epidote, albite, and opaline silica. This kind of calcite is present in all ore zones without preference.

Calcite is also extended as an alteration mineral replacing primary (volcanogenic) minerals or disseminated in the groundmass of volcanic rocks. In basalts it replaces olivine, pyroxene, and calcic plagioclase; in rhyodacites it alters ferromagnesian minerals and plagioclase. This style of calcite may occur in association with disseminated copper sulphides, but it is also present in background, barren rocks.

Microprobe and XRD analyses confirm that the carbonate is exclusively calcite. Manganese (0.3-2.7 %) was detected in almost all samples probed. Other minor
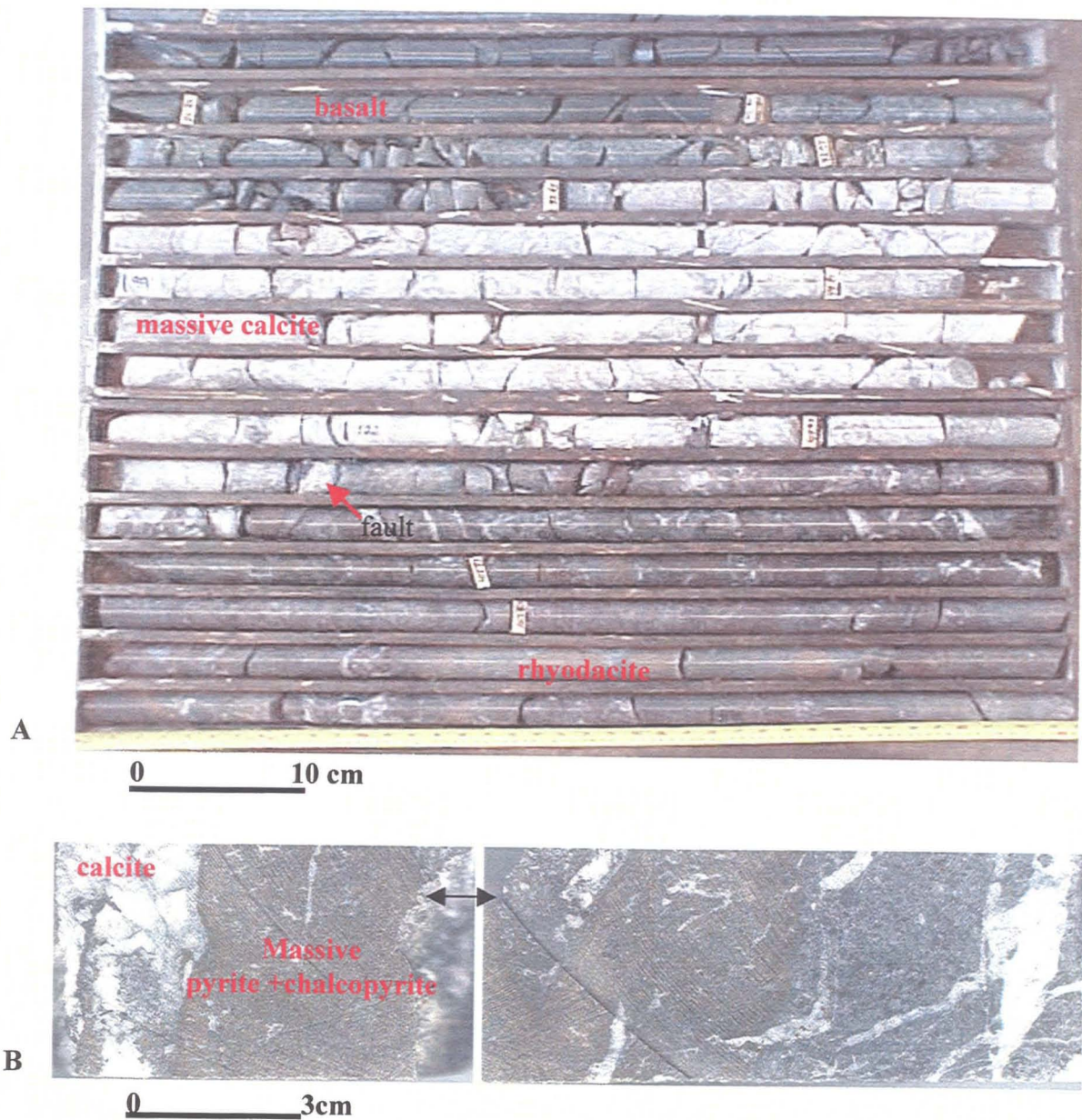
Figure 6.1. Photographs of calcite as a gangue in DDH samples.

A) Massive calcite vein adjacent to a fault zone (Manto Rojo mine block);

B) Calcite veinlets cross-cutting massive pyrite-chalcopyrite vein (Valdivia Sur orebody).

impurities are silica, magnesium and iron (Appendix 3.1)

The widespread presence of calcite is probably the result of precipitation of this mineral during very-low-grade metamorphism, diagenetic Stage I, but mostly later, during the hydrothermal Stage II. Calcite has been reported as a metamorphic mineral in rocks of the Lo Prado Formation in regional studies (e.g. Levi, 1969), thus calcite altering volcanogenic minerals in background rocks, probably formed during very-low-grade metamorphism. This generation could be favoured by the liberation of Ca during the albitisation of calcic plagioclases (*spilitisation* see Chapter 4). Some proportion of the calcite associated with bitumen and pyrite probably formed during diagenesis, but crosscutting relationships indicate that the bulk of the calcite precipitated later than solidification of petroleum to form bitumen, thus probably at temperatures above 100°C. Textural and analytical evidence support the notion that calcite infilling open spaces and associated with copper sulphides was formed during hydrothermal Stage II. Fluid inclusion studies indicate maximum homogenisation temperatures between 145 and 303°C (without pressure correction) for this calcite associated with copper sulphides (Appendix 7.2), confirming it was deposited during hydrothermal Stage II. Later barren veins yield lower maximum temperatures of homogenisation, but still higher than diagenetic (e.g. 104 to 170°C, Appendix 7.2). $\delta^{13}C$ in sparry calcite associated with copper sulphides, yields a wide range between -4.2 to -20.2 ‰ indicating that part of hydrothermal calcite incorporated light C by oxidation of bitumen previously formed during diagenesis (Wilson, 1998a).

Chlorite - $Si_3O_{10} (Mg,Fe)_5 (Al,Fe)_2 (OH)_8$

Chlorite is less abundant than calcite, but it is also an important secondary mineral altering host rocks, and as a gangue mineral accompanying copper sulphides.

Chlorite is very common in basalts altering olivine, pyroxene, and plagioclase crystals, replacing glass in groundmass and infilling amygdules. In rhyodacites, is is less abundant but still frequent, altering ferromagnesian minerals, plagioclase, and in the groundmass. In volcanic sediments chlorite is common in the cement-matrix and in volcanic fragments.

As a gangue mineral, chlorite occurs filling veins, pores and amygdules associated with pyrite, and copper sulphides (Figure 6.2a) in all host rocks. This kind of chlorite is much more frequent in the core of orebodies, within the bornite and bornite-chalcocite ore zones, and it is less abundant in the external haloes (chalcopyrite and pyrite ore zones). Chlorite filling open spaces and related to copper sulphides occurs associated with calcite, K-feldspar, quartz and, to a lesser extent, with epidote, albite, and bitumen.

According to microprobe analyses, the composition of chlorite varies between pychnochlorite and ripidolite, although a few samples classify as diabantite. (Appendices 3.1. and 3.2). Contrary to previous studies (e.g. Holmgren, 1987; Klohn, et al., 1990) the microprobe analyses performed during this thesis do not suggest a clear variation in the composition of chlorite in relation to copper ore as opposed to other settings (Appendix 3.2).

Similarly to calcite, chlorite was deposited in successive events. Chlorite that rims vesicles filled with bitumen must have formed very early in the diagenesis of lavas (Wilson, 1998a). The pervasive alteration of the host rocks (including background rocks) where chlorite replaces mafic minerals was probably a result of the very-low-grade metamorphism of the sequence, although it could also be partially the result of hydrothermal alteration. Chlorite closely associated with copper sulphides, particularly within the bornite and bornite-chalcocite ore zones, must have been deposited during Stage II.

Albite - Si_3AlO_8Na

Albite is a very important alteration mineral at El Soldado, less common as a gangue phase related to copper ore. As was previously described in Chapter 4, phenocrysts and microlites of both rhyodacites and basalts have been altered to albite during very-low-grade metamorphism. This albitisation, not directly related to the copper mineralisation process, has a regional distribution (e.g. Levi et al., 1982), and within the mine camp affected both background (barren) and mineralised rocks. It was more intense in rhyodacites where albite fully mimics the primary plagioclase; in basalts this early

A) Sample RB99-01, rhyodacite, bornite-chalcocite ore zone

B) Sample RB99-03, rhyodacite, pyrite ore zone

C) Sample MP770, rhyodacitic dyke, pyrite ore zone

D) Sample RB9867, rhyodacite bornite ore zone
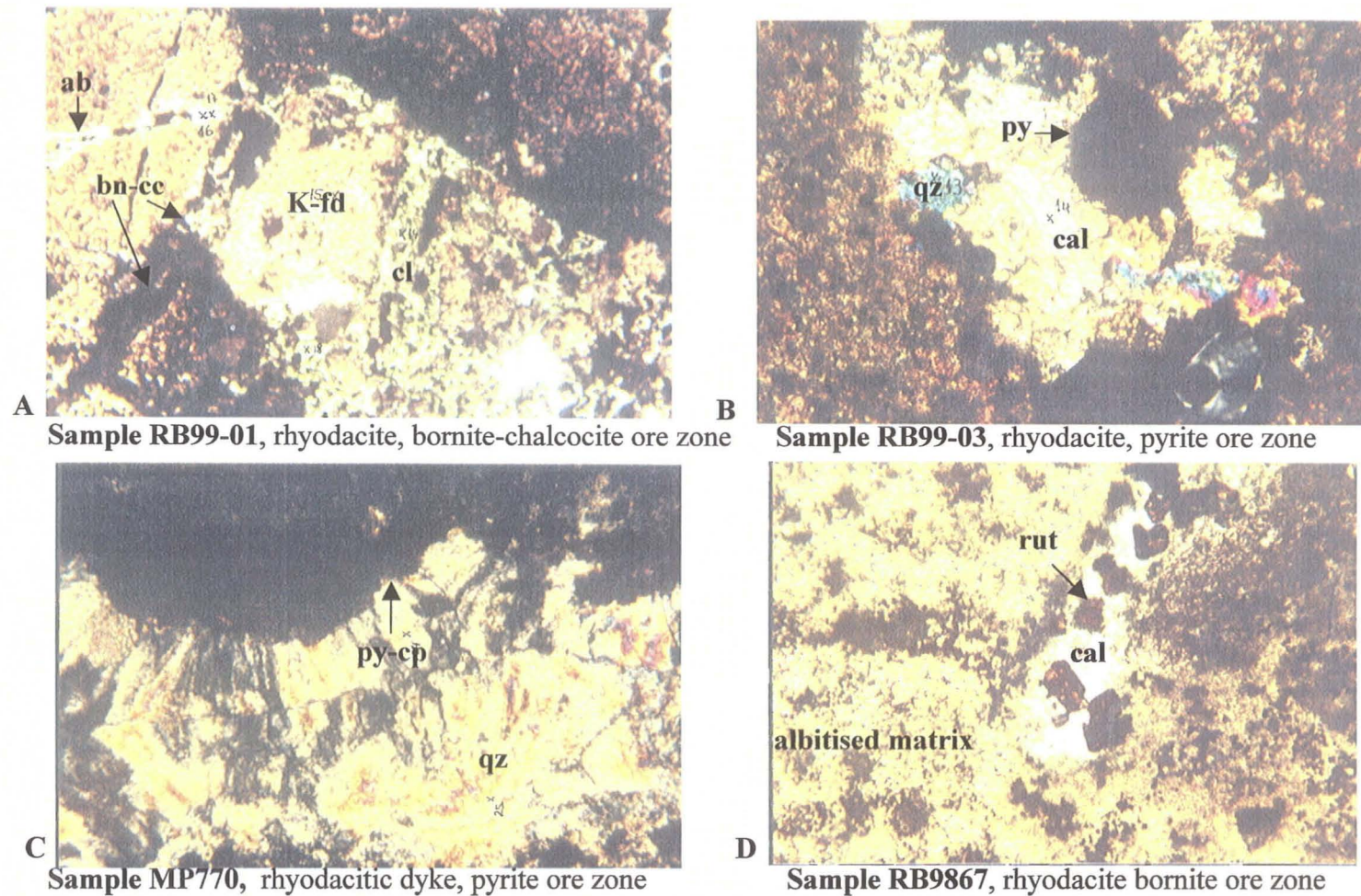
Figure 6.2. Microphotographs of gangue minerals.
A) Chlorite (green) and albite (white) in a brecciated K-feldspar altered rock with bornite-chalcocite (black);
B) Calcite (white) and quartz (blue) filling in pores with pyrite (black);
C) Quartz in vein associated with pyrite-chalcopyrite (black);
D) Rutile and calcite in albitised rhyodacite.

albitisation was not complete and some basalts from background zones preserve their original more calcic plagioclase (bytownite-labradorite; see Appendix 3.1). As a result of this alteration rocks acquired characteristics of *spilites* and *keratophyres* (see discussion in Chapter 4).

Pervasive albitisation has been recognised as well in association with copper mineralisation, and affecting all types of host rocks. This albitisation is stronger in the richest zones of orebodies, particularly within the chalcopyrite-bornite, bornite, and bornite-chalcocite ore zones. In the external haloes of orebodies the albitisation is weaker and less pervasive although it is clearly noticeable. This kind of albitisation is also important following narrow zones along the contact between country rocks and mafic impervious dykes. Rocks affected by albitisation have a light pink to white colour (Figure 6.3b, c, d) and in the most altered rocks the original composition and texture are difficult to establish.

Albite within these altered zones occurs replacing pre-existing feldspars and less commonly infilling veinlets and pores as minute crystals, which are usually difficult to identify optically. Albite was identified by XRD and microprobe analyses but the most useful tool to recognise the grade and extension of albitisation was the Na-cobaltinitrite staining (Figure 6.3; Appendix 6).

This albitisation related to copper ore is more relevant in rhyodacites, where it replaces the abundant K-feldspar originally present in the groundmass (Figures 6.3 and 6.4). In the bornite and bornite-chalcocite ore zones, this replacement is strongest and in some samples almost all potassium has been removed from the rocks (Figure 6.4b; see also Section 6.3). In mineralised basalts, albitisation is recognised by fine aggregates of albite in the groundmass (possible replacing K-feldspar) and by a small increase in the Na content of albite phenocrysts with respect to barren (background) basalts (background basalts: average of albite phenocrysts: An_6; mineralised basalts: average An_2; see Appendix 3.1). In volcanic sediments albite occurs as fine aggregates in the matrix-cement and altering feldspar within volcanic fragments. In all these mineralised rocks, albite occurs also infilling veinlets, pores and amygdules (basalts), generally as a minor phase accompanying calcite, quartz, K-feldspar, chlorite and/or copper sulphides. More
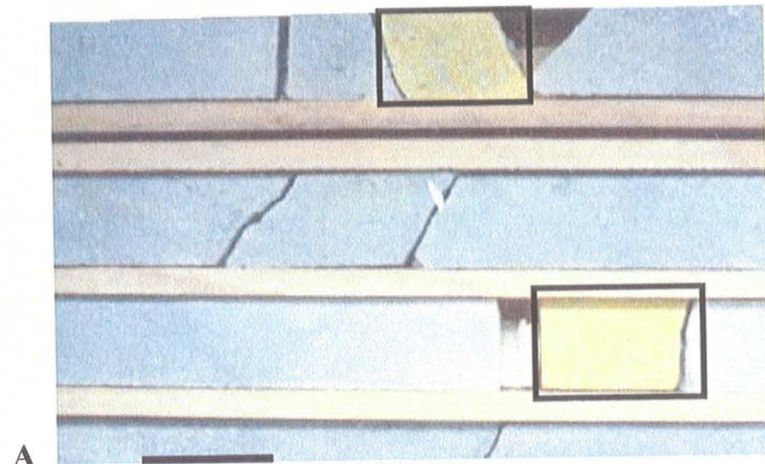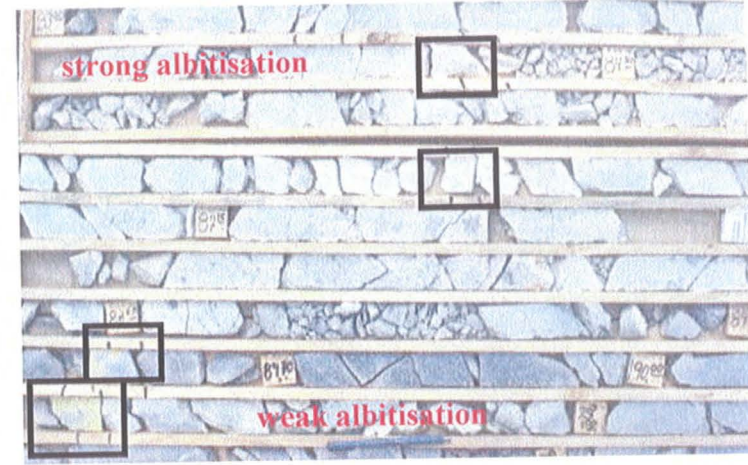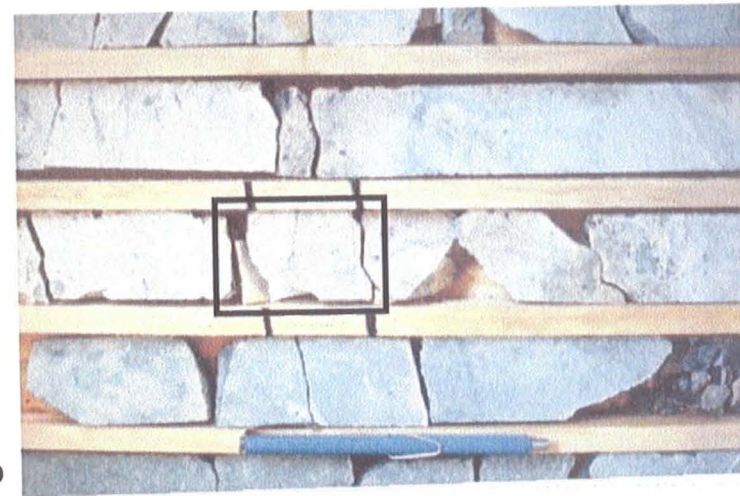
Figure 6.3. Photographs of DDH samples of background and albitised rhyodacites.
A) Background unmineralised rhyodacite;
B) C) & D) Albitised rhyodacite mineralised with bornite-chalcocite.
Insets show sections stained with Na-cobaltinitrite; lack of yellow tint is indicative of removal of K (K-feldspar replaced by albite).

Sample RB9805, background rhyodacite
Na_2O: 5.49%, K_2O: 3.16%

Sample RB9867, albitised rhyodacite in bornite-chalcocite zone:
Na_2O: 10.54%, K_2O: 0.01%

Sample MP778, K-feldspar altered rhyodacite in bornite-chalcocite zone:
Na_2O: 3.49%, K_2O: 6.39%
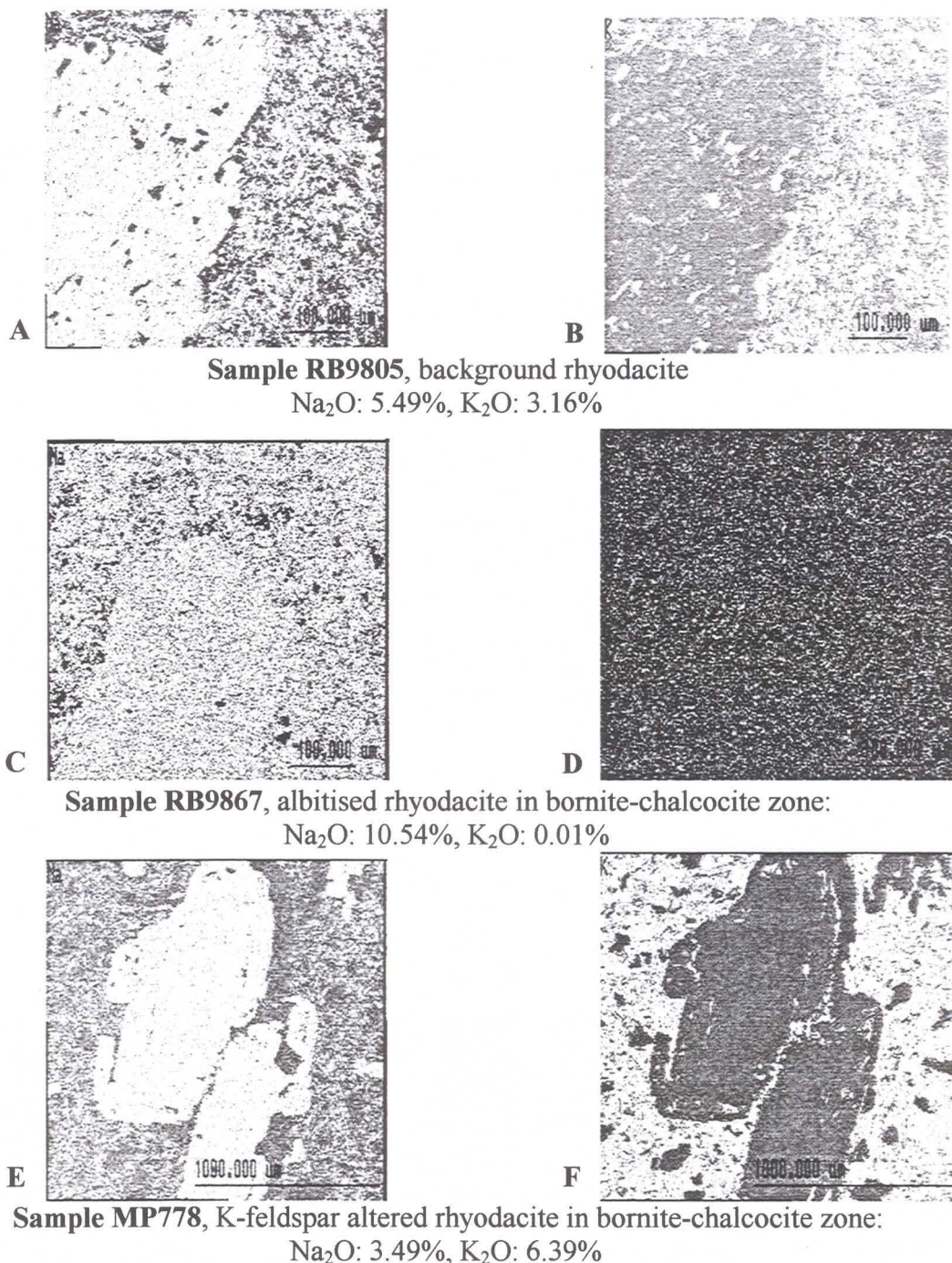
Figure 6.4. X-Ray microprobe images of Na (left) and K (right) in background and altered rhyodacites.
A) & **B)** Background rhyodacite (sample RB 9805);
C) & **D)** albitised rhyodacite in bornite-chalcocite zone (sample RB9867);
E) & **F)** K-feldspar altered rhyodacite in bornite-chalcocite zone (sample MP778).
Note the presence of K (K-feldspar) in the groundmass of the background sample; the complete replacement of K by Na in the albitised sample; and, the increase of K (K-feldspar) in groundmass of the K-feldspar altered sample.

commonly, albite can be detected as small crystals (< 0.2 mm) riming veinlets or vugs and intimately associated with K-feldspar (microcline), suggesting a simultaneous formation of both phases.

In summary, textural evidence supports the hypothesis that albite formed during two separate episodes. Early albite, not directly related to copper ore, was generated during regional very-low-grade metamorphism, altering the more calcic plagioclase of volcanic rocks. Late albite directly associated with copper sulphides precipitated during hydrothermal Stage II. This albite is more abundant in the core of orebodies where an extensive and pervasive albitisation is noted.

K-Feldspar - Si_3AlO_8K

K-feldspar is a common gangue and alteration mineral at El Soldado although less abundant than calcite, chlorite, and albite. It has been recognised in all types of host rocks, being more important in rhyodacites. K-feldspar was identified at El Soldado as an important secondary mineral associated with copper sulphides only in the most recent studies (e.g. Boric, 1997; Wilson, 1998a); in the past it was considered to be a primary component of the rhyodacites (e.g. Klohn et al., 1990). This thesis shows evidence of at least two different styles of occurrence of K-feldspar, formed during two separate stages.

In background (barren) rhyodacites, K-feldspar is found as microcrystalline aggregates in the groundmass. This fine-grained K-feldspar is not easily distinguished from albite and quartz using the optical microscope, but it can be identified in microprobe X-ray images and by Na-cobaltinitrite staining (Figures 6.3 and 6.4; Appendices 3.3 and 6). This K-feldspar does not show any relationship with copper ore and probably crystallised during regional metamorphism, simultaneously with replacement of plagioclase phenocrysts by albite, after a generalised mobilisation of alkalis, yet a primary origin cannot be totally ruled out. Traces of K-feldspar of probably similar origin have been recognised in groundmass of background basalts.

K-feldspar of clearly secondary origin has been identified in all types of host rocks, altering albite phenocrysts, infilling vugs, amygdules and veinlets, or as fine aggregates in groundmass or matrix-cement of rocks. This K-feldspar is more abundant

within orebodies, where it occurs accompanied by bornite, chalcocite, chalcopyrite and/or hematite, but it is also found as a rarity in external, background, barren rocks. In basalts, this K-feldspar typically infills open spaces (veins, amygdules; Figure 6.5c) and is accompanied by calcite, minor copper sulphides, chlorite, epidote and albite, and it is rare as an alteration of plagioclase (Figure 4.2f). K-feldspar filling pores is well crystallised, and XRD indicatse it to be microcline (Appendices 4.1 and 4.2). In volcanic sediments it can be observed as fine aggregates in cement-matrix and infilling veinlets having a patchy or irregular distribution mostly in mineralised rocks (Figure 6.5d). In rhyodacites K-feldspar is found altering albite phenocrysts (patches and veinlets; Figure 4.8), infilling veinlets associated with calcite and chlorite, and as fine aggregates in groundmass where it replaces albite microlites (Figures 6.5a-b, 6.4e-f). This alteration to K-feldspar (which implies an increase in K-feldspar content and a decrease in the albite content with respect to background rhyodacites) has been observed in irregular and narrow areas (<10 m of width) close to structures (faults, dykes), particularly within the core of orebodies (e.g. Valdivia Sur Chimney; Figure 5.6). In these areas, K-feldspar is associated with calcite, chlorite, bornite, chalcocite, chalcopyrite, and hematite and rocks have a characteristic pink to reddish coloration (Figure 6.5a-b). It is difficult to determine the mineralogical composition of this late K-feldspar in rhyodacites because in these rocks both phase coexist; however most XRD analyses indicated a microcline composition (Appendix 4.1).

Microprobe analyses show that K-feldspar has sodium (up to 3 %), barium (up to 1.7 %), and less frequently iron (up to 1.7%) and calcium (up to 0.4%) as main impurities (Appendix 3.1).

In summary, K-feldspar present in the groundmass of rhyodacites without relationship with copper mineralisation, was probably formed during early regional metamorphism of the sequence. On the contrary, later-formed K-feldspar (microcline) associated with copper sulphides formed during the hydrothermal Stage II, altering all host rocks. $^{40}Ar/^{39}Ar$ dating of microcline samples associated with copper sulphides yield ages from 106 to 101 Ma (Table 3.4; Appendix 7.1), an age range ascribed to the copper mineralisation event (Wilson, 1998a; Wilson et al., in press a). $\delta^{18}O$ in this K-feldspar yield a restricted range of 12.0 to 12.7‰ (average: 12.5 ‰), which suggests a
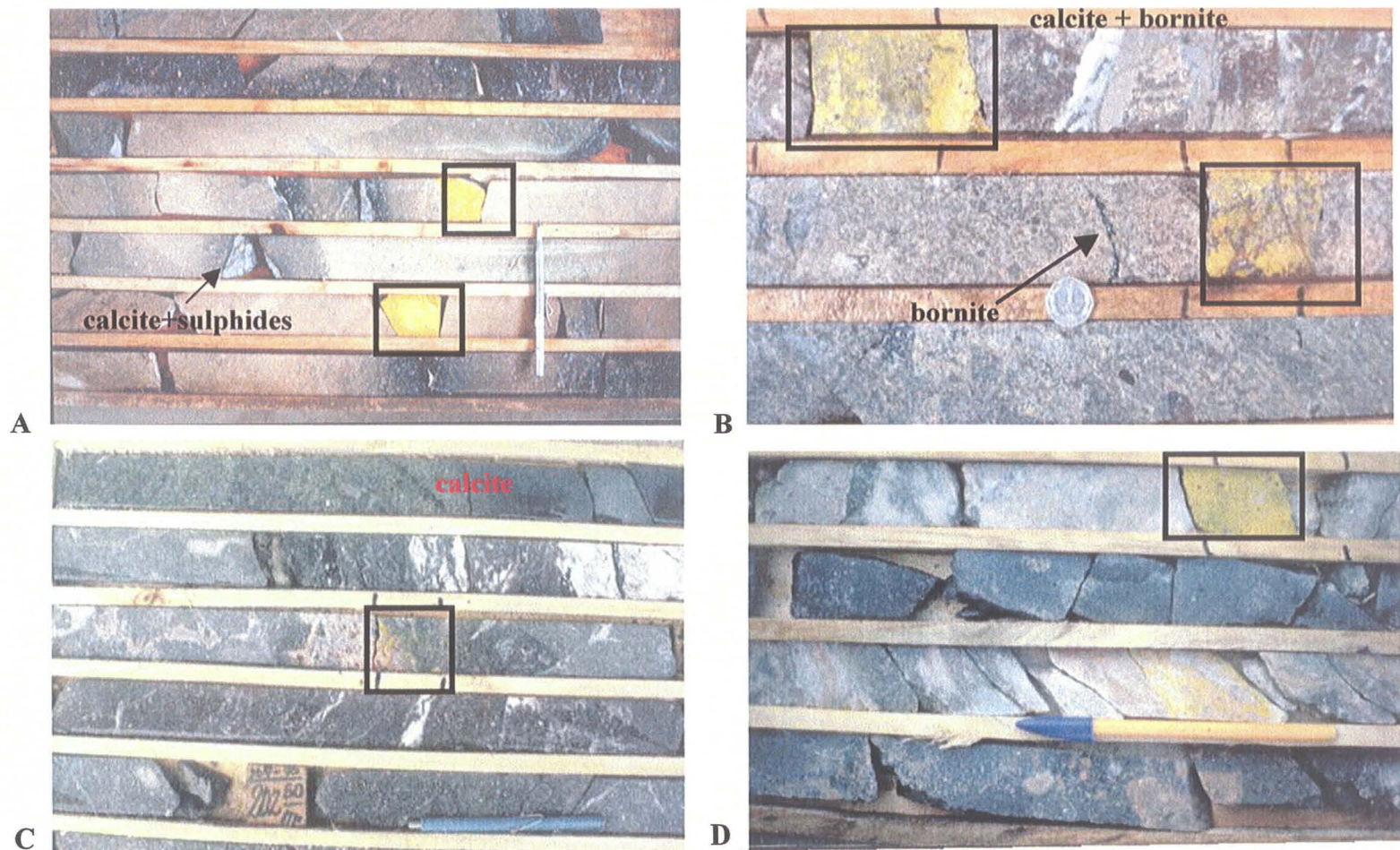
Figure 6.5. Photographs of K-feldspar alteration in DDH samples.

A) Pervasive K-feldspar alteration in rhyodacite, bornite-chalcocite zone;

B) Patches of K-feldspar in brecciated rhyodacite, bornite zone;

C) K-feldspar and calcite veinlets in basalt, bornite zone;

D) K-feldspar in volcanic sediment, bornite-chalcocite zone.

Insets show sections stained with Na-cobaltinitrite (yellow).

metamorphic (not magmatic) origin for this late K-feldspar (Wilson 1998a).

Bitumen - Graphitic Carbon (Solid Organic Matter)

In El Soldado organic matter associated with pyrite and copper sulphides occurs as bitumen and rare graphitic carbon. Bitumen is common in all kind of rocks (including basalts, rhyodacites, and dykes) and in all orebodies, although it is relatively more abundant in the Filo mine block in the southern part of the camp. Graphitic carbon has been identified only in the Morro mine block located in the northern part of the camp.

The distribution, petrography, maturity, and composition (chemical, isotopic) of the organic matter was studied in detail by Nicholas Wilson in his Ph.D. thesis (Wilson, 1998a), and its role in the genesis of El Soldado has been discussed in recent papers by Zentilli et al. (1994,1997), Wilson and Zentilli (1999), and Wilson (2000) (see Chapter 3). Consequently the organic matter was not studied in detail in this thesis and the following description is a summary totally based on the papers mentioned above.

Bitumen occurs as spherical (globular), angular and irregular grains, which fill in primary and secondary porosity of host rocks. Bitumen is interpreted to represent liquid petroleum solidified during burial of the sequence. Globules of bitumen represent droplets of petroleum, which usually have degassing bubbles and fractures ("shrinkage cracks") produced during solidification.

Bitumen is very commonly associated with framboidal pyrite in background barren rocks and pyrite ore zones but it has also been documented in all copper sulphide ore zones. Bitumen has abundant inclusions of framboidal pyrite and rare of sphalerite, chalcopyrite and small euhedral quartz crystals. Textures suggest that all of these minerals grew during diagenetic Stage I, before solidification of the bitumen. Bitumen is cut by calcite, quartz, and copper sulphides, which filled in the post-solidification fractures, and therefore must have formed during hydrothermal Stage II. Bitumen is also associated with copper sulphides within orebodies where they replaced framboidal pyrite.

Physical and chemical composition of bitumen changes from background rocks to orebodies. Wilson (1998a) demonstrated that in the Filo orebody, the reflectance under oil (R_o) (a measure of organic matter maturity) increases from about 3.5% in pyritic

haloes to about 4.5 % in the ore core. Most of the bitumen is isotropic to weakly anisotropic under cross-polarised light, but bitumen associated with copper sulphides in the richest ore zones usually presents the highest degree of anisotropy. This anisotropy appears to be related to the content of impurities in the bitumen. Microprobe analyses indicate that besides C, S is the major component of bitumen (0.4-3.5 %). Other minor components are, Cu, Fe, Cl, and Pb, which are more abundant (>1 %) where bitumen is anisotropic and associated with copper sulphides (Wilson, 1998a, 2000).

$\delta^{13}C$ analyses of bitumen samples associated with ore yield values from -25.9 to -30.8 % (Appendix 7.3) a range compatible with bitumen generated from petroleum (Zentilli et al., 1997). A couple of samples of bitumen from the matrix of sedimentary rocks of Lo Prado Formation and not related to ore yield $\delta^{13}C$ values of -28.9 to -29.0 ‰ (Zentilli et al., 1997; Appendix 7.3).

Graphitic carbon has been identified in the northern Morro mine block associated with fine (millimetre scale) chalcopyrite-bornite veinlets. The graphictic carbon is highly anisotropic with high bireflectance and it is considered to represent bitumen thermally altered to temperatures around 200-250 °C (Wilson, 2000). Microprobe analyses detected S (0.68-1.06%) and traces of Cu and Fe (<0.3%) as minor elements in this graphitic carbon (Wilson 2000).

In summary, according to previous studies, bitumen represents petroleum that migrated from the underlying lower, sedimentary member of the Lo Prado Formation into the volcanic and volcaniclastic upper member. Pyrite (± sphalerite, ± chalcopyrite) developed by biodegradation of petroleum when it was still not solid during diagenetic Stage I. During the continuing burial in the basin, petroleum solidified into bitumen, forming degassing structures and shrinking. Later, bitumen was thermally altered around the orebodies, developed anisotropy, and was locally graphitised by the hydrothermal fluids of Stage II. Bitumen chemically reduced the mineralising fluids, incorporated some components (Cl, Cu, Fe) and favoured the precipitation of copper sulphides during Stage II (Wilson, 1998a; Wilson and Zentilli, 1999; Wilson, 2000).

Quartz and Silica - SiO₂

Quartz is a minor gangue and alteration phase at El Soldado; it is relatively more abundant in rhyodacites and is rare in basalts and sediments.

In rhyodacites quartz, and less frequently opaline silica occur infilling pores and veinlets associated with calcite, bitumen and pyrite within background and external pyrite ore zones (Figure 6.2b). In some samples minute quartz (doubly-terminated, euhedral) crystals occur within bitumen, suggesting it formed early during diagenesis (Wilson, 1998a). In rhyodacites, quartz also occurs within orebodies infilling veinlets and vugs, associated with calcite and copper sulphides (Figure 6.2c), particularly within the bornite and bornite-chalcocite ore zones. Within these zones quartz is always a minor gangue mineral subordinate to calcite. In addition, secondary quartz also occurs in rhyodacites altering albite phenocrysts and as fine aggregates in their groundmass. In basalts and sedimentary units, quartz has been documented mostly in the bornite and bornite-chalcocite ore zones, infilling veins and pores associated with the copper sulphides and calcite.

Fluid inclusions analysed in samples from veinlets associated with copper sulphides yield maximum homogenisation temperatures from 119 to 257 °C (without pressure corrections; Appendix 7.2), confirming the hydrothermal nature of this quartz. Quartz is quite pure according to microprobe analyses (Appendix 3.1).

In summary, quartz intergrown with bitumen and pyrite formed during diagenesis (Stage I) at lower temperatures according to their textures (< 120 °C; Wilson, 1998a). Quartz in veinlets associated with copper sulphides crystallised as part of hydrothermal Stage II at higher temperatures (>120 °C). Quartz re-crystallised in the groundmass of rhyodacites and altering albite phenocrysts may have formed during hydrothermal Stage II. Alternatively, it may be the result of regional metamorphism (in part devitrification of glassy groundmass).

Epidote - $Ca_2(Al,Fe)_3(OH)(SiO_4)_3$

Epidote is a common but volumetrically restricted secondary phase in the El Soldado deposit. Epidote is much more abundant in basalts, although it is also present in rhyodacites and sediments. This mineral is more conspicuous in the deeper levels of the

mine and in narrow haloes surrounding mafic dykes (Figure 3.12a) and the gabbro stock.

In basalts, epidote occurs altering augite, olivine, and plagioclase and infilling veinlets and amygdules accompanied by calcite, chlorite, microcline, hematite and rare albite. In rhyodacites it replaces plagioclase and ferromagnesian minerals and is rare in veinlets. In sedimentary rocks, epidote is rare and occurs mostly disseminated in the cement-matrix. Epidote is scarce as gangue mineral, although it can be observed to be associated with chalcopyrite, bornite, and or chalcocite, mostly infilling rims of amygdules in basalts.

XRD and microprobe spot analyses indicate that the epidote phase presents at El Soldado is pistacite, the more ferric variety of the epidote family (Appendices 3.1 and 4.1)

The bulk of the epidote does not show any relationship with copper mineralisation, and probably formed as a product of regional metamorphism and local contact metamorphism (surrounding subvolcanic bodies). Calcium and alumina released during albitisation could favour its formation. Nevertheless epidote infilling open spaces and associated with copper sulphides, calcite, chlorite and microcline (particularly in basalts) was definitely a minor phase formed during hydrothermal Stage II.

Titanite ($CaTiSiO_5$) and Rutile (TiO_2)

Although volumetrically non-important these titanium-bearing minerals are widespread at El Soldado, occurring as minor secondary phases in basalts and rhyodacites.

Titanite (sphene) and leucoxene (an amorphous hydrous titanium dioxide) are common in background rocks altering titano-magnetite (basalts) and or altering ferromagnesian minerals. They frequently occur associated with disseminated pyrite, calcite, and rutile (Figure 4.7). Titanite is less abundant within orebodies as a minor gangue phase, associated with calcite and copper sulphides infilling veinlets or surrounding disseminated sulphides.

Rutile, by the contrary, is more abundant within orebodies, particularly in the bornite and bornite-chalcocite ore zones, where it occurs associated with calcite, copper

sulphides, and minor titanite and hematite (Figures 6.2d and 5.12b). In background rocks it is present more sparsely altering ferromagnesian crystals or titano-magnetite, generally associated with titanite, pyrite, and calcite. Holmgren (1987) demonstrated this polarity in distribution of titanite and rutile pointing out that titanite content decreases within copper orebodies.

Titanite and rutile were identified optically and with the microprobe (spot analyses and X-ray images; Appendices 3.1 and 3.2).

Titanite, leucoxene, (and possible some rutile) disseminated in background barren rocks formed previously to copper sulphides probably during regional metamorphism. Both phases are described as typical accessories components of spilites and keratophyres (e.g. Battey, 1955; Cann, 1969; Hughes, 1975; see Section 4.3.2.2). Most rutile, in particular where associated with copper sulphides, probably formed during hydrothermal Stage II, replacing pre-existing titanite (Figure 5.12b). A similar observation has been made in Mantos Blancos in Northern Chile (Figure 2.1; Chapter 2) where titanite predominates in background volcanic rocks whereas rutile is more abundant in altered-mineralised rocks (Chavez, 1985).

The widespread presence of titanite and rutile indicates that alteration processes affected originally titanium-bearing minerals and that titanium had some grade of local mobility in volcanic host rocks at El Soldado. Nevertheless lithochemistry indicates that titanium behaved as an immobile element in whole rock analyses (see Sections 4.3 and 6.2).

Muscovite - $KAl_2(OH)_2(AlSi_3O_{10})$

Fine muscovite (sericite) is a relatively common phase altering plagioclase phenocrysts and microlites in basalts (Figure 4.2e, f) and it is less abundant altering albite crystals and in the groundmass of rhyodacites. Muscovite also has been identified by XRD analyses in the matrix of barren volcano-clastic sediments (e.g. sample MP855, Appendix 4.1). Microprobe analyses show that muscovite contains iron, magnesium, manganese, calcium and sodium as minor constituents (Appendix 3.1).

Muscovite has not been recognised associated with copper ore, and probably

formed during very-low-grade regional metamorphism.

Clay Minerals - Montmorillonite - $(Mg,Ca) \cdot Al_2O_3 \cdot 5SiO_2 \cdot nH2O$ /
Illite - $KAl_2(OH)_2[AlSi_3(O,OH)_{10}]$

Clay minerals of the montmorillonite - illite families have been recognised by XRD analyses in the cement-matrix of volcano-clastic rocks associated with chlorite-calcite, which are the major components. XRD analyses also suggest that these minerals occur as minor phases in the groundmass of volcanic host rocks, where they are very difficult to distinguish from sericite.

Apatite - $Ca_5(PO_4)_3(F,Cl,OH)$

Apatite is a common accessory mineral present in both rhyodacites and basalts. It occurs as fine grains (10-100 μm) disseminated in groundmass or included within albite phenocrysts or infilling thin veinlets (< 10 μm width). Microprobe X-ray images show that apatite is relatively more frequent within altered-mineralised rocks than in background barren rocks (Appendix 3.2), suggesting that it formed as an alteration product. Lithochemistry analyses confirm that hypothesis (see Section 6.3).

6.3. Lithochemistry

6.3.1. Introduction

This section presents a lithochemical analysis of the hydrothermal alteration comparing the chemical composition of altered-mineralised host rocks and their unmineralised equivalents. The aim was to know the chemical behaviour of the main host rocks estimating the gain and losses of major oxides and trace elements associated with the process of alteration and copper mineralisation. The ultimate goal was to recognise any geochemical pattern associated with copper ore, which allows developing some criteria useful for future exploration.

The study was based on analysing representative samples of the main host rocks collected from the different mineralogical ore-zones and from background barren areas. Most of samples were collected along a detailed transect between Filo and Valdivia

orebodies in the central-south part of the mine (cross sections -750 and -900 North; see Figures 5.5 and 5.6). A few samples from other areas of the mine were also incorporated (Figures 5.7 and 5.8). The overall geochemical data sorted by rock type and ore-zone are shown in Appendix 2.2 and a summary with the average values is shown in Table 6.1.

For this comparison, the average compositions of basalts, rhyodacites and rhyodacitic dykes of the different ore zones defined, were normalised against the average compositions of their background counterparts sampled distal to ore. Specific gravity (S.G.) and magnetic susceptibility (M.S.) were also considered in the comparison. For the sake of simplicity, the alteration effects on basalts are referred to 3 mineral zones: pyrite (including pyrite and pyrite-chalcopyrite ore zones of Chapter 5), chalcopyrite (including chalcopyrite and chalcopyrite-bornite ore zones of Chapter 5), and bornite-chalcocite (including bornite and bornite-chalcocite ore zones of Chapter 5). For the rhyodacites, the alteration effects are described using the same pyrite and chalcopyrite zones of basalts, but the bornite-chalcocite zone is divided in 2 sub-zones: sodic and potassic, to emphasise the redistribution of alkalis. For rhyodacitic dykes, the alteration effects are referred only to 2 zones located at the roots of orebodies (the deep levels of the underground mine): pyrite and "pyrite-sphalerite-galena", the latter one describing samples from Paso Riel background area, which carries traces of those sulphides.

The results are presented in Table 6.2 and are plotted on semi-log graphs (Figures 6.6 to 6.10).

6.3.2. Rhyodacites Lithochemistry

In the rhyodacite flows (Figures 6.6 and 6.7) all mineralised zones are enriched with copper in comparison to background rocks, although the increment is less relevant in the pyrite zone. Sulphur also increases in most zones with the exception of bornite-chalcocite (sodic) subzone where it decreases slightly. There is no significant change in specific gravity and magnetic susceptibility (which is in general very close to zero; Figure 6.6, Table 6.1). Among major oxides SiO_2, TiO_2, Al_2O_3, and CaO show no significant changes; on the contrary, Na_2O, FeO (total), MgO, and P_2O_5 show a

Table 6.1 Geochemical Composition by Rock Type and Ore Zone. Average Values for Major and Selected Trace Elements

A) Major Elements

Host rock	Ore Zone (n)	Cu[1]	SG[2]	MS[3]	SiO_2	TiO_2	Al_2O_3	FeOT	MnO	MgO	CaO	Na_2O	K_2O	P_2O_5	LOI	C[4]	S	$Na_2O/$
		%	g/cm^3	K2	%	%	%	%	%	%	%	%	%	%	%	%	%	(Na_2O+K_2O)
rhyodacite	(background) (5)	0.05	2.58	0.00	69.46	0.41	14.34	2.02	0.12	0.31	4.40	4.85	3.96	0.13	3.88	0.79	0.81	0.55
rhyodacite	(py)+(py-cp) (8)	0.28	2.63	0.00	69.73	0.43	13.91	2.63	0.09	0.55	4.53	5.53	2.49	0.11	3.98	0.77	1.36	0.69
rhyodacite	(cp)+(cp-bn) (5)	3.23	2.61	0.00	67.72	0.41	15.03	2.79	0.09	0.31	4.28	6.44	2.74	0.20	2.79	0.73	1.95	0.70
rhyodacite	(sodic) (bn)+(bn-cc) (13)	2.65	2.60	0.01	68.71	0.48	15.23	2.19	0.08	0.36	3.79	7.32	1.66	0.18	2.73	0.65	0.72	0.82
rhyodacite	(potassic) (bn-cc) (4)	3.66	2.63	0.01	66.46	0.44	14.31	3.89	0.07	0.71	4.13	3.41	6.27	0.31	3.08	0.69	1.66	0.35
rhyodacitic dyke	background (py-sp-ga) (2)	0.01	2.61	0.01	69.12	0.45	13.25	3.04	0.10	2.24	3.46	3.47	4.79	0.09	3.32	0.55	0.29	0.42
rhyodacitic dyke	(py)+(py-cp) (4)	0.27	2.68	0.04	68.67	0.42	14.15	4.22	0.10	1.32	2.79	3.69	4.52	0.13	4.37	0.48	2.44	0.45
basalt	(background) (4)	0.01	2.90	2.03	51.56	0.69	19.17	7.97	0.46	5.49	9.44	3.03	2.05	0.13	2.62	0.11	0.01	0.60
basalt	(py)+(py-cp) (7)	0.15	2.79	0.35	52.70	0.71	18.44	7.67	0.53	4.76	8.28	5.34	1.45	0.12	6.50	1.04	1.21	0.79
basalt	(cp)+(cp-bn) (5)	2.08	2.78	0.04	51.03	0.73	18.14	8.26	0.58	3.56	9.43	5.91	2.05	0.31	6.64	1.41	1.15	0.74
basalt	(bn)+(bn-cc) (sodic) (6)	2.09	2.79	0.15	51.71	0.75	19.33	9.21	0.81	5.86	5.83	5.33	1.03	0.14	6.18	0.77	0.40	0.84

B) Selected Trace Elements

Host rock	Ore Zone (n)	Ag	As	Cu[5]	Co	Ni	Pb	Zn	Ba	Rb	Sr	Y	Zr	Hf	Nb	Th	U	V
		ppm	ppm	ppm	ppm	ppm	ppm	ppm	ppm	ppm	ppm	ppm	ppm	ppm	ppm	ppm	ppm	ppm
rhyodacite	(background) (5)	<1	4	115	7.6	23	4	9	561	96	60	24	185	5	6	9	2.5	53
rhyodacite	(py)+(py-cp) (8)	<1	58	755	10.1	9	5	15	415	58	66	26	204	6	6	9	2.3	41
rhyodacite	(cp)+(cp-bn) (5)	3	36	25660	2.7	7	<5	12	411	55	47	26	194	5	6	8	2.2	35
rhyodacite	(sodic) (bn)+(bn-cc) (13)	4	2	16828	2.9	11	5	20	158	35	43	26	194	5	6	8	2.3	48
rhyodacite	(potassic) (bn-cc) (4)	11	66	44600	1.6	<5	6	<5	711	135	33	23	179	6	5	7	2.0	65
rhyodacitic dyke	background (py-sp-ga) (2)			100					580	79	47	27	210		5			
rhyodacitic dyke	(py)+(py-cp) (4)			4816					476	84	56	23	181		6			
basalt	(background) (4)	<1	3	66	30.3	32	<5	172	543	67	363	15	43	<1	<1	<1	<0.5	243
basalt	(py)+(py-cp) (7)	<1	29	916	44.4	44	39	153	201	57	175	15	50	<1	1	1	0.6	241
basalt	(cp)+(cp-bn) (5)	<1	<1	2968	22.8	32	<5	155	507	53	168	13	35	<1	1	1	<0.5	263
basalt	(bn)+(bn-cc) (sodic) (6)	2	15	9772	28.0	30	<5	213	283	34	125	16	57	<1	2	<1	<0.5	253

1) Cu assay value for 3 m drill core interval, 2) Specific gravity, 3) Magnetic susceptibility, 4) Inorganic carbon, 5) Cu value for whole rock chemical analysis

Table 6.2.- Geochemical Comparison Between Mineralised and Background Rocks.

Ore Zones / Background Ratios* for Major and Selected Trace Elements

A.- Major Elements

Host rock	Ratios	Cu[1]	SG[2]	MS[3]	SiO_2	TiO_2	AL_2O_3	FeO_T	MnO	MgO	CaO	Na_2O	K_2O	P_2O_5	LOI	C[4]	S	$Na_2O / (Na_2O+K_2O)$
rhyodacite	(py)+(py-cp) / background	5.05	1.02		1.00	1.05	0.97	1.30	0.78	1.74	1.03	1.14	0.63	0.84	1.03	0.97	1.67	1.25
rhyodacite	(cp)+(cp-bn) / background	58.7	1.01		0.97	1.00	1.05	1.38	0.75	1.00	0.97	1.33	0.69	1.50	0.72	0.92	2.40	1.28
rhyodacite	sodic (bn)+(bn-cc) / background	48.3	1.01		0.99	1.18	1.06	1.08	0.65	1.15	0.86	1.51	0.42	1.32	0.70	0.83	0.88	1.48
rhyodacite	potassic (bn)+(bn-cc) / background	81.3	1.02		0.96	1.06	1.00	1.93	0.60	2.26	0.94	0.70	1.58	2.34	0.79	0.87	2.05	0.64
basalt	(py)+(py-cp) / background	11.3	0.96	0.17	1.02	1.03	0.96	0.96	1.15	0.87	0.88	1.77	0.71	0.95	2.48	9.83	121	1.32
basalt	(cp)+(cp-bn) / background	156	0.96	0.02	0.99	1.06	0.95	1.04	1.27	0.65	1.00	1.95	1.00	2.37	2.54	13.3	115	1.25
basalt	(bn)+(bn-cc) / background	157	0.96	0.07	1.00	1.08	1.01	1.15	1.77	1.07	0.62	1.76	0.50	1.06	2.36	7.22	40	1.40

B.- Selected Trace Elements

Host rock	Ratios	Ag	As	Cu[5]	Co	Ni	Pb	Zn	Ba	Rb	Sr	Y	Zr	Hf	Nb	Th	U	V
rhyodacite	(py)+(py-cp) / background	1.0	15.5	6.6	1.3	0.38	1.0	1.7	0.74	0.60	1.10	1.09	1.10	1.12	1.01	0.93	0.92	0.78
rhyodacite	(cp)+(cp-bn) / background	5.0	9.6	223	0.3	0.30	0.6	1.3	0.73	0.58	0.80	1.09	1.05	1.00	1.07	0.83	0.87	0.67
rhyodacite	sodic (bn)+(bn-cc) / background	8.7	0.6	146	0.4	0.48	1.1	2.2	0.28	0.36	0.73	1.09	1.05	1.00	1.11	0.83	0.93	0.92
rhyodacite	potassic (bn)+(bn-cc) / background	23	17.6	388	0.2	0.11	1.4	0.3	1.27	1.40	0.55	0.96	0.96	1.10	0.86	0.76	0.80	1.24
basalt	(py)+(py-cp) / background	1.0	10.1	14	1.5	1.38	16	0.9	0.37	0.85	0.48	1.00	1.17					0.99
basalt	(cp)+(cp-bn) / background	1.0	0.2	45	0.8	1.00	1.0	0.9	0.93	0.79	0.46	0.87	0.83					1.08
basalt	(bn)+(bn-cc) / background	4.0	5.3	147	0.9	0.95	1.0	1.2	0.52	0.51	0.34	1.11	1.34					1.04

(*) Ratios calculated using averages of Table 6.1. When an average was below than a detection limit, half of this limit was used to calculate the ratio

1) Cu assay value for 3 m drill core interval, 2) Specific gravity, 3) Magnetic susceptibility, 4) Inorganic carbon, 5) Cu value for whole rock chemical analysis
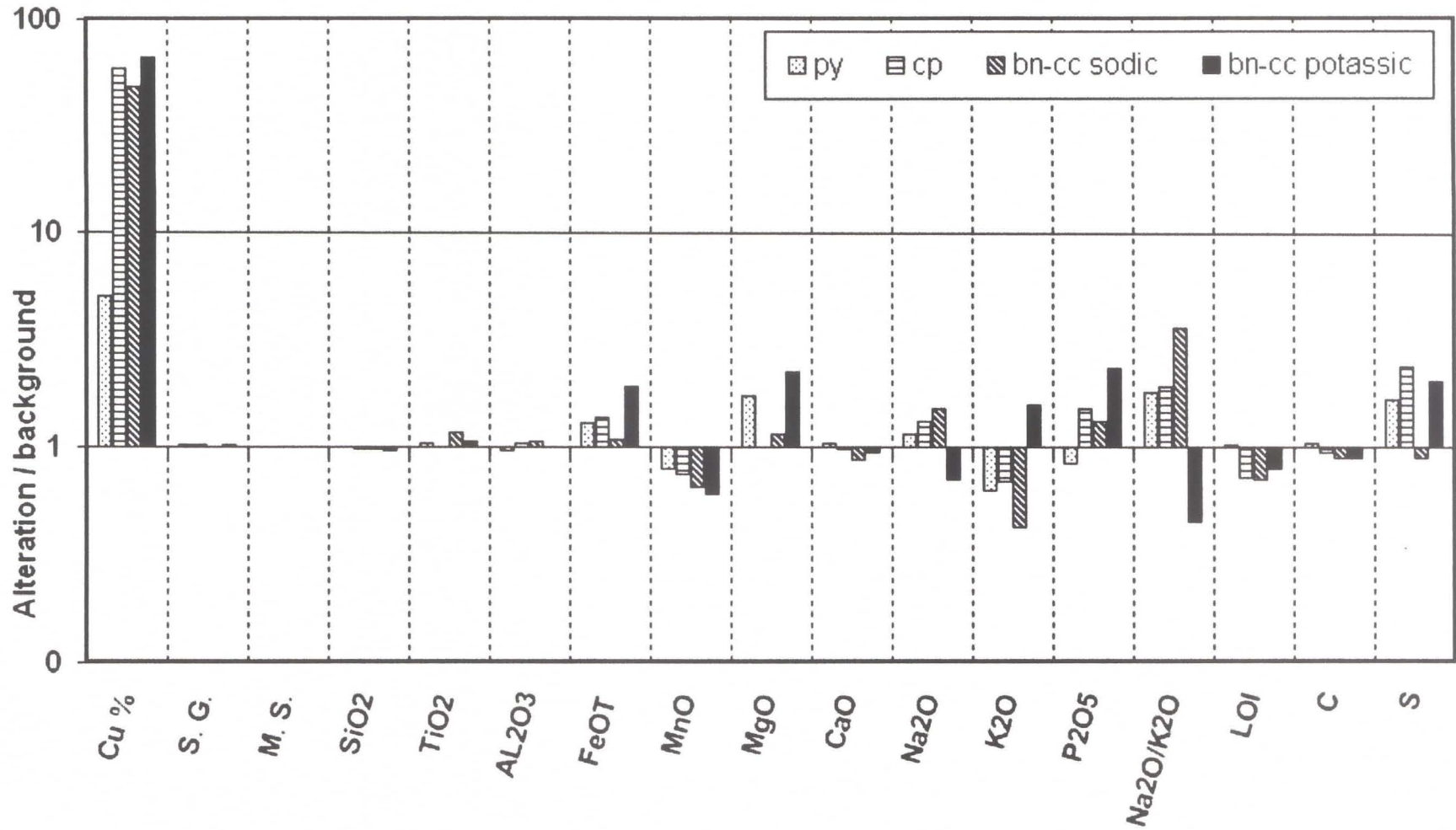
Figure 6.6. Alteration of host rhyodacites, El Soldado Mine – major elements
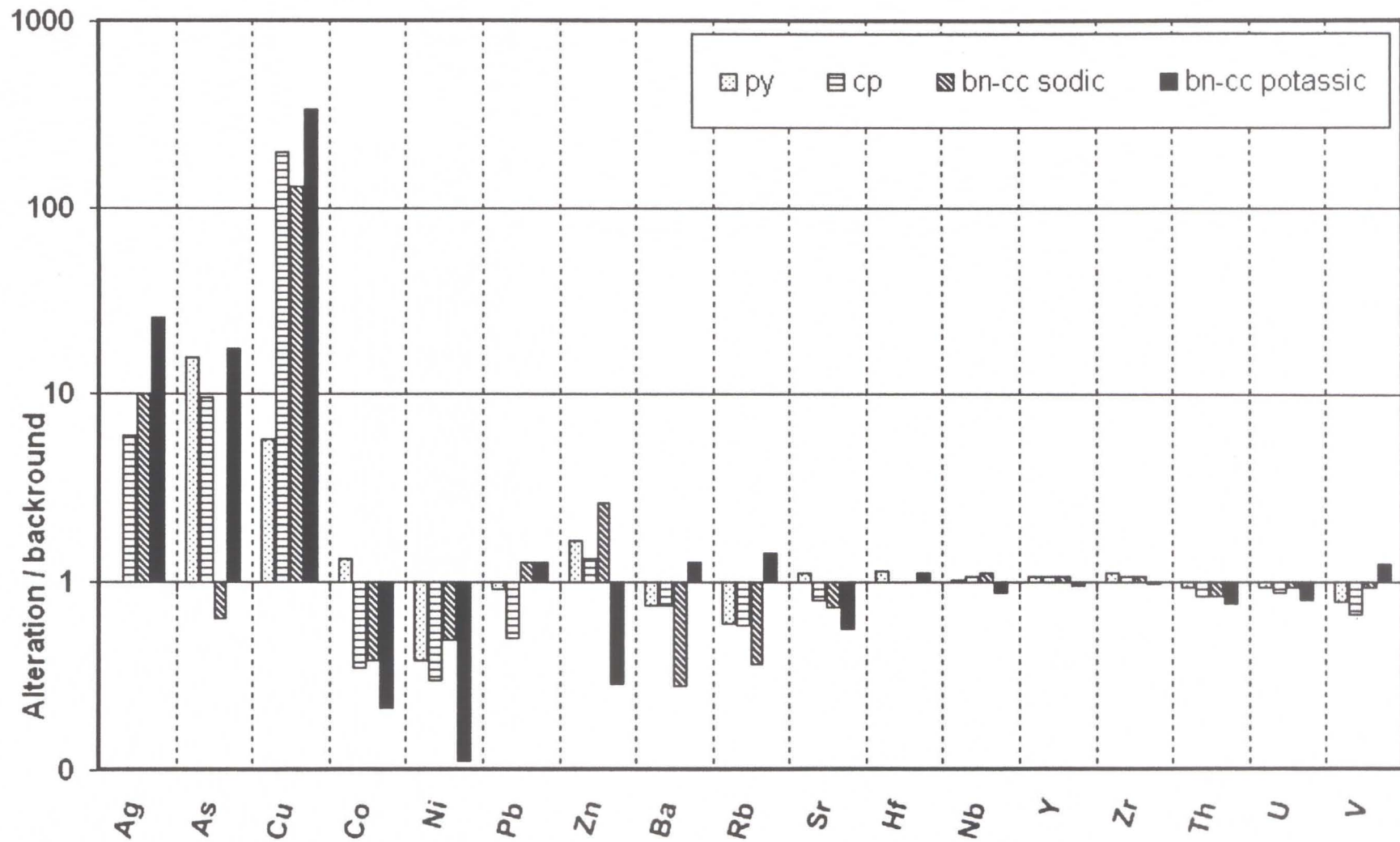
Figure 6.7. Alteration of host rhyodacites, El Soldado Mine – selected trace elements.

moderate increase, and K_2O and MnO exhibit an important decrease in all zones (Figure 6.6). These changes can be related to albitisation (gain of Na_2O and loss of K_2O), chloritisation (gain of MgO and FeO), hematitisation (gain of FeO) and the presence of secondary apatite (increase of P_2O_5) in mineralised rhyodacites, all alteration types that were described in the previous section. An important exception is the presence of a sub-zone with an enrichment in K_2O (values up to 9.4 wt %) and a decrease in Na_2O (values down to 1.1 wt %), within the bornite-chalcocite ore zone, which was detected in the vicinity of major faults in the core of Valdivia Sur chimney (Figure 6.12, below). This anomaly is explained by the deposition in this sub-zone of K-feldspar (microcline) replacing albite (Figure 6.5a, b). The decrease in MnO is correlated with a slight decrease of CaO, because MnO is a minor constituent in calcite (Appendix 3.1). Inorganic C and LOI show a similar behaviour than MnO reflecting that rocks selected as background rhyodacite were somewhat enriched in carbonate in comparison with the mineralised ones. This fact is in apparent contradiction with the widespread calcite alteration related with ore zones (see previous section), but could be explained because calcite occurs mostly in veins (Figure 6.1), which were not included in the analysed samples. In retrospect, other samples, preferably with no carbonate veining should have been selected as background samples.

It is important to emphasise that major-oxide data in rhyodacites reflect very well the widespread alteration to albite and chlorite and the locally important alteration to K-feldspar present within orebodies. A good indicator of albitisation is the ratio: $Na_2O/(Na_2O+K_2O)$, which steadily increases from an average of 0.55 in background rhyodacites to 0.69 in the pyrite zone, 0.70 in the chalcopyrite zone, and 0.82 in the bornite-chalcocite (sodic) sub-zone (Table 6.1; Figure 6.11 through 6.14, below). According to whole rock analyses in most albitised samples, Na_2O increases up to values above 10 wt % (from an average in background rhyodacites of 4.85 wt %) whereas K_2O decreases down to values of 0.01 wt % (from an average in background rhyodacites of 3.96 wt %; Appendix 2.2). Conversely within the potassic rich bornite-chalcocite sub-zone, K_2O increases up to 9.9 wt % and Na_2O decreases down to 1.1 %, and consequently the $Na_2O/(Na_2O+K_2O)$ ratio has lower values (average 0.35) reflecting the alteration to

microcline (Appendix 2.2). Chloritisation, represented by increase in FeO and MgO is also evident in all zones but particularly in the potassic rich bornite-chalcocite sub-zone, where those oxides have the major increments (Table 6.2; Figure 6.6); their change is consistent with the abundant chlorite associated with microcline observed as gangue in this sub-zone.

The metallic trace elements have different behaviours although Ag, As, Pb, and Zn show in general important increments within mineralised zones (Figure 6.7). Ag increases in the chalcopyrite and bornite-chalcocite (sodic and potassic) zones but was not detected in the pyrite zone (Table 6.1). This relationship indicates that Ag was deposited associated with copper mineralisation during Stage II as an impurity incorporated within copper sulphides (particularly bornite and chalcocite; see Appendix 3.1), yet Ag is not present in pyrite (mostly diagenetic in origin). Most ore zones (including pyrite zone) are enriched in Zn and As (Figure 6.7), suggesting that these elements where incorporated into the rhyodacites during Stage I as sphalerite and arsenopyrite (both phases described as diagenetic; see Chapter 5). Pb shows minor increments in the bornite-chalcocite zones (sodic and potassic), but decreases in the chalcopyrite zone and shows no change in the pyrite zone (Figure 6.7). Co and Ni are depleted in most ore zones but these results are not reliable taking in account that their values are too close to the detection limits (Table 6.1). In any case it is clear that those metals are not enriched in the ore zones. As expected, Ba and Rb have a behaviour parallel to that of K_2O (Figure 6.7), with important depletions in all zones with the exception of the potassic bornite-chalcocite sub-zone where both are enriched. This implies that Ba and Rb can be used as good indicators of alteration (albitisation) related to copper ore. Yet Sr behaves similarly to CaO, C, and LOI, indicating that it is included within calcite (figure 6.7). The mobility pattern for Rb and Sr has instructive implications for any geochronological and petrogenetic use of Sr isotopes in investigating these systems. As expected, generally immobile Y, Zr, Hf, and Nb show no change (Tables 6.1, 6.2). Th, U, and V display weak depletions (Figure 6.7) although again those results are not very reliable because the values are very close to detection limits.

6.3.3. Lithochemsitry of Rhyodacitic Dykes

As a complement to previous analyses the alteration of rhyodacitic dykes was investigated in a few samples collected from the southern dyke in Valdivia Sur and Paso Riel mining blocks, representing the deep roots of orebodies. The dyke was normalised against the same background rhyodacite flows above (Tables 6.1 and 6.2) because of the absence of samples of unaltered dyke protoliths. As expected, the lithochemical behaviour of the rhyodacitic dyke (Figure 6.8) is similar to rhyodacite flows, although there are some relevant differences (compare Figures 6.8, 6.6, and 6.7).

The pyrite zone (Valdivia Sur mine block) shows no significant gain or loss in SiO_2, TiO_2 and Al_2O_3; an important enrichment in Cu, S, FeO (total), and MgO, and depletions in CaO, and MnO. All these major-oxides and elements have similar behaviours in the dyke than in flow rocks (Figures 6.6 and 6.8). The gain in MgO and FeO (total) is related to chloritisation. The main difference with respect to flows is that the dyke in the pyrite zone shows increments in K_2O (up to 7.75 wt %) and depletions in Na_2O. The average value for $Na_2O/(Na_2O+ K_2O)$ is 0.45 (Table 6.2, Figure 6.12, below). This alkali mobility in the rhyodacitic dyke rock may imply an alteration to microcline (which was not revealed petrographically), similar to that observed in the bornite-chalcocite sub-zone in the flows (see previous section), but it could simply represent a different content of alkalis in the dyke, product of early low-grade metamorphism. The relatively low values of Ba do not support the presence of microcline (Table 6.1; Figure 6.8). In any case albitisation related to mineralisation was not detected in this dyke.

The sphalerite-pyrite-galena zone in the dyke (Paso Riel mining block) has a similar behaviour to that of the pyrite zone, highlighting a gain in MgO that implies a strong chloritisation. The main difference is that Cu and S are depleted (Figure 6.8).

In summary, the southern rhyodacitic dyke mineralised with pyrite-(chalcopyrite) or traces of sphalerite-pyrite-galena at deep levels of the mine, shows an important alteration to chlorite (gain in MgO and FeO) and relatively highest potassium values which could reflect an alteration to K-feldspar or a different original content of alkalis previous to copper mineralisation. Albitisation, which is the main alteration related to ore in other host rocks, was not detected in this unit.
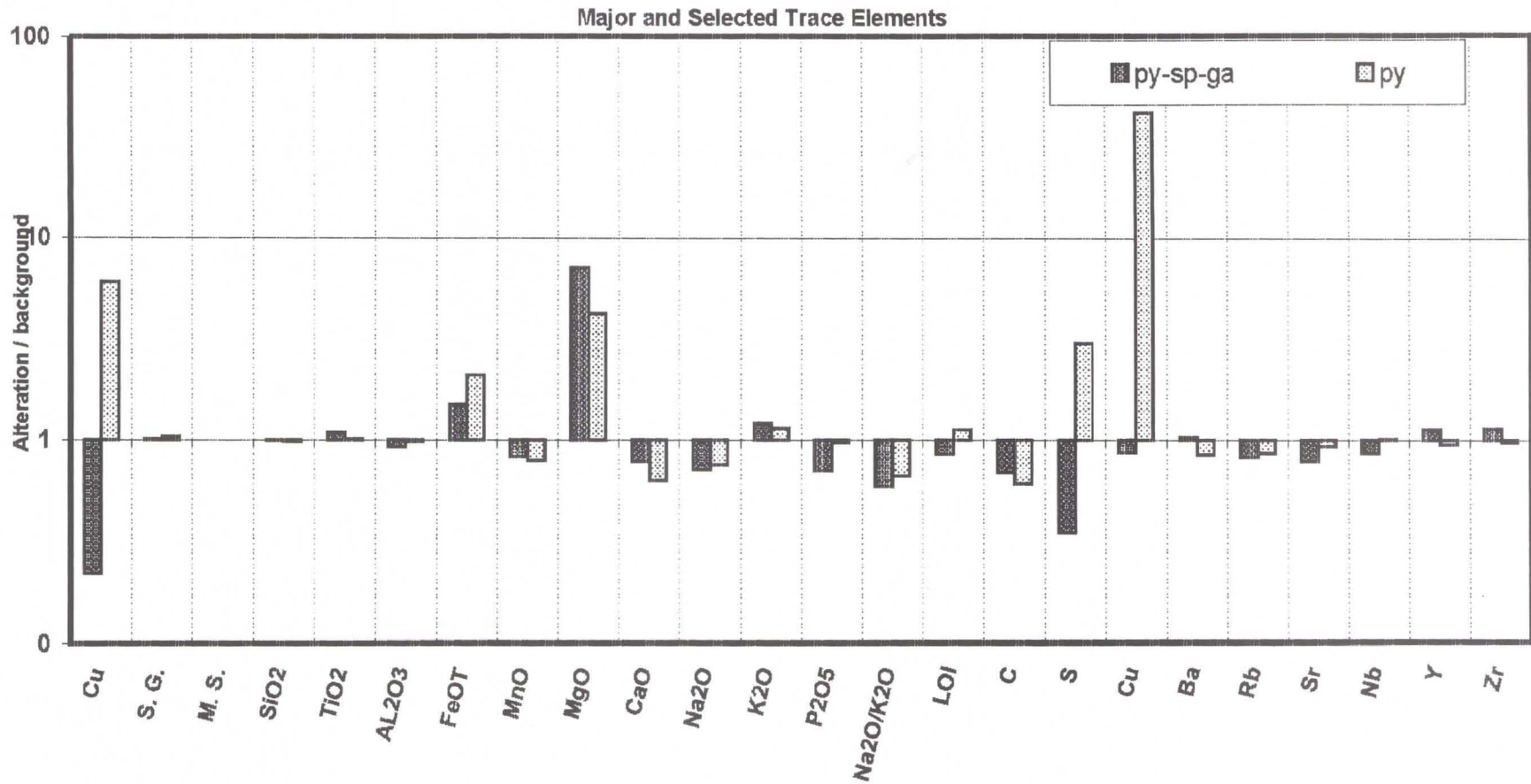
Figure 6.8. Alteration of host rhyodacitic dykes, El Soldado mine, major and selected trace elements.

6.3.4. Lithochemistry of Basalts

The lithochemistry behaviour of basalts (Figures 6.9 and 6.10) is, in general, similar to that in rhyodacites, although there are some minor differences. Again, all mineralised zones are enriched in Cu and S and there is no change in specific gravity. In contrast with the rhyodacites, in the basalts there is a drastic loss of magnetic susceptibility in all mineralised zones, reflecting the wholesale sulphidation of magnetite, associated with a large gain in S; this extreme effect should be useful in exploration. Among the major oxides again there is no relevant change in TiO_2, Al_2O_3, and SiO_2 (no hint of silicification, even in the bornite-chalcocite zone), and also (and contrary to rhyodacites) in FeO (total). More significant are the increment in Na_2O and the depletion in K_2O in all zones, which reflect the widespread albitisation observed in mineralised basalts (see previous section). $Na_2O/(Na_2O+K_2O)$ ratio shows an increment from 0.60 in background basalts to 0.79 in the pyrite zone, 0.74 in the chalcopyrite zone and 0.84 (Table 6.2, Figures 6.11 through 6.14) in the bornite-chalcocite zone, backing up the albitisation. CaO and MgO show weak depletions in most zones indicating that despite of noticeable deposition of calcite, chlorite and epidote, these elements were slightly depleted in mineralised basalts, after alteration of primary minerals such as plagioclase and pyroxene. Yet MgO shows a small increment in the bornite-chalcocite zone, which can be associated with the strong chloritisation observed there. Again P_2O_5 shows an important increment, particularly in the chalcopyrite zone, which is related to the presence of secondary apatite. In contrast with the rhyodacites, inorganic C, MnO, and LOI all increment in mineralised zones, reflecting the alteration to calcite.

Most of metallic trace elements show increments in mineralised basalts (Tables 6.1 and 6.2; Figure 6.10) but the analysis of them is complicated because many samples yield values below detection limits (Appendix 2.2; Table 6.1). Ag was detected only in the bornite-chalcocite zone corroborating it is a minor constituent of these two sulphides. Arsenic is lost within the chalcopyrite zone, but increases in the other two zones. Zentilli et al. (1997) showed how arsenopyrite, probably formed early (Stage I), has been almost totally replaced by bornite-chalcocite; it appears that some of the As was redistributed in Cu sulphides later during stage II. Pb was detected only in the pyrite zone (Table 6.1) and
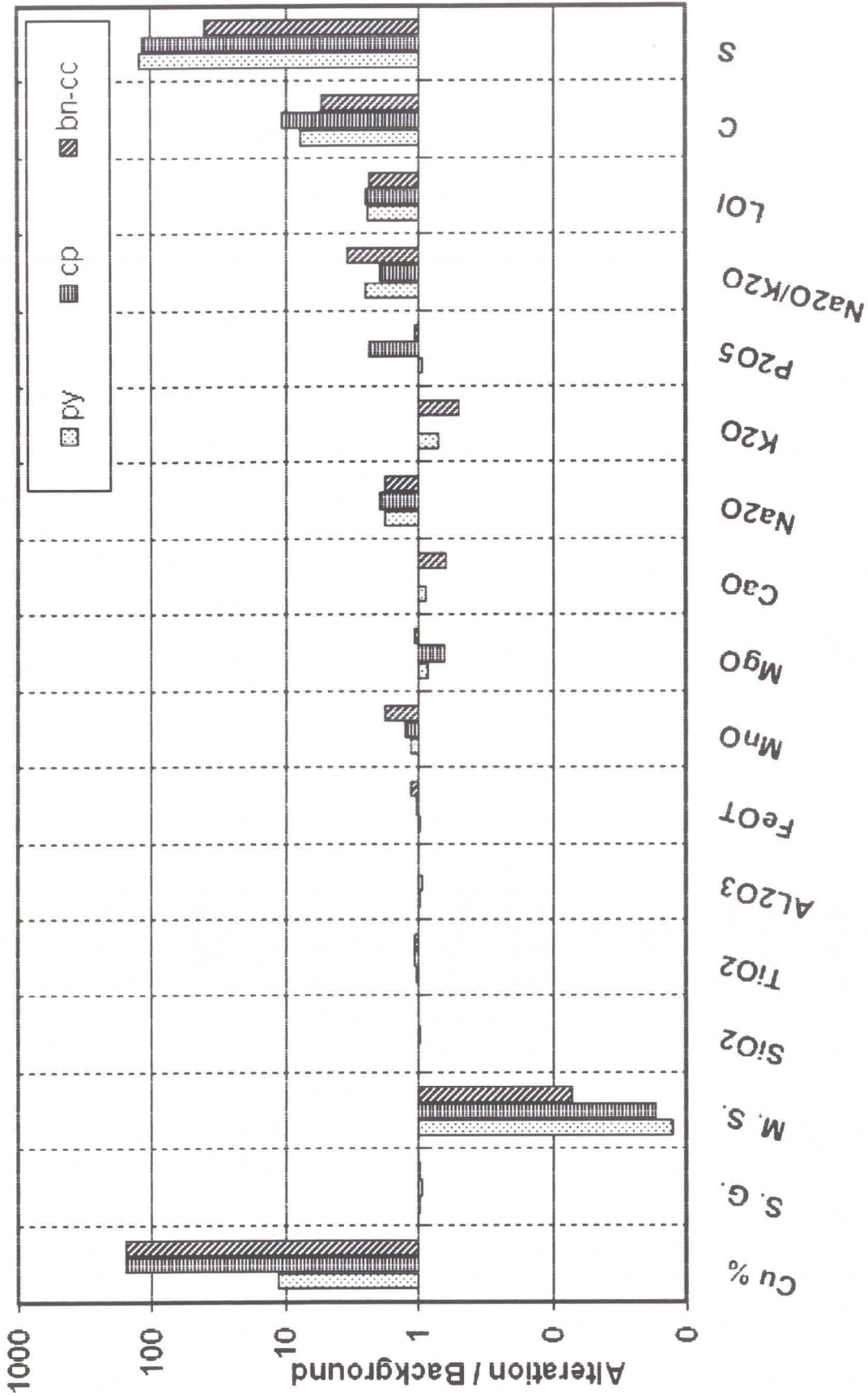
Figure 6.9. Alteration of host basalts, El Soldado Mine – major elements.
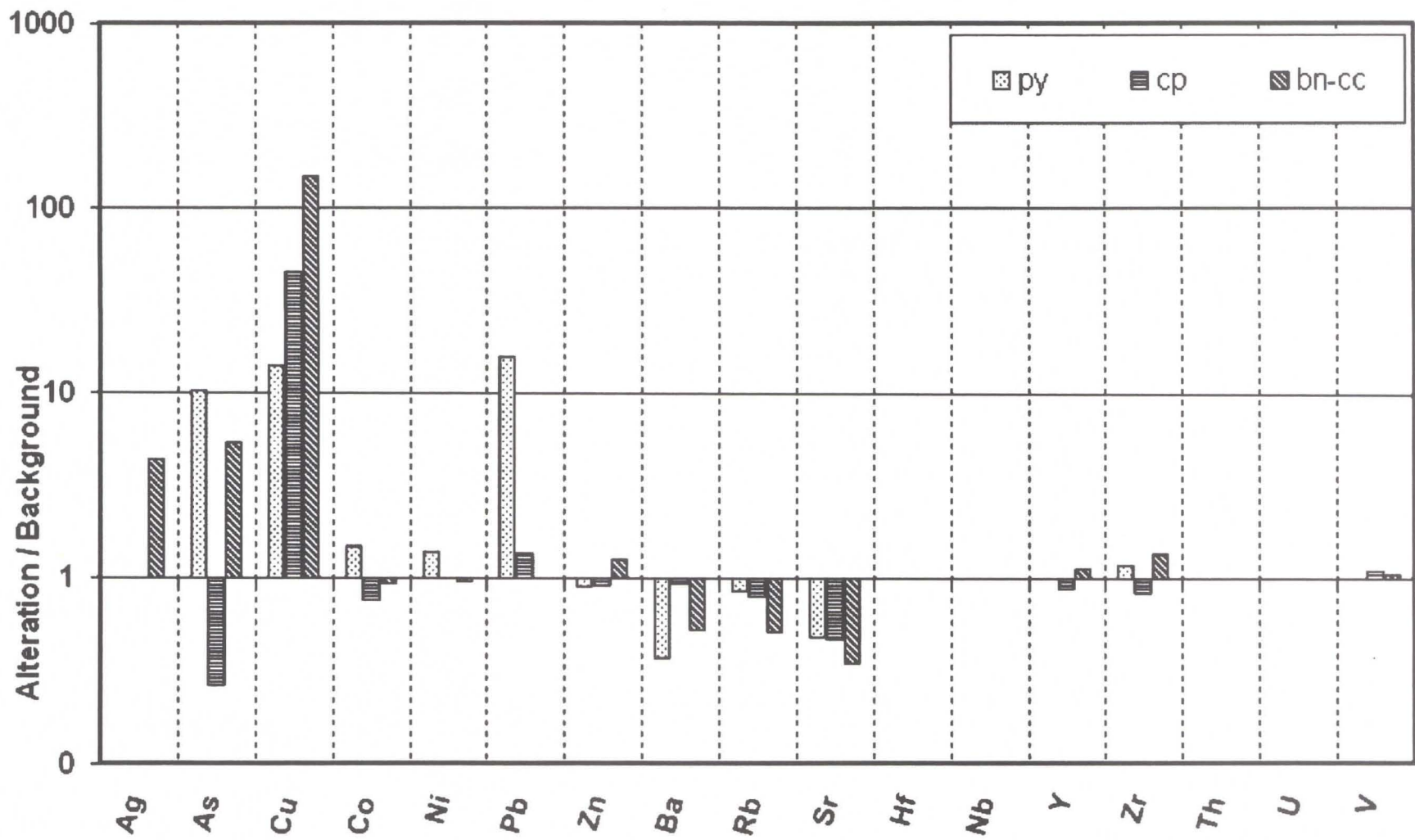
Figure 6.10. Alteration of host basalts, El Soldado Mine – selected trace elements.

it is associated with the scarce galena observed with pyrite and deposited during Stage I (see Chapter 5). Co and Ni show weak increments in the pyrite zone and depletions or no change in the other two (Figure 6.10). These results suggest these elements are associated with pyrite (Co was detected as a minor constituent in pyrite by microprobe) and were incorporated into the basalts during diagenesis (Stage I). Zn shows no important changes. More significant are the depletions in Ba, and Rb (which behave similarly to K_2O) and Sr (which behaves akin to CaO). Again Ba and Rb are good indicators of albitisation related to copper ore and could be used for exploration. Y, Zr, and V show no significant changes and Th, U, Hf, and Nb were not statistically analysed because most samples yield values below detection limits (Table 6.1).

6.3.5. Lithochemistry of Sedimentary-Volcaniclastic Rocks and Mafic Dykes

The alteration effects on these rocks were not studied in detail because they are not important as host rocks, yet some observations based on limited analysed samples are described.

Volcanic sedimentary rocks have a variable composition; thus it is not possible to select a background precursor to be compared with the altered-mineralised samples. Whole rock analyses of altered-mineralised volcanic sediments show a great dispersion in all major-oxides and trace elements (Appendix 2.2), which reflects the varied composition of rocks and the superimposed alteration effects. Albite, calcite, chlorite, and K-feldspar (Figure 6.5d) have all been observed to alter mineralised sediments, and this observation is supported by the relatively high values of Na_2O, CaO, MgO and K_2O of some mineralised samples (Appendix 2.2). Albitisation related to copper ore is also evident considering the $Na_2O/(Na_2O + K_2O)$ ratio, which increases from an average value of 0.78 in barren sediments with traces of pyrite-chalcopyrite to 0.84 and 0.83 in sediments mineralised with chalcopyrite and bornite-chalcocite (Appendix 2.2, Figures 6.12 and 6.13). Albitisation can be illustrated comparing samples MP855 and MP854 collected in the same sedimentary horizon in the apical part of Valdivia Sur orebody (Figures 5.6 and 6.12). Sample MP855 is a green rock, barren (Cu: 0.04 %) with traces of pyrite, which has a high content of K_2O (6.67 wt %) possibly associated with the Figure
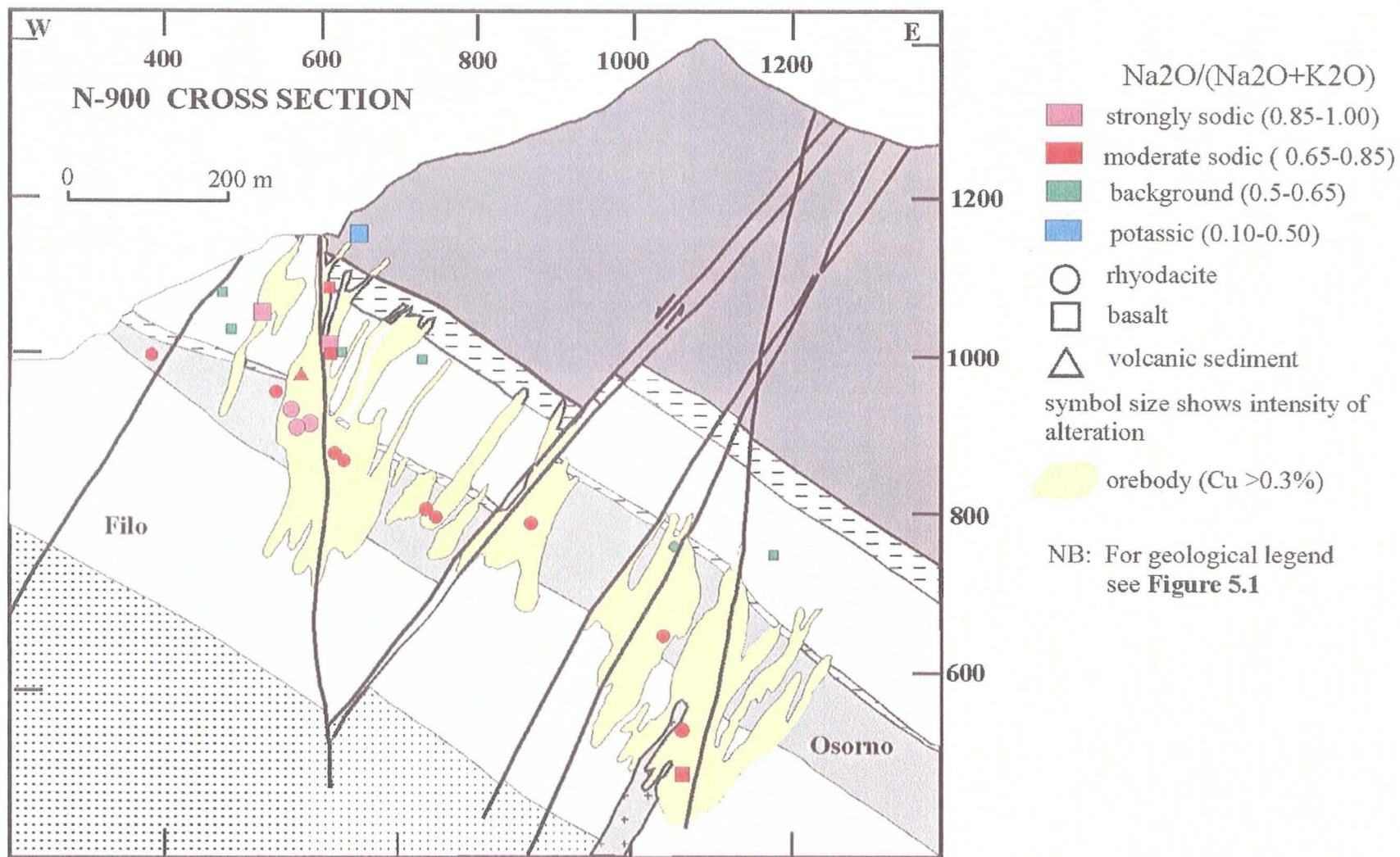
Figure 6.11. Sodic alteration related to copper mineralisation, cross-section −900 N.

Na2O/(Na2O+K2O)

strongly sodic (0.85-1.00)

moderate sodic (0.65-0.85)

background (0.5-0.65)

potassic (0.10-0.50)

○ rhyodacite

□ basalt

△ volcanic sediment

symbol size shows intensity of alteration

orebody (Cu >0.3%)

NB: For geological legend see **Figure 5.1**
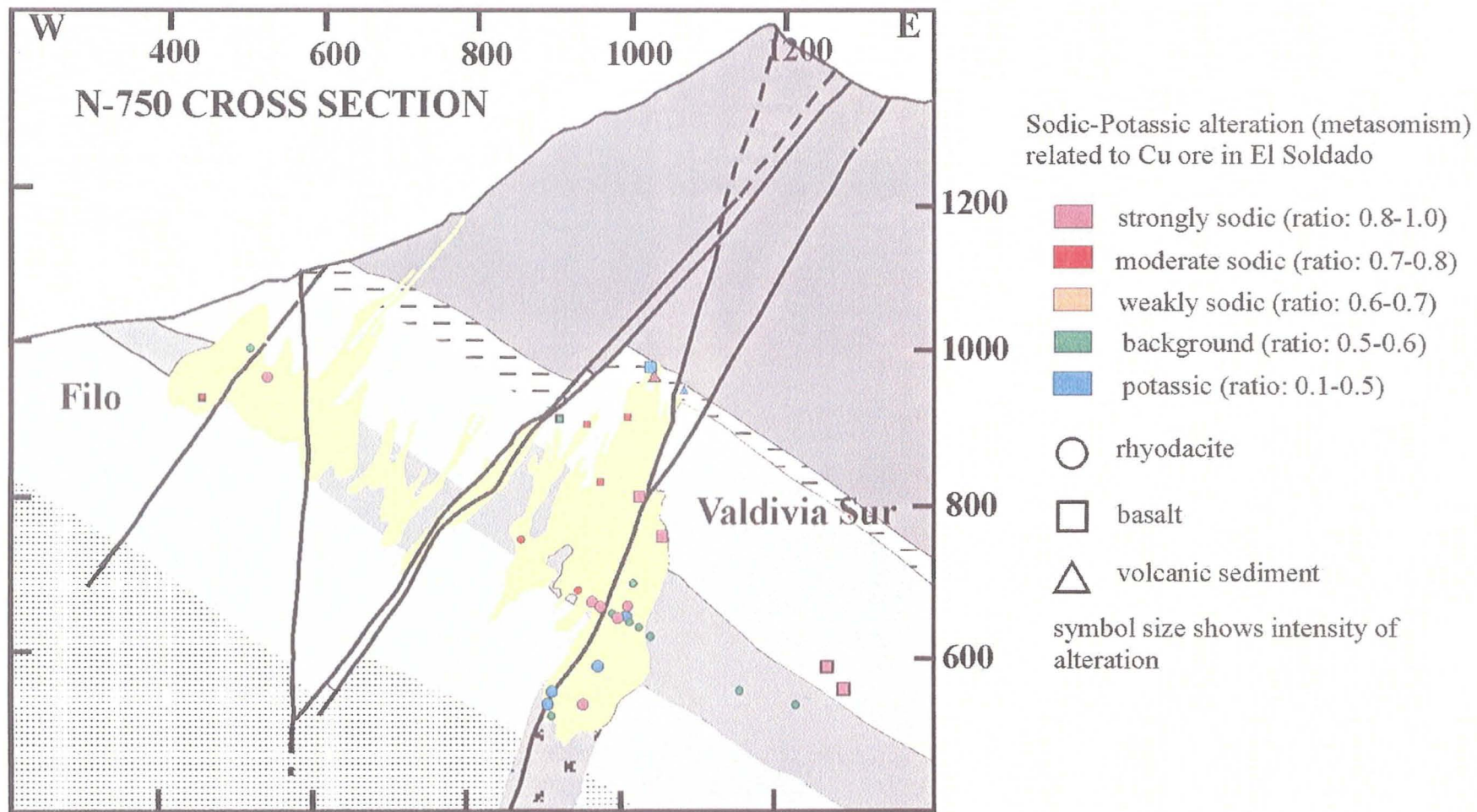
Figure 6.12. Sodic-potassic alteration related to copper mineralisation, cross-section –750 N.
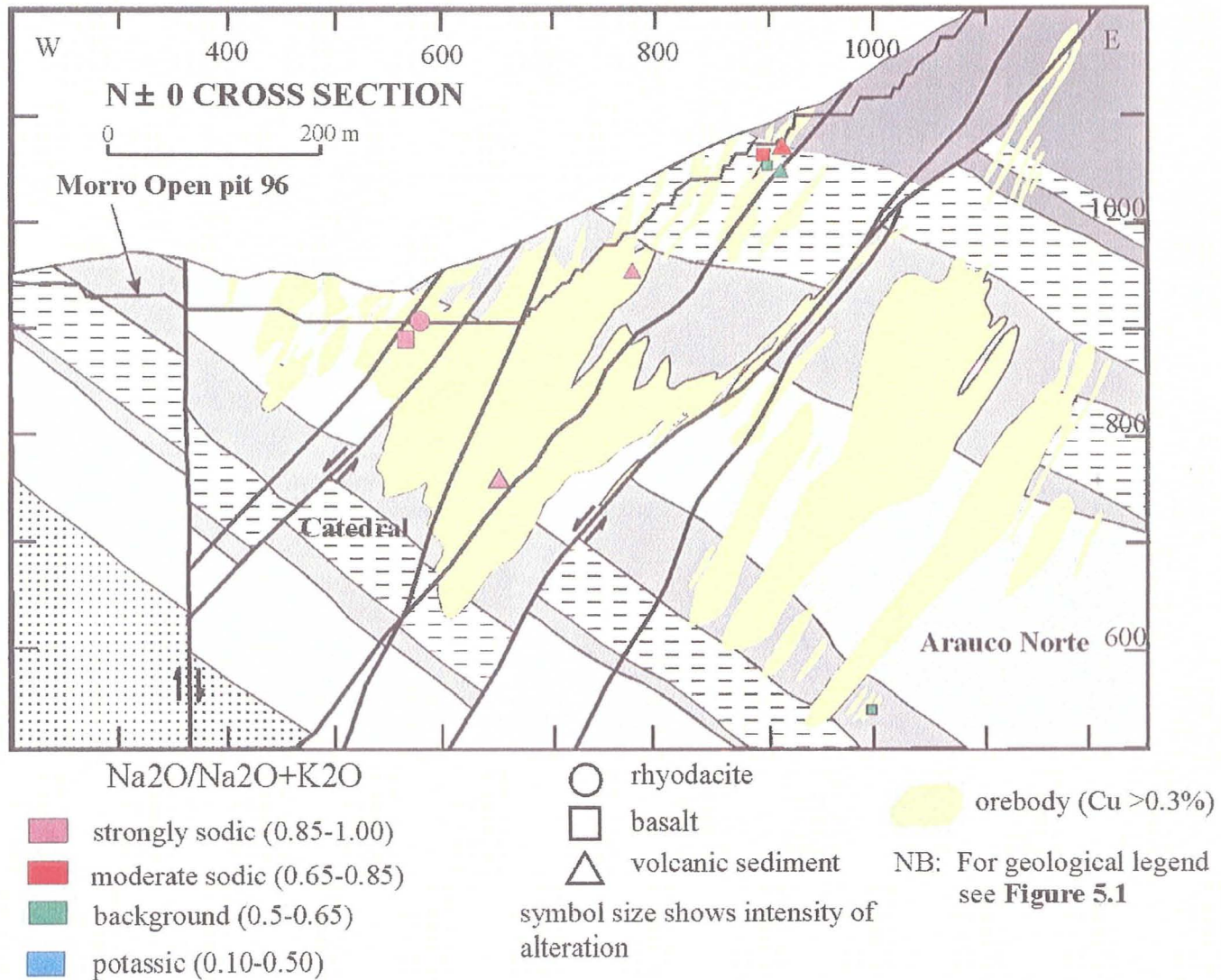
Figure 6.13. Sodic alteration related to copper mineralisation, cross-section +/- 0 N.

The figure contains the following labels and legend:

N ± 0 CROSS SECTION

W   400   600   800   1000   E

0   200 m

Morro Open pit 96

Catedral

Arauco Norte 600

1000

800

Na2O/Na2O+K2O

strongly sodic (0.85-1.00)
moderate sodic (0.65-0.85)
background (0.5-0.65)
potassic (0.10-0.50)

○ rhyodacite
□ basalt
△ volcanic sediment

symbol size shows intensity of alteration

orebody (Cu >0.3%)

NB: For geological legend see Figure 5.1
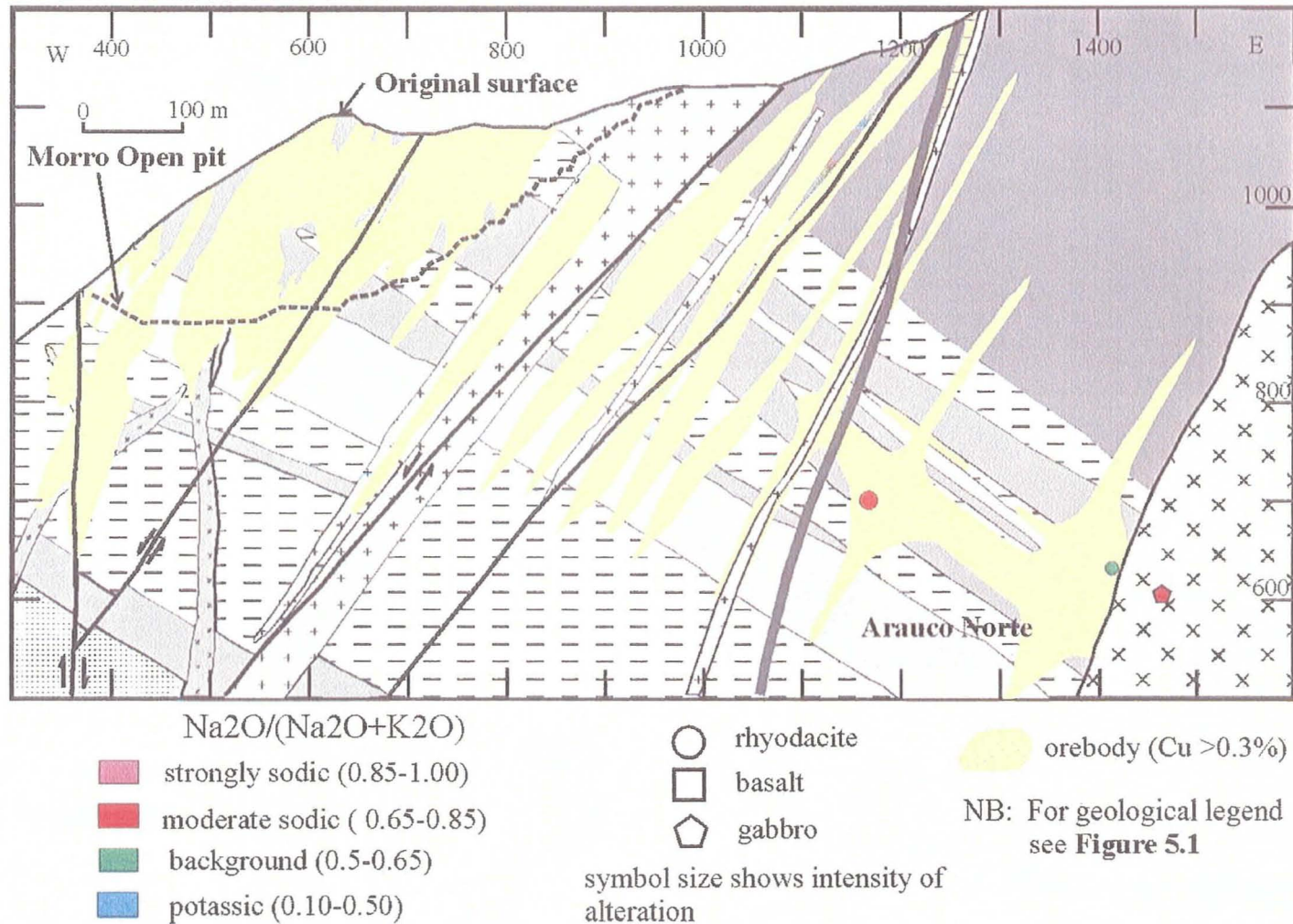
N+250 CROSS SECTION

Figure 6.14. Sodic alteration related to copper mineralisation, cross-section +250 N.

presence of illite-sericite in its matrix-cement and a low content of Na_2O (0.58 wt %). Sample MP854, taken 45 m away than the previous, is a light pink rock mineralised with bornite (Cu: 0.91 %) that has high Na_2O (4.89 wt %) and low K_2O (0.30 wt %) values. These example shows the extreme remobilisation of alkalis associated with the hydrothermal mineralisation of copper (see also microprobe images in Appendix 3.3).

Mafic dykes are not important as host rocks and most of them are barren. Yet copper mineralisation and hydrothermal alteration is commonly observed concentrated only along their borders (Figure 3.12a) suggesting they acted as impervious barriers to the mineralising fluids. Nevertheless many dykes, particularly the thinner ones (<2 m of thickness) are mineralised and present a strong alteration to calcite, chlorite, albite, K-feldspar, and or epidote. One dyke from the upper part of Valdivia Sur that is mineralised with bornite-chalcocite (sample MP772) has a relatively high value of K_2O (6.35 %, Appendix 2.2; Figures 5.6 and 6.12) indicating a potassic alteration confirmed by cobaltinitrite staining (Appendix 6). According to drill-core-mapping, albitisation is the most extended alteration in mineralised mafic dykes, but no chemical analyses of albitised dykes are available.

6.4. Comparison with Other Major Strata-Bound Copper Deposits

Hydrothermal alteration associated with volcanic hosted Chilean strata-bound copper deposit has been subject of much discussion and controversy and contrary to other major deposits, such as porphyry coppers or epithermal gold-silver deposits, there is still no generally accepted model which describes and explains the phenomenon. Originally the alteration effects were sub-estimated and the strata-bound deposits were though to be syngenetic (e.g. Ruiz et al., 1965). Later it became evident that, despite the relatively paucity of gangue minerals and the fact that host rocks preserve their original textures, these deposits have an associated hydrothermal alteration. This alteration is characterised by the assemblage of albite-calcite-chlorite-hematite-quartz-epidote-titanite ± K-feldspar-minor sericite (e.g. Sato, 1984; Camus, 1985). In general the view that this local hydrothermal alteration is weak and difficult to distinguish from regional low-grade metamorphism (prehnite-pumpellyte and greenschist facies) that affects the barren

volcanic country rocks, has predominated (e.g. overviews by Sato, 1984; Sillitoe, 1992). Although this concept might be valid for some deposits hosted by volcano-sedimentary units (e.g. Talcuna, Cerro Negro), detailed petrographic and lithochemical studies performed at larger (and economically more relevant) strata-bound volcanic-hosted deposit such as Mantos Blancos, Punta del Cobre and Mantos Blancos, have unequivocally established, similarly to this thesis, that hydrothermal alteration related to ore is stronger than previously assumed and characterised by pervasive alkali metasomatism, particularly sodium and locally potassium (Chavez, 1985; Marschik and Fontboté, 1996; Boric et al., 2002).

6.4.1. Mantos Blancos (based on Chavez, 1985)

Mantos Blancos (Chapter 2; Figure 2.2) is the largest strata-bound Cu-(Ag) deposit of Chile and has many similarities to El Soldado in its pattern of mineralisation-alteration. At Mantos Blancos pyrite-chalcopyrite-bornite-chalcocite-hematite hypogene ore is hosted by a bimodal volcanic Upper Triassic(?)-Lower Jurassic sequence composed of calc-alkaline rhyodacites and andesites, which present an extensive regional albitisation and are called "*keratophyres*". Petrography indicates that main alterations related to ore are albitisation, chloritisation, and hematitisation. Calcite is also a widespread and an important alteration mineral. Silicification and sericitisation, although recognised, are not significant in comparison to the extensive albitisation. Titanite predominates in background volcanic rocks and rutile in altered-mineralised ones. Lithochemistry confirmes a pervasive metasomatism, which includes widespread addition of Na_2O and removal of CaO, and K_2O (and Rb) associated with albitisation. Local MgO, and FeO enrichments are observed associated with chloritisation. Chavez (1985) concluded that chloritisation, and hematitisation were simultaneous with copper mineralisation but he did not specify if albitisation was a local phenomena related to ore or an expression of the regional low-grade metasomatism. Geochemical data from samples from deep drill holes presented by Tassinari et al., (1993) indicate that barren andesites deep in the deposit have less sodic alteration than their upper mineralised equivalents, which suggests that there is a local albitisation directly related with copper

ore. K-feldspar alteration has not been reported and the highest K_2O values are 3.4 wt % in andesites and 3.1 wt % in rhyodacites (Chavez, 1985; Tassinari et al., 1993). The similarities in the pattern of alteration between Mantos Blancos and El Soldado are striking.

The age of alteration-mineralisation at Mantos Blancos is considered to be about 150 Ma, according to Rb/Sr, Ar/Ar, and K/Ar dating of altered host rocks (Tassinari et al., 1993; Cortés, 1998), and K/Ar ages of barren dykes that cut orebodies (Chavez, 1985). This age is broadly coeval with the emplacement of plutonic rocks in the district (K/Ar: 147 Ma; Chavez, 1985; and with sinistral activity of major faults (K/Ar in biotite from mylonites: 152 Ma; Cortés, 1998). The source of metals and the nature of hydrothermal fluids are still uncertain. A direct magmatic source for copper mineralisation related with subvolcanic intrusives (Chavez, 1985), or plutonic rocks (Cortés, 1998) has been proposed. In addition, Chavez (1985) suggested a seawater source for sodium (albite) and magnesium (chlorite). Yet Tassinari et al. (1993) based on Sr and C isotopic data, concluded that "the hydrothermal fluids could not have been purely magmatic, nor seawater in origin" and invoked a mixture of different fluids to explain the mineralisation.

6.4.2. Punta del Cobre (based on Marschik and Fontboté, 1996)

Punta del Cobre (Figure 2.3) is a Cu-(Ag-Au) strata-bound deposit located in the same district as La Candelaria Cu-(Au-Fe) mine, which is considered transitional between Cu-(Ag) mantos (Mantos Blancos, El Soldado) and Cu-(Au-Fe) deposits (Chapter 2.)

At Punta del Cobre the chalcopyrite-hematite-magnetite hypogene ore is hosted by the Upper Jurassic (?)-Lower Cretaceous Punta del Cobre Formation composed of a bimodal sequence of calc-alkaline mafic (basalts, andesites) and felsic (dacites) lavas. Host rocks have suffered a strong and pervasive alkali early metasomatism followed by a late hydrothermal event associated with emplacement of a Lower Cretaceous batholith exposed in the western side of the district.

The alkali metasomatism is directly associated with copper mineralisation and is

characterised by sodic and potassic assemblages. Sodic alteration is relatively more extensive and is defined by the association albite-quartz-chlorite±sericite±calcite. This alteration affected all rocks but particularly the dacite, where the original feldspar has been completely transformed to albite. This fact led many authors to name this rock an "*albitofiro*" (Ruiz et al., 1965) or trachyte (Hopf, 1990). This sodic metasomatism implies an addition of Na_2O (up to 10 wt %), low values of K_2O and depletions of CaO and MgO. The potassic alteration has a more restrict distribution and is defined by the assemblage K-feldspar-quartz-chlorite±biotite±tourmaline and is characterised by high K_2O values (5 to 11 wt %). Potassic alteration is also the most important alteration at La Candelaria (Ryan et al., 1995; Chapter 2).

A late contact metamorphic event produced north-northeast trending zones, which from west to east are characterised by Ca-amphibole±biotite±sericite, biotite±chlorite ±sericite±epidote, and epidote±chlorite±quartz±calcite assemblages. These zones overprinted with variable intensity the areas affected by alkali metasomatism. Geochemical data indicate that this late event did not involve large metasomatic mass transfer. The alkali metasomatism present at Punta del Cobre is considered a local event independent and superimposed to regional low-grade metamorphism, taking into account that many rocks of the host Punta del Cobre Formation are unaffected by this alteration. This alkali metasomatism shows important similarities with the alteration described at El Soldado, although the potassic alteration is clearly more developed at Punta del Cobre. This fact implies a higher temperature (up to 400-500 °C, Hopf, 1990) and a possible direct relation with an intrusive source (Hopf, 1990; Marshick and Fontboté, 1996), which is not the case at El Soldado.

The age of copper mineralisation and alkali alteration had occurred at 116-114 Ma based on Ar/Ar and Rb/Sr dating of altered-mineralised rocks, and the age of the late contact metamorphism at 112-110 Ma according to Ar/Ar dating of intrusives (Arévalo, et al., 2000). Similar ages have been recorded for the Cu-(Au-Fe) La Candelaria deposit located 4 km Southwest of Punta del Cobre, where the main pulse of mineralisation had occured at 117-114 Ma and a second pulse, related to nearby batholitic intrusions, at 112-110 Ma (Marschick and Fontboté, 2001).

The ore and alteration mineralogy at Punta del Cobre indicates a relatively hot hydrothermal system probably related to a deep intrusive source (Hopf, 1990; Marschick and Fontboté, 1996; 2001). The potassic alteration (including La Candelaria area) are considered to represent the more internal parts of the hydrothermal centres and albitisation the more distal parts. Based on fluid inclusion and isotopic data, Marschik and Fontboté (2001) have proposed that the main precipitation mechanism at Punta del Cobre-La Candelaria, was probably a mixing and cooling of magmatic fluids (bearing metals and sulphur) with basinal brines or meteoric fluids. In conclusion, Punta del Cobre is considered a relatively distal intrusion-related deposit and it has suggested that it occupies an intermediate position between magnetite-apatite and porphyry copper deposits (Marschik and Fontboté, 1996).

6.5. Summary

Mineralogical and lithochemical data presented in this chapter allows establishing the following generalisations:

1) Barren volcanic rocks distal to orebodies at El Soldado present a relatively weak alteration characterised by the presence of calcite, chlorite, albite, K-feldspar, epidote, titanite, sericite, bitumen, and pyrite altering primary components or infilling open spaces. These minerals are interpreted to be product of diagenesis and subsequent very-low-grade metamorphism, which affected the sequence at a regional scale. During diagenesis (Stage I) were deposited scarce quartz, opaline silica, calcite, and chlorite accompanying a widespread generation of pyrite whose growth was associated with petroleum, later solidified into bitumen. Framboidal and colloform textures of pyrite are indicative of lower temperatures (< 120 ° C) for this stage. The metamorphism included the widespread albitisation of original, more calcic, plagioclase, which favoured the precipitation of Ca bearing minerals such as calcite and epidote and inhibited the occurrence of quartz. Rocks acquired characteristics of *spilites* (basalts) and *keratophyres* (rhyodacites) (Chapter 4). Mineralogical assemblages recognised at the mine during this study are not diagnostic to assign a metamorphic grade. Previous regional studies (Levi, 1969; Levi et al., 1982) indicated a prehnite-pumpellyte facies (very-low-grade) for rocks

of the upper member of Lo Prado Formation, that constrain the temperature to the range of c.a. 200-350 ° C (Winkler, 1974).

2) Mineralised volcanic rocks present a hydrothermal alteration, which overprints the effects of previous diagenesis-regional metamorphism. This local phenomenon is characterised by the abundant presence of calcite, chlorite, albite, K-feldspar (microcline), hematite, and minor quartz, and rutile, which replaced original components or infilled open spaces, and occur in direct association with copper sulphides. Spatial distribution and intensity of alteration coincides in general with copper orebodies; alteration is more pervasive and stronger within the bornite-chalcocite inner cores of orebodies, and weaker in the pyrite-chalcopyrite external haloes. Restricted fluid-inclusion homogenisation temperature data in calcite and quartz associated with copper sulphides suggest a maximum temperature c.a. 300-350 °C for this hydrothermal stage, which is compatible with the observed mineralogical assemblage.

3) The alteration is characterised by a generalised increase in Na_2O and a decrease in K_2O contents in all ore zones, thus reflecting the widespread albitisation related to copper mineralisation. Yet narrow zones within the bornite-chalcocite ore cores show gains in K_2O and losses in Na_2O values, reflecting a local and structurally controlled alteration to microcline. A good indicator of alkali metasomatism is the ratio $Na_2O/(Na_2O+K_2O)$ that represents very well the albitisation and local potassic alteration. The oxides MgO, and FeO, also show relevant increments associated with chloritisation, particularly within bornite-chalcocite ore zones. Rb and Ba behave like K_2O and also can be used as indicators of alteration.

4) Ag shows significant increments only within the bornite-chalcocite ore zone, which implies it was deposited accompanying these sulphides during hydrothermal Stage II. On the contrary, As, Ni, Co, Zn, and Pb show increments in the pyrite ore zone, which suggests these metals were incorporated in to the rocks during diagenesis.

5) In basalts, the alteration included a loss of magnetic susceptibility in all mineralised zones reflecting the sulphidisation of magnetite, which should be useful for exploration.

6) The alteration pattern of El Soldado has many similarities with that of other

major Chilean strata-bound volcanic-hosted deposits, which suggests a similar mode of origin. In all these deposits a pervasive local alkali metasomatism (widespread sodic, locally potassic) is recognised, accompanied by the crystallization of chlorite, calcite and subordinate quartz, sericite, and rutile. The age of mineralisation-alteration post-dates the deposition of host sequences by c.a.15-25 My, and was broadly coeval with emplacements of batholiths and regional brittle-shear faulting. Faults were relevant in focussing hydrothermal fluids, and the role of intrusives is not totally clear. Albitisation (sodic metasomatism) predominates in Cu-(Ag) deposits such as El Soldado and Mantos Blancos, which are located distal to plutonic rocks. On the contrary potassic alteration, possibly implying higher temperatures of formation, is more relevant (yet still subordinate to sodic one) in Punta del Cobre, which is more proximal to plutonic rocks than El Soldado and Mantos Blancos.

CHAPTER 7. EVOLUTION OF THE EL SOLDADO DEPOSIT

7.1. Introduction

Data presented in previous chapters lead to propose a genetic model for El Soldado deposit, which essentially considered two phases of mineralisation: a first diagenetic stage (**Stage** I) of rock preparation and deposition of low-temperature pyrite, related to petroleum migration, and a second hydrothermal phase (**Stage II**) of deposition of copper-(silver) sulphides replacing pre-existing pyrite. An intervening metamorphic stage can be assumed, involving the burial of the sequence until the time of batholith emplacement. This model, with minor adjustments, is similar to that proposed by Wilson (1998a) and Wilson and Zentilli (1999), but significantly different from the interpretation reached by the geological staff of the mine more than a decade ago (e.g. Klohn et al., 1990).

Figures 7.1 and 7.2 present a generalised summary of the evolution of El Soldado, taking into account the general geology, mineral paragenesis, fluid inclusion constraints, and the geochronology. Figure 7.3 (below) shows the theoretical conditions of pH and fO_2 that probably prevailed during copper mineralisation (Stage II).

7.2. Evolution of the Deposit

The evolution of El Soldado deposit can be inferred to have taken place in the following steps (modified and incremented from Wilson, 1988a; Wilson and Zentilli, 1999; Boric et al., 2002; Wilson et al., in press a and b):

7.2.1. Deposition of the Volcano - Sedimentary Sequence

During Early Cretaceous the deposition of a thick sedimentary-volcanic sequence took place in a marine-terrestrial environment representing an "intra-arc" basin at an active continental margin.

a) Deposition of the Lower Member of Lo Prado Formation: deposition of over 1200 m of calcareous and organic-rich sediments of the Lower Member of Lo Prado
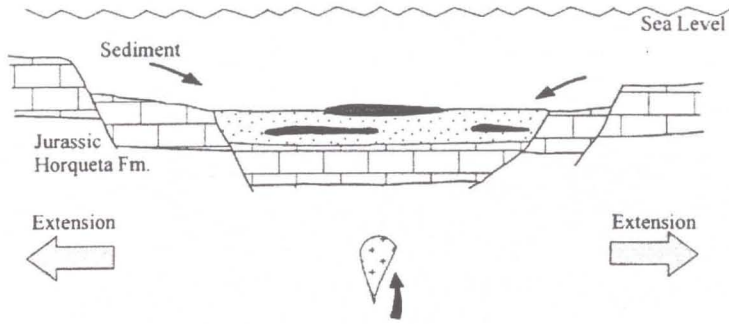
I - Deposition of the lower Lo Prado Fm.

~145 - 135 Ma
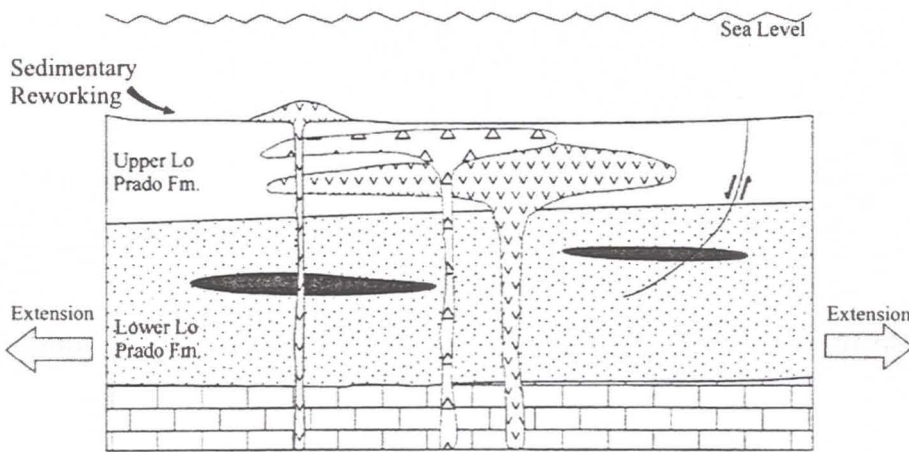
II - Deposition of the upper Lo Prado Fm.

~135 - 127 Ma
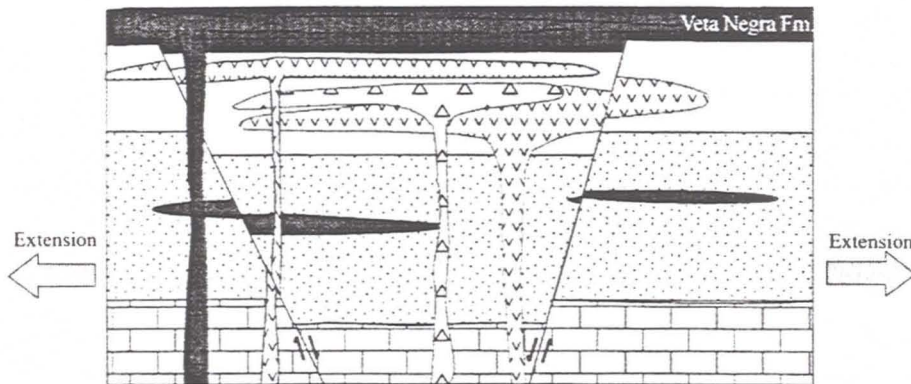
III - Deposition of the Veta Negra Fm.

~127 - 110 Ma

Figure 7.1. Schematic diagrams for the formation of El Soldado.
(Modified from Wilson, 1998).
See text for discussion. Not to scale.

~127 - 110 Ma
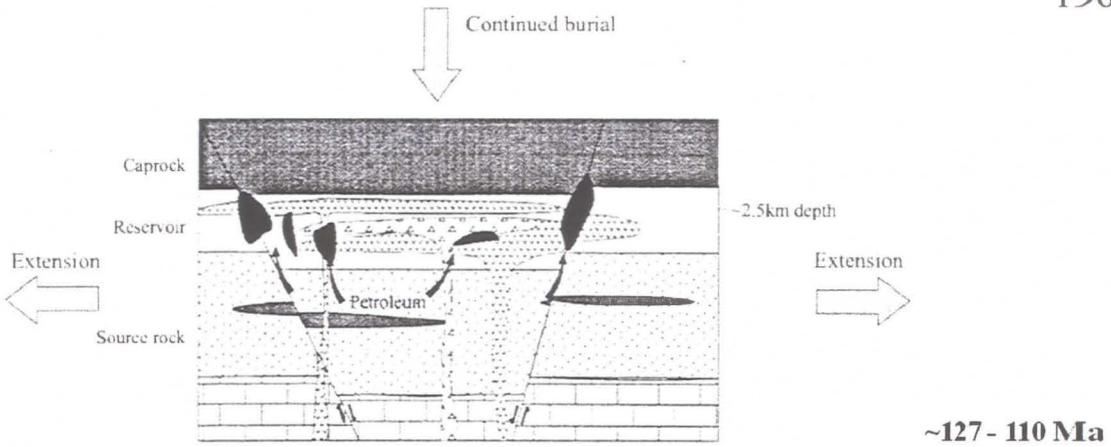
IV – Petroleum generation, migration and accumulation. Biodegradation formed. Pyrite (As rich) and later basinal burial solidified the semi-solid petroleum into solid bitumen. Development of very low grade metamorphism produced "spilites" and " keratophyres".

~106 - 101 Ma
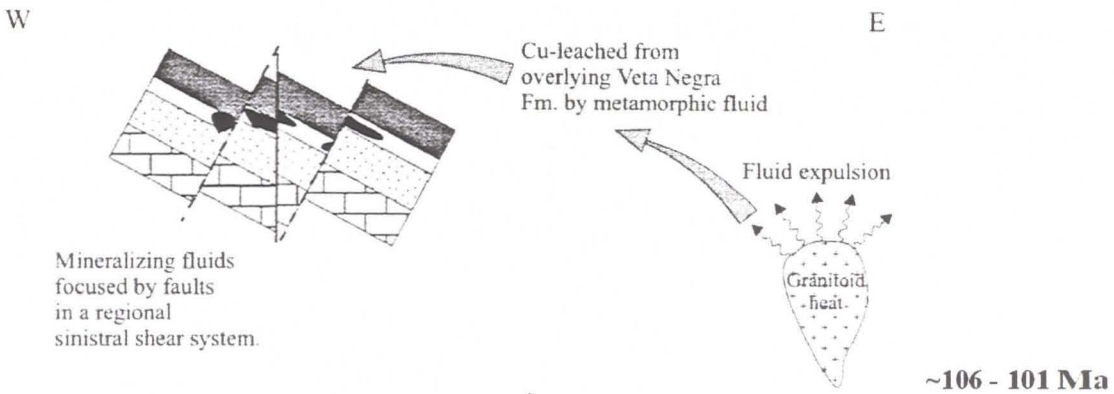
a) section

Development of a dilational jog within a sinistral shear system.

b) plan view
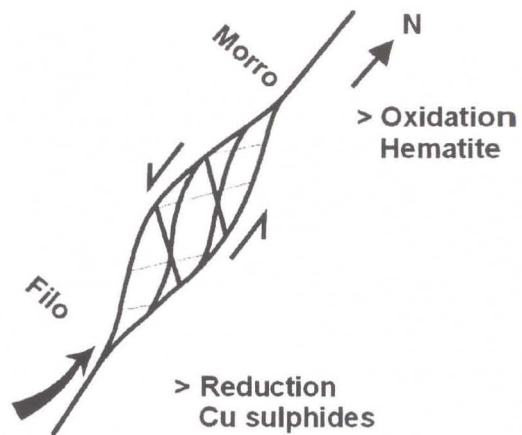
V – Cu-(Ag) mineralisation. Cu leached from overlying Veta Negra Fm by oxidising metamorphic fluids, focussed by faults in a sinistral shear system and deposited in the reduced rocks of Lo Prado Fm replacing diagenetic pyrite.

Figure 7.1. Continued.
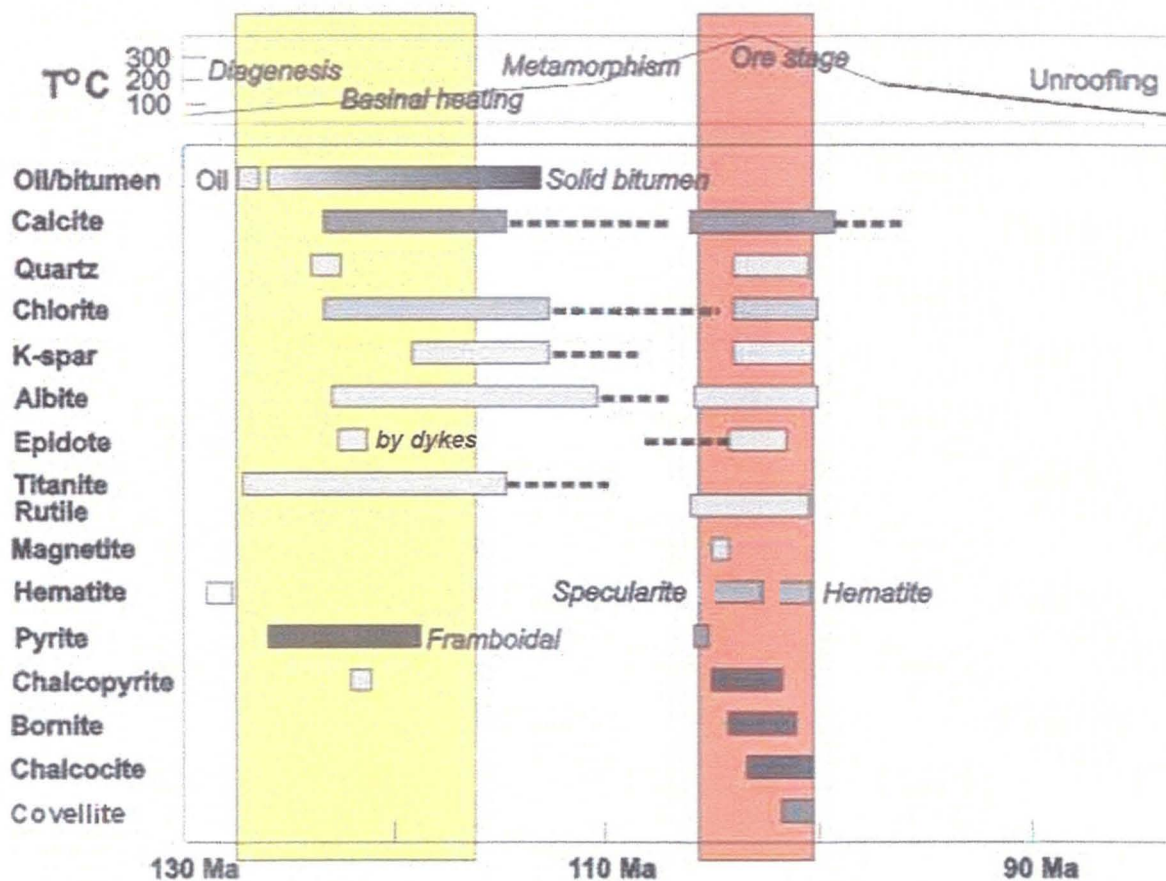
Figure 7.2. Paragenetic sequence and schematic evolutionary history of El Soldado, taking into consideration all available data.

Temperatures and ages are approximate only. Darker bars indicate most important phases. (From Boric et al., 2002.)

Formation on to the Upper Jurassic Horqueta Formation occurred during Berriasian to Valanginian? (145-132 Ma). Fossils indicate a bathial to sublittoral environment for this sedimentation.

b) **Deposition of the Upper Member of Lo Prado Formation:** during the Hauterivian (132-127 Ma) a bimodal sequence (about 650 m thick) of basalts and rhyodacites was extruded to form the Upper Member of Lo Prado Formation, which conformably rests over the Lower Member of Lo Prado Formation. Intercalated sedimentary beds with marine fossils indicate a shallow marine environment of deposition. Rhyodacites were extruded fed by dykes and formed domes, which show typical textures of subaqueous effusion. Volcanic rocks were exposed to high-energy erosion that led to the formation of volcaniclastic, poorly sorted, sediments (breccias, sandstones), which accumulated preferentially at the top of this upper member. These upper sediments are more impervious than the volcanic rocks, which developed primary porosity in vesicular top flows (basalts), columnar joints (rhyodacites), and brecciated lavas.

c) **Deposition of Veta Negra Formation:** a thick sequence of basalts, basaltic andesites, andesites, pyroclastic and epiclastic rocks was deposited conformably onto the Upper Member of Lo Prado Formation, during the Barremian to the Albian(?). Intercalations of lacustrine siltstones with plant remains indicate terrestrial conditions of deposition. Deuteric alteration after extrusion in an oxidised subaerial environment generated widespread hematitisation in the lavas, which acquired a characteristic reddish brown colour. The lower volcanic strata of this unit have a basaltic composition, similar to the Upper Lo Prado Formation, and were fed by dykes intersected in the workings of the El Soldado mine. The upper flows are relatively more andesitic, reflecting an evolutionary trend in the volcanism during its deposition. Total thickness of the Veta Negra Formation has been estimated to be 5 to 7 Km, but it could be less considering tectonic repetition by extensional faults.

According to previous regional studies, the sedimentary-volcanic rocks of the three units described above were accumulated within an intra-arc basin at an active continental margin. The great thickness of the sequence (> 6.5 Km) and the presence of

Lower Cretaceous marine fossils in the overlying Las Chilcas Formation, are indicative of extensional faulting and subsidence in the basin during the deposition of the rocks. This fact is in agreement with a deep and relatively low-stress subduction ("Marianas" type) postulated for central Chile during this period of time. Petrography and geochemical data presented in this thesis confirm that the volcanic rocks of the upper Lo Prado and Veta Negra Formations represent a volcanic-arc suite. Bimodal lavas of the Upper Member of Lo Prado Formation have a typical calk-alkaline, low-K signature; basalts represents the primitive parental magmas and rhyodacites were generated by crustal contamination which is demonstrated by xenocrystic zircons with Proterozoic and Paleozoic U/Pb ages. The basaltic-andesitic rocks of Veta Negra Formation might represent a more evolved potassic suite.

7.2.2. Diagenetic Stage I: Pyrite Mineralisation

a) **Generation, Migration, and Accumulation of Petroleum:** During burial the organic-rich sediments of the Lower Member of Lo Prado Formation reached oil-window temperatures (~ 60 °C) and liquid petroleum was generated in these rocks. The petroleum migrated upwards through extensional normal faults (growth faults?) that must have been active during sedimentation and volcanism that filled the basin, and accumulated in the Upper Member of Lo Prado Formation. Permeability was provided by primary porosity such as columnar jointing, synvolcanic breccias, interparticle spaces in coarse volcaniclastic rocks, vesicular zones in basalts, and secondary fracture porosity related to faults. The uppermost sedimentary unit of the Lo Prado Formation and/or the lowest tuffaceous strata of Veta Negra Formation acted as a relatively impervious cap for the petroleum reservoir. Degassing bubbles (geopetal structures) show that oil migration occurred when strata where still horizontal (Wilson, 1998 a; Wilson and Zentilli, 1999).

b) **Pyrite Deposition (Stage I):** a first stage of mineralisation, characterised by widespread deposition of framboidal and spheroidal pyrite, and traces of sphalerite, chalcopyrite, galena, pyrrhotite and arsenopyrite, occurred within rocks of the Upper Member of Lo Prado Formation. Small amounts of quartz, silica, chlorite and calcite precipitated accompanying these sulphides. Petrographic observations show that

framboidal pyrite grew within and around petroleum, before it solidified, which is indicative of a low-temperature (<120 °C) process. Isotopic studies indicate that sulphur was derived from low-temperature (probably bacterial) reduction of sulphate from the oilfield pore waters (Wilson et al., in press b). Reduction of sulphate produced H_2S that in the presence of iron formed pyrite. Since iron is not easily transported in oxidised waters (e.g. Love, 1967), it was most likely derived from the reduced pore waters accompanying the petroleum in their rise through the normal faults. This concept is totally consistent with the Re-Os data on diagenetic pyrite (Ruiz et al., 1997).

Pyrite occurring in basalts and rhyodacites of the Upper Member of Lo Prado Formation, which replaces titano-magnetite and ferromagnesian minerals and is associated with titanite-leucoxene, probably formed also during this diagenetic stage from a similar source, although not direct connection with petroleum has been observed. Alternatively it could have been generated later during metamorphism.

c) Formation of Bitumen: On continued burial the Upper Member of Lo Prado Formation reached temperatures of 100-120 °C and liquid petroleum was not stable, was degassed and solidified into bitumen. Solidification produced shrinkage fracturing of bitumen and calcite crystallised in the open spaces. Carbon isotope data show that this calcite was in part generated by the oxidation of organic matter (Wilson el al., in press b).

The age of this diagenetic Stage I is poorly constrained but it must have developed between deposition of the volcanic host rocks of the Upper Member of Lo Prado Formation at ca. 130 Ma, and peak metamorphism when temperatures in the basin increased well over 200 °C (lower temperature for prehnite-pumpellyte facies).

7.2.3. Very Low-Grade Metamorphism: Alteration to *Spilites* and *Keratophyres*

After continued burial, the temperature and pressure increased in the basin and the rocks of the Upper Member of Lo Prado Formation were affected by non-penetrative, very-low-grade metamorphism. Calcite, chlorite, albite, epidote, K-feldspar, sericite, and titanite altered original components or filling in open spaces. The metamorphism included the widespread albitisation of plagioclase phenocrysts, a process led by diffusion that mimics the original textures, and the volcanic rocks acquired characteristics

of spilites (basalts) and keratophyres (rhyodacites). Metamorphism had regional extent and reached the prehnite-pumpellyte facies (Levi, 1969; Levi et al., 1982; 1989) that constrain the temperature to the range of c.a. 200-350 °C (Winkler, 1974).

The metamorphism was probably a long-term process (more than one episode?) that occurred between diagenesis and main plutonic emplacement dated at about 106-103 Ma. in the region (Rivano et al, 1993). Some $^{40}Ar/^{39}Ar$ dates from interstitial K-feldspar in rhyodacites yields ages from 112 to 109 Ma (Wilson, 1998a), which can be attributed to this phenomenon (Boric et al., 2002).

The secondary mineralogy produced in the Upper Member of Lo Prado Formation at El Soldado after diagenesis-very-low-grade metamorphism is similar to that described in previous studies for the same stratigraphic unit away from the mine camp, with the sole difference that at El Soldado there is abundant pyrite. This anomalous pyrite is related to the abundance of organic matter and was a crucial factor that favoured the subsequent copper mineralisation at El Soldado (Wilson, 1988a).

7.2.4. Hydrothermal Stage II: Copper-(Silver) Mineralisation

The main hydrothermal event at El Soldado included the precipitation of copper sulphides replacing previous diagenetic pyrite and an associated alteration characterised by pervasive albitisation and local K-feldspar development. This process was broadly contemporaneous with sinistral brittle shear faulting and a regional peak in batholith emplacement. Chalcopyrite, bornite, chalcocite, and minor covellite were the ore minerals generated during this stage. Silver was introduced into the system and was precipitated as a minor constituent of bornite and chalcocite. Associated gangue-alteration minerals formed were specularite, fine-grained hematite, calcite, chlorite, albite, microcline, and scarce pyrite, rutile, quartz, and epidote.

The mineralisation-alteration process was strongly controlled by brittle faults. Hydrothermal fluids were channelled along a dilational jog (cymoid loop) developed in a regional sinistral shear system. Copper sulphides precipitated preferentially in the more brittle fractured volcanic rocks of the Upper Member of Lo Prado Formation, but scarce ore is found at the lower strata of Veta Negra Formation. Mineral zoning suggests that the

mineralising fluids flowed from the south towards the north along the structural dominated system. In the northern extreme of the deposit specular hematite developed instead of copper sulphides reflecting a deficit in sulphur and copper.

The salinity of fluid inclusions (21-26% NaCl-equivalent) indicates that the solutions that transported the copper were high-salinity brines, which could be present in the volcanic sequence as a consequence of hydration reactions during pro-grade metamorphism (e.g. Westra, 1988a). The oxygen and carbon isotope data, the strontium isotopes and the presence of atmospheric argon in the alteration and gangue K-feldspar are compatible with the fluids having been connate, in part meteoric waters within the subaerial volcanic Veta Negra Formation, in partial equilibrium with the rocks during metamorphism.

Sulphur was inherited wholesale from diagenetic pyrite, as indicated by the matching extremely wide range in sulphur isotopic ratios in pyrite and copper sulphides, (Wilson, 1998a; Collins, 2002) and there is little evidence for sulphur addition during this Stage II. The source of the Cu is speculative, but as forcefully put forward by Westra (1988a) for El Soldado, by analogy with other low-grade metamorphic sequences hosting copper ores such as the Karmutsen volcanics in British Columbia (Lincoln, 1981), the Keweenawan tholeiitic lavas of northern Michigan (Jolly and Smith, 1972), it is most likely that the copper deposited at El Soldado was extracted during prograde low-grade metamorphism from the overlying oxidised Veta Negra Formation volcanic rocks.

Copper was most probably transported by chloride complexes in the oxidised fluids, as evidenced by the presence of chlorine in the bitumen associated with high copper ores (Wilson and Zentilli, 1999). The energy source for fluid migration may have been the regional tectonic tilting of the strata and the intrusion of the huge Cretaceous batholith. Focusing was provided by the development of a brittle shear system parallel to the Andean margin in response to oblique subduction (e.g. Maksaev and Zentilli, 2002) generating transtensional regimes such as the cymoid loop at El Soldado.

Copper precipitated when the copper-rich oxidised chlorine brines reacted with reduced volcanic rocks of Upper Lo Prado Formation. Copper precipitated mainly where mineralising fluids reacted with pyrite and bitumen from Stage I. Bitumen acted as active

carbon to destabilise the chloride complexes (Wilson and Zentilli, 1999). Copper-rich solutions reacted with pyrite to form first chalcopyrite and then bornite and chalcocite. The replacement of pyrite by chalcopyrite only requires the addition of copper, but any further replacement by copper leads to an excess of iron, which results in the co-precipitation of hematite. As a result of this process the cores of mineralising conduits contain chalcocite-bornite-hematite, with bornite, bornite-chalcopyrite, and chalcopyrite zones developed outward from the cores. The pyritic external and deep zone represents mostly the remnant of non-replaced Stage I pyrite (Wilson, 1998a) although minor deposition of pyrite also occurred (Collins, 2002) particularly in the northern side of the deposit.

Temperatures of fluids reached a maximum of 300-350 °C during the mineralisation event, according to fluid inclusion data, and diminished progressively during waning phases (Holmgren, 1987). Figure 7.3 summarises the conditions of pH and fO_2 that probably prevailed during ore deposition (modified from Lincoln, 1981), to explain the coexistence of bitumen, pyrite, chalcopyrite, bornite, chalcocite, hematite and minor magnetite, and calcite. The solutions were oxidised (upper part of the red oval inset), and reacted with the reduced host rocks (lower part of the red oval inset). The oval should be placed at slightly higher pH to allow for calcite stability; the stability relationships are not very different for 300°C.

Age of mineralisation was probably close to 103 ± 2 Ma, on the basis of the $^{40}Ar/^{39}Ar$ dates obtained in previous and current work for K-feldspar associated with copper sulphides (Boric and Munizaga, 1994; Wilson, 1998a). This age is similar to $^{40}Ar/^{39}Ar$ dates obtained for an altered-mineralised dacitic porphyry at La Isla Cu mine, in the Chacana area, 10 Km South of El Soldado (Boric and Munizaga, 1994). Also the age is comparable with $^{40}Ar/^{39}Ar$ dates yield for K-feldspar and sericite in Veta Negra Formation lavas in the same Chacana area interpreted as representing metamorphism (Fuentes et al., 2001) and with biotite K/Ar ages for plutonic rocks exposed Northeast of the mine (Rivano et al., 1993). Mineralisation was not restricted to El Soldado camp and was coincident with a peak in regional metamorphism probably associated with a pulse in plutonic activity.
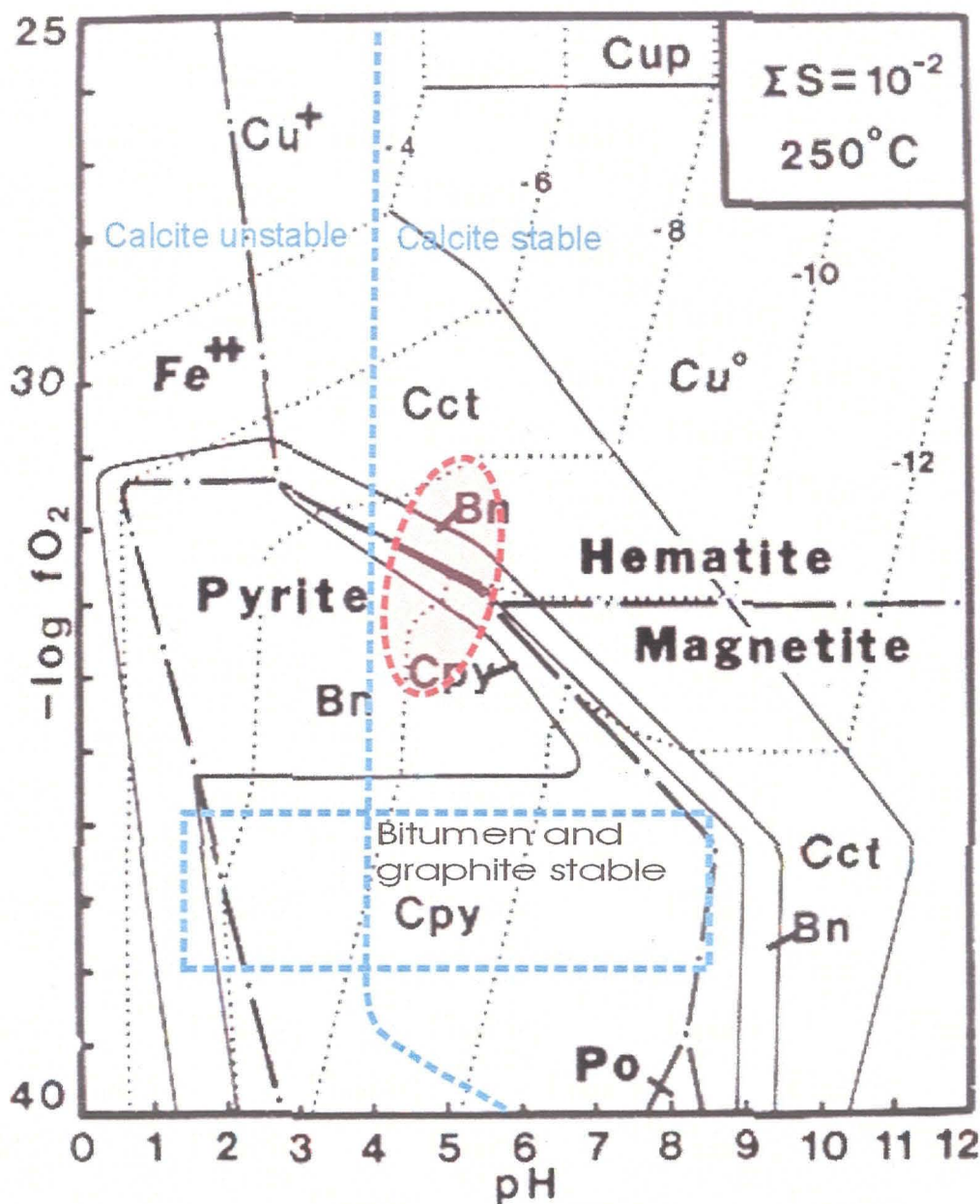
Figure 7.3. Probable conditions prevailing during the main phase (stage II) of mineralisation at El Soldado (red-filled oval).

The stabilities of copper-bearing minerals are shown superimposed on the stabilities of iron minerals in the system Cu-Fe-S-O-H. Cct = chalcocite, Cpy = chalcopyrite, Cup = cuprite, Cu° = native copper, Bn = bornite, and Po = pyrrhotite. The boundaries between iron phases are shown with heavy dash-dot lines. The boundaries between Fe^{2+} and iron minerals are drawn at an activity of Fe^{2+} in solution of 10^{-3}. The boundaries between copper-bearing minerals are shown with solid lines. The log of the activity of Cu^{+} in equilibrium with each copper mineral is contoured with dotted lines. The diagrams are from Lincoln (1981) and were constructed from data contained in Helgeson (1969). The fields for calcite and bitumen-graphite are adapted from Barnes (1979).

7.2.5. Uplift, Unroofing, Erosion, and Supergene Mineralisation

After ore formation and batholith intrusion, the region underwent rapid cooling and exhumation during tectonic inversion of the Early Cretaceous basin related with a major plate tectonic reorganisation (Ramos and Alemán, 2000; Figure 2.5). This interpretation is supported by apatite fission track dates of ca. 88 Ma at El Soldado, and 82-95 Ma at the Caleu Pluton (28 Km Southeast of El Soldado; Parada and Larrondo, 1999; Gana and Zentilli, 2000), which revealed rapid denudation during the Late Cretaceous and that by 90 Ma the Early Cretaceous rocks had cooled to ca. 100 °C and were never substantially reheated (Boric et al., 2002; Wilson et al., in press a).

After continuous denudation the deposit was exposed to weathering and erosion and probably part of its western flank was removed along a west-draining (El Gallo) gulch as indicated by the surface-truncated orebodies and asymmetric mineral zoning. Supergene oxidation is not insignificant, in particular in the upper levels of the El Soldado mine near the surface, and in the proximity of open faults, such that mixed sulphide-oxide ores are exploited by leaching. However, oxidation has led to a decrease in copper grades rather than to supergene enrichment. The lack of sufficient pyrite to generate sulphuric acid during oxidative weathering, the presence of reducing bitumen, and of abundant calcite to neutralise any acid formed, have worked against supergene enrichment (e.g. González and Holmgren, 1993).

CHAPTER 8. CONCLUSIONS AND OTHER CONSIDERATIONS

8.1. Protolith

One of the main objectives of this thesis was to, once and for all, define the nature of the protolith of the host volcanic rocks at El Soldado, and determine their absolute age.

8.1.1 Rocks Not Alkaline. Petrological and lithochemical evidence, including immobile trace elements, indicates that the volcanic-subvolcanic host rocks at El Soldado are a bimodal calc-alkaline suite composed of basalts and rhyodacites. The rocks were affected by a regional very-low-grade metamorphism (prehnite-pumpellyte facies) and have an intense albitisation at the mine related to the copper mineralisation. These factors led to their misidentification as alkaline trachytes and andesites in previous studies. The regionally metamorphosed background ("least altered") rocks have characteristics that in the past led to designation of them as *spilite* (basalts) and *keratophyre* (rhyodacite).

Major, minor and trace elements, including REE suggest the host volcanic rocks of the Upper member of Lo Prado Formation are arc-related calc-alkaline magmas. Alkalis have been strongly remobilised and cannot be used for rock characterisation. The basalts might represent the primitive parental magmas with little evolution/contamination and the rhyodacites were generated by crustal contamination, which is demonstrated by resorbed xenocrist zircons with Proterozoic and Paleozoic U/Pb ages. The basaltic-andesitic rocks of the overlying Veta Negra Formation are more evolved and have relatively high contents of K_2O.

8.1.2. Age of Host Rocks. The age of the Lo Prado Formation is Berriasian - Hauterivian, and the Upper member, hosting the ores at El Soldado, is probably restricted to the Hauterivian (132-127 Ma; Okulitch, 1999 and pers. comm. 2002) on the basis of regional correlation and paleontological chronology. Dating by U/Pb of zircon on a rhyodacite host dyke yielded a (high-error) age of 138±3 to 126±28 Ma, which is consistent with the paleontological age and a few previous $^{40}Ar/^{39}Ar$ dates. Therefore the host volcanic rocks were formed ca. 25 My before the copper mineralisation event (c.a

206

103 ± 2 Ma. according to $^{40}Ar/^{39}Ar$ dating of K-feldspar associated with ore), and their extrusion has nothing to do with the hydrothermal event.

8.2. Zoning

A second objective of the thesis was to better define, at the scale of the mine, the mineral zoning of ore and alteration minerals, and explain it on the basis of ore-forming processes.

8.2.1. Zoning at Various Scales. The study has confirmed semi quantitatively the zoning in individual orebodies, consisting of an external pyrite zone, followed inward by chalcopyrite-pyrite, chalcopyrite, chalcopyrite-bornite, bornite, and a central zone of bornite-chalcocite-hematite.

On a camp scale, bornite and bornite chalcocite (copper sulphides) are more abundant to the south and along the west flank of the mine, mostly along the main NS (sinistral) shear fault. In contrast, pyrite and chalcopyrite are more abundant to the north and to the east, away to the main shear faults. Copper sulphides are more abundant in the south and specular hematite in the north, reflecting a higher fO_2 and/or a relatively deficit of sulphur and copper during ore mineralisation in the northern side of the deposit. Pyrite is also more abundant in the lower levels (roots) of orebodies, and conversely, hematite (fine crystalline and as specularite) is relatively more abundant in the upper levels, also reflecting a change in the redox conditions with depth (oxidation at upper levels, reduction at lower levels).

8.2.2. Descending Fluids. This global pattern can be explained by generation of copper orebodies by *descending* oxidised, copper-rich fluids, which precipitated copper sulphides within fractured and chemically reduced rocks of the Upper Member of Lo Prado Formation. Mineralising fluids were channelled along the main shear faults and probably flowed from the south to the north. Precipitation was caused by reaction with pyrite and bitumen generated early during low-temperature diagenesis, confirming a two-stage model of ore generation (Wilson, 1998a; Wilson and Zentilli, 1999). Copper-rich

solutions reacted with pyrite to form first chalcopyrite and then bornite and chalcocite; the resulting excess of iron formed hematite. As a consequence of this process the centres of mineralising conduits contain chalcocite-bornite-hematite, with bornite, bornite-chalcopyrite, and chalcopyrite zones developed outward from the cores. The pyritic external and deep zone represents mostly the remnant of non-replaced diagenetic pyrite although minor deposition of euhedral pyrite (Collins, 2002) also occurred.

8.3. Alteration

The third objective was to document any chemical changes experienced by the rocks as a result of ore forming processes, which would be useful in exploration.

8.3.1. Alteration Related to Ore. Mineralogical and chemical data shows that copper mineralisation is spatially associated with a strong hydrothermal alteration that overprints the effects of previous diagenesis and regional metamorphism. The alteration is characterised by a generalised increase in Na_2O and depletion in K_2O contents related to a pervasive albitisation of host rocks within orebodies. Nevertheless, there are localised zones of K_2O increase in bornite-chalcocite orebody cores near structures, where K-feldspar (microcline) precipitated. A good indicator of alteration related to copper ore is the ratio $Na_2O/(Na_2O+K_2O)$, which reflects very well the albitisation and local potassic alteration. MgO and FeO, associated with chloritisation, also increase in the cores of orebodies. Rb and Ba behave similarly to K_2O and also can be used as indicators of alteration.

8.3.2. Loss of Magnetic Susceptibility. The complete disappearance of magnetic susceptibility in basalts as they approach mineralised bodies resulted from sulphidation of titano-magnetite, and should be a useful empirical tool in logging and geophysical exploration.

8.4. Other Considerations

Two main ore controls at El Soldado are:

8.4.1. Pyrite and Bitumen: Copper minerals replaced pre-existing pyrite, which developed within a degraded petroleum reservoir, probably with the interaction of sulphur reducing bacteria, at temperatures below 120 $^{\circ}$C (Wilson and Zentilli, 1999). Petroleum migration and pyrite growth preceded tilting of the strata (Wilson, 1998a). Therefore the locus for pyrite within the potential petroleum reservoir could extend long distances down dip and to the east. Solid bitumen acted as a reductant for hydrothermal solutions and probably destabilised chloride complexes carrying copper. Other paleo-petroleum reservoirs within the Early Cretaceous basin could be the locus of mineralisation even if no pyrite was developed. As pointed out by Zentilli et al. (1997) interaction of hydrothermal solutions with petroleum source rocks (organic-rich Lo Prado Formation or any other), migrating hydrocarbons or hydrocarbon reservoirs could be good loci for sulphide precipitation. Petroleum has had both physical roles, such as preserving pore spaces by preventing cementation, providing new porosity during shrinking to a solid, and because of its negligible tensile and shear strength, enhancing reactivation of bitumen-sealed faults (Zentilli et al., 1997), and chemical roles, such as promoting pyrite growth, and acting as a reductant to oxidizing solutions.

8.4.2. Structural Permeability: Early formed extensional faults controlled the migration of petroleum and localised the formation of the essential pyrite, before and during petroleum migration. Later remobilisation of these faults and development of a sinistral strike-slip regime with a transtensional zone (cymoid loop) responding to a horizontal maximum principal stress $\sigma 1$ oriented NNW-SSE. The best extensional structures should have an orientation parallel to the above, and the permeability zones formed should have a sub-vertical extension, parallel to the intermediate stress direction (e.g. Sibson, 2001). Within this brittle regime, the most favourable rocks types for ore were the brittle rhyodacites, and basaltic lavas of the Upper Member of the Lo Prado Formation, whereas the more ductile fine-grained clastic sediments are relatively less favourable.

8.4.3. Basinal Brines. The El Soldado deposit is epigenetic, but the fluids that formed it were not magmatic. The isotopic and fluid inclusion data available suggest that the fluids were highly saline basinal brines, modified by prograde metamorphism, but with a significant component of meteoric water. Evaporites may have been involved, although they have not been recognized in the basin.

8.5. Generalisations About Very Large Manto-Type Cu Deposits.

This study suggests that very large Chilean manto type Cu-(Ag) deposits hosted by volcanic rocks, such as El Soldado, Mantos Blancos and Punta del Cobre have some common features, perhaps suggesting that these deposits form part of a continuum between the Cu-(Ag) and Cu-(Au-Fe) strata-bound deposits (Boric et al., 2002; Maksaev and Zentilli, 2002):

- They were generated during the Upper Jurassic-Early Cretaceous; a particular period of Andean evolution characterised by the development of a volcanic arc and trans-tensional and tensional regimes within intra-arc and back-arc basins. These features were explained by an oblique and low-stress subduction during the interval.

- They are hosted by bimodal calc-alkaline volcanic sequences including basaltic-andesites and rhyodacite extrusive-subvolcanic units that have been strongly albitised.

- They have a similar paragenesis that starts with specular hematite, followed by increasingly copper-rich sulphides.

- They are associated with strong sodic and local potassic alteration, clearly distinguishable from regional metamorphic assemblages. Potassic alteration is relevant only in Punta del Cobre district (Cu-Ag-Au).

- Mineralisation-alteration post-date deposition of host sequences in c.a 15-25 Ma and was broadly coeval with plutonic emplacement and brittle sinistral (transtensional) shear. Faults focussed hydrothermal fluids but the role of plutons was not clear. Mantos Blancos and El Soldado are distal to plutonic rocks and a direct genetic relationship with intrusives is not evident. Punta del Cobre deposit is proximal to a batholith and a deep intrusive source has been postulated for its genesis.

- The importance of petroleum involvement, or the generation of diagenetic pyrite as rock preparation is important in El Soldado, but has not been associated with Mantos Blancos and Punta del Cobre; possibly El Soldado is an anomaly.

8.6. Recommendations for Further Work

8.6.1. At a Mine Scale

- To complete the study of distribution and paragenetic position of the specularite found in the northern extreme of the El Soldado. It is important to know if this specularite represents an early phase presents in other Chilean manto type copper deposits (e.g. Punta del Cobre, Mantos Blancos) or simply a lateral change in the redox conditions at the time of deposition of copper sulphides.
- To perform a fluid inclusion study based on the new two-stage model of ore deposition to better define the variations in temperature and salinity of the mineralising fluids.

8.6.2. At a District Scale

- To study other mines hosted by the Upper Member of Lo Prado Formation southern and northern of El Soldado (Figure 3.1), in order to know if these deposits formed in the same manner than El Soldado. The particular interest will be the study of skarnoid deposits located at Cabildo (El Sauce mine) and La Campana districts to establish if they formed during the same mineralisation event than El Soldado and from the same metamorphic-hydrothermal source or if they represent intrusive related deposits.

REFERENCES

Aberg, G., Aguirre, L., Levi, B., and Nystrom, J.O., 1984. Spreading subsidence and generation of ensialic marginal basins, an example from the Early Cretaceous of central Chile, *In* Kokelaar, B.P. and Howells, M.F. (eds.) Marginal Basin Geology, Geol. Soc. Spec. Publ.16, p.185-193.

Ahumada, R., 1985 a. Eventos intrusivos en el yacimiento cuprífero El Soldado, V region. Unpublished B. Sc. Thesis, Universidad de Chile, Departamento de Geología y Geofísica, Santiago, Chile 115 p.

Ahumada, R., 1985 b. Eventos intrusivos en el yacimiento cuprífero El Soldado, V Región, Chile, IV Congr. Geol. Chileno, Antofagasta, IV, p.752-773.

Ahumada, R. and González, F., 1995. Uso de restricciones geológicas en la estimación geostadística de reservas en el yacimiento El Soldado, VII Congr. Geol. Chileno, Concepción, II, p.709-713.

Allen, R., 1988. False pyroclastic textures in altered silicic lavas, with implications for volcanic-associated mineralization, Economic Geology, v.83, p.1424-1446.

Amstutz, G.C., 1968. Les laves spilitiques et leurs gites mineraux, Geol. Rdsch., 57, p.936-954.

Arévalo, C., Grocott, J., Pringle, M. and Martin, W., 2000. Edad $^{40}Ar/^{39}Ar$ de la mineralización en el yacimiento Candelaria, Región de Atacama, IX Congr. Geol. Chileno, Puerto Varas, Chile, v. 2, p.92-98.

Atkin, B.P., Injoque-Espinoza, J.L. and Harvey, P.K., 1985. Cu-Fe amphibole mineralization in the Arequipa segment, *In* Pitcher W.S. et al. (eds.) Magmatism at a plate edge: the Peruvian Andes, Blackie, Glascow, London, New York, p.261-270.

Barnes, H.L., 1979. Solubilities of ore minerals, *In* Barnes, H.L. (*ed.*) Geochemistry of hydrothermal ore deposits: New York, Wiley Interscience, p. 404-460.

Bassi, H., 1984. El Soldado, a Chilean, apparently stratiform disseminated ore deposit, with tectonic and lithological controls, *In* Bogdanov, N.A. (ed.) Tezisy; 27-y mezhdunarodnyy gelogicheskiy kongress- Abstracts, 27th International Geological Congress, 27; 6, p.27.

Bassi, H., 1985. Results of extrapolating metallogenic controls of the El Soldado Mine to strategic prospecting in the Aconcagua Region, central Chile, *In* Kutinajan (ed.) Parameters controlling the distribution of large ore deposits, ore clusters, mineral belts and metallogenic provinces; Part III, global tectonics and metallogeny, 3, 1,

36 p.

Bassi, H., 1988. Evolución en el Conocimiento Geológico del Yacimiento Cuprífero Diseminado El Soldado, 5a Región, Chile, V Congr. Geol. Chileno, Santiago, III, p.G53-G70.

Battey, M.H.,1955. Alkali metasomatism and the petrology of some keratophyres, Geol. Mag. 92, p.104-126.

Boric, R., 1985. Geología y yacimientos metálicos del distrito Talcuna, Región de Coquimbo, Revista Geológica de Chile, N° 25-26, p.57-75.

Boric, R., 1995. Mineral zoning at El Soldado copper deposit, central Chile, GSA Meeting New Orleans, Abstracts, p. 1473.

Boric, R., 1997. Nuevos antecedentes sobre el modelo genético del yacimiento de cobre El Soldado, Chile central, VIII Congr. Geol. Chileno, Antofagasta, p.862-866.

Boric, R., Díaz, F., and Maksaev, V., 1990. Geología y yacimientos metalíferos de la Región de Antofagasta, Servicio Nacional de Geología y Minería, Boletín N° 40, Santiago, 246 p.

Boric, R. and Munizaga, F., 1994. Geocronología Ar-Ar y Rb-Sr del depósito estratoligado de cobre El Soldado (Chile central), Comunicaciones, Universidad de Chile, v. 25-26, p.57-75.

Boric, R. and Zentilli, M., 2001. Geology, mineral zoning and lithogeochemistry of hydrothermal alteration at the El Soldado manto type copper deposit, Chile, Abstracts Atlantic Geosciencie Society Colloquium and Annual Meeting, Moncton New Brunswick, v. 37.

Boric, R., Holmgren, C., Wilson, N.S.F. and Zentilli, M., 2002. The geology of the El Soldado Cu-(Ag) deposit, Central Chile, *In* Porter T.M. (ed.) Hydrothermal iron-oxide copper-gold & related deposits: a global perspective, Volume 2, p.163-184.

Caddey, S., 2001. Investigación estructural y control de la mineralización en el yacimiento de cobre El Soldado, unpublished CMD internal report, 19 p. plus 79 p. appendix, Technical Archives El Soldado Mine.

Camus, F., 1985. Los yacimientos estratoligados de Cu, Pb-Zn y Ag de Chile, *In* Frutos, J., et al. (eds.) Geología y recursos minerales de Chile, Editorial Universitaria, Concepción, Chile. p.574-635.

Camus, F., 1990. Geological characteristics of stratabound deposits associated with lacustrine sediments, Central Chile, *In* Fontboté, L. et al. (eds.) Stratabound ore deposits in the Andes, Springer Verlag, p.79-110.

Camus, F. and Dilles, J.H., 2001. A special issue devoted to porphyry copper deposits of northern Chile, Economic Geology, v. 96, p.233-237.

Cann, J.R., 1969. Spilites from the Carlsberg Ridge, Indian Ocean, Journal of Petrology, 10, p.1-9.

Cardozo, M., 1990. The Copara metallotect in Central Peru: Geologic evolution and ore formation, *In* Fontboté, L. et al. (eds.) Stratabound ore deposits in the Andes, Springer Verlag, p.395-412.

Carter, W.D., 1961. Yacimientos de cobre tipo manto, su distribución en franjas mineralizadas, Provincia de Aconcagua, Boletín N° 10, Instituto de Investigaciones Geológicas, Chile, 30 p.

Cas, R.A.F. and Wright, J.V., 1987. Volcanic succesions: modern and ancient: a geological approach to processes, products and succesions, London, Allen and Unwin, 528 p.

Cisternas, M. E., Frutos, J., Galindo, E., Spiro, B., 1999. Lavas con bitumen en el Cretácico inferior de Copiapó, Región de Atacama, Chile: petroquímica e importancia metalogénica, Revista Geológica de Chile, v. 26, 2, p.205-226.

Charrier, R., and Muñoz, N., 1994. Jurassic Cretaceous paleogeographic evolution of the Chilean Andes at 23°-24°S and 34°-35°S latitude: a comparative analysis, *In* Reuter, K.J. et al. (eds.) Tectonics of the Southern Central Andes, Springer Verlag, p.233-242.

Chávez, A., 1988. Relaciones entre fracturas, campos de esfuerzos y mineralización en el yacimiento El Soldado, V Región, unpublished B.Sc.Thesis, Departamento de Geología y Geofisica, Universidad de Chile, Santiago, 141 p.

Chavez, W., 1984. Alteration mineralogy and chemistry of rhyolitic and andesitic volcanic rocks of the Mantos Blancos copper-silver district, Chile, Society of Mining Engineers of AIME, Pre-print, N° 84-153, 5 p.

Chavez, W., 1985. Geological setting and the nature and distribution of disseminated copper mineralization of the Mantos Blancos district, Antofagasta Province, Chile, unpublished Ph.D. Thesis, California University, Berkeley, USA, 142 p.

Clark, A.H., 1993. Are outsized porphyry copper deposits either anatomically or environmentally distinctive? *In* Giant Ore Deposits, Society of Economic Geologists, Special Publication 2, p. 213-283.

Collao, S., 1993. Inclusiones fluídas en el Yacimiento Mantos Blancos, unpublished

report, Departamento de Ciencias de la Tierra, Universidad de Concepción, Concepción, Chile, 27 p.

Collins, P. 2002. Fixation of sulphur during framboidal pyrite development in a petroleum reservoir in Cretaceous volcanics in the Andes: implications for Cu metallogenesis, unpublished B.Sc. Thesis, Dalhousie University, 147 p.

Contador N., and Glavic, M., 2001. Sublevel open stoping at El Soldado mine: a geomechanic challenge, underground mining methods, engineering fundamentals and international case studies, Society for Mining, Metallurgy, and Exploration, Inc. (SME), Chapter 29, p.263-269.

Cornejo, P., Tosdal, R.M., Mpodozis, C., Tomlinson, A.J., Rivera, O., and Fanning, C.M., 1997. El Salvador, Chile, porphyry copper deposit revisited: Geologic and geochronological framework. International Geology Review, v. 39, p. 22-54..

Cortés, J. 1998. Geología y geoquímica preliminar del distrito minero de Mantos Blancos, cordillera de la costa, Segunda Región de Antofagasta, Chile, unpublished B. Sc. thesis, Universidad Católica del Norte, 137 p., 2 appendices.

Cox, K.G., Bell, J.D., and Pankhurst R.T.J., 1979. The interpretation of igneous rocks, London, Allen and Unwin, 455 p.

Cox, S.F., Knackstedt, M.A., and Braun, J., 2001. Principles of structural control on permeability and fluid flow in hydrothermal systems, Chapter 1, *In* Richards J.P. and Tosdal R.M. (eds.) Structural controls on ore genesis, Reviews in Economic Geology, v. 14, p.1-24.

Cuesta Research Limited, 1995a. Asesoría en estudios microscópicos: mineralogy, mineral and rock chemistry of samples from the El Soldado copper deposit, data report-1, unpublished CMD internal report, 50 p., Technical Archives El Soldado Mine.

Cuesta Research Limited, 1995b. Asesoría en estudios microscópicos: mineralogy, mineral and rock chemistry of samples from the El Soldado copper deposit, data report-2, unpublished CMD internal report, 156 p., Technical Archives El Soldado Mine.

Cuesta Research Limited, 1995c. Asesoría en estudios microscópicos: mineralogy, mineral and rock chemistry of samples from the El Soldado copper deposit, data report-3, unpublished CMD internal report 30 p., Technical Archives El Soldado Mine.

Cuesta Research Limited, 1996. Asesoría en estudios microscopicos: mineralogy, mineral and rock chemistry of samples from the El Soldado copper deposit, summary

report, unpublished CMD internal report, 10 p. plus 11 p., tables, Technical Archives El Soldado Mine.

Dallmeyer, R.D., Brown, M., Grocott, J., Taylor, G.K., and Treolar, P.J., 1996. Mesozoic magmatic and tectonic events within the Andean plate boundary zone, 26°-27°30'S, north Chile: constraints from 40Ar/39Ar mineral ages, The Journal of Geology, University of Chicago, v. 104, p.19-40.

Davidson, J. and Mpodozis, C., 1991. Regional geologic setting of epithermal gold deposits, Chile, Economic Geology, v. 86, p.1174-1186.

Definis, A. 1985. Antecedentes geológicos del yacimiento de cobre Santo Domingo, Taltal y discusión acerca de su relación con un sistema de filones gabrodioríticos, IV Congr. Geol. Chileno, Antofagasta, Chile, v.2, p.204-215.

Elders, W.A., Hoagland, J.R., McDowell, S.D., and Cobo, J.M., 1979. Hydrothermal mineral zones in the geothermal reservoir of Cerro Prieto, In Elders W.A. (ed.) Geology and geothermics of the Salton Trough, Field Trip Guidebook No. 7, Geological Society of America 92nd Annual Meeting, San Diego, November 1979, p.36-43.

Espinoza, S., 1981. Esbozo metalogénico del distrito de Michilla, II Región, Chile, Primer Coloquio sobre volcanismo y metalogénesis, Departamento de Geociencias, Universidad del Norte, Antofagasta, Chile, p.71-81.

Espinoza, S., Véliz, H., Esquivel, J., Arias, J., y Moraga, A., 1996. The Cupriferous Province of the Coastal Range, Northern Chile, In Camus, F. et al. (eds.) Andean Copper Deposits: New Discoveries, Mineralization, Styles and Metallogeny, Society of Economic Geologists, Special Publication Number 5, p.19-32.

Evans 1993. Introduction to ore geology, Oxford, Blackwell, 231 p.

Fontboté, L., 1990. Stratabound ore deposits in the Andes; a review and a classification according to their geotectonic setting, In Fontboté, L. et al. (eds.) Stratabound ore deposits in the Andes, Springer Verlag, p.79-110.

Fuentes, F., Féraud, G., Aguirre, L., and Morata, D., 2001. Convergent strategy to date metamorphic minerals in sub-greenschist facies metabasites by the $^{40}Ar/^{39}Ar$ method, III South American Symposium on Isotope Geology, Extended Abstract Volume (CD), Sociedad Geológica de Chile, Santiago, p.34-36.

Fuenzalida, H. 1965. Clima, In Geografía Económica de Chile, Corporación de Fomento de la Producción, Santiago, Chile, p.98-152.

Gana, P., Wall, R., Gutiérrez, A., 1996. Mapa Geológico del área de Valparaíso-

Curacaví, Región de Valparaíso y Región Metropolitana, Servicio Nacional de Geología y Minería, Chile, Mapas Geológicos, N° 1, Escala 1:100,000, 1 mapa, 1 anexo.

Gana, P. and Zentilli, M., 2000. Historia termal y exhumación de intrusivos de la Cordillera de la Costa de Chile Central, IX Congr. Geol. Chileno, Puerto Varas, Chile, v. 2, p.664-668.

Gilluly, J., 1935. Keratophyres of Eastern Oregon and the spilite problem, American Journal of Science, v. XXIX, n° 171, p.225-252, and p.336-349.

González, F. and Holmgren, C., 1993. Características mineralógicas de la zona de oxidación y su implicancia en la recuperación de sulfuros en el yacimiento El Soldado, Congreso Internacional de Ingeniería de Minas, III Región, Copiapó, Chile, Actas, p.270-279.

Heaman, H. and Parish, R., 1991. U-Pb geochronology of accesory minerals, In Heaman L., and Ludden, N.J. (eds.) Mineralogical Association of Canada, short course handbook on applications of radiogenic isotope systems to problems in geology, Toronto, May, 1991, Chapter 3, p.59-102.

Helgeson, H.C., 1969. Complexing and hydrotermal ore deposition, New York, Macmillan, 85 p.

Holmgren, C., 1985. Antecedentes para un modelo genético del yacimiento El Soldado, V Región, IV Congr. Geol. Chileno, Antofagasta, IV, p.626-650.

Holmgren, C., 1987. Antecedentes para un modelo genético del yacimiento El Soldado, V Región de Valparaíso, Chile, Revista Geológica de Chile, 30, p.3-18.

Holmgren, C. and González, F., 1988. Zonación mineralógico-metalúrgica del yacimiento El Soldado, V Región, V Congr. Geol. Chileno, Santiago, III, p.G147-G160.

Hopf, S., 1990. The Agustina mine, a volcanic-hosted copper deposit in Northern Chile, In Fontboté, L. et al. (eds.) Stratabound ore deposits in the Andes, Springer Verlag, p.421-434.

Hughes, C.J., 1973. Spilites, keratophyres, and the igneous spectrum, Geol. Mag. 109, 6, p.513-527.

Hughes, C.J., 1975. Keratophyres defined, Neues Jahrb. Mineral., Monatsh., p.425-430.

Hughes, 1982. C.J., Igneous petrology, Elsevier, 551 p.

Irvine, T.N. and Baragar, W.R.A., 1971. A guide to chemical classification of the common rocks, Can. J. Earth Sc. 8, p.523-548.

Jolly W.T. and Smith, R.E., 1972. Degradation and metamorphic differentiation of the Keweenawan tholeiitic lavas of northern Michigan, USA, Journal of Petrology, v.13, p.273-309.

Kirkham, R.V., 1989. Distribution, settings, and genesis of sediment-hosted stratiform copper deposits, Geol.Assoc. Canada Special Paper 36, p.3-38.

Kirkham, R.V., 1996. Volcanic redbed copper, *In* Eckstrand O.R., et al. (eds.) Geology of Canadian mineral deposit types, Geological Survey of Canada, Geology of Canada, N° 8, p. 241-252.

Klohn, E., Holmgren, C., and Ruge, H., 1986. El Soldado, a peculiar copper deposit associated with anomalous alkaline volcanism in the Central Chilean Coastal Range, Proc., 115th Annual Meeting, Soc. Mining Eng., New Orleans, AIME, 8 p.

Klohn, E., Holmgren, C., and Ruge, H., 1990. El Soldado, a strata-bound copper deposit associated with alkaline volcanism in the central Chilean Coastal Range, *In* Fontboté, L. et al. (eds.) Stratabound ore deposits in the Andes, Springer Verlag, p.435-448.

Le Maitre, R.W., Batteman, P., Dudek, A., Keller, J., Lameyre Le Bas, M.J., Sabine, P.A., Schmid, R., Sorensen, H., Streckeisen A., Wooley, A.R., and Zanettin, B., 1989. A classification of igneous rocks and glossary of terms, Blackwell, Oxford.

Levi, B., 1969. Burial metamorphism of a Cretaceous volcanic sequence west from Santiago, Chile, Contrib. Mineral Petrol., 24, p.30-49.

Levi, B., 1985. Resultados de análisis geoquímicos de muestras de El Soldado, unpublished CMD report, 22 p. with chemycal anlayses, Technical Archives, El Soldado Mine.

Levi, B., Aguirre, L., and Nystrom, J.O., 1982. Metamorphic gradients in burial metamorphosed vesicular lavas: comparison of basalt and spilite in Cretaceous basic flows from central Chile, Contrib. Mineral Petrol., 80, p.49-58.

Levi, B., Nystrom, J.O., Thiele. R., and Aberg, G., 1988. Geochemical trends in Mesoszoic-tertiary volcanic rocks from the Andes in Central Chile, and tectonic implications, Journal of South American Earth Sciences, v. 1, p.63-74.

Levi, B., Aguirre, L., Nyström, J.O., Padilla, H. And Vergara, M., 1989. Low-grade regional metamorphism in the Mesozoic-Cenozoic volcanic sequences of the Central Andes, Journal of Metamorphic Geology, v. 7, p.487-495.

Lincoln, T.N., 1981. The redistribution of copper during low-grade metamorphism of the Karmunsen volcanics, Vancouver Island, British Columbia, Economic Geology v.76, p.2147-2161.

Losert, J., 1973. Genesis of copper mineralization and associated alterations in the Jurassic volcanics rocks of Buena Esperanza mining area, publicación N°40, Departamento de Geología, Universidad de Chile, Santiago, 104 p.

Losert, J., 1974. Alteration and associated copper mineralization in the Jurassic volcanic rocks of Buena Esperanza mining area (Antofagasta Province, northern Chile), *In* Klohn E. (ed.), Coloquio sobre fenómenos de alteración y metamorfismo en rocas volcánicas e intrusivas, p.51-85.

Love, L.G., 1967. Sulphides of metals in recent sediments, Proceedings of the 15th Inter-University Geological Congress, University of Leicester, England, p.30-60.

Maksaev, V., 1990. Metallogeny, geological evolution, and thermochronology of the Chilean Andes between latitudes 21° and 26° South and the origin of major porphyry copper deposits, unpublished Ph.D. Thesis, Dalhousie University, Halifax, Nova Scotia, Canada, 554 p.

Maksaev, V., and Zentilli, M., 2002. Chilean strata-bound Cu-(Ag) deposits: an overview, *In* Porter, T.M. (ed.) Hydrothermal iron-oxide copper-gold & related deposits: a global perspective, v.2, p. 185-205.

Marschik, R., and Fontboté, L., 1996. Copper (iron) mineralization and superposition of alteration events in the Punta del Cobre belt, northern Chile, SEG, Special Publication N°5, p.171-189.

Marschik, R. and Fontboté, L., 2001. The Candelaria-Punta del Cobre Iron Oxide Cu–Au (-Zn-Ag) deposits, Chile, Economic Geology, v.96, p.1799-1826.

Martin, W., 1981. Distribución de la mineralización en el yacimiento cuprífero El Soldado, V Región, unpublished B. Sc. thesis, Departamento de Geología y Geofísica, Universidad de Chile, Santiago, 92 p.

McKinstry, H.E., 1948. Mining Geology: Englewood Cliffs, NJ, Prentice Hall, 680 p.

Mcphie J., Doyle, M. and Allen, R., 1993. Volcanic textures: a guide to the interpretation of textures in volcanic rocks, Centre for Ore Deposit and Exploration Studies Unversity of Tasmania, 198 p.

Middlemost, E.A.K., 1975. The basalt clan, Earth Sci. Rev., 11, 337-364.

Morata, D., Aguirre, L., Féraud, G., Fuentes, F., Parada, M.A. and Vergara, M., 2001. The Lower Cretaceous volcanism in the coastal range of central Chile: Geochronology and isotopic geochemistry, III South American Symposium on Isotope Geology, Extended Abstract Volume (CD), Sociedad Geológica de Chile, Santiago, p.321-324.

Mpodozis, C., and Ramos, V., 1989. The Andes of Chile and Argentina, *In* Ericksen, G.E., et al. (eds.) Geology of the Andes and its relation to hydrocarbon and mineral resources, Circum-Pacific Council for Energy and Mineral Resources, Earth Science Series, v. 11, p.59-90.

Munizaga, F., 1992. Informe yacimiento El Soldado, proyecto FONDECYT # 1033/89, unpublished internal CMD report, Technical Archives, El Soldado Mine.

Munizaga, F., Holmgren, C., Huete, C., and Kawashita, K., 1988. Geocronología de los yacimientos de cobre El Soldado y Lo Aguirre, Chile central, V Congr. Geol. Chileno, Santiago, III, p. G177-193.

Munizaga, F. and Zentilli, M., 1994. Caracterización isotópica del azufre de los depósitos estratoligados de Cu en Chile, Comunicaciones, Universidad de Chile, v. 25–26, p.127-134.

Munizaga, F., Zentilli, M., Tassinari, C., Boric, R., Ramírez, R. and Reynolds, P.H., 1995. Geochronological and isotopic signatures of Mesozoic stratabound "manto-type" copper deposits of Chile (abstract), GSA Annual Meeting, New Orleans, Geological Society of America, Abstract with Programs, 27, 6, p.A-410.

Nisterenko, G.V., Losert, J., Chávez, L., and Naumov, V.B., 1973. Temperaturas y presiones de formación de algunos yacimientos cupríferos de Chile, Revista Geológica de Chile, N°1, p.74-84.

Olcay, L., and Alarcón B., 1975. Alteración hidrotermal sódica de mina El Soldado, provincia de Valparaíso, Chile, II Congr. Geol. Iberoam. Geol. Econ., Buenos Aires, II, p.1-9.

Okulitch, A.V., 1999. Geological time scale 1999, Geological Survey of Canada, Open File 3040, National Earth Science Series, Geological Atlas, Revised.

Ortiz, F.J., Araya, R., Franquesa, F., Moraga, A. and Zentilli, M., 1966. Informe geológico del distrito minero de Punta del Cobre, Instituto de Investigaciones Geológicas, Chile, Special Publication N°1, 4 volumes, 86 maps.

Oyarzún, R., Ortega, L., Sierra, J., Lunar, R., and Oyarzún, J., 1998. Cu, Mn, and Ag mineralization in the Quebrada Marquesa Quadrangle, Chile: the Talcuna and Arqueros districts, Mineralium Deposita, v. 33, p.547-559.

Palacios, C., 1986. Subvolcanic Copper deposits in the coastal range of northern Chile, Zentralblatt für Geologie und Paläontologie, Teil I, 1985, H.9/10, Stuttgart, p.1605-1615.

Palacios, C. and Definis A., 1981. Geología del yacimiento estratiforme Susana, distrito Michilla, Antofagasta. Primer Coloquio sobre volcanismo y metalogénesis, Departamento de Geociencias, Universidad del Norte, Antofagasta, Chile, p.82-91.

Parada, M.A. and Larrondo, P., 1999. Thermochronology of the Lower Cretaceous Caleu pluton in the coast range of central Chile: tectono-stratigraphic implications, Fourth ISAG, Goettingen (Germany), p.563-566.

Pearce, J. A., 1996. A user's guide to basalt discrimination diagrams, *In* Wyman, D.A. (ed.) trace element geochemistry of volcanic rocks: applications for massive sulphide exploration, Geol. Assoc. Can., short course notes, v. 12, p.79-113.

Pearce J.A.and Cann J.R., 1973. Tectonic setting of basaltic rocks determined using trace element analyses, Earth and Planetary Sciences Letters, 19, p.290-300.

Philpotts, A.R., 1990. Igneous and metamorphic petrology, Englewood Cliffs, N.J., Prentice Hall.

Pichowiak, S., Buchelt, M., and Damm, K.W., 1990. Magmatic activity and tectonic setting of early stages of Andean cycle in northern Chile, Geological Society of America, Special Paper 241, p.127-144.

Piracés, R. and Maksaev, V., 1977. Geología de la Hoja Quillota, Instituto de Investigaciones Geológicas, Chile, unpublished report, 64 p., 1 map scale 1:250,000.

Ponce, R., 2001. Geología, mineralización y distribución de elementos en trazas en el sector Filo, mina El Soldado, V Región, Universidad de Chile, Departamento de Geología, unpublished B. Sc.Thesis, Universidad de Chile, Santiago, 104 p.

Pop, N., Heaman, L., Edelsein, O., Isache, C., Zentilli, M., Pecskay, Z., Valdman, S., and Rusu, C., 2000. Geocronología de las rocas ígneas y los productos de alteración hidrotermal relacionadas a la mineralización de Cu-Fe-(Au) del sector Adriana - Carola - Cobriza (parte este del Distrito Punta del Cobre - Candelaria) en base a dataciones U-Pb (en circón), $^{40}Ar/^{39}Ar$ y K-Ar. IX Congr. Geol. Chileno, Puerto Varas, Chile, v. 2, p.155-160.

Porter, T.M. 2000. Hydrothermal iron-oxide copper-gold & related ore deposits, *In* Porter T.M. (ed.) Hydrothermal iron oxide copper-gold & related deposits: a global

perspective, v. 1, PGC Publishing, Adelaide, p.3-5.

Ramos, V. and Alemán, A., 2000. Tectonic evolution of the Andes, *In* Cordani, U.G. et al. (eds.), Tectonic evolution of South America, Rio de Janeiro, Brazil, p.635-685.

Reid, W. P., 1969. Mineral staining tests, Mineral Industries Bulletin, v. 12, 3, May 1969, p.11.

Rivano, S. 1996. Geología de las Hojas Quillota y Portillo, Servicio Nacional de Geología y Minería, limited circulation, preliminary report 7644C1, 202 p, plus 29 p. appendix, to accompany Rivano, S., Sepúlveda, P., Boric, R., and Espiñeira, D., 1993, Hojas Quillota y Portillo, Servicio Nacional de Geología y Minería, Carta Geológica de Chile N° 73.

Rivano, S., Sepúlveda, P., Boric, R., Espiñeira, D., 1993. Hojas Quillota y Portillo (1:250,000), SERNAGEOMIN, Carta Geológica de Chile, No.73.

Roedder, E. 1979. Fluid inclusions as samples of ore fluids, *In* Geochemistry of hydrothermal ore deposits, 2nd ed., John Wiley, London, p.684-737.

Robinson, D., 1987. The transitionfrom diagenesis to metamorphism at very low grades and possible high grade analogues, Earth and Planetary Science Letters, 92, p.81-88.

Ruge, H., 1985. Geología y Mineralización del Yacimiento de Cobre El Soldado, V Región, Chile, IV Congr. Geol. Chileno, Antofagasta, IV, p.855-872.

Ruge, H., and Vera, I., 1985. Evaluation of sampling an grade control methods at the El Soldado underground copper mine, Chile, *In* Metz, R. A. (ed.) Applied mining geology; problems of sampling and grade control, SME. Am. Inst. Min. Metall. and Pet. Eng., New York, NY, p.147-156.

Ruiz, C. and Peebles, F., 1988. Geología, distribución y génesis de los yacimientos metalíferos Chilenos: Santiago, Editorial Universitaria, 334 p.

Ruiz, C., Aguirre, L., Corvalán, J., Klohn, C., Klohn, E., and Levi, B., 1965. Geología y yacimientos metalíferos de Chile, Instituto de Investigaciones Geológicas, Santiago, Chile, 302 p.

Ruiz, C., Aguilar, A., Egert, E., Espinosa, W., Peebles, F., Quezada, R. and Serrano, M., 1971. Strata-bound copper sulphide deposits of Chile, *In* Proceedings IMA-IAGOD, 7th General Meeting, Tokyo-Kyoto, Japan, 1970, Soc. Min. Geol. Japan, Special Issue 3, p.252-260.

Ruiz, J., Freydier, C., McCandless, T., Chesley, J. and Munizaga, F., 1997. Re-Os-Isotope systematics of sulfides from base-metal porphyry and manto type

mineralization in Chile, International Geology Review, v. 39, 4, p.317-324.

Ryan, P., Lawrence, A., Jenkins, R., Matthews. J., Zamora, J., Marino, E., and Urqueta, I., 1995. The Candelaria copper-gold deposit, Chile. *In* Pierce, F.W. and Bolm, J.G. (eds.) Porphyry copper deposits of the American Cordillera, Arizona Geological Society Digest, 20, p.625-645.

Sato, T., 1984. Manto-type copper deposits of Chile, *In* Research on calc-alkaline magmatism and related mineralization in Chile: Report of research and development cooperation ITIT project no.7911, Geological Survey of Japan: March 1984, p.57-72.

Scheuber, E. and Andriessen, P.A.M., 1990. The kinematic and geodynamic significance of the Atacama fault zone, northern Chile, Journal of Structural Geology, v. 12, No 2, p.243-257.

Scheuber, E., and Reuter, K.J. 1992. Relation between tectonics and magmatism in the Andes of northern Chile and adjacent areas between 21 and 25° S. Tectonophysics, 205, p.127-140.

Scheuber, E., Bogdanovic, T., Jensen, A., and Reuter, K., 1994. Tectonic development of the north Chilean Andes in relation to plate convergence and magmatism since the Jurassic, *In* Reuter, K., J., et al. (eds.) Tectonics of the southern Andes, Springer Verlag, p.121-153.

Sibson, R.H., 2001. Seismogenic framework for hydrotermal transport and ore deposition, *In* Richards J.P. and.Tosdal R.M. (eds.) Structural controls on ore genesis, Reviews in Economic Geology, vol. 14, p.25-50.

Sillitoe, R. H., 1990. Copper deposits and Andean evolution, Earth Science Series, Circum-Pacific Council Energy Mineral Resource, v.11, p.285–311.

Sillitoe, R. H., 1992. Gold and copper metallogeny of the Central Andes: past, present and future exploration objectives, Economic Geology v. 87, p.2205-2216.

Skewes, A., 1987a. Estudio de inclusiones fluídas en la mina El Soldado, unpublished internal CMD report, Technical Archives, El Soldado Mine, 12 p.

Skewes, A., 1987b. Inclusiones fluídas en muestras del sondaje 250/88 de El Soldado, unpublished internal CMD report, Technical Archives, El Soldado Mine, 4 p.

Skewes, A., 1988. Inclusiones fluídas en muestra de El Soldado, unpublished internal CMD report, Technical Archives, El Soldado Mine, 2 p.

Steinmüller, K., Chacón N., and Grant, B., 2000. Volcanogenic massive sulphide deposits

in Perú, *In* Sherlock, R.L. and Logan, M.A. (eds.) VMS deposits of Latin America, Special Publication n° 2, Mineral Deposit Division, Geological Association of Canada, p.423-437.

Subbarao, K.V., 2000. Sr isotopic evidence on the spilitic degradation of the Deccan Basalt, *In* Subbarao, K.V. (ed.) Deccan volcanic province (geomorphology, mineralogy, petrology, and geochemistry) Lonar Lake Memoir, Geological Society of India, Bangalore, 43, Part 2; p.49-55.

Tassinari, C., Munizaga, F. y Ramírez, R., 1993. Edad y geoquímica isotópica Rb-Sr del yacimiento de cobre Mantos Blancos: relación temporal con el magmatismo Jurásico, Revista Geológica de Chile, v. 20, N° 2, p.193-206.

Terrazas, R., 1977. Petrografia, alteración hidrotermal y mineralización del yacimiento cuprífero El Soldado, Provincia Valparaíso, Chile, unpublished Ph.D. thesis Universidad de Chile, 105 p.

Tosdal, R. M., 1996. The Amazon-Laurentian connection as viewed from the Middle Proterozic rocks in the central Andes, western Bolivia and northern Chile, Tectonics, v.15, No. 4, p.827 (95TC03248).

Trista, D., 2001. Mineralización y microtermometría de inclusiones fluidas de yacimientos cupríferos de la Cordillera de la Costa, entre los 22°04' - 22°44' latitud Sur, II Región de Antofagasta, Chile, unpublished B.Sc. Thesis, Departamento de Ciencias Geológicas, Universidad Católica del Norte, Antofagasta, Chile, 127 p.

Ullrich, T.D. and Clark, A.H., 1999. The Candelaria copper-gold deposit, Region III, Chile: Paragenesis, geochronology and fluid composition, *In* Stanley, C.J. et al. (eds.), Mineral Deposits: Processes to Processing, Balkema, Rotterdam, p.201-114.

Vallance, T.G., 1999. Spilitic degradation of a tholeiitic basalt, spilitic degradation of a tholeiitic basalt, *In* Subbarao, K.V. (ed.) Deccan volcanic province (geomorphology, mineralogy petrology, and geochemistry) Lonar Lake Memoir, Geological Society of India, Bangalore. 43, Part 2; p.855-866.

Vergara, M., Levi, B., Nyström, J.O., and Cancino, A., 1995. Jurassic and Early Cretaceous island arc volcanism, extension, and subsidence in the Coast range of central Chile, Geological Society of America Bulletin, v. 107, N°12, p.1427-1440.

Vidal, C., Injoque-Espinoza, J., Sidder, G.B., and Mukasa, S.B., 1990. Amphibolitic Cu- Fe skarn deposits in the central coast of Peru, Economic Geology v. 85, p.1447-1461.

Vila, T., Lindsay, N. and Zamora, R., 1996. Geology of the Manto Verde copper deposit,

northern Chile: a specularite-rich, hydrothermal-tectonic breccia related to the Atacama Fault Zone, *In* Camus, F. et al. (eds.), Andean copper deposits: new discoveries, mineralization styles and metallogeny, Soc. of Economic Geologists Special Publication N° 5, p.157-170.

Villalobos, H., 1995. Antecedentes para un modelo genético del yacimiento Veta Negra y su relación con el yacimiento de cobre El Soldado, V Región, unpublished B.Sc, Thesis, Universidad de Concepción, 91 p.

Vivallo, W. and Henríquez, F., 1998. Génesis común de los depósitos estratoligados y vetiformes de cobre del Jurásico Medio a Superior en la Cordillera de la Costa, Región de Antofagasta, Chile, Revista Geológica de Chile, v. 25, N° 2, p.199-228.

Wall, R., Gana, P., and Gutiérrez, A., 1996. Mapa Geológico del área de San Antonio-Melipilla, Regiones de Valparaíso, Metropolitana y del Libertador General Bernardo O'Higgins, Servicio Nacional de Geología y Minería, Chile, Mapas Geológicos, N° 2, Escala 1:100,000, 1 mapa, 1 anexo.

Wall, R., Selles, D., and Gana, P., 1999. Área Tiltil-Santiago, Región Metropolitana, Servicio Nacional de Geología y Minería, Chile, Mapas Geológicos, N°11, Escala 1:100,000, 1 mapa, 1 anexo.

Westra, G., 1988a. La importancia del metamorfismo de carga en la formación de yacimientos de cobre de tipo manto: preprint, Keynote Address, V Cong. Geol. Chileno, Santiago, 18 p.

Westra, G., 1988b. A critical appraisal of the evidence for a magmatic hydrothermal origin for the El Soldado copper deposit, unpublished internal CMD report. Technical Archives, el Soldado mine, 21 p.

Willson, M., 1989. Igneous petrogenesis: a global tectonic approach, London, Unwin Hyman, 466 p.

Wilson, N.S.F., 1996. Framboidal copper sulphides associated with bitumen: implications to genesis of the El Soldado copper deposit, Atlantic Geology, v. 32, 1, p.91.

Wilson, N.S.F, 1997. The role of petroleum in the genesis of central Chilean strata-bound copper deposits, GSA Abstracts with programs, 1997, p.A-208.

Wilson, N.S.F., 1998a. The role of petroleum in the formation of the El Soldado copper deposit, Chile: Hydrothermal replacement of a biodegraded petroleum reservoir, unpublished Ph.D. Thesis, Dalhousie University, Canada, 418 p.

Wilson, N.S.F, 1998b. Organic petrology of pyro-bitumen from the El Soldado copper deposit, Chile, Abstracts of the 15th Annual Meeting of The Society for Organic

Petrology, v.15, p.47-50.

Wilson, N.S.F., 2000. Organic petrology, chemical composition, and reflectance of pyrobitumen from the El Soldado Cu deposit, Chile, International Journal of Coal Geology, 43, p.53-82.

Wilson, N.S.F and Zentilli, M., 1997a. Copper sulphides formed in a degraded petroleum reservoir of the Cretaceous Andean arc basin, central Chile *In* Henry J.P. et al. (eds.) Proceedings, Geofluids Conference, p.488-491.

Wilson, N.S.F and Zentilli, M., 1997b. The role of petroleum in the formation of stratabound copper deposits in central Chile, GAC/MAC Abstracts, May 1997, p.A-158.

Wilson, N.S.F and Zentilli, M., 1998. The formation of stratabound copper deposits in degraded petroleoum reservoirs, central Chile, The Gangue, v. 57, p.16-17.

Wilson N.S.F. and Zentilli M., 1999. The role of organic matter in the genesis of the El Soldado volcanic-hosted manto-type Cu deposit, Chile, Economic Geology, v. 94, p.1115-1136.

Wilson, N.S.F., Zentilli, M., Reynolds, P.H. and Boric, R. (in press a). $^{40}Ar/^{39}Ar$ Geochronology of K-feldspar (Adularia) from the El Soldado manto-type copper deposit, Chile, submitted to Chemical Geology.

Wilson, N. S. F., Zentilli, M., and Spiro, B. (in press b). The essential role of bacteria and petroleum in the formation of the volcanic-hosted El Soldado manto-type Cu deposit, Chile: a sulfur, carbon, oxygen, and strontium isotope study, submitted to Economic Geology.

Williams, H., Turner F.J., and Gilbert, C.M., 1968. Petrografia, introducción al estudio de las rocas en secciones delgadas, Cía editoral Continental, S.A., México, 430 p.

Winchester J.A. and Floyd, P.A., 1977. Geochemical discrimination of different magma series and their differentiation products using immobile elements, Chemical Geology, v. 20, p.325-343.

Winkler, H.G F., 1974. Petrogenesis of metamorphic rocks, Springer Verlag, Berlin, 320 p.

Wood D.A., Joron, J.L., and Treuil, M., 1979. A re-appraisal of the use of trace elements to classify and discriminate between magma series erupted in different tectonics settings, Earth and Planetary Science Letters, 45, p.326-336.

Zentilli, M., 1974. Geological evolution and metallogenetic relationships in the Andes of

northern Chile between 26° and 29° South, unpublished Ph.D. thesis, Queen's University, Kingston, Ontario, Canada, 446 p.

Zentilli, M., Boric, R., Munizaga, F., and Graves, M.C., 1994. Petroleum involvement in the genesis of some strata-bound copper deposits of Chile, VII Congr. Geol. Chileno, Concepción, II, p.542-1546.

Zentilli, M., Munizaga, F., Graves, M. C., Boric. R., Wilson. N.S.F., Mukhopadhyay, P. K., and Snowdon, L.R., 1997, Hydrocarbon involvement in the genesis of ore deposits: an example in Cretaceous strata-bound (manto type) copper deposits of central Chile, International Geology Review, v.39, p.1-21.

Zentilli, M, Heaman, L., Pop, N., and Boric, R., 2001. Evidence of Precambrian crust under the Coastal Cordillera of Chile: xenocrystic zircons in Cretaceous volcanic rocks, (Abstract published, not presented), III South American Symposium on Isotope Geology, Comunicaciones, Universidad de Chile.

Appendices

APPENDIX 1. SAMPLE LIST WITH INDICATIONS OF THE ANALYSIS DONE

- Abbreviations:
    - bckd: background
    - bckd mt: background with magnetite
    - bckd py: background with pyrite
    - bckd py-mt: background with pyrite-magnetite
    - bckd py-ht: background with pyrite-hematite
    - bckd ht: background with hematite
    - bckd ht-cp: background with hematite-chalcopyrite
    - bckd py-sph-ga: background with pyrite-sphalerite-galena
    - py: pyrite
    - py-cp: pyrite-chalcopyrite
    - py-cp-sp: pyrite-chalcopyrite-specularite
    - cp: chalcopyrite
    - cp-bn: chalcopyrite-bornite
    - bn: bornite
    - bn-cc: bornite-chalcocite
    - cc: chalcocite

Appendix 1.- Sample List with Indication of Analyses Done

Sample #	North	East	Elevation	Code	Meters	Mine Block	Rock Type	Ore Zone	% Cu in drill core 3 m interval	Petrography	Ore Petrography	Chemical	Microprobe Points	Microprobe X Ray	XRD	Dating	Cobaltinitrite tintion	Specific Gravity	Magnetic Susceptibility
Z614-95	175	680	910			Morro	microdioritic dike	bckd		X	X	X	X				X		X
Z617-95	163	673	909			Morro	mafic dyke	cp											X
Z618-95	254	579	909			Morro	mafic dyke	cp											X
Z619-95	-10	381	920			Morro	volcanic sediment	bckd											X
Z622-95	250	1423	628	S250/88	910.0-910.2	Arauco N	gabbro	bckd	0.02	X	X	X					X		X
Z623-95	250	1423	628	S250/88	870.2-870.3	Arauco Norte	gabbro	altered	0.03						X		X		X
Z624-95	250	1420	629	S250/88	866.5-866.6	Arauco Norte	rhyodacite	py	0.03										
Z625-95	250	1405	633	S250/88	850.0-850.1	Arauco Norte	brecciated rhyodacite	py	0.01						X		X		X
Z626-95	300	810	959	SAQ20/86	108.8-109.0	Morro	basaltic dyke	bckd	0.02	X	X	X	X				X		X
Z629-95	-950	1311	565	S139/91	184.0-84.2	Osorno	rhyodacite	bckd	0.01										X
Z630-95				S160/94	256.7-256.8	Catedral	mafic dyke	py	0.07									X	X
Z631-95	-650	1174	601			Valdivia Sur	rhyodacite	bckd	0.02										X
Z632-95	-650	1274	556	S651/87	366.0-366.3	Valdivia Sur	basalt	bckd py	0.01	X	X	X	X				X		X
Z634-95	-1150	682	744	S24/95	292.3-292.6	Malvas	basalt	bckd py	0.01										X
RB2000-2	-2264	61	1245	ST5/00	21.0 - 21.6	Tardones	basalt	py-cp								Ar/Ar			
MP2001-01				S195/00	104.7-104.8	Manto Rojo Norte	brecciated rhyodacite	py-cp-spe		X	X								
MP2001-02				S195/00	115.7-115.8	Manto Rojo Norte	brecciated rhyodacite	py-cp		X	X								
MP2001-03				S195/00	163.1-163.2	Manto Rojo Norte	brecciated rhyodacite	py-cp-spe		X	X								
MP2001-04				S195/00	168.5-168.6	Manto Rojo Norte	brecciated rhyodacite	cp-bn-spe		X	X								
MP2001-05				S195/00	173.5-173.6	Manto Rojo Norte	brecciated rhyodacite	cp-bn		X	X								
MP2001-06				S195/00	215.5-215.6	Manto Rojo Norte	rhyodacite	py-cp-spe		X	X								
MP2001-07				S195/00	271.3-271.4	Manto Rojo Norte	brecciated rhyodacite	py-cp-spe		X	X								
MP2001-30				S115/01	330.2-330.3	Manto Rojo Norte	rhyodacite	py-cp-spe		X	X								

Appendix 1.- Sample List with Indication of Analyses Done

Sample #	Location			Drill core		Mine Block	Rock Type	Ore Zone	% Cu in drill core 3 m interval	Analyses									
	North	East	Elevation	Code	Meters					Petrography	Ore Petrography	Chemical	Microprobe Points	Microprobe X Ray	XRD	Dating	Cobaltinitrite tintion	Specific Gravity	Magnetic Susceptibility
RB9907	-750	987	664	S751	207.7-207.9	Valdivia Sur	vein	cp-bn	4.46								X		
RB9908	-750	1038	637	S751	265.6-265.7	Valdivia Sur	breccia	py	0.04								X		
RB9909	-750	988	664	S751	209.7-209.9	Valdivia Sur	vein	py-cp	4.46								X		
RB9910	-750	1008	654	S751	231.0-231.2	Valdivia Sur	rhyodacite	bn	3.57								X		
RB9911	-750	1014	650	S751	238.6-238.8	Valdivia Sur	rhyodacite	bn-cc	6.14								X		
RB9912	-750	1485	390	S751	775.9-776.0	Valdivia Sur	sandstone	py-cp	0.14						X		X		
RB9913	-750	893	593	S507/84	190.4-190.6	Valdivia Sur	basalt	bckd	0.02						X		X		
RB9914	-750	895	587	S507/84	196.7-196.9	Valdivia Sur	basalt	py-cp	0.35								X		
RB9915	-750	918	545	S507/84	244.7-244.8	Valdivia Sur	rhyodacite	py	0.07								X		
RB9916	-750	948	607	S463/84	212.2-212.3	Valdivia Sur	rhyodacite	cp-bn	3.33								X		
RB9917	-750	968	584	S463/84	242.0-242.1	Valdivia Sur	rhyodacite	bn-cc	5.84								X		
RB9918	-750	945	740	S133/84	145.6-145.8	Valdivia Sur	rhyodacite	bn	0.21								X		
RB9919	-750	922	826	S117/84	50.0-50.1	Valdivia Sur	rhyodacite	cp	3.38								X		
RB9920	-750	927	825	S117/84	54.9-55.0	Valdivia Sur	rhyodacite breccia	bn-cc	3.17								X		
RB9921	-750	960	898	S145/87	103.9-104.0	Valdivia Sur	basalt	cp-bn	0.10						X		X		
RB9922	-750	1012	1034	S145/87	169.0-169.2	Valdivia Sur	basalt	cp-bn	3.43						X		X		
RB9923	-750	1039	1051	S145/87	200.4-200.6	Valdivia Sur	basaltic dike	bn	0.99								X		
RB9924	-750	1041	1053	S145/87	202.0-202.2	Valdivia Sur	vein in basaltic dike	bn	0.94						X		X		
RB9925	-775	1013	908	S101/89	97.3-97.4	Valdivia Sur	basalt	bckd	0.06								X		
RB9926	-775	1033	908	S101/89	76.9-77.1	Valdivia Sur	volcanic sed.	cp-bn	2.34						X		X		
RB9927	-750	1073	935	S99/89	47.9-48.0	Valdivia Sur	volcanic sed.	bckd	0.04								X		
RB9928	-750	1069	936	S99/89	52.3-52.5	Valdivia Sur	volcanic sed.	bckd	0.09						X		X		
RB9929	-750	1062	940	S99/89	60.6-60.8	Valdivia Sur	volcanic sed - basaltic dike	bckd	0.06								X		
RB9930	-900	459	1081	S42/91	21.9-22.0	Filo	basalt	bckd	0.14				X		X		X		
RB9931	-900	460	1081	S42/91	22.3-22.4	Filo	basalt	bckd	0.06								X		
RB9932	-900	471	1075	S42/91	35.6-35.7	Filo	basalt	bckd	0.09						X		X		
RB9933	-900	457	1082	S42/91	21.0-21.1	Filo	basalt	bckd	0.14						X		X		
RB9934	-900	593	1014	S42/91	170.8-170.9	Filo	basalt	bn-cc	1.51								X		
RB9935	-750	1034	949	S145/87	194.4-194.5	Valdivia Sur	volcanic sediment	bn-cc	1.50						X		X		
Z603-95	-853	659	1154			Filo	basalt Veta Negra Fm	bckd		X	X	X	X				X		X
Z604-95	-1022	418	1052			Filo	basalt	bkd											X
Z607-95	-108	619	923			Morro	microdioritic dike	bkd											X
Z612-95	100	666	909			Morro	rhyodacite	cp							X		X		X

Sample #	Location			Drill core		Mine Block	Rock Type	Ore Zone	% Cu	Analyses									
	North	East	Elevation	Code	Meters				in drill core 3 m intervale	Petrography	Ore Petrography	Chemical	Microprobe Points	Microprobe X Ray	XRD	Dating	Cobaltinitrite tintion	Specific Gravity	Magnetic Susceptibility
RB98-47	-900	612	1004	S42/91	194.2-194.6	Filo	basalt	bn-cc	1.05	X	X	X					X	X	X
RB98-48	-900	615	1003	S42/91	197.1-197.4	Filo	basalt	py-cp	0.32	X	X	X					X	X	X
RB98-49	-900	624	999	S42/91	206.6-207.0	Filo	basalt	bckd py	<0.01	X	X	X					X	X	X
RB98-50	-900	735	988	S902	266.7-266.9	Filo	basalt	bckd py	0.03	X	X	X					X	X	X
RB98-51	-900	739	985	S902	272.0-272.1	Filo	basalt	py	0.03								X		
RB98-52	-900	696	1010	S902	222.4-222.7	Filo	basalt	bn-cc	2.05	X	X	X	X	X			X	X	X
RB98-53	-900	1003	830	S902	577.4-557.6	Filo	basalt	py	0.01								X		
RB98-54	-900	817	940	S902	363.0-363.6	Filo	basalt	py-cp	0.13								X		
RB98-55	-900	633	898	S903	42.1-42.3	Filo	basalt	bn-cc	0.38								X		
RB98-56	-900	640	892	S903	50.3-50.6	Filo	rhyodacite	bn-cc	1.88	X	X	X					X	X	X
RB98-57	-900	671	862	S903	94.4-94.7	Filo	rhyodacite	bn	0.31								X		
RB98-58	-900	701	836	S903	132.5-132.8	Filo	rhyodacite	cp-bn	0.45								X		
RB98-59	-900	719	820	S903	157.5-157.7	Filo	rhyodacite	bn-cc	1.24								X		
RB98-60	-900	741	801	S903	186.7-187.0	Filo	rhyodacite	cp-bn	0.95								X		
RB98-61	-900	751	790	S903	199.8-200.0	Filo	rhyodacite	bckd cp-ht	0.26	X	X	X					X	X	X
RB98-62	-900	772	772	S903	228.5-228.7	Filo	rhyodacite	bn-cc	0.71								X		
RB98-63	-900	787	758	S903	248.3-248.5	Filo	rhyodacite	bckd cp-ht	0.10								X		
RB98-64	-900	623	854	S219/96	20.0-20.2	Filo	rhyodacite	bckd cp-ht	0.22	X	X	X					X	X	X
RB98-65	-900	617	861	S219/96	28.4-28.8	Filo	rhyodacite	bn	1.04	X	X	X					X	X	X
RB98-66	-900	698	884	S219/96	58.5-58.9	Filo	rhyodacite	bn	1.67								X		
RB98-67	-900	680	906	S219/96	87.0-87.3	Filo	rhyodacite	bn	0.74	X	X	X	X	X	X		X	X	X
RB98-68	-900	671	916	S219/96	99.5-99.8	Filo	rhyodacite	bn-cc	1.21								X		
RB98-69	-900	664	925	S219/96	113.6-113.8	Filo	rhyodacite	bn-cc	1.44	X	X	X					X	X	
RB98-70	-900	642	951	S219/96	146.4-146.6	Filo	rhyodacite	bckd ht	0.08	X	X	X					X	X	X
RB98-71	-900	640	953	S219/96	149.8149.9	Filo	rhyodacite	bckd cp-ht	0.04								X		
RB98-72	-750	1247	524	S182/96	150.0-222.0	Valdivia Sur	rhyodacite	bckd py	0.04	X						U/Pb	X	X	X
RB98-73 (composite)	-900	1030	490	S121/94	113.0-154.0	Osorno	rhyodacitic dike	py-cp	0.86	X						U/Pb	X		X
	-900	1025	470	S232/94	123.0-155.0	Osorno		py-cp	1.02								X		
	-900	1045	508	110/94	120.0-155.0	Osorno		py-cp	0.92								X		
RB98-74 (composite)	250	1520	770	S316/97	499.0-527.0	Arauco	gabbro	bckd	0.02	X						U/Pb	X	X	X
	250	1485	642	S266/97	722.0-760.0	Arauco		bckd	0.00								X		
	250	1450	620	S250/88	889.0-899.0	Arauco		bckd	0.03								X		
RB98-75	-750	1052	754	SP116/84	196.0-196.1	Valdivia Sur	basalt	bckd	0.03								X		
RB98-76	-750	1043	800	SP117/84	173.0-173.2	Valdivia Sur	basalt	py-cp	0.18	X	X	X					X	X	X
RB9901	-750	995	660	S751	217.5-217.6	Valdivia Sur	rhyodacite	bn-cc	4.51	X	X	X	X	X	X		X		X
RB9902	-750	1004	655	S751	227.3-227.4	Valdivia Sur	rhyodacite	cp-bn	3.32	X	X	X			X		X		X
RB9903	250	1164	692	S250/88	597.4-597.5	Arauco Norte	rhyodacite	py	0.05	X	X	X	X	X	X		X		X
RB9904	250	1415	630	S250/88	856.5-856.7	Arauco Norte	rhyodacite	py	0.04	X	X	X			X		X		X
RB9905	-750	968	675	S751	186.5-186.7	Valdivia Sur	vein	cp-bn	1.90								X		
RB9906	-750	985	666	S751	205.8-206.0	Valdivia Sur	vein	cp-bn	5.90								X		

Appendix 1.- Sample List with Indication of Analyses Done

Sample #	Location			Drill core		Mine Block	Rock Type	Ore Zone	% Cu	Analyses									
	North	East	Elevation	Code	Meters				in drill core 3 m intervals	Petrography	Ore Petrography	Chemical	Microprobe Points	Microprobe X Ray	XRD	Dating	Cobaltinitrite tintion	Specific Gravity	Magnetic Susceptibility
RB98-07	-750	829	805	S90/85	68.1-68.4	Valdivia Sur	rhyodacite	bckd py	0.02								X		
RB98-08	-750	910	705	S751	122.0-122.3	Valdivia Sur	rhyodacite-andesite	bckd py	0.03								X		
RB98-09	-750	844	745	S132/84	45.0-45.3	Valdivia Sur	rhyodacite	py	0.05	X	X	X					X	X	X
RB98-10	-750	949	686	S751	164.7-65.0	Valdivia Sur	rhyodacite	py	0.07	X	X	X					X	X	X
RB98-11	-750	966	676	S751	184.1-184.3	Valdivia Sur	rhyodacite	py-cp	0.37	X	X	X	X	X			X	X	X
RB98-12	-750	985	665	S751	206.1-206.3	Valdivia Sur	rhyodacite	cp	5.90	X	X	X					X	X	X
RB98-13	-750	973	673	S751	192.0-192.3	Valdivia Sur	rhyodacite	cp-bn	1.06	X	X	X					X	X	X
RB98-14	-750	983	668	S751	203.9-204.0	Valdivia Sur	rhyodacite	cp-bn	1.71								X		
RB98-15	-750	1002	658	S751	224.3-224.6	Valdivia Sur	rhyodacite	bn-cc	4.91	X	X	X	X	X	X		X	X	X
RB98-16	-750	1005	655	S751	227.6-227.7	Valdivia Sur	rhyodacite	bn-cc	3.32								X		
RB98-17	-750	1009	654	S751	232.0-232.2	Valdivia Sur	rhyodacite	bn-cc	3.57								X		
RB98-18	-750	1015	650	S751	238.6-238.7	Valdivia Sur	rhyodacite	bn	6.14						X		X		
RB98-19	-750	1019	642	SP131/84	247.5-247.7	Valdivia Sur	rhyodacite	cp-bn	4.47	X	X	X					X	X	X
RB98-20	-750	1018	648	S751	243.0-243.2	Valdivia Sur	rhyodacite	cp-bn	0.37								X		
RB98-21	-750	1047	632	S751	276.6-276.8	Valdivia Sur	rhyodacite	bckd py	0.07	X	X	X					X	X	
RB98-22	-750	1111	594	S751	351.0-351.3	Valdivia Sur	rhyodacite	bckd py	0.02	X	X	X	X	X			X	X	X
RB98-23	-750	1155	570	S751	401.5-401.7	Valdivia Sur	rhyodacite	bckd py	0.02								X		
RB98-24	-750	1160	428	S182/96	334.6-334.8	Valdivia Sur	rhyodacite	bckd py	0.09								X		
RB98-25	-750	1532	418	S751	716.7-717.0	Valdivia Sur	rhyodacite	py	0.03								X		
RB98-26	-750	445	1015	S28/91	36.7-37.0	Filo	basalt	bckd py	0.01								X		
RB98-27	-750	709	908	S28/91	322.0-322.3	Filo	basalt	bckd	0.02						X		X		
RB98-28	-750	770	888	SP508/84	194.3-194.6	Filo	basalt	bckd	0.05								X		
RB98-29	-775	902	908	S101/89	210.4-210.7	Valdivia Sur	basalt	bckd mt	0.02	X	X	X	X	X			X	X	X
RB98-30	-775	890	908	S101/89	222.2-222.3	Valdivia Sur	basalt	bn	0.08								X		
RB98-31	-775	927	908	S101/89	185.7-185.8	Valdivia Sur	basalt	py-cp	0.17	X	X	X					X	X	X
RB98-32	-775	946	908	S101/89	166.0-166.3	Valdivia Sur	basalt	bn-cc	0.64								X		
RB98-33	-775	967	908	S101/89	145.9-146.0	Valdivia Sur	basalt	bn-cc	1.93						X		X		
RB98-34	-775	973	908	S101/89	139.5-139.8	Valdivia Sur	basalt	bn-cc	2.60								X		
RB98-35	-775	989	907	S101/89	123.8-123.9	Valdivia Sur	basalt	cp	0.86								X		
RB98-36	-775	986	907	S101/89	126.8-127.1	Valdivia Sur	basalt	cp	0.55	X	X	X					X	X	X
RB98-37	-775	1028	907	S101/89	84.4-84.8	Valdivia Sur	basalt	py	0.80								X		
RB98-38	-775	1041	907	S101/89	70.6-71.0	Valdivia Sur	basalt	bn	0.97								X		
RB98-39	-775	1058	925	S118/87	205.7-205.8	Valdivia Sur	volcanic sed.	bn	0.63						X		X		
RB98-40	-900	1178	741	S111/91	147.5-147.7	Osorno	basalt	bckd mt	0.01	X	X	X					X	X	X
RB98-41	-900	1251	574	S88/91	131.9-132.2	Osorno	basalt	bckd py	<0.01								X		
RB98-42	-900	467	1076	S42/91	31.8-32.1	Filo	basalt	bckd mt	0.01	X	X	X	X	X			X	X	X
RB98-43	-900	477	1072	S42/91	42.5-43.0	Filo	basalt	bn	0.18				X		X		X		
RB98-44	-900	527	1047	S42/91	98.0-98.3	Filo	basalt	bn-cc	0.87	X	X	X	X				X	X	X
RB98-45	-900	584	1019	S42/91	162.2-162.9	Filo	basalt	cp-bn	0.49	X	X	X					X	X	X
RB98-46	-900	602	1010	S42/91	182.5-182.6	Filo	basalt	bn-cc	0.33						X		X		

Appendix 1.- Sample List with Indication of Analyses Done

Sample #	Location			Drill core		Mine Block	Rock Type	Ore Zone	% Cu	Analyses									
	North	East	Elevation	Code	Meters				in drill core 3 m intervals	Petrography	Ore Petrography	Chemical	Microprobe Points	Microprobe X Ray	XRD	Dating	Cobaltinitrite tintion	Specific Gravity	Magnetic Susceptibility
MP-831	50	698	754	SP392/84	85.3-85.5	Morro	volcanic sediment	cp	1.13	X	X	X							
MP-833	50	786	943	S24/94	50.1-50.3	Morro	volcanic sediment	cp	2.36	X	X	X							
MP-839	-750	921	541	SP507/84	250.7-250.9	Valdivia Sur	rhyodacitic dike	py	0.11	X	X	X	X				X	X	X
MP840						Morro	basaltic dike rhyodacite	cp		X			X	X	X		X		
MP-842	-750	1233	569	S111/94	147.0-147.1	Valdivia Sur	rhyodacite	py-cp	0.17										X
MP-844	-900	484	1018	S17/92	97.5-97.7	Filo	rhyodacitic dike	bckd mt	0.01	X	X	X	X				X	X	X
MP-845	-900	359	1011	S43/92	27.6-27.8	Filo	rhyodacitic dike	bckd py-mt	0.01	X	X	X	X				X	X	X
MP-846	200	341	845	S46/85	33.9-34.2	Morro	rhyodacitic dike	bckd py	0.07	X	X	X	X				X	X	X
MP-848	400	836	898	S66/94	279.2-279.4	Morro	rhyodacitic dike	bckd py	0.03	X	X	X	X				X	X	X
MP-849	-825	649	1066	S803	77.2-77.3	Filo	basalt	cc	0.42						X				
MP-850	-825	652	1066	S803	74.7-74.9	Filo	basalt	bn	0.47				X		X		X		X
MP-851	-800	728	1106	S158/90	52.7-52. 9	Filo	basalt Veta Negra Fm	bn-cc	5.14						X				X
MP-854	-750	1040	958	S99/89	87.7-87.9	Valdivia Sur	volcanic sediment	bn	0.91	X	X	X	X	X	X		X	X	X
MP-855	-750	1079	939	S99/89	39.5-39.8	Valdivia Sur	volcanic sediment	bkd py	0.04	X	X	X	X	X	X		X	X	X
MP-856	-750	991	658	SP131/84	216.3-216.5	Valdivia Sur	rhyodacite	bn	7.82	X	X	X	X				X	X	X
MP-858	50	906	1044	S144/93	36.5 to 36.7	Morro	volcanic sed.	py	0.34	X	X	X					X		X
MP-860	-900	380	1001	S43/92	50.8-51.0	Filo	rhyodacite	py	0.04	X	X	X	X				X	X	X
MP-861	-900	440	968	S43/92	119.0-119.2	Filo	volcanic sed.	py-cp	0.09	X	X	X					X		X
MP-864	350	385	893	S124/95	2.0-2.4	Morro	rhyodacite	bn-cc	1.06	X	X	X	X		X		X	X	X
MP-865	-750	1026	909	S116/87	168.0-168.2	Valdivia Sur	basalt	py	2.26	X	X	X	X	X			X	X	X
MP-866	0	991	550	S160/94	8.0-8.2	Arauco	andesitic dike	py	0.04	X	X	X	X				X		X
MP-869	-750	1011	936	S145/87	173.1-173.3	Valdivia Sur	volcanic sed.	cp	1.61	X	X	X							X
MP880	-1100	679	653	S27/93	253.5-253.6	Malvas	basalt	bn	1.00						X				
RB98-01	250	1515	776	S316/97	498.0-511.0	Arauco N	gabbro	bckd	0.01						X		X	X	X
RB98-02	250	1483	645	S266/97	733.0-747.0	Arauco N	gabbro	bckd	0.00						X				
RB98-03	250	1434	679	S266/97	681.6- 681.7	Arauco N	gabbro-rhyodacite	bckd	0.00						X				
RB98-04	-900	1032	516	S110/94	114.0-129.0	Osorno	rhyodacite dike	py-cp	0.71						X				
RB98-05	-750	1245	527	S182/96	178.0-188.0	Valdivia Sur	rhyodacite	bckd py	0.06	X	X	X	X	X			X	X	X
RB98-06	-750	1320	552	S160/96	226.0-237.0	Valdivia Sur	basalt	bckd py	0.09	X	X	X	X	X			X	X	X

234

Appendix 1.- Sample List with Indication of Analyses Done

Sample #	Location			Drill core		Mine Block	Rock Type	Ore Zone	% Cu in drill core 3 m interval	Analyses									
	North	East	Elevation	Code	Meters					Petrography	Ore Petrography	Chemical	Microprobe Points	Microprobe X Ray	XRD	Dating	Cobaltinitrite titration	Specific Gravity	Magnetic Susceptibility
MP-664	-900	875	768	S157/89	72.4-72.5	Osorno	rhyodacite	bn-cc	2.74	X	X	X	X		X		X	X	X
MP-674	-900	1033	637	S186/89	260.5-260.7	Osorno	rhyodacite	cp	0.43	X	X	X					X	X	X
MP-677	-875	1063	739	S16/89	260.0-260.3	Osorno	rhyodacite	bn	3.77	X	X	X	X		X		X	X	X
MP-701	-900	1054	506	S110/94	144.4-144.5	Osorno	rhyodacite	py	0.90	X	X	X					X	X	X
MP-703	-900	1058	470	S121/94	166.7-166.8	Osorno	basalt	py	0.30	X	X	X	X				X	X	X
MP-713	350	610	975	S27/92	17.1-17.2	Morro	brecciated rhyodacite	bn	1.07	X	X	X	X				X	X	X
MP-716	350	364	804	S46/92	44.2-44.4	Morro	rhyodacite	cp	0.59										X
MP-718	100	438	962	S46/92	48.5-49.4	Morro	rhyodacite	bn	1.42	X	X	X	X		X		X	X	X
MP-719	350	380	792	S51/85	58.4-58.6	Morro	rhyodacite	py	0.13	X	X	X	X				X	X	X
MP-723	51.3	904	1044	S144/93	21.0-21.2	Morro	basalt	cp-bn	1.31	X	X	X	X				X	X	
MP-724	51.3	905	1038	S144/93	27.5-27.7	Morro	basalt	cp	7.40	X	X	X	X				X	X	X
MP-728	-101	572	905	S30/94	75.7-75.9	Morro	basalt	py	0.06	X	X	X	X				X	X	X
MP-737	-900	575	895	S43/92	274.3-274.5	Filo	rhyodacite	cc	2.23	X	X	X	X		X		X	X	X
MP-739	-750	509	952	S11/92	125.5-125.7	Filo	rhyodacite	cp	2.31	X	X	X	X		X		X	X	X
MP-746	-750	493	996	S28/91	90.1-90.3	Filo	rhyodacite	bn-cc	1.15	X	X	X	X				X	X	X
MP-747	-900	573	897	S43/92	295.1-295.2	Filo	sandstone	bn	1.56	X	X	X					X	X	X
MP-754	-25	-390	610	S178/90	226.6-226.8	Paso Riel	rhyodacitic dike	bckd py-sp-ga	0.01	X	X	X	X				X	X	X
MP-757	-25	-428	610	S178/90	177.5-177.7	Paso Riel	rhyodacitic dike	bckd py-sp-ga	0.01	X	X	X					X	X	X
MP-761	-25	-445	610	S178/90	169.8-170.0	Paso Riel	sandstone	bckd py-sp-ga	0.02	X	X	X	X						
MP-764	-750	947	536	S75/88	1.4-1.6	Valdivia Sur	rhyodacitic dike	cp	0.69	X	X	X	X				X	X	X
MP-768	-750	929	517	SP507/84	229.1-229.3	Valdivia Sur	rhyodacitic dike	py-cp	0.03	X	X	X	X				X	X	X
MP-770	-750	927	531	SP507/84	260.8-261.0	Valdivia Sur	rhyodacitic dike	py	0.05	X	X	X	X	X	X		X	X	X
MP-772	-750	1035	960	S99/89	84.20- 84.5	Valdivia Sur	basaltic dike	cc	4.92	X	X	X	X	X			X	X	X
MP-775	-750	1027	945	S145/87	185.2-185.5	Valdivia Sur	rhyodacite	cp	2.39	X	X	X	X				X	X	X
MP-776	-750	1022	941	S145/87	179.2-179.5	Valdivia Sur	rhyodacite	py	1.08	X	X	X					X	X	X
MP-778	-750	970	587	SP463/84	240.6-240.8	Valdivia Sur	rhyodacite	bn-cc	5.75	X	X	X	X	X			X	X	X
MP-782	-750	1005	696	SP132/84	210.0-210.2	Valdivia Sur	rhyodacite	bn-cc	4.30	X	X	X	X				X	X	X
MP-786	-750	1019	806	SP117/84	147.7-147.9	Valdivia Sur	basalt	cp	0.64	X	X	X	X	X			X	X	X
MP-787	-750	975	815	SP117/84	102.2-102.5	Valdivia Sur	basalt	bn	1.49	X	X	X	X				X	X	
MP-788	-750	446	911	S12/92	124.4-124.6	Filo	basalt	py	0.01	X	X	X					X		
MP-790	-900	574	761	S54/88	223.5-223.7	Filo	basalt	cp-bn	0.90	X	X	X	X				X	X	X
MP-791	-900	581	962	S17/92	211.1-211.4	Filo	volcanic sediment	cc	1.28	X	X	X	X				X		
MP-793	-900	614	1073	S167/90	210.3-210.5	Filo	basalt	cc	3.86	X	X	X	X				X		
MP-805	200	433	918	S14/94	15.0-15.2	Morro	basalt	bn-cc	3.23	X	X	X	X				X	X	X
MP-817	-100	922	1103	S156/93	7.5 to 7.7	Morro	volcanic sediment	bn-cc	3.71	X	X	X							X

APPENDIX 2. ROCK GEOCHEMISTRY DATA

2.1.- Rock geochemistry (major, minor, trace, and rare earth elements), listed by sample number.

2.2.- Geochemical composition by rock type and ore zone (major, minor, selected trace, and rare earth elements).

2.3.- CIPW norm calculations for less altered basalts.

Appendix 2.1.- Rock Geochemistry

- Major, minor, trace, and rare earth elements.

- Listed by sample number

- Abbreviations:
    - Rock Type:
        - rhy: rhyodacite
        - rhydk: rhyodacitic dyke
        - bas: basalt
        - basdk: basaltic dyke
        - volcsed: volcanic sediment
        - sand: sandstone
        - diordk: microdioritic dyke
        - anddk: andesitic dyke
        - basVN: basalt of Veta Negra Formation

    - Ore zone:
        - bckd: background
        - bckd mt: background with magnetite
        - bckd py: background with pyrite
        - bckd py-mt: background with pyrite-magnetite
        - bckd py-ht: background with pyrite-hematite
        - bckd ht: background with hematite
        - bckd ht-cp: background with hematite-chalcopyrite
        - bckd py-sph-ga: background with pyrite-sphalerite-galena
        - py: pyrite
        - py-cp: pyrite-chalcopyrite
        - cp: chalcopyrite
        - cp-bn: chalcopyrite-bornite
        - bn: bornite
        - bn-cc: bornite-chalcocite
        - cc: chalcocite

Appendix 2.1.- Rock Geochemistry

Sample	Rock Type	Ore Zone	Mine Block	Cu[1] %	Spec. Grav.	Mag. Susc.	SiO₂ %	TiO₂ %	Al₂O₃ %	Fe₂O₃T %	MnO %	MgO %	CaO %	Na₂O %	K₂O %	P₂O₅ %	LOI %	Cr₂O₃ %	Total %	FeO %	FeOT[2] %
MP664	rhy	bn-cc	Osorno	2.74	2.56	0.01	59.81	0.49	15.21	4.19	0.17	1.10	6.16	6.19	2.92	0.24	4.57	< 0.01	101.05	3.63	3.77
MP674	rhy	py-cp	Osorno	0.43	2.58	0.00	64.11	0.38	14.37	0.62	0.06	0.15	6.21	6.63	2.28	0.08	4.14	< 0.01	99.03	0.67	0.56
MP677	rhy	bn	Osorno	3.77	2.65	0.00	66.10	0.47	16.33	0.84	0.06	0.19	3.56	5.78	4.35	0.26	2.98	0.01	100.95	1.29	0.76
MP701	rhydk	py	Osorno	0.90	2.76	0.14	69.36	0.41	13.92	3.81	0.02	0.36	1.55	4.64	2.10	0.10	2.86	0.01	99.14	1.52	3.43
MP703	bas	py	Osorno	0.30	2.95	0.00	47.03	0.55	15.29	9.45	0.31	5.55	7.66	3.51	1.13	0.09	9.05	0.02	99.64	4.62	8.50
MP713	rhy	bn	Morro	1.07	2.60	0.02	68.00	0.36	12.63	1.52	0.08	0.07	4.96	6.20	0.64	0.07	4.27	0.01	98.81	1.37	1.37
MP718	rhy	bn	Morro	1.42	2.59	0.00	64.65	0.56	16.64	0.80	0.02	0.10	3.02	10.55	0.25	0.15	2.25	< 0.01	98.99	0.93	0.72
MP719	rhy	py	Morro	0.13	2.71	0.02	66.88	0.47	14.04	3.27	0.06	1.06	2.37	3.95	3.72	0.10	3.29	0.01	99.22	2.03	2.94
MP723	bas	cp-bn	Morro	1.31	2.78		45.53	0.56	15.33	9.41	0.29	1.74	7.78	5.96	2.74	0.64	3.58	0.09	93.65	11.20	8.47
MP724	bas	cp	Morro	7.40	2.87	0.00	48.33	0.87	16.81	6.71	0.35	2.41	7.44	5.70	3.07	0.43	6.00	0.07	98.19	6.40	6.04
MP728	bas	py	Morro	0.06	2.76	0.04	50.96	0.73	17.11	8.37	0.45	5.73	5.46	5.91	0.34	0.18	4.70	0.02	99.96	5.70	7.53
MP737	rhy	cc	Filo	2.23	2.57	0.01	72.00	0.38	15.90	0.75	0.05	0.22	0.68	8.65	0.11	0.22	0.89	0.01	99.86	0.95	0.67
MP739	rhy	cp	Filo	2.31	2.49	0.00	63.98	0.38	18.36	3.36	0.02	0.06	0.65	10.55	0.06	0.22	1.44	< 0.01	98.08	3.09	3.02
MP746	rhy	bn-cc	Filo	1.15	2.59	0.00	62.71	0.33	13.12	0.29	0.10	0.07	7.46	5.08	4.22	0.07	5.55	< 0.01	99.00	0.43	0.26
MP747	volcsed	bn	Filo	1.56			63.07	0.46	13.60	9.07	0.24	3.45	0.99	4.92	0.21	0.11	3.18	0.01	99.31	6.42	8.16
MP754	rhydk	bckd py-sph-ga	Paso Riel	0.01	2.63	0.01	64.95	0.38	11.57	3.07	0.12	2.15	5.00	2.91	4.42	0.07	4.28	< 0.01	98.92	2.01	2.76
MP757	rhydk	bckd py-sph-ga	Paso Riel	0.01	2.58	0.00	66.69	0.48	13.68	3.36	0.07	2.11	1.55	3.71	4.70	0.11	2.36	0.01	98.83	2.34	3.02
MP761	sand	bckd py-sph-ga	Paso Riel	0.02			52.83	1.07	17.28	8.77	0.23	5.29	2.84	2.59	3.48	0.29	4.92	< 0.01	99.59	6.20	7.89
MP764	rhydk	cp	Valdivia S	0.69	2.57	0.00	60.89	0.42	17.23	1.86	0.06	0.19	4.17	10.08	0.22	0.11	3.32	0.01	98.56	1.36	1.67
MP768	rhydk	py-cp	Valdivia S	0.03	2.73	0.00	67.00	0.37	12.76	4.42	0.09	1.01	3.23	3.62	3.42	0.20	4.88	0.01	101.00	2.23	3.98
MP770	rhydk	py	Valdivia S	0.05	2.56	0.00	58.96	0.43	14.49	5.83	0.15	2.66	2.08	2.45	7.27	0.10	4.62	0.02	99.06	2.11	5.25
MP772	anddk	cc	Valdivia S	4.92	2.74	0.29	57.42	0.79	20.43	3.14	0.11	0.59	2.56	4.44	6.01	0.12	2.84	0.04	98.49	3.04	2.83
MP775	rhy	cp	Valdivia S	2.39	2.66	0.00	63.00	0.51	12.91	3.86	0.09	0.07	6.08	4.96	3.71	0.32	2.14	0.01	97.66	3.59	3.47
MP776	rhy	py-cp	Valdivia S	1.08	2.66	0.00	67.36	0.50	12.61	2.53	0.10	0.06	4.09	4.91	3.65	0.12	3.11	0.01	99.05	0.67	2.28
MP778	rhy	bn-cc	Valdivia S	5.75	2.68	0.00	67.65	0.37	13.35	4.41	0.02	0.27	0.48	3.35	6.14	0.44	1.23	0.01	97.72	6.22	3.97
MP782	rhy	bn-cc	Valdivia S	4.30	2.63	0.00	67.98	0.35	10.73	3.34	0.06	0.27	5.04	4.08	3.13	0.30	2.50	0.02	97.80	4.33	3.01
MP786	bas	cp	Valdivia S	0.64	2.72	0.05	44.08	0.61	16.43	9.16	1.06	4.65	9.23	5.09	0.43	0.08	9.12	0.09	100.03	6.96	8.24
MP787	bas	bn	Valdivia S	1.49	2.73		49.59	0.88	18.80	8.93	0.33	3.82	4.19	5.46	1.79	0.12	5.25	0.04	99.20	6.93	8.04
MP788	bas	py	Filo	0.01			48.89	0.68	17.26	9.80	0.45	5.55	9.90	2.22	0.96	0.11	3.92	0.01	99.75	4.20	8.82
MP790	bas	cp-bn	Filo	0.90	3.46	0.02	42.07	0.60	18.97	6.33	0.33	2.93	22.91	< 0.01	0.08	0.09	4.55	0.02	98.88	5.20	5.70
MP791	volcsed	cc	Filo	1.28			72.40	0.36	10.95	0.60	0.05	0.19	3.75	5.17	1.80	0.26	3.66	0.02	99.21	1.67	0.54

(1) Cu assay value for 3 m drillcore interval, (2) FeOT=(Fe₂O₃T * 0.8998)

Appendix 2.1.- Rock Geochemistry, Continued

Sample	S %	C(3) %	C(4) %	CO₂ %	+H₂O %	-H₂O %	Ag ppm	As ppm	Ba ppm	Cl ppm	Co ppm	Cu ppm	Hg ppm	Ni ppm	Pb ppm	Rb ppm	Sb ppm	Sn ppm	Sr ppm	U ppm	V ppm	W ppm	Zn ppm
MP664	0.74	1.28		4.30	0.75	0.19			285							60			52				
MP674	0.26	1.27		4.30	0.18	0.04			245							54			42				
MP677	0.50	0.70		2.30	0.30	0.08			540							98			52				
MP701	2.54	0.33		1.20	0.82	0.08			155							62			48				
MP703	3.16	1.59		5.20	4.00	0.45			50							46			62				
MP713	0.39	1.00	1.03		0.28	0.15			40			10000				16			24				
MP718	0.22	0.63		1.80	0.08	0.07			20							4			42				
MP719	0.47	0.47		1.30	1.37	0.20			380							84			52				
MP723	2.43	1.54		5.00	1.22	0.04			680							44			84				
MP724	2.58	1.40		4.40	1.99	0.49			1235							70			132				
MP728	0.47	0.68		2.00	3.37	0.25			85							12			308				
MP737	0.40	0.05	0.06		0.22	0.08			40			13100				6			38				
MP739	2.37	<0.05	0.04		0.07	0.07			40			24600				4			40				
MP746	0.17	1.45	1.56		0.06	0.03			270							84			8				
MP747	0.20	0.15	0.15		3.00	0.20			40			3600				12			26				
MP754	0.41	0.90	1.01		1.43	0.07			525			100				74			30				
MP757	0.16	0.20	0.24		1.60	0.05			635							84			64				
MP761	0.77	0.20	0.53		3.99	0.21			850			100				90			168				
MP764	1.21	0.75	0.84		0.17	0.12			40			9100				4			52				
MP768	2.64	0.50	0.63		1.12	0.13			415			12700				80			68				
MP770	2.53	0.35	0.40		1.59	0.08	0.6	141	674		14.0	648	70	20	40	100.3	1.2	3	24	1.5	10	<1	260
MP772	0.66	0.25	0.29		1.25	0.28			2010			19000				206			186				
MP775	2.77	1.15	1.16		0.14	0.06			810			29700				68			46				
MP776	1.62	0.70	0.75		0.20	0.06			730			3300				78			104				
MP778	1.73	0.05	0.06		0.31	0.06			900			52000				132			32				
MP782	1.11	1.05	1.05		0.31	0.04			270			200				66			8				
MP786	0.23	1.70	1.76		3.72	0.30	<0.2		57		25.5	4850	50	45	5	12.9	<0.2	<1	100	0.5	210	<1	220
MP787	0.45	0.70	0.60		3.32	0.19			275			1070				78			54				
MP788	2.41	0.20	0.21		1.86	0.28			270			200				34			292				
MP790	1.66	0.65	0.59		3.99	0.22			45			23900				4			14				
MP791	0.62	0.75	1.96		0.10	0.02			250			21800				46			36				

(3) Inorganic carbon, (4) Total carbon

Appendix 2.1.- Rock Geochemistry, Continued

Sample	Cs ppm	Ga ppm	Hf ppm	Nb ppm	Ta ppm	Th ppm	Tl ppm	Y ppm	Zr ppm	La ppm	Ce ppm	Pr ppm	Nd ppm	Sm ppm	Eu ppm	Gd ppm	Tb ppm	Dy ppm	Ho ppm	Er ppm	Tm ppm	Yb ppm	Lu ppm
MP664				6				26	189	9	19	2.9	12	3.3	0.9	2.8	0.6	3.2	0.9	2.1	0.4	2.5	0.5
MP674				8				28	252	5	14	2.7	10	2.4	0.7	2.4	0.4	3.4	0.8	2.3	0.4	2.8	0.5
MP677				6				32	231	6	17	3.0	12	2.8	1.0	2.8	0.5	3.3	0.8	1.9	0.3	2.4	0.5
MP701				8				20	213	5	19	2.3	9	2.3	0.6	1.9	0.3	2.2	0.5	1.4	0.2	1.9	0.3
MP703				< 2				12	27	1	5	0.9	4	1.1	0.4	1.1	0.2	1.5	0.6	0.9	0.1	1.5	0.2
MP713				8				22	183	9	26	3.3	10	1.6	0.5	1.6	0.4	2.5	0.6	1.5	0.3	2.3	0.3
MP718				10				36	312	6	17	2.9	11	2.7	0.7	2.6	0.6	3.7	1.0	2.3	0.4	3.1	0.5
MP719				6				28	225	21	42	6.2	23	4.8	0.9	4.0	0.6	3.7	0.9	2.2	0.4	2.9	0.5
MP723				< 2				12	21	3	12	1.8	7	1.8	1.1	1.8	0.3	2.0	0.5	0.9	0.2	1.1	0.1
MP724				2				16	51	5	17	2.4	10	2.7	1.3	2.3	0.4	2.1	0.6	1.5	0.2	1.3	0.2
MP728				2				22	123	20	37	5.6	22	4.2	1.9	3.5	0.6	3.8	0.8	2.0	0.2	1.8	< 0.1
MP737				8				28	198	22	48	5.5	20	3.7	0.9	3.0	0.5	2.4	0.6	1.5	0.3	1.8	0.3
MP739				8				30	243	1	10	1.7	7	1.5	0.5	2.3	0.6	3.8	0.8	1.9	0.4	2.4	0.4
MP746				4				28	147	5	14	2.1	6	1.2	0.5	1.8	0.4	2.4	0.7	1.4	0.3	1.8	0.3
MP747				6				18	138														
MP754				6				26	210	5	15	2.2	10	2.1	0.7	1.9	0.5	2.5	0.8	1.6	0.3	2.4	0.3
MP757				4				28	210														
MP761				6				28	138	10	29	3.9	15	2.5	1.1	3.3	0.6	4.2	0.9	2.1	0.3	2.3	0.4
MP764				10				30	222	4	15	2.2	12	2.0	0.7	2.2	0.4	2.9	0.7	1.8	0.4	2.4	0.3
MP768				6				24	171	15	35	4.8	34	5.0	0.8	3.0	0.5	4.2	0.6	1.7	0.3	1.7	0.2
MP770	0.6	10	3	3.5	<0.5	6	1.5	22	160	11.00	27.00	3.70	15.0	3.80	0.70	3.70	0.50	2.80	0.50	1.50	0.30	1.80	0.20
MP772				< 2				20	60	5	17	2.7	10	1.7	1.2	2.2	0.3	2.2	0.5	0.9	0.2	0.9	0.2
MP775				6				32	186	23	51	6.3	22	3.9	1.4	3.3	0.6	3.5	0.7	1.9	0.3	2.0	0.3
MP776				6				32	207	13	33	4.3	15	2.6	0.8	3.0	0.6	3.2	0.7	1.9	0.3	1.9	0.3
MP778				4				24	162	6	15	2.5	14	2.4	0.4	1.6	0.4	2.9	0.8	1.6	0.3	1.7	0.3
MP782				6				28	162	13	33	4.2	17	2.8	1.3	3.4	0.7	3.5	0.9	1.7	0.4	2.1	0.3
MP786	0.4	16	<1	1.5	<0.5	1	<.5	12	39	66.5	116.5	11.0	35.0	4.1	1.2	3.9	0.5	2.0	0.4	1.0	0.1	1.0	0.1
MP787				< 2				24	66														
MP788				4				18	48	5	15	2.2	10	1.9	0.9	1.5	0.3	2.3	0.5	0.8	0.2	1.3	0.3
MP790				2				12	36	3	14	1.9	6	1.6	0.8	1.4	0.3	1.4	0.4	1.0	0.2	0.8	0.2
MP791				6				24	120	4	12	1.8	10	1.7	0.5	1.6	0.4	2.5	0.6	1.3	0.2	1.6	0.3

Appendix 2.1.- Rock Geochemistry, Continued

Sample	Rock Type	Ore Zone	Mine Block	Cu[1] %	Spec. Grav.	Mag. Susc.	SiO$_2$ %	TiO$_2$ %	AL$_2$O$_3$ %	Fe$_2$O$_3$T %	MnO %	MgO %	CaO %	Na$_2$O %	K$_2$O %	P$_2$O$_5$ %	LOI %	Cr$_2$O$_3$ %	Total %	FeO %	FeOT[2] %
MP793	bas	cc	Filo	3.86			51.75	0.72	19.17	11.87	1.02	3.90	1.58	4.19	1.81	0.14	3.56	0.05	99.76	10.10	10.68
MP805	bas	bn-cc	Morro	3.23	2.82	0.03	50.91	0.73	16.74	8.86	0.56	6.15	3.55	5.01	0.39	0.17	5.69	0.02	98.78	7.49	7.97
MP817	volcsed	bn-cc	Morro	3.71			42.58	0.50	13.90	8.26	0.44	4.36	9.39	3.99	1.48	0.08	8.08	0.02	93.08	8.43	7.43
MP831	volcsed	cp	Morro	1.13			67.69	0.41	13.46	2.30	0.02	0.07	3.18	7.43	0.58	0.09	3.55	0.02	98.80	0.33	2.07
MP833	volcsed	cp	Morro	2.36			52.59	0.60	16.75	6.64	0.14	2.14	4.72	7.65	1.08	0.29	5.43	0.01	98.08	4.95	5.97
MP839	rhydk	py	Valdivia S	0.11	2.67	0.00	64.96	0.38	12.45	3.71	0.10	0.95	3.69	3.29	4.26	0.09	5.12	0.02	99.02	1.17	3.34
MP844	bas	bckd mt	Filo	< 0.01	2.85	2.99	49.74	0.86	17.66	9.93	0.48	5.38	7.33	3.71	2.21	0.16	2.34	0.03	99.83	5.90	8.94
MP845	rhy	bckd py-mt	Filo	< 0.01	2.60	1.12	62.65	0.52	15.49	7.19	0.20	2.44	0.84	5.37	2.57	0.11	1.98	0.02	99.38	4.97	6.47
MP846	rhydk	bckd py	Morro	0.07	2.56	0.01	67.54	0.50	14.14	3.58	0.13	1.27	1.71	4.85	3.38	0.11	2.20	0.03	99.44	2.65	3.22
MP848	rhy	bckd py	Morro	< 0.01	2.52	0.00	64.79	0.37	14.19	1.90	0.07	0.42	3.86	4.98	5.00	0.07	3.56	0.02	99.23	0.90	1.71
MP854	volcsed	bn	Valdivia S	0.91	2.56	0.00	75.85	0.21	8.06	1.12	0.04	0.21	3.20	4.57	0.28	0.04	2.73	0.01	96.32	0.81	1.01
MP855	volcsed	bckd py	Valdivia S	0.04	2.58	0.00	64.47	0.40	14.73	5.62	0.20	2.28	0.77	0.55	6.33	0.07	3.54	0.01	98.97	2.66	5.06
MP856	rhy	bn	Valdivia S	7.82	2.80	0.00	59.11	0.42	13.62	5.37	0.06	0.47	2.89	8.05	1.11	0.22	1.73	0.01	93.06	9.56	4.83
MP858	volcsed	py-cp	Morro	0.34			48.92	0.66	15.83	9.30	0.13	0.66	6.82	5.80	2.94	0.14	7.45	0.02	98.67	0.74	8.37
MP860	rhy	bckd py	Filo	0.04	2.54	0.02	65.90	0.34	10.26	0.94	0.08	0.19	6.27	4.70	2.21	0.07	4.77	0.01	95.74	0.58	0.85
MP861	volcsed	py-cp	Filo	0.12			51.96	0.71	12.86	8.73	0.22	3.63	8.41	3.90	0.44	0.15	8.24	0.01	99.26	7.05	7.86
MP864	rhy	bn-cc	Morro	1.06	2.63	0.01	65.56	0.48	12.72	2.11	0.03	0.17	2.16	4.32	4.53	0.11	1.23	0.02	93.44	3.88	1.90
MP865	bas	py	Valdivia S	0.01	2.88	0.00	43.54	0.64	17.32	2.67	0.38	1.01	13.91	4.65	3.19	0.09	11.92	0.01	99.33	1.44	2.40
MP866	anddk	bckd	Arauco	0.04		5.00	59.16	0.69	15.57	3.95	0.13	2.11	3.99	4.35	4.38	0.14	4.69	0.02	99.18	2.69	3.55
MP869	volcsed	cp	Valdivia S	1.61			52.50	0.53	12.81	7.58	0.45	1.88	8.50	3.35	1.88	0.09	7.03	0.02	96.62	6.64	6.82
RB98-05	rhy	bckd py	Valdivia S	0.06	2.62	0.00	64.73	0.39	13.49	2.79	0.12	0.27	4.85	5.20	2.99	0.14	4.65	0.01	99.63	0.66	2.51
RB98-06	bas	bckd py	Valdivia S	0.09	2.77	0.02	45.97	0.84	17.63	9.28	0.72	5.00	5.62	5.46	0.78	0.13	6.23	<0.01	97.66	6.86	8.35
RB98-09	rhy	py	Valdivia S	0.05	2.64	0.00	64.44	0.38	13.19	3.99	0.10	0.63	4.76	5.51	2.25	0.13	4.19	0.01	99.58	1.14	3.59
RB98-10	rhy	py	Valdivia S	0.07	2.65	0.00	64.52	0.33	12.24	3.79	0.15	0.60	5.99	4.89	1.98	0.13	5.28	0.01	99.91	0.92	3.41
RB98-11	rhy	py-cp	Valdivia S	0.37	2.56	0.00	63.91	0.35	13.59	1.16	0.13	0.35	6.19	7.67	0.20	0.13	4.75	0.01	98.44	0.75	1.04
RB98-12	rhy	cp	Valdivia S	5.90	2.69	0.01	59.14	0.36	13.92	3.08	0.12	0.13	6.87	4.83	3.96	0.12	4.14	0.01	96.68	3.23	2.77
RB98-13	rhy	cp-bn	Valdivia S	1.06	2.63	0.01	65.52	0.35	12.89	1.48	0.12	0.57	5.15	6.14	1.58	0.13	4.18	0.01	98.12	1.31	1.33
RB98-15	rhy	bn-cc	Valdivia S	4.91	2.64	0.00	66.15	0.34	13.42	2.97	0.07	0.31	3.54	7.17	<0.01	0.13	2.87	0.01	96.98	4.79	2.67
RB98-19	rhy	cp-bn	Valdivia S	4.47	2.60	0.00	67.12	0.35	12.80	2.82	0.07	0.63	1.29	4.03	3.47	0.15	2.04	0.01	94.78	6.12	2.54
RB98-21	rhy	bckd py	Valdivia S	0.07		0.00	68.01	0.41	13.70	1.90	0.11	0.34	3.19	4.22	3.62	0.14	2.90	0.01	98.55	1.37	1.71
RB98-22	rhy	bckd py	Valdivia S	0.02	2.60	0.00	65.01	0.38	12.91	2.21	0.16	0.18	5.53	4.16	3.70	0.14	5.19	0.01	99.58	0.56	1.99

(1) Cu assay value for 3 m drillcore interval, (2) FeOT=(Fe$_2$O$_3$T * 0.8998)

Appendix 2.1.- Rock Geochemistry, Continued

Sample	S %	C(3) %	C(4) %	CO2 %	H2O+ %	H2O- %	Ag ppm	As ppm	Ba ppm	Cl ppm	Co ppm	Cu ppm	Hg ppm	Ni ppm	Pb ppm	Rb ppm	Sb ppm	Sn ppm	Sr ppm	U ppm	V ppm	W ppm	Zn ppm
MP793	0.75	0.15	0.15		3.67	0.21			870			23800				54			92				
MP805	0.59	0.45	0.45		4.10	0.40			105			14400				12			158				
MP817	1.40	1.80	1.86		2.75	0.25			220			39500				28			56				
MP831	1.61	0.70	0.64		0.16	0.05			40			1600				16			62				
MP833	3.12	0.85	0.79		1.38	0.15			280			31800				26			84				
MP839	2.04	0.75	0.76		1.12	0.09			660			1100				92			82				
MP844	0.01	0.05	0.07		2.37	0.24			815			<100				52			394				
MP845	< 0.01	< 0.05	0.04		2.08	0.12			465			<100				64			96				
MP846	0.02	0.25	0.29		1.28	0.08			505			<100				74			52				
MP848	0.49	0.85	0.76		0.49	0.07			755			<100				106			38				
MP854	0.14	0.60	0.64		0.17	0.06			60			3200				8			28				
MP855	0.09	0.10	0.13		2.92	0.43			785			300				252			18				
MP856	2.77	0.55	0.57		0.43	0.07	12.1	<1	89.5		2.0	70250	<10	25	15	15.6	0.8	1	55	2.0	25	<1	55
MP858	6.19	1.20	1.21		0.95	0.20			475			600				88			94				
MP860	0.12	1.25	1.24		0.35	0.08	0.4	42	271		40.5	417.5	10	35	135	49.6	0.4	1	76	2.5	35	<1	25
MP861	0.22	1.60	1.61		3.28	0.27			80			1200				12			44				
MP864	1.08	0.40	0.40		0.37	0.10			670			29400				88			40				
MP865	0.10	2.80	2.78		1.97	0.35	0.2	60	274		28	1007.5	40	35	105	159	2.2	1	110	0.5	210	<1	55
MP866	0.22	0.85	0.77		1.86	0.16			405			<100				100			48				
MP869	1.59	1.55	1.62		2.12	0.27			360			15700				70			86				
RB98-05	1.63	0.90					<1	4	415	<140	8.0	95	10	20	5	74	<0.2	<1	54	2.5	50	1	10
RB98-06	1.46	0.90					1	13	94.0	400	33.0	700	40	15	10	37.8	<0.2	<1	87	<0.5	245	<1	300
RB98-09	2.24	0.80					<1	14	361	<240	14.0	350	20	15	10	50.6	<0.2	<1	108	2.0	50	<1	15
RB98-10	2.19	1.10					<1	36	314	<220	11.5	70	30	20	5	50.8	<0.2	<1	87	2.0	40	<1	15
RB98-11	0.31	1.25					<1	2	19.0	<290	5.0	230	10	5	<5	4	<0.2	<1	51	2.0	40	<1	10
RB98-12	2.27	1.35					1	2	535	<220	1.5	25000	50	5	<5	93.4	<0.2	<1	52	2.0	35	<1	10
RB98-13	0.26	0.95					<1	<1	167.0	300	3.0	2100	<10	10	<5	35.2	<0.2	<1	60	2.0	40	<1	15
RB98-15	1.16	0.70					7	8	9.0	<240	2.0	27700	10	15	<5	2.8	<0.2	<1	35	2.5	20	<1	10
RB98-19	2.06	0.15					6	105	501	<200	3.5	46900	40	5	<5	76.8	0.2	<1	39	2.5	30	<1	10
RB98-21	0.21	0.60					<1	3	559	<220	7.0	250	<10	45	<5	104	<0.2	<1	64	2.5	50	<1	10
RB98-22	1.33	1.00					<1	6	573	<220	7.5	70	10	10	5	95.6	<0.2	<1	80	2.5	50	<1	10

(3) Inorganic carbon, (4) Total carbon

Appendix 2.1.- Rock Geochemistry, Continued

Sample	Cs ppm	Ga ppm	Hf ppm	Nb ppm	Ta ppm	Th ppm	Tl ppm	Y ppm	Zr ppm	La ppm	Ce ppm	Pr ppm	Nd ppm	Sm ppm	Eu ppm	Gd ppm	Tb ppm	Dy ppm	Ho ppm	Er ppm	Tm ppm	Yb ppm	Lu ppm
MP793				2				14	51	1	7	1.1	5	0.8	0.9	1.3	0.3	2.1	0.6	0.9	0.2	1.3	0.2
MP805				4				18	135														
MP817				2				12	54														
MP831				8				26	177	7	21	2.9	11	1.9	0.4	1.8	0.4	2.5	0.8	1.9	0.4	2.2	0.4
MP833				4				16	84	18	43	5.5	18	3.0	0.9	3.0	0.5	2.6	0.6	1.5	0.2	1.5	0.3
MP839				6				26	180	16	46	5.8	27	9.5	0.1	7.2	1.0	9.2	0.7	2.0	0.3	7.3	0.6
MP844				2				20	75	9	31	5.5	26	5.8	1.3	4.2	2.1	6.5	1.5	3.1	0.6	1.7	0.3
MP845				6				30	249	29	75	9.6	38	8.6	0.6	9.1	1.3	6.8	2.0	2.0	0.8	6.6	0.8
MP846				6				24	228	11	34	6.4	28	6.7	0.5	4.8	0.8	3.6	1.8	2.5	0.3	5.4	0.6
MP848				6				28	210	6	20	5.4	18	1.8	< 0.2	5.4	0.7	4.9	0.6	4.9	0.8	5.7	0.9
MP854				6				12	114														
MP855				2				26	198														
MP856	0.1	10	5	5.5	<0.5	7	<0.5	24	174	13.0	32.5	4.3	18.5	4.8	1.1	4.9	0.7	4.1	0.8	2.8	0.5	2.9	0.4
MP858				< 2				16	57														
MP860	0.3		4	6	<0.5	8	3.5	25	160	19.5	42.5	5.2	22.0	5.0	0.8	4.4	0.8	4.2	0.9	2.6	0.4	2.4	0.4
MP861				6				24	99														
MP864				6				30	195														
MP865	11.2		1	<1	<0.5	1	2.0	17	43	9.5	18.5	2.4	11.0	2.7	0.9	3.0	0.4	2.4	0.5	1.5	0.1	1.4	0.2
MP866				6				24	180	6	26	7.4	27	4.4	< 0.2	1.4	0.9	10.6	0.8	1.1	1.3	3.3	0.9
MP869				2				18	84														
RB98-05	0.5	14	5	6	<0.5	9	<0.5	22	170	14.0	26.0	3.4	13.5	3.0	0.7	3.2	0.6	3.4	0.8	2.4	0.4	2.4	0.4
RB98-06	1.1	17	1	1	<0.5	<1	1.5	17	51	5.5	9.5	1.6	7.5	2.3	0.9	2.9	0.5	2.8	0.6	1.6	0.2	1.6	0.2
RB98-09	0.4	15	6	6	<0.5	8	0.5	30	187	18.5	36.5	5.2	21.5	5.1	0.9	5.7	0.9	5.0	1.1	3.3	0.4	3.2	0.4
RB98-10	0.7	15	5	5	<0.5	8	1.5	24	177	11.0	21.5	3.1	13.0	3.5	0.6	4.1	0.6	4.0	0.8	2.6	0.4	2.7	0.4
RB98-11	0.1	15	5	6	<0.5	7	<0.5	24	188	8.0	15.5	2.1	10.0	2.6	0.5	2.9	0.6	3.5	0.8	2.7	0.4	3.1	0.4
RB98-12	0.4	11	5	6	<0.5	8	0.5	26	189	13.0	26.0	3.8	15.5	4.5	0.8	4.1	0.8	4.4	0.9	2.5	0.4	3.0	0.5
RB98-13	0.1	13	5	6	<0.5	7	<0.5	27	193	13.5	25.5	3.6	15.0	4.0	0.8	4.5	0.8	4.6	1.0	3.1	0.4	3.2	0.4
RB98-15	<0.1	11	4	5	<0.5	8	<0.5	24	153	14.5	31.0	4.3	15.5	3.8	0.9	3.7	0.8	3.5	1.0	2.5	0.6	2.7	0.5
RB98-19	0.3	9	5	5	<0.5	8	<0.5	16	160	12.0	25.5	3.5	14.0	3.1	0.6	3.0	0.6	2.6	0.6	1.8	0.4	2.3	0.4
RB98-21	1.4	16	5	6	<0.5	9	0.5	24	186	13.0	26.0	3.5	14.5	3.7	0.8	3.8	0.7	3.6	0.9	2.3	0.4	2.5	0.4
RB98-22	0.7	14	5	5	<0.5	9	0.5	23	172	9.5	19.0	2.6	10.5	2.4	0.5	3.0	0.5	3.3	0.8	2.4	0.3	2.7	0.4

Appendix 2.1.- Rock Geochemistry, Continued

Sample	Rock Type	Ore Zone	Mine Block	Cu[1] %	Spec. Grav.	Mag. Susc.	SiO_2 %	TiO_2 %	AL_2O_3 %	Fe_2O_3T %	MnO %	MgO %	CaO %	Na_2O %	K_2O %	P_2O_5 %	LOI %	Cr_2O_3 %	Total %	FeO %	$FeOT^{[2]}$ %
RB98-29	bas	bckd mt	Valdivia S	0.02	2.98	1.20	49.11	0.60	19.47	7.88	0.54	4.80	10.17	2.47	1.90	0.11	2.83	0.01	99.89	5.53	7.09
RB98-31	bas	py-cp	Valdivia S	0.17	2.70	1.95	51.37	0.80	19.46	9.19	0.48	3.35	1.80	5.79	1.82	0.14	3.68	0.02	97.90	7.40	8.27
RB98-36	bas	cp	Valdivia S	0.55	2.75	0.05	43.42	0.58	16.00	8.69	0.51	1.96	12.44	5.42	1.23	0.11	9.97	0.01	100.35	5.82	7.82
RB98-40	bas	bckd mt	Osorno	0.01	2.88	2.07	49.31	0.62	17.04	8.70	0.36	6.35	9.13	2.86	1.54	0.12	3.20	0.01	99.24	5.68	7.83
RB98-42	bas	bckd mt	Filo	0.01	2.89	1.84	50.56	0.59	19.75	7.63	0.39	4.61	9.74	2.62	2.26	0.11	2.11	0.01	100.40	4.79	6.87
RB98-44	bas	bn-cc	Filo	0.87	2.80	0.49	45.32	0.54	18.07	9.02	0.45	6.62	6.50	4.60	0.56	0.11	6.23	0.01	98.03	7.07	8.12
RB98-45	bas	cp-bn	Filo	0.49	2.77	0.04	49.84	0.70	17.64	7.52	0.42	5.46	5.66	4.56	1.81	0.13	4.54	0.01	98.29	6.34	6.77
RB98-47	bas	bn-cc	Filo	1.05	2.85	0.04	42.89	0.64	16.97	8.80	0.84	6.23	9.16	4.95	0.60	0.11	9.10	0.01	100.30	8.10	7.92
RB98-48	bas	py-cp	Filo	0.32	2.72	0.03	48.58	0.62	15.55	7.95	0.82	6.35	6.82	4.99	1.36	0.12	5.81	0.01	98.98	6.31	7.15
RB98-49	bas	bckd py	Filo	< 0.01	2.84	0.02	47.26	0.66	17.10	8.89	1.33	6.20	6.45	3.28	2.02	0.12	4.44	0.01	97.76	7.72	8.00
RB98-50	bas	bckd py	Filo	0.03	2.75	0.03	40.05	0.55	14.82	9.02	1.42	3.96	13.06	3.32	1.74	0.10	9.71	0.01	97.76	6.01	8.12
RB98-52	bas	bn-cc	Filo	2.05	2.77	0.02	45.61	0.64	17.18	9.17	1.29	5.60	7.01	5.21	0.61	0.11	7.26	0.01	99.70	8.42	8.25
RB98-56	rhy	bn-cc	Filo	1.88	2.52	0.01	68.82	0.39	14.16	2.33	0.10	0.49	2.73	6.08	1.44	0.13	2.07	<0.01	98.74	2.13	2.10
RB98-61	rhy	bckd cp-ht	Filo	0.26	2.56	0.00	68.03	0.39	13.37	3.35	0.07	0.10	3.51	5.82	2.88	0.14	2.67	<0.01	100.35	0.43	3.01
RB98-64	rhy	bckd cp-ht	Filo	0.22	2.58	0.06	68.44	0.41	13.70	4.97	0.11	0.99	1.46	5.25	2.39	0.14	1.79	0.01	99.66	3.06	4.47
RB98-65	rhy	bn	Filo	1.04	2.56	0.00	67.34	0.42	14.82	1.93	0.10	0.30	3.86	5.98	2.42	0.13	2.96	<0.01	100.25	2.40	1.74
RB98-67	rhy	bn	Filo	0.74	2.56	0.01	63.28	0.55	19.48	1.58	0.04	0.33	1.75	10.25	<0.01	0.14	1.56	<0.01	98.96	3.36	1.42
RB98-69	rhy	bn-cc	Filo	1.44	2.53		70.22	0.40	13.91	4.14	0.06	0.57	1.33	7.26	<0.01	0.13	1.24	0.01	99.27	1.32	3.73
RB98-70	rhy	bckd ht	Filo	0.08	2.53	0.22	66.78	0.42	14.67	3.90	0.06	0.68	1.92	6.95	1.70	0.14	1.90	0.01	99.13	1.15	3.51
RB98-76	bas	py	Valdivia S	0.18	2.71	0.06	50.00	0.59	17.00	7.89	0.52	3.38	7.44	7.45	0.40	0.07	6.45	<0.01	101.20	4.59	7.10
RB98-79	rhy	bckd py	Valdivia S	0.07			67.58	0.41	13.85	1.84	0.11	0.28	3.44	4.49	3.54	0.14	3.09	0.01	98.78	1.11	1.66
RB99-01	rhy	bn-cc	Valdivia S	4.51		0.02	45.00	0.38	13.43	6.83	0.12	1.72	5.98	0.90	7.67	0.38	5.47	<0.01	87.88		6.15
RB99-02	rhy	bn-cc	Valdivia S	3.32		0.00	63.00	0.35	11.94	1.85	0.08	0.24	5.81	3.98	3.99	0.18	4.39	0.01	95.82		1.66
RB99-03	rhy	py	Morro	0.05		0.00	73.50	0.34	13.32	0.88	0.01	0.21	1.63	4.17	1.78	0.03	2.41	<0.01	98.28	0.15	0.79
RB99-04	rhy	py	Morro	0.04		0.00	64.00	0.52	12.13	5.86	0.10	1.07	3.05	4.16	3.04	0.12	4.68	0.01	98.74	1.60	5.27
Z603-95	basVN	bckd	Filo	0.01		0.62	46.08	0.75	19.91	8.74	1.81	6.63	4.22	2.48	4.58	0.11	4.41	0.01	99.73	3.92	7.86
Z614-95	diordk	bckd	Morro	0.01			52.03	0.62	18.03	10.00	0.53	3.41	2.88	6.20	2.29	0.25	3.08	0.01	99.33	5.80	9.00
Z622-95	gabbro	bckd	Morro	0.02		4.16	50.75	0.90	17.57	10.07	0.17	5.22	10.00	2.77	0.72	0.15	1.30	0.01	99.63	6.03	9.06
Z626-95	basdk	bckd	Morro	0.02		0.42	48.31	0.76	18.81	10.27	0.94	5.80	3.92	4.77	1.68	0.16	4.37	0.05	99.84	6.91	9.24
Z632-95	bas	bckd py	Valdivia S	< 0.01		0.12	44.76	0.76	19.20	9.54	1.47	5.23	6.49	5.16	0.39	0.12	6.52	0.03	99.67	6.67	8.58

(1) Cu assay value for 3 m drillcore interval, (2) $FeOT = (Fe_2O_3T * 0.8998)$

Appendix 2.1.- Rock Geochemistry, Continued

Sample	S %	C(3) %	C(4) %	CO₂ %	+H2O %	-H₂O %	Ag ppm	As ppm	Ba ppm	Cl ppm	Co ppm	Cu ppm	Hg ppm	Ni ppm	Pb ppm	Rb ppm	Sb ppm	Sn ppm	Sr ppm	U ppm	V ppm	W ppm	Zn ppm
RB98-29	0.01	0.10					<1	4	539	<340	27.5	50	<10	30	5	77.6	<0.2	<1	465	<0.5	225	<1	190
RB98-31	0.20	0.10					<1	<1	319	500	31.5	1100	20	45	<5	97.8	<0.2	<1	113	0.5	305	<1	175
RB98-36	0.40	2.40						<1	198.5	<300	21.0	3200	10	25	<5	63	<0.2	<1	139	<0.5	260	<1	110
RB98-40	0.01	0.25					<1	4	342	<200	37.0	25	<10	40	<5	46	<0.2	<1	309	<0.5	265	<1	205
RB98-42	0.01	<0.05					<1	<1	476	<200	26.5	140	<10	25	<5	93.4	<0.2	<1	283	<0.5	240	<1	120
RB98-44	0.01	0.45					<1	5	157.5	<260	32.5	2560	10	25	<5	21.4	<0.2	<1	163	<0.5	240	<1	235
RB98-45	0.12	0.40						1	366	<250	22.0	855	<10	25	<5	77.2	<0.2	<1	383	<0.5	320	<1	135
RB98-47	0.11	1.70					3	1	140.5	<330	22.0	9200	<10	30	<5	18	<0.2	<1	119	0.5	235	<1	210
RB98-48	0.43	0.90					<1	17	301	<340	29.5	1940	<10	30	<5	36.8	<0.2	<1	125	<0.5	230	<1	205
RB98-49	0.06	0.15					<1	26	3,440	<840	39.5	45	<10	35	5	74.4	<0.2	<1	424	0.5	270	<1	245
RB98-50	1.81	2.20					<1	181	731	<450	39.5	55	70	15	10	55.8	<0.2	<1	212	0.5	240	<1	165
RB98-52	0.50	1.15					3	39	148.0	<410	29.5	7600	120	35	<5	21.2	<0.2	<1	163	0.5	285	<1	195
RB98-56	0.25	0.35					<1	<1	215	<250	2.5	4500	10	5	5	38	<0.2	4	86	2.0	70	<1	20
RB98-61	0.04	0.70					<1	<1	530	<220	3.0	700	<10	<5	<5	66.6	<0.2	<1	57	2.0	45	<1	10
RB98-64	0.02	0.25					<1	<1	256	<230	8.0	200	<10	10	<5	55.8	<0.2	<1	56	2.5	55	<1	20
RB98-65	0.47	0.65					1	1	251	<250	3.5	9700	80	5	<5	57.6	<0.2	<1	64	2.5	70	<1	5
RB98-67	1.09	0.25					5	1	7.0	<310	2.5	26000	10	10	<5	1.4	<0.2	<1	44	3.0	60	<1	<5
RB98-69	0.03	0.15					<1	<1	10.5	<250	5.0	475	<10	5	<5	2.4	<0.2	<1	58	2.0	45	<1	25
RB98-70	0.01	0.30					1	5	115.0	<270	5.0	160	<10	10	<5	40.2	<0.2	3	59	2.5	50	<1	10
RB98-76	1.72	1.35					0.2	37	105.0		88.5	330	110	65	45	15	0.2	1	213	1.0	220	<1	175
RB98-79	0.40	0.60					<1	2	501	<220	8.0	110	<10	15	5	102	<0.2	<1	63	2.5	60	<1	5
RB99-01	2.70	1.20					16.8	1	865		3.0	73400	<10	<5	10	220	0.2	1	28	2.0	90	7	<5
RB99-02	1.14	1.10					5.9	131	408		<0.5	23600	<10	<5	<5	100.5	0.2	1	32	2.0	40	5	<5
RB99-03	0.58	0.25					<0.2	5	865		2.0	160	<10	<5	<5	62	<0.2	<1	31	3.0	20	5	<5
RB99-04	3.21	0.50					<0.2	234	408		18.0	420	20	<5	<5	78.2	0.2	2	53	2.5	55	5	30
Z603-95	0.05	0.05	0.04		4.26	0.28	<0.2	23	4420		35.0	50	<10	35	15	50	0.4	<1	445	0.5	210	<1	650
Z614-95	0.22	0.25	0.21		2.57	0.57	<0.2	5	658		22.0	120	<10	15	5	49.6	0.2	<1	278	0.5	95	<1	325
Z622-95	0.12	< 0.05	0.03		1.39	0.20	<0.2	<1	223		31.5	95	<10	35	5	49.6	<0.2	<1	385	0.5	255	<1	85
Z626-95	0.13	0.15	0.12		4.22	0.38	0.2	3	542.5		26.5	725	10	30	15	47	<0.2	<1	322	0.5	225	<1	260
Z632-95	0.03	0.75	0.75		4.41	0.29	<0.2	3	87.75		32.5	20	<10	20	15	10	<0.2	<1	284	<0.5	195	<1	425

(3) Inorganic carbon, (4) Total carbon

Appendix 2.1.- Rock Geochemistry, Continued

Sample	Cs ppm	Ga ppm	Hf ppm	Nb ppm	Ta ppm	Th ppm	Tl ppm	Y ppm	Zr ppm	La ppm	Ce ppm	Pr ppm	Nd ppm	Sm ppm	Eu ppm	Gd ppm	Tb ppm	Dy ppm	Ho ppm	Er ppm	Tm ppm	Yb ppm	Lu ppm
RB98-29	1.9	18	<1	<1	<0.5	1	<0.5	13	36	6.0	12.0	1.7	7.5	2.2	0.8	2.2	0.4	2.2	0.5	1.3	0.1	1.3	0.1
RB98-31	3.8	21	1	<1	<0.5	1	0.5	10	44	7.5	14.0	1.8	8.0	2.0	0.9	2.7	0.4	1.8	0.4	1.0	0.1	1.2	0.1
RB98-36	0.9	15	<1	<1	<0.5	1	<0.5	10	31	6.5	11.5	1.8	7.0	2.0	0.6	2.2	0.3	1.7	0.4	1.0	0.1	1.0	0.1
RB98-40	2.2	17	<1	<1	<0.5	1	<0.5	13	32	8.5	17.0	2.4	10.5	2.5	1.0	2.8	0.4	2.0	0.5	1.0	0.1	1.0	0.1
RB98-42	1.8	17	<1	<1	<0.5	<1	<0.5	13	28	6.5	11.5	1.7	6.5	2.1	0.7	2.5	0.4	2.2	0.4	1.1	0.1	1.2	0.1
RB98-44	1.4	17	<1	<1	<0.5	<1	<0.5	14	25	9.0	14.5	2.1	8.5	2.3	1.1	2.8	0.5	2.6	0.5	1.4	0.2	1.4	0.1
RB98-45	2.7	17	<1	<1	<0.5	1	<0.5	14	36	9.5	17.5	2.5	10.5	2.4	1.0	2.8	0.5	2.6	0.5	1.4	0.2	1.3	0.1
RB98-47	0.3	16	<1	<1	<0.5	1	<0.5	16	31	12.0	21.5	2.9	13.0	3.7	1.3	4.1	0.6	3.2	0.5	1.2	0.1	1.2	0.1
RB98-48	0.3	13	<1	<1	<0.5	1	0.5	12	33	9.5	17.0	2.5	9.5	2.5	0.8	2.4	0.4	1.9	0.4	1.2	0.1	1.0	0.1
RB98-49	3.0	20	1	<1	<0.5	2	0.5	14	45	10.5	19.5	2.6	12.0	2.8	1.1	2.6	0.5	2.5	0.5	1.4	0.2	1.2	0.1
RB98-50	0.6	16	<1	<1	<0.5	1	7.0	12	33	8.0	13.5	2.1	8.0	2.2	0.7	2.3	0.4	2.0	0.4	1.1	0.1	1.2	0.1
RB98-52	0.6	18	<1	1	<0.5	1	1.5	12	36	10.5	22.0	3.1	11.5	2.7	0.9	2.9	0.4	2.0	0.4	1.1	0.1	1.2	0.1
RB98-56	0.5	15	5	6	<0.5	8	<0.5	23	168	23.0	48.0	6.4	25.0	4.9	1.4	5.0	0.8	3.8	0.8	2.2	0.3	2.4	0.4
RB98-61	0.5	16	5	5	<0.5	9	<0.5	21	181	13.0	26.5	3.4	12.0	2.5	0.5	2.7	0.5	2.9	0.7	2.2	0.3	2.5	0.3
RB98-64	0.2	18	5	5	<0.5	8	<0.5	27	183	15.5	31.0	4.0	14.5	3.4	0.8	3.7	0.7	4.7	0.9	2.9	0.4	2.8	0.4
RB98-65	0.3	16	5	6	<0.5	9	<0.5	27	192	24.0	47.0	6.0	22.5	4.9	0.9	4.7	0.7	4.4	0.8	2.6	0.4	2.7	0.4
RB98-67	<0.1	16	6	7	<0.5	6	<0.5	21	221	14.0	26.0	3.5	13.5	3.2	0.5	3.1	0.5	2.9	0.7	2.3	0.5	3.1	0.5
RB98-69	0.1	14	5	6	<0.5	8	<0.5	22	197	18.0	37.0	5.0	20.0	4.1	0.8	3.8	0.6	3.6	0.8	2.0	0.3	2.6	0.4
RB98-70	0.1	15	5	6	<0.5	9	<0.5	25	191	22.5	43.5	5.4	20.5	4.2	1.0	4.3	0.7	3.6	0.8	2.3	0.4	2.9	0.4
RB98-76	0.4	18	1	1	<0.5	1	2.0	12	34	5.5	11.5	1.7	8.5	2.3	0.9	2.5	0.4	2.0	0.5	1.1	0.1	1.2	0.2
RB98-79	1.3	16	5	6	<0.5	10	0.5	24	190	13.5	26.5	3.4	14.0	3.9	0.9	3.7	0.7	3.6	0.7	2.4	0.4	2.8	0.4
RB99-01	0.5	10	6	5	<0.5	7	0.5	18	189	10.5	21.5	2.8	10.5	3.1	1.2	3.1	0.6	2.9	0.6	2.4	0.4	2.8	0.5
RB99-02	0.3	8	5	5	<0.5	7	<0.5	21	169	3.5	9.5	1.5	6.5	2.1	0.5	2.4	0.5	3.2	0.7	2.7	0.4	2.9	0.4
RB99-03	1.1	15	6	5	<0.5	10	<0.5	23	211	20.5	42.5	5.2	18.5	3.5	0.5	3.5	0.6	3.4	0.8	2.9	0.5	3.2	0.5
RB99-04	0.4	12	6	5	<0.5	10	<0.5	22	188	11.5	26.0	3.6	14.0	3.2	0.6	3.3	0.6	3.3	0.7	2.7	0.4	2.6	0.4
Z603-95	2.4	17	1	1	<0.5	1	<0.5	18	54	6.5	15.0	2.2	11.0	5.7	1.1	3.4	0.5	2.9	0.6	1.7	0.3	1.7	0.3
Z614-95	0.3	15	1	1.5	<0.5	1	<0.5	20	89	12.5	28.0	3.9	18.0	4.4	1.1	4.2	0.6	3.3	0.7	1.6	0.2	1.9	0.3
Z622-95	0.5	18	1	1	<0.5	1	<0.5	17	52	9.0	20.0	2.9	13.0	2.9	0.9	3.7	0.5	2.9	0.6	1.7	0.3	1.7	0.3
Z626-95	1.4	18	1	1.5	<0.5	2	<0.5	13	47	13.5	27.5	3.8	15.5	3.6	1.1	3.3	0.4	2.6	0.5	1.4	0.2	1.4	0.1
Z632-95	0.4	17	1	1.5	<0.5	<1	<0.5	16	50	6.0	13.5	2.1	9.0	2.6	1.0	3.5	0.5	2.7	0.6	1.6	0.2	1.8	0.2

Appendix 2.2.-Geochemical Composition by Rock Type and Ore Zone

- Major, minor, selected trace, and rare earth elements.
- Major elements recalculated to 100% wt (volatile free).
- Listed by rock type and ore zone.

- Abbreviations:
  - Ore zone:
    - bckd: background
    - bckd mt: background with magnetite
    - bckd py: background with pyrite
    - bckd py-mt: background with pyrite-magnetite
    - bckd py-ht: background with pyrite-hematite
    - bckd ht: background with hematite
    - bckd ht-cp: background with hematite-chalcopyrite
    - bckd py-sph-ga: background with pyrite-sphalerite-galena
    - py: pyrite
    - py-cp: pyrite-chalcopyrite
    - cp: chalcopyrite
    - cp-bn: chalcopyrite-bornite
    - bn: bornite
    - bn-cc: bornite-chalcocite
    - cc: chalcocite

Appendix 2.2.- Geochemical Composition by Rock Type and Ore Zone

Sample	Rock Type	Ore Zone	Cu % in ddh	Spec. Grav.	Mag. Susc.	Mine Block	SiO$_2$ %	TiO$_2$ %	AL$_2$O$_3$ %	FeOT %	MnO %	MgO %	CaO %	Na$_2$O %	K$_2$O %	P$_2$O$_5$ %	Total %	Na$_2$O/ K$_2$O	Na$_2$O / Na$_2$O+K$_2$O	LOI %	S %	C (inor) %
MP848	rhyodacite	bckd py	<0.01	2.52	0.00	Morro	67.87	0.39	14.86	1.79	0.07	0.44	4.04	5.22	5.24	0.07	100.00	1.00	0.50	3.56	0.49	0.85
RB98-05	rhyodacite	bckd py	0.06	2.62	0.00	Valdivia S	68.36	0.41	14.25	2.65	0.13	0.29	5.12	5.49	3.16	0.15	100.00	1.74	0.63	4.65	1.63	0.90
RB98-21	rhyodacite	bckd py	0.07		0.00	Valdivia S	71.25	0.43	14.35	1.79	0.12	0.36	3.34	4.42	3.79	0.15	100.00	1.17	0.54	2.90	0.21	0.60
RB98-22	rhyodacite	bckd py	0.02	2.60	0.00	Valdivia S	69.04	0.40	13.71	2.11	0.17	0.19	5.87	4.42	3.93	0.15	100.00	1.12	0.53	5.19	1.33	1.00
RB98-79	rhyodacite	bckd py	0.07			Valdivia S	70.77	0.43	14.50	1.73	0.12	0.29	3.60	4.70	3.71	0.15	100.00	1.27	0.56	3.09	0.40	0.60
Average	**rhyodacite**	**bckd py**	**0.05**	**2.58**	**0.00**		**69.46**	**0.41**	**14.34**	**2.02**	**0.12**	**0.31**	**4.40**	**4.85**	**3.96**	**0.13**	**100.00**	**1.22**	**0.55**	**3.88**	**0.81**	**0.79**
MP845	rhyodacite	bckd py-mt	<0.01	2.60	1.12	Filo	64.82	0.54	16.03	6.69	0.21	2.52	0.87	5.56	2.66	0.11	100.00	2.09	0.68	1.98	<0.01	<0.05
MP860	rhyodacite	bckd py-ht	0.04	2.54	0.02	Filo	72.52	0.37	11.29	0.93	0.09	0.21	6.90	5.17	2.43	0.08	100.00	2.13	0.68	4.77	0.12	1.25
RB98-70	rhyodacite	bckd ht	0.08	2.53	0.22	Filo	68.97	0.43	15.15	3.62	0.06	0.70	1.98	7.18	1.76	0.14	100.00	4.09	0.80	1.90	0.01	0.30
Average	**rhyodacite**	**bckd py,ht,mt**	**0.04**	**2.56**	**0.45**		**68.77**	**0.45**	**14.16**	**3.75**	**0.12**	**1.15**	**3.25**	**5.97**	**2.28**	**0.11**	**100.00**	**2.62**	**0.72**	**3.12**	**0.05**	**0.53**
RB98-61	rhyodacite	bckd cp-ht	0.26	2.56	0.00	Filo	69.90	0.40	13.74	3.10	0.07	0.10	3.61	5.98	2.96	0.14	100.00	2.02	0.67	2.67	0.04	0.70
RB98-64	rhyodacite	bckd cp-ht	0.22	2.58	0.06	Filo	70.29	0.42	14.07	4.59	0.11	1.02	1.50	5.39	2.45	0.14	100.00	2.20	0.69	1.79	0.02	0.25
Average	**rhyodacite**	**bckd cp-ht**	**0.24**	**2.57**	**0.03**		**70.10**	**0.41**	**13.90**	**3.85**	**0.09**	**0.56**	**2.55**	**5.69**	**2.71**	**0.14**	**100.00**	**2.10**	**0.68**	**2.23**	**0.03**	**0.48**
MP719	rhyodacite	py	0.13	2.71	0.02	Morro	69.96	0.49	14.69	3.08	0.06	1.11	2.48	4.13	3.89	0.10	100.00	1.06	0.51	3.29	0.47	0.35
RB99-03	rhyodacite	py	0.05		0.00	Morro	76.74	0.35	13.91	0.83	0.01	0.22	1.70	4.35	1.86	0.03	100.00	2.34	0.70	2.41	0.58	0.25
RB99-04	rhyodacite	py	0.04		0.00	Morro	68.48	0.56	12.98	5.64	0.11	1.14	3.26	4.45	3.25	0.13	100.00	1.37	0.58	4.68	3.21	0.50
RB98-09	rhyodacite	py	0.05	2.64	0.00	Valdivia S	67.85	0.40	13.89	3.78	0.11	0.66	5.01	5.80	2.37	0.14	100.00	2.45	0.71	4.19	2.24	0.80
RB98-10	rhyodacite	py	0.07	2.65	0.00	Valdivia S	68.46	0.35	12.99	3.62	0.16	0.64	6.36	5.19	2.10	0.14	100.00	2.47	0.71	5.28	2.19	1.10
MP674	rhyodacite	py-cp	0.43	2.58	0.00	Osorno	67.61	0.40	15.15	0.59	0.06	0.16	6.55	6.99	2.40	0.08	100.00	2.91	0.74	4.14	0.26	1.17
MP776	rhyodacite	py-cp	1.08	2.66	0.00	Valdivia S	70.40	0.52	13.18	2.38	0.10	0.06	4.27	5.13	3.81	0.13	100.00	1.35	0.57	3.11	1.62	0.70
RB98-11	rhyodacite	py-cp	0.37	2.56	0.00	Valdivia S	68.31	0.37	14.52	1.12	0.14	0.37	6.62	8.20	0.21	0.14	100.00	38.4	0.97	4.75	0.31	1.25
Average	**rhyodacite**	**py, py-cp**	**0.28**	**2.63**	**0.00**		**69.73**	**0.43**	**13.91**	**2.63**	**0.09**	**0.55**	**4.53**	**5.53**	**2.49**	**0.11**	**100.00**	**2.22**	**0.69**	**3.98**	**1.36**	**0.77**
MP739	rhyodacite	cp	2.31	2.49	0.00	Filo	65.75	0.39	18.87	3.11	0.02	0.06	0.67	10.84	0.06	0.23	100.00	180.7	0.99	1.44	2.37	<0.05
MP775	rhyodacite	cp	2.39	2.66	0.00	Valdivia S	66.23	0.54	13.57	3.65	0.09	0.07	6.39	5.21	3.90	0.34	100.00	1.34	0.57	2.14	2.77	1.15
RB98-12	rhyodacite	cp	5.90	2.69	0.01	Valdivia S	64.13	0.39	15.09	3.01	0.13	0.14	7.45	5.24	4.29	0.13	100.00	1.22	0.55	4.14	2.27	1.35
RB98-13	rhyodacite	cp-bn	1.06	2.63	0.01	Valdivia S	69.86	0.37	13.74	1.42	0.13	0.61	5.49	6.55	1.68	0.14	100.00	3.89	0.80	4.18	0.26	0.95
RB98-19	rhyodacite	cp-bn	4.47	2.60	0.00	Valdivia S	72.60	0.38	13.85	2.74	0.08	0.68	1.40	4.36	3.75	0.16	100.00	1.16	0.54	2.04	2.06	0.15
Average	**rhyodacite**	**cp, cp-bn**	**3.23**	**2.61**	**0.00**		**67.72**	**0.41**	**15.03**	**2.79**	**0.09**	**0.31**	**4.28**	**6.44**	**2.74**	**0.20**	**100.00**	**2.35**	**0.70**	**2.79**	**1.95**	**0.73**
RB98-65	rhyodacite	bn	1.04	2.56	0.00	Filo	69.35	0.43	15.26	1.79	0.10	0.31	3.98	6.16	2.49	0.13	100.00	2.47	0.71	2.96	0.47	0.65
RB98-67	rhyodacite	bn	0.74	2.56	0.01	Filo	65.07	0.57	20.03	1.46	0.04	0.34	1.80	10.54	0.01	0.14	100.00	2108	1.00	1.56	1.09	0.25
MP713	rhyodacite	bn	1.07	2.60	0.02	Morro	72.05	0.38	13.38	1.45	0.08	0.07	5.26	6.57	0.68	0.07	100.00	9.69	0.91	4.27	0.39	1.00
MP718	rhyodacite	bn	7.82	2.59	0.00	Morro	66.88	0.58	17.22	0.74	0.02	0.10	3.12	10.91	0.26	0.16	100.00	42.2	0.98	2.25	0.22	0.49
MP677	rhyodacite	bn	3.77	2.65	0.00	Osorno	67.55	0.48	16.69	0.77	0.06	0.19	3.64	5.91	4.45	0.27	100.00	1.33	0.57	2.98	0.50	0.63
MP856	rhyodacite	bn	1.42	2.80	0.00	Valdivia S	65.11	0.46	15.00	5.32	0.07	0.52	3.18	8.87	1.22	0.24	100.00	7.25	0.88	1.73	2.77	0.55
MP746	rhyodacite	bn-cc	1.15	2.59	0.00	Filo	67.13	0.35	14.04	0.28	0.11	0.07	7.99	5.44	4.52	0.07	100.00	1.20	0.55	5.55	0.17	1.45
RB98-56	rhyodacite	bn-cc	1.88	2.52	0.01	Filo	71.36	0.40	14.68	2.17	0.10	0.51	2.83	6.30	1.49	0.13	100.00	4.22	0.81	2.07	0.25	0.35
RB98-69	rhyodacite	bn-cc	1.44	2.53		Filo	71.50	1.02	14.16	3.79	0.06	0.58	1.35	7.39	0.01	0.13	100.00	1479	1.00	1.24	0.03	0.15
MP664	rhyodacite	bn-cc	2.74	2.56	0.01	Osorno	62.26	0.51	15.83	3.92	0.18	1.15	6.41	6.44	3.04	0.25	100.00	2.12	0.68	4.57	0.74	1.17
MP782	rhyodacite	bn-cc	4.30	2.63	0.00	Valdivia S	71.60	0.37	11.30	3.17	0.06	0.28	5.31	4.30	3.30	0.32	100.00	1.30	0.57	2.5	1.11	1.05
RB98-15	rhyodacite	bn-cc	4.91	2.64	0.00	Valdivia S	70.52	0.36	14.31	2.85	0.07	0.33	3.77	7.64	0.01	0.14	100.00	1529	1.00	2.87	1.16	0.70
MP737	rhyodacite	cc	2.23	2.57	0.01	Filo	72.81	0.38	16.08	0.68	0.05	0.22	0.69	8.75	0.11	0.22	100.00	78.6	0.99	0.89	0.4	0.05
Average	**rhyodacite**	**bn, bn-cc, cc**	**2.65**	**2.60**	**0.01**		**68.71**	**0.48**	**15.23**	**2.19**	**0.08**	**0.36**	**3.79**	**7.32**	**1.66**	**0.18**	**100.00**	**4.41**	**0.82**	**2.73**	**0.72**	**0.65**

Appendix 2.2.- Geochemical Composition by Rock Type and Ore Zone, Continued

Sample	Rock Type	Ore Zone	Ag ppm	As ppm	Ba ppm	Co ppm	Cu ppm	Hg ppm	Ni ppm	Pb ppm	Rb ppm	Sr ppm	U ppm	V ppm	Zn ppm
MP848	rhyodacite	bckd py			755		<100				106	38			
RB98-05	rhyodacite	bckd py	<1	4	415	8.0	95	10	20	5	74	54	2.5	50	10
RB98-21	rhyodacite	bckd py	<1	3	559	7.0	250	<10	45	<5	104	64	2.5	50	10
RB98-22	rhyodacite	bckd py	<1	6	573	7.5	70	10	10	5	96	80	2.5	50	10
RB98-79	rhyodacite	bckd py	<1	2	501	8.0	110	<10	15	5	102	63	2.5	60	5
Average	**rhyodacite**	**bckd py**	**<1**	**4**	**561**	**7.6**	**115**	**<10**	**23**	**4**	**96**	**60**	**2.5**	**53**	**9**
MP845	rhyodacite	bckd py-mt			465		<100				64	96			
MP860	rhyodacite	bckd py-ht	0.4	42	271	40.5	418	10	35	135	50	76	2.5	35	25
RB98-70	rhyodacite	bckd ht	1	5	115	5.0	160	<10	10	<5	40	59	2.5	50	10
Average	**rhyodacite**	**bckd py,ht,mt**	**<1**	**24**	**284**	**22.8**	**209**	**<10**	**23**	**69**	**51**	**77**	**2.5**	**43**	**1**
RB98-61	rhyodacite	bckd cp-ht	<1	<1	530	3.0	700	<10	<5	<5	67	57	2.0	45	10
RB98-64	rhyodacite	bckd cp-ht	<1	<1	256	8.0	200	<10	10	<5	56	56	2.5	55	20
Average	**rhyodacite**	**bckd cp-ht**	**<1**	**<1**	**393**	**5.5**	**450**	**<10**	**6**	**<5**	**61**	**57**	**2.3**	**50**	**15**
MP719	rhyod low	py			380						84	52			
RB99-03	rhyod low	py	<0.2	5	865	2.0	160	<10	<5	<5	62	31	3.0	20	<5
RB99-04	rhyod low	py	<0.2	234	408	18.0	420	20	<5	<5	78	53	2.5	55	30
RB98-09	rhyodacite	py	<1	14	361	14.0	350	20	15	10	51	108	2.0	50	15
RB98-10	rhyodacite	py	<1	36	314	11.5	70	30	20	5	51	87	2.0	40	15
MP674	rhyodacite	py-cp			245						54	42			
MP776	rhyodacite	py-cp			730		3300				78	104			
RB98-11	rhyodacite	py-cp	<1	2	19	5.0	230	10	5	<5	4	51	2.0	40	10
Average	**rhyodacite**	**py, py-cp**	**<1**	**58**	**415**	**10.1**	**755**	**17**	**9**	**5**	**58**	**66**	**2.3**	**41**	**15**
MP739	rhyodacite	cp			40		24600				4	40			
MP775	rhyodacite	cp			810		29700				68	46			
RB98-12	rhyodacite	cp	1	2	535	1.5	25000	50	5	<5	93	52	2.0	35	10
RB98-13	rhyodacite	cp-bn	<1	<1	167	3.0	2100	<10	10	<5	35	60	2.0	40	15
RB98-19	rhyodacite	cp-bn	6	105	501	3.5	46900	40	5	<5	77	39	2.5	30	10
Average	**rhyodacite**	**cp, cp-bn**	**3**	**36**	**411**	**2.7**	**25660**	**32**	**7**	**<5**	**55**	**47**	**2.2**	**35**	**12**
RB98-65	rhyodacite	bn	1	1	251	3.5	9700	80	5	<5	58	64	2.5	70	5
RB98-67	rhyodacite	bn	5	1	7	2.5	26000	10	10	<5	1	44	3.0	60	<5
MP713	rhyodacite	bn			40		10000				16	24			
MP718	rhyodacite	bn			20						4	42			
MP677	rhyodacite	bn			540						98	52			
MP856	rhyodacite	bn	12.1	<1	90	2	70700	<10	25	15	16	55	2.0	25	55
MP746	rhyodacite	bn-cc			270		5900				84	8			
RB98-56	rhyodacite	bn-cc	<1	<1	215	2.5	4500	10	5	5	38	86	2.0	70	20
RB98-69	rhyodacite	bn-cc	<1	<1	11	5.0	475	<10	5	<5	2	58	2.0	45	25
MP664	rhyodacite	bn-cc			285						60	52			
MP782	rhyodacite	bn-cc			270		200				66	8			
RB98-15	rhyodacite	bn-cc	7	8	9	2.0	27700	10	15	<5	3	35	2.5	20	10
MP737	rhyodacite	cc			40		13100				6	38			
Average	**rhyodacite**	**bn, bn-cc, cc**	**4**	**2**	**158**	**2.9**	**16828**	**20**	**11**	**5**	**35**	**43**	**2.3**	**48**	**20**

Appendix 2.2.- Geochemical Composition by Rock Type and Ore Zone, Continued

Sample	Rock Type	Ore Zone	Cs ppm	Ga ppm	Hf ppm	Nb ppm	Ta ppm	Th ppm	Y ppm	Zr ppm	La ppm	Ce ppm	Pr ppm	Nd ppm	Sm ppm	Eu ppm	Gd ppm	Tb ppm	Dy ppm	Ho ppm	Er ppm	Tm ppm	Yb ppm	Lu ppm
MP848	rhyodacite	bckd py				6			28.0	210	6	20	5.4	18	1.8	< 0.2	5.4	0.7	4.9	0.6	4.9	0.8	5.7	0.9
RB98-05	rhyodacite	bckd py	0.5	14	5	6	<0.5	9	22.0	170	14.0	26.0	3.4	13.5	3.0	0.7	3.2	0.6	3.4	0.8	2.4	0.4	2.4	0.4
RB98-21	rhyodacite	bckd py	1.4	16	5	6	<0.5	9	23.5	186	13.0	26.0	3.5	14.5	3.7	0.8	3.8	0.7	3.6	0.9	2.3	0.4	2.5	0.4
RB98-22	rhyodacite	bckd py	0.7	14	5	5	<0.5	9	22.5	172	9.5	19.0	2.6	10.5	2.4	0.5	3.0	0.5	3.3	0.8	2.4	0.3	2.7	0.4
RB98-79	rhyodacite	bckd py	1.3	16	5	6	<0.5	10	24.0	190	13.5	26.5	3.4	14.0	3.9	0.9	3.7	0.7	3.6	0.7	2.4	0.4	2.8	0.4
Average	rhyodacite	bckd py	1.0	15	5	6	<0.5	9	24.0	185	11	24	3.7	14.1	3.0	0.6	3.8	0.6	3.8	0.8	2.9	0.5	3.2	0.5
MP845	rhyodacite	bckd py-mt				6			30.0	249	29	75	9.6	38	8.6	0.6	9.1	1.3	6.8	2.0	2.0	0.8	6.6	0.8
MP860	rhyodacite	bckd py-ht	0.3	8	4	6	<0.5	8	25.0	160	19.5	42.5	5.2	22.0	5.0	0.8	4.4	0.8	4.2	0.9	2.6	0.4	2.4	0.4
RB98-70	rhyodacite	bckd ht	0.1	15	5	6	<0.5	9	24.5	191	22.5	43.5	5.4	20.5	4.2	1.0	4.3	0.7	3.6	0.8	2.3	0.4	2.9	0.4
Average	rhyodacite	bckd py,ht,mt	0.2	12	5	6	<0.5	9	26.5	200	19	42.2	5.5	21.7	4.9	0.8	5.1	0.8	4.4	1.0	2.4	0.5	3.6	0.5
RB98-61	rhyodacite	bckd cp-ht	0.5	16	5	5	<0.5	9	20.5	181	13.0	26.5	3.4	12.0	2.5	0.5	2.7	0.5	2.9	0.7	2.2	0.3	2.5	0.3
RB98-64	rhyodacite	bckd cp-ht	0.2	18	5	5	<0.5	8	27.0	183	15.5	31.0	4.0	14.5	3.4	0.8	3.7	0.7	4.7	0.9	2.9	0.4	2.8	0.4
Average	rhyodacite	bckd cp-ht	0.4	17	5	5	<0.5	9	23.8	182	14.3	28.8	3.7	13.3	3.0	0.7	3.2	0.6	3.8	0.8	2.6	0.4	2.7	0.4
MP719	rhyod low	py				6			28.0	225	21	42	6.2	23	4.8	0.9	4.0	0.6	3.7	0.9	2.2	0.4	2.9	0.5
RB99-03	rhyod low	py	1.1	15	6	5	<0.5	10	22.5	211	20.5	42.5	5.2	18.5	3.5	0.5	3.5	0.6	3.4	0.8	2.9	0.5	3.2	0.5
RB99-04	rhyod low	py	0.4	12	6	5	<0.5	10	21.5	188	11.5	26.0	3.6	14.0	3.2	0.6	3.3	0.6	3.3	0.7	2.7	0.4	2.6	0.4
RB98-09	rhyodacite	py	0.4	15	6	6	<0.5	8	29.5	187	18.5	36.5	5.2	21.5	5.1	0.9	5.7	0.9	5.0	1.1	3.3	0.4	3.2	0.4
RB98-10	rhyodacite	py	0.7	15	5	5	<0.5	8	24.0	177	11.0	21.5	3.1	13.0	3.5	0.6	4.1	0.6	4.0	0.8	2.6	0.4	2.7	0.4
MP674	rhyodacite	py-cp				8			28.0	252	5	14	2.7	10	2.4	0.7	2.4	0.4	3.4	0.8	2.3	0.4	2.8	0.5
MP776	rhyodacite	py-cp				6			32.0	207	13	33	4.3	15	2.6	0.8	3.0	0.6	3.2	0.7	1.9	0.3	1.9	0.3
RB98-11	rhyodacite	py-cp	0.1	15	5	6	<0.5	7	23.5	188	8.0	15.5	2.1	10.0	2.6	0.5	2.9	0.6	3.5	0.8	2.7	0.4	3.1	0.4
Average	rhyodacite	py, py-cp	0.5	14	5.6	6	<0.5	9	26.1	204	14	28.9	4.1	15.6	3.5	0.7	3.6	0.6	3.7	0.8	2.6	0.4	2.8	0.4
MP739	rhyodacite	cp				8			30.0	243	1	10	1.7	7	1.5	0.5	2.3	0.6	3.8	0.8	1.9	0.4	2.4	0.4
MP775	rhyodacite	cp				6			32.0	186	23	51	6.3	22	3.9	1.4	3.3	0.6	3.5	0.7	1.9	0.3	2.0	0.3
RB98-12	rhyodacite	cp	0.4	11	5	6	<0.5	8	25.5	189	13.0	26.0	3.8	15.5	4.5	0.8	4.1	0.8	4.4	0.9	2.5	0.4	3.0	0.5
RB98-13	rhyodacite	cp-bn	0.1	13	5	6	<0.5	7	27.0	193	13.5	25.5	3.6	15.0	4.0	0.8	4.5	0.8	4.6	1.0	3.1	0.4	3.2	0.4
RB98-19	rhyodacite	cp-bn	0.3	9	5	5	<0.5	8	16.0	160	12.0	25.5	3.5	14.0	3.1	0.6	3.0	0.6	2.6	0.6	1.8	0.4	2.3	0.4
Average	rhyodacite	cp, cp-bn	0.3	11	5	6	<0.5	8	26.1	194	12.5	27.6	3.8	14.7	3.4	0.8	3.4	0.7	3.8	0.8	2.2	0.4	2.6	0.4
RB98-65	rhyodacite	bn	0.3	16	5	6	<0.5	9	26.5	192	24.0	47.0	6.0	22.5	4.9	0.9	4.7	0.7	4.4	0.8	2.6	0.4	2.7	0.4
RB98-67	rhyodacite	bn	<0.1	16	6	7	<0.5	6	20.5	221	14.0	26.0	3.5	13.5	3.2	0.5	3.1	0.5	2.9	0.7	2.3	0.5	3.1	0.5
MP713	rhyodacite	bn				8			22.0	183	9	26	3.3	10	1.6	0.5	1.6	0.4	2.5	0.6	1.5	0.3	2.3	0.3
MP718	rhyodacite	bn				10			36.0	312	6	17	2.9	11	2.7	0.7	2.6	0.6	3.7	1.0	2.3	0.4	3.1	0.5
MP677	rhyodacite	bn				6			32.0	231	6	17	3.0	12	2.8	1.0	2.8	0.5	3.3	0.8	1.9	0.3	2.4	0.5
MP856	rhyodacite	bn	0.1	10	5	6	<0.5	7	24.3	174	13.0	32.5	4.3	18.5	4.8	1.1	4.9	0.7	4.1	0.8	2.8	0.5	2.9	0.4
MP746	rhyodacite	bn-cc				4			28.0	147	5	14	2.1	6	1.2	0.5	1.8	0.4	2.4	0.7	1.4	0.3	1.8	0.3
RB98-56	rhyodacite	bn-cc	0.5	15	5	6	<0.5	8	22.5	168	23.0	48.0	6.4	25.0	4.9	1.4	5.0	0.8	3.8	0.8	2.2	0.3	2.4	0.4
RB98-69	rhyodacite	bn-cc	0.1	14	5	6	<0.5	8	22.0	197	18.0	37.0	5.0	20.0	4.1	0.8	3.8	0.6	3.6	0.8	2.0	0.3	2.6	0.4
MP664	rhyodacite	bn-cc				6			26.0	189	9	19	2.9	12	3.3	0.9	2.8	0.6	3.2	0.9	2.1	0.4	2.5	0.5
MP782	rhyodacite	bn-cc				6			28.0	162	13	33	4.2	17	2.8	1.3	3.4	0.7	3.5	0.9	1.7	0.4	2.1	0.3
RB98-15	rhyodacite	bn-cc	<0.1	11	4	5	<0.5	8	23.5	153	14.5	31.0	4.3	15.5	3.8	0.9	3.7	0.8	3.5	1.0	2.5	0.6	2.7	0.5
MP737	rhyodacite	cc				8			28.0	198	22	48	5.5	20	3.7	0.9	3.0	0.5	2.4	0.6	1.5	0.3	1.8	0.3
Average	rhyodacite	bn, bn-cc, cc	0.2	14	5	6	<0.5	8	26.1	194	13.6	30.4	4.1	15.6	3.4	0.9	3.3	0.6	3.3	0.8	2.1	0.4	2.5	0.4

Appendix 2.2.- Geochemical Composition by Rock Type and Ore Zone, Continued

Sample	Rock Type	Ore Zone	Cu % in ddh	Spec. Grav.	Mag. Susc.	Mine Block	SiO$_2$ %	TiO$_2$ %	AL$_2$O$_3$ %	FeOT %	MnO %	MgO %	CaO %	Na$_2$O %	K$_2$O %	P$_2$O$_5$ %	Total %	Na$_2$O/ K$_2$O	Na$_2$O/ Na$_2$O+K$_2$O	LOI %	S %	C (inor) %
MP864	rhyodacite	bn-cc	1.06	2.63	0.01	Morro	71.28	0.52	13.83	2.06	0.03	0.18	2.35	4.70	4.93	0.12	100.00	0.95	0.49	1.23	1.08	0.40
MP778	rhyodacite	bn-cc	5.75	2.68	0.00	Valdivia S	70.44	0.39	13.90	4.13	0.02	0.28	0.50	3.49	6.39	0.46	100.00	0.55	0.35	1.23	1.73	0.05
RB99-01	rhyodacite	bn-cc	4.51	2.58	0.02	Valdivia S	55.06	0.46	16.43	7.52	0.15	2.10	7.32	1.10	9.39	0.46	100.00	0.12	0.11	5.47	2.70	1.20
RB99-02	rhyodacite	bn-cc	3.32		0.00	Valdivia S	69.05	0.38	13.09	1.82	0.09	0.26	6.37	4.36	4.37	0.20	100.00	1.00	0.50	4.39	1.14	1.10
Average	**rhyodacite**	**bn-cc**	**3.66**	**2.63**	**0.01**		**66.46**	**0.44**	**14.31**	**3.89**	**0.07**	**0.71**	**4.13**	**3.41**	**6.27**	**0.31**	**100.00**	**0.54**	**0.35**	**3.08**	**1.66**	**0.69**
MP846	**rhyod dyke**	**bckd py**	**0.07**	**2.56**	**0.01**	**Morro**	**69.74**	**0.52**	**14.60**	**3.33**	**0.13**	**1.31**	**1.77**	**5.01**	**3.49**	**0.11**	**100.00**	**1.43**	**0.59**	**2.2**	**0.02**	**0.25**
MP754	rhyod dyke	bckd py-sp-ga	0.01	2.63	0.01	Paso Riel	68.85	0.40	12.27	2.93	0.13	2.28	5.30	3.08	4.69	0.07	100.00	0.66	0.40	4.28	0.41	0.90
MP757	rhyod dyke	bckd py-sp-ga	0.01	2.58	0.00	Paso Riel	69.38	0.50	14.23	3.15	0.07	2.20	1.61	3.86	4.89	0.11	100.00	0.79	0.44	2.36	0.16	0.20
Average	**rhyod dyke**	**bckd py-sp-ga**	**0.01**	**2.61**	**0.01**		**69.12**	**0.45**	**13.25**	**3.04**	**0.10**	**2.24**	**3.46**	**3.47**	**4.79**	**0.09**	**100.00**	**0.73**	**0.42**	**3.32**	**0.29**	**0.55**
MP701	rhyod dyke	py	0.90	2.76	0.14	Osorno	72.33	0.43	14.52	3.58	0.02	0.38	1.62	4.84	2.19	0.10	100.00	2.21	0.69	2.86	2.54	0.33
MP770	rhyod dyke	py	0.05	2.56	0.00	Valdivia S	62.83	0.46	15.44	5.59	0.16	2.83	2.22	2.61	7.75	0.11	100.00	0.34	0.25	4.62	2.53	0.35
MP839	rhyod dyke	py	0.11	2.67	0.00	Valdivia S	69.47	0.41	13.31	3.57	0.11	1.02	3.95	3.52	4.56	0.10	100.00	0.77	0.44	5.12	2.04	0.75
MP768	rhyod dyke	py-cp	0.03	2.73	0.00	Valdivia S	70.03	0.39	13.34	4.16	0.09	1.06	3.38	3.78	3.57	0.21	100.00	1.06	0.51	4.88	2.64	0.50
Average	**rhyod dyke**	**py, py-cp**	**0.27**	**2.68**	**0.04**		**68.67**	**0.42**	**14.15**	**4.22**	**0.10**	**1.32**	**2.79**	**3.69**	**4.52**	**0.13**	**100.00**	**0.82**	**0.45**	**4.37**	**2.44**	**0.48**
MP764	**rhyod dyke**	**cp**	**0.69**	**2.57**	**0.00**	**Valdivia S**	**64.07**	**0.44**	**18.13**	**1.76**	**0.06**	**0.20**	**4.39**	**10.61**	**0.23**	**0.12**	**100.00**	**45.8**	**0.98**	**3.32**	**1.21**	**0.75**
MP844	basalt	bckd mt	< 0.01	2.85	2.99	Filo	51.56	0.89	18.31	9.26	0.50	5.58	7.60	3.85	2.29	0.17	100.00	1.68	0.63	2.34	0.01	0.05
RB98-42	basalt	bckd mt	0.01	2.89	1.84	Filo	51.86	0.61	20.26	7.04	0.40	4.73	9.99	2.69	2.32	0.11	100.00	1.16	0.54	2.11	0.01	<0.05
RB98-40	basalt	bckd mt	0.01	2.88	2.07	Osorno	51.82	0.65	17.91	8.23	0.38	6.67	9.59	3.01	1.62	0.13	100.00	1.86	0.65	3.20	0.01	0.25
RB98-29	basalt	bckd mt	0.02	2.98	1.20	Valdivia S	51.02	0.62	20.23	7.37	0.56	4.99	10.57	2.57	1.97	0.11	100.00	1.30	0.57	2.83	0.01	0.10
Average	**basalt**	**bckd mt**	**0.01**	**2.90**	**2.03**		**51.56**	**0.69**	**19.17**	**7.97**	**0.46**	**5.49**	**9.44**	**3.03**	**2.05**	**0.13**	**100.00**	**1.48**	**0.60**	**2.62**	**0.01**	**0.11**
RB98-49	basalt	bckd py	< 0.01	2.84	0.02	Filo	51.14	0.71	18.50	8.66	1.44	6.71	6.98	3.55	2.19	0.13	100.00	1.62	0.62	4.44	0.06	0.15
RB98-50	basalt	bckd py	0.03	2.75	0.03	Filo	45.96	0.63	17.01	9.31	1.63	4.54	14.99	3.81	2.00	0.11	100.00	1.91	0.66	9.71	1.81	2.20
Z632-95	basalt	bckd py	< 0.01	2.81	0.12	Valdivia S	48.57	0.82	20.83	9.31	1.59	5.67	7.04	5.60	0.42	0.13	100.00	13.2	0.93	6.52	0.03	0.75
RB98-06	basalt	bckd py	0.09	2.77	0.02	Valdivia S	50.80	0.93	19.48	9.23	0.80	5.52	6.21	6.03	0.86	0.14	100.00	7.00	0.88	6.23	1.46	0.90
Average	**basalt**	**bckd py**	**0.03**	**2.79**	**0.05**		**49.12**	**0.77**	**18.96**	**9.13**	**1.36**	**5.61**	**8.80**	**4.75**	**1.37**	**0.13**	**100.00**	**3.47**	**0.78**	**6.73**	**0.84**	**1.00**
MP788	basalt	py	0.01			Filo	51.55	0.72	18.20	9.30	0.47	5.85	10.44	2.34	1.01	0.12	100.00	2.31	0.70	3.92	2.41	0.20
MP728	basalt	py	0.06	2.76	0.04	Morro	53.98	0.77	18.12	7.98	0.48	6.07	5.78	6.26	0.36	0.19	100.00	17.4	0.95	4.7	0.47	0.55
MP703	basalt	py	0.30	2.95	0.00	Osorno	52.48	0.61	17.06	9.49	0.35	6.19	8.55	3.92	1.26	0.10	100.00	3.11	0.76	9.05	3.16	1.42
MP865	basalt	py	0.01	2.88	0.00	Valdivia S	49.97	0.73	19.88	2.76	0.44	1.16	15.96	5.34	3.66	0.10	100.00	1.46	0.59	11.92	0.10	2.80
RB98-76	basalt	py	0.18	2.71	0.06	Valdivia S	53.22	0.63	18.09	7.56	0.55	3.60	7.92	7.93	0.43	0.07	100.00	18.6	0.95	6.45	1.72	1.35
RB98-48	basalt	py-cp	0.32	2.72	0.03	Filo	52.60	0.67	16.84	7.74	0.89	6.88	7.38	5.40	1.47	0.13	100.00	3.67	0.79	5.81	0.43	0.90
RB98-31	basalt	py-cp	0.17	2.70	1.95	Valdivia S	55.07	0.86	20.86	8.86	0.51	3.59	1.93	6.21	1.95	0.15	100.00	3.18	0.76	3.68	0.20	0.10
Average	**basalt**	**py, py-cp**	**0.15**	**2.79**	**0.35**		**52.70**	**0.71**	**18.44**	**7.67**	**0.53**	**4.76**	**8.28**	**5.34**	**1.45**	**0.12**	**100.00**	**3.69**	**0.79**	**6.50**	**1.21**	**1.04**

Appendix 2.2.- Geochemical Composition by Rock Type and Ore Zone, Continued

Sample	Rock Type	Ore Zone	Ag ppm	As ppm	Ba ppm	Co ppm	Cu ppm	Hg ppm	Ni ppm	Pb ppm	Rb ppm	Sr ppm	U ppm	V ppm	Zn ppm
MP864	rhyodacite	bn-cc			670		29400				88	40			
MP778	rhyodacite	bn-cc			900		52000				132	32			
RB99-01	rhyodacite	bn-cc	17	1	865	3.0	73400	<10	<5	10	220	28	2.0	90	<5
RB99-02	rhyodacite	bn-cc	5.9	131	408	<0.5	23600	<10	<5	<5	101	32	2.0	40	<5
Average	**rhyodacite**	**bn-cc**	**11**	**66**	**711**	**1.6**	**44600**	**<10**	**<5**	**6**	**135**	**33**	**2.0**	**65**	**<5**
MP846	**rhyod dyke**	**bckd py**			**505**		**<100**				**74**	**52**			
MP754	rhyod dyke	bckd py-sp-ga			525		100				74	30			
MP757	rhyod dyke	bckd py-sp-ga			635						84	64			
Average	**rhyod dyke**	**bkcd py-es-ga**			**580**		**100**				**79**	**47**			
MP701	rhyod dyke	py			155						62	48			
MP770	rhyod dyke	py	<1	141	674	14	648	70	20	40	100	24	1.5	10	260
MP839	rhyod dyke	py			660		1100				92	82			
MP768	rhyod dyke	py-cp			415		12700				80	68			
Average	**rhyod dyke**	**py, py-cp**	**<1**	**141**	**476**	**14**	**4816**	**70**	**20**	**40**	**84**	**56**	**1.5**	**10**	**260**
MP764	**rhyod dyke**	**cp**			**40**		**9100**				**4**	**52**			
MP844	basalt	bckd mt			815		<100				52	394			
RB98-42	basalt	bckd mt	<1	<1	476	26.5	140	<10	25	<5	93.4	283	<0.5	240	120
RB98-40	basalt	bckd mt	<1	4	342	37.0	25	<10	40	<5	46.0	309	<0.5	265	205
RB98-29	basalt	bckd mt	<1	4	539	27.5	50	<10	30	5	77.6	465	<0.5	225	190
Average	**basalt**	**bckd mt**	**<1**	**3**	**543**	**30.3**	**66**	**<10**	**32**	**<5**	**67**	**363**	**<0.5**	**243**	**172**
RB98-49	basalt	bckd py	<1	26	3440	39.5	45	<10	35	5	74.4	424	0.5	270	245
RB98-50	basalt	bckd py	<1	181	731	39.5	55	70	15	10	55.8	212	0.5	240	165
Z632-95	basalt	bckd py	<0.2	3	88	32.5	20	<10	20	15	10	284	<0.5	195	425
RB98-06	basalt	bckd py	1	13	94	33.0	700	40	15	10	37.8	87	<0.5	245	300
Average	**basalt**	**bckd py**	**<1**	**56**	**1088**	**36.1**	**205**	**30**	**21**	**10**	**44.5**	**252**	**<0.5**	**238**	**284**
MP788	basalt	py			270		200				34	292			
MP728	basalt	py			85						12	308			
MP703	basalt	py			50						46	62			
MP865	basalt	py	0.2	60	274	28	1008	40	35	105	159	110	0.5	210	55
RB98-76	basalt	py	0.2	37	105	88.5	330	110	65	45	15.0	213	1.0	220	175
RB98-48	basalt	py-cp	<1	17	301	29.5	1940	<10	30	<5	36.8	125	<0.5	230	205
RB98-31	basalt	py-cp	<1	<1	319	31.5	1100	20	45	<5	97.8	113	0.5	305	175
Average	**basalt**	**py, py-cp**	**<1**	**29**	**201**	**44.4**	**916**	**44**	**44**	**39**	**57.2**	**175**	**0.6**	**241**	**153**

Appendix 2.2.- Geochemical Composition by Rock Type and Ore Zone, Continued

Sample	Rock Type	Ore Zone	Ag ppm	As ppm	Ba ppm	Co ppm	Cu ppm	Hg ppm	Ni ppm	Pb ppm	Rb ppm	Sr ppm	U ppm	V ppm	Zn ppm
MP864	rhyodacite	bn-cc			670		29400				88	40			
MP778	rhyodacite	bn-cc			900		52000				132	32			
RB99-01	rhyodacite	bn-cc	17	1	865	3.0	73400	<10	<5	10	220	· 28	2.0	90	<5
RB99-02	rhyodacite	bn-cc	5.9	131	408	<0.5	23600	<10	<5	<5	101	32	2.0	40	<5
Average	**rhyodacite**	**bn-cc**	**11**	**66**	**711**	**1.6**	**44600**	**<10**	**<5**	**6**	**135**	**33**	**2.0**	**65**	**<5**
MP846	**rhyod dyke**	**bckd py**			**505**		**<100**				**74**	**52**			
MP754	rhyod dyke	bckd py-sp-ga			525		100				74	30			
MP757	rhyod dyke	bckd py-sp-ga			635						84	64			
Average	**rhyod dyke**	**bkcd py-es-ga**			**580**		**100**				**79**	**47**			
MP701	rhyod dyke	py			155						62	48			
MP770	rhyod dyke	py	<1	141	674	14	648	70	20	40	100	24	1.5	10	260
MP839	rhyod dyke	py			660		1100				92	82			
MP768	rhyod dyke	py-cp			415		12700				80	68			
Average	**rhyod dyke**	**py, py-cp**	**<1**	**141**	**476**	**14**	**4816**	**70**	**20**	**40**	**84**	**56**	**1.5**	**10**	**260**
MP764	**rhyod dyke**	**cp**			**40**		**9100**				**4**	**52**			
MP844	basalt	bckd mt			815		<100				52	394			
RB98-42	basalt	bckd mt	<1	<1	476	26.5	140	<10	25	<5	93.4	283	<0.5	240	120
RB98-40	basalt	bckd mt	<1	4	342	37.0	25	<10	40	<5	46.0	309	<0.5	265	205
RB98-29	basalt	bckd mt	<1	4	539	27.5	50	<10	30	5	77.6	465	<0.5	225	190
Average	**basalt**	**bckd mt**	**<1**	**3**	**543**	**30.3**	**66**	**<10**	**32**	**<5**	**67**	**363**	**<0.5**	**243**	**172**
RB98-49	basalt	bckd py	<1	26	3440	39.5	45	<10	35	5	74.4	424	0.5	270	245
RB98-50	basalt	bckd py	<1	181	731	39.5	55	70	15	10	55.8	212	0.5	240	165
Z632-95	basalt	bckd py	<0.2	3	88	32.5	20	<10	20	15	10	284	<0.5	195	425
RB98-06	basalt	bckd py	1	13	94	33.0	700	40	15	10	37.8	87	<0.5	245	300
Average	**basalt**	**bckd py**	**<1**	**56**	**1088**	**36.1**	**205**	**30**	**21**	**10**	**44.5**	**252**	**<0.5**	**238**	**284**
MP788	basalt	py			270		200				34	292			
MP728	basalt	py			85						12	308			
MP703	basalt	py			50						46	62			
MP865	basalt	py	0.2	60	274	28	1008	40	35	105	159	110	0.5	210	55
RB98-76	basalt	py	0.2	37	105	88.5	330	110	65	45	15.0	213	1.0	220	175
RB98-48	basalt	py-cp	<1	17	301	29.5	1940	<10	30	<5	36.8	125	<0.5	230	205
RB98-31	basalt	py-cp	<1	<1	319	31.5	1100	20	45	<5	97.8	113	0.5	305	175
Average	**basalt**	**py, py-cp**	**<1**	**29**	**201**	**44.4**	**916**	**44**	**44**	**39**	**57.2**	**175**	**0.6**	**241**	**153**

Appendix 2.2.- Geochemical Composition by Rock Type and Ore Zone, Continued

Sample	Rock Type	Ore Zone	Cu % in ddh	Spec. Grav.	Mag. Susc.	Mine Block	SiO₂ %	TiO₂ %	AL₂O₃ %	FeOT %	MnO %	MgO %	CaO %	Na₂O %	K₂O %	P₂O₅ %	Total %	Na₂O/ K₂O	Na₂O/ Na₂O+K₂O	LOI %	S %	C (inor) %
MP724	basalt	cp	7.40	2.87	0.00	Morro	52.85	0.95	18.38	6.60	0.38	2.64	8.14	6.23	3.36	0.47	100.00	1.86	0.65	6.00	2.58	1.20
MP786	basalt	cp	0.64	2.72	0.05	Valdivia S	49.03	0.68	18.28	9.17	1.18	5.17	10.27	5.66	0.48	0.09	100.00	11.8	0.92	9.12	0.23	1.70
RB98-36	basalt	cp	0.55	2.75	0.05	Valdivia S	48.52	0.65	17.88	8.74	0.57	2.19	13.90	6.06	1.37	0.12	100.00	4.41	0.82	9.97	0.40	2.40
RB98-45	basalt	cp-bn	0.49	2.77	0.04	Filo	53.60	0.75	18.97	7.28	0.45	5.87	6.09	4.90	1.95	0.14	100.00	2.52	0.72	4.54	0.12	0.40
MP723	basalt	cp-bn	1.31	2.78		Morro	51.14	0.63	17.22	9.51	0.33	1.95	8.74	6.69	3.08	0.72	100.00	2.18	0.69	3.58	2.43	1.36
Average	**basalt**	**cp, cp-bn**	**2.08**	**2.78**	**0.04**		**51.03**	**0.73**	**18.14**	**8.26**	**0.58**	**3.56**	**9.43**	**5.91**	**2.05**	**0.31**	**100.00**	**2.89**	**0.74**	**6.64**	**1.15**	**1.41**
MP787	basalt	bn	1.49	2.73		Valdivia S	53.31	0.95	20.21	8.64	0.35	4.11	4.50	5.87	1.92	0.13	100.00	3.05	0.75	5.25	0.45	0.70
RB98-44	basalt	bn-cc	0.87	2.80	0.49	Filo	49.86	0.59	19.88	8.93	0.50	7.28	7.15	5.06	0.62	0.12	100.00	8.21	0.89	6.23	0.01	0.45
RB98-47	basalt	bn-cc	1.05	2.85	0.04	Filo	47.49	0.71	18.79	8.77	0.93	6.90	10.14	5.48	0.66	0.12	100.00	8.25	0.89	9.10	0.11	1.70
RB98-52	basalt	bn-cc	2.05	2.77	0.02	Filo	49.84	0.70	18.77	9.02	1.41	6.12	7.66	5.69	0.67	0.12	100.00	8.54	0.90	7.26	0.50	1.15
MP805	basalt	bn-cc	3.23	2.82	0.03	Morro	55.23	0.79	18.16	8.65	0.61	6.67	3.85	5.43	0.42	0.18	100.00	12.8	0.93	5.69	0.59	0.45
MP793	basalt	cc	3.86			Filo	54.50	0.76	20.19	11.25	1.07	4.11	1.66	4.41	1.91	0.15	100.00	2.31	0.70	3.56	0.75	0.15
Average	**basalt**	**bn, bn-cc, cc**	**2.09**	**2.79**	**0.15**		**51.71**	**0.75**	**19.33**	**9.21**	**0.81**	**5.86**	**5.83**	**5.33**	**1.03**	**0.14**	**100.00**	**5.15**	**0.84**	**6.18**	**0.40**	**0.77**
MP855	**volcsed**	**bckd py**	**0.04**	**2.58**	**0.00**	**Valdivia S**	**67.97**	**0.42**	**15.53**	**5.33**	**0.21**	**2.40**	**0.81**	**0.58**	**6.67**	**0.07**	**100.00**	**0.09**	**0.08**	**3.54**	**0.09**	**0.10**
MP861	volcsed	py-cp	0.12			Filo	57.65	0.79	14.27	8.71	0.24	4.03	9.33	4.33	0.49	0.17	100.00	8.86	0.90	8.24	0.22	1.60
MP858	volcsed	py-cp	0.34			Morro	54.19	0.73	17.54	9.27	0.14	0.73	7.56	6.43	3.26	0.16	100.00	1.97	0.66	7.45	6.19	1.20
Average	**volcsed**	**py-cp**	**0.23**				**55.92**	**0.76**	**15.90**	**8.99**	**0.19**	**2.38**	**8.44**	**5.38**	**1.87**	**0.16**	**100.00**	**2.87**	**0.74**	**7.85**	**3.21**	**1.40**
MP831	volcsed	cp	1.13			Morro	71.25	0.43	14.17	2.18	0.02	0.07	3.35	7.82	0.61	0.09	100.00	12.8	0.93	3.55	1.61	0.70
MP833	volcsed	cp	2.36			Morro	57.20	0.65	18.22	6.50	0.15	2.33	5.13	8.32	1.17	0.32	100.00	7.08	0.88	5.43	3.12	0.85
MP869	volcsed	cp	1.61			Valdivia S	59.11	0.60	14.42	7.68	0.51	2.12	9.57	3.77	2.12	0.10	100.00	1.78	0.64	7.03	1.59	1.55
Average	**volcsed**	**cp**	**1.70**				**62.52**	**0.56**	**15.60**	**5.45**	**0.23**	**1.51**	**6.02**	**6.64**	**1.30**	**0.17**	**100.00**	**5.10**	**0.84**	**5.34**	**2.11**	**1.03**
MP747	volcsed	bn	1.56			Filo	66.24	0.48	14.28	8.57	0.25	3.62	1.04	5.17	0.22	0.12	100.00	23.4	0.96	3.18	0.2	0.15
MP854	volcsed	bn	0.91	2.56	0.00	Valdivia S	81.15	0.22	8.62	1.08	0.04	0.22	3.42	4.89	0.30	0.04	100.00	16.3	0.94	2.73	0.14	0.60
MP791	volcsed	cc	1.28			Filo	75.84	0.38	11.47	0.57	0.05	0.20	3.93	5.42	1.89	0.27	100.00	2.87	0.74	3.66	0.62	0.75
MP817	volcsed	bn-cc	3.71			Morro	50.60	0.59	16.52	8.83	0.52	5.18	11.16	4.74	1.76	0.10	100.00	2.70	0.73	8.08	1.4	1.80
Average	**volcsed**	**bn, bn-cc, cc**	**1.87**				**68.46**	**0.42**	**12.72**	**4.76**	**0.22**	**2.31**	**4.89**	**5.05**	**1.04**	**0.13**	**100.00**	**4.85**	**0.83**	**4.41**	**0.59**	**0.83**
MP761	sediment	bckd	0.02			Paso Riel	56.33	1.14	18.42	8.41	0.25	5.64	3.03	2.76	3.71	0.31	100.00	0.74	0.43	4.92	0.77	0.20
MP866	and dyke	bckd py-sp-ga	0.04		5.00	Arauco	62.89	0.73	16.55	3.78	0.14	2.24	4.24	4.62	4.66	0.15	100.00	0.99	0.50	4.69	0.22	0.85
MP772	and dyke	cc	4.92	2.74	0.29	Valdivia S	60.25	0.83	21.44	2.96	0.12	0.62	2.69	4.66	6.31	0.13	100.00	0.74	0.42	2.84	0.66	0.25
Z614-95	dior dyke	bckd	0.01			Morro	54.63	0.65	18.93	9.45	0.56	3.58	3.02	6.51	2.40	0.26	100.00	2.71	0.73	3.08	0.22	0.25
Z626-95	basdk	bckd	0.02		0.42	Morro	51.18	0.81	19.93	9.79	1.00	6.14	4.15	5.05	1.78	0.17	100.00	2.84	0.74	4.37	0.13	0.15
Z622-95	gabbro	bckd	0.02		4.16	Morro	52.15	0.92	18.06	9.31	0.17	5.36	10.28	2.85	0.74	0.15	100.00	3.85	0.79	1.3	0.12	< 0.05
Z603-95	basalt VN	bckd	0.01		0.62	Filo	48.80	0.79	21.08	8.33	1.92	7.02	4.47	2.63	4.85	0.12	100.00	0.54	0.35	4.41	0.05	0.05

Appendix 2.2.- Geochemical Composition by Rock Type and Ore Zone, Continued

Sample	Rock Type	Ore Zone	Ag ppm	As ppm	Ba ppm	Co ppm	Cu ppm	Hg ppm	Ni ppm	Pb ppm	Rb ppm	Sr ppm	U ppm	V ppm	Zn ppm
MP724	basalt	cp			1235						70	132			
MP786	basalt	cp	<0.2		57	25.5	4850	50	45	5	13	101	0.5	210	220
RB98-36	basalt	cp	<1	<1	199	21.0	3200	10	25	<5	63.0	139	<0.5	260	110
RB98-45	basalt	cp-bn	<1	1	366	22.0	855	<10	25	<5	77.2	383	<0.5	320	135
MP723	basalt	cp-bn			680						44	84			
Average	basalt	cp, cp-bn	<1	<1	507	22.8	2968	22	32	<5	53	168	<0.5	263	155
MP787	basalt	bn			275		1070				78	54			
RB98-44	basalt	bn-cc	<1	5	158	32.5	2560	10	25	<5	21.4	163	<0.5	240	235
RB98-47	basalt	bn-cc	3	39	148	29.5	7600	120	35	<5	21.2	163	0.5	285	195
RB98-52	basalt	bn-cc	3	1	141	22.0	9200	<10	30	<5	18.0	119	0.5	235	210
MP805	basalt	bn-cc			105		14400				12	158			
MP793	basalt	cc			870		23800				54	92			
Average	basalt	bn, bn-cc, cc	2	15	283	28.0	9772	45	30	<5	34.1	125	<0.5	253	213
MP855	volcsed	bckd py			785		300				252	18			
MP861	volcsed	py-cp			80		1200				12	44			
MP858	volcsed	py-cp			475		600				88	94			
Average	volcsed	py-cp			278		900				50	69			
MP831	volcsed	cp			40		1600				16	62			
MP833	volcsed	cp			280		31800				26	84			
MP869	volcsed	cp			360		15799				70	86			
Average	volcsed	cp			227		16400				37	77			
MP747	volcsed	bn			40		3600				12	26			
MP854	volcsed	bn			60		3200				8	28			
MP791	volcsed	cc			250		21800				46	36			
MP817	volcsed	bn-cc			220		39500				28	56			
Average	volcsed	bn, bn-cc, cc			143		17025				24	37			
MP761	sediment	bckd py-sp-ga			850		100				90	168			
MP866	and dyke	bckd			405						100	48			
MP772	and dyke	cc			2010		19000				206	186			
Z614-95	dior dyke	bckd	<0.2	5	658	22	120	<10	15	5	75	278	0.5	95	325
Z626-95	basdk	bckd	0.2	3	543	26.5	725	10	30	15	47	322	0.5	225	260
Z622-95	gabbro	bckd	<0.2	<1	223	31.5	95	<10	35	5	19	385	0.5	255	85
Z603-95	basalt VN	bckd	<0.2	23	4420	35	50	<10	35	15	139	445	0.5	210	650

Appendix 2.2.- Geochemical Composition by Rock Type and Ore Zone, Continued

Sample	Rock Type	Ore Zone	Cs ppm	Ga ppm	Hf ppm	Nb ppm	Ta ppm	Th ppm	Y ppm	Zr ppm	La ppm	Ce ppm	Pr ppm	Nd ppm	Sm ppm	Eu ppm	Gd ppm	Tb ppm	Dy ppm	Ho ppm	Er ppm	Tm ppm	Yb ppm	Lu ppm
MP724	basalt	cp				2			16.0	51	5	17	2.4	10	2.7	1.3	2.3	0.4	2.1	0.6	1.5	0.2	1.3	0.2
MP786	basalt	cp	0.4	16	<1	2	<0.5	1	11.8	39	66.5	116.5	11.0	35.0	4.1	1.2	3.9	0.5	2.0	0.4	1.0	0.1	1.0	0.1
RB98-36	basalt	cp	0.9	15	<1	<1	<0.5	1	10.0	31	6.5	11.5	1.8	7.0	2.0	0.6	2.2	0.3	1.7	0.4	1.0	0.1	1.0	0.1
RB98-45	basalt	cp-bn	2.7	17	<1	<1	<0.5	1	14.0	36	9.5	17.5	2.5	10.5	2.4	1.0	2.8	0.5	2.6	0.5	1.4	0.2	1.3	0.1
MP723	basalt	cp-bn				<2			12.0	21	3	12	1.8	7	1.8	1.1	1.8	0.3	2.0	0.5	0.9	0.2	1.1	0.1
Average	**basalt**	**cp, cp-bn**	**1.3**	**16**	**<1**	**1**	**<0.5**	**1**	**12.8**	**35**	**18**	**34.9**	**3.9**	**13.9**	**2.6**	**1.0**	**2.6**	**0.4**	**2.1**	**0.5**	**1.2**	**0.2**	**1.1**	**0.1**
MP787	basalt	bn				<2			24.0	66														
RB98-44	basalt	bn-cc	1.4	17	<1	<1	<0.5	<1	14.0	25	9.0	14.5	2.1	8.5	2.3	1.1	2.8	0.5	2.6	0.5	1.4	0.2	1.4	0.1
RB98-47	basalt	bn-cc	0.6	18	<1	1	<0.5	1	11.5	36	12.0	21.5	2.9	13.0	3.7	1.3	4.1	0.6	3.2	0.5	1.2	0.1	1.2	0.1
RB98-52	basalt	bn-cc	0.3	16	<1	<1	<0.5	1	16.0	31	10.5	22.0	3.1	11.5	2.7	0.9	2.9	0.4	2.0	0.4	1.1	0.1	1.2	0.1
MP805	basalt	bn-cc				4			18.0	135														
MP793	basalt	cc				2			14.0	51	1	7	1.1	5	0.8	0.9	1.3	0.3	2.1	0.6	0.9	0.2	1.3	0.2
Average	**basalt**	**bn, bn-cc, cc**	**0.8**	**17**	**<1**	**2**	**<0.5**	**<1**	**16.3**	**57**	**8**	**16**	**2.3**	**10**	**2.4**	**1.1**	**2.8**	**0.5**	**2.5**	**0.5**	**1.2**	**0.2**	**1.3**	**0.1**
MP855	**volcsed**	**bckd py**				2			26.0	198														
MP861	volcsed	py-cp				6			24.0	99														
MP858	volcsed	py-cp				< 2			16.0	57														
Average	**volcsed**	**py-cp**				**4**			**20.0**	**78**														
MP831	volcsed	cp				8			26.0	177	7	21	2.9	11	1.9	0.4	1.8	0.4	2.5	0.8	1.9	0.4	2.2	0.4
MP833	volcsed	cp				4			16.0	84	18	43	5.5	18	3.0	0.9	3.0	0.5	2.6	0.6	1.5	0.2	1.5	0.3
MP869	volcsed	cp				2			18.0	84														
Average	**volcsed**	**cp**				**5**			**20.0**	**115**	**13**	**32**	**4.2**	**15**	**2.5**	**0.7**	**2.4**	**0.5**	**2.6**	**0.7**	**1.7**	**0.3**	**1.9**	**0.4**
MP747	volcsed	bn				6			18.0	138														
MP854	volcsed	bn				6			12.0	114														
MP791	volcsed	cc				6			24.0	120	4	12	1.8	10	1.7	0.5	1.6	0.4	2.5	0.6	1.3	0.2	1.6	0.3
MP817	volcsed	bn-cc				2			12.0	54														
Average	**volcsed**	**bn, bn-cc, cc**				**5**			**16.5**	**107**	**4**	**12**	**1.8**	**10**	**1.7**	**0.5**	**1.6**	**0.4**	**2.5**	**0.6**	**1.3**	**0.2**	**1.6**	**0.3**
MP761	sediment	bckd py-sp-ga				6			28.0	138	10	29	3.9	15	2.5	1.1	3.3	0.6	4.2	0.9	2.1	0.3	2.3	0.4
MP866	and dyke	bckd				6			24.0	180	6	26	7.4	27	4.4	< 0.2	1.4	0.9	10.6	0.8	1.1	1.3	3.3	0.9
MP772	and dyke	cc				< 2			20.0	60	5	17	2.7	10	1.7	1.2	2.2	0.3	2.2	0.5	0.9	0.2	0.9	0.2
Z614-95	dior dyke	bckd	0.3	15	1	2	<0.5	1	20.0	89	12.5	28.0	3.9	18.0	4.4	1.1	4.2	0.6	3.3	0.7	1.6	0.2	1.9	0.3
Z626-95	basdk	bckd	1.4	18	1	2	<0.5	2	13.0	47	13.5	27.5	3.8	15.5	3.6	1.1	3.3	0.4	2.6	0.5	1.4	0.2	1.4	0.1
Z622-95	gabbro	bckd	0.5	18	1	1	<0.5	1	16.5	52	9.0	20.0	2.9	13.0	2.9	0.9	3.7	0.5	2.9	0.6	1.7	0.3	1.7	0.3
Z603-95	basalt VN	bckd	2.4	17	1	1	<0.5	1	18.0	54	6.5	15.0	2.2	11.0	5.7	1.1	3.4	0.5	2.9	0.6	1.7	0.3	1.7	0.3

Appendix 2.3.- CIPW norm calculations for less altered basalts.

Appendix 2.3. Norm calculation for sample RB98 40 (basalt)

Oxide	Wt %	Mol. Wt. oxide	Mole proportion	ap	ilm	or	ab	an	mt	di wo	di en	di fs	hy en	hy fs	ol fo	ol fa	qz
SiO2	51.69	60.08	0.8603			0.7575	0.4673	0.2479			0.1319		-0.0425				
TiO2	0.65	79.88	0.0081		0.0000												
Al2O3	17.86	101.96	0.1752			0.1580	0.1097	0.0000									
Fe2O3	2.50	159.69	0.0157						0.0000								
FeO	5.95	71.85	0.0829		0.0747				0.0672			0.0504		0.0246		0.0000	
MnO	0.38	70.94	0.0053														
MgO	6.66	40.3	0.1652								0.1239		0.0604		0.0000		
CaO	9.57	56.08	0.1707	0.1677				0.0580		0.0000							
Na2O	3.00	61.98	0.0484				0.0000										
K2O	1.61	94.2	0.0171			0.0000											
P2O5	0.13	141.9	0.0009	0.0000													
Total	100.00																
Mole proportion of normative mineral				0.0009	0.0081	0.0171	0.0484	0.1097	0.0157	0.0580	0.0412	0.0168	0.0636	0.0259	0.0604	0.0246	
Mole to weigth conversion factor				336.21	151.73	556.64	524.43	278.20	231.54	116.16	100.38	131.93	100.38	131.93	70.34	101.89	60.08
Wt% of normative minerals				0.30	1.23	9.54	25.37	30.51	3.63	6.74	4.14	2.21	6.38	3.41	4.25	2.50	
Sum of normative minerals				100.21							0.1239	0.0504	0.0849				
Color Index				34.8							0.0894						
Normative anortite				55							0.0894						

258

Appendix 2.3. Norm calculation for sample RB98 42 (basalt)

Oxide	Wt %	Mol. Wt. oxide	Mole proportion	ap	ilm	or	ab	an	mt	di wo	di en	di fs	hy en	hy fs	ol fo	ol fa	qz
SiO2	51.74	60.08	0.8611			0.7138	0.4543	0.1935			0.1041		-0.0217				
TiO2	0.60	79.88	0.0076		0.0000												
Al2O3	20.21	101.96	0.1982			0.1737	0.1304	0.0000									
Fe2O3	2.36	159.69	0.0148						0.0000								
FeO	4.90	71.85	0.0682		0.0607				0.0534			0.0394		0.0136		0.0000	
MnO	0.40	70.94	0.0056														
MgO	4.72	40.3	0.1171								0.0864		0.0298		0.0000		
CaO	9.97	56.08	0.1777	0.1751				0.0447		0.0000							
Na2O	2.68	61.98	0.0433				0.0000										
K2O	2.31	94.2	0.0245			0.0000											
P2O5	0.11	141.9	0.0008	0.0000													
Total	100.00																
Mole proportion of normative mineral				0.0008	0.0076	0.0245	0.0433	0.1304	0.0148	0.0447	0.0307	0.0140	0.0566	0.0258	0.0298	0.0136	
Mole to weigth conversion factor				336.21	151.73	556.64	524.43	278.20	231.54	116.16	100.38	131.93	100.38	131.93	70.34	101.89	60.08
Wt% of normative minerals				0.27	1.15	13.67	22.68	36.28	3.42	5.19	3.08	1.85	5.68	3.41	2.09	1.38	
Sum of normative minerals			100.15										0.0864	0.0394	0.0434		
Color Index			27.5										0.0825				
Normative anortite			62										0.0825				

259

Appendix 2.3. Norm calculation for sample RB98 29 (basalt)

Oxide	Wt %	Mol. Wt. oxide	Mole proportion	ap	ilm	or	ab	an	mt	wo	di en	di fs	hy en	hy fs	ol fo	ol fa	qz
SiO2	50.93	60.08	0.8476			0.7221	0.4742	0.2026			0.1034		-0.0390				
TiO2	0.62	79.88	0.0078		0.0000												
Al2O3	20.19	101.96	0.1980			0.1771	0.1358	0.0000									
Fe2O3	1.80	159.69	0.0113						0.0000								
FeO	5.73	71.85	0.0798		0.0720				0.0685			0.0508		0.0279		0.0000	
MnO	0.56	70.94	0.0079														
MgO	4.98	40.3	0.1235								0.0916		0.0502		0.0000		
CaO	10.55	56.08	0.1881	0.1854				0.0496		0.0000							
Na2O	2.56	61.98	0.0413				0.0000										
K2O	1.97	94.2	0.0209			0.0000											
P2O5	0.11	141.9	0.0008	0.0000													
Total	100.00																
Mole proportion of normative mineral				0.0008	0.0078	0.0209	0.0413	0.1358	0.0113	0.0496	0.0319	0.0177	0.0414	0.0230	0.0502	0.0279	
Mole to weigth conversion factor				336.21	151.73	556.64	524.43	278.20	231.54	116.16	100.38	131.93	100.38	131.93	70.34	101.89	60.08
Wt% of normative minerals				0.27	1.18	11.64	21.67	37.77	2.61	5.76	3.20	2.34	4.16	3.03	3.53	2.84	
Sum of normative minerals			100.01										0.0916	0.0508	0.0780		
Color Index			28.9										0.0644				
Normative anortite			64										0.0644				

Appendix 2.3. Norm calculation for sample MP844 (basalt)

Oxide	Wt %	Mol. Wt. oxide	Mole proportion	ap	ilm	or	ab'	an	mt	wo	di en	fs	hy en	fs	ol fo	fa	qz	ne	ab
SiO2	51.38	60.08	0.8552			0.7098	0.3388	0.1531			0.0765		0.0861	0.0048				0.2426	
TiO2	0.89	79.88	0.0111		0.0000														
Al2O3	18.24	101.96	0.1789			0.1547	0.0929	0.0000											
Fe2O3	3.48	159.69	0.0218						0.0000										
FeO	6.09	71.85	0.0848		0.0737				0.0630					0.0510		0.0000			
MnO	0.50	70.94	0.0070																
MgO	5.56	40.3	0.1379								0.1116				0.0000				
CaO	7.57	56.08	0.1350	0.1311				0.0383		0.0000									
Na2O	3.83	61.98	0.0618				0.0000												
K2O	2.28	94.2	0.0242			0.0000													
P2O5	0.17	141.9	0.0012	0.0000															
Total	100.00																		
Mole proportion of normative mineral				0.0012	0.0111	0.0242	0.0618	0.0929	0.0218	0.0383	0.0263	0.0120			0.1116	0.0510		0.0012	#####
Mole to weigth conversion factor				336.21	151.73	556.64	524.43	278.20	231.54	116.16	100.38	131.93	100.38	131.93	70.34	101.89	60.08	284.1	#####
Wt% of normative minerals				0.39	1.69	13.49		25.83	5.05	4.45	2.64	1.58			7.85	5.20		0.34	31.80
Sum of normative minerals				100.31									0.1116	0.0510	0.1626				
Color Index				28.8									0.1626						
Normative anortite				45															

APPENDIX 3.- MICROPROBE DATA

3.1.- Results of microprobe spot analyses of rock-forming and alteration - gangue
   minerals, listed by mineral and host rock.
3.2.- Mineral plots for selected spot analyses.
3.3.- Back-scatter and X-ray microprobe images, listed by ore zone and host rock.
3.4.- Results of microprobe spot analyses of sulphides, listed by mineral and host rock.

Appendix 3.1.- Results of microprobe spot analyses of rock-forming and alteration-gangue minerals, listed by mineral and host rock.

Appendix 3.1.- Analyses of K-Feldspar (microcline)

Spot	Grain	SiO₂ %	Al₂O₃ %	FeO %	MnO %	MgO %	CaO %	Na₂O %	K₂O %	Cl %	P₂O₅ %	BaO %	SrO %	ZrO %	Total %	Or	Ab	An	Mineral	Si	Al	O	K	Na	Ca	Fe	Mn	Ba	# Ions	Remarks
Sample MP850, basalt, Filo mine block, bornite ore zone																														
4	4	64.90	18.77					0.22	15.68			0.65			100.21	0.98	0.02	0.00	K-fd	2.99	1.02	8.00	0.92	0.02				0.01	12.97	in vein
5	5	64.63	18.62					0.24	16.44						99.92	0.98	0.02	0.00	K-fd	2.99	1.02	8.00	0.97	0.02					13.00	in vein
8	8	63.12	18.08						15.75						96.94	1.00	0.00	0.00	K-fd	3.00	1.01	8.00	0.96	0.00					12.97	in vein
10	10	64.90	18.77					0.22	15.91	0.10					99.90	0.98	0.02	0.00	K-fd	3.00	1.02	8.00	0.94	0.02					12.98	in vein
Sample RB9843, basalt, Filo mine block, bornite ore zone																														
1	1	64.33	18.51					0.23	16.16						99.22	0.98	0.02	0.00	K-fd	2.99	1.02	8.00	0.96	0.02					12.99	in vein
2	2	64.80	18.73				0.43	0.28	15.74						99.97	0.95	0.03	0.02	K-fd	2.99	1.02	8.00	0.93	0.02	0.02				12.98	in vein
3	3	64.72	18.78	0.48				0.20	15.85			0.50			100.52	0.98	0.02	0.00	K-fd	2.98	1.02	8.00	0.93	0.02		0.02		0.01	12.98	in vein
6	6	63.38	18.32					0.31	15.78			0.56			98.34	0.97	0.03	0.00	K-fd	2.99	1.02	8.00	0.95	0.03				0.01	12.99	in vein
7	7	64.10	18.57					0.27	16.06						99.01	0.97	0.03	0.00	K-fd	2.99	1.02	8.00	0.96	0.02					12.99	in vein
12	12	64.20	18.50						16.05						98.75	1.00	0.00	0.00	K-fd	3.00	1.02	8.00	0.96	0.00					12.97	in vein
13	13	64.69	18.57					0.29	16.32			0.57			100.43	0.97	0.03	0.00	K-fd	2.99	1.01	8.00	0.96	0.03				0.01	13.00	in vein
14	14	64.03	18.63					0.30	16.22						99.19	0.97	0.03	0.00	K-fd	2.98	1.02	8.00	0.96	0.03					13.00	in vein
Sample RB9930, basalt, Filo mine block, background ore zone (unmineralized)																														
7	6	63.82	18.91					0.37	15.46			1.70			100.26	0.96	0.04	0.00	K-fd	2.97	1.04	8.00	0.92	0.03				0.03	12.99	in phenocryst
Sample MP866, andesitic dyke, Arauco mi8ne block, background ore zone (unmineralized)																														
26	1	62.69	19.54					0.23	15.16			1.54			99.16	0.98	0.02	0.00	K-fd	2.94	1.08	8.00	0.91	0.02		0.00		0.03	12.98	in phenocryst
Sample MP844, basalt, Filo mine block, background ore zone (unmineralized)																														
2	1	60.79	23.70	0.39	0.30		0.28	0.99	12.88						99.32	0.90	0.10	0.00	Kfd +albite?	2.80	1.29	8.00	0.76	0.09		0.01	0.01		12.96	in phenocryst
Sample RB9805, rhyodacite, Valdivia Sur mine block, background ore zone (unmineralized)																														
9	5	62.30	18.33					2.74	11.06		0.31		0.44		95.19	0.73	0.27	0.00	Kfd +albite?	2.97	1.03	8.00	0.67	0.25				0.01	12.97	in phenocryst
19	12	66.13	19.00					1.34	12.96	0.12					99.55	0.86	0.14	0.00	Kfd +albite?	3.02	1.02	8.00	0.75	0.12					12.92	groundmass
Sample RB9822, rhyodacite, Valdivia Sur mine block, background ore zone (unmineralized)																														
2	1	65.36	18.90					0.23	16.05						100.54	0.95	0.02	0.03	K-fd	3.01	1.08	8.00	0.66	0.01	0.02				12.79	in phenocryst
2	2	64.02	18.74					0.29	15.58			0.55			99.18	0.97	0.03	0.00	K-fd	2.98	1.03	8.00	0.93	0.03				0.01	12.98	in phenocryst
3	3	62.77	18.59	1.74		0.61		1.98	13.03						98.72	0.81	0.19	0.00	K-fd	2.94	1.03	8.00	0.78	0.18		0.07	0.04		13.03	veinlet
4	2	65.72	19.03					3.03	11.54						99.14	0.72	0.28	0.00	Kfd +albite?	3.00	1.02	8.00	0.67	0.27					12.96	in phenocryst
12	8	64.81	18.55	0.58				0.23	15.94						100.12	0.98	0.02	0.00	K-fd	2.99	1.01	8.00	0.94	0.02		0.02			12.98	groundmass
15	11	64.59	18.51					0.29	15.44					0.60	99.42	0.97	0.03	0.00	K-fd	2.99	1.01	8.00	0.91	0.03					12.96	in xenolith
Sample MP840, rhyodacite, Morro mine block, chalcopyrite ore zone																														
32	6	65.31	18.88					0.35	14.98						99.52	0.97	0.03	0.00	K-fd	3.00	1.02	8.00	0.88	0.03					12.94	in phenocryst
Sample MP778, rhyodacite, Valdivia Sur mine block, bornite-chalcocite ore zone																														
18	14	68.22	18.12					0.29	14.21	0.11					100.95	0.97	0.03	0.00	K-fd	3.07	0.96	8.00	0.82	0.02					12.89	in vein
21	15	65.43	18.97						16.01						100.41	1.00	0.00	0.00	K-fd	3.00	1.02	8.00	0.94						12.96	in phenocryst
26	16	66.96	18.22					0.22	14.22						99.61	0.98	0.02	0.00	K-fd	3.05	0.98	8.00	0.83	0.02					12.88	in phenocryst
22	15	65.53	19.11					1.60	14.35						100.59	0.86	0.14	0.00	K-fd	2.99	1.03	8.00	0.83	0.14					12.99	in phenocryst

Appendix 3.1.- Analyses of Calcite

Spot	Grain	SiO₂ %	Al₂O₃ %	FeO %	MnO %	MgO %	CaO %	Na₂O %	K₂O %	TiO₂ %	P₂O₅ %	SrO %	Cl %	Total %	Mineral	Remarks
Sample RB9805, rhyodacite Valdivia Sur mine block, background ore zone (unmineralized)																
3	1	0.26		0.38	0.64		51.89		0.32					53.49	calcite	in albite phenocryst
25	14	0.18			1.07		52.93							54.18	calcite	in vein
30	16				1.38		53.21							54.59	calcite	in albite phenocryst
16	11	8.38			1.73		49.43							59.54	calcite+quartz	in albite phenocryst
15	10	19.26	5.54		0.88		39.79	2.29						67.76	calcite+albite	crystal aggregate
31	16	7.70	4.16	0.67	0.50	0.37	47.56		1.66					62.63	calcite+mica	in albite phenocryst
Sample RB9811, rhyodacite, Valdivia Sur mine block, pyrite-chalcopyrite ore																
13	10				0.63		54.51							55.14	calcite	replacing phenocryst
5	4	0.39			0.63		56.54							57.55	calcite	in vug
Sample RB9815, rhyodacite, Valdivia Sur mine block, bornite-chalcocite ore																
2	2				0.55		57.37							57.92	calcite	vein
3	3	0.28			0.56		57.77							58.62	calcite	in albite phenocryst
Sample RB9822, rhyodacite, Valdivia Sur mine block, background ore zone																
3a	1	0.26			1.17		57.17							58.60	calcite	in albite phenocryst
8	3				0.81		54.78							55.59	calcite	in albite phenocryst
9	3				0.87		58.09							58.96	calcite	in albite phenocryst
10	3	0.22			0.82		58.61							59.65	calcite	in albite phenocryst
11	3	2.65	0.84		1.80		52.84	0.46						58.59	calcite	in albite phenocryst
12	4	0.17			2.69		55.08						0.11	58.05	calcite	in ferromagnesian crystal
13	5	0.53			1.17		54.56							56.25	calcite	in ferromagnesian crystal
17	8	0.25			1.20		51.60							53.05	calcite	in albite phenocryst
19	9	0.30		0.37	2.71		56.31							59.69	calcite	in albite phenocryst
14	6	5.59			1.59		49.79			2.62				59.58	calcite+titanite	in ferromagnesian crystal
Sample RB9867, rhyodacite, Valdivia Sur mine block, bornite-chalcocite ore zone																
3	3	0.17			2.41		57.26							59.85	calcite	in vug
6	6				2.01	0.16	57.72							59.89	calcite	in altered phenocrist?
7	7				1.80		57.49							59.29	calcite	in vug
21	15				1.46		57.61							59.07	calcite	in vein
4	4				0.33		40.75			24.16				65.23	calcite+rutile	in vug
Sample RB9903, rhyodacite, Morro mine block, pyrite ore zone																
6	2	1.01	0.28		0.44		56.45		0.31					58.47	calcite	in albite phenocryst
14	10	0.18					57.61							57.79	calcite	in vein/vug
Sample MP770, rhyodacitic dyke, Valdivia Sur mine block, pyrite zone																
11	7	0.16			0.61	0.32	48.89							59.39	calcite	in vein
Sample MP778, rhyodacite, Valdivia Sur mine block, bornite-chalcocite ore zone																

Appendix 3.1.- Analyses of Calcite (continued)

Spot	Grain	SiO₂ %	Al₂O₃ %	FeO %	MnO %	MgO %	CaO %	Na₂O %	K₂O %	TiO₂ %	P₂O₅ %	SrO %	Cl %	Total %	Mineral	Remarks
7	6	2.60	0.62		0.64		55.46	0.22						59.54	calcite	in albite phenocryst
8	6	0.41	0.16		0.44	0.32	59.52							60.85	calcite	in albite phenocryst
MP845, rhyodacite, Filo mine block, background ore zone (unmineralized)																
62	a	0.12			0.63		52.07							52.82	calcite	in vug
66	b	1.03		0.95		0.27	54.11						1.02	57.38	calcite	in ferromagnesian crystal
MP846, rhyodacitic dyke, Morro mine block, background ore zone (unmineralized)																
52	b	0.11		0.43	0.33		54.81							55.67	calcite	in ferromagnesian crystal
MP848, rhyodacite, Morro mine block, background ore zone (unmineralized)																
1	17	0.14		0.29	1.30		53.99							55.72	calcite	in ferromagnesian crystal
Sample RB9806, basalt, Valdivia Sur mine block, pyrite background ore zone																
7	3				0.72		58.48							59.20	calcite	in pyroxene phenocryst
10	4	0.18			0.72		58.62							59.52	calcite	in pyroxene phenocryst
11	4	0.21		0.33	1.47		56.25							58.26	calcite	in pyroxene phenocryst
12	5				0.77		54.34							55.16	calcite	in pyroxene phenocryst
25	13	0.20					54.50							54.70	calcite	in vein
Sample RB9844, basalt, Filo mine block, bornite-chalcocite ore zone																
11	2			0.40	3.86		56.04						0.09	60.38	calcite	in pyroxene phenocryst
13	2				0.89		41.51							42.40	calcite	in pyroxene phenocryst
14	2				2.97		57.24							60.20	calcite	in pyroxene phenocryst
Sample RB9852, basalt, Filo mine block, bornite-chalcocite ore zone																
8	7	0.25			0.97		57.44							58.65	calcite	in vein
18	13	0.17			1.60		58.19							59.96	calcite	in pyroxene phenocryst
7	6	44.29			0.89		31.92							77.10	calcite+quartz	in vein (mixture)
Sample MP840, basaltic dyke, Morro mine block, chalcopyrite ore zone																
4	2				0.85		57.50							58.34	calcite	in vein
5	4						57.35							57.35	calcite	in vein
6	5			0.57	1.81		57.07							59.45	calcite	in vein
16	15	0.65	0.18	0.31	0.56		58.22							59.92	calcite	in pyroxene phenocryst
27	17	2.04	0.56		0.48		54.18							57.26	calcite	in plagioclase phenocryst
12a	11	0.23		0.35	1.70		57.38				0.23			59.90	calcite	in amygdule
Sample MP850, basalt, Filo mine block, bornite chalcocite																
3	3				0.49		57.13							57.62	calcite	in vein
6	6						57.95							57.95	calcite	in vein
Sample Z614-95 microdioritic dyke, Morro mine block, background ore zone (unmineralized)																
42	1	0.21		0.28	0.16		58.18							58.83	calcite	in ferromagnesian crystal
Sample Z622-95, gabbro, Arauco Norte mine block, background ore zone (unmineralized)																

Appendix 3.1.- Analyses of Calcite (continued)

Spot	Grain	SiO$_2$ %	Al$_2$O$_3$ %	FeO %	MnO %	MgO %	CaO %	Na$_2$O %	K$_2$O %	TiO$_2$ %	P$_2$O$_5$ %	SrO %	Cl %	Total %	Mineral	Remarks
37	1	1.06		0.67		0.22	54.32						0.80	56.26	calcite	in pyroxene crystal
Sample MP866, andesitic dyke, Arauco mine block, background ore zone (unmineralized)																
27	1	0.42	0.16	0.31	0.63	0.42	56.80							58.74	calcite	in ferromagnesian crystal

Appendix 3.1.- Analyses of Chlorite

Spot	Grain	SiO₂ %	Al₂O₃ %	FeO %	MnO %	MgO %	CaO %	Na₂O %	K₂O %	Total %	Mineral	Si	O	Mg	Fe	Al	Mn	Ca	Na	K	OH	# ions	Remarks
Mineral Formula Si₃O₁₀(Mg,Fe)₅(Al,Fe)₂(OH)₈																							
Sample RB9829, basalt, Valdivia Sur mine block, background ore zone (unmineralized)																							
3	1	29.13	16.42	19.81	1.83	19.23	0.17			86.60	chlorite	3.04	10.00	2.13	1.23	1.44	0.12	0.01	0.00	0.00	8.00	25.98	in pyroxene phenocryst
6	3	29.10	16.22	19.76	1.83	19.41	0.24			86.57	chlorite	3.04	10.00	2.16	1.23	1.43	0.12	0.02	0.00	0.00	8.00	25.99	in plagioclase phenocryst
10	5	29.27	16.03	19.85	1.68	18.69	0.50			86.03	chlorite	3.07	10.00	2.09	1.25	1.42	0.11	0.04	0.00	0.00	8.00	25.97	in pyroxene phenocryst
Sample RB9842, basalt, Filo mine block, background ore zone (unmineralized)																							
15	10	21.87	8.14	36.71	0.52	8.01	8.08			83.33	chlorite?	2.79	10.00	1.09	2.79	0.88	0.04	0.79	0.00	0.00	8.00	26.37	in pyroxene phenocryst
Sample RB9843, basalt, Filo mine block, background ore zone (unmineralized)																							
5	5	29.88	19.31	16.07	1.33	16.89	5.85			89.33	chlorite?	2.99	10.00	1.80	0.96	1.63	0.08	0.45	0.00	0.00	8.00	25.91	in vein
Sample RB9930, basalt, Filo mine block, background ore zone (unmineralized)																							
3	3	28.61	18.39	17.28	0.89	21.14	0.16			86.46	chlorite	2.93	10.00	2.31	1.06	1.59	0.05	0.01	0.00	0.00	8.00	25.95	in vug
4	4	27.27	19.50	17.10	1.91	20.26	0.21			86.25	chlorite	2.82	10.00	2.23	1.06	1.70	0.12	0.02	0.00	0.00	8.00	25.94	in vein
6	5	28.90	18.29	16.90	1.23	21.37				86.68	chlorite	2.95	10.00	2.32	1.03	1.57	0.08	0.00	0.00	0.00	8.00	25.95	in albite phenocryst
Sample MP844, basalt, Filo mine block, background ore zone (unmineralized)																							
3	1	28.25	17.89	21.76	1.60	18.22	0.26	0.36		88.35	chlorite	2.92	10.00	2.00	1.34	1.56	0.10	0.02	0.05	0.00	8.00	26.00	in vug
Sample Z632-95, basalt, Valdivia Sur mine block, pyrite background ore zone																							
7	1	26.66	19.26	22.18	3.75	15.70	0.27	0.23		88.05	chlorite	2.81	10.00	1.76	1.39	1.71	0.24	0.02	0.03	0.00	8.00	25.96	in vug
9	1	27.69	20.41	21.88	3.72	16.34	0.11	0.38		90.52	chlorite	2.81	10.00	1.77	1.33	1.75	0.23	0.01	0.05	0.00	8.00	25.95	in groundmass
Sample RB9806, basalt, Valdivia Sur mine block, pyrite-background ore zone																							
3	1	27.33	20.68	20.83	2.08	15.35	0.17		0.45	86.89	chlorite	2.86	10.00	1.71	1.30	1.82	0.13	0.01	0.00	0.04	8.00	25.88	border of phenocryst
24	12	26.20	20.89	22.65	2.10	15.46				87.29	chlorite	2.76	10.00	1.73	1.42	1.85	0.13	0.00	0.00	0.00	8.00	25.89	in border of vein
33	21	27.36	19.15	21.63	1.64	17.40	0.14			87.31	chlorite	2.86	10.00	1.93	1.35	1.68	0.10	0.01	0.00	0.00	8.00	25.93	in vein
8	3	27.07	19.22	22.26	2.27	16.93	0.16			87.91	chlorite?	2.83	10.00	1.88	1.39	1.69	0.14	0.01	0.00	0.00	8.00	25.94	in pyroxene phenocryst
9	3	25.31	21.11	22.81	3.76	14.29				87.27	chlorite?	2.69	10.00	1.62	1.45	1.89	0.24	0.00	0.00	0.00	8.00	25.90	in pyroxene phenocryst
13	5	26.43	19.75	23.25	1.55	15.73	0.16			86.87	chlorite?	2.80	10.00	1.77	1.47	1.76	0.10	0.01	0.00	0.00	8.00	25.92	in pyroxene phenocryst
14	5	25.94	20.82	22.86	1.76	15.29	0.20	0.28		87.14	chlorite?	2.74	10.00	1.72	1.44	1.85	0.11	0.02	0.04	0.00	8.00	25.92	in pyroxene phenocryst
Sample RB9844, basalt, Filo mine block, bornite-chalcocite ore zone																							
12	2	28.13	18.48	20.06	1.18	19.08	0.35			87.23	chlorite	2.91	10.00	2.10	1.24	1.61	0.07	0.03	0.00	0.00	8.00	25.95	in pyroxene phenocryst
15	2	31.62	21.12	13.13	0.85	14.17	8.03			88.91	chlorite	3.12	10.00	1.49	0.77	1.75	0.05	0.61	0.00	0.00	8.00	25.79	in pyroxene phenocryst
21	5	27.15	18.14	19.70	1.19	18.53	0.17	0.29		85.16	chlorite	2.88	10.00	2.10	1.25	1.62	0.08	0.01	0.04	0.00	8.00	25.99	in vein
22	6	17.45	11.87	12.78	1.02	12.99	21.75			77.85	chlorite/calcite	2.22	10.00	1.76	0.97	1.27	0.08	2.12	0.00	0.00	8.00	26.41	in vein
Sample RB9852, basalt, Filo mine block, bornite-chalcocite ore zone																							
1	1	27.41	17.49	21.86	3.78	15.96				86.50	chlorite	2.93	10.00	1.82	1.40	1.57	0.24	0.00	0.00	0.00	8.00	25.96	in vein
2	2	27.56	17.36	22.52	3.62	15.60		0.27		86.91	chlorite	2.94	10.00	1.77	1.44	1.56	0.23	0.00	0.04	0.00	8.00	25.98	in vein
14	11	27.35	17.67	23.09	3.50	14.83	0.16			86.61	chlorite	2.93	10.00	1.69	1.48	1.60	0.23	0.01	0.00	0.00	8.00	25.94	vein in albite phenocryst
17	12	27.28	16.92	21.11	3.24	16.46	0.15	0.66		85.82	chlorite	2.93	10.00	1.88	1.36	1.53	0.21	0.01	0.10	0.00	8.00	26.03	in a vug
Sample Z603-95, basalt Veta Negra Formation, background ore zone (unmineralized)																							
55	1	30.60	16.52	11.60	3.23	24.84	0.22	0.20		87.20	chlorite	3.05	10.00	2.64	0.69	1.39	0.19	0.02	0.03	0.00	8.00	26.01	in pyroxene phenocryst
Sample Z614-95 microdioritic dyke, Morro mine block, background ore zone (unmineralized)																							
43	1	28.45	15.72	23.22	1.42	17.39	0.22	0.33		86.74	chlorite	3.02	10.00	1.97	1.47	1.41	0.09	0.02	0.05	0.00	8.00	26.03	in vug

Appendix 3.1.- Analyses of Chlorite (continued)

Spot	Grain	SiO$_2$ %	Al$_2$O$_3$ %	FeO %	MnO %	MgO %	CaO %	Na$_2$O %	K$_2$O %	Total %	Mineral	Mineral Formula Si$_3$O$_{10}$(Mg,Fe)$_5$(Al,Fe)$_2$(OH)$_8$										# ions	Remarks
												Si	O	Mg	Fe	Al	Mn	Ca	Na	K	OH		
Sample Z622-95, gabbro, Arauco Norte mine block, background ore zone (unmineralized)																							
39	1	45.69	7.36	16.11		20.61	1.06	0.36		91.19	chlorite?	4.26	10.00	2.05	0.90	0.58	0.00	0.08	0.05	0.00	8.00	25.91	in pyroxene phenocryst
Sample Z626-95 basaltic dyke, Morro mine block, background ore zone (unmineralized)																							
24	a	28.53	16.19	22.31	2.10	17.66	0.49	0.29		87.56	chlorite	3.00	10.00	1.98	1.40	1.43	0.13	0.04	0.04	0.00	8.00	26.02	in pyroxene phenocryst
MP866, andesitic dyke, Arauco mine block, background ore zone (unmineralized)																							
28	1	28.54	18.39	18.10	2.15	18.32	0.37	0.29		86.16	chlorite	2.97	10.00	2.03	1.13	1.61	0.14	0.03	0.04	0.00	8.00	25.94	in groundmass
Sample MP840, basaltic dyke, Morro mine block, chalcopyrite ore zone																							
13	12	27.00	18.92	21.48	5.50	14.93				87.84	chlorite?	2.86	10.00	1.68	1.36	1.69	0.35	0.00	0.00	0.00	8.00	25.93	in amygdule
18	15	26.46	18.81	22.07	5.98	13.55				86.88	chlorite?	2.85	10.00	1.55	1.42	1.71	0.39	0.00	0.00	0.00	8.00	25.92	in pyroxene phenocryst
21	16	26.83	17.82	23.37	5.46	13.00	0.31	0.27		87.05	chlorite?	2.91	10.00	1.50	1.51	1.62	0.36	0.03	0.04	0.00	8.00	25.96	in plagioclase phenocryst
25	16	35.64	18.37	17.45	4.21	11.42	0.27	2.26		89.63	chlorite?	3.53	10.00	1.20	1.03	1.53	0.25	0.02	0.31	0.00	8.00	25.88	in plagioclase phenocryst
38	15	26.97	18.79	20.92	5.63	14.99		0.30		87.60	chlorite?	2.86	10.00	1.69	1.32	1.68	0.36	0.00	0.04	0.00	8.00	25.96	in pyroxene phenocryst
10a	9	28.84	18.53	22.41	5.23	13.86		0.48		89.35	chlorite?	3.00	10.00	1.53	1.39	1.62	0.33	0.00	0.07	0.00	8.00	25.94	in pyroxene phenocryst
Sample RB9805, rhyodacite, Valdivia Sur mine block, background ore zone (unmineralized)																							
5	2	24.53	20.16	32.20	0.89	8.79				86.57	chlorite	2.74	10.00	1.46	3.00	2.65	0.08	0.00	0.00	0.00	8.00	27.94	in albite phenocryst
MP846, rhyodacitic dyke, Morro mine block, background ore zone (unmineralized)																							
48	a	23.04	18.79	28.20	1.01	10.74				81.78	chlorite	2.69	10.00	1.87	2.76	2.59	0.10	0.00	0.00	0.00	8.00	28.01	in groundmass
Sample RB9901, rhyodacite, Valdivia Sur mine block, bornite-chalcocite ore zone																							
9	5	26.31	18.11	21.94	0.81	14.64			0.53	82.35	chlorite	2.93	10.00	2.43	2.04	2.39	0.08	0.00	0.00	0.08	8.00	27.94	in matrix
13	9	25.89	20.18	24.16	1.46	15.34				87.02	chlorite	2.75	10.00	2.43	2.15	2.53	0.13	0.00	0.00	0.00	8.00	27.99	in matrix
14	10	26.65	19.24	21.24	0.76	17.58				85.46	chlorite	2.83	10.00	2.78	1.89	2.41	0.07	0.00	0.00	0.00	8.00	27.97	in matrix
18	13	25.96	19.63	22.86	1.13	15.93				85.51	chlorite	2.79	10.00	2.55	2.05	2.48	0.10	0.00	0.00	0.00	8.00	27.97	in matrix
Sample MP770 rhyodacitic dyke, Valdivia Sur mine block, pyrite ore zone																							
3	1	24.80	18.43	15.32	0.80	17.65	0.18			77.18	chlorite	2.84	10.00	3.02	1.47	2.49	0.08	0.02	0.00	0.00	8.00	27.91	in albite phenocryst
13	9	25.71	19.58	14.90	0.67	18.83				79.69	chlorite	2.83	10.00	3.09	1.37	2.54	0.06	0.00	0.00	0.00	8.00	27.90	in veinlet
Sample RB9867, rhyodacite, Filo mine block, bornite-chalcocite ore zone																							
16	11	23.73	14.64	19.08	0.67	7.43	0.39	0.62	0.23	66.80	chlorite?	3.25	10.00	1.52	2.19	2.37	0.08	0.06	0.17	0.04	8.00	27.67	in vein with sulfides
Sample MP778, rhyodacite, Valdivia Sur mine block, bornite-chalcocite ore zone																							
1	1	28.46	19.77	20.91	1.10	19.44				89.68	chlorite?	2.86	10.00	2.91	1.76	2.34	0.09	0.00	0.00	0.00	8.00	27.97	in vein with sulphides
3	3	31.12	17.23	24.35	0.59	13.56				86.86	chlorite?	3.26	10.00	2.12	2.13	2.13	0.05	0.00	0.00	0.00	8.00	27.68	in vein with sulphides
9	7	27.54	18.77	20.93	1.07	18.20				86.50	chlorite?	2.88	10.00	2.84	1.83	2.31	0.09	0.00	0.00	0.00	8.00	27.96	in microcystaline aggregate

Appendix 3.1.- Analyses of Muscovite

Spot	Grain	SiO$_2$ %	Al$_2$O$_3$ %	FeO %	MnO %	MgO %	CaO %	Na$_2$O %	K$_2$O %	Total %	Mineral	Si	O	K	Al	Fe	Mn	Mg	Ca	Na	OH	# ions	Remarks
Sample RB9829, basalt, Valdivia Sur mine block, background ore zone (unmineralized)																							
12	6	46.48	36.44	1.22	0.66	0.20			10.40	95.40	muscovite	3.08	10.00	0.88	2.85	0.07	0.04	0.02	0.00	0.00	2.00	18.93	in plagioclase phenocryst
13	6	46.45	35.48	1.10	0.36				9.61	92.99	muscovite	3.14	10.00	0.83	2.82	0.06	0.02	0.00	0.00	0.00	2.00	18.87	in plagioclase phenocryst
14	7	48.19	34.08	1.16		0.26	0.22	1.27	9.81	94.99	muscovite	3.20	10.00	0.83	2.67	0.06	0.00	0.03	0.02	0.15	2.00	18.95	in plagioclase phenocryst
16	9	46.97	34.77	2.17		0.58			9.98	94.47	muscovite	3.14	10.00	0.85	2.74	0.12	0.00	0.06	0.00	0.00	2.00	18.91	in plagioclase phenocryst
18	11	57.71	25.46	1.17		0.57	2.01	5.09	5.47	97.47	muscovite?	3.67	10.00	0.44	1.91	0.06	0.00	0.05	0.14	0.57	2.00	18.85	in plagioclase phenocryst
Sample RB9842, basalt, Filo mine block, background ore zone (unmineralized)																							
6	4	47.81	35.38	0.93			0.21	0.46	9.83	94.62	muscovite	3.17	10.00	0.83	2.76	0.05	0.00	0.00	0.02	0.05	2.00	18.89	in plagioclase phenocryst
1	1	46.37	34.64	1.17	0.58	0.52			10.90	94.18	muscovite	3.13	10.00	0.94	2.75	0.07	0.03	0.05	0.00	0.00	2.00	18.97	in plagioclase phenocryst
7	5	46.82	35.30	1.28		0.69	0.21	0.21	9.83	94.35	muscovite	3.12	10.00	0.84	2.78	0.07	0.00	0.07	0.01	0.02	2.00	18.92	in plagioclase phenocryst
8	5	46.62	36.31	0.88	0.34	0.23			10.41	94.78	muscovite	3.10	10.00	0.88	2.85	0.05	0.02	0.02	0.00	0.00	2.00	18.92	in plagioclase phenocryst
12	9	46.28	36.10	1.17		0.22			10.74	94.51	muscovite	3.09	10.00	0.92	2.84	0.07	0.00	0.02	0.00	0.00	2.00	18.94	in plagioclase phenocryst
13	9	46.17	36.08	0.65	0.41				10.50	93.81	muscovite	3.10	10.00	0.90	2.86	0.04	0.02	0.00	0.00	0.00	2.00	18.92	in plagioclase phenocryst
Sample RB9844, basalt, Filo mine block, bornite-chalcocite ore zone																							
5	1	60.33	19.49	1.03		0.50	3.66	0.57	13.38	98.50	muscovite?	3.91	10.00	1.11	1.49	0.06	0.00	0.05	0.25	0.06	2.00	18.93	in large phenocryst
Sample RB9852, basalt, Filo mine block, bornite-chalcocite ore zone																							
12	10	41.81	18.25	14.21	2.59	9.12			5.76	91.74	muscovite+ chlorite	3.12	10.00	0.55	1.61	0.89	0.16	1.02	0.00	0.00	2.00	19.35	in amygdule
Sample MP772, andesitic dike, Valdivia Sur mine block, chalcocite ore zone																							
5	5	57.11	21.82	2.89		1.70		0.92	11.42	95.86	muscovite?	3.79	10.00	0.97	1.70	0.16	0.00	0.17	0.00	0.11	2.00	18.89	in plagioclase phenocryst
6	6	60.51	21.37	1.51		0.81		0.33	13.41	97.94	muscovite?	3.91	10.00	1.11	1.63	0.08	0.00	0.08	0.00	0.04	2.00	18.84	in plagioclase phenocryst
Sample RB9805, rhyodacite, Valdivia Sur mine block, background ore zone (unmineralized)																							
11	7	50.03	29.67	4.41		1.46			9.46	95.02	moscovite?	3.35	10.00	0.81	2.34	0.25		0.15	0.00	0.00	2.00	18.89	radial mineral
Sample RB9822, rhyodacite, Valdivia Sur mine block, background ore zone (unmineralized)																							
18	9	55.29	22.30	0.95		0.48		0.51	12.32	91.85	muscovite?	3.80	10.00	1.08	1.81	0.05		0.05	0.00	0.07	2.00	18.87	in albite phenocryst

Mineral Formula Si$_3$O$_{10}$KAl$_3$(OH)$_2$

Appendix 3.1.- Analyses of Epidote

Spot	Grain	SiO2	Al2O3	FeO	MnO	MgO	CaO	Na2O	K2O	SrO	Total	Mineral	Mineral Formula (SiO₄)₃Ca₂(Al,Fe)₃(OH)									#	Remarks
		%	%	%	%	%	%	%	%	%	%		Si	O	Ca	Al	Fe	Mn	Mg	Na	OH	ions	
Sample RB9842, basalt, Filo mine block, background ore zone (unmineralized)																							
2	2	36.01	8.02	18.40	0.38	0.35	34.28				97.44	epidote	3.23	12.00	3.30	0.85	1.38	0.03	0.05		1.00	21.84	phenocryst
3	2	35.35	8.89	17.30	0.57	1.40	32.50				96.01	epidote	3.20	12.00	3.15	0.95	1.31	0.04	0.19		1.00	21.83	phenocryst
11	8	49.80	25.88	6.62			10.13	4.63	0.19		98.43	epidote + albite	3.70	12.00	0.81	2.27	0.41	0.00	0.00	0.67	1.00	20.87	in groundmass
Sample RB9843, basalt, Filo mine block, background ore zone (unmineralized)																							
4	4	37.10	21.29	13.53			22.73				94.64	epidote	3.14	12.00	2.06	2.13	0.96	0.00	0.00		1.00	21.29	in vein
9	9	36.77	23.23	13.08	1.30	1.63	21.18				97.19	epidote	3.03	12.00	1.87	2.26	0.90	0.09	0.20		1.00	21.34	in vein
10	10	37.12	20.67	15.65			23.39				96.82	epidote	3.12	12.00	2.10	2.04	1.10	0.00	0.00		1.00	21.36	in vein
11	11	37.13	21.05	14.98	0.61		22.91				96.67	epidote	3.11	12.00	2.06	2.08	1.05	0.04	0.00		1.00	21.35	in vein
Sample RB9930, basalt, Valdivia Sur mine block, background ore zone (unmineralized)																							
2	2	37.59	23.92	11.25	0.28		23.54				96.58		3.08	12.00	2.07	2.31	0.77	0.02	0.00		1.00	21.26	in vug
Sample RB9806, basalt, Valdivia Sur mine block, pyrite background ore zone																							
15	6	37.65	22.72	12.72			23.84				96.93	epidote	3.10	12.00	2.11	2.21	0.88				1.00	21.29	in vein
16	7	37.64	22.25	13.26	0.27		23.37				96.79	epidote	3.12	12.00	2.07	2.17	0.92	0.02			1.00	21.30	in vein
19	10	37.83	22.81	12.45	0.40		23.53				97.02	epidote	3.11	12.00	2.07	2.21	0.86	0.03			1.00	21.28	in vein
29	17	37.81	24.14	11.41	0.46		23.69				97.50	epidote	3.08	12.00	2.07	2.32	0.78	0.03			1.00	21.27	in vein
Sample RB9844, basalt, Filo mine block, bornite chalcocite ore zone																							
8	1	40.91	23.29	5.78		3.08	21.54	1.48			96.08	epidote	3.26	12.00	1.84	2.19	0.39	0.00	0.37	0.24	1.00	21.28	in plagioclase phenocryst
9	1	37.09	20.60	15.10			23.32				96.12	epidote	3.13	12.00	2.11	2.05	1.07				1.00	21.35	in plagioclase phenocryst
10	1	37.17	21.77	13.61			23.24				95.78	epidote	3.12	12.00	2.09	2.15	0.95				1.00	21.31	in plagioclase phenocryst
1	1	37.09	23.95	12.18			23.62				96.84	epidote	3.05	12.00	2.08	2.32	0.84				1.00	21.29	in plagioclase phenocryst
4	1	37.22	23.39	6.48		2.90	22.98				92.96	epidote	3.10	12.00	2.05	2.30	0.45	0.00	0.36		1.00	21.25	in plagioclase phenocryst
16	3	36.81	23.70	6.54		2.34	22.86				92.24	epidote	3.09	12.00	2.06	2.34	0.46	0.00	0.29		1.00	21.24	in plagioclase phenocryst
6	1	48.48	21.58	4.13		1.35	14.04		5.89		95.46	epidote + mica	3.80	12.00	1.18	2.00	0.27	0.00	0.16		1.00	20.99	in large phenocryst
Sample MP840 basaltic dyke, Morro mine block, chalcopyrite ore zone																							
4a	3	36.25	19.60	15.57	0.43		22.39				94.24	epidote	3.14	12.00	2.08	2.00	1.13	0.03	0.00		1.00	21.37	in vein
36	13	35.19		28.02			33.42				96.62	epidote	3.39	12.00	3.43	0.00	2.26	0.00	0.00		1.00	22.08	in vein
37	14	35.48	22.63	10.96	0.80		22.49			0.35	92.70	epidote	3.06	12.00	2.08	2.30	0.79	0.06	0.00		1.00	21.29	in vein
8a	7	37.03	22.62	12.98	1.04	0.31	22.62				96.60	epidote	3.08	12.00	2.01	2.21	0.90	0.07	0.04		1.00	21.32	in phenocryst
Z603-95, basalt, Veta Negra Formation, background ore zone (unmineralized)																							
57	1	35.12	25.18	5.18	0.92	1.64	22.79				90.83	epidote	2.99	12.00	2.08	2.53	0.37	0.07	0.21		1.00	21.24	in plagioclase phenocryst
Sample RB9805, rhyodacite, Valdivia Sur mine block, background ore zone (unmineralized)																							
28	16	33.32	20.53	9.65	0.37		18.03				81.90	epidote?	3.19	12.00	1.85	2.31	0.77	0.03			1.00	21.15	in albite phenocryst
29	16	32.33	20.06	9.03	1.08		16.35				78.85	epidote?	3.20	12.00	1.74	2.34	0.75	0.09			1.00	21.12	in albite phenocryst
Sample RB9903, rhyodacite, Arauco Norte mine block, pyrite ore zone																							
9	5	30.90	19.16	9.34			14.12				73.51	epidote?	3.26	12.00	1.59	2.38	0.82				1.00	21.05	in vein

Appendix 3.1.- Analyses of Quartz

Spot	Grain	SiO₂ %	Al₂O₃ %	FeO %	MgO %	CaO %	Na₂O %	K₂O %	P₂O₅ %	Cl %	Total %	Mineral	Si	O	Mg	Ca	Na	K	Al	# ions	Remarks
Sample RB9903, rhyodacite, Arauco Norte mine block, pyrite ore zone																				
7	3	96.49	1.30					0.41			98.20	quartz	0.99	2.00				0.01		2.99	in vein
8	4	97.56	0.71								98.27	quartz	0.99	2.00						2.99	in vein
10	6	99.41									99.41	quartz	1.00	2.00						3.00	in vein
13	9	99.61									99.61	quartz	1.00	2.00						3.00	in vein/vug
Sample RB9811, Valdivia Sur mine block, pyrite-chalcopyrite ore zone																				
4	3	100.12									100.12	quartz	1.00	2.00						3.00	in vug
6	5	96.55				1.34					97.89	quartz	0.99	2.00		0.01				3.01	in vug
16	13	96.91							0.40		97.31	quartz	1.00	2.00						3.00	in vein
Sample RB9815, rhyodacite, Valdivia Sur mine block, bornite-chalcocite ore zone																				
23	16	94.46					0.24		0.38	0.09	95.16	quartz	0.99	2.00			0.00			3.00	in groudmass
25	18	99.89									99.89	quartz	1.00	2.00						3.00	in vein
26	19	99.87									99.87	quartz	1.00	2.00						3.00	in vein
27	20	99.80	0.57								100.37	quartz	0.99	2.00						2.99	in vein
24	17	89.15	8.70				5.11				102.96	quartz+albite	0.90	2.00			0.10			3.00	in groudmass
Sample MP778, rhyodacite, Valdivia Sur mine block, bornite-chalcocite ore zone																				
2	2	100.51									100.51	quartz	1.00	2.00						3.00	in vein
4	4	99.83									99.83	quartz	1.00	2.00						3.00	in vein
5	5	99.04	0.74								99.77	quartz	1.02	2.00						3.02	in vein
10	8	100.71		0.36							100.07	quartz	1.00	2.00						3.00	in vein
12	10	100.22									100.22	quartz	1.00	2.00						3.00	in vein
17	13	100.08									100.08	quartz	1.00	2.00						3.00	in vein
29	17	98.61	0.31		0.23						99.15	quartz	1.00	2.00	0.00					3.00	in vein
30	18	99.86									99.86	quartz	1.00	2.00						3.00	in vein
Sample MP770, Valdivia Sur mine block, A12 rhyodacitic dyke, pyrite ore zone																				
4	2	98.02	0.46								99.48	quartz	1.00	2.00						3.00	in groundmass
5	1	99.15	0.66								99.81	quartz	0.99	2.00						2.99	in albite phenocryst
6	3	99.19									99.19	quartz	1.00	2.00						3.00	secondary
7	4	98.65	0.94								99.59	quartz	0.99	2.00						2.99	secondary
8	5	99.60									99.60	quartz	1.00	2.00						3.00	in albite phenocryst
10	6	99.97									99.97	quartz	1.00	2.00						3.00	in vein
12	8	98.57	0.43								99.00	quartz	1.00	2.00						3.00	in veinlet
14	10	99.43									99.43	quartz	1.00	2.00						3.00	in veinlet
15	11	98.56	0.43								98.98	quartz	1.00	2.00						3.00	in veinlet

Appendix 3.1.- Analyses of Quartz (continued)

Spot	Grain	SiO$_2$ %	Al$_2$O$_3$ %	FeO %	MgO %	CaO %	Na$_2$O %	K$_2$O %	P$_2$O$_5$ %	Cl %	Total %	Mineral	Mineral Formula (SiO$_2$)							# ions	Remarks
													Si	O	Mg	Ca	Na	K	Al		
16	12	99.73									99.73	quartz	1.00	2.00						3.00	in veinlet
17	13	100.11								0.38	100.48	quartz	1.00	2.00						3.00	in major vein
18	14	99.84									99.84	quartz	1.00	2.00						3.00	in major vein
19	15	100.06									100.06	quartz	1.00	2.00						3.00	in vug
20	16	99.72								0.35	100.06	quartz	1.00	2.00						3.00	in vug
22	18	99.58									99.58	quartz	1.00	2.00						3.00	in vug
24	20	99.27									99.27	quartz	1.00	2.00						3.00	in vein
25	21	99.94									99.94	quartz	1.00	2.00						3.00	in vein
27	23	98.95									98.95	quartz	1.00	2.00						3.00	in vein
28	24	99.48	0.23								99.72	quartz	1.00	2.00						3.00	in vein
29	25	99.16	0.30								99.46	quartz	1.00	2.00						3.00	in vein
Sample MP772, andesitic dike, Valdivia Sur mine block, bornite ore zone																					
2	2	98.64									98.64	quartz	1.00	2.00						3.00	fine aggregate
3	3	100.43									100.43	quartz	1.00	2.00						3.00	large crystal
4	4	98.73	0.50			0.19					99.42	quartz	0.99	2.00		0.00			0.01	3.00	in veinlet
Sample RB9852, basalt, Filo mine block, bornite-chalcocite ore zone																					
6	5	99.98									99.98	quartz	1.00	2.00						3.00	in vein
9	8	99.31									99.31	quartz	1.00	2.00						3.00	in vein
Sample Z622-95 Gabbro, Arauco Norte mine block, background ore zone (unmineralized)																					
38	1	97.23	0.15	0.52	1.18						99.08	quartz	1.12	2.00	0.02				0.00	3.15	in ferromagnesian crystal

Appendix 3.1.- Analyses of Rutile

Spot	Grain	SiO$_2$ %	TiO$_2$ %	Al$_2$O$_3$ %	FeO %	CaO %	Na$_2$O %	K$_2$O %	BaO %	ZrO$_2$ %	Cl %	Total %	Mineral	Ti	O	Si	Al	Fe	Ca	Na	# ions	Remarks
Sample RB9822, rhyodacite, Valdivia Sur mine block, background ore zone (unmineralized)																						
15	7	1.23	93.65			1.63			0.28			98.06	rutile	0.97	2.00	0.02			0.02		3.02	replacing ferromagnesian
Sample MP845, rhyodacite, Filo mine block, background ore zone (unmineralized)																						
63	b	0.21	94.65		0.35	0.94						96.15	rutile	0.99	2.00	0.00		0.00	0.01		3.01	replacing Ti magnetite
Sample MP848, rhyodacite, Morro mine block, background ore zone (unmineralized)																						
1	16	0.23	94.66		0.48	0.27						95.64	rutile	0.99	2.00	0.00		0.01	0.00		3.00	replcing Ti magnetite
Sample MP846, rhyodacitic dyke, Morro mine block, background ore zone (unmineralized)																						
50	b		95.67		0.33	1.00						97.00		0.99	2.00	0.00		0.00	0.01		3.01	replacing phenocryst
51	b	0.45	93.14		0.21	1.64						95.43		0.98	2.00	0.01		0.00	0.02		3.01	replacing phenocryst
Sample MP839, rhyodacitic dyke, Valdivia Sur mine block, pyrite ore zone																						
10	1	2.59	87.81	0.35	2.43	0.86		0.10			0.07	94.21		0.94	2.00	0.04	0.01	0.03	0.01		3.02	associated with pyrite
10b	1	0.27	94.06		0.43	0.39						95.14		0.99	2.00	0.00		0.01	0.01		3.01	associated with pyrite
Sample RB9811, rhyodacite, Valdivia Sur mine block, pyrite chalcopyrite ore zone																						
3	2		95.80		0.59	0.17						96.56	rutile	1.00	2.00			0.01	0.00		3.02	in vug
9	7	0.34	96.33									96.67	rutile	1.00	2.00	0.00					3.02	in vug
11	8	0.20	95.26		0.53							95.99	rutile	0.99	2.00	0.00		0.01			3.02	in vug
14	11	0.31	95.23			2.10						97.65	rutile	0.98	2.00	0.00			0.03		3.02	replacing phenocryst?
Sample RB9867, rhyodacite, Filo mine block, bornite ore zone																						
1	1		95.99		0.66	2.20						98.85	rutile	0.98	2.00			0.01	0.03		3.02	in vug
5	5	0.47	94.86		0.76	1.37						97.45	rutile	0.98	2.00	0.01		0.01	0.02		3.01	in vug
17	12	0.63	95.32		0.49					0.70		97.14	rutile	0.98	2.00	0.01		0.01			3.00	in vein
20	14	0.81	94.95		0.61	0.83						97.21	rutile	0.98	2.00	0.01		0.01	0.01		3.01	in vein
22	16	0.35	96.14		0.47	0.55						97.51	rutile	0.99	2.00	0.00		0.01	0.01		3.01	in vein
Sample RB9815, rhyodacite, Valdivia Sur mine block, bornite-chalcocite ore zone																						
18	12	1.89	95.25	0.62	0.45		0.44					98.65	rutile	0.96	2.00	0.03	0.01	0.01		0.01	3.01	cristaline
22	15	6.72	31.64	2.20			1.94					42.50	rutile+albite	0.71	2.00	0.20	0.08			0.17	3.16	in groudmass

Appendix 3.1.- Analyses of Titanite

Spot	Grain	SiO₂ %	Al₂O₃ %	FeO %	MnO %	MgO %	CaO %	Na₂O %	K₂O %	TiO₂ %	P₂O₅ %	Cl %	Total	Mineral	Mineral Formula (SiO₅CaTi)												# ions	Remarks
															Si	O	Ca	Ti	Al	Fe	Mn	Mg	Na	K	P	Cl		
Sample RB9805, rhyodacite, valdivia Sur mine block, background ore zone (unmineralized)																												
4	2	30.29	2.88	0.88			29.34			35.12	0.40		98.90	titanite	1.00	5.00	1.04	0.87	0.11	0.02					0.01		8.06	in albite phenocryst
13	8	31.38	5.17	0.34			30.10			31.72			98.71	titanite	1.03	5.00	1.06	0.78	0.20	0.01							8.08	in albite phenocryst
32	17	30.13	2.03				29.15			36.51			97.83	titanite	1.00	5.00	1.04	0.92	0.08	0.00							8.04	in albite phenocryst
34	11	30.31	3.08				29.69					0.10	97.60	titanite	1.01	5.00	1.06	0.86	0.12	0.00						0.01	8.07	in albite phenocryst
Sample Z626-95, basaltic dyke, Morro mine block, background ore zone (unmineralized)																												
20	1	30.87	4.09	2.83	0.30	0.52	27.49			29.75			95.85	titanite	1.05	5.00	1.00	0.76	0.16	0.08	0.01	0.03					8.10	replacing Ti-magnetite
Sample MP845, basalt, Filo mine block, background ore zone (unmineralized)																												
64	b	30.87	6.27	0.68			29.95			30.15			97.91	titanite	1.02	5.00	1.06	0.75	0.24	0.02							8.10	replacing Ti-magnetite
Sample MP840, basaltic dyke/rhyodacite, Morro mine block, chalcopyrite ore zone																												
31	6	50.49	13.08	0.76			9.23	0.23	9.43	13.21			96.42	titanite + feldspar	1.57	5.00	0.31	0.31	0.48	0.02			0.01	0.37			8.07	in albite phenocryst

Appendix 3.1.- Analysis of Apatite

Spot	Grain	SiO₂ %	Al₂O₃ %	FeO %	MgO %	CaO %	Na₂O %	P₂O₅ %	Cl %			Total %	Mineral	Mineral Formula Ca₅(PO₄)₃ (F,Cl,OH)										# ions	Remarks
														Ca	P	O	Si	Al	Fe	Mg	Na	Cl	OH		
Sample MP770 rhyodacitic dyke, Valdivia Sur mine block, pyrite ore zone																									
21	17	0.52				56.37		41.59	0.54			99.02	apatite	5.05	2.94	12.00	0.04				0.08	0.92		21.04	in vug
23	19	0.38		0.46	0.21	55.18		41.60	1.38			99.20	apatite	4.97	2.96	12.00	0.03		0.03	0.03	0.20	0.80		21.02	in vug
Sample RB9815, rhyodacite, Valdivia Sur mine block, bornite-chalcocite ore zone																									
12	6	1.05	0.36			56.14	0.35	41.92				99.82	apatite	4.95	2.92	12.00	0.09	0.03			0.06		1.00	21.05	in albite phenocryst

Appendix 3.2.- Mineral plots for selected spot analyses.

- Appendix 3.2 a. Pyroxene phenocrysts in basalts, dykes and gabbro.
- Appendix 3.2 b. Plagioclase phenocrysts in basalts, dykes and gabbro.
- Appendix 3.2 c. Albite (secondary) phenocrysts in rhyodacites.
- Appendix 3.2 d. Secondary albite in basalts.
- Appendix 3.2 e. Secondary albite in rhyodacites.
- Appendix 3.2 f. Secondary microcline in basalts.
- Appendix 3.2 g. Secondary microcline in rhyodacites.
- Appendix 3.2.h. Chlorite in basalts
- Appendix 3.2 i. Chlorite in rhyodacites.

Appendix 3.2.a
Pyroxene Phenocrysts in Basalt, Dykes and Gabbro
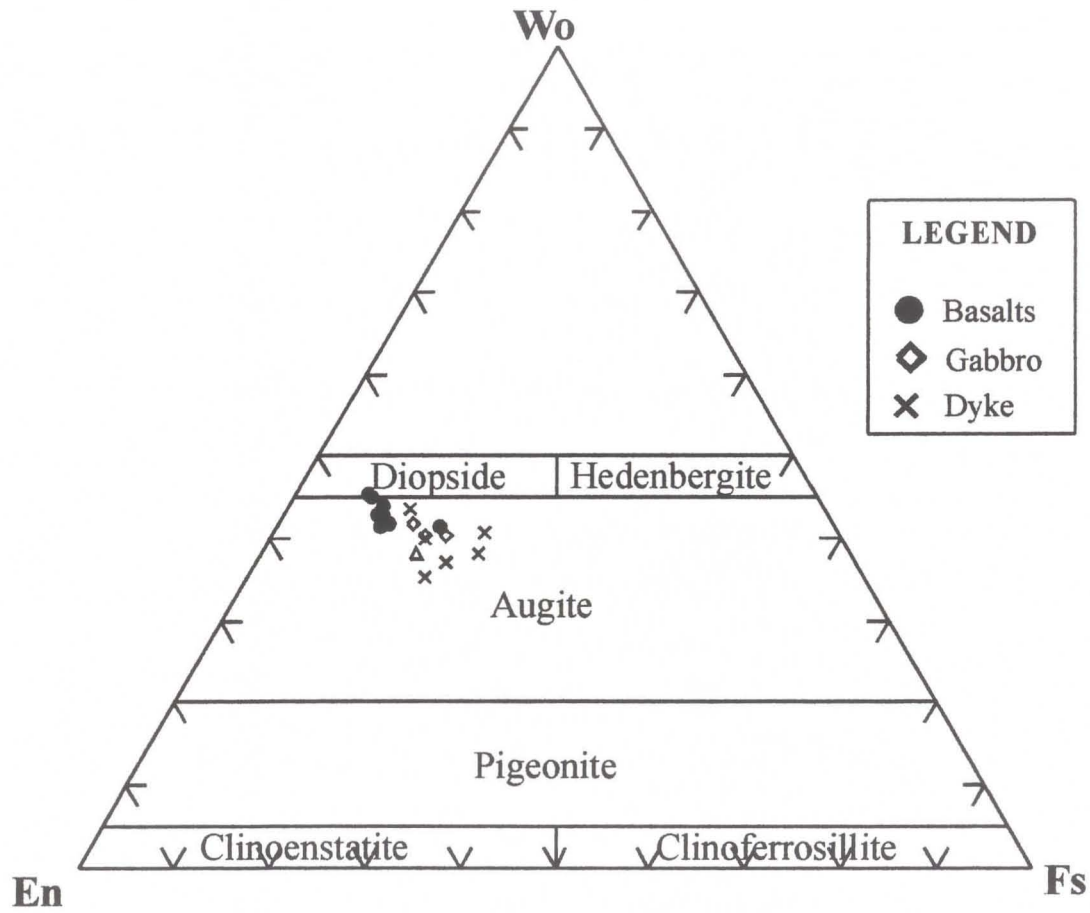
Appendix 3.2.b
Plagioclase Phenocrysts in Basalts, Dykes and Gabbro
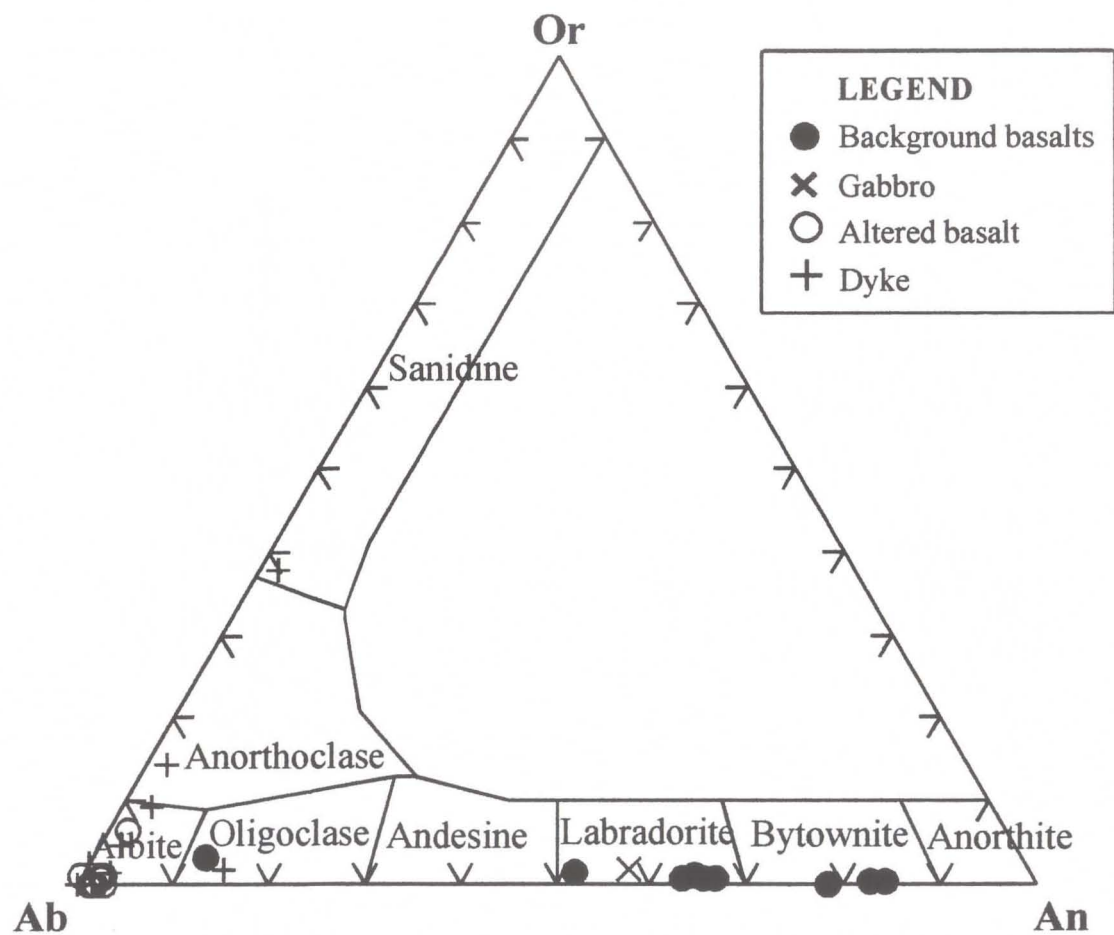
Appendix 3.2.c
Albite Phenocryst in Rhyodacite
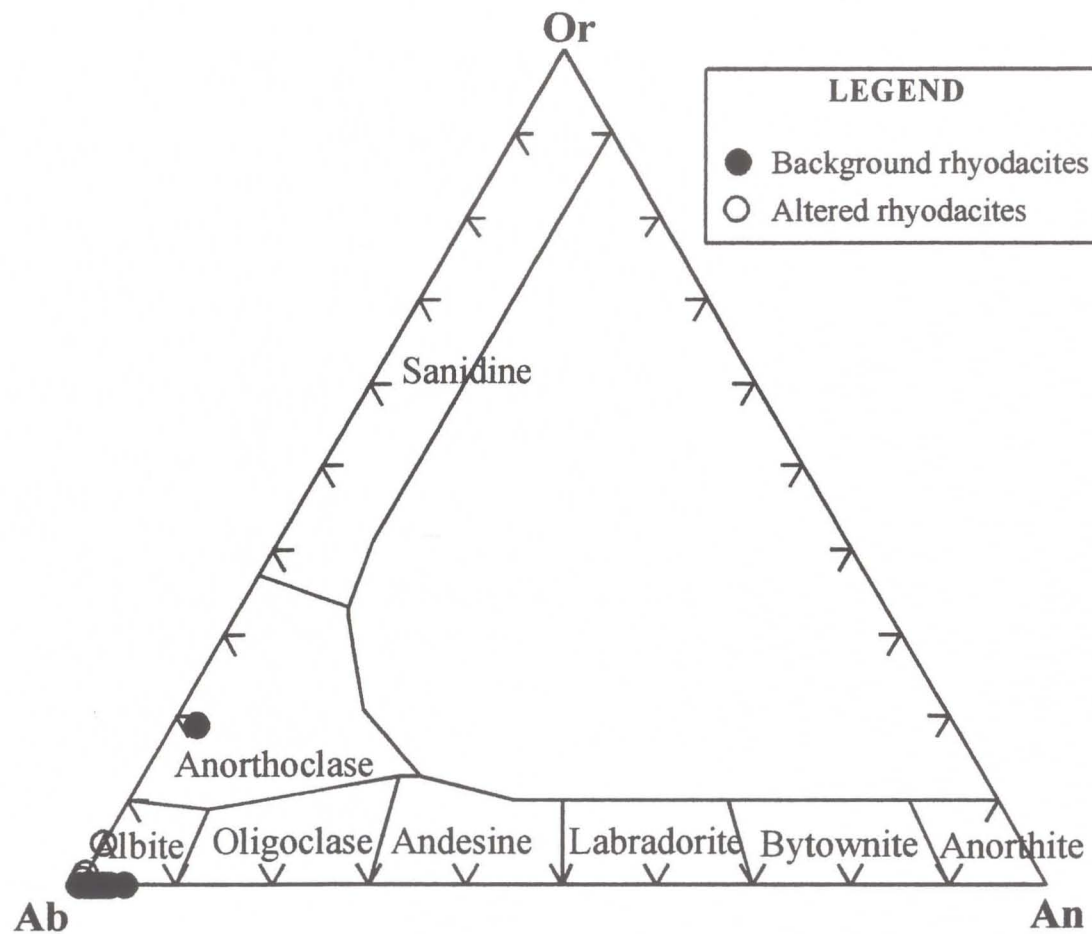
Appendix 3.2.d
Secondary Albite in Basalts
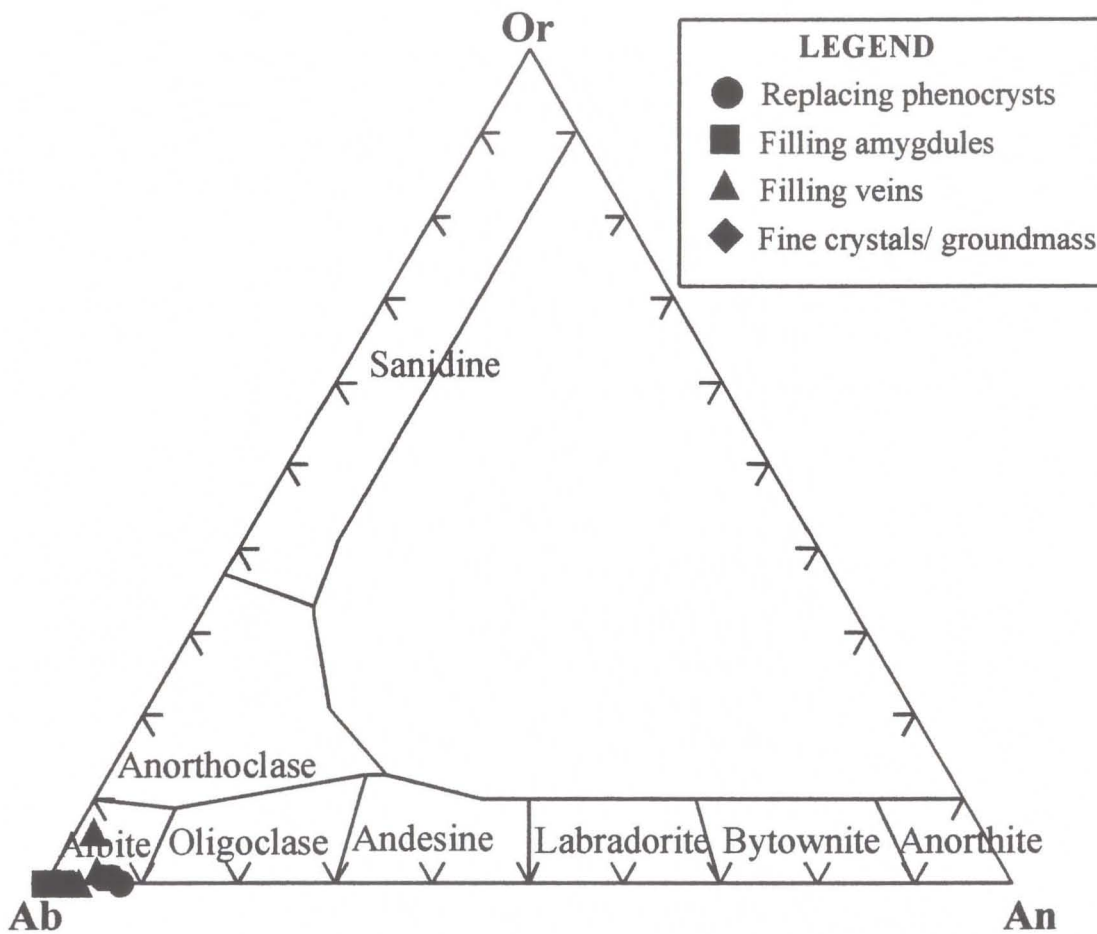
Appendix 3.2.e
Secondary Albite in Rhyodacites
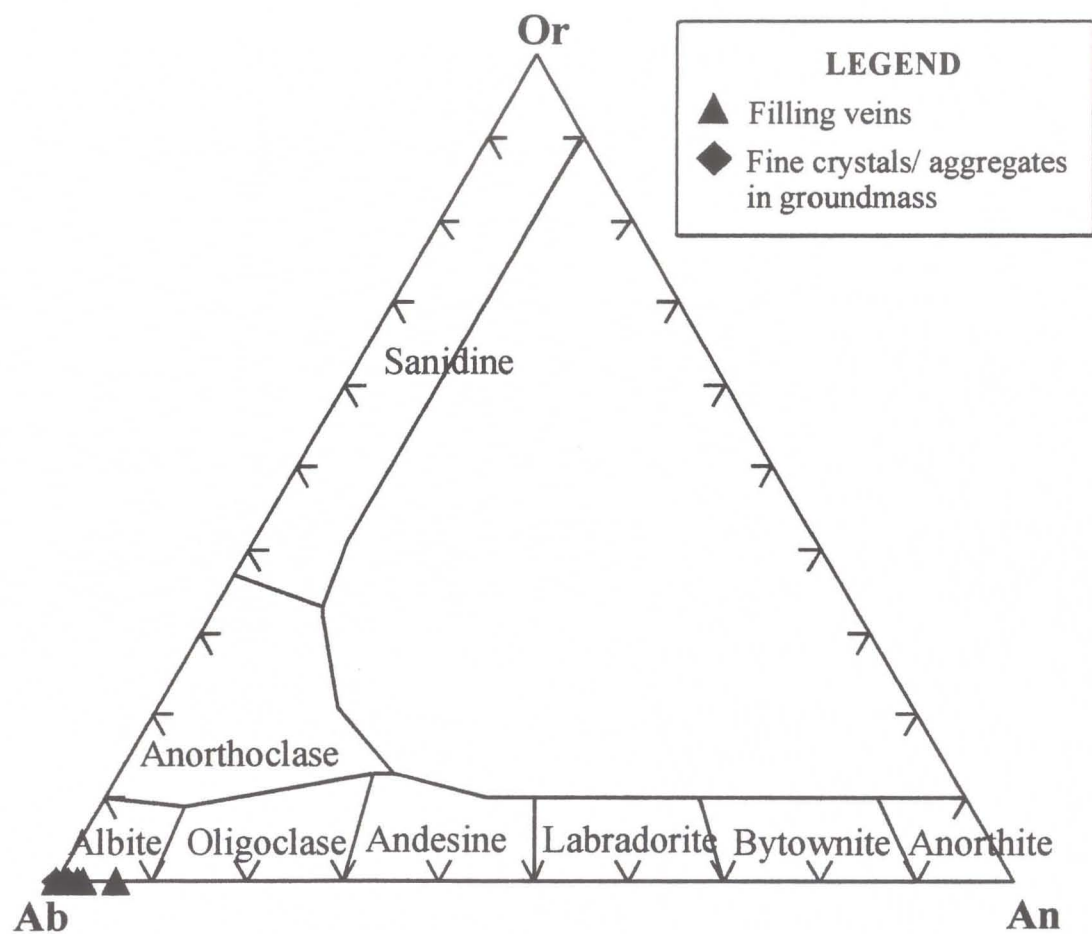
Appendix 3.2.f
Secondary K-feldspar (Microcline) in Basalts

283
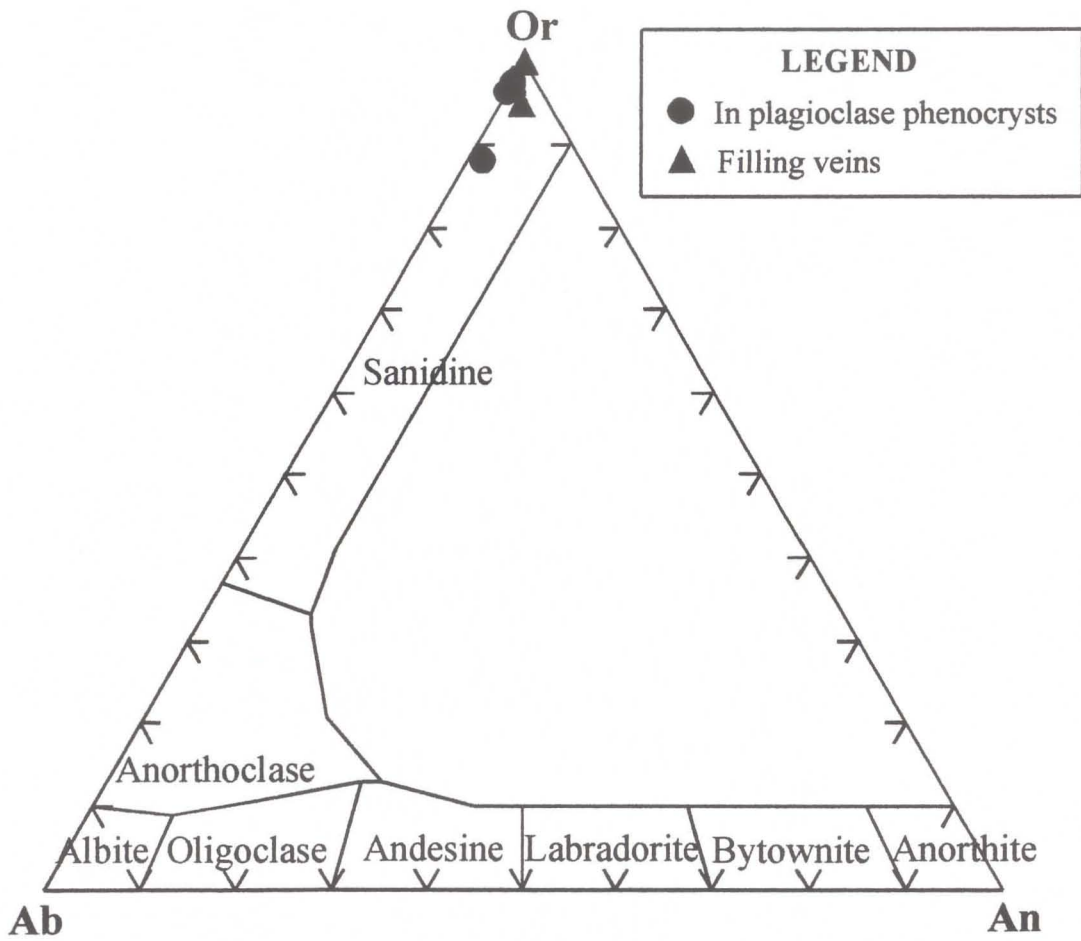
Appendix 3.2.g
Secondary K-feldspar (Microcline) in Rhyodacites

Appendix 3.2.h
Chlorite in Basalts

Figure axes: Y-axis labeled **Fe2+Fe3** (0 to 12), X-axis labeled **Si** (4 to 8).

Field labels within diagram: Daphnite, Pseudothuringite, Brunsvigite, Ripidolite, Diabantite, Corundophilite, Pycnochlorite, Clinochlore, Sheridanite, Penninite, Talc-chlorite
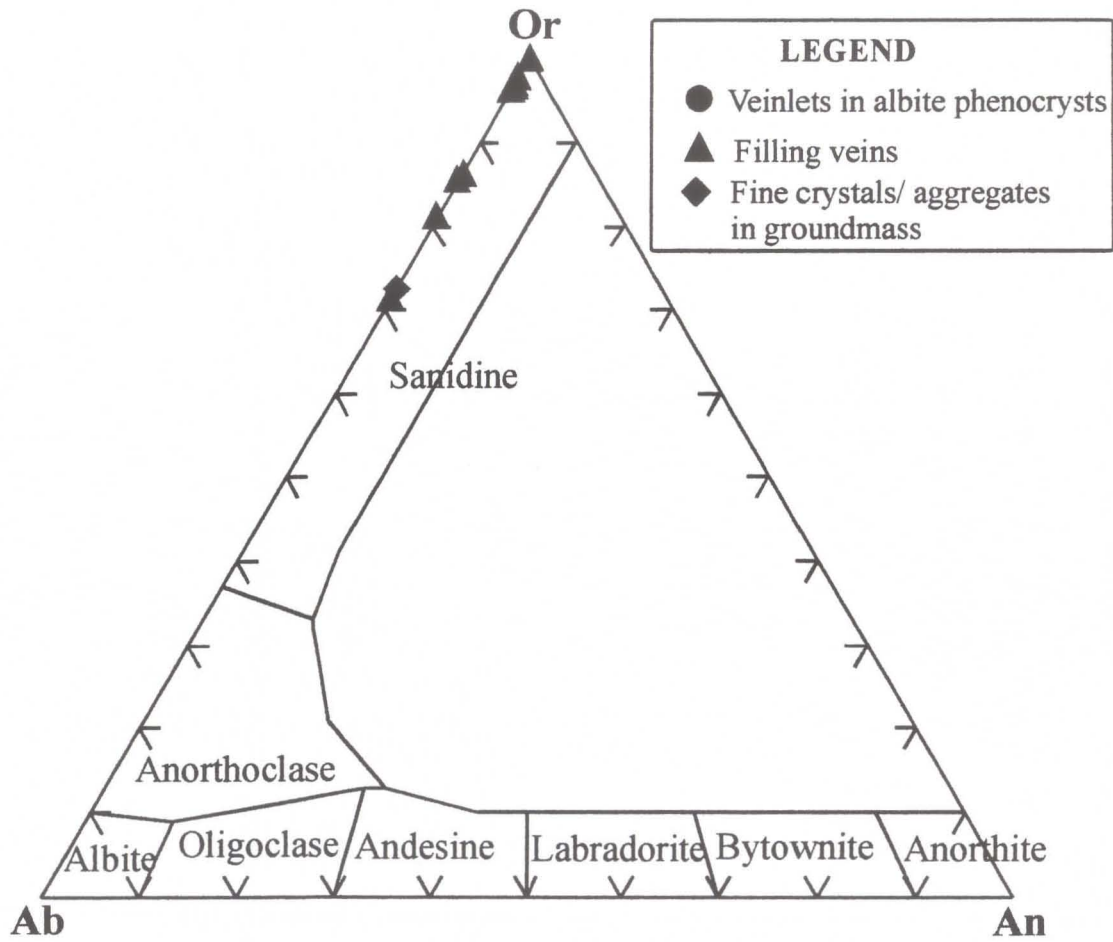
LEGEND
- ● Replacing ferromagnesium, barren rock
- ○ ,Replacing ferromagnesium, mineralized rock
- ▲ Filling veins, barren rock
- △ Filling veins, mineralized rock

Appendix 3.2.i
Chlorite in Rhyodacites

Appendix 3.3. Microprobe Back-Scatter and X-Ray Images

- For each rock sample, data are presented in the following order:

  Image a):
  - top left: back-scatter image
  - top right: Al X-ray map
  - Bottom left: Na X-ray map
  - Bottom right: K X-ray map

  Image b):
  - top left: Si X-ray map
  - top right: Mg X-ray map
  - Bottom left: Ca X-ray map
  - Bottom right: P X-ray map

  Image c):
  - top left: S X-ray map
  - top right: Mn X-ray map
  - Bottom left: Fe X-ray map
  - Bottom right: Ti X-ray map

- Samples listed by rock type and ore zone

- Abbreviations used in annotations:
  - ab: albite
  - ap: apatite
  - amgd: amygdule
  - aug: augite
  - bn: bornite
  - cal: calcite
  - cc: chalcocite
  - cp: chalcopyrite
  - chl: chlorite
  - diss: disseminated
  - ep: epidote
  - ferromg: ferromagnesian minerals
  - gm: groundmass
  - hem: hematite
  - kfd: potassium feldspar
  - mt: magnetite
  - mc: microcline
  - pg: pigeonite
  - phen: phenocryst
  - poss: possible
  - py: pyrite
  - qz: quartz
  - ru: rutile
  - ser: sericite
  - sur: surrounding
  - ti: titanite
  - vns: veins
  - x: crystal
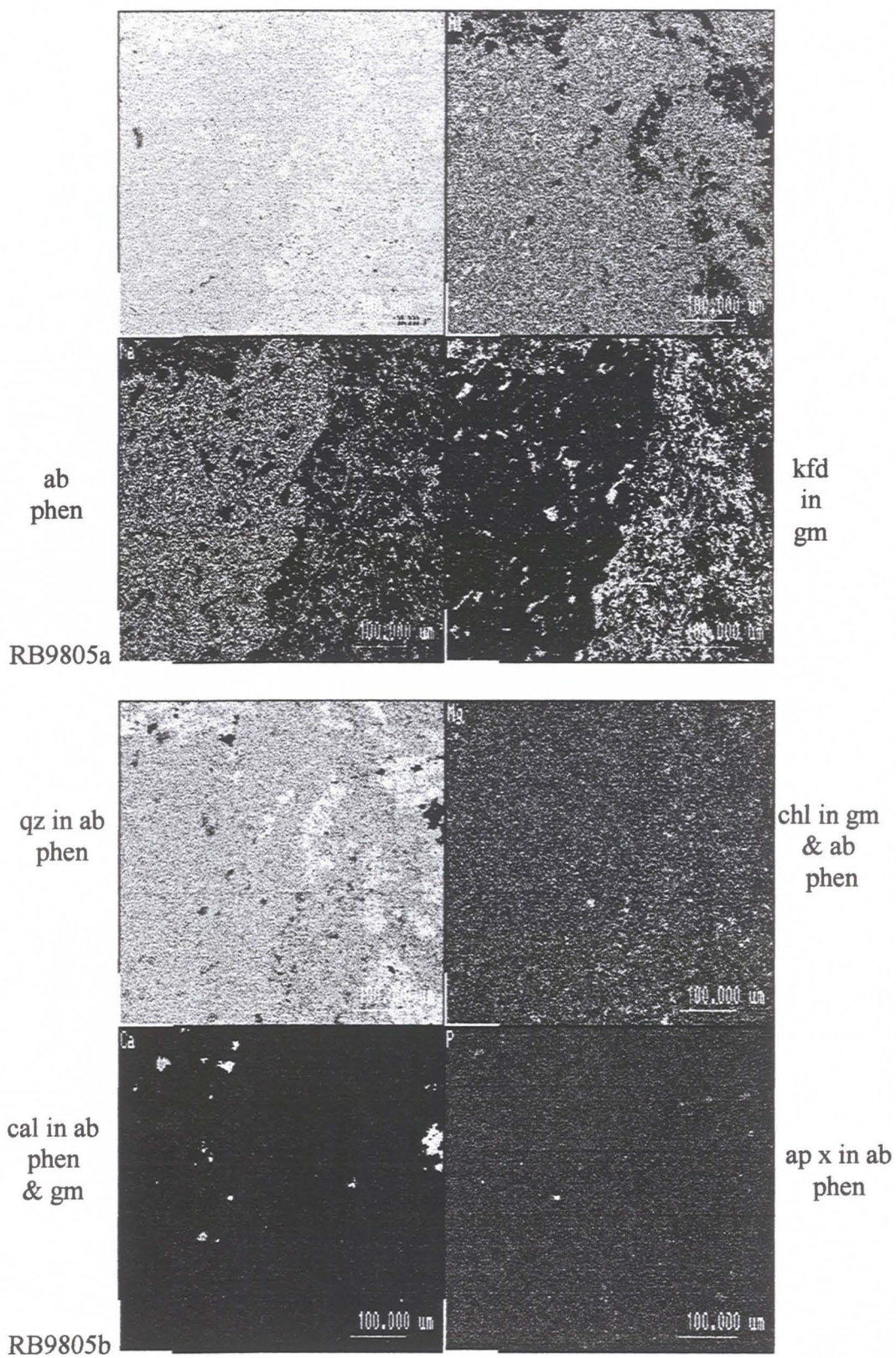
ab
phen

kfd
in
gm

RB9805a

qz in ab
phen

chl in gm
& ab
phen

cal in ab
phen
& gm

ap x in ab
phen

RB9805b

Sample RB9805, Rhyodacite, background zone, Valdivia Sur.

288

py in
gm
& ab

ti x
in gm
& ab

RB9805c

kfd in
gm &
ab phen
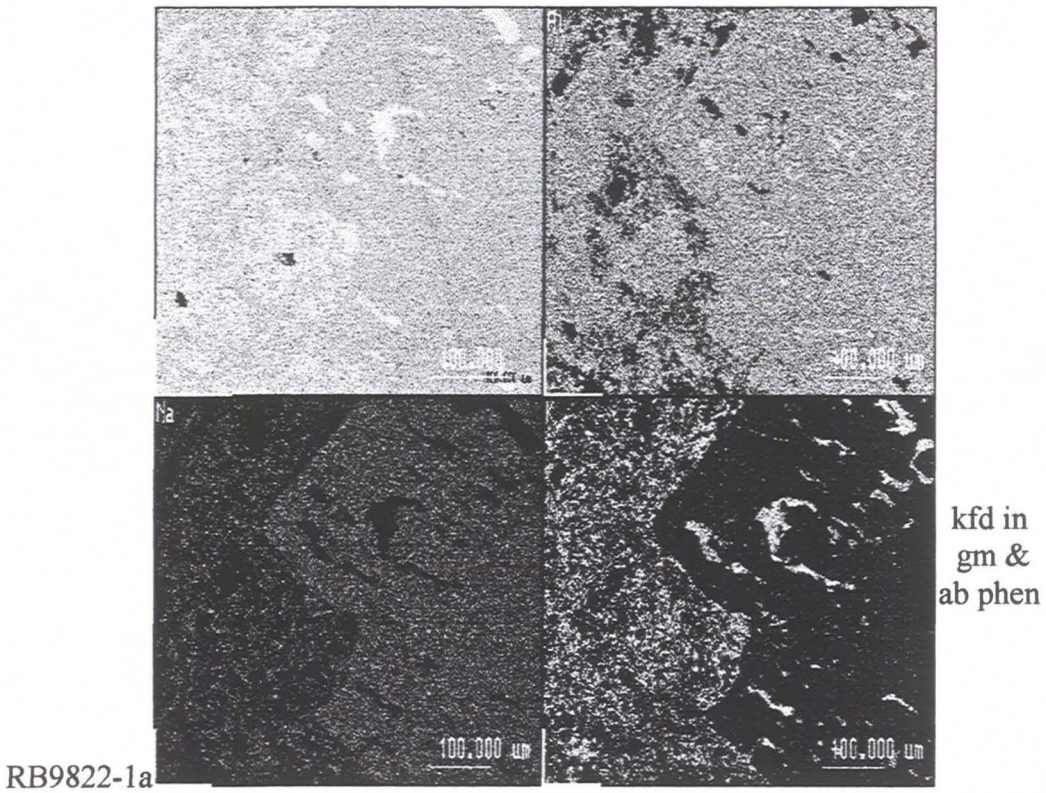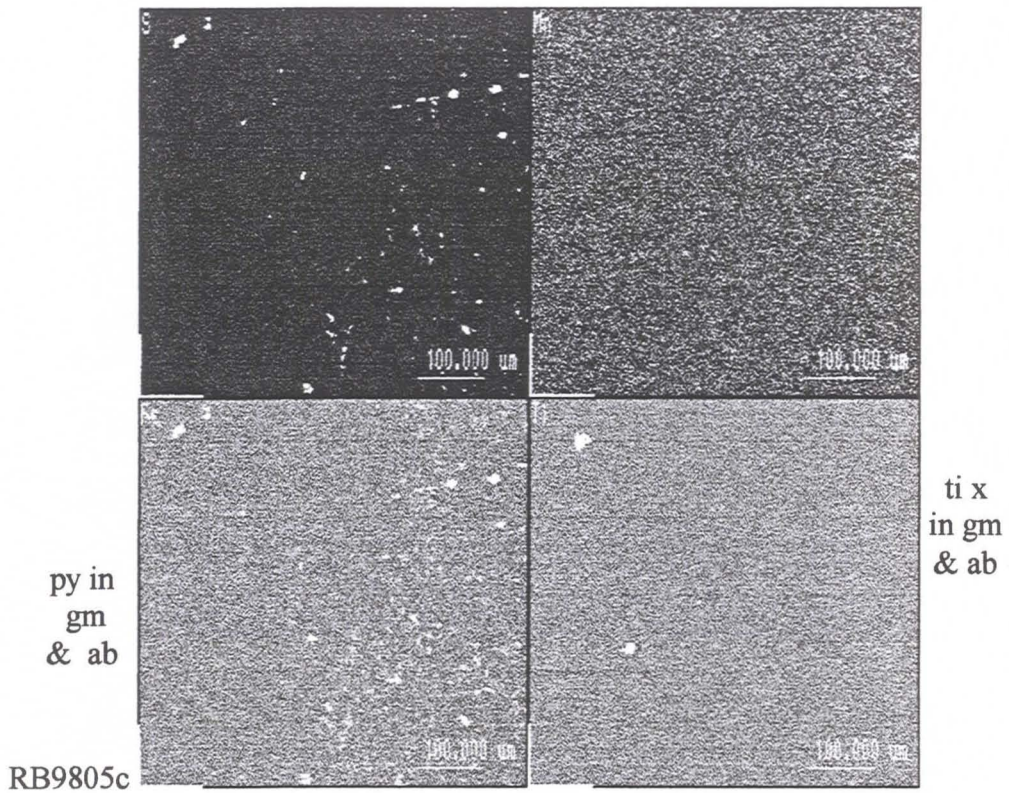
RB9822-1a

Sample RB9805, Rhyodacite, background zone, Valdivia Sur.
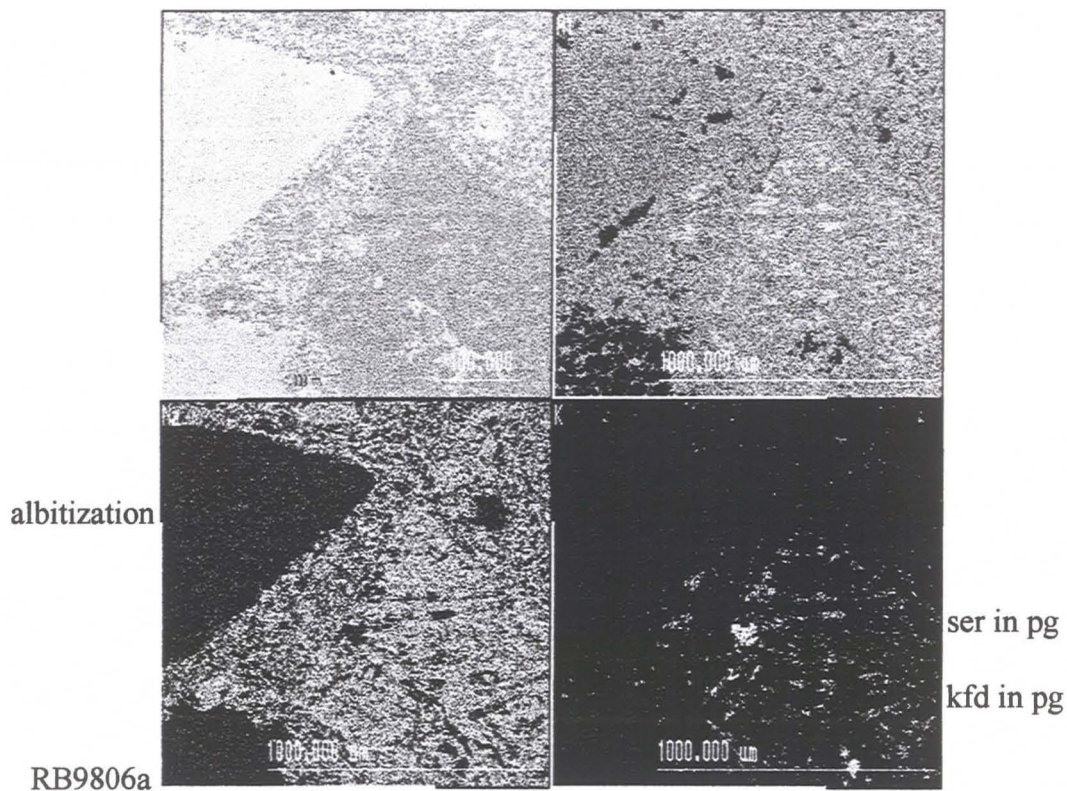Sample RB9822-1, Rhyodacite, background zone, Valdivia Sur.

qz in gm
& in
ab phen
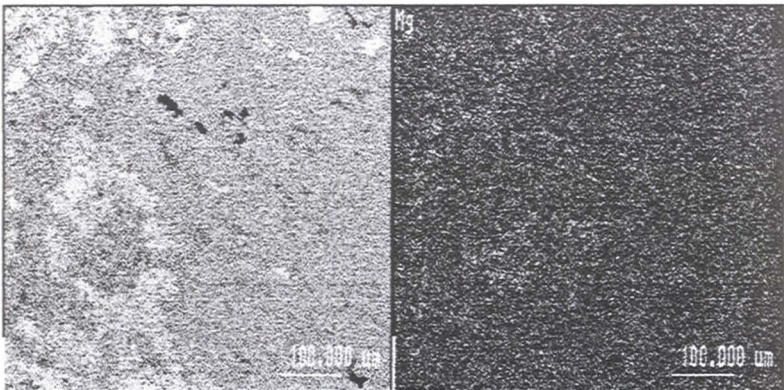
cal in
ab phen
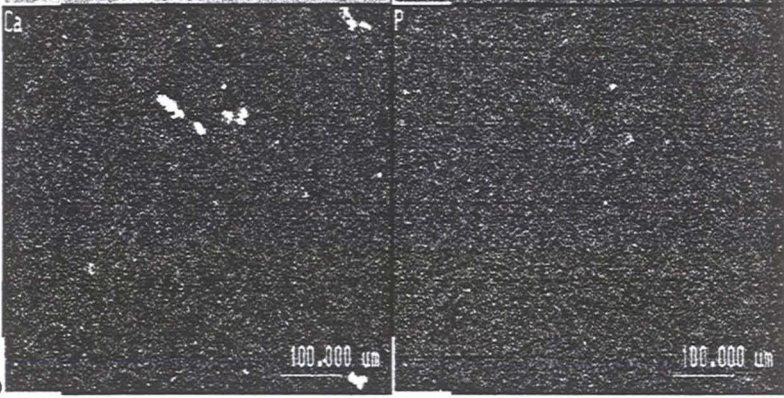
scarce
ap diss

RB9822-1b

py diss
in gm &
phen
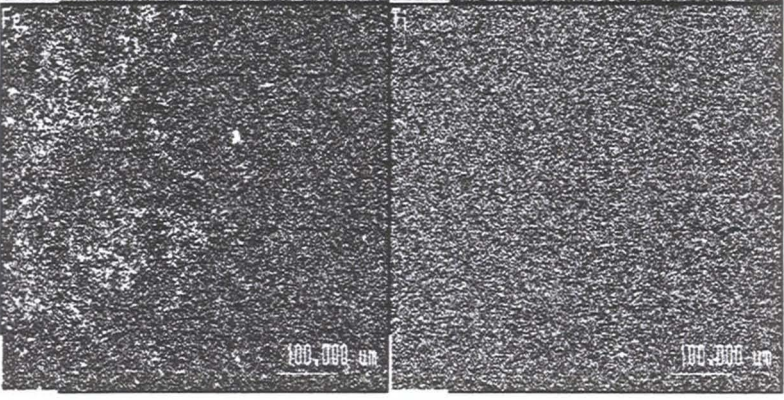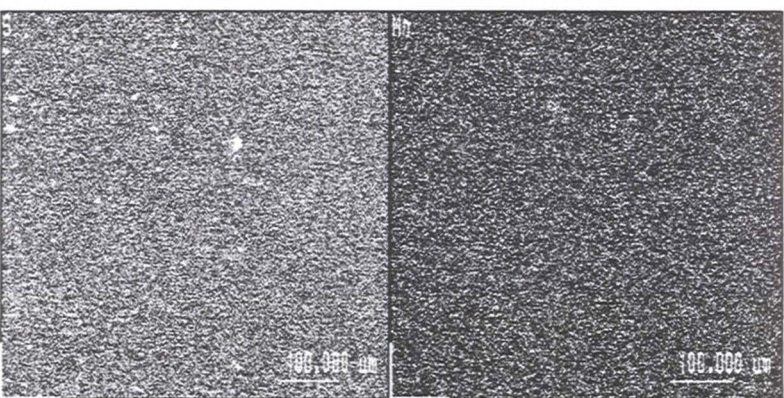
RB9822-1c

Sample RB9822-1, Rhyodacite, background zone, Valdivia Sur.

RB9822-2a

Some qz
in bands

cal
bands
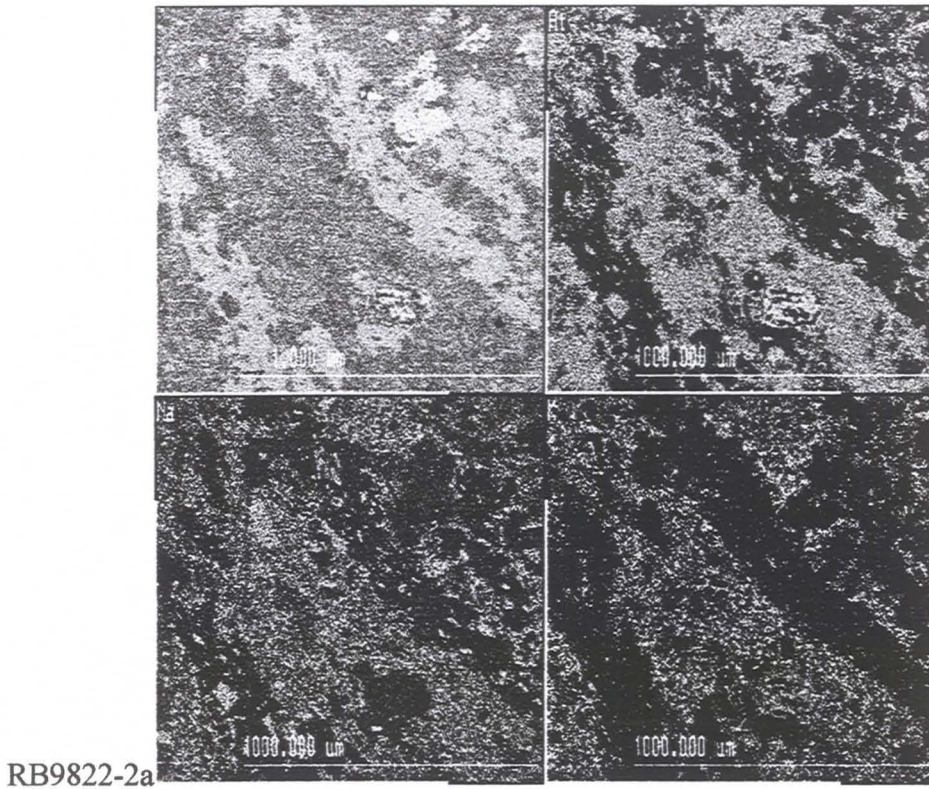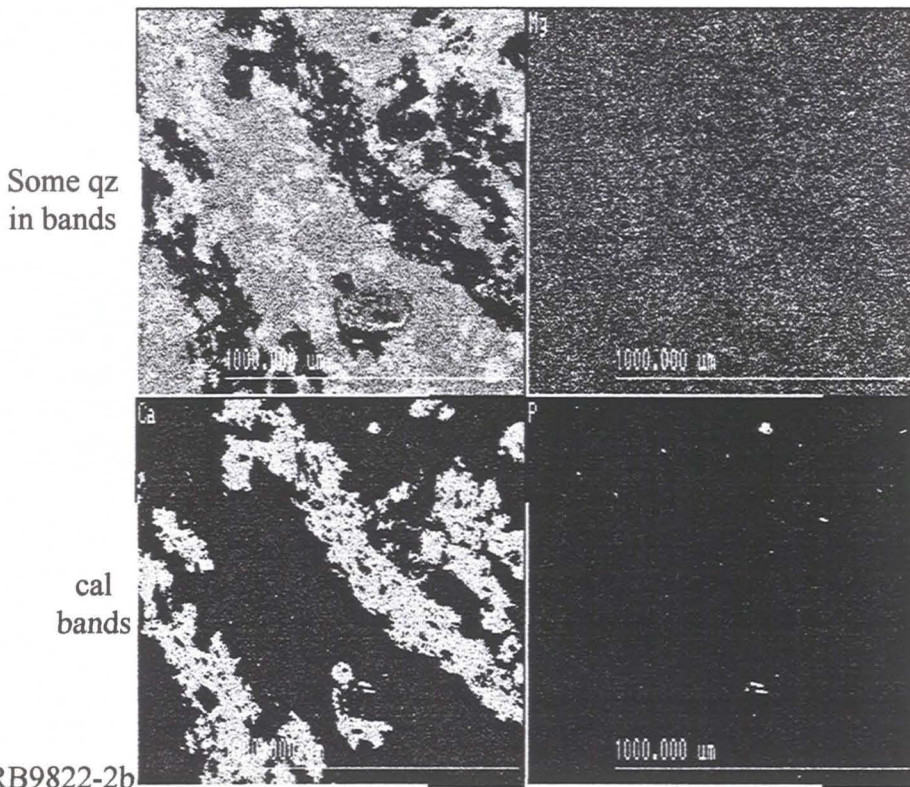
RB9822-2b

ap diss
in gm &
replacing
ferromg or
mt

Sample RB9822-2, Rhyodacite, background zone, Valdivia Sur.
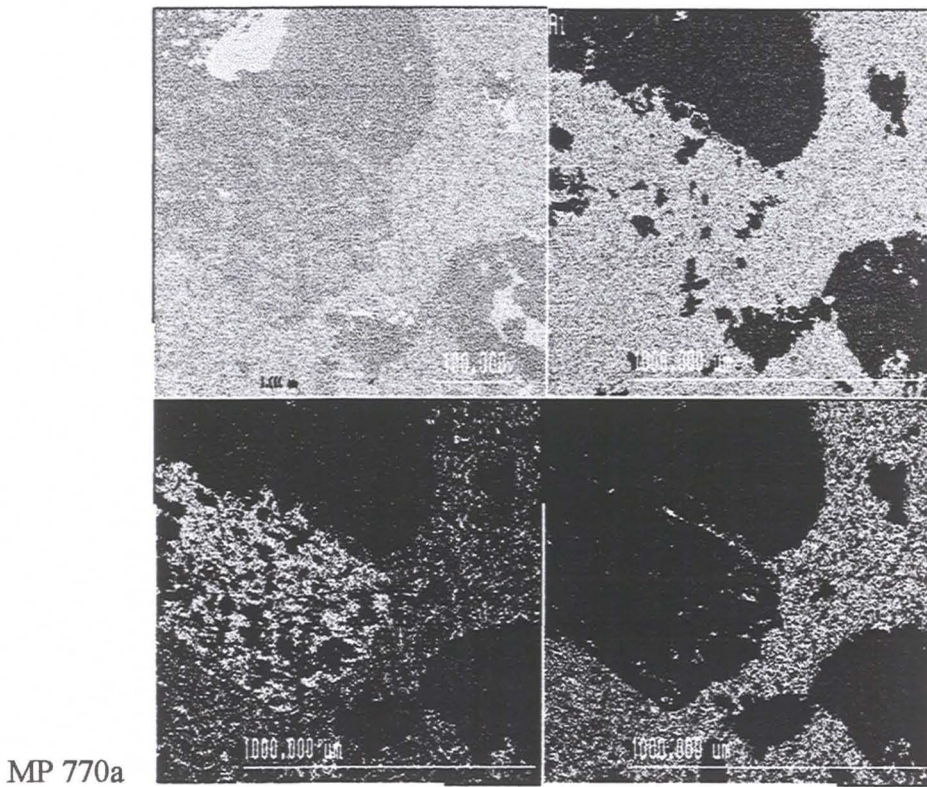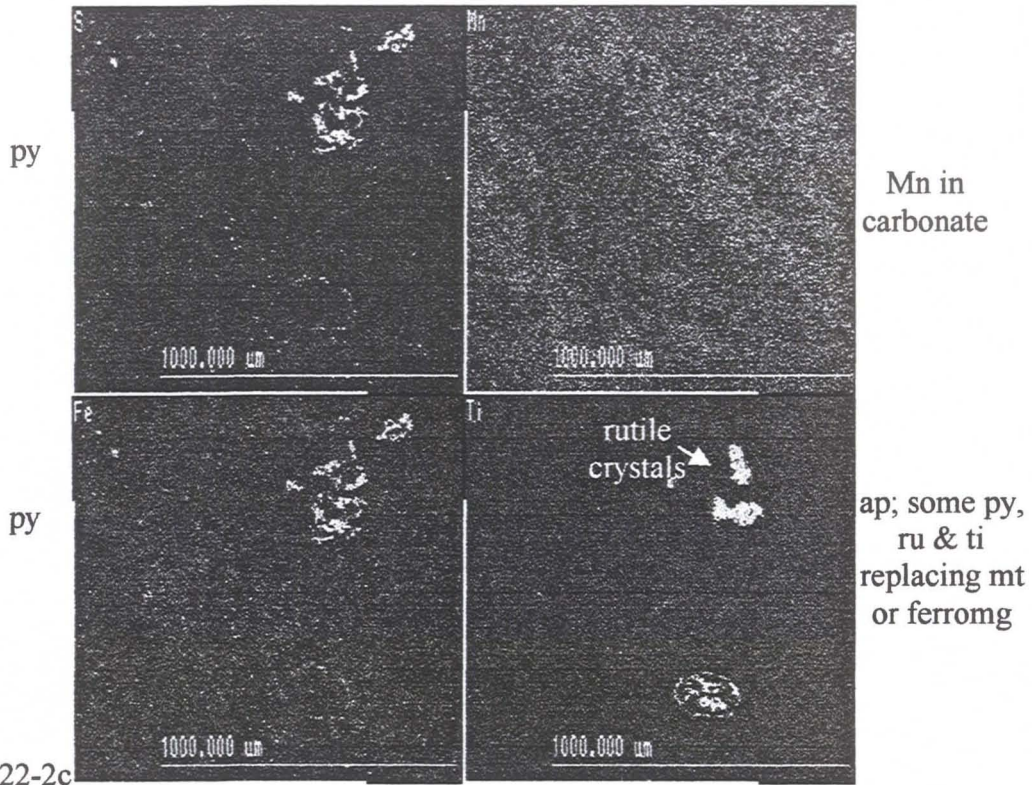
py

Mn in
carbonate

py

rutile
crystals

ap; some py,
ru & ti
replacing mt
or ferromg

RB9822-2c

MP 770a

Sample RB9822-2, Rhyodacite, background zone, Valdivia Sur.
Sample MP 770, Rhyodacitic dyke, pyrite zone, Valdivia Sur.

qz in
ab in
vugs

chl in
ab

cal in
vugs

ap

MP 770b

rutile
+
titanite

MP 770c

Sample MP 770, Rhyodacitic dyke, pyrite zone, Valdivia Sur.

ab phen
no zoning

RB9811a

qz vns

chl vns

ap in ab

RB9811b

Sample RB9811, Rhyodacite, chalcopyrite-pyrite zone, Valdivia Sur.

py x

chl vns

RB9811c

kfd in
ab
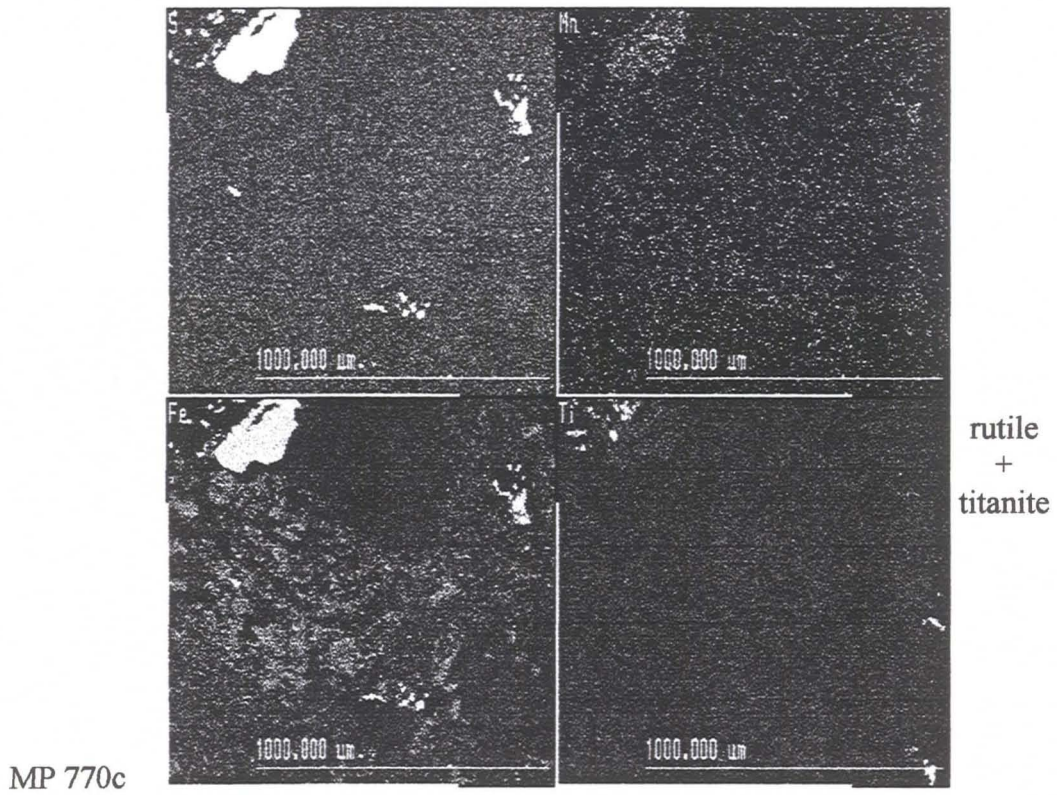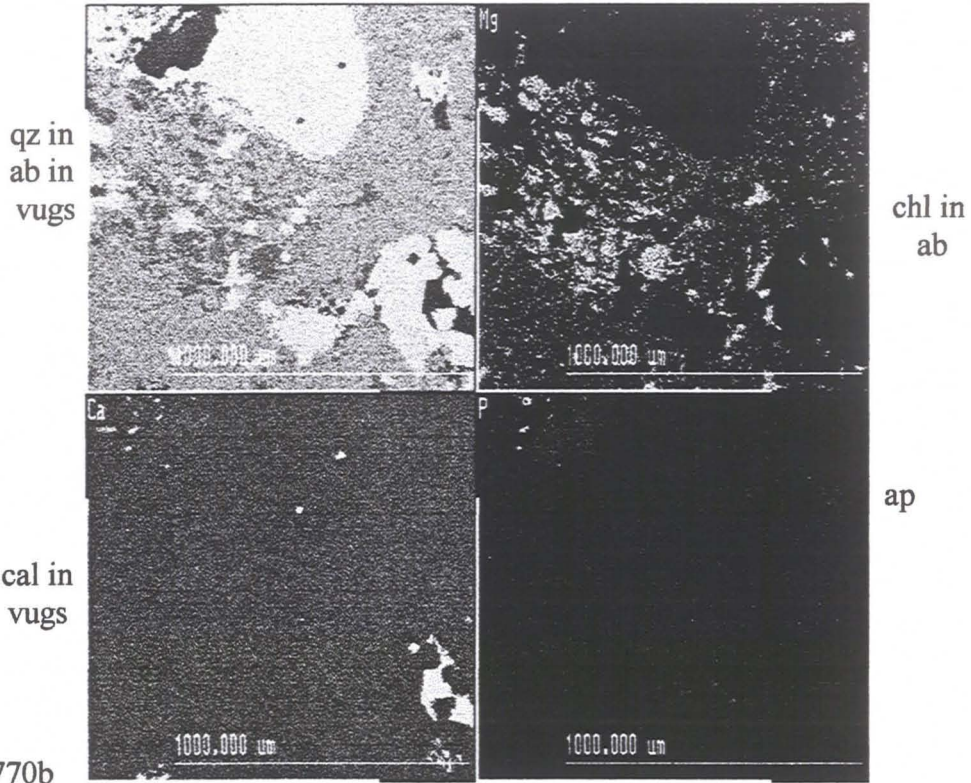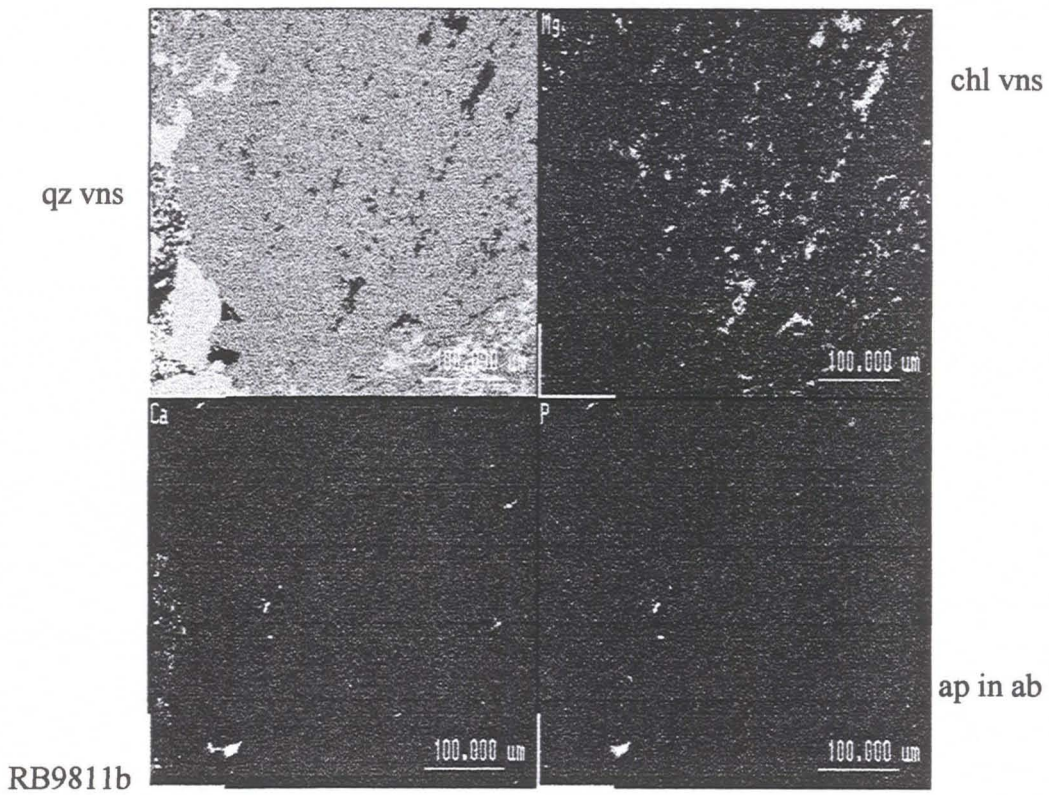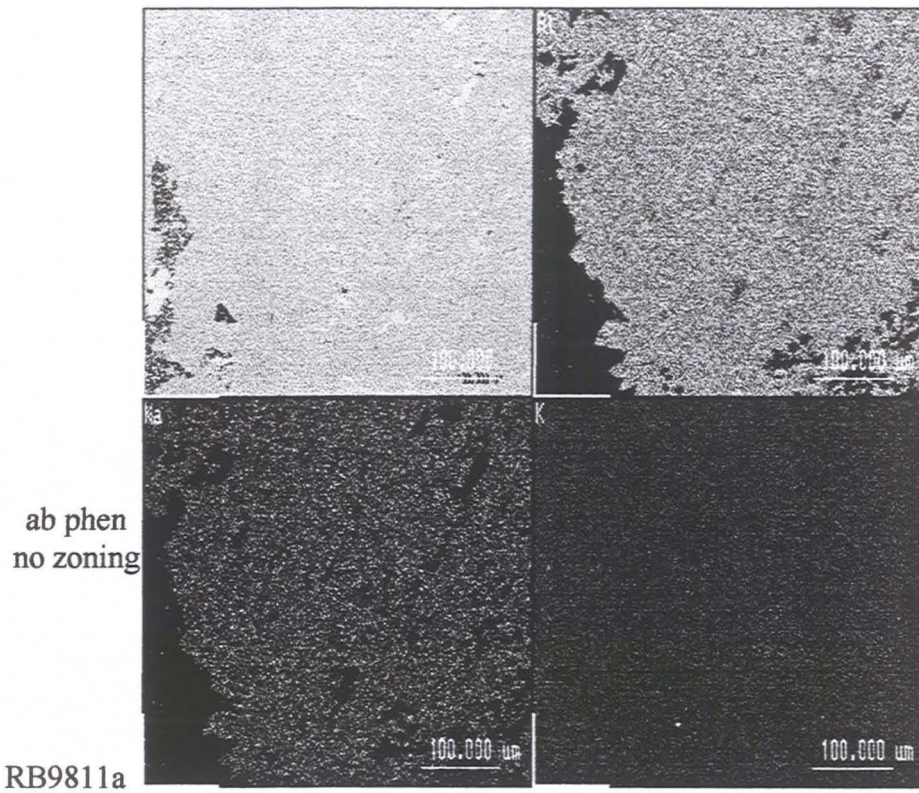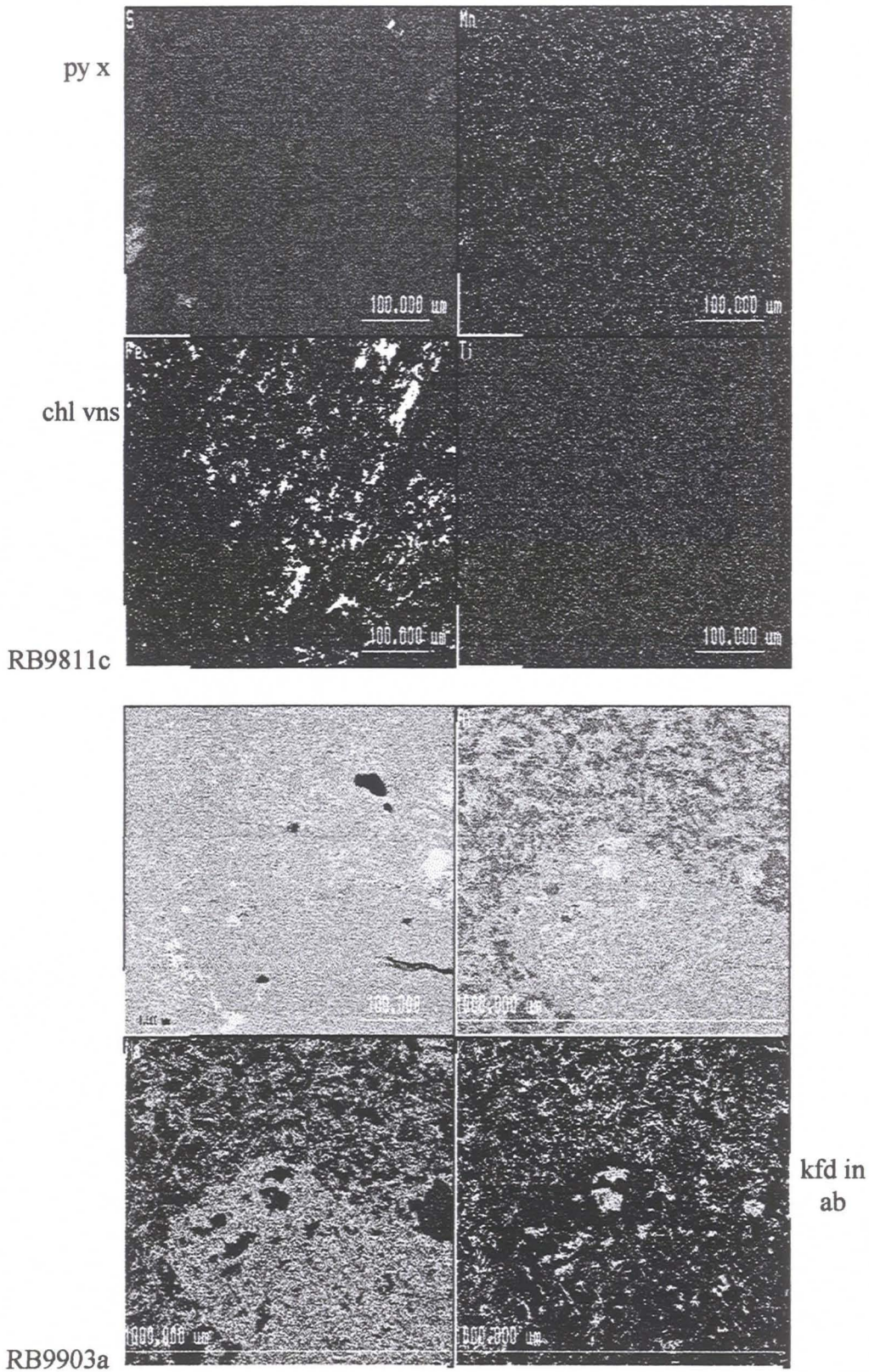
RB9903a

Sample RB9811, Rhyodacite, chalcopyrite-pyrite zone, Valdivia Sur.
Sample RB9903, Rhyodacite, chalcopyrite-pyrite zone, Morro.

qz in ab

Mg

Ca

P

ap in gm

cal sur.
ab phen

RB9903b

S

Mn

sulfides
(py-cp)
in gm
& ab
phen

Fe

Ti
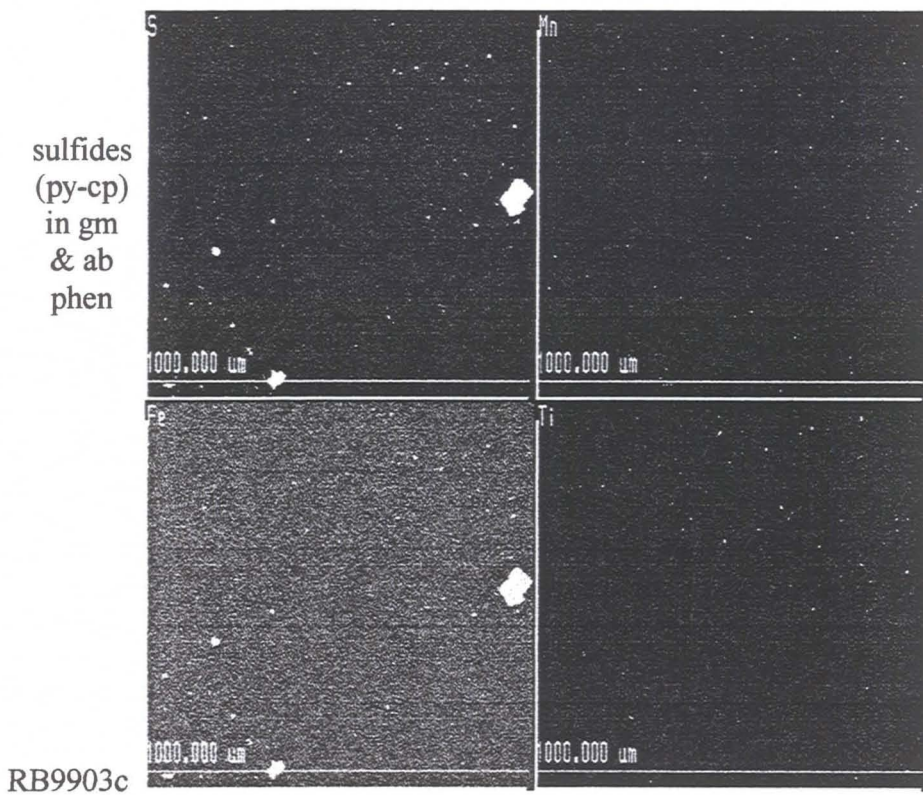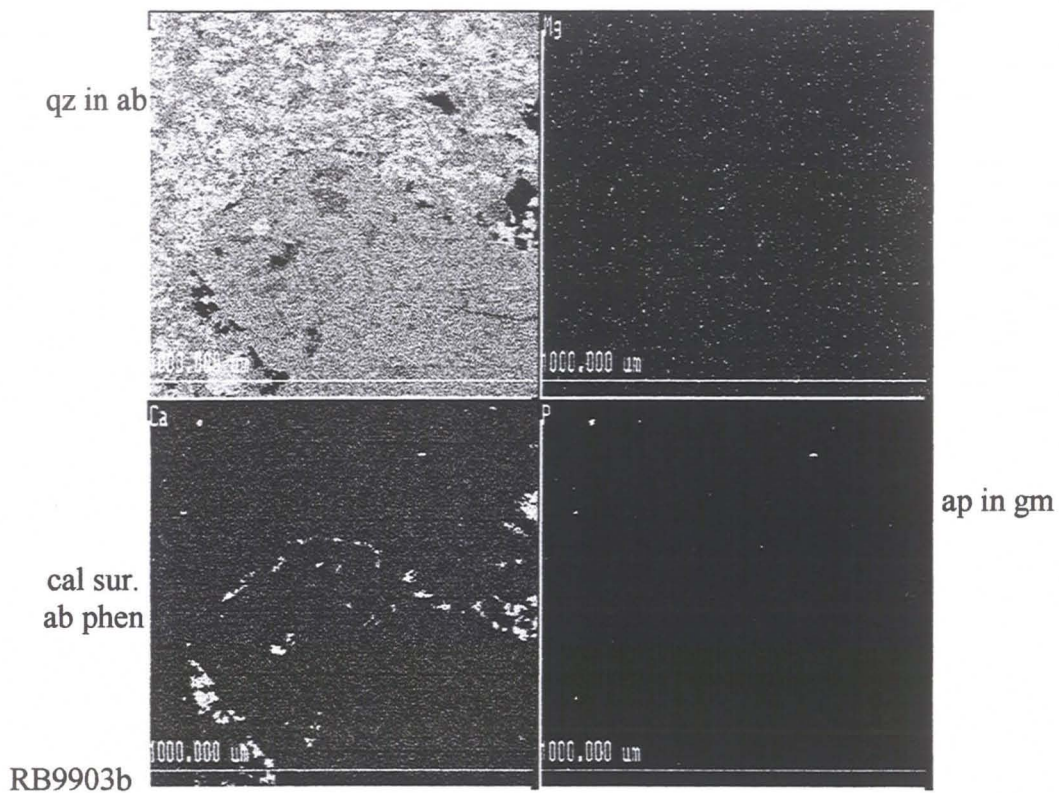
RB9903c

Sample RB9903, Rhyodacite, chalcopyrite-pyrite zone, Morro.

Sample RB9815, Rhyodacite, bornite-chalcocite zone, Valdivia Sur.
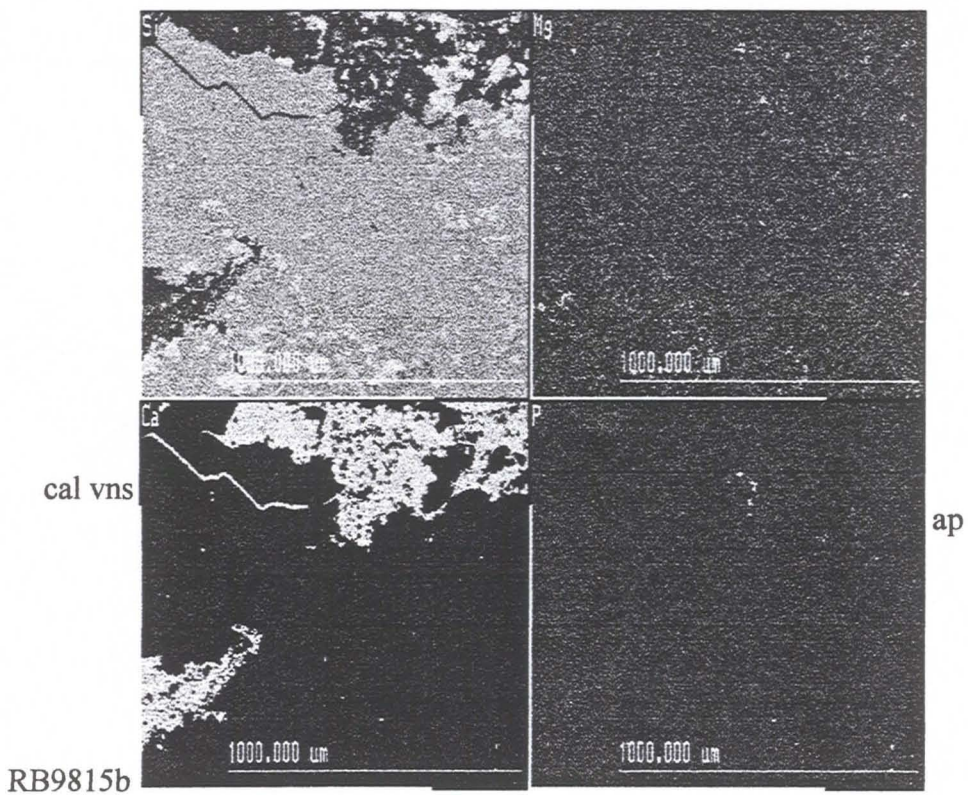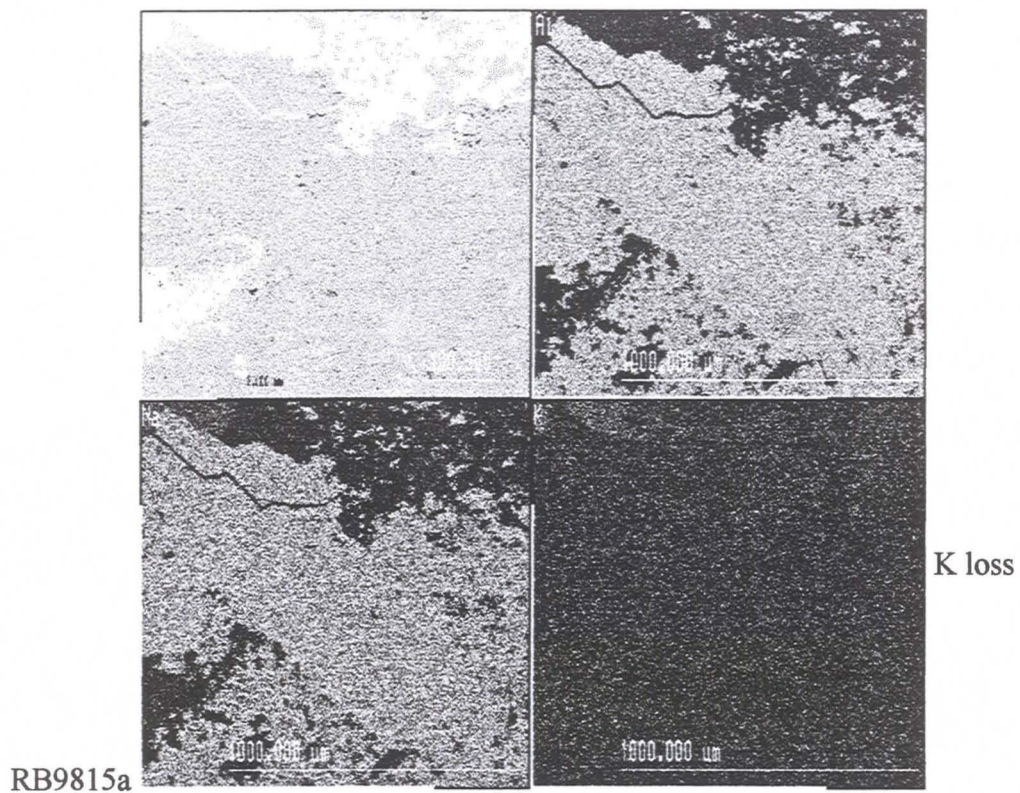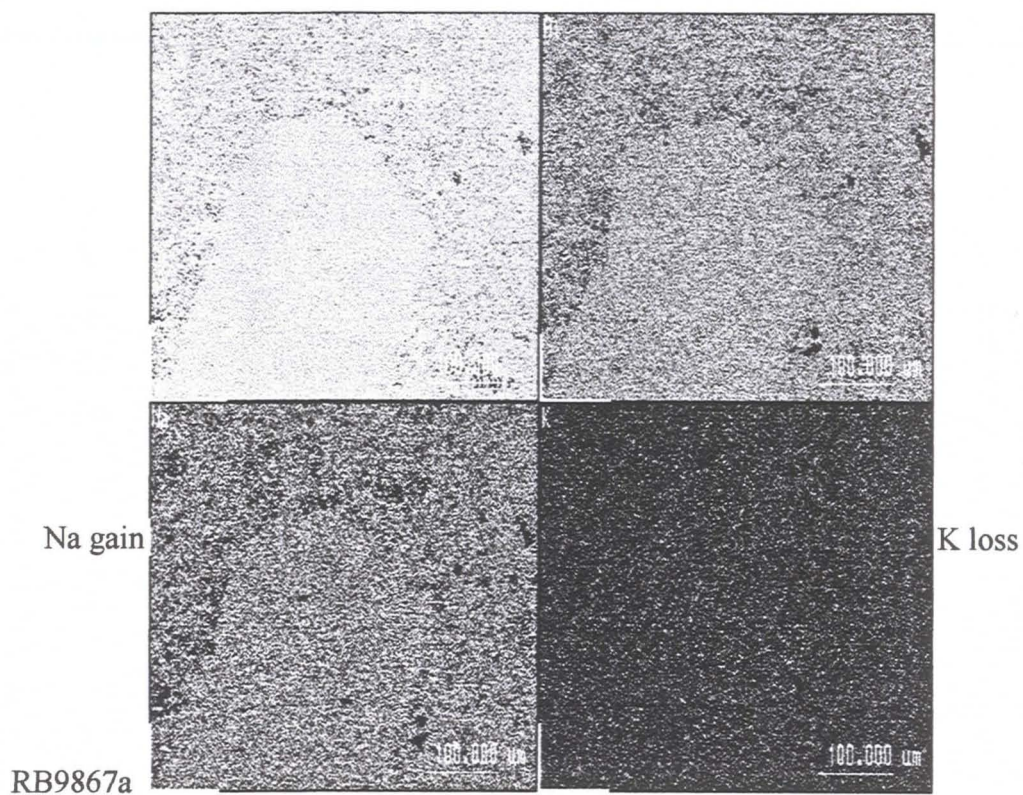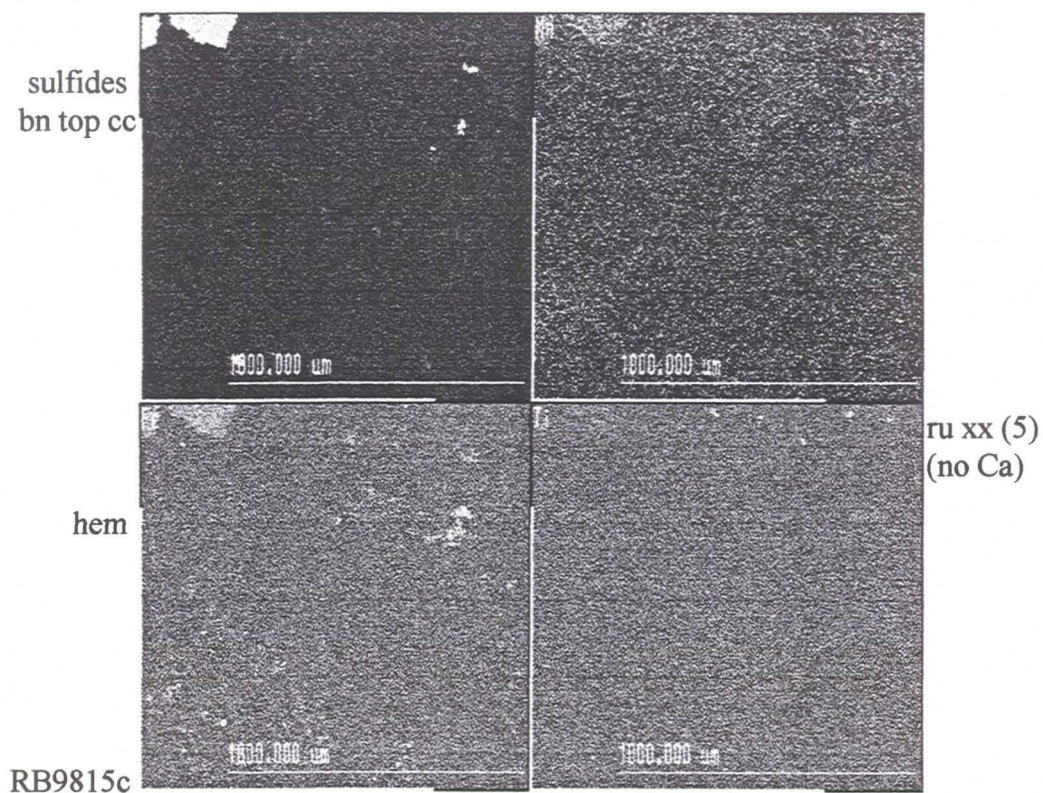
297

Sample RB9815, Rhyodacite, bornite-chalcocite zone, Valdivia Sur.
Sample RB9867, Rhyodacite, bornite-chalcocite zone, Valdivia Sur.
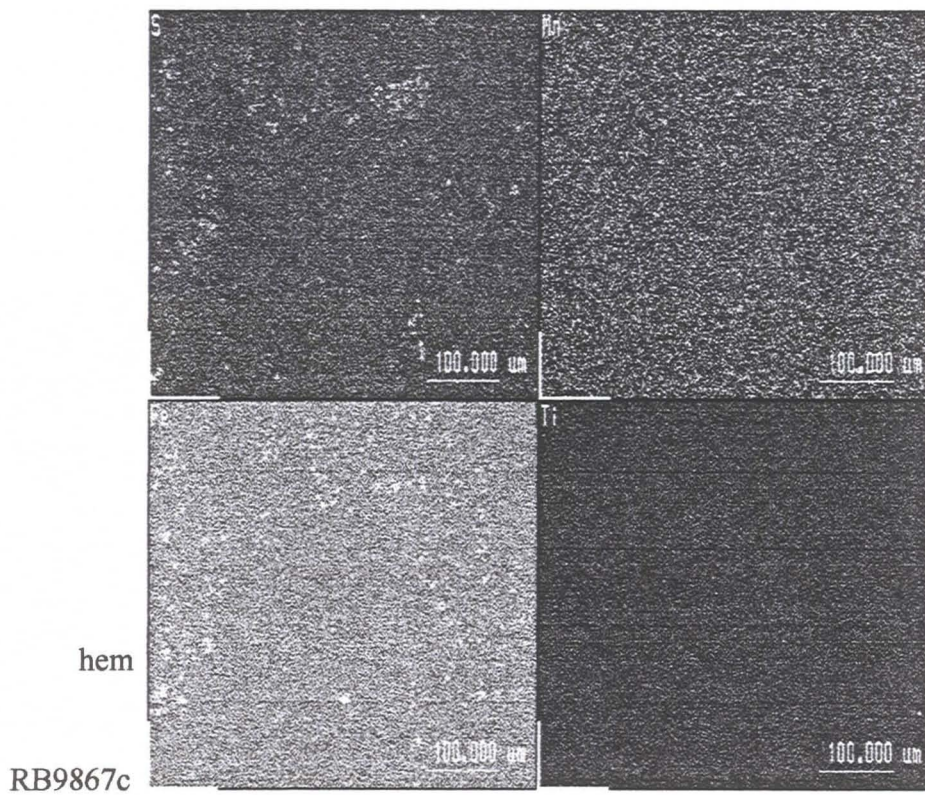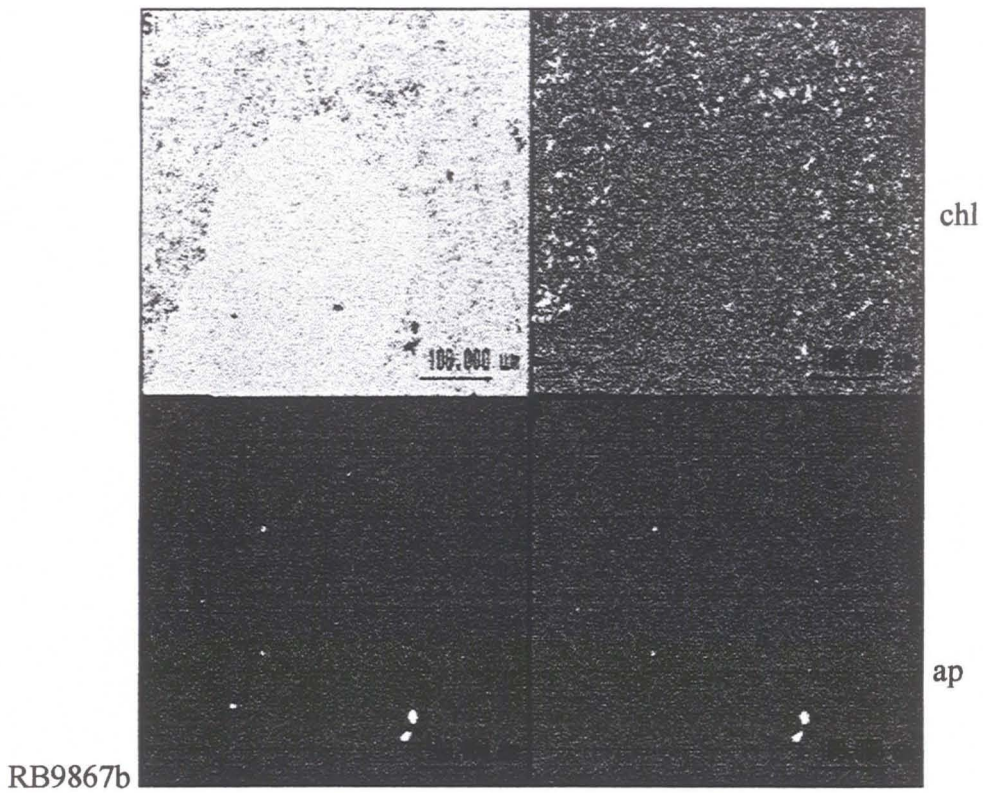
RB9867b

chl

ap

hem

RB9867c

Sample RB9867, Rhyodacite, bornite-chalcocite zone, Valdivia Sur.

ab vns

kfd
in gm

RB9901a

chl
vugs &
veinlets

ap

RB9901b

Sample RB9901, Rhyodacite, bornite-chalcocite zone, Valdivia Sur.

300
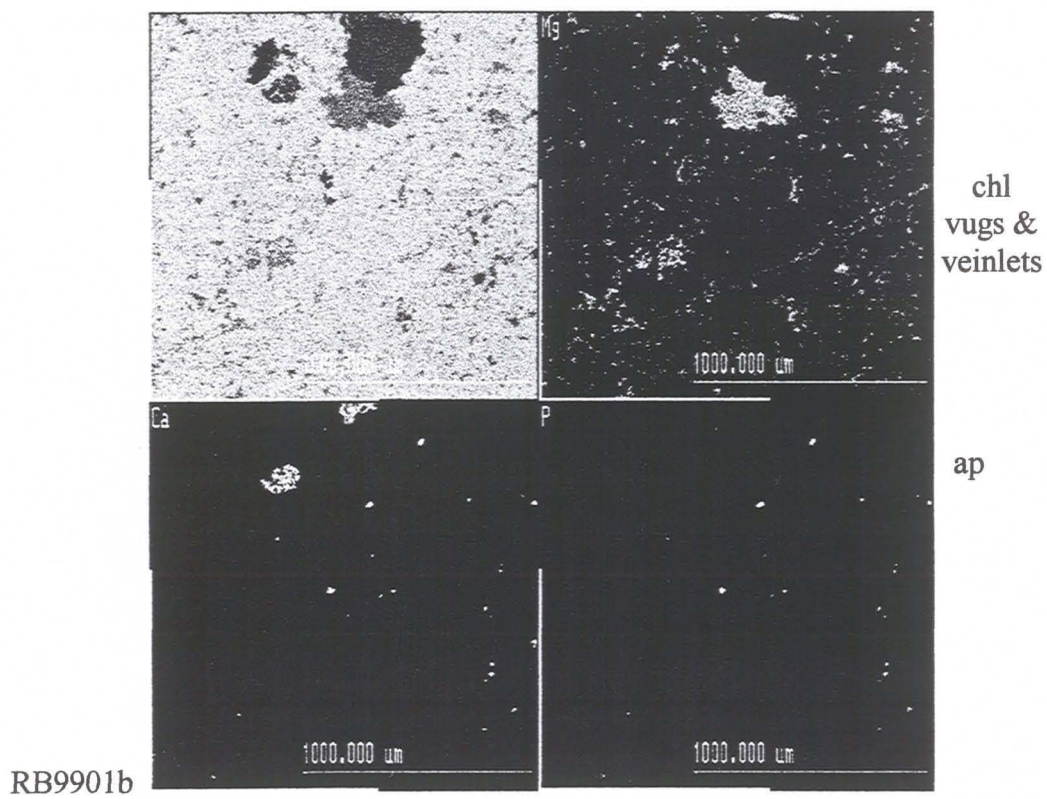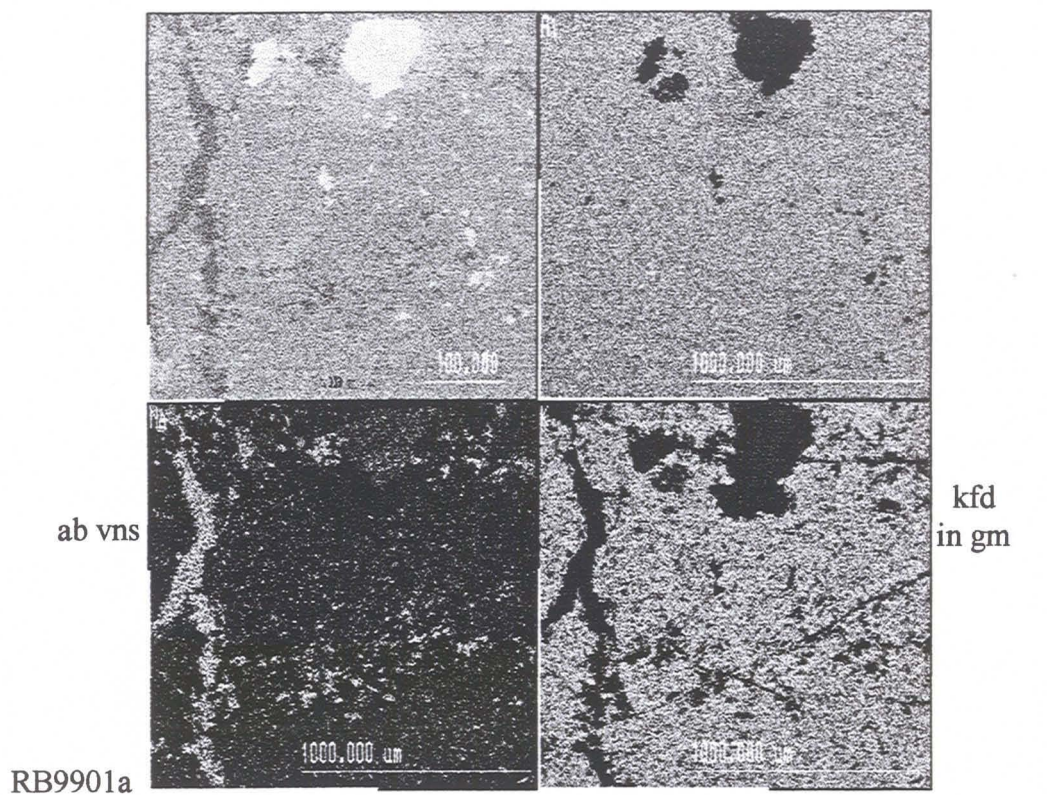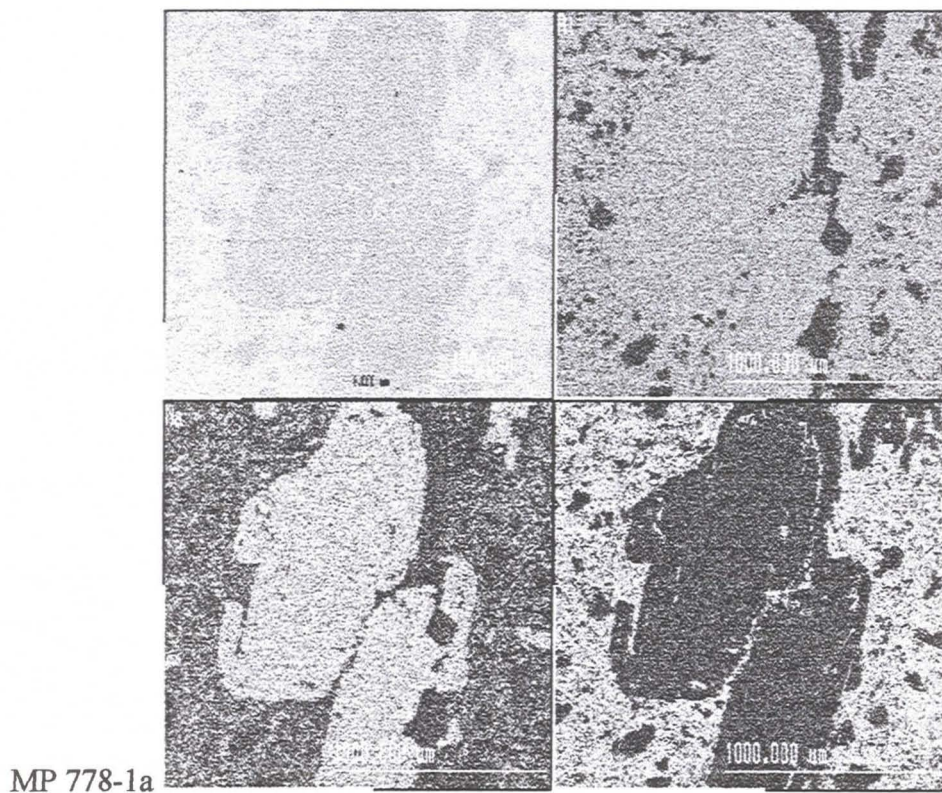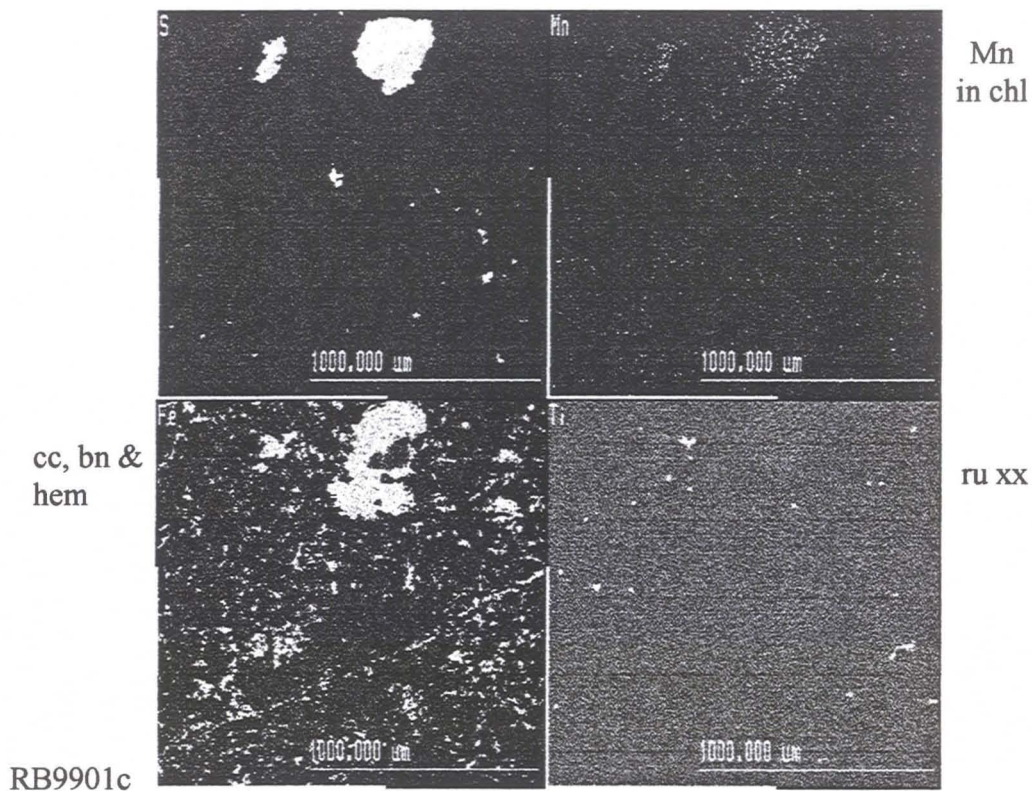
Sample RB 9901, Rhyodacite, bornite-chalcocite zone, Valdivia Sur.
Sample MP 778-1, Rhyodacite, bornite-chalcocite zone, Valdivia Sur.

qz vns
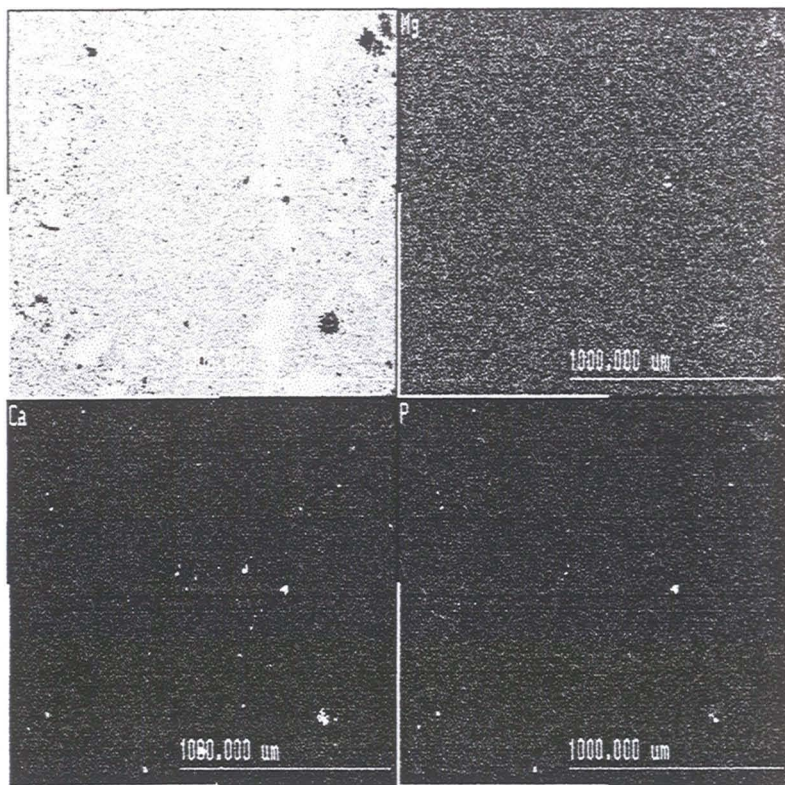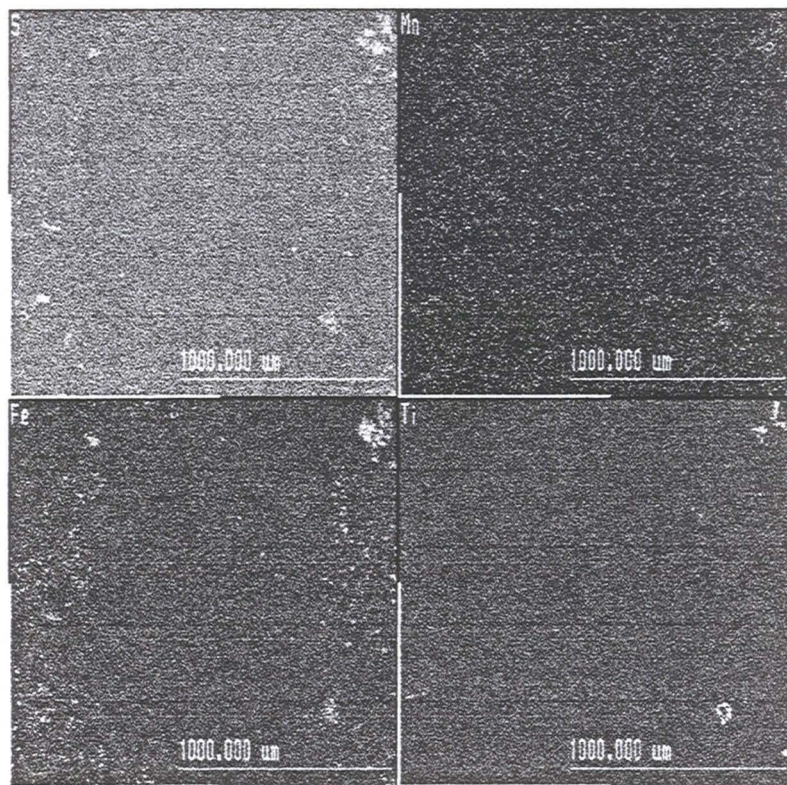
ap

MP 778-1b

ru

MP 778-1c

Sample MP 778-1, Rhyodacite, bornite-chalcocite zone, Valdivia Sur.

MP 778-2a

MP 778-2b

Sample MP 778-2, Rhyodacite, bornite-chalcocite zone, Valdivia Sur.

cc vn
bn-cc

rare ru

MP 778-2c

Sample MP 778-2, Rhyodacite, bornite-chalcocite zone, Valdivia Sur.

ab in gm
& pg

mc in pg

K
almost
all in pg

RB9829a

chl in pg, gm
& Femg or
amgd

no ap

cal in pg
& gm

RB9829b

Sample RB9829, Basalt, background zone, Valdivia Sur.

no py

ep in pg

hem in
Femg

RB9829c

Ti-not in gm
poss ru or
sphene
in gm

ab in gm
an in Fe x

mc in gm

RB9842a

Sample RB9829, Basalt, background zone, Valdivia Sur.
Sample RB9842, Basalt, background zone, Filo.

chl in
FeMg

chl in
pg

cal in
FeMg

no ap !

RB9842b

no py

Fe in
border
of aug

ti-mt

RB9842c

Sample RB9842, Basalt, background zone, Filo.

albitization

RB9806a

ser in pg

kfd in pg

chl in gm

chl in pg

cal +chl
+sph
replacing
FeMg
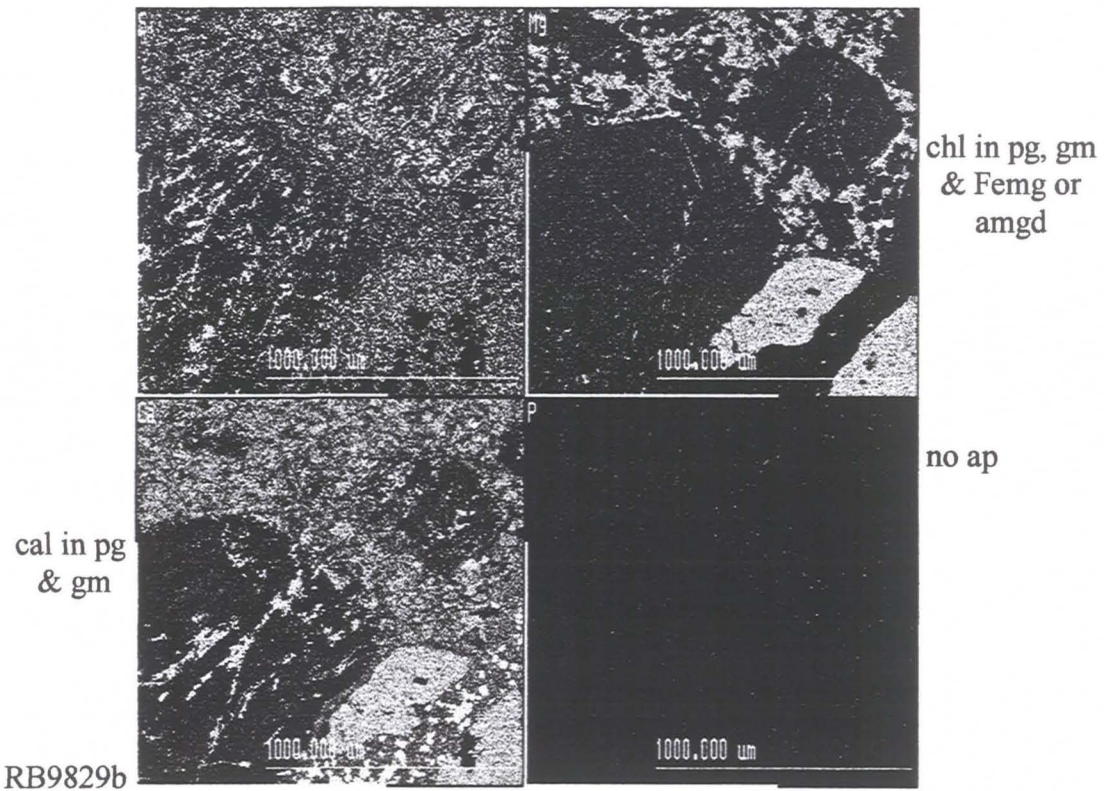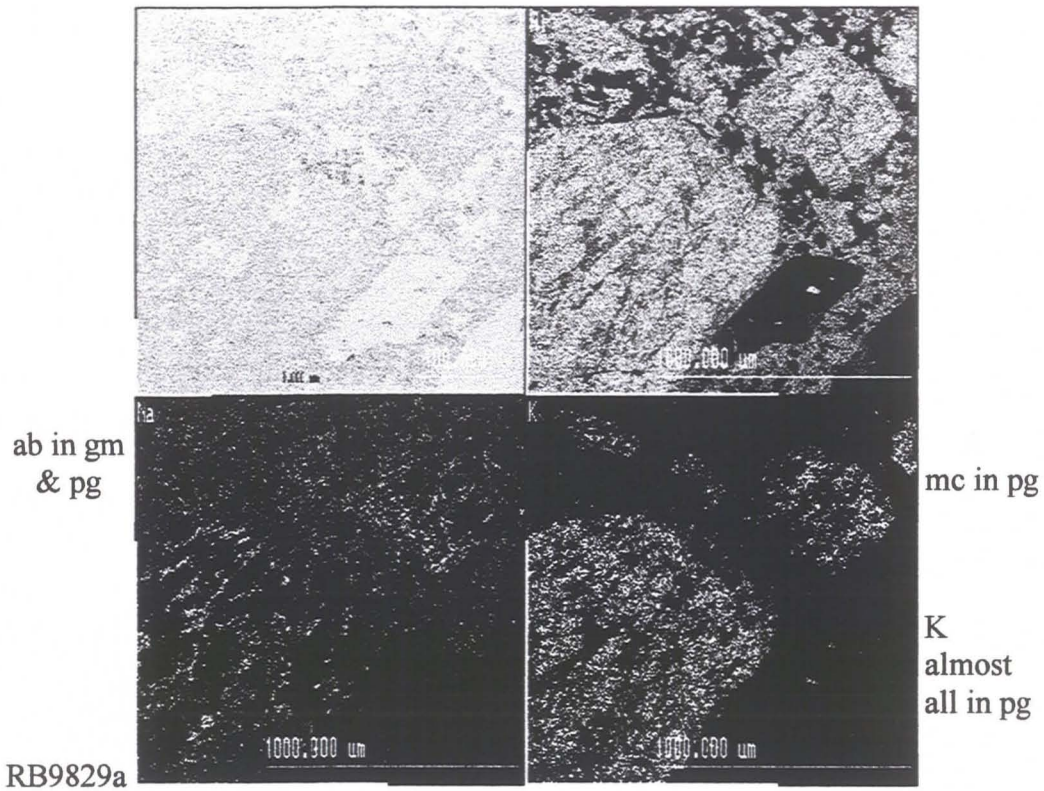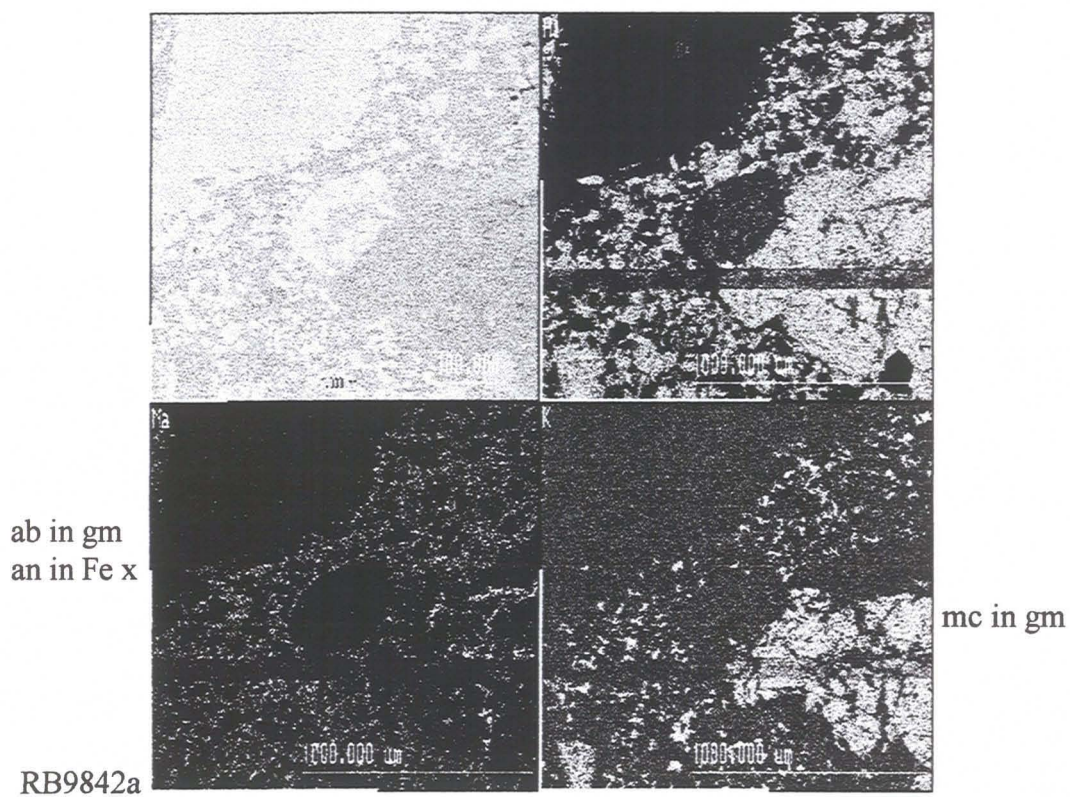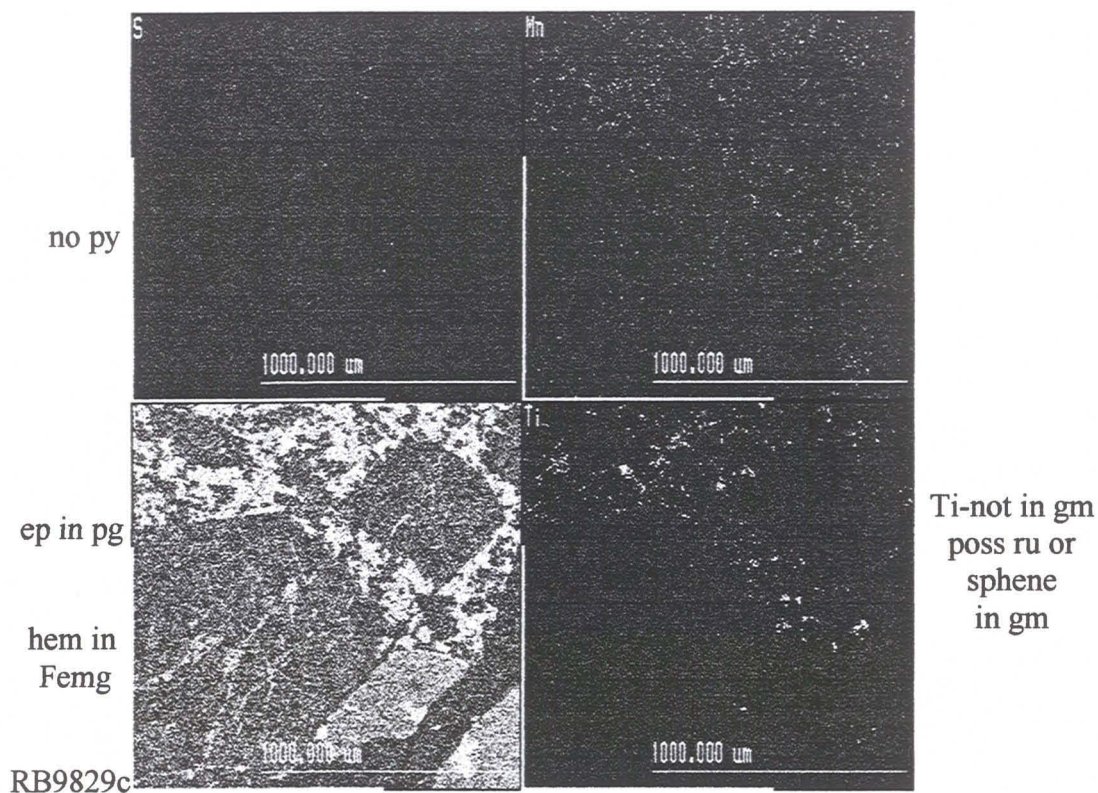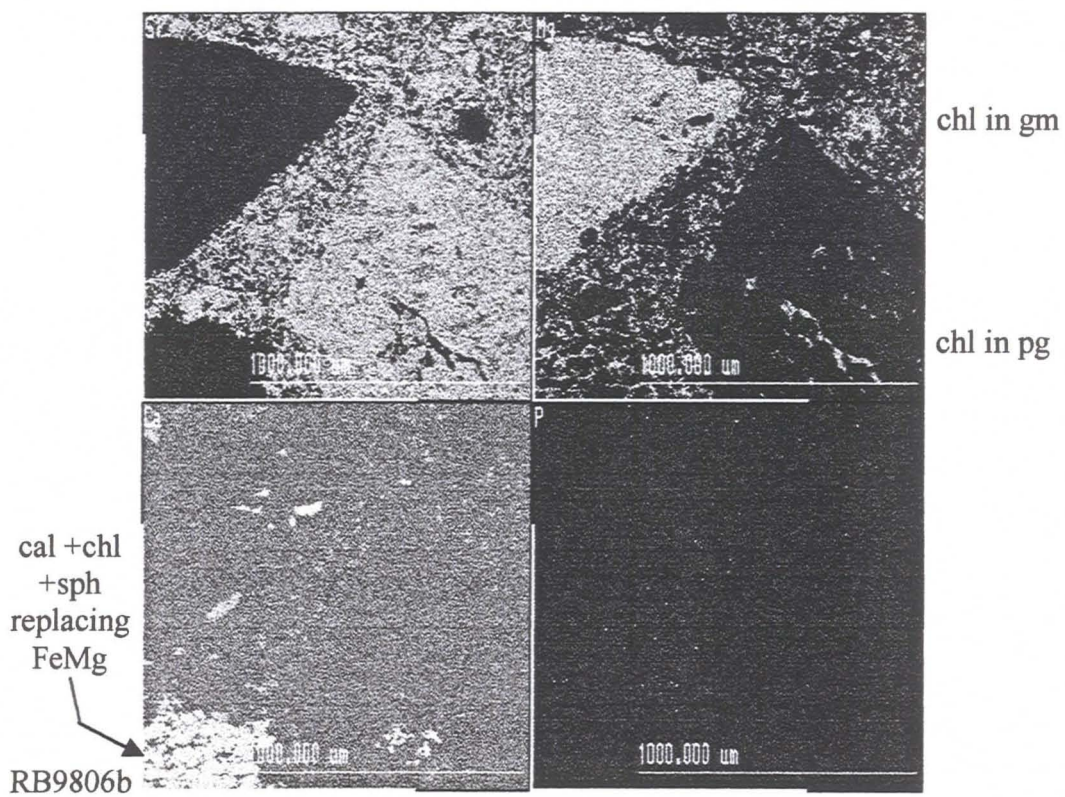
RB9806b

Sample RB9806, Basalt, pyritic background zone, Valdivia Sur

py in gm
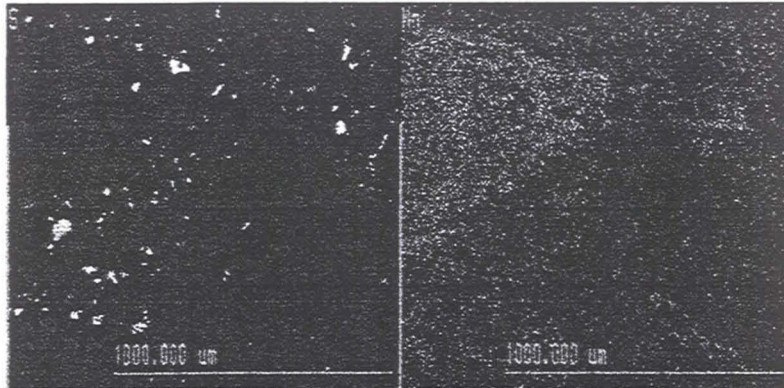
py +chl
replacing
FeMg
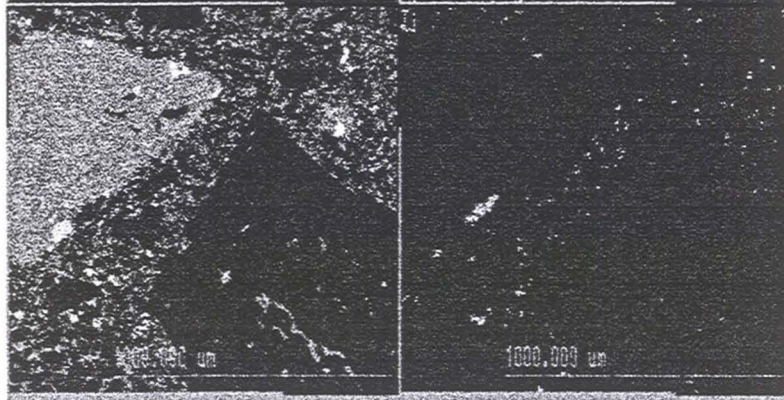
sphene in
border of
FeMg

poss ti-mt
or ru?

RB9806c
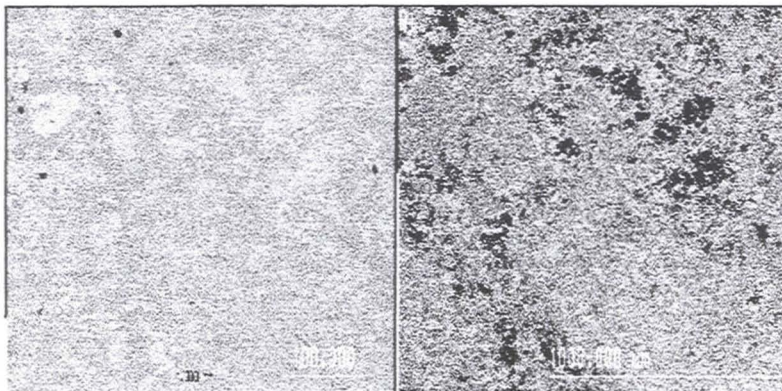
ab in
rims
of gm
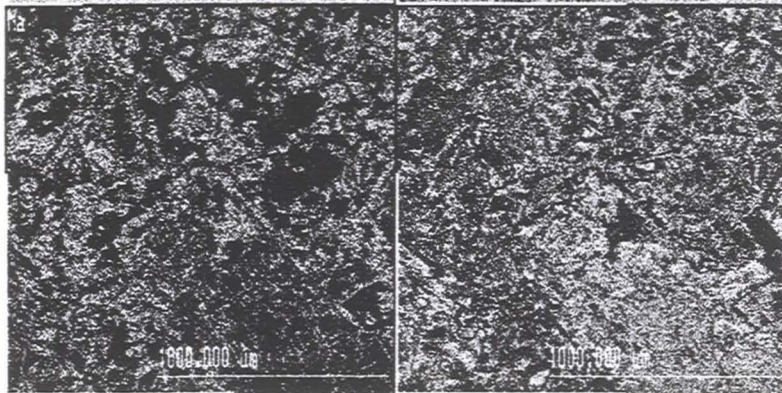
MP 865a

Sample RB9806, Basalt, pyritic background zone, Valdivia Sur
Sample MP 865, Basalt, pyritic zone, Valdivia Sur
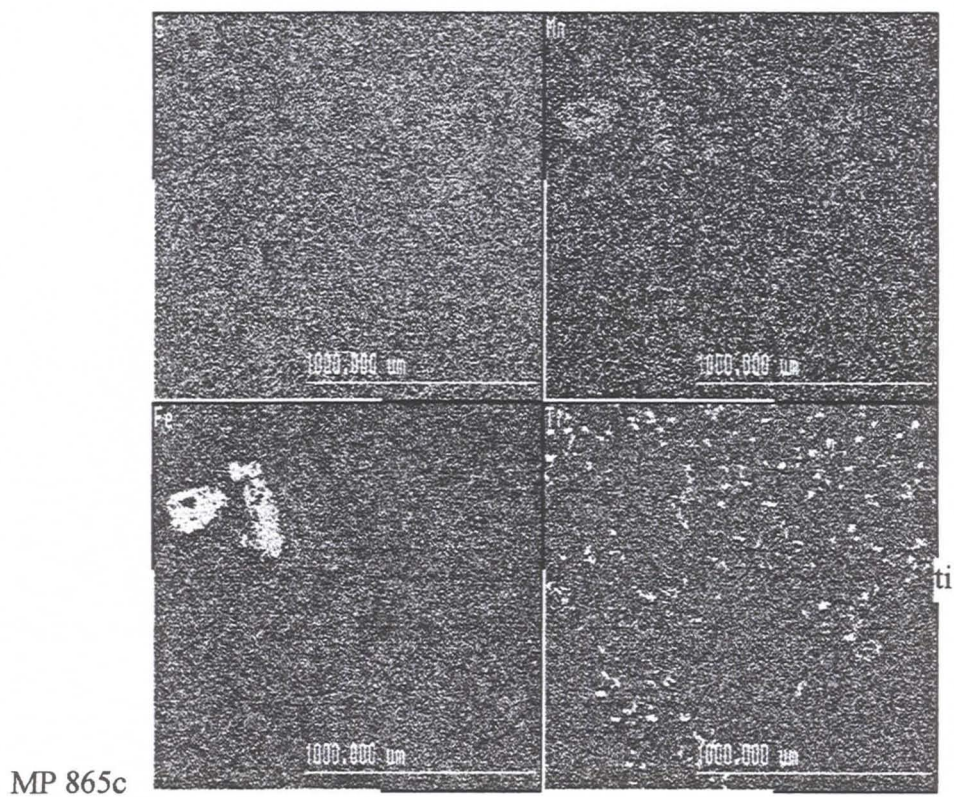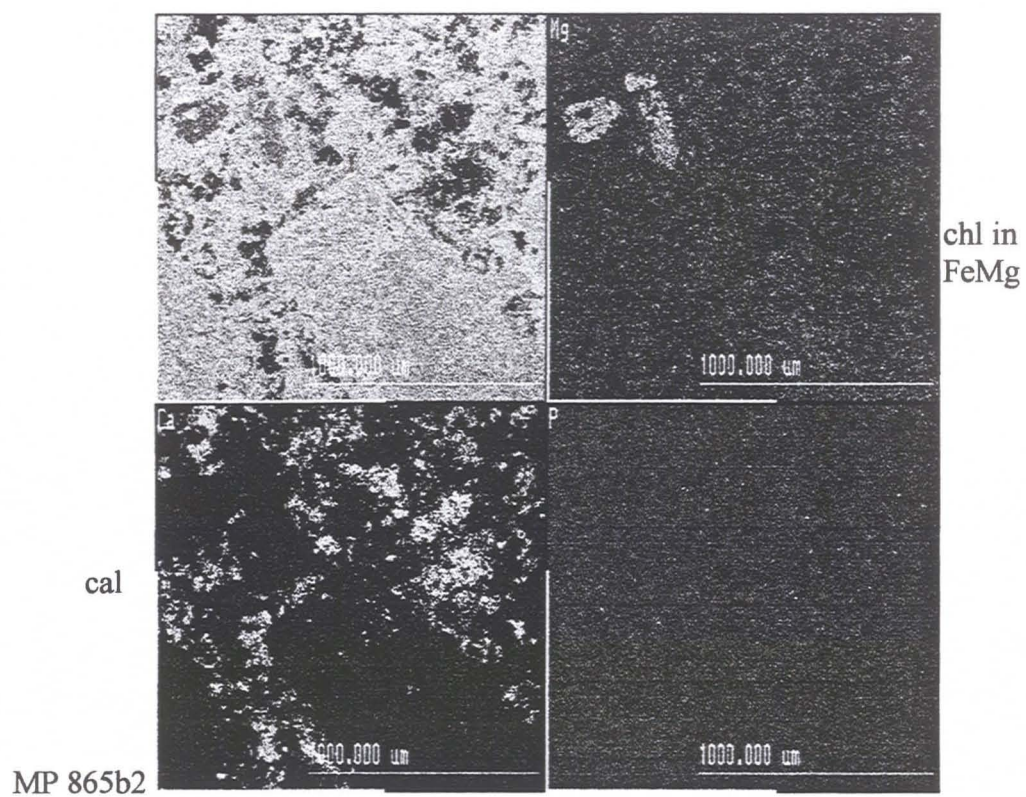
chl in FeMg

cal

MP 865b2

ti

MP 865c

Sample MP 865, Basalt, pyritic zone, Valdivia Sur

MP 786a

MP 786b
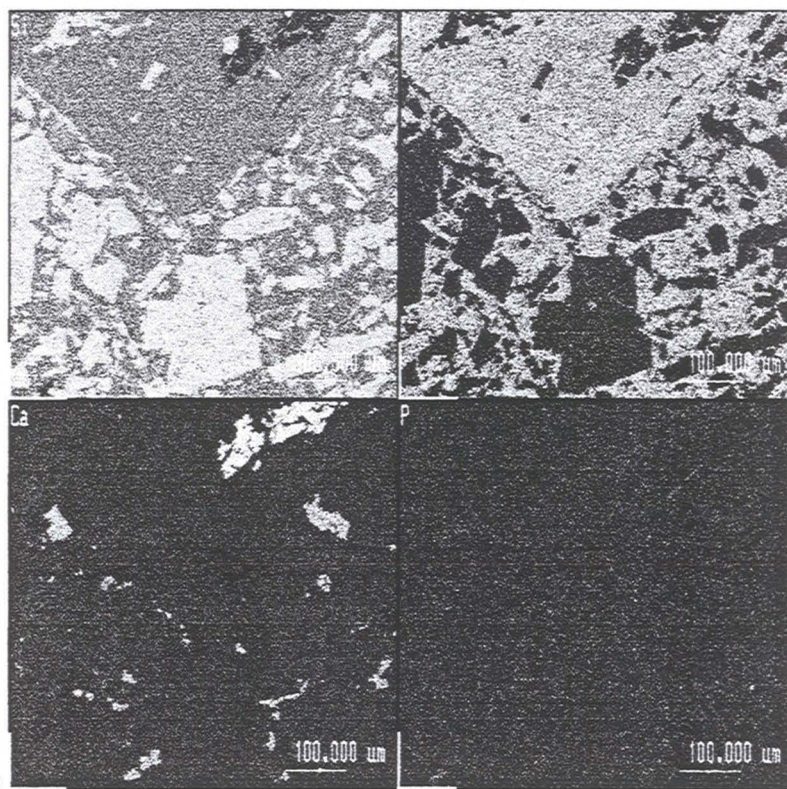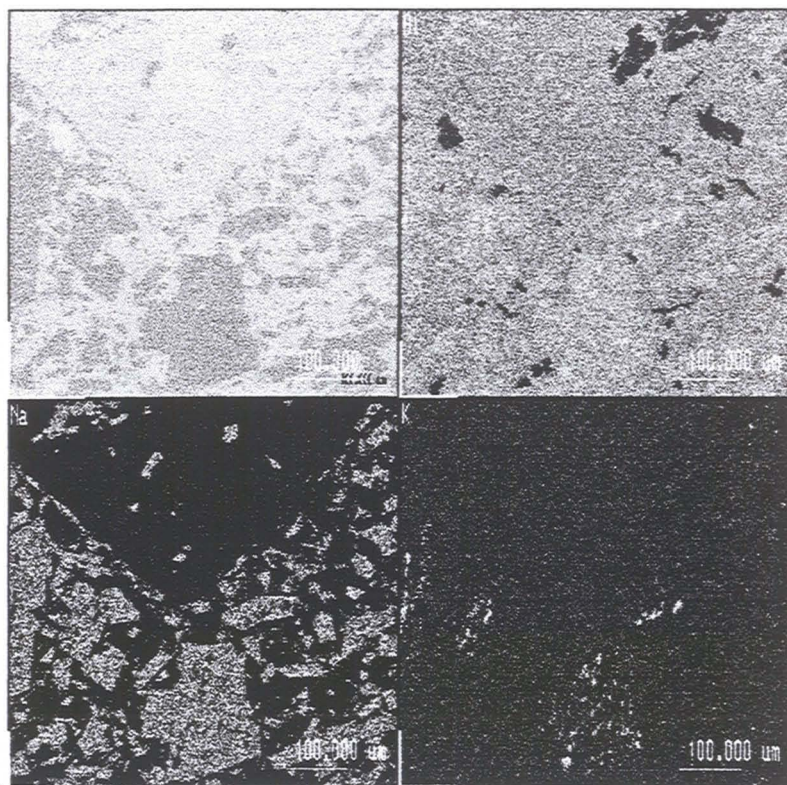
Sample MP 786, Basalt, chalcopyritic zone, Valdivia Sur
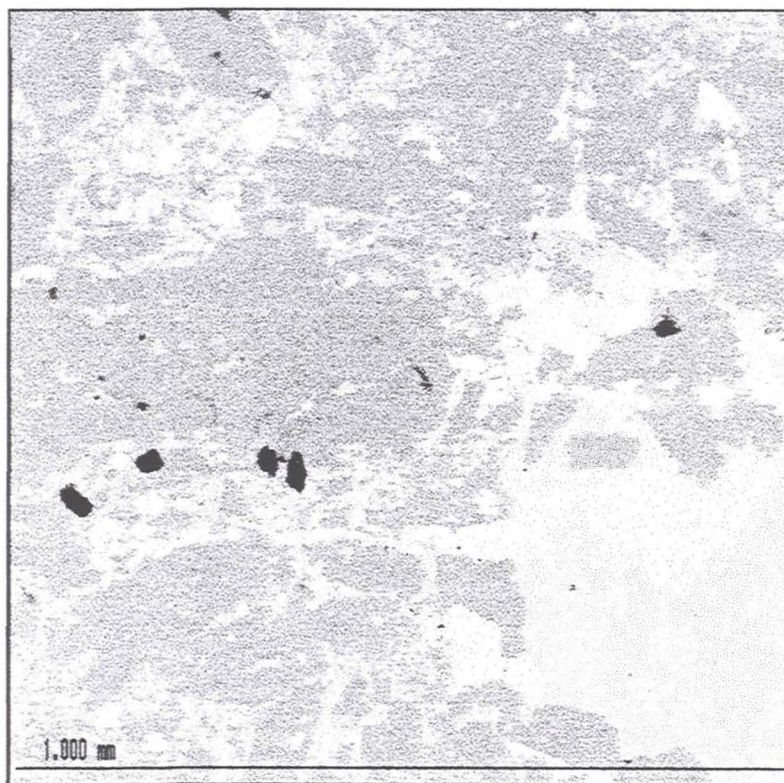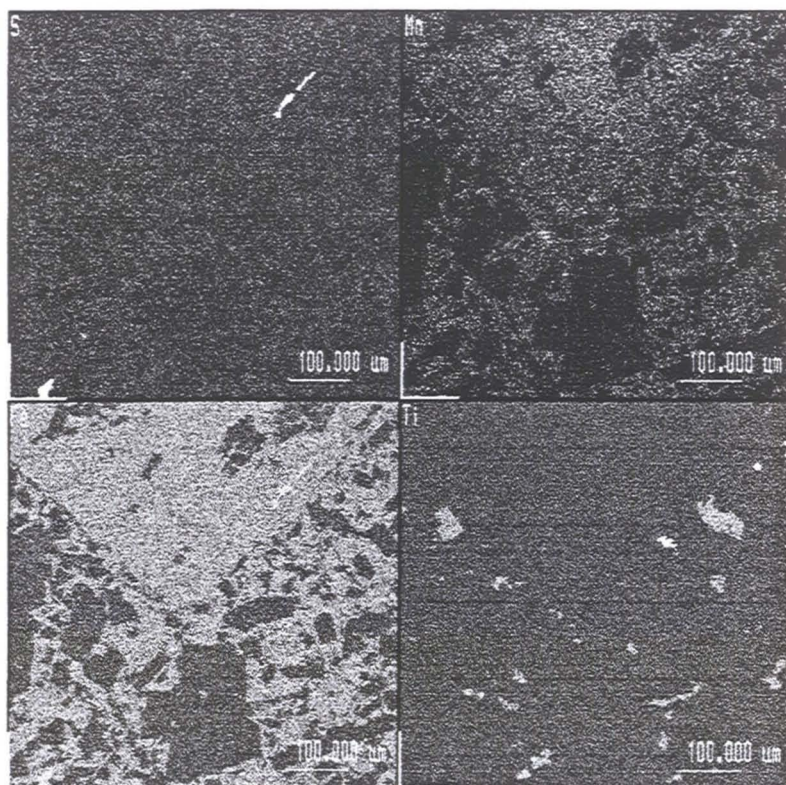
MP 786c

RB9852

Back Scatter Image
Sample MP 786, Basalt, chalcopyritic zone, Valdivia Sur.
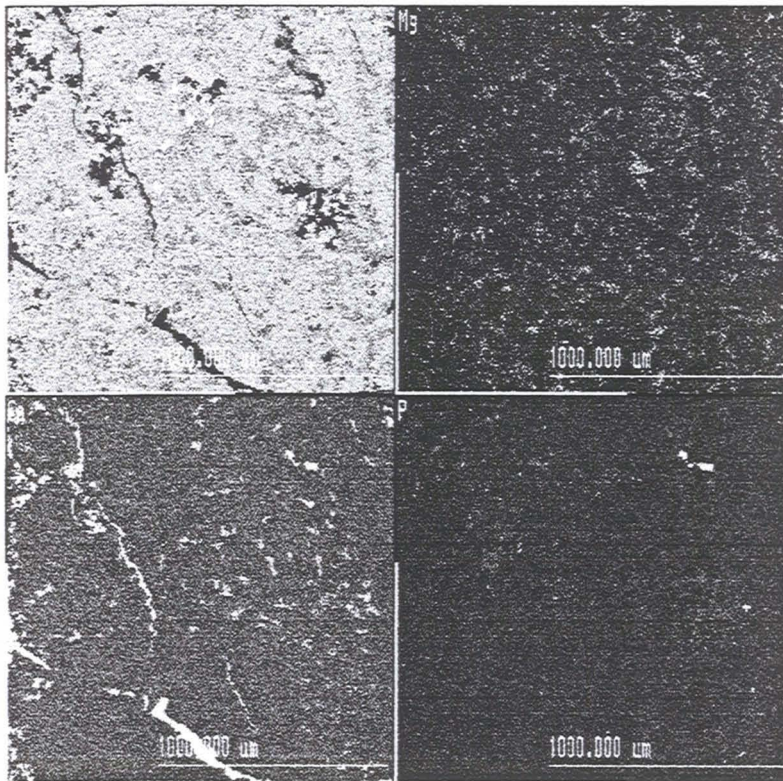Sample RB 9852, Basalt, bornite-chalcocite zone, Filo.
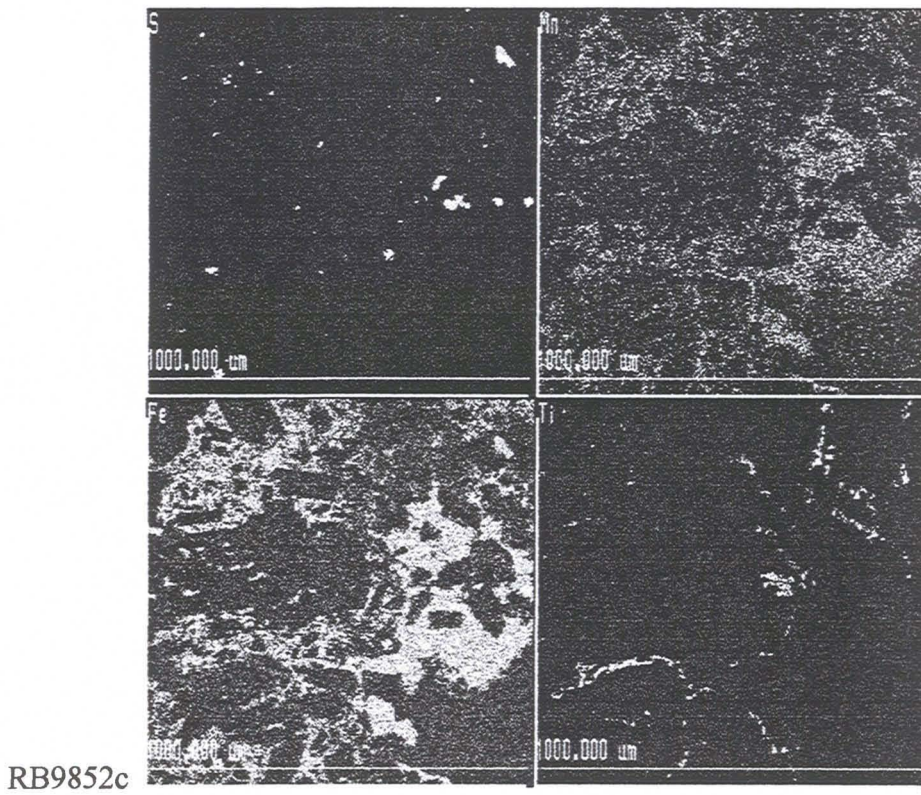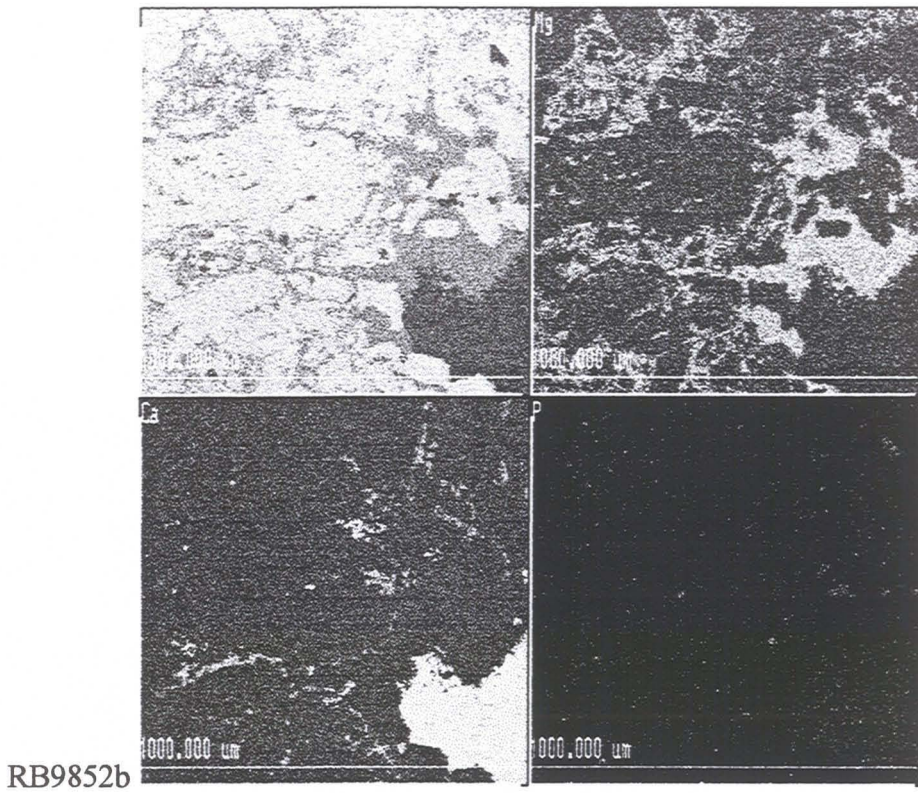
RB9852b

RB9852c

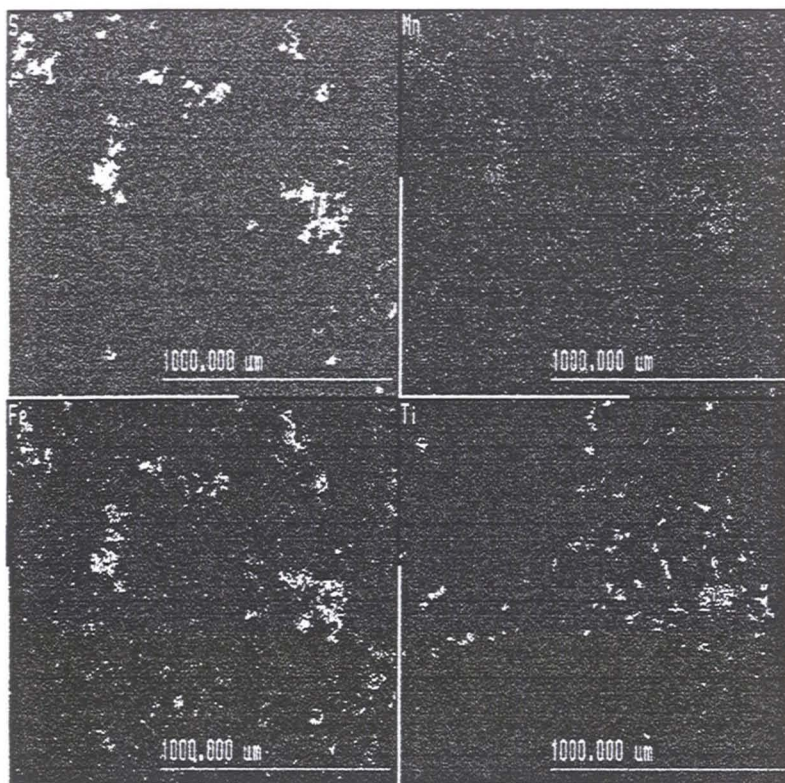Sample RB9852, Basalt, bornite-chalcocite zone, Filo.
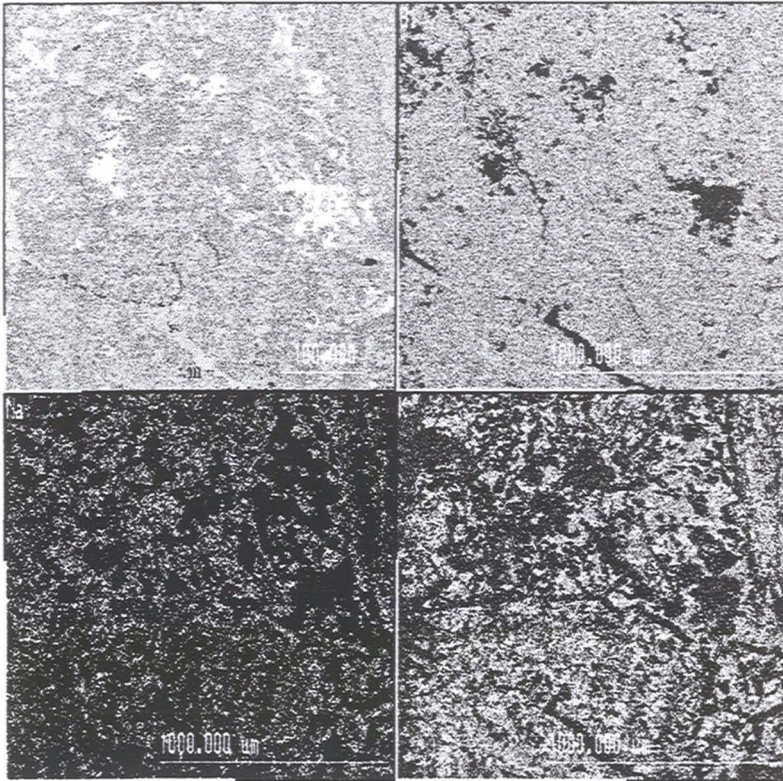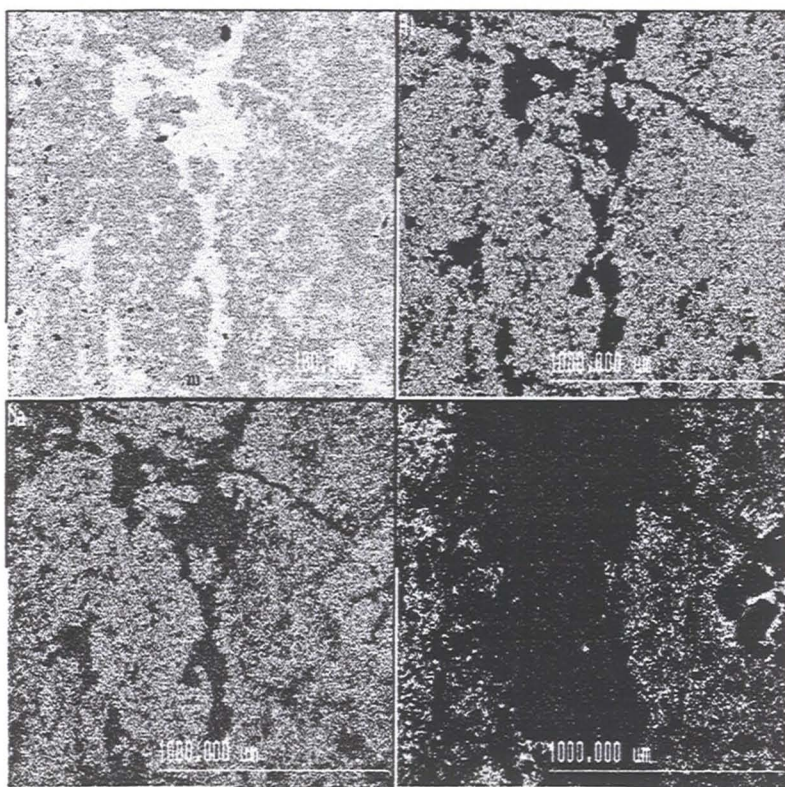
MP 772a

MP 772b

Sample MP 772, Basaltic dyke, chalcocite zone, Valdivia Sur.
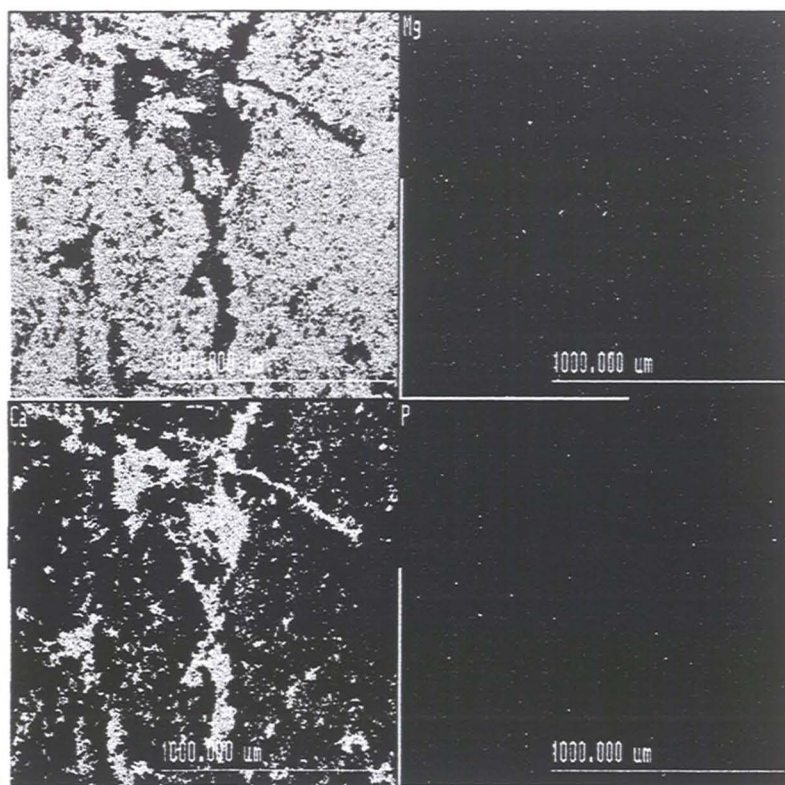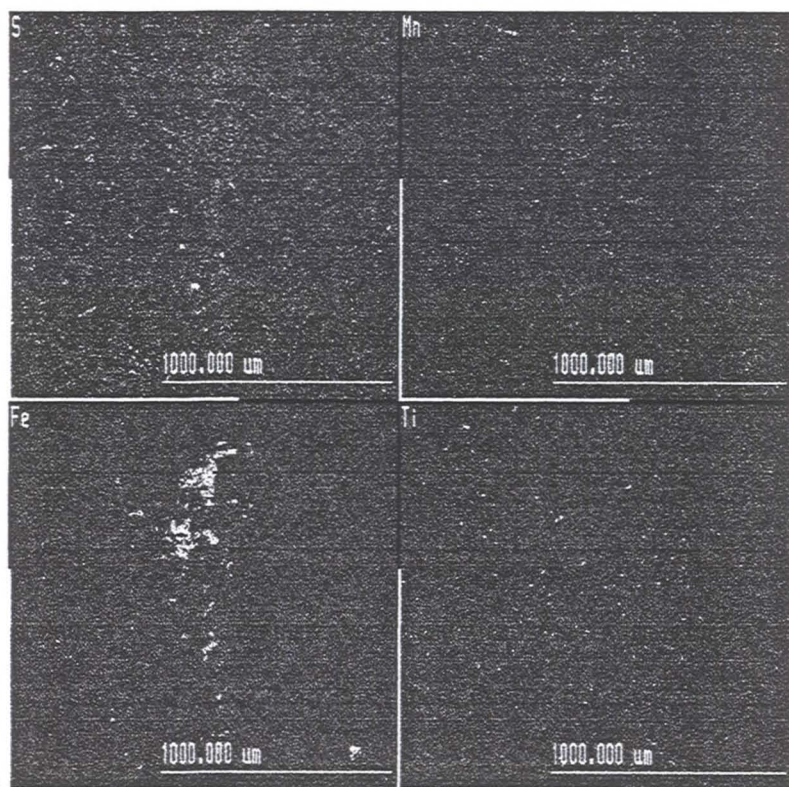
314

MP 772c

MP 840a

Sample MP 772, Basaltic dyke, chalcocite zone, Valdivia Sur.
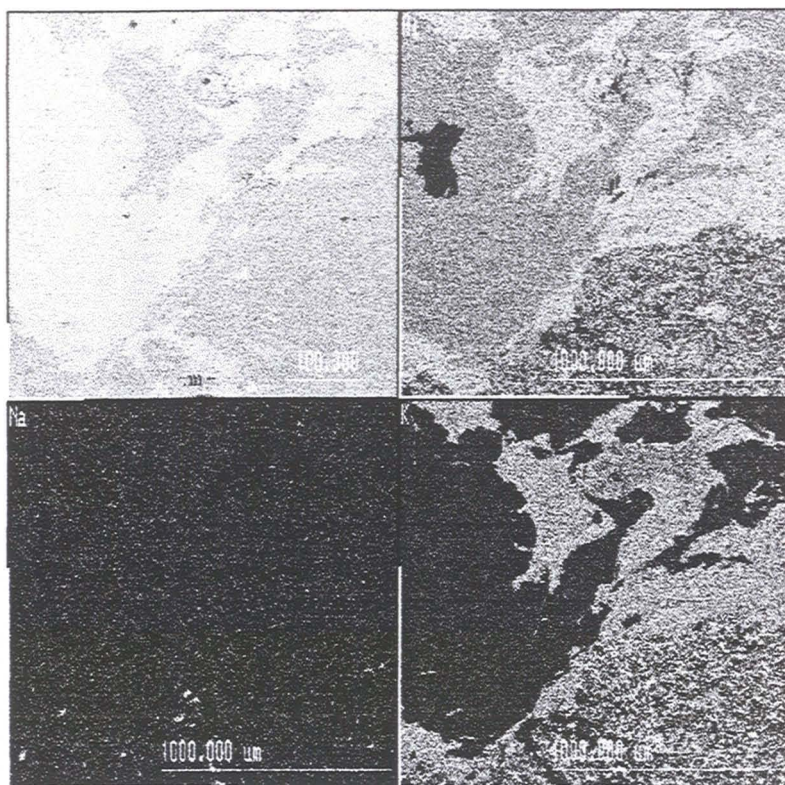Sample MP 840, Rhyodacite, in contact with basaltic dyke, Morro.

MP 840b

MP 840c

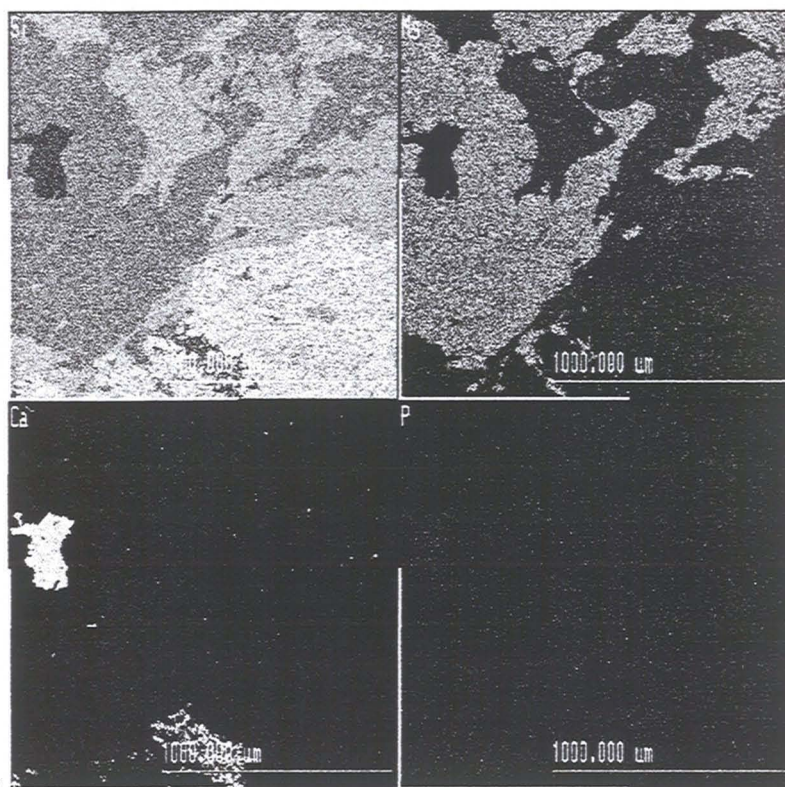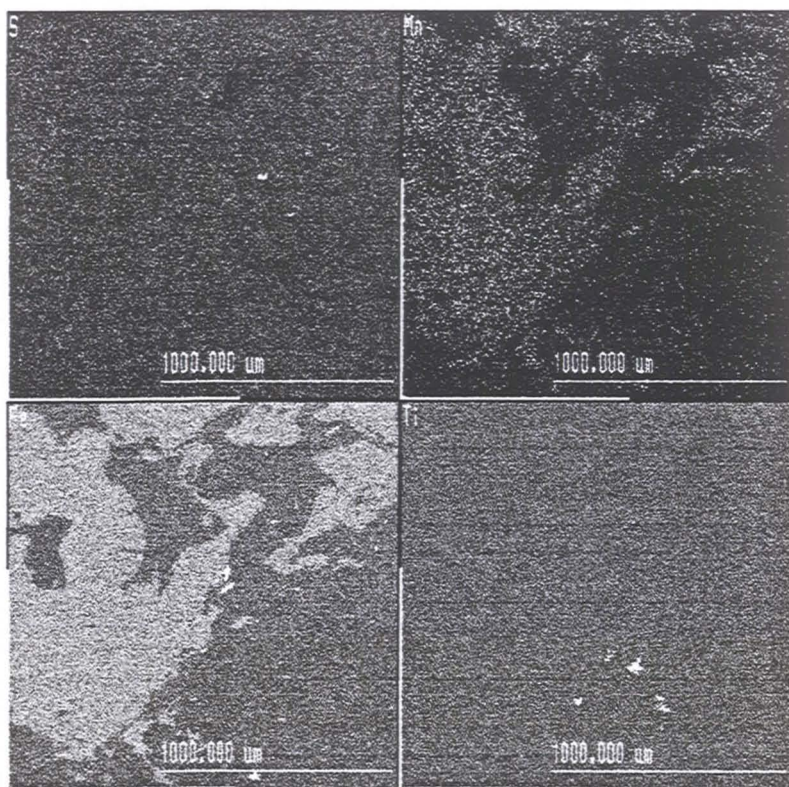Sample MP 840, Rhyodacite, in contact with basaltic dyke, Morro.
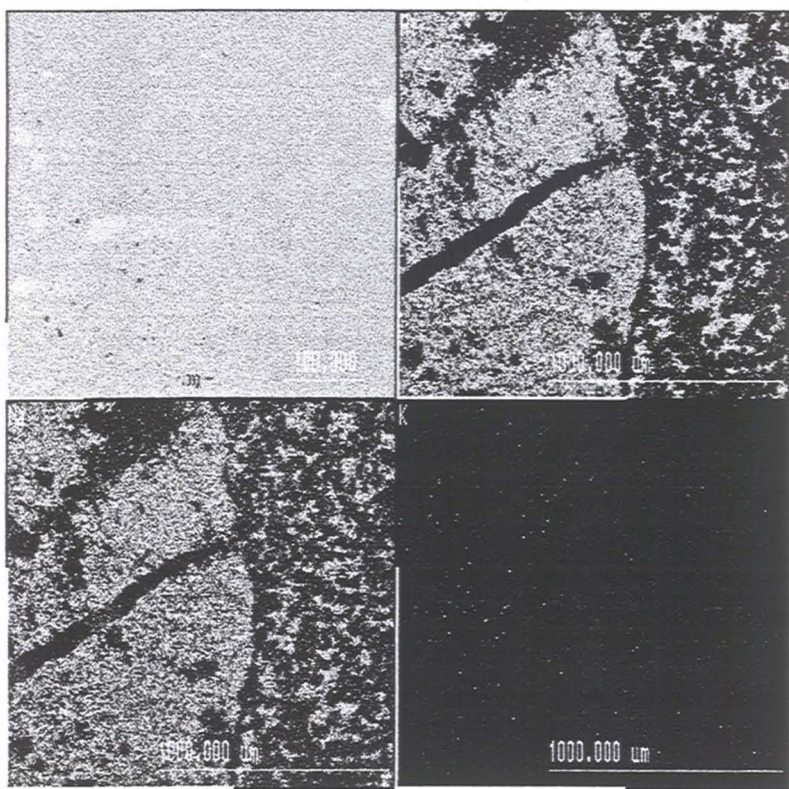
MP 855a

MP 855b

Sample MP 855, Volcaniclastic rock, background zone, Valdivia Sur.

317

MP 855c

MP 854a

Sample MP 855, Volcaniclastic rock, background zone, Valdivia Sur.
Sample MP 854, Volcaniclastic rock, bornite-chalcocite zone, Valdivia Sur.
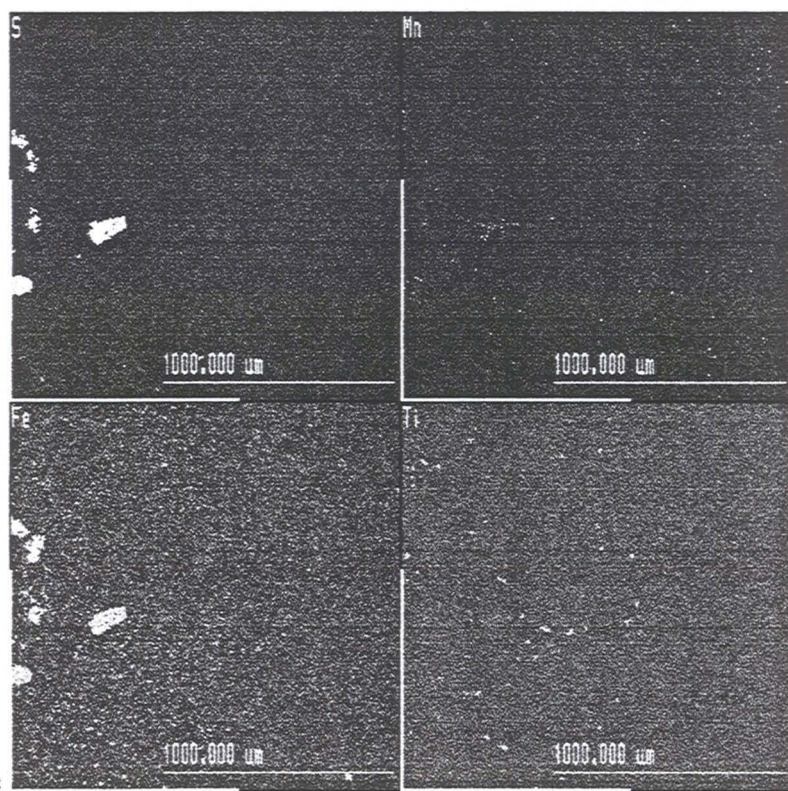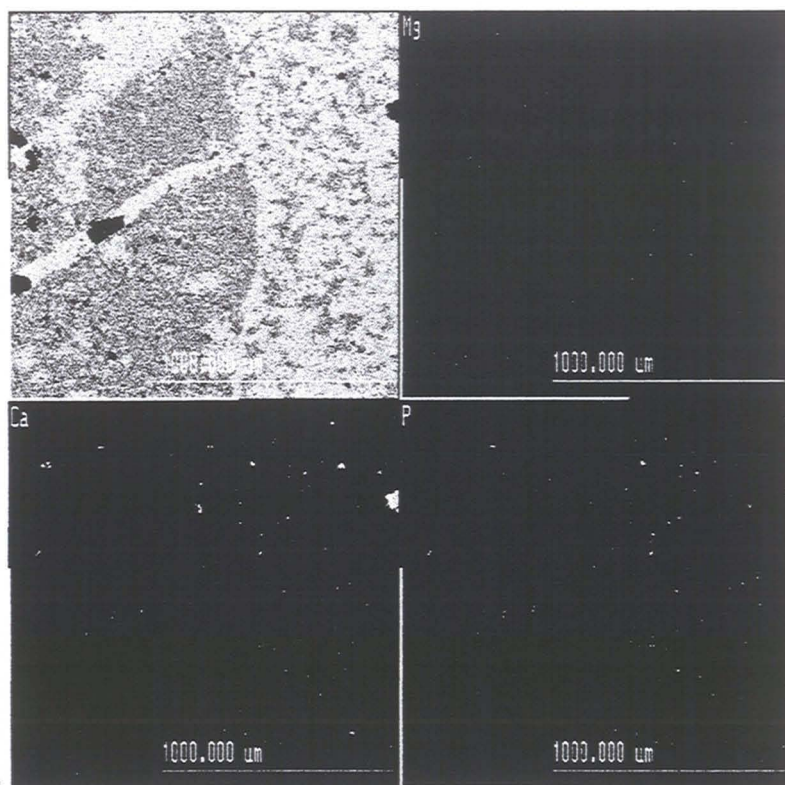
MP 854b

MP 854c

Sample MP 854, Volcaniclastic rock, bornite-chalcocite zone, Valdivia Sur.

Appendix 3.4.- Results of microprobe spot analyses of sulphides, listed by mineral and host rock.

- Abbreviations:
    - Ore zone:
        - bckd py: background with pyrite
        - bckd py-sph-ga: background with pyrite-sphalerite-galena
        - py: pyrite
        - py-cp: pyrite-chalcopyrite
        - cp: chalcopyrite
        - cp-bn: chalcopyrite-bornite
        - bn: bornite
        - bn-cc: bornite-chalcocite
        - cc: chalcocite

- References:
    - (1) This work
    - (2) Cuesta Research 1995, b (microprobe data by Milton Graves)

Appendix 3.4.- Analyses of Pyrite

Rock Type	Ore zone	Mine block	Sample	Grain	Point	Cu %	Fe %	S %	As %	Sb %	Zn %	Ti %	W %	Mn %	Co %	Si %	Total %	Mineral	Comments	Reference
basalt	py	Osorno	MP703	1	17		45.84	53.07									98.91	pyrite		2
basalt	py	Valdivia Sur	MP865	b	4		46.89	53.70	0.35								100.94	pyrite	main grain	2
basalt	py	Valdivia Sur	MP865		1		47.71	53.94							0.56		101.65	pyrite		1
basalt	py	Valdivia Sur	MP865		2	3.43	45.6	51.19	0.28								97.07	pyrite		1
basalt	py	Valdivia Sur	MP865		5		47.9	53.79									101.69	pyrite		1
basalt	py	Valdivia Sur	MP865		7		46.77	53.64									100.41	pyrite		1
basalt	py	Valdivia Sur	MP865		8		45.41	52.54							0.83		97.95	pyrite		1
basalt	py	Valdivia Sur	MP865		9		46.87	53.19									100.06	pyrite		1
basalt	py	Valdivia Sur	MP865		11	0.57	47.29	53.69									100.98	pyrite		1
basalt	py	Valdivia Sur	MP865		12		46.89	54.14	0.5								101.53	pyrite		1
basalt	py	Valdivia Sur	MP865		14		47.67	53.64									101.31	pyrite		1
basalt	py	Filo	RB9850		1		47.47	53.64									101.11	pyrite		1
basalt	py	Filo	RB9850		2		47.02	53.31									100.33	pyrite		1
basalt	py	Filo	RB9850		3		46.16	53.05	1.28				0.36				100.49	pyrite		1
basalt	py	Filo	RB9850		5		46.75	53.17									99.92	pyrite		1
basalt	py	Morro	MP728	1	2		46.90	54.79	t		0.80						102.48	pyrite		2
basalt	cp	Morro	MP724	1	19		46.97	54.14									101.11	pyrite		2
basalt	cp-bn	Filo	MP790	b	46	1.07	46.65	53.39									101.10	pyrite	inclusion in cp	2
basalt	cp-bn	Filo	MP790	e	51	1.16	47.10	55.87									104.13	pyrite		2
rhyodacite	bkd-py	Valdivia Sur	RB9805		1		46.91	54.10									101.01	pyrite		1
rhyodacite	bkd-py	Valdivia Sur	RB9805		2		46.68	53.68									100.36	pyrite		1
rhyodacite	bkd-py	Valdivia Sur	RB9805		3		47.10	53.47									100.57	pyrite		1
rhyodacite	bkd-py	Valdivia Sur	RB9805		4		45.25	53.23									98.48	pyrite		1
rhyodacite	bkd-py	Valdivia Sur	RB9805		5		45.91	53.83									99.74	pyrite		1
rhyodacite	bkd-py	Valdivia Sur	RB9805		6		45.67	53.70									99.37	pyrite		1
rhyodacite	bkd-py	Valdivia Sur	RB9805		7		45.73	53.77						0.94			99.50	pyrite		1
rhyodacite	bkd-py	Valdivia Sur	RB9805		8		45.99	53.69						0.31			99.68	pyrite		1
rhyodacite	py	Morro	MP719	1	10		46.62	54.09	t								100.71	pyrite		2
rhyodacite	py	Valdivia Sur	MP770	a	17		46.64	53.79	0.39			0.62					100.81	pyrite		2
rhyodacite	py	Valdivia Sur	MP770	d	22		47.42	54.44	0.37	0.16	.						102.39	pyrite		2
rhyodacite	py-cp	Valdivia Sur	RB9811		2		45.77	52.19	0.26								98.22	pyrite	euhedral	1
rhyodacite	py-cp	Valdivia Sur	RB9811		6		47.10	53.46									100.56	pyrite		1
rhyodacite	py-cp	Valdivia Sur	RB9811		7		46.90	54.04									100.94	pyrite		1

Appendix 3.4.- Analyses of Pyrite

Rock Type	Ore zone	Mine block	Sample	Grain	Point	Cu %	Fe %	S %	As %	Sb %	Zn %	Ti %	W %	Mn %	Co %	Si %	Total %	Mineral	Comments	Reference
rhyodacite	py-cp	Valdivia Sur	RB9811		8		47.26	53.52	0.24								101.02	pyrite		1
rhyodacite	py-cp	Valdivia Sur	RB9811		9		46.21	53.73									99.94	pyrite		1
rhyodacite	cp	Valdivia Sur	MP764	1	48	0.32	46.22	54.15									100.68	pyrite		2
rhyodacite	cp	Filo	MP739	b	33	1.11	46.64	54.01	1.56								103.32	pyrite	inclusion in cp	2
rhyodacite	cp	Filo	MP739	a	35		47.75	54.75									102.50	pyrite	cubic crystal rim	2
rhyodacite	cp	Filo	MP739	a	36		47.59	54.84									102.42	pyrite	cubic crystal centre	2
rhyodacitic dyke	bkd-py-sp-ga	Paso Riel	MP754	1	41		46.61	53.85									100.46	pyrite		2
rhyodacitic dyke	py-cp	Valdivia Sur	MP768	1	19		48.06	55.27	0.35								103.68	pyrite		2
rhyodacitic dyke	py-cp	Valdivia Sur	MP768	3	22		47.55	55.33	0.35								103.22	pyrite		2
rhyodacitic dyke	py-cp	Valdivia Sur	MP768	4	24		48.19	55.71	0.19								104.08	pyrite		2
rhyodacitic dyke	py-cp	Valdivia Sur	MP768	5	26		48.23	55.52	0.27								104.02	pyrite		2
rhyodacitic dyke	py-cp	Valdivia Sur	MP768	f	2		47.98	55.17	0.40								103.54	pyrite		2
sandstone	bkd-py-sp-ga	Paso Riel	MP761	1	72		45.92	53.55									99.47	pyrite		2
basalt	py	Filo	RB9850		6		44.78	50.01	4.99								99.78	Arsenial pyrite		1
basalt	py	Filo	RB9850		7		46.80	51.97	2.04								100.81	Arsenial pyrite		1
basalt	py	Filo	RB9850		8		45.35	51.05	0.97							0.59	97.37	Arsenial pyrite		1
basalt	py	Filo	RB9850		9		45.63	50.76	4.63							0.14	101.02	Arsenial pyrite		1
basalt	py	Filo	RB9850		10		47.33	53.05	0.82								101.20	Arsenial pyrite		1
basalt	py	Filo	RB9850		11		44.94	50.37	4.72								100.03	Arsenial pyrite		1
basalt	py	Filo	RB9850		12		44.17	49.19	7.53								100.89	Arsenial pyrite		1
basalt	py	Filo	RB9850		13		44.40	49.96	5.71								100.07	Arsenial pyrite		1
basalt	py	Filo	RB9850		14		47.25	52.94	0.29							0.55	100.48	Arsenial pyrite		1
basalt	py	Filo	RB9850		15		46.88	53.28	0.80								100.96	Arsenial pyrite		1

Appendix 3.4.- Analyses of Chalcopyrite

Rock Type	Ore zone	Mine block	Sample	Grain	Point	Cu %	Fe %	S %	As %	Zn %	Ag %	Bi %	W %	Total %	Mineral	Comments	Reference
basalt	py	Osorno	MP703	1	18	34.67	30.57	34.73						99.97	chalcopyrite		2
basalt	py	Osorno	MP703	1	20	34.13	30.92	34.90				t		99.95	chalcopyrite		2
basalt	py	Osorno	MP703	1	21	33.73	30.93	34.79						99.44	chalcopyrite		2
basalt	py	Morro	MP728	1	1	35.29	30.93	35.57						101.78	chalcopyrite		2
basalt	py	Morro	MP728	1	6	35.62	30.44	35.49						101.54	chalcopyrite		2
basalt	py	Valdivia Sur	MP865	b	5	34.75	30.35	34.36						99.47	chalcopyrite	main grain	1
basalt	py	Valdivia Sur	MP865	b	1	35.01	30.24	34.41						99.67	chalcopyrite	satellite grain	1
basalt	py	Valdivia Sur	MP865		10	35.06	31.04	34.72						65.76	chalcopyrite		1
basalt	py	Valdivia Sur	MP865		13	35.22	30.54	35.08						65.62	chalcopyrite		1
basalt	cp	Morro	MP724	1	17	34.85	30.91	34.79						100.55	chalcopyrite		2
basalt	cp	Morro	MP724	1	18	35.22	30.49	34.73						100.44	chalcopyrite		2
basalt	cp	Morro	MP724	1	16	35.28	30.55	35.52						101.36	chalcopyrite		2
basalt	cp	Valdivia Sur	MP786	f	10	35.48	31.64	35.46						102.58	chalcopyrite		2
basalt	cp-bn	Filo	MP790	b	47	35.04	31.27	35.88						102.18	chalcopyrite		2
basalt	cp-bn	Filo	MP790	e	50	35.33	30.82	35.14						101.29	chalcopyrite		2
basalt	cp-bn	Morro	MP723	1	13	34.91	30.24	34.67				t		99.82	chalcopyrite		2
basalt	cp-bn	Morro	MP723	1	15	35.34	30.26	34.90						100.50	chalcopyrite		2
basalt	bn-cc	Filo	RB9852		9	31.51	27.76	34.81					0.36	62.57	chalcopyrite	one small grain	1
rhyodacite	py	Morro	MP719	1	11	31.20	32.00	37.14						100.34	chalcopyrite		2
rhyodacite	py	Morro	MP719	1	9	34.98	30.86	35.42	t			t		101.26	chalcopyrite		2
rhyodacite	py	Valdivia Sur	MP770	a	16	34.31	30.19	34.79						99.29	chalcopyrite	main phase with py	2
rhyodacite	py	Valdivia Sur	MP770	d	21	34.85	31.19	35.09						101.13	chalcopyrite		2
rhyodacite	cp	Valdivia Sur	MP764	1	49	33.66	30.42	35.43						99.52	chalcopyrite		2
rhyodacite	cp	Valdivia Sur	MP764	1	50	34.59	31.07	35.07	0.22					100.94	chalcopyrite		2
rhyodacite	cp	Valdivia Sur	MP775	2	56	33.79	30.77	34.88						99.44	chalcopyrite		2
rhyodacite	cp	Valdivia Sur	MP775	2	60	34.01	30.72	34.79						99.52	chalcopyrite		2
rhyodacite	cp	Valdivia Sur	MP775	3	62	34.24	31.08	35.02						100.35	chalcopyrite		2
rhyodacite	cp	Valdivia Sur	MP775	1	51	34.42	30.89	35.05						100.36	chalcopyrite		2
rhyodacite	cp	Filo	MP739	b	31	34.42	30.54	35.01						99.97	chalcopyrite	inclusion in bitumen	2
rhyodacite	cp	Filo	MP739	a	34	33.82	31.25	35.36						100.43	chalcopyrite	main phase	2
rhyodacite	cp	Filo	MP739	b	30	34.03	31.17	35.18						100.37	chalcopyrite	main phase	2

Appendix 3.4.- Analyses of Chalcopyrite

Rock Type	Ore zone	Mine block	Sample	Grain	Point	Cu %	Fe %	S %	As %	Zn %	Ag %	Bi %	W %	Total %	Mineral	Comments	Reference
rhyodacite	bn	Morro	MP713	b	7	35.95	30.96	35.68						102.60	chalcopyrite		2
rhyodacite	bn	Morro	MP713	b	8	35.72	30.62	35.16						101.50	chalcopyrite		2
rhyodacite	bn	Morro	MP713	d	11	36.37	30.99	35.03						102.39	chalcopyrite		2
rhyodacite	bn	Morro	MP713	d	11b	34.33	30.26	34.79						99.39	chalcopyrite		2
rhyodacite	bn	Morro	MP718	3	13	34.84	30.94	34.95						100.72	chalcopyrite		2
rhyodacite	bn	Morro	MP718	3	11	35.62	30.35	34.94						100.91	chalcopyrite		2
rhyodacite	bn	Valdivia Sur	MP856	a	58	36.45	30.55	34.91						101.90	chalcopyrite	cp-bn veinlet	2
rhyodacite	bn-cc	Morro	MP864	d	54	35.01	31.37	34.33						100.71	chalcopyrite	minor phase with bn	2
rhyodacite	bn-cc	Valdivia Sur	MP782	2	37	35.25	30.27	34.93						100.44	chalcopyrite		2
rhyodacite	cc	Filo	MP737	i	1	35.54	29.50	34.85						99.89	chalcopyrite	main phase with bn	2
rhyodacite	py-cp	Valdivia Sur	RB9811		3	36.00	30.43	34.64						101.07	chalcopyrite	large grain	1
rhyodacite	py-cp	Valdivia Sur	RB9811		4	34.29	30.38	34.75						99.42	chalcopyrite	large grain	1
rhyodacite	py-cp	Valdivia Sur	RB9811		5	35.64	31.09	34.74						101.47	chalcopyrite		1
rhyodacite	py-cp	Valdivia Sur	RB9811		1	34.82	30.38	34.88						100.08	chalcopyrite		1
rhyodacitic dyke	py-cp	Valdivia Sur	MP768	1	18	33.82	31.93	36.40	0.24					102.39	chalcopyrite		2
rhyodacitic dyke	py-cp	Valdivia Sur	MP768	3	21	33.25	31.56	36.14	0.15					101.09	chalcopyrite		2
rhyodacitic dyke	py-cp	Valdivia Sur	MP768	4	23	34.43	32.19	36.08	0.15					102.86	chalcopyrite		2
rhyodacitic dyke	py-cp	Valdivia Sur	MP768	4	25	33.99	31.38	35.68						101.04	chalcopyrite		2
rhyodacitic dyke	py-cp	Valdivia Sur	MP768	f	1	36.72	31.43	35.15						103.30	chalcopyrite		2
volcanic sediment	bn	Valdivia Sur	MP854	b	56	35.21	29.38	34.02						98.61	chalcopyrite	minor phase with bn	2
sandstone	bkd-py-sph-ga	Paso Riel	MP761	1	68	33.26	29.98	34.84		1.16				99.24	chalcopyrite		2
sandstone	bkd-py-sph-ga	Paso Riel	MP761	2	64	33.94	30.43	34.94			0.18			99.48	chalcopyrite		2

Appendix 3.4.- Analyses of Bornite

Rock Type	Ore zone	Mine block	Sample	Grain	Point	Cu %	Fe %	S %	As %	Ag %	Bi %	Co %	Total %	Mineral	Comments	Reference
basalt	cp-bn	Filo	MP790	b	38	63.13	11.65	26.06					100.84	bornite	bn-py-cp grain	2
basalt	cp-bn	Filo	MP790	b	39	63.32	11.71	25.92					100.95	bornite	bn-py-cp grain	2
basalt	cp-bn	Filo	MP790	b	40	63.20	11.68	25.86					100.74	bornite	bn-py-cp grain	2
basalt	cp-bn	Filo	MP790	b	41	63.68	11.79	25.84					101.30	bornite	bn-py-cp grain	2
basalt	cp-bn	Filo	MP790	b	42	62.09	11.26	26.15					99.50	bornite	in bitumen vein	2
basalt	cp-bn	Filo	MP790	e	49	62.93	11.95	26.16					101.04	bornite		2
basalt	cp-bn	Morro	MP723	1	14	63.31	11.83	25.63					100.76	bornite		2
basalt	cp-bn	Morro	MP723	1	12	63.52	11.34	25.49					100.36	bornite		2
basalt	bn	Valdivia Sur	MP787	a	7	64.19	11.72	24.99					100.90	bornite	main phase	2
basalt	bn	Valdivia Sur	MP787	b	15	63.39	11.09	25.24					99.72	bornite	main phase	2
basalt	bn-cc	Filo	RB9852		1	63.78	11.24	25.37					100.39	bornite		1
basalt	bn-cc	Filo	RB9852		2	64.10	11.27	25.03					100.40	bornite		1
basalt	bn-cc	Filo	RB9852		3	64.26	11.35	25.11					100.72	bornite		1
basalt	bn-cc	Filo	RB9852		5	63.51	11.14	25.22					99.87	bornite		1
basalt	bn-cc	Filo	RB9852		6	63.77	11.67	25.25					100.69	bornite		1
basalt	bn-cc	Filo	RB9852		7	61.52	12.76	25.96					100.24	bornite		1
basalt	bn-cc	Filo	RB9852		8	62.56	11.68	25.12					99.36	bornite		1
basalt	bn-cc	Morro	MP805	e	12	64.83	11.31	25.61					101.76	bornite		2
basalt	bn-cc	Morro	MP805	c	17	64.64	10.91	25.17					100.71	bornite		2
basalt	bn-cc	Morro	MP805	a	20	65.08	11.02	24.91					101.01	bornite		2
basalt	bn-cc	Morro	MP805	d	22	65.22	10.94	25.47					101.63	bornite		2
basalt	bn-cc	Morro	MP805	e	62	63.89	11.18	25.12					100.18	bornite		2
basalt	cc	Filo	MP793	e	19	64.73	10.23	24.47					99.43	bornite	main phase	2
basalt	cc	Filo	MP793	c	26	64.82	10.15	24.82					99.79	bornite	vein in bitumen	2
basalt	cc	Filo	MP793	d	27	63.39	11.83	25.22					100.44	bornite	major phase	2
basalt	cc	Filo	MP793	b	31	65.00	10.73	24.81					100.54	bornite	major phase	2
basalt	cc	Filo	MP793	a	33	63.96	10.60	24.67					99.23	bornite	major phase	2
rhyodacite	cp	Valdivia Sur	MP775	2	61	60.15	12.53	26.33					99.01	bornite		2
rhyodacite	cp	Valdivia Sur	MP775	2	58	60.75	12.33	26.21	0.23				99.51	bornite		2
rhyodacite	cp	Valdivia Sur	MP775	2	57	60.99	12.17	26.06	0.20	0.10			99.51	bornite		2
rhyodacite	cp	Valdivia Sur	MP775	1	53	67.92	10.38	22.97					101.27	bornite		2
rhyodacite	bn	Morro	MP718	2	8	62.99	11.42	25.31					99.73	bornite		2
rhyodacite	bn	Morro	MP718	3	12	63.11	11.38	25.50	t				99.99	bornite		2
rhyodacite	bn	Morro	MP718	1	7	63.88	11.76	25.42					101.06	bornite		2
rhyodacite	bn	Morro	MP718	1	1	64.17	11.25	25.39					100.82	bornite		2

Appendix 3.4.- Analyses of Bornite

Rock Type	Ore zone	Mine block	Sample	Grain	Point	Cu %	Fe %	S %	As %	Ag %	Bi %	Co %	Total %	Mineral	Comments	Reference
rhyodacite	bn	Morro	MP713	a	3	65.64	12.50	26.20					104.34	bornite		2
rhyodacite	bn	Morro	MP713	a	4	64.11	12.31	26.09					102.52	bornite		2
rhyodacite	bn	Morro	MP713	b	5	64.40	12.14	25.96					102.51	bornite		2
rhyodacite	bn	Morro	MP713	b	9	65.49	11.58	26.23					103.31	bornite		2
rhyodacite	bn	Morro	MP713	d	12	65.89	12.08	26.29					104.26	bornite		2
rhyodacite	bn	Morro	MP713	d	12b	63.10	11.73	25.95					100.78	bornite		2
rhyodacite	bn	Valdivia Sur	MP856	a	59	63.51	11.68	25.61					100.80	bornite	main phase of vein	2
rhyodacite	bn	Valdivia Sur	MP856	c	62	64.22	11.60	25.49					101.32	bornite		2
rhyodacite	bn	Valdivia Sur	MP856	g	65	64.06	12.10	25.47					101.63	bornite	main phase	2
rhyodacite	bn-cc	Filo	MP746	b	35	62.34	10.94	25.11					98.38	bornite		2
rhyodacite	bn-cc	Filo	MP746	c	39	65.10	9.28	24.33					98.71	bornite		2
rhyodacite	bn-cc	Filo	MP746	a	42	63.64	10.76	24.96					99.36	bornite		2
rhyodacite	bn-cc	Morro	MP864	e	48	61.70	10.20	24.05					95.94	bornite	main phase	2
rhyodacite	bn-cc	Morro	MP864	b	51	62.47	12.29	25.10					99.86	bornite		2
rhyodacite	bn-cc	Morro	MP864	d	53	64.67	11.39	25.06					101.11	bornite	main phase	2
rhyodacite	bn-cc	Osorno	MP664	2	13	63.16	11.06	25.33	t				99.54	bornite		2
rhyodacite	bn-cc	Osorno	MP664	1	10	63.40	11.17	25.51			t		100.07	bornite		2
rhyodacite	bn-cc	Osorno	MP664	1	4	63.42	11.20	25.32					99.94	bornite		2
rhyodacite	bn-cc	Osorno	MP664	1	2b	63.59	11.16	25.20	t	t			99.94	bornite		2
rhyodacite	bn-cc	Osorno	MP664	1	1	64.00	11.73	25.48	0.32				101.53	bornite		2
rhyodacite	bn-cc	Osorno	MP664	1	2	64.21	11.28	25.58		0.19			101.26	bornite		2
rhyodacite	bn-cc	Valdivia Sur	MP778	1	29	62.59	11.52	25.50					99.61	bornite		2
rhyodacite	bn-cc	Valdivia Sur	MP778	1	26	62.94	11.42	25.69		0.10			100.15	bornite		2
rhyodacite	bn-cc	Valdivia Sur	MP778	1	24	63.77	11.24	25.49					100.50	bornite		2
rhyodacite	bn-cc	Valdivia Sur	MP782	1	34	62.65	11.33	25.38					99.36	bornite		2
rhyodacite	bn-cc	Valdivia Sur	MP782	2	36	62.68	12.14	25.30					100.12	bornite		2
rhyodacite	bn-cc	Valdivia Sur	MP782	1	31	62.98	11.27	25.38					99.63	bornite		2
rhyodacite	bn-cc	Valdivia Sur	RB9815		1	60.71	12.49	25.04					98.24	bornite?		1
rhyodacite	cc	Filo	MP737	i	2	62.52	11.14	25.91					99.57	bornite	main phase	2
rhyodacite	cc	Filo	MP737	j	7	63.88	11.72	25.66					101.26	bornite		2
rhyodacite	cc	Filo	MP737	d	13	64.67	11.22	25.44					101.33	bornite		2
rhyodacitic dyke	cc	Valdivia Sur	MP772	1	19	62.77	11.43	25.30		0.32	0.64		100.47	bornite		2
rhyodacitic dyke	cc	Valdivia Sur	MP772	1	21	62.86	11.58	25.39	0.28	0.14			100.25	bornite		2
rhyodacitic dyke	cc	Valdivia Sur	MP772	2	17	63.06	11.52	26.15					100.73	bornite		2
rhyodacitic dyke	cc	Valdivia Sur	MP772	2	15	63.22	11.02	25.45	0.21	0.17			100.06	bornite		2

Appendix 3.4.- Analyses of Bornite

Rock Type	Ore zone	Mine block	Sample	Grain	Point	Cu %	Fe %	S %	As %	Ag %	Bi %	Co %	Total %	Mineral	Comments	Reference
rhyodacitic dyke	cc	Valdivia Sur	MP772			63.48	11.35	25.44					100.27	bornite		2
volcanic sediment	bn	Valdivia Sur	MP854	b	55	62.65	11.01	24.73					98.39	bornite	main phase	2

Appendix 3.4.- Analyses of Chalcocite Group

Rock Type	Ore zone	Mine block	Sample	Grain	Point	Cu %	Fe %	S %	As %	Sb %	Ag %	Bi %	Total %	Mineral	Formula Cu	Formula S	Comments	Reference
basalt	bn	Valdivia Sur	MP787	a	8	77.71	0.76	21.89					100.35	digenite	1.79	1.00	rare phase	2
basalt	bn	Valdivia Sur	MP787	b	14	77.93	0.42	21.20					99.55	digenite	1.85	1.00	blue minor phase	2
basalt	bn-cc	Morro	MP805	a	19	81.50		19.86					101.36	chalcocite	2.07	1.00		2
basalt	bn-cc	Morro	MP805	c	15	79.77		21.56					101.33	digenite	1.87	1.00		2
basalt	bn-cc	Morro	MP805	e	11	80.47		21.74					102.21	digenite	1.82	1.00		2
basalt	bn-cc	Morro	MP805	e	13	79.87		21.93					101.80	digenite	1.84	1.00		2
basalt	bn-cc	Morro	MP805	c	18	78.14	0.43	21.66					100.23	digenite	1.82	1.00		2
basalt	bn-cc	Morro	MP805	d	21	80.65	0.42	22.05					103.13	digenite	1.84	1.00		2
basalt	bn-cc	Morro	MP805	e	61	78.44		21.42					99.86	digenite	1.85	1.00		2
basalt	cc	Filo	MP793	e	18	80.25		19.66					99.91	chalcocite	2.06	1.00	main phase	2
basalt	cc	Filo	MP793	c	25	79.68	0.29	20.29					100.26	chalcocite	1.98	1.00	vein in bitumen	2
basalt	cc	Filo	MP793	b	32	79.35		20.03					99.38	chalcocite	2.00	1.00	major phase	2
basalt	cc	Filo	MP793	a	34	80.13		20.10					100.24	chalcocite	2.01	1.00	major phase	2
basalt	cc	Filo	MP793	d	28	78.93	1.69	20.21					100.83	chalcocite	1.97	1.00	other major phase	2
basalt	cc	Filo	MP793	e	20	77.45	4.46	20.73					102.63	digenite	1.88	1.00	veinlet in bitumen	2
rhyodacite	bn	Morro	MP718	2	10	79.47	1.17	20.92	0.46				102.02	djurleite	1.92	1.00		2
rhyodacite	bn	Morro	MP718	2	9	78.45	1.31	21.28	0.38			t	101.43	digenite	1.86	1.00		2
rhyodacite	bn	Morro	MP718	1	2	77.25	1.59	21.62	t				100.46	digenite	1.80	1.00		2
rhyodacite	bn	Morro	MP718	1	3	77.57	0.94	21.80	0.30			t	100.61	digenite	1.80	1.00		2
rhyodacite	bn	Morro	MP718	3	14	77.89	1.44	21.96	t				101.29	digenite	1.79	1.00		2
rhyodacite	bn-cc	Filo	MP746	c	38	80.19	0.32	20.13					100.64	chalcocite	2.01	1.00		2
rhyodacite	bn-cc	Filo	MP746	a	41	80.00		20.08					100.08	chalcocite	2.10	1.00		2
rhyodacite	bn-cc	Filo	MP746	b	36	78.56		20.12					98.68	chalcocite	1.97	1.00		2
rhyodacite	bn-cc	Morro	MP864	b	50	75.31	2.41	22.83					100.54	digenite	1.66	1.00		2
rhyodacite	bn-cc	Morro	MP864	b	52	76.05	1.95	22.46					100.46	digenite	1.71	1.00		2
rhyodacite	bn-cc	Osorno	MP664	1	1b	78.61		19.85					98.46	chalcocite	2.00	1.00		2
rhyodacite	bn-cc	Osorno	MP664	1	3	79.70	0.28	20.22	t		t		100.19	chalcocite	1.99	1.00		2
rhyodacite	bn-cc	Osorno	MP664	2	14	80.11	0.62	20.55	0.36				101.63	chalcocite	1.99	1.00		2
rhyodacite	bn-cc	Osorno	MP664	1	9	80.94	0.52	20.44	0.40				102.30	chalcocite	2.00	1.00		2
rhyodacite	bn-cc	Osorno	MP664	1	12	81.01		20.28					101.30	chalcocite	2.02	1.00		2
rhyodacite	bn-cc	Osorno	MP664	1	8	81.21	t	20.62	0.29				102.12	chalcocite	1.99	1.00		2
rhyodacite	bn-cc	Osorno	MP664		15	79.01	1.28	20.63	t		t		100.91	djurleite?	1.93	1.00		2
rhyodacite	bn-cc	Osorno	MP664	1	6	79.63	t	20.68	0.37				100.67	djurleite?	1.94	1.00		2
rhyodacite	bn-cc	Osorno	MP664	1	3	79.83	t	20.63	t		t		100.46	djurleite?	1.95	1.00		2
rhyodacite	bn-cc	Osorno	MP664	1	2	79.88	0.54	20.57	0.33				101.31	djurleite?	1.96	1.00		2
rhyodacite	bn-cc	Osorno	MP664	1	5	80.98	0.50	20.74	t				102.21	djurleite?	1.97	1.00		2
rhyodacite	bn-cc	Osorno	MP664	2	16	81.09	0.66	20.52	t				102.26	djurleite?	1.97	1.00		2

Appendix 3.4.- Analyses of Chalcocite Group

Rock Type	Ore zone	Mine block	Sample	Grain	Point	Cu %	Fe %	S %	As %	Sb %	Ag %	Bi %	Total %	Mineral	Formula Cu	Formula S	Comments	Reference
rhyodacite	bn-cc	Valdivia Sur	MP778	1	25	78.72		20.64	0.47				99.84	djurleite?	1.92	1.00		2
rhyodacite	bn-cc	Valdivia Sur	MP778	1	27	79.45	0.63	20.75	0.31				101.14	djurleite?	1.93	1.00		2
rhyodacite	bn-cc	Valdivia Sur	MP782	1	33	78.24	0.71	20.15	0.26		0.16		99.52	djurleite?	1.96	1.00		2
rhyodacite	bn-cc	Valdivia Sur	MP782	1	30	79.18		20.33	0.36				99.88	djurleite?	1.96	0.96		2
rhyodacite	bn-cc	Valdivia Sur	MP782	1	35	79.31	0.22	20.28	0.32		0.10		100.22	djurleite?	1.97	0.97		2
rhyodacite	bn-cc	Valdivia Sur	MP782	1	32	79.54		20.43	0.19				100.15	djurleite?	1.96	1.00		2
rhyodacite	cc	Filo	MP737	d	14	80.28	0.41	20.20					100.89	chalcocite	2.00	1.00		2
rhyodacite	cc	Filo	MP737	e	15	80.81		20.27					101.07	chalcocite	2.01	1.00		2
andesitic dyke	cc	Valdivia Sur	MP772	2	13	80.57		20.11	0.29		0.17		101.14	chalcocite	2.02	1.00		2
andesitic dyke	cc	Valdivia Sur	MP772	2	14	82.37		20.47	0.44		0.18		103.46	chalcocite	2.03	1.00		2
andesitic dyke	cc	Valdivia Sur	MP772	2	13	82.49		20.30	0.34				103.13	chalcocite	2.05	1.00		2
andesitic dyke	cc	Valdivia Sur	MP772	1	20	78.18	1.57	20.46	0.41	0.24			100.86	djurleite	1.93	1.00		2
andesitic dyke	cc	Valdivia Sur	MP772	2	13	78.19		20.21	0.45		0.20		99.05	djurleite?	1.95	1.00		2
andesitic dyke	cc	Valdivia Sur	MP772	1	22	78.59	1.11	20.60			0.13		100.43	djurleite?	1.92	1.00		2
andesitic dyke	cc	Valdivia Sur	MP772	2	16	78.71	0.95	20.55	0.27			0.63	101.12	djurleite?	1.93	1.00		2
andesitic dyke	cc	Valdivia Sur	MP772	2	13	79.02		20.37	0.32				99.70	djurleite?	1.96	1.00		2
andesitic dyke	cc	Valdivia Sur	MP772	2	18	79.26	0.63	20.32	0.26		0.09		100.55	djurleite?	1.97	1.00		2
volcanic sediment	bn	Valdivia Sur	MP854	b	57	73.95	2.25	22.04					98.23	digenite	1.69	1.00	minor phase in bn	2
volcanic sediment	cc	Filo	MP791	h	27	77.31		22.03					99.34	digenite	1.77	1.00		2
volcanic sediment	cc	Filo	MP791	h	28	72.61		21.86			0.54		95.02	digenite	1.68	1.00		2
volcanic sediment	cc	Filo	MP791	h	29	72.24		21.90			0.71		94.85	digenite	1.66	1.00		2

Appendix 3.4.- Analyses of Covellite

Rock Type	Ore zone	Mine block	Sample	Grain	Point	Cu	Fe	S	As	Sb	Ag	Co	Total	Mineral	Formula S	Formula Cu	Comments	Reference
rhyodacite	cp	Valdivia Sur	MP775	2	54	67.21	1.30	31.00	0.29		0.10		99.90	covellite	1.09	1.00		2
rhyodacite	cp	Valdivia Sur	MP775	2	59	69.14	1.16	30.45	0.25				101.00	covellite	1.15	1.00		2
rhyodacite	cp	Valdivia Sur	MP775	2	55	71.30	1.15	27.75	0.26				100.45	covellite	1.30	1.00		2
rhyodacite	bn	Valdivia Sur	MP856	g	64	63.82	4.45	29.36					97.63	covellite	1.08	1.00	inclusion in bn	2
rhyodacite	bn-cc	Morro	MP864	e	47	71.16	0.33	29.58					101.07	covellite	1.21	1.00	minor phase	2
rhyodacite	bn-cc	Morro	MP864	e	49	70.02		29.86			0.40		100.28	covellite	1.18	1.00	minor phase	2
volcanic sediment	bn	Valdivia Sur	MP854	b	58	66.84	2.35	31.73					100.92	covellite	1.06	1.00	inclusion in bn	2
volcanic sediment	cc	Filo	MP791	h	25	69.67	0.26	30.11				0.56	100.61	covellite	1.17	1.00		2

Appendix 3.4.- Analyses of Galena

Rock Type	Ore zone	Mine block	Sample	Grain	Point	Cu %	Fe %	S %	Sb %	Zn %	Pb %		Total %	Mineral	Reference
basalt	py	Morro	MP728	2	7		2.45	13.24			86.63		102.32	galena	2
basalt	py	Valdivia Sur	MP865		3		2.08	12.67			88.21		102.96	galena	1
rhyodacitic dyke	bkd py-sph-ga	Paso Riel	MP754	1	43			12.24		1.50	88.58		102.32	galena	2
rhyodacitic dyke	bkd py-sph-ga	Paso Riel	MP754	1	46			12.51			86.52		99.03	galena	2
rhyodacitic dyke	bkd py-sph-ga	Paso Riel	MP754	1	42		0.91	12.66			86.04		99.61	galena	2
rhyodacitic dyke	bkd py-sph-ga	Paso Riel	MP754	1	40		1.29	12.70	0.32		86.53		100.84	galena	2
sandstone	bkd py-sph-ga	Paso Riel	MP761	1	69			12.25		0.90	87.69		100.83	galena	2
sandstone	bkd py-sph-ga	Paso Riel	MP761	2	66	0.59		12.41		1.22	87.55		101.76	galena	2
basalt	py	Valdivia Sur	MP865		4		24.84	31.14			46.81		102.79	galena+pyrite	1
basalt	py	Valdivia Sur	MP865		6		38.55	46.62			14.4		99.57	galena+pyrite	1
basalt	py	Filo	RB9850		4		43.17	50.37			4.72		98.26	galena+pyrite	1

Appendix 3.4.- Analyses of Sphalerite

Rock Type	Ore zone	Mine block	Sample	Grain	Point	Cu %	Fe %	S %	As %	Sb %	Zn %	Bi %	Total %	Mineral	Reference
basalt	py	Morro	MP728	1	5	0.61	0.70	33.10			68.93	t	103.34	sphalerite	2
basalt	py	Morro	MP728	1	3	0.75	0.75	33.13	t		67.72		102.35	sphalerite	2
rhyodacitic dyke	bkd py-sph-ga	Paso Riel	MP754	1	45	0.74	6.37	32.90			61.63	0.68	102.32	sphalerite	2
rhyodacitic dyke	bkd py-sph-ga	Paso Riel	MP754	1	47	0.89	3.17	33.00	0.38		62.95		100.39	sphalerite	2
rhyodacitic dyke	bkd py-sph-ga	Paso Riel	MP754	1	44	2.82	5.96	32.59			58.32		99.68	sphalerite	2
sandstone	bkd py-sph-ga	Paso Riel	MP761	1	67	0.02	5.90	32.73	0.34		60.58		99.56	sphalerite	2
sandstone	bkd py-sph-ga	Paso Riel	MP761	2	65	0.23	8.02	33.24			58.83		100.32	sphalerite	2

Appendix 3.4.- Analyses of Anilite

Rock Type	Ore zone	Mine block	Sample	Grain	Point	Cu %	Fe %	S %					Total %	Mineral	Reference
basalt	bn-cc	Morro	MP805	c	16	74.74	0.71	26.91					102.36	anillite?	2
rhyodacite	cc	Filo	MP737	j	5	75.99	0.49	24.42					100.90	anilite?	2
rhyodacite	cc	Filo	MP737	j	8	74.89	0.51	24.87					100.27	anilite?	2

Appendix 3.4.- Analyses of Cobaltite

Rock Type	Ore zone	Mine block	Sample	Grain	Point	Cu %	Fe %	S %	As %	Ni %	Co %	Mg %	Total %	Mineral	Reference
basalt	cc	Filo	MP793	e	17	4.29	1.36	18.47	43.83	1.72	30.00		99.65	cobaltite	2
volcanic sediment	cc	Filo	MP791	h	24		1.16	19.46	43.70	3.36	31.00	1.24	99.91	cobaltite	2

4.- X-RAY DIFFRACTION DATA

4.1. Sample list with X-Ray diffractograms results
4.2. Diffractograms for selected samples

Appendix 4.1 Sample Lists with X-Ray Diffractograms results

Appendix 4.1.- X-Ray Diffractograms Results

Sample	Rock	Ore Zone	Analysed Mineral	Result	Plots
RB9833c	basalt	bckd	pink feldspar concentrated	microcline ord, microcline int	
RB9833e	basalt	bckd	bornite concentrated	bornite	normal
RB9913a	basalt	bckd	hematite in vein	quartz, hematite,	normal
RB9921b	basalt	bckd	pink feldspar concentrated	microcline int.	detailed, normal
RB9921c	basalt	bckd	black mineral vein	albite ordered	normal
RB9930a	basalt	bckd	pink feldspar concentrated	microcline int, (microcline ord), (orthoclase)	detailed, normal
RB9930b	basalt	bckd	chlorite concentrated	clinochlore, (chamosite)	normal
RB9930c	basalt	bckd	calcite concentrated	calcite	normal
RB9930e	basalt	bckd	epidote concentrated	epidote, (clinozoisite), (piemontite)	normal
RB9932a	basalt	bckd	epidote concentrated in veins	epidote, clinozoisite, piemontite	normal
RB9932b	basalt	bckd	kfd veins in epidotized basalt	microcline ord, pigeonite, piemontite	detailed, normal
RB9933a	basalt	bckd	pink feldspar concentrated	microcline ord, microcline int	detailed, normal
RB9933b	basalt	bckd	chlorite concentrated	pumpellyte Mg, pumpellyte Fe, clinochlore	normal
RB9933c	basalt	bckd	red mineral concentrated	hematite, ferrihydrite, clinochlore, microcline ord, rutile	normal
RB9922a	basalt	cp-bn	albite and kfeldspar in vein	albite ord, anorthoclase dis	
RB9922b	basalt	cp-bn	albite and kfeldspar in vein	albite ord, microcline int, microcline ord	detailed, normal
MP850a	basalt	bn	pink feldspar concentrated	unclear	
MP850b	basalt	bn	pink feldspar concentrated	microcline ord, microcline int	detailed, normal
RB9843a	basalt	bn	pink feldspar concentrated	microcline ord, albite ord, microcline int	detailed, normal
RB9846a	basalt	bn-cc	chlorite in amygdule	clinochlore, (chamosite)	normal
RB9846b	basalt	bn-cc	pink feldspar in matrix, brecciated rock	microcline int, clinochlore, microcline ord	detailed, normal
MP851a	basalt V. Negra	bn-cc	altered phenenocrysts	albite ord, microcline int	detailed, normal
MP851b	basalt V. Negra	bn-cc	K-feldspar in vugs	(microcline int)	normal
MP880a	basalt, V. Negra	bn	Kfeldspar vein	microcline int, orthoclase	detailed, normal
RB9924a	basaltic dyke	bn	albite and kfeldspar in vein	albite, microcline, orthoclase	detailed, normal
Z62395a	gabbro	altered	chlorite veintlets in gabbro	clinochlore, chamosite, (albite dis, albite ord)	normal
Z62395b	gabbro	altered	pink feldspar in gabbro	albite or, microcline or, microcline int	detailed, normal
RB9902a	rhyodacite	py	groundmass concentrated, potassic altered rock	quartz, albite ord, orthoclase barian	normal
RB9903a	rhyodacite	py	groundmass concentrated, albitised rock	quartz, albite ord,	normal
RB9904a	rhyodacite	py	chlorite vein, potassic altered rock	quartz, clinochlore, albite ord,	normal
RB9904b	rhyodacite	py	groundmass concentrated, potassic altered rock	quartz, albite ord, clinochlore, microcline int	detailed, normal
Z62595b	rhyodacite	py	groundmass concentrated, albitised rock	albite ord, quartz	normal
Z62595c	rhyodacite	py	whole rock, albitised rock	albite ord,	normal
Z61295a	rhyodacite	cp	groundmass, potassic altered rock	quartz, albite ord, microcline int	detailed, normal
Z61295b	rhyodacite	cp	kfeldspar concentrated, potassic altered rock	albite ord, quartz, anorthoclase dis	detailed, normal
Z61295c	rhyodacite	cp	groundmass concentrated, potassic altered rock	pumpellite (microcline or)	normal
MP739a	rhyodacite	cp-bn	groundmass concentrated, albitised rock	quartz, albite ord,	normal
MP677a	rhyodacite	bn	groundmass concentrated, potassic altered rock	quartz, montmorillonite, albite ord	normal
MP677b	rhyodacite	bn	groundmass concentrated, potassic altered rock	quartz, albite ord, montmorillonite, (microcline)	detailed, normal
MP718a	rhyodacite	bn	groundmass concentrated, albitised rock	quartz, albite ord,	normal
RB9818a	rhyodacite	bn	chlorite in matrix	clinoclhore, quartz, albite ord, chamosite	
RB9818b	rhyodacite	bn	pink fragments, brecciated rock	pumpellyte Fe, microcline	normal
RB9818c	rhyodacite	bn	whole rock, brecciated	quartz, clinochlore, chamosite	normal

Appendix 4.1.- X-Ray Diffractograms Results

Sample	Rock	Ore Zone	Analysed Mineral	Result	Plots
RB9818d	rhyodacite	bn	pink fragment in brecciated rock	quartz, microcline ord	detailed, normal
MP664a	rhyodacite	bn-cc	groundmass concentrated, potassic altered rock	microcline int, orthoclase barian	detailed, normal
MP864a	rhyodacite	bn-cc	kfd veinlet in albite phenocryst, potassic altered rock	quartz, albite ord,	normal
RB9815a	rhyodacite	bn-cc	matrix concentrated, albitised rock	quartz, albite ord	normal
RB9867a	rhyodacite	bn-cc	groundmass concentrated, albitised rock	albite ord	normal
RB9901a	rhyodacite	bn-cc	altered fragment concentrated, brecciated rock	(sanidine)	normal
RB9901b	rhyodacite	bn-cc	matrix concentrated, potassic altered rock	quartz, clinochlore,epidote	normal
RB9935a	rhyodacite	bn-cc	matrix concentrated,	quartz, albite ord, sanidine potassian dis, (microcline int)	normal
RB9935b	rhyodacite	bn-cc	whole rock, potassic altered rock	quartz, albite ord, anorthoclase dis, (mic ord, mic int, orthoclase)	normal
MP737a	rhyodacite	cc	dark chlorite	clinochlore fe, clinochlore ferr, chamosite, albite ord	normal
MP737b	rhyodacite	cc	groundmass concentrated, albitised rock	quartz, albite ord,	
MP737c	rhyodacite	cc	whole rock, albitised	quartz, albite ord,	normal
MP770a	rhyodacitic dyke	py	whole rock, potassic altered rock	quartz, orthoclase bar, (microcline int, orthoclase)	normal
MP855a	volcanic sediment	bckd	chlorite in matrix	clinochlore, chamosite?	normal
MP855b	volcanic sediment	bckd	clay in matrix	quartz, celadonite, muscovite, montmorillonite, illite	2 normal
MP855c	volcanic sediment	bckd	kfd in matrix	quartz, celadonite, corrensite, gedrite, (muscovite, ort ba)	normal
RB9927a	volcanic sediment	bckd	chlorite-mica in vugs	muscovite, celadonite, clinochlore, glauconite	normal
RB9928a	volcanic sediment	bckd	whole rock, altered	quartz, microcline int, albite ord	normal
RB9912a	volcanic sediment	py-cp	white vein, potassic altered sediment	quartz, orthoclase bar, illite, orthoclase, albite ord	detailed, normal
RB9912b	volcanic sediment	py-cp	whole rock, potassic altered sediment	quartz, albite ord, (sanidine, microcline int, sanidine dis)	normal
RB9926a	volcanic sediment	cp-bn	cream mineral in vein	laumontite	normal
MP854a	volcanic sediment	bn	whole rock, albitised	quartz, albite ord, albite cal ord	normal
MP854b	volcanic sediment	bn	groundmass concentrated, albitised rock	quartz, albite ord, albite cal ord	normal
RB9839a	volcanic sediment	bn	matrix concentrated, albitised rock	albite ord, quartz, albite cal ord	normal

Abbreviations:

Ore Zone:

bckd:background
py:pyrite
py-cp:pyrite-chalcopyrite
cp:chalcopyrite
cp-bn:chalcopyrite-bornite
bn:bornite
bn-cc:bornite-chalcocite
cc:chalcocite

Results

ord: ordered
int: intermediate
dis: disordered

Appendix 4.2.- X-Ray Diffractograms for selected samples.

- Listed by host rock and ore zone
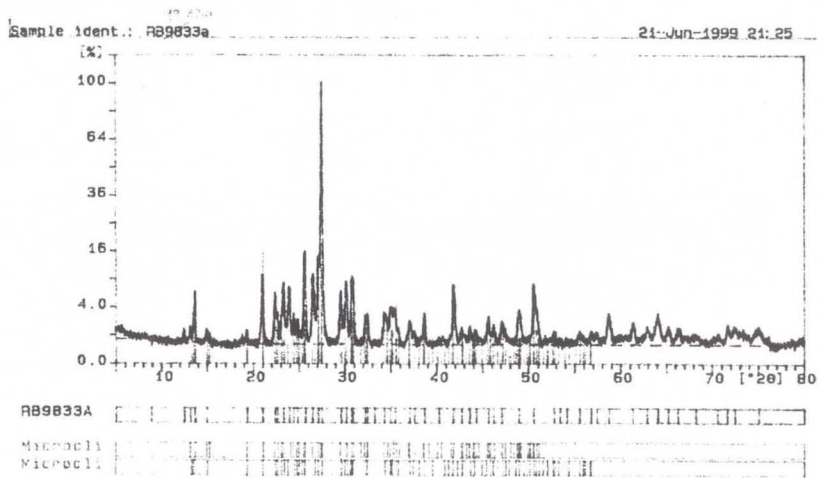
RB9933 basalt, background zone
microcline in vug
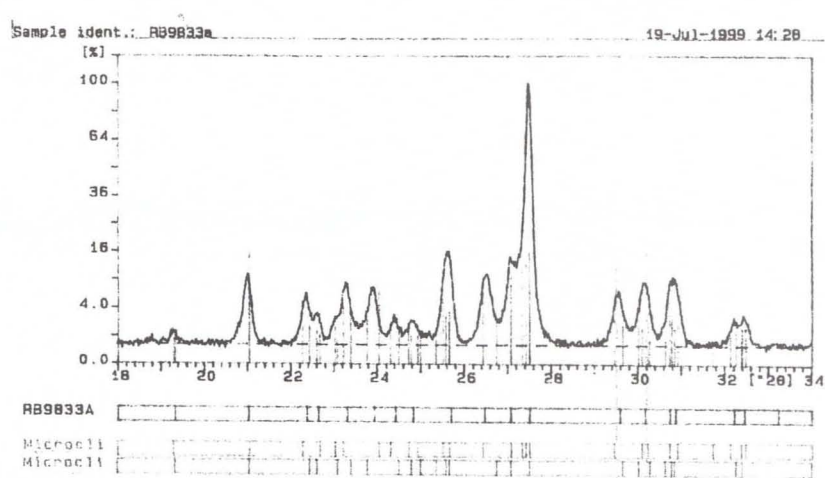
RB9933 basalt, background zone
microcline in vug
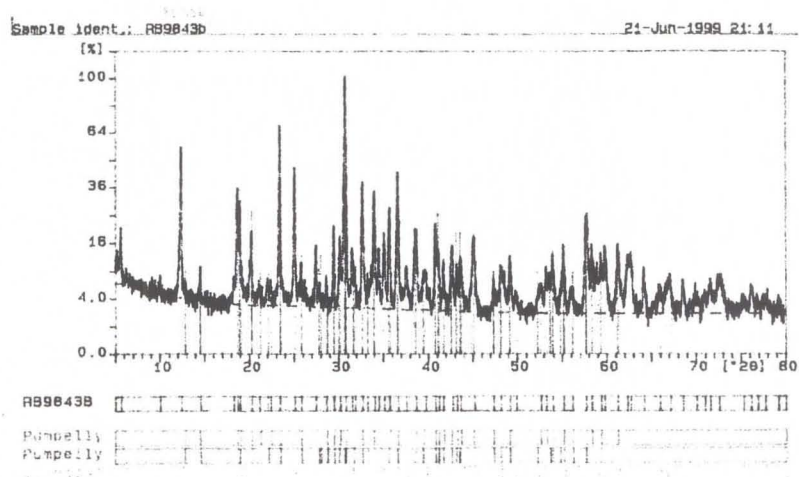
RB9933 basalt, background zone
chlorite – pumpellyte? in vug
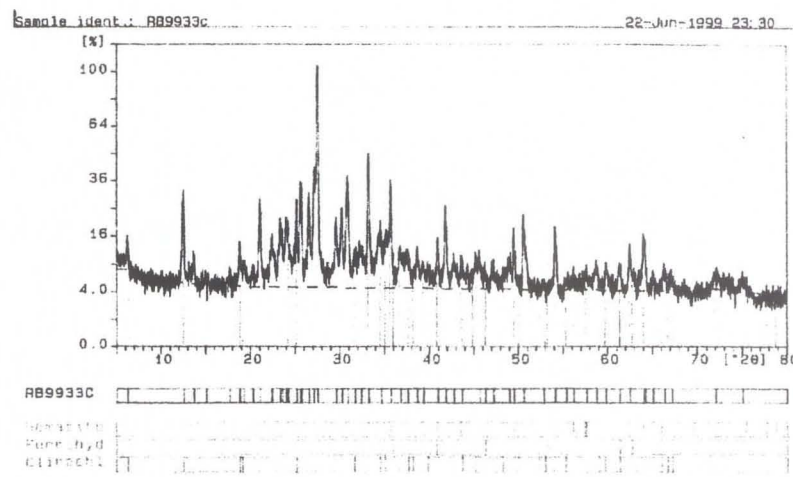
RB9933 basalt, background zone
hematite in vug
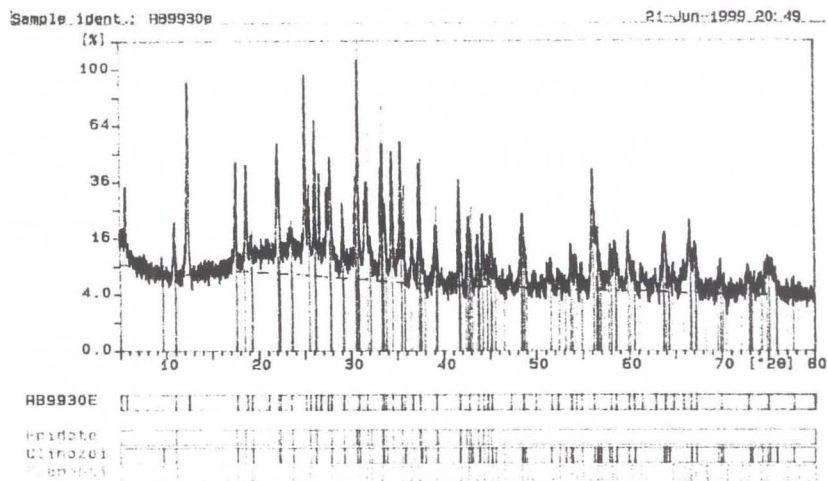
RB9930 basalt, background zone
epidote in vug
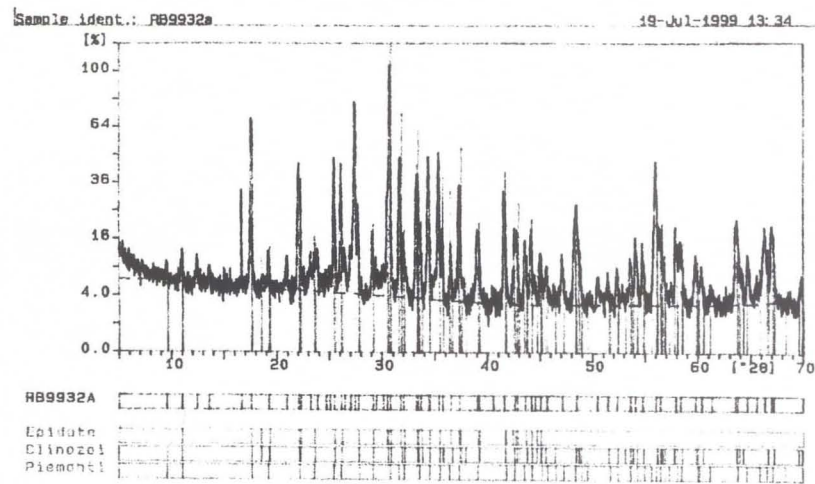
RB9932 basalt, background zone
epidote in vein
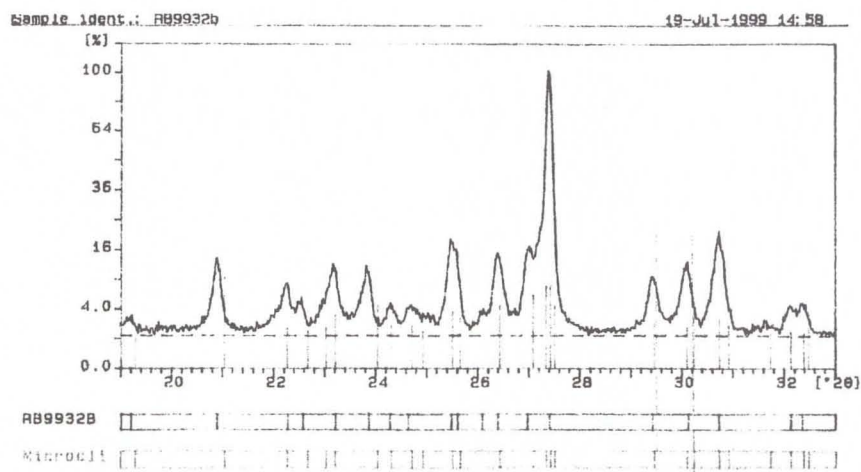
RB9932 basalt, background zone
microcline in vein
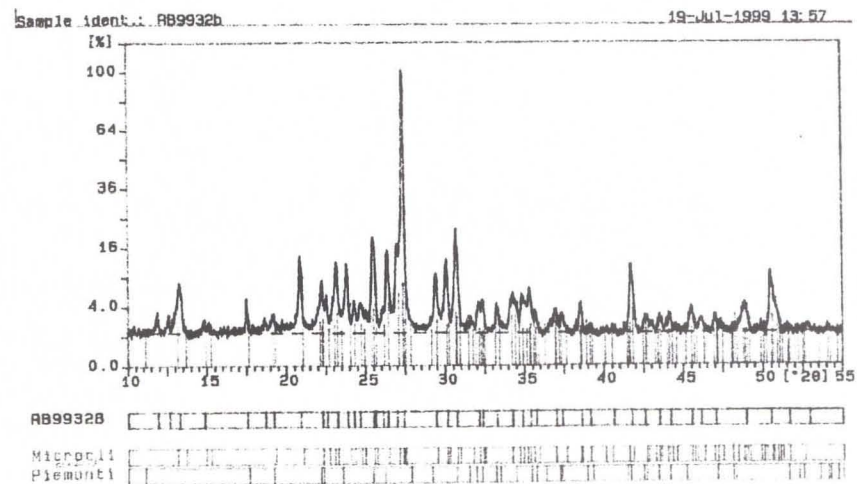
RB9932 basalt, background zone
microcline, epidote in vein
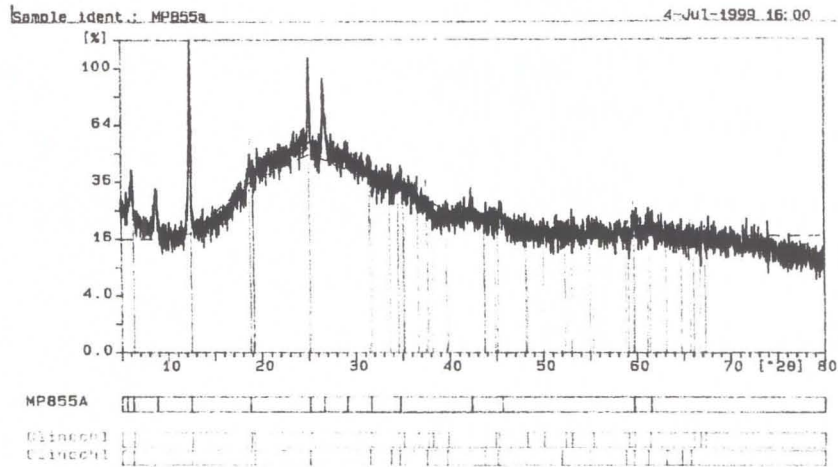
MP 855 vol. sed., background zone
chlorite in matrix
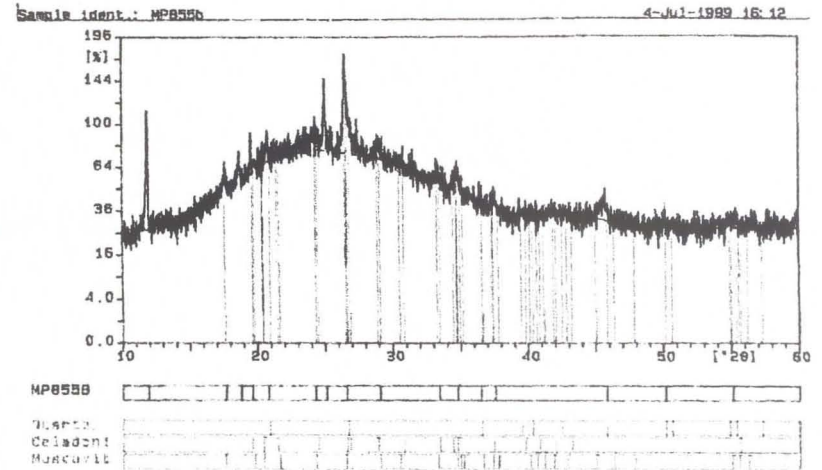
MP 855 vol. sed., background zone
celadonite, muscovite in matrix
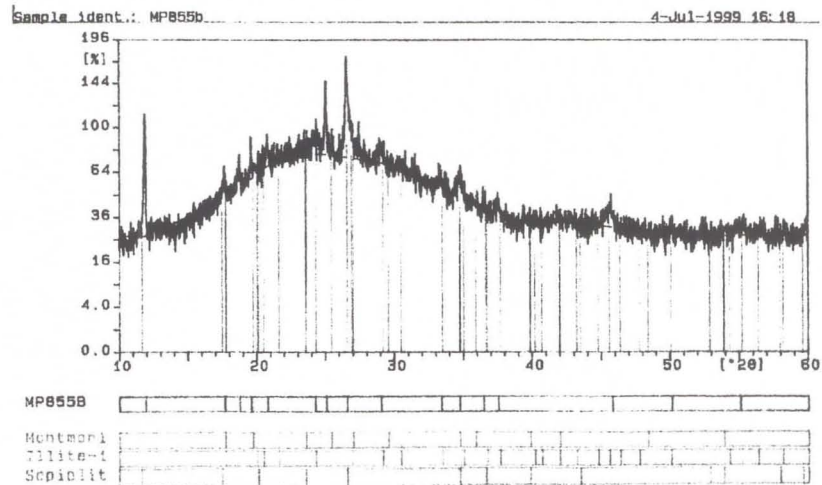
MP 855 vol. sed., background zone
montmorillonite, illite in matrix
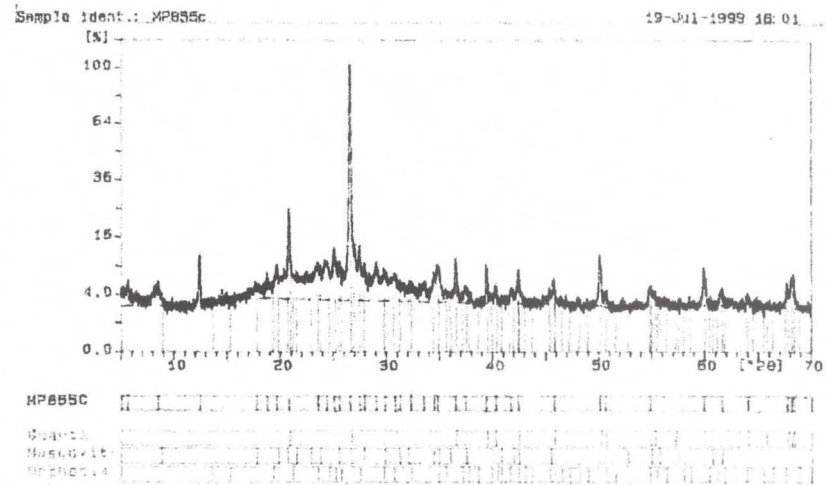
MP 855 vol. sed., background zone
orthoclase? in vein
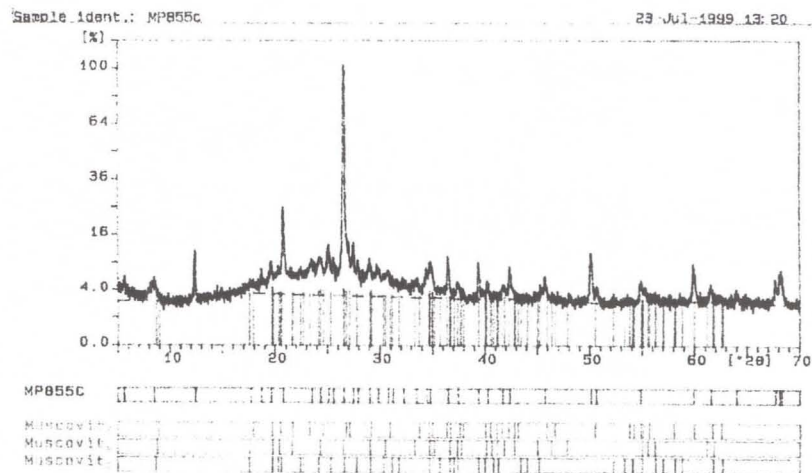
MP 855 vol. sed., background zone
muscovite
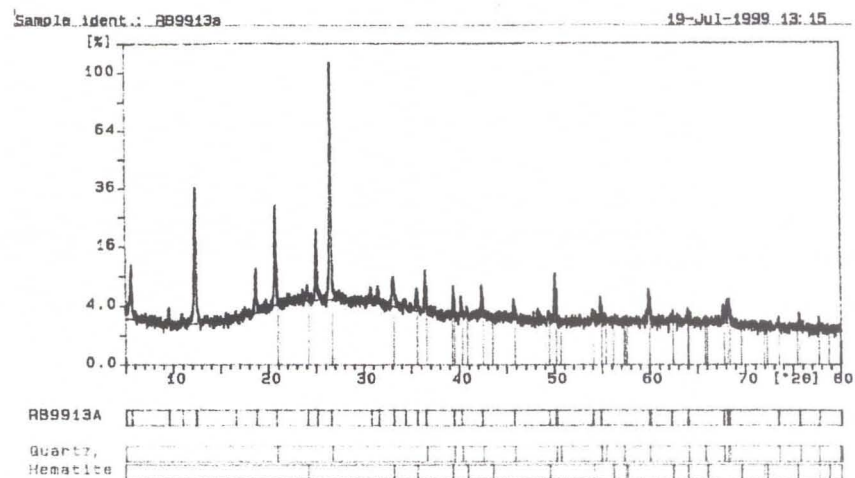
RB9913 basalt, background zone
hematite, quartz in vein
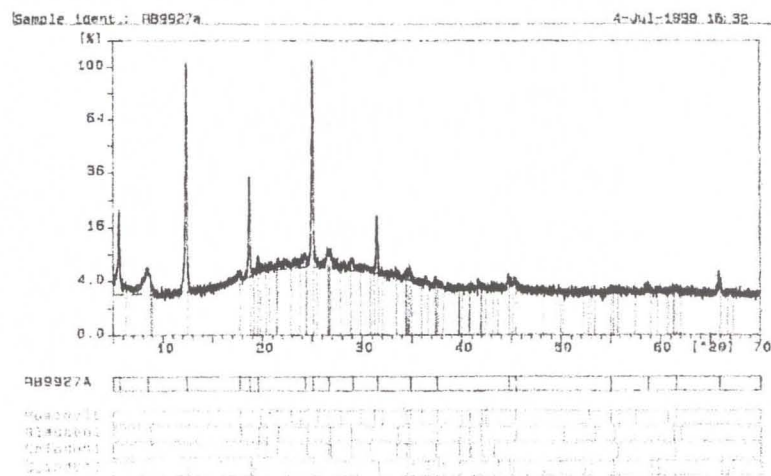
RB9927 vol. sed., background zone
chlorite, muscovite in vugs
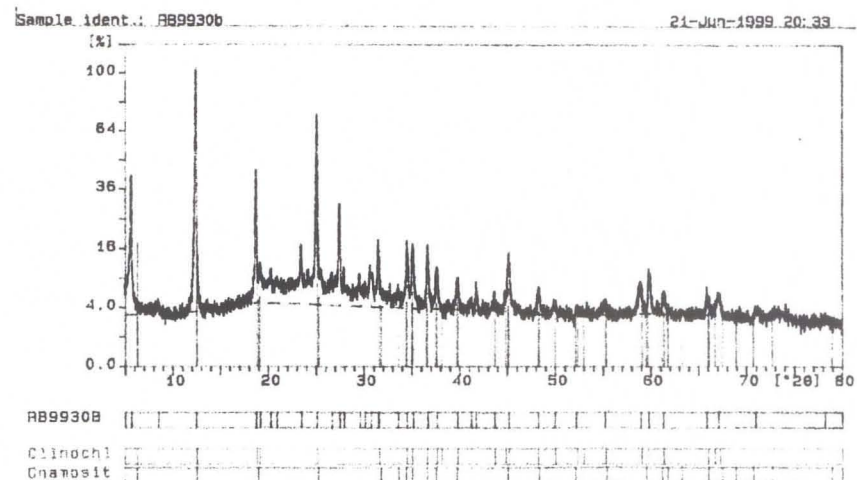
RB9930 basalt, background zone
chlorite in vug
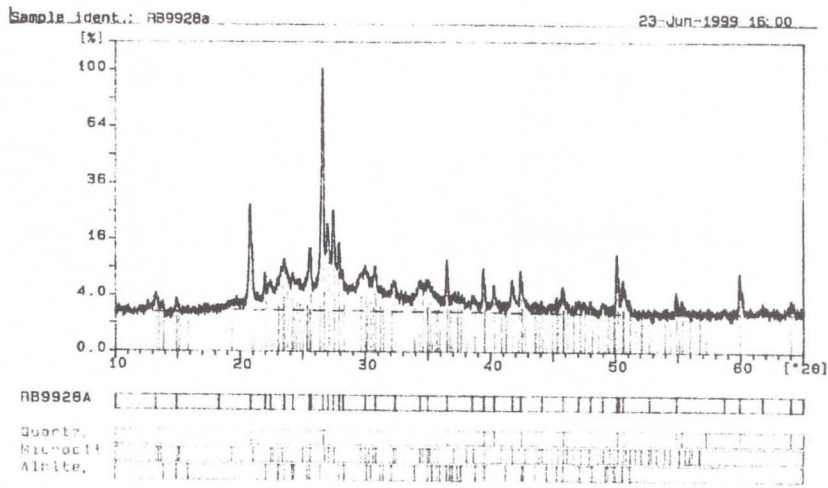
RB9928 vol. sed., close to dyke
quartz, microcline, albite in groundmass
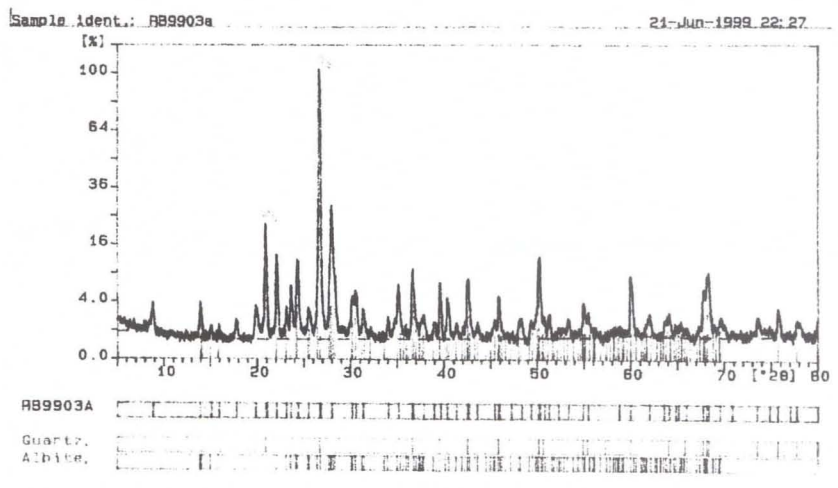
RB9903 rhyodacite, py zone
quartz, albite in groundmass
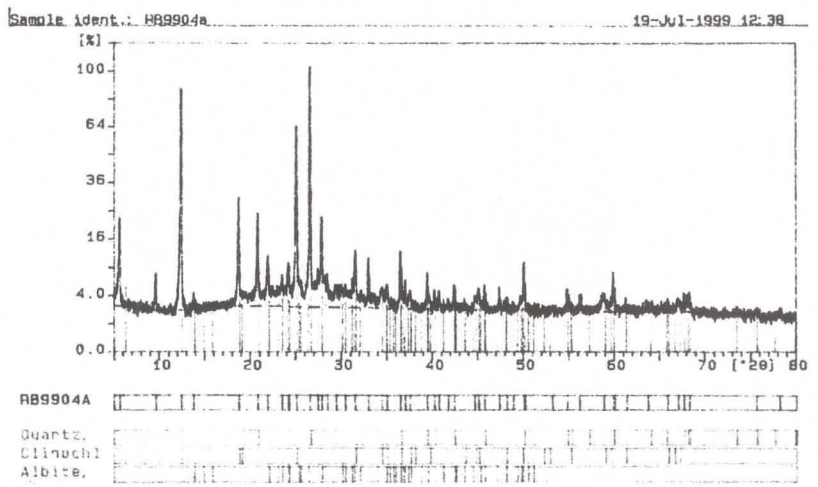
RB9904 rhyodacite, py zone
quartz, chlorite, albite in vein
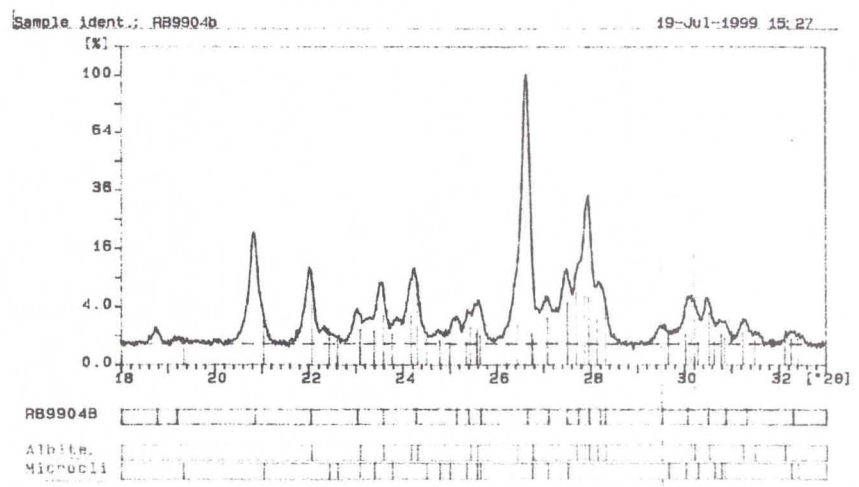
RB9904 rhyodacite, py zone
albite, microcline in vein
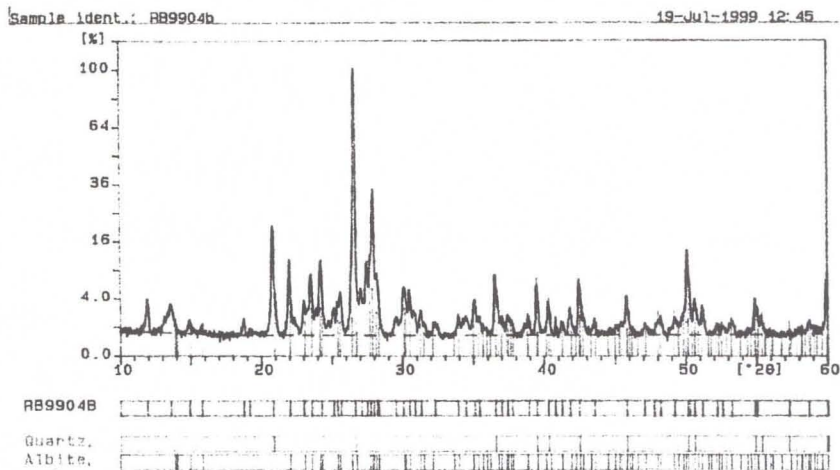
RB9904 rhyodacite, py zone
albite, quartz in groundmass
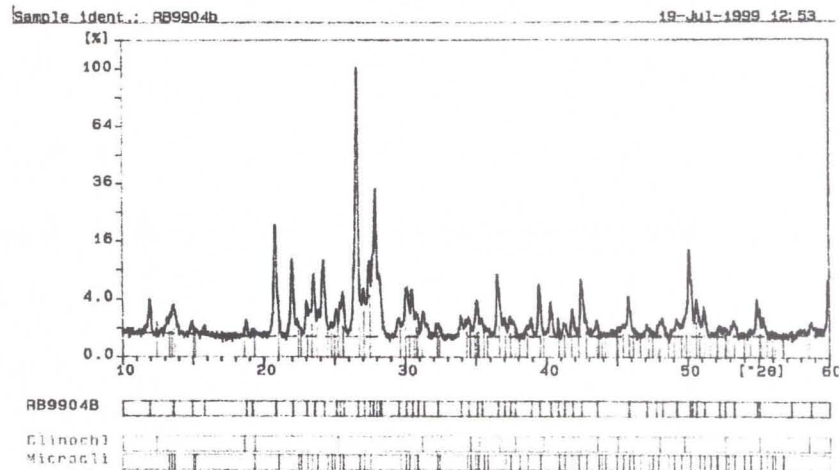
RB9904 rhyodacite, py zone
microcline, chlorite in groundmass
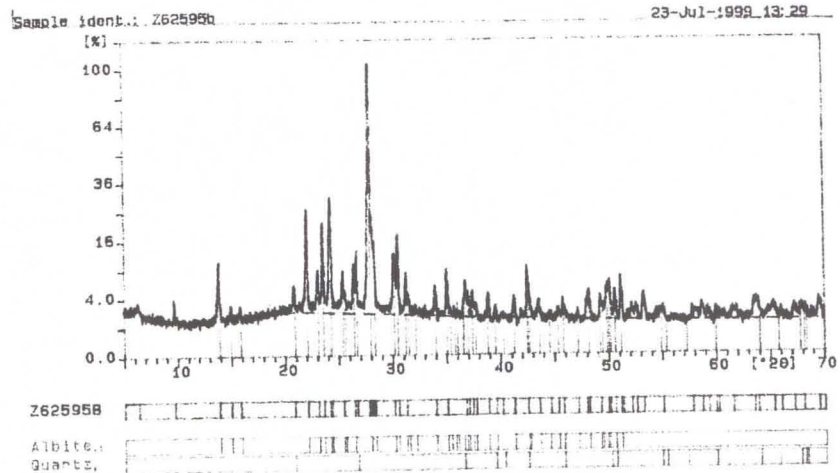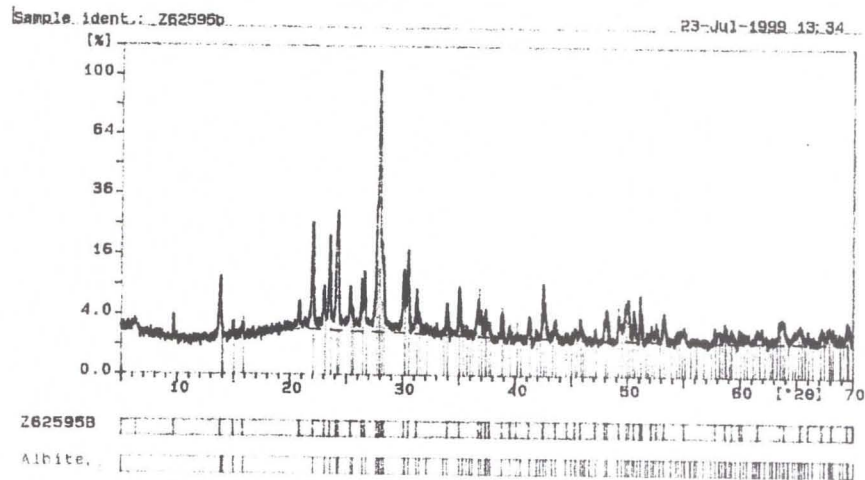
Z62595 rhyodacite, py zone
albite, quartz in groundmass

Z62595 rhyodacite, py zone
albite in groundmass
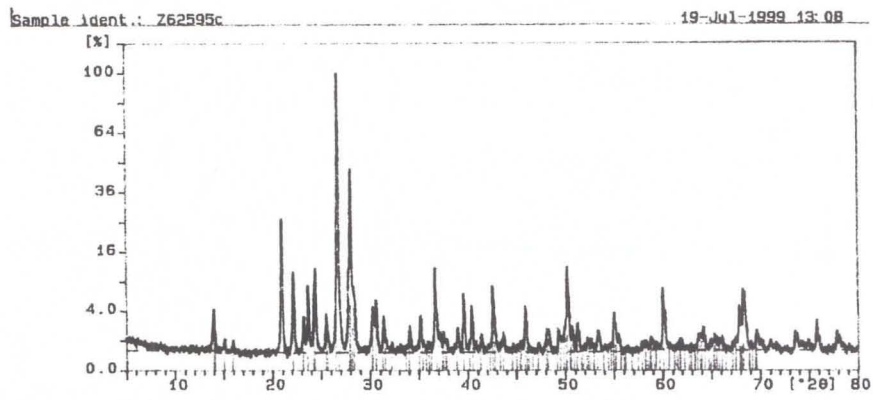
Z62595 rhyodacite, py zone
albite in groundmass
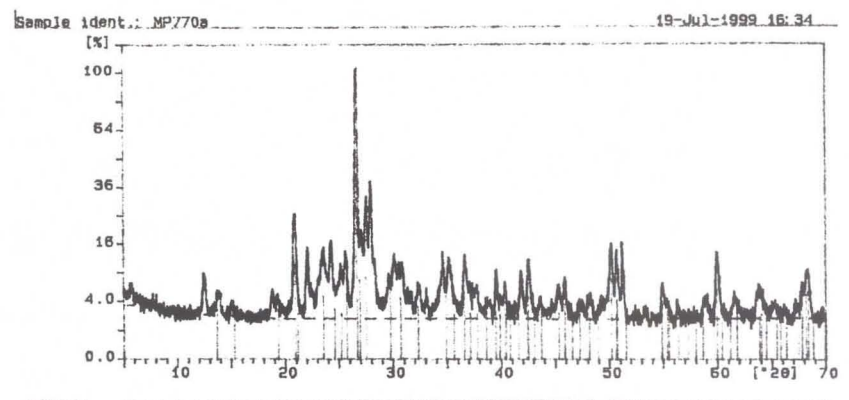
MP 770 rhyodacitic dyke, py zone
quartz, orthoclase
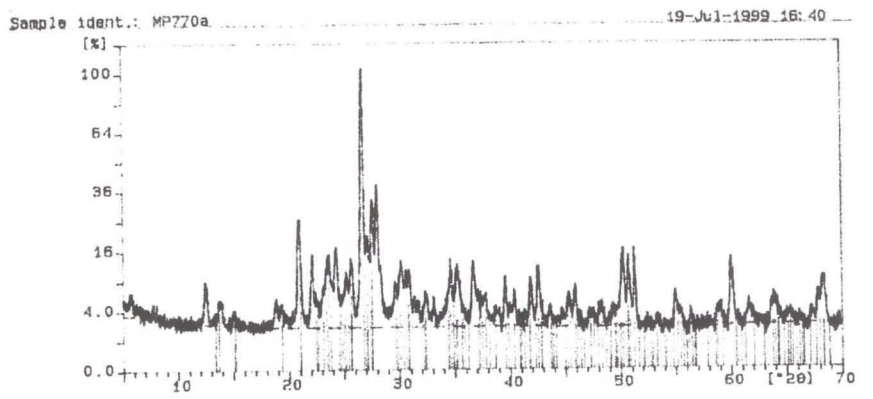
MP 770 rhyodacitic dyke, py zone
microcline
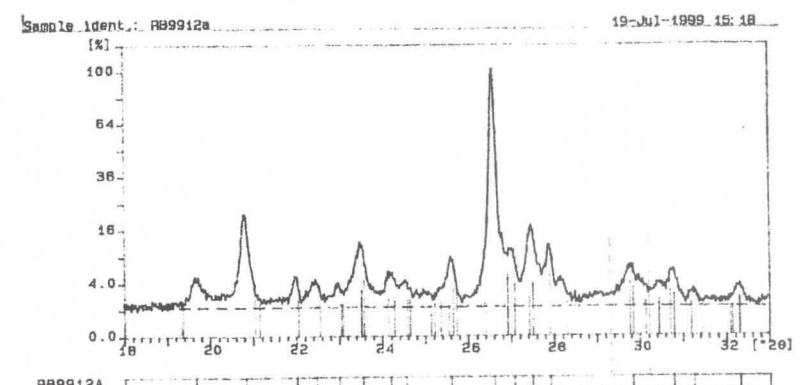
RB9912 volcanic sediment, py-cp zone
orthoclase, albite in vein
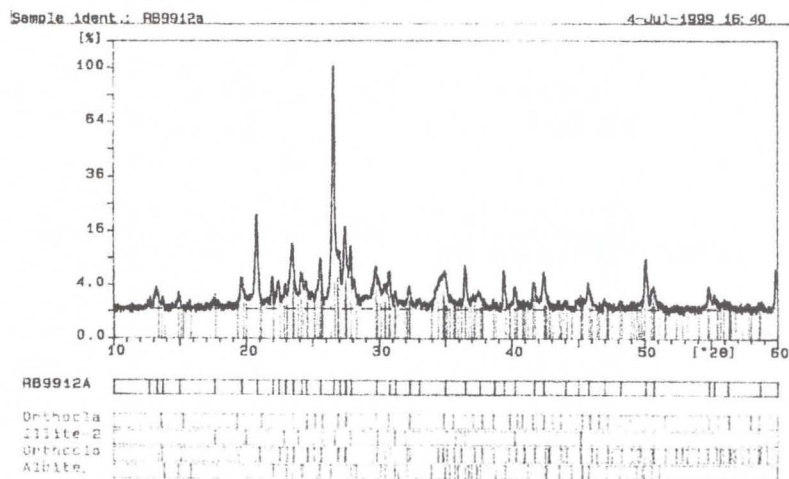
RB9912 volcanic sediment, py-cp zone
orthoclase, illite in vein
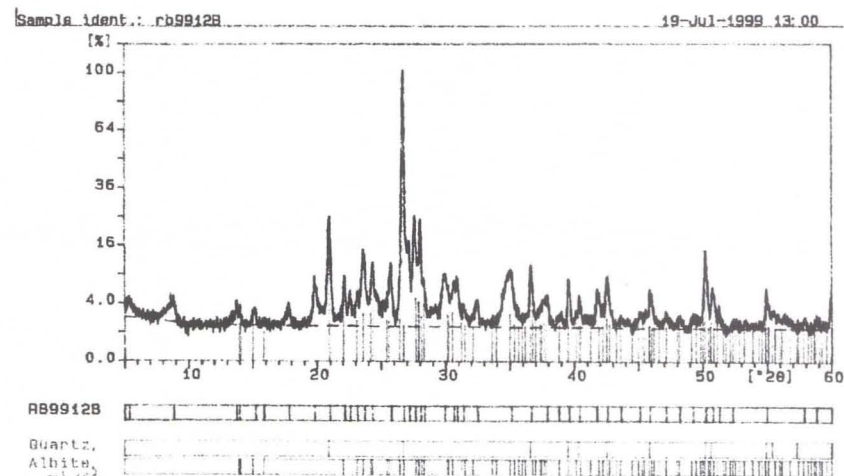
RB9912 volcanic sediment, py-cp zone
quartz, albite in whole rock
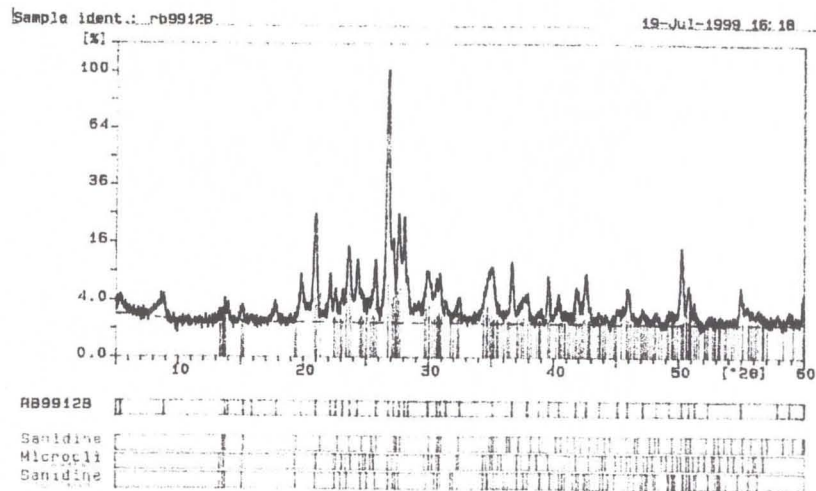
RB9912 volcanic sediment, py-cp zone
microcline in whole rock
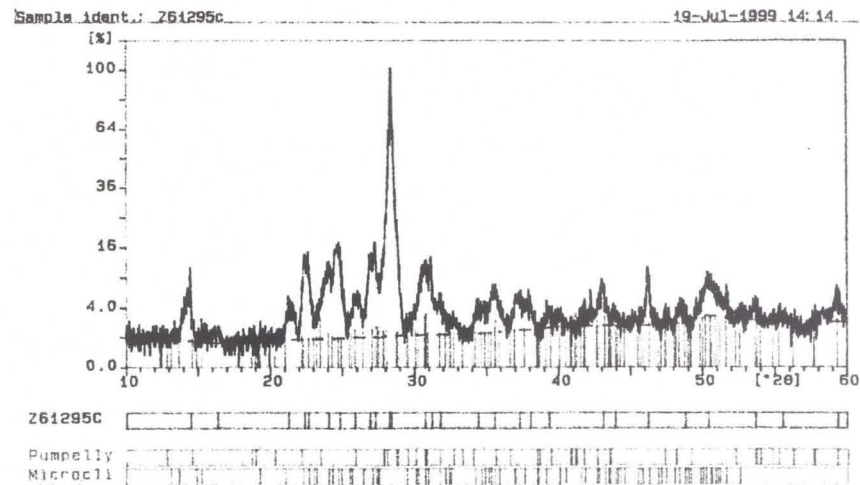
Z61295 rhyodacite, cp zone
microcline-pumpellyte? in groundmass
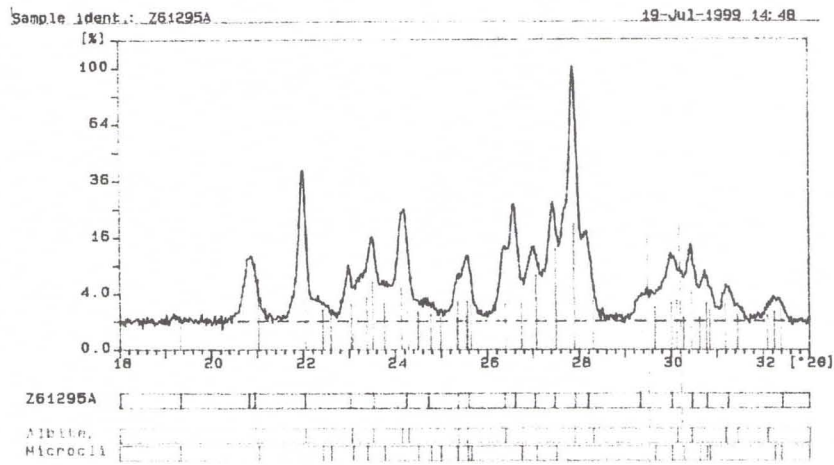
Z61295 rhyodacite, cp zone
microcline, albite in groundmass
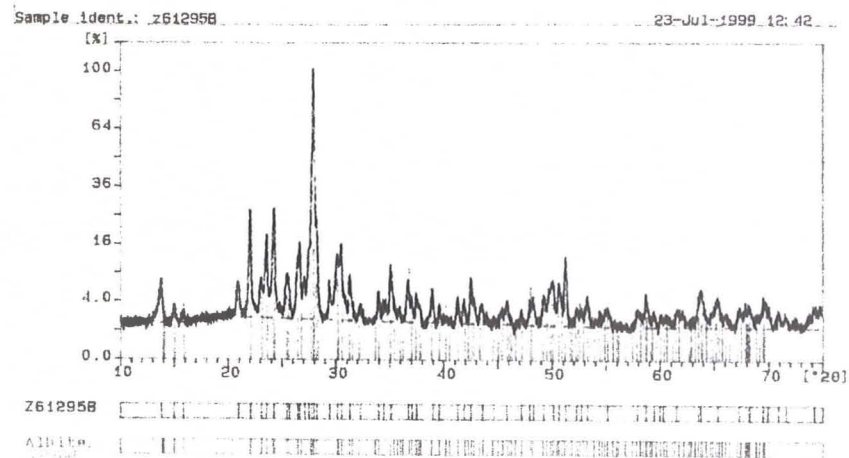
Z61295 rhyodacite, cp zone
albite, quartz in groundmass
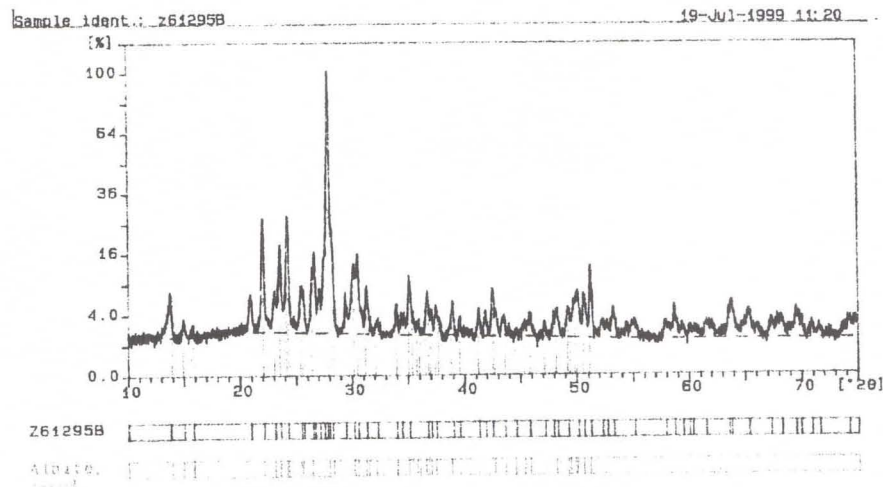
Z61295 rhyodacite, cp zone
albite in groundmass
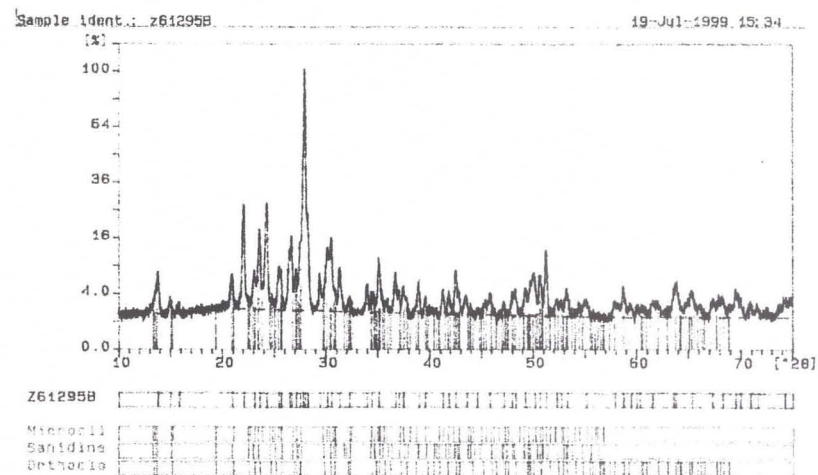
Z61295 rhyodacite, cp zone
microcline in groundmass
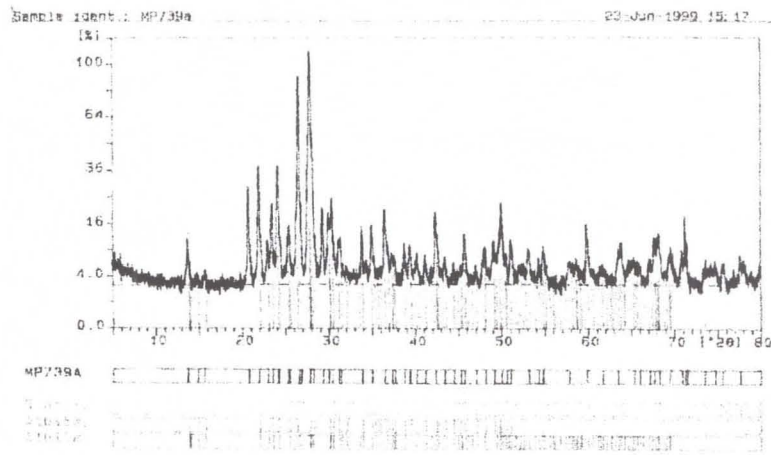
MP 739 rhyodacite, cp-bn zone
quartz, albite in groundmass
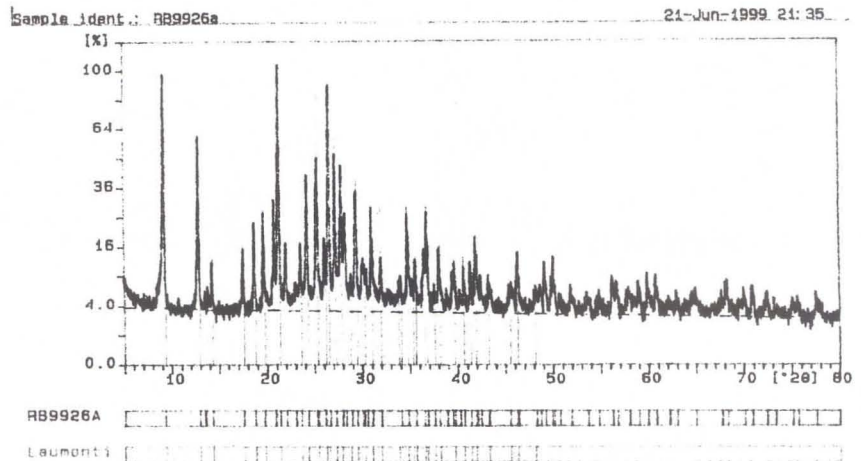
RB9925 volcanic sediment, cp-bn zone
laumontite in vein
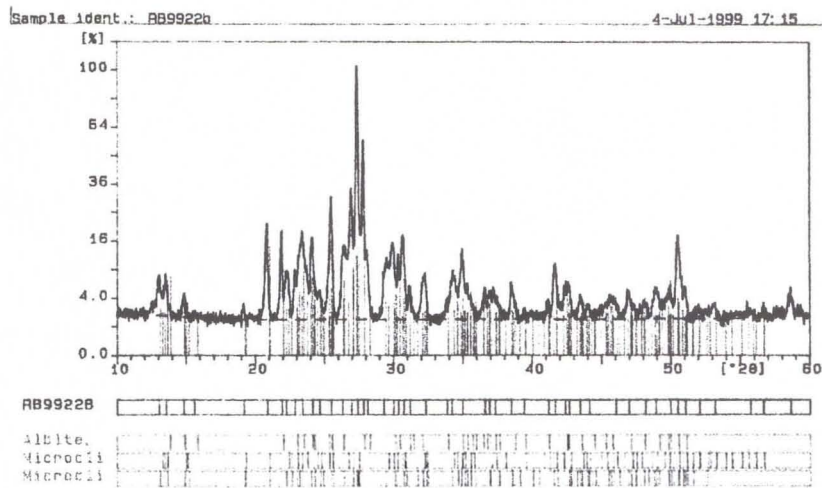
RB9922 basalt, cp-bn zone
albite and microcline in vein
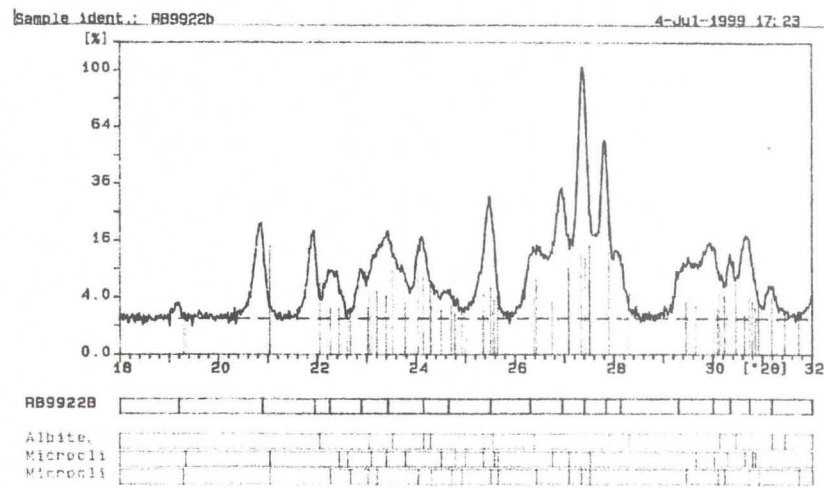
RB9922 basalt, cp-bn zone
albite and microcline in vein
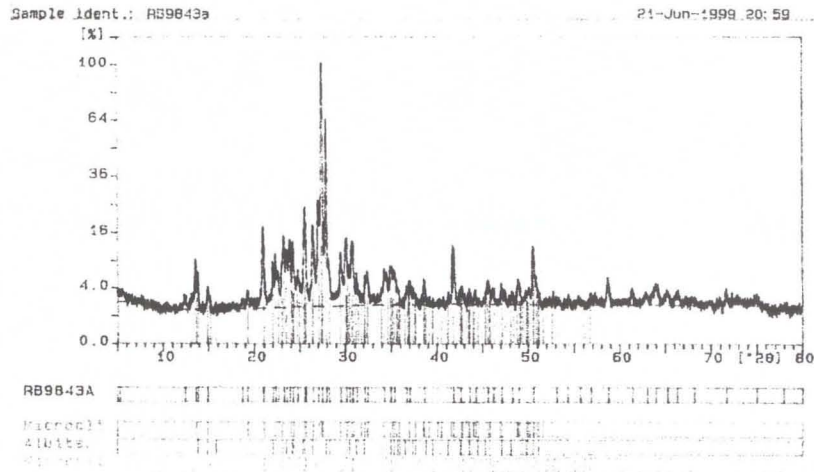
RB9843 basalt, bn zone
microcline and albite in vug
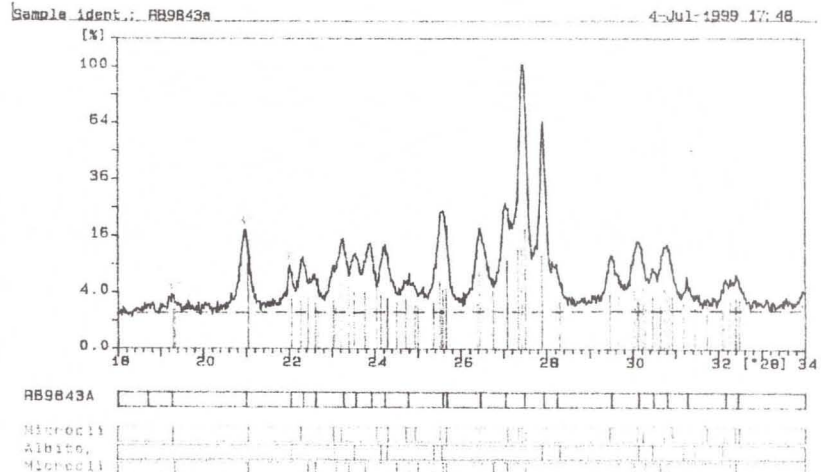
RB9843 basalt, bn zone
microcline and albite in vug
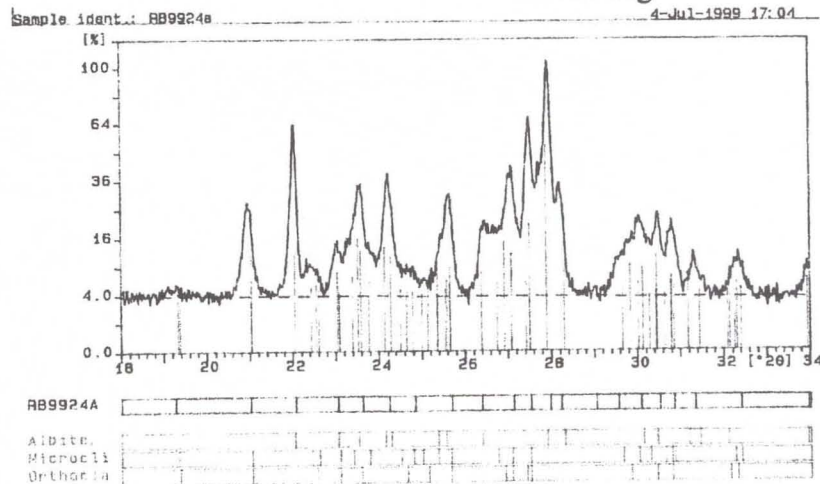
RB9924 basaltic dyke, bn zone
albite and microcline in vein
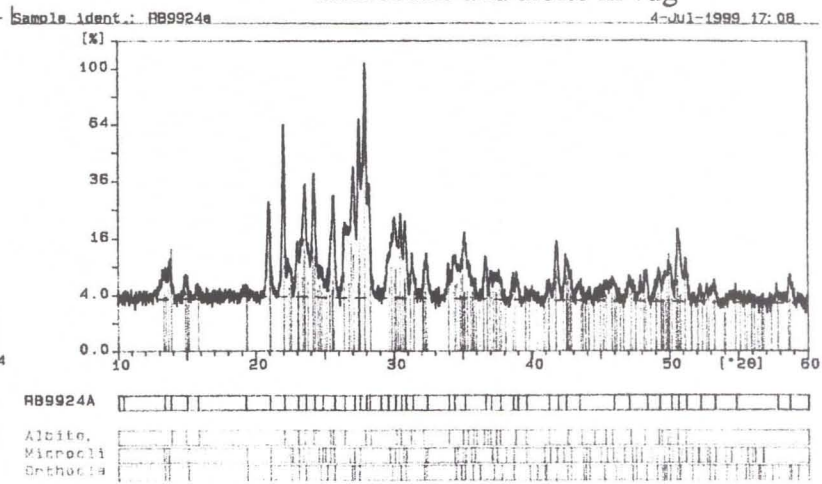
RB9924 basaltic dyke, bn zone
albite and microcline in vein
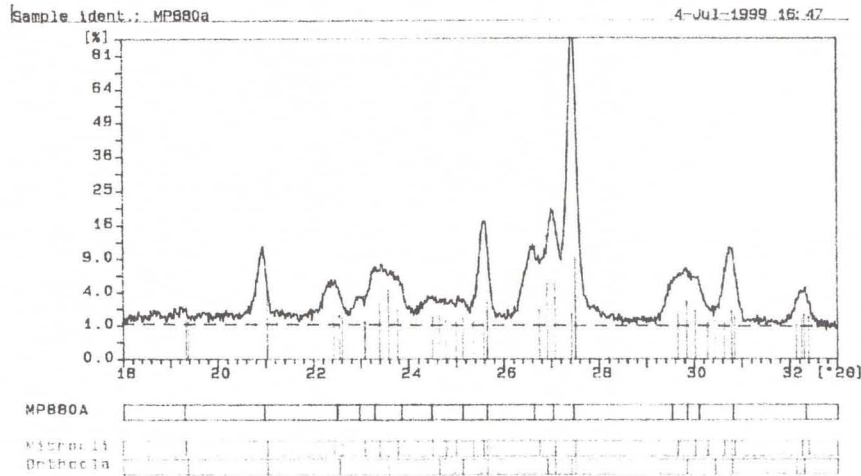
MP 880 basalt Veta Negra Fm, bn zone
microcline in vein
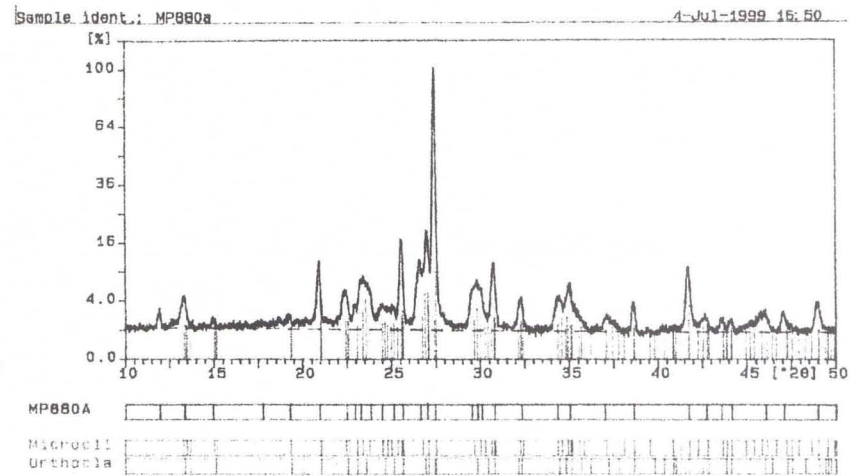
MP 880 basalt Veta Negra Fm, bn zone
microcline in vein
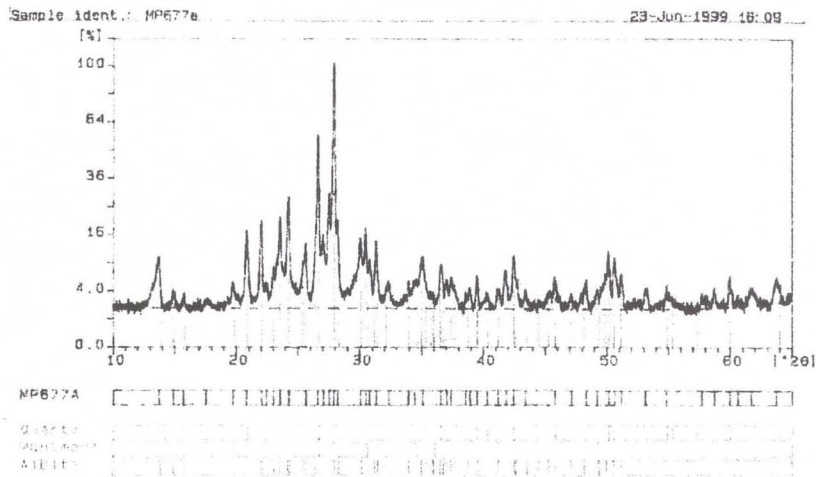
MP 677 rhyodacite, bn zone
quartz, montmrillonite, albite in groundmass
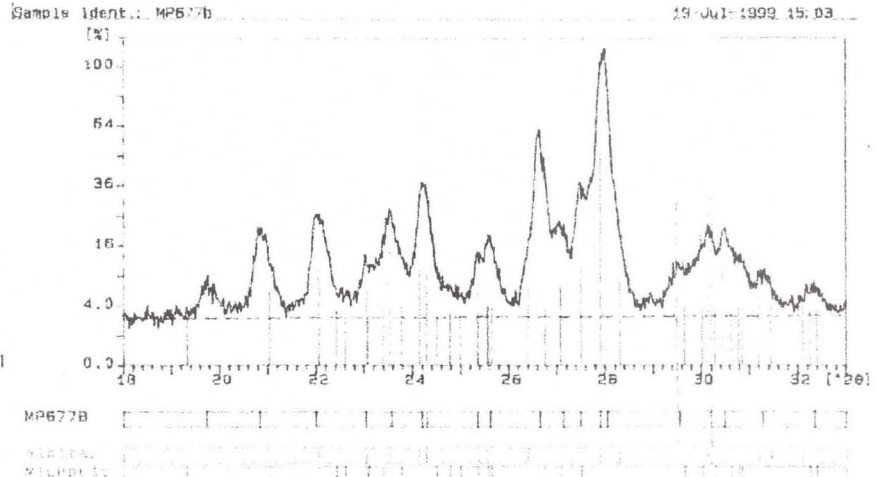
MP 677 rhyodacite, bn zone
albite, microcline in groundmass
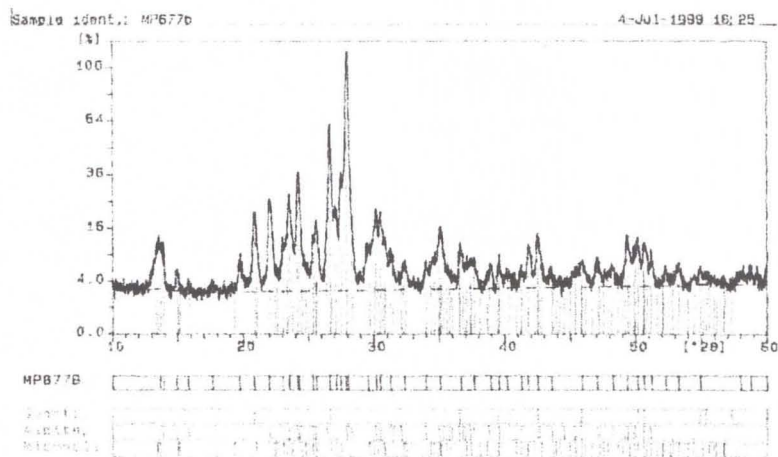
MP 677 rhyodacite, bn zone
albite, microcline in groundmass
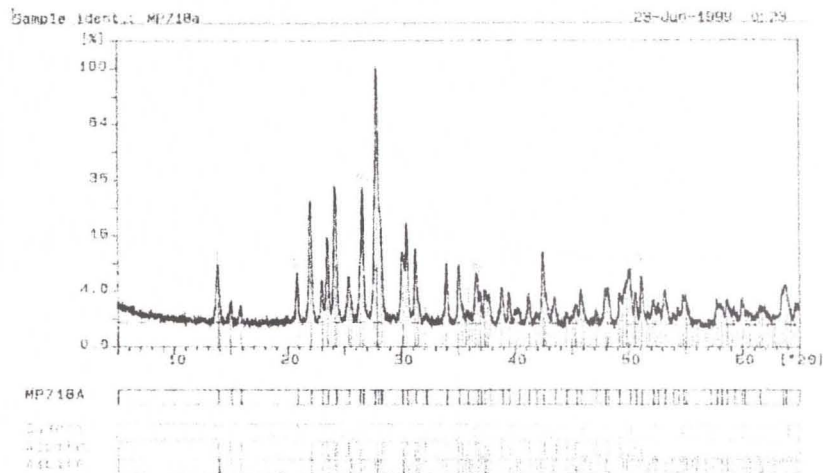
MP 718 rhyodacite, bn zone
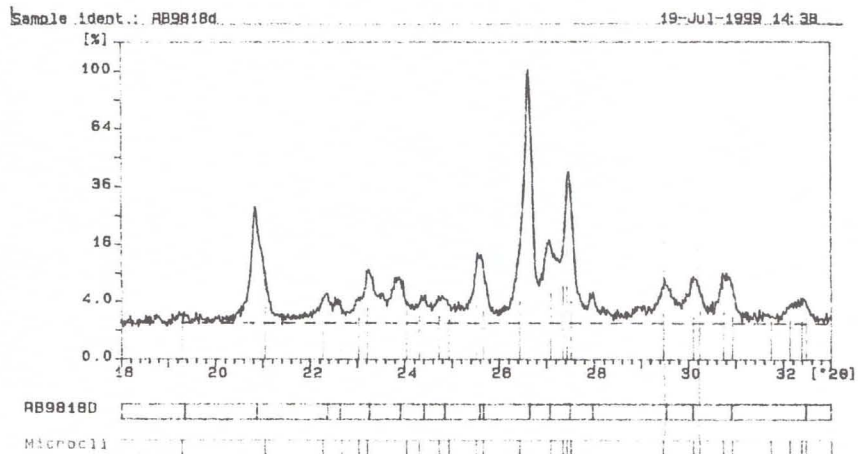albite, quartz in groundmass
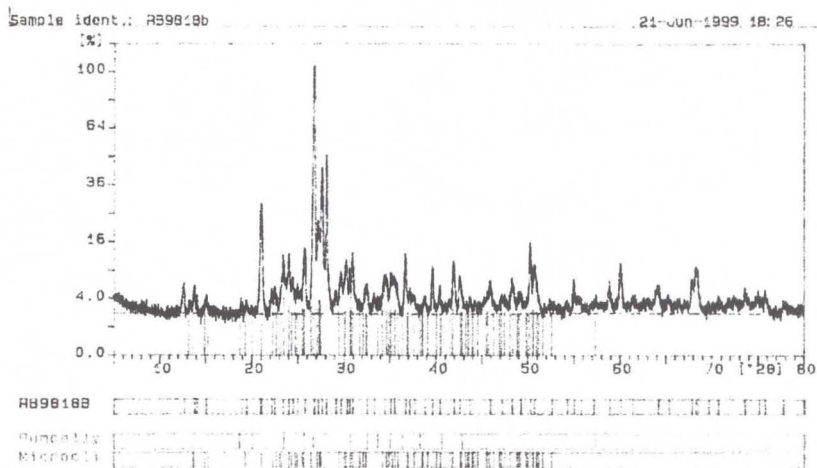
RB9818 rhyodacite, bn zone
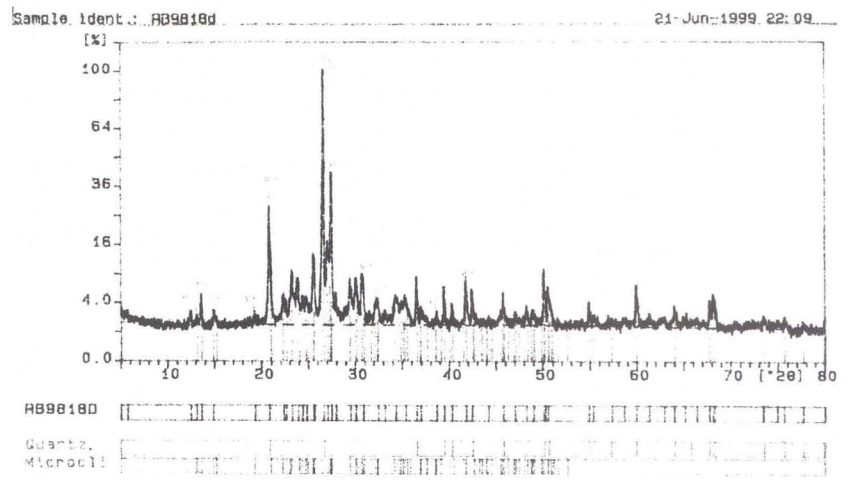microcline, pumpellyte in matrix
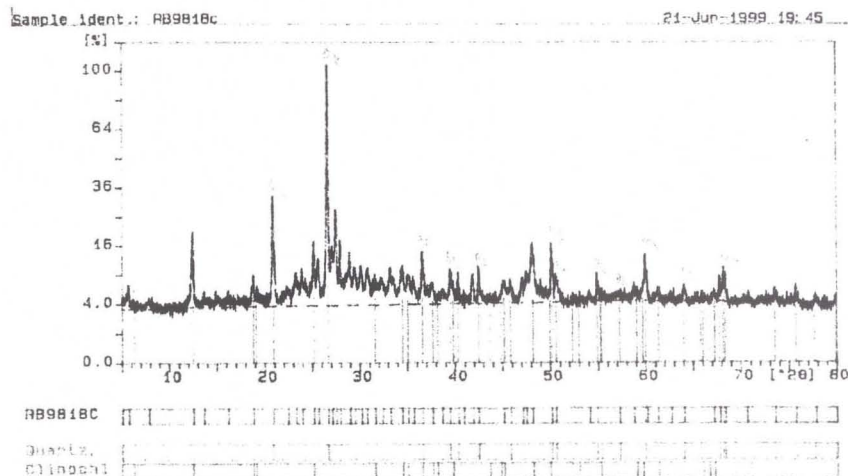
RB9818 rhyodacite, bn zone
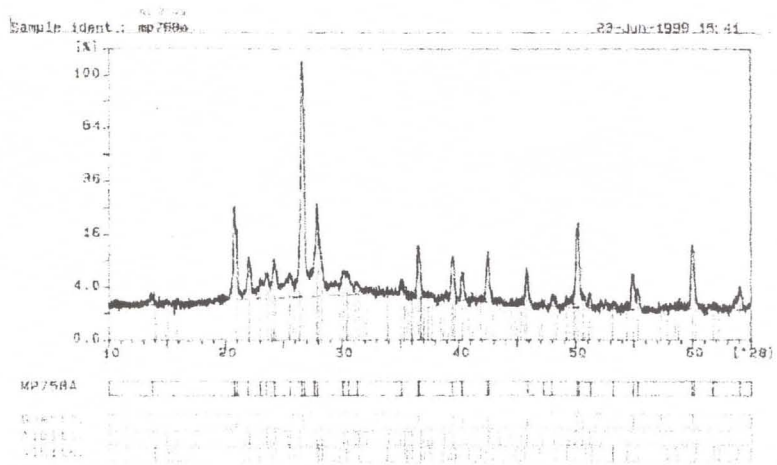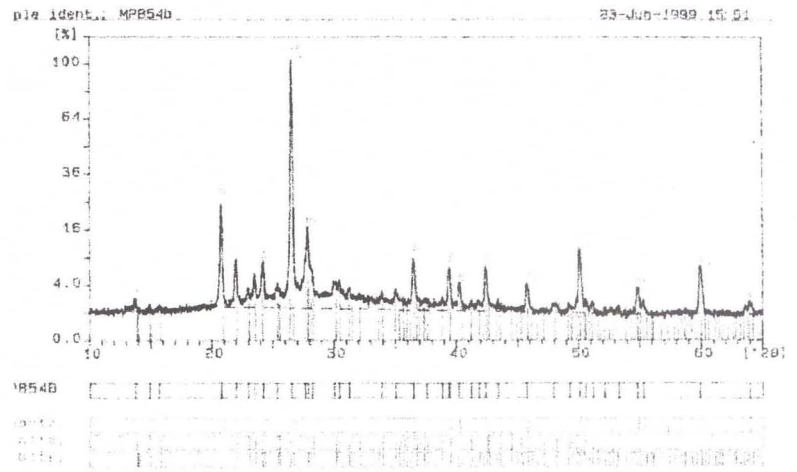chlorite, quartz in matrix

RB9818 rhyodacite, bn zone
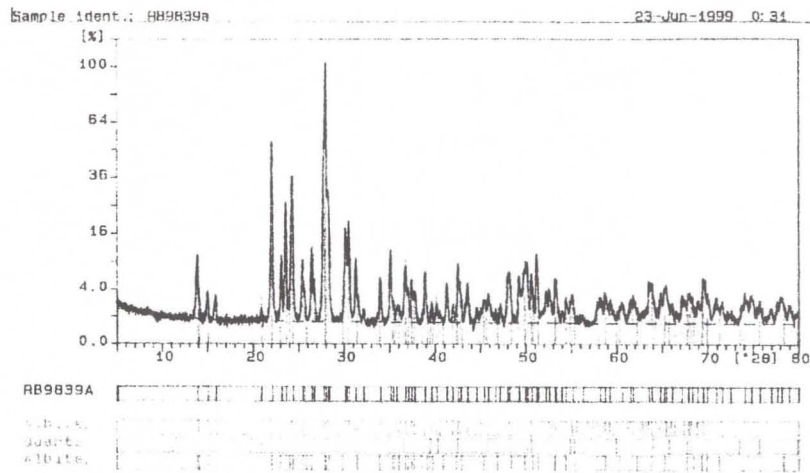microcline in matrix

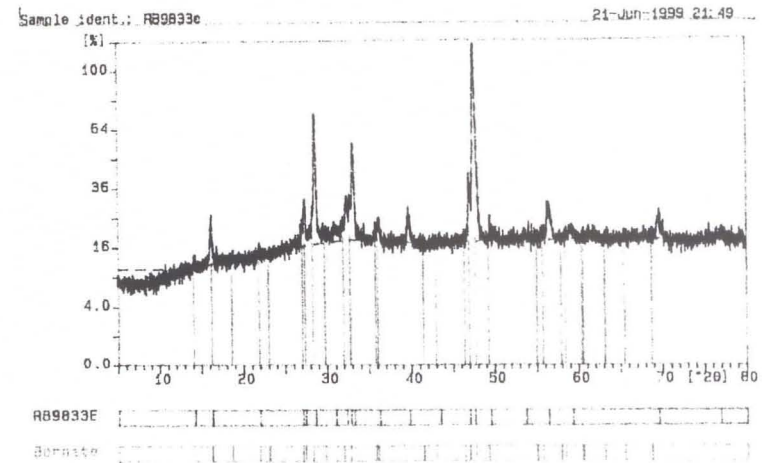RB9818 rhyodacite, bn zone
microcline, quartz in fragment
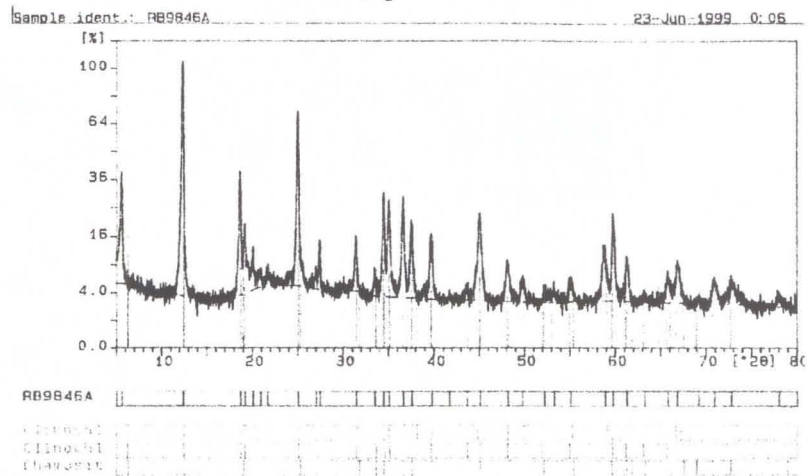

MP 854 volcanic sediment, bn zone
albite in groundmass

MP 854 volcanic sediment, bn zone
albite in groundmass

RB9839 volcanic sediment, bn zone
albite, quartz in matix

RB9833 basalt, bn-cc zone
bornite in amygdule

RB9846 basalt, bn-cc zone
chlorite in amygdule
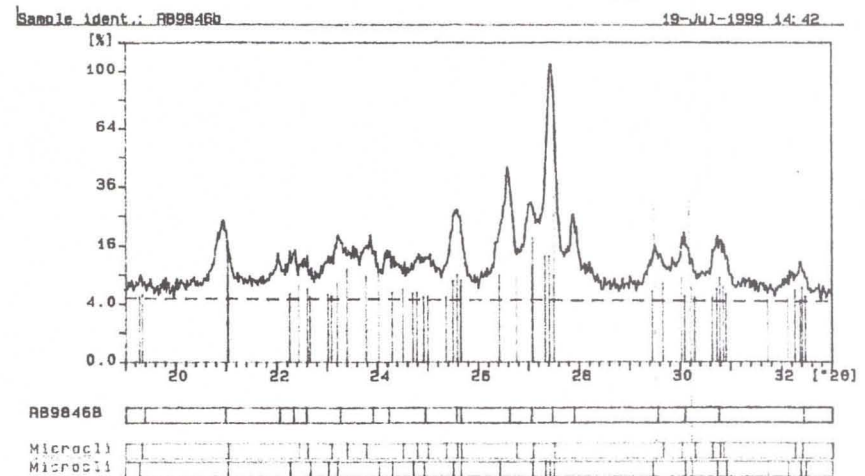
RB9846 basalt, bn-cc zone
microcline in amygdule
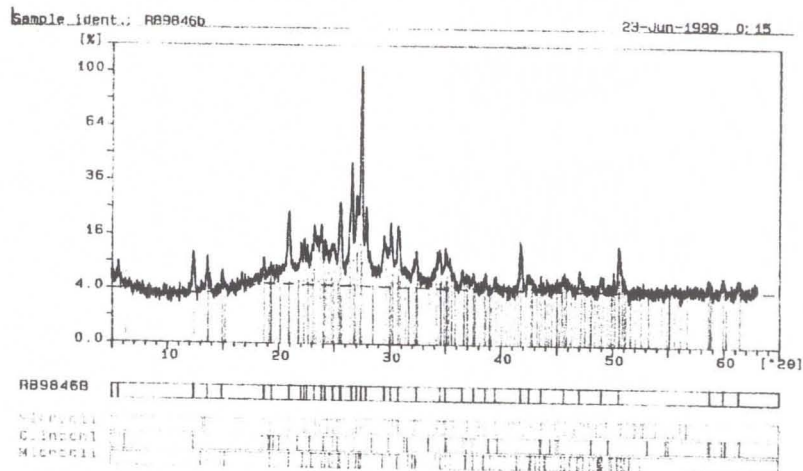
RB9846 basalt, bn-cc zone
microcline in amygdule
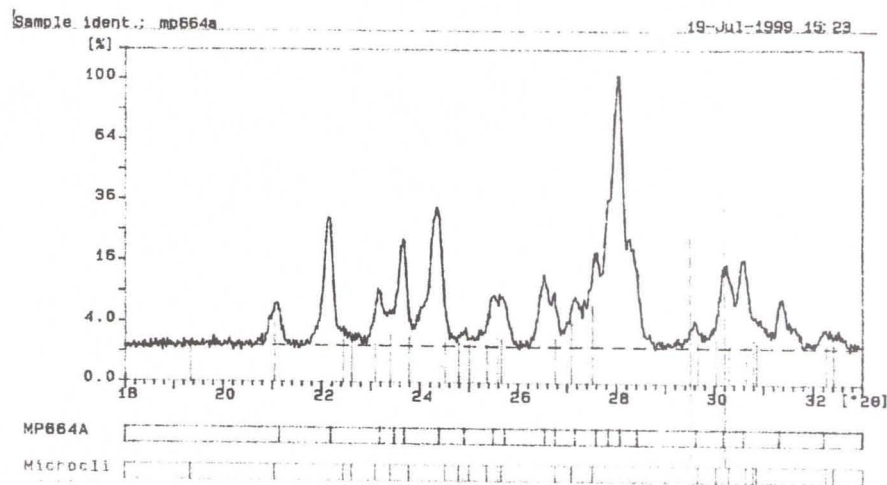
MP 664 rhyodacite, bn-cc zone
microcline in groundmass
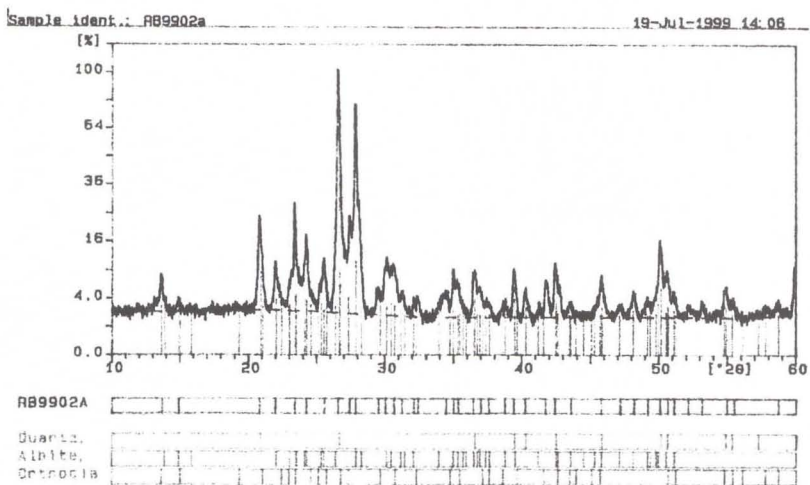
RB9902 rhyodacite, py zone
quartz, albite, orthoclase in groundmass
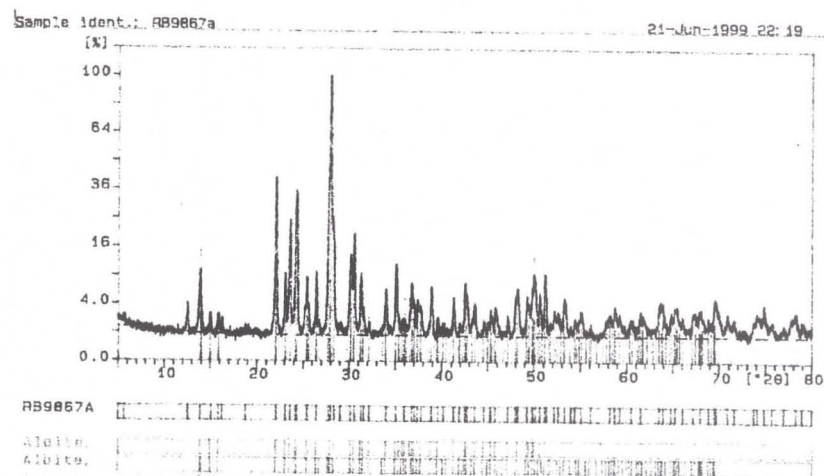
RB9867 rhyodacite, bn-cc zone
albite in groundmass

Sample ident.: MP864a   23-Jul-1999 12:52
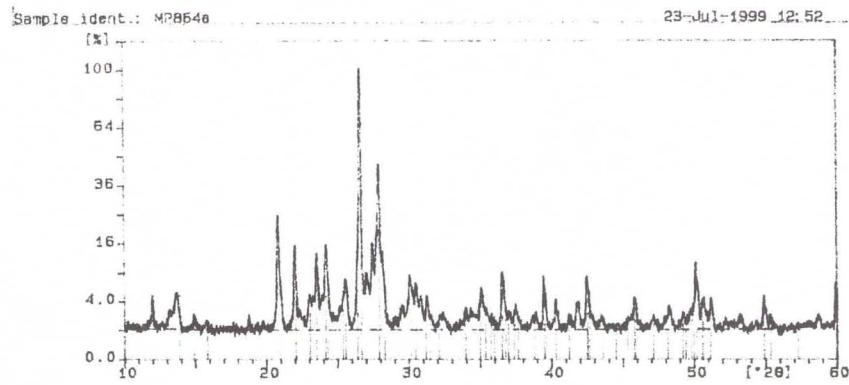
MP 864 rhyodacite, bn-cc zone
albite phenocryst
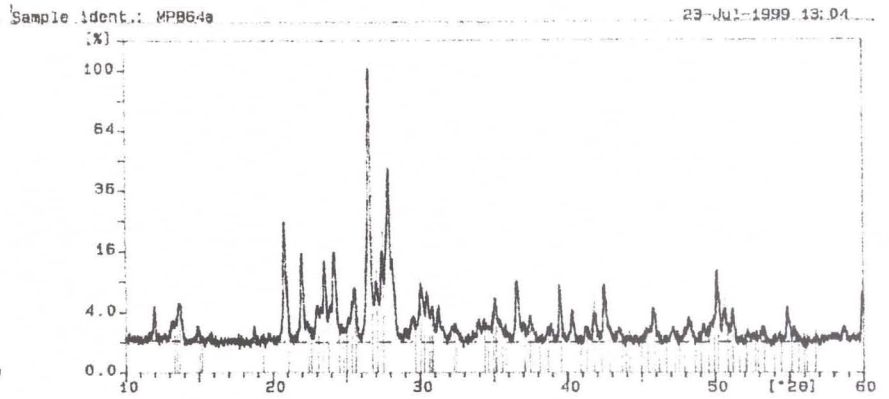
Sample ident.: MP864a   23-Jul-1999 13:04

MP 864 rhyodacite, bn-cc zone
microcline in veinlet

Sample ident.: RB9815a   19-Jul-1999 12:10

RB9815 rhyodacite, bn-cc zone
albite in matriz

Sample ident.: RB9901a   19-Jul-1999 15:54
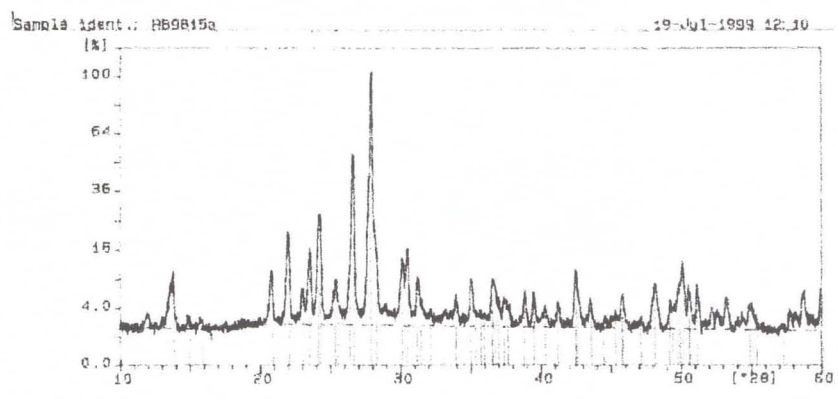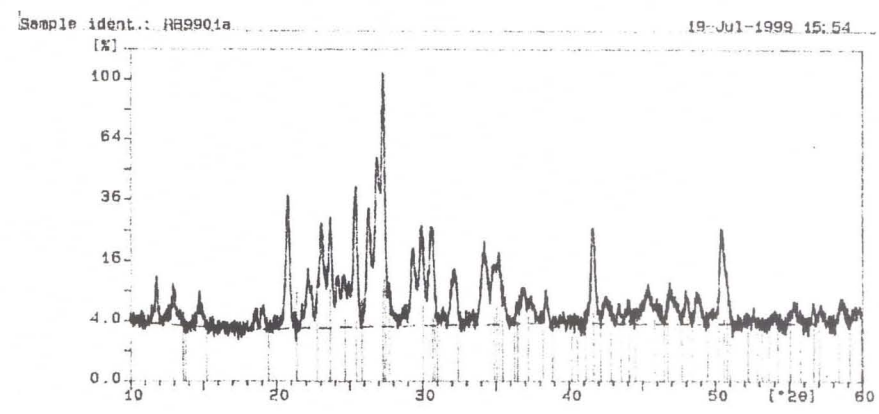
RB9901 rhyodacite, bn-cc zone
sanidine in altered fragment
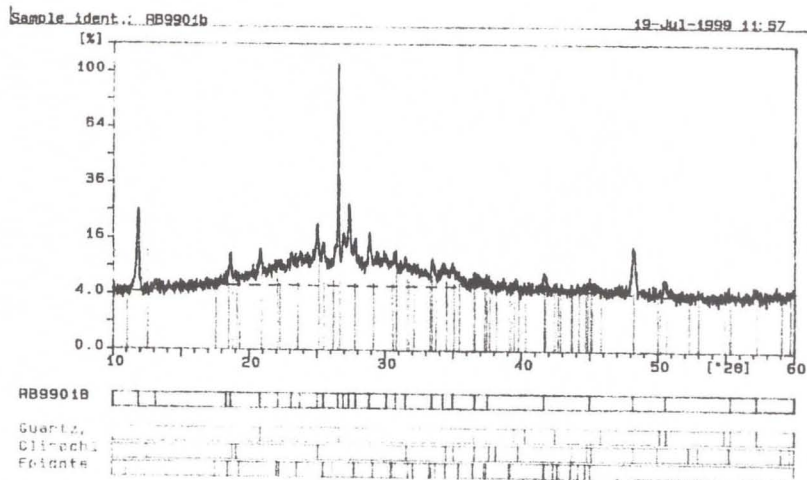
RB9901 rhyodacite, bn-cc zone
quartz, chlorite, epidote in matrix
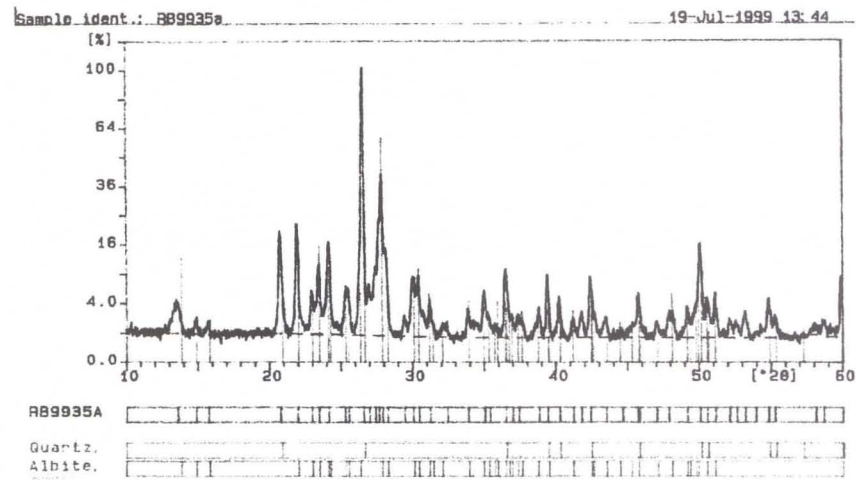
RB9935 rhyodacite, bn-cc zone
quartz, albite in matrix
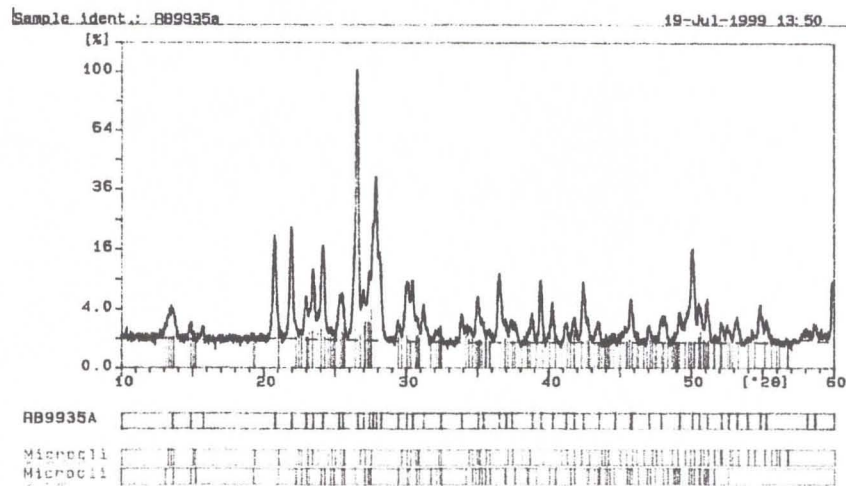
RB9935 rhyodacite, bn-cc zone
microcline in matrix
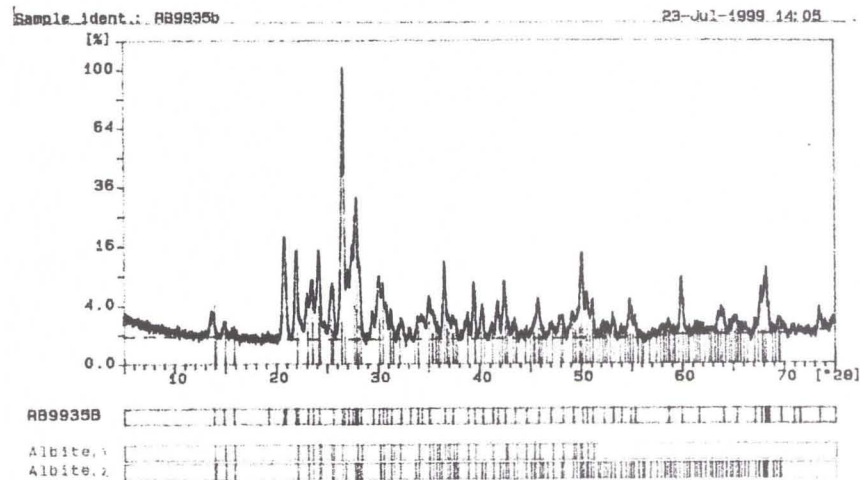
RB9935 rhyodacite, bn-cc zone
albite in matrix
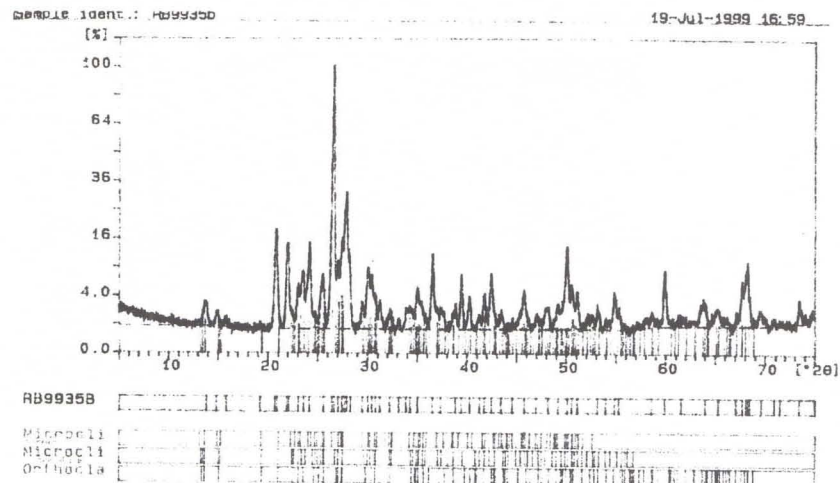
RB9935 rhyodacite, bn-cc zone
microcline in matrix
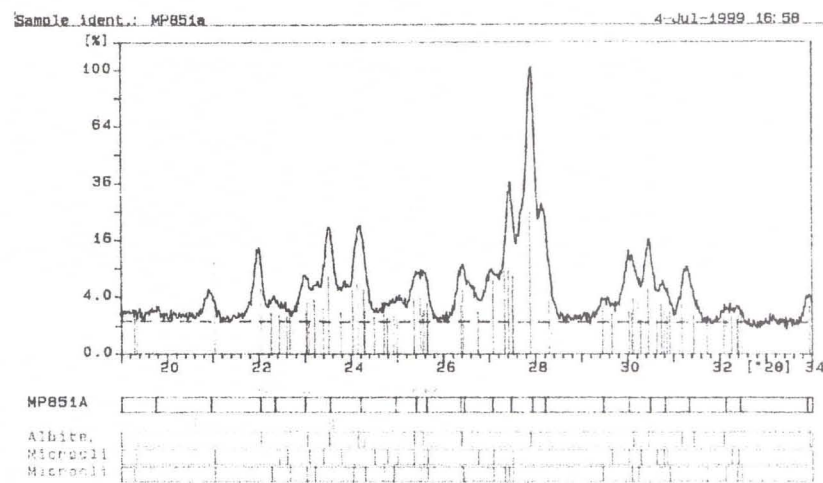
MP 851 basalt Veta Negra Fm, bn-cc zone
microcline in albite phenocryst
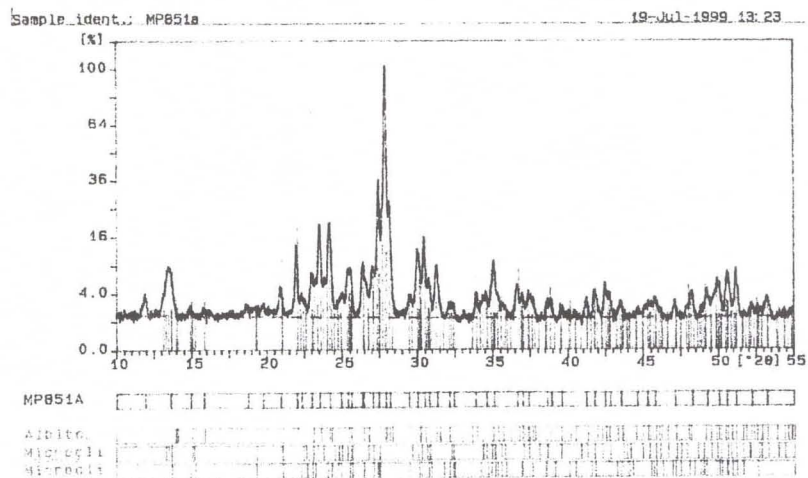
MP 851 basalt Veta Negra Fm, bn-cc zone
microcline vein in albite phenocryst
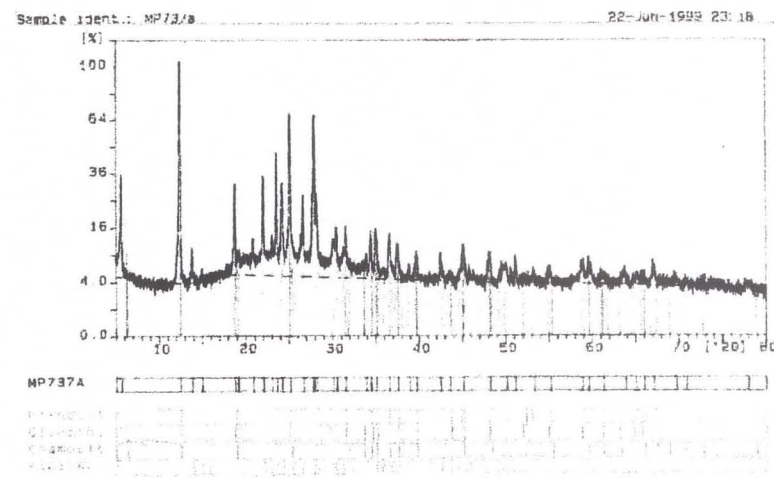
MP 737 rhyodacite, cc zone
chlorite in matrix

Z62395 gabbro, contact zone
chlorite
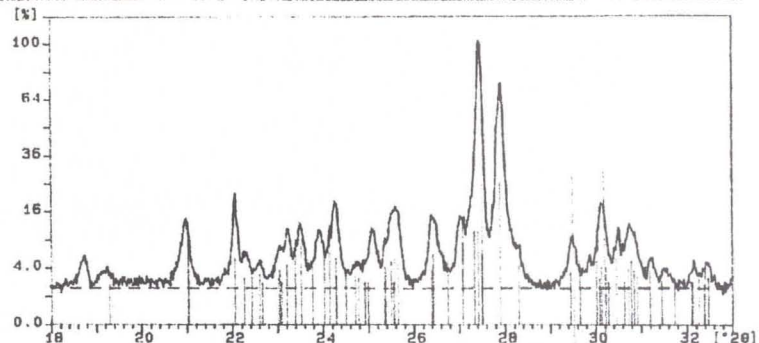
Z62395 gabbro, contact zone
albite, microcline
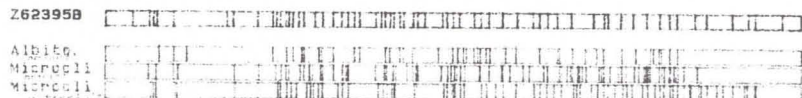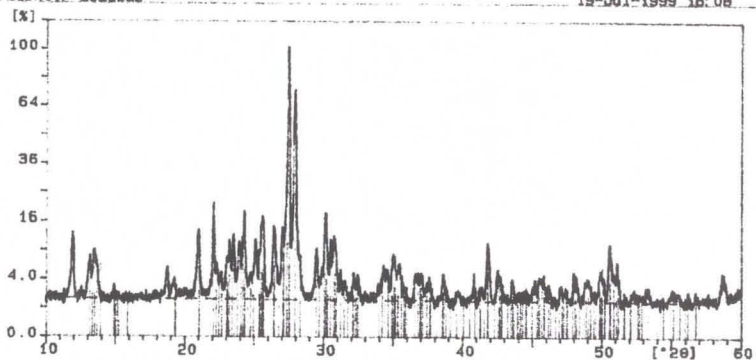
Z62395 gabbro, contact zone
albite, microcline

5.- MAGNETIC SUSCEPTIBILITY AND SPECIFIC GRAVITY DATA

- Listed by rock type and ore zone

Appendix 5.- Specific Gravity and Magnetic Susceptibility Data

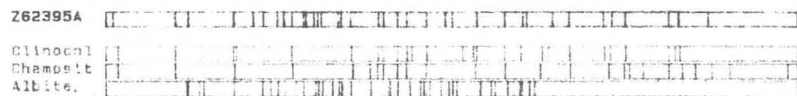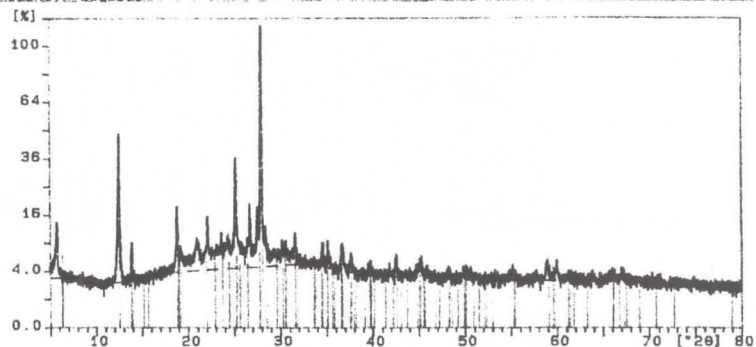| Sample	Rock Type	Ore Zone	Specific Gravity (g/cm³)	Magnetic Susceptibility
RB98-29	basalt	background magnetite	2.98	1.20
MP-844	basalt	background magnetite	2.85	2.99
RB98-40	basalt	background magnetite	2.88	2.07
RB98-42	basalt	background magnetite	2.89	1.84
Z634-95	basalt	background magnetite		2.00
Z604-95	basalt	background magnetite		2.70
Z632-95	basalt	background pyrite		0.16
RB98-06	basalt	background pyrite	2.77	0.02
RB98-49	basalt	background pyrite	2.84	0.02
RB98-50	basalt	background pyrite	2.75	0.03
MP-703	basalt	pyrite	2.95	0.00
MP-728	basalt	pyrite	2.76	0.04
MP-865	basalt	pyrite	2.88	0.00
RB98-76	basalt	pyrite	2.71	0.06
RB98-31	basalt	pyrite-chalcopyrite	2.70	1.95
RB98-48	basalt	pyrite-chalcopyrite	2.72	0.03
MP842	basalt	pyrite-chalcopyrite		0.00
MP-724	basalt	chalcopyrite	2.87	0.00
MP-786	basalt	chalcopyrite	2.72	0.05
RB98-36	basalt	chalcopyrite	2.75	0.05
MP-723	basalt	chalcopyrite-bornite	2.78	
RB98-45	basalt	chalcopyrite-bornite	2.77	0.04
MP-790	basalt/ calcite vein	chalcopyrite-bornite	3.46	0.02
MP-787	basalt	bornite	2.73	
MP-805	basalt	bornite-chalcocite	2.82	0.03
MP-850	basalt	bornite-chalcocite		0.12
RB98-44	basalt	bornite-chalcocite	2.80	0.49
RB98-47	basalt	bornite-chalcocite	2.85	0.04
RB98-52	basalt	bornite-chalcocite	2.77	0.02
RB98-01	gabbro	background	2.95	4.30
RB98-74	gabbro	background	2.89	4.00
Z622-95	gabbro	background		4.16
Z623-95	gabbro	altered		0.03
MP-866	mafic dyke	background		5.00
Z626-95	mafic dyke	background		2.00
Z618-95	mafic dyke	background		2.00
Z626-95	mafic dyke	background		2.00
Z630-95	mafic dyke	pyrite	2.73	0.40
Z617-95	mafic dyke	chalcopyrite		0.03
MP-772	mafic dyke	bornite-chalcocite	2.74	0.29
Z607-95	microdioritic dyke	background		5.60
Z614-95	microdioritic dyke	background		7.00
MP-848	rhyodacite	background pyrite	2.52	0.00
MP-860	rhyodacite	background pyrite	2.54	0.02
RB98-05	rhyodacite	background pyrite	2.62	0.00
RB98-21	rhyodacite	background pyrite		0.00
RB98-22	rhyodacite	background pyrite	2.60	0.00
RB98-72	rhyodacite	background pyrite	2.60	0.01
Z629-95	rhyodacite	background pyrite		0.05
Z631-95	rhyodacite	background pyrite		0.40
MP-845	rhyodacite	background pyrite	2.60	1.12
RB98-61	rhyodacite	background chalcopyrite-hematite	2.56	0.00
RB98-64	rhyodacite	background chalcopyrite-hematite	2.58	0.06
RB98-70	rhyodacite	background hematite	2.53	0.22
MP-719	rhyodacite	pyrite	2.71	0.02
RB98-09	rhyodacite	pyrite	2.64	0.00

Appendix 5.- Specific Gravity and Magnetic Susceptibility Data

Sample	Rock Type	Ore Zone	Specific Gravity (g/cm^3)	Magnetic Susceptibility
RB98-10	rhyodacite	pyrite	2.65	0.00
RB98-11	rhyodacite	pyrite	2.56	0.00
RB99-03	rhyodacite	pyrite		0.00
RB99-04	rhyodacite	pyrite		0.00
Z624-95	rhyodacite	pyrite		0.07
MP-674	rhyodacite	pyrite-chalcopyrite	2.58	0.00
MP-776	rhyodacite	pyrite-chalcopyrite	2.66	0.00
MP-716	rhyodacite	chalcopyrite		0.00
MP-739	rhyodacite	chalcopyrite	2.49	0.00
MP-775	rhyodacite	chalcopyrite	2.66	0.00
RB98-12	rhyodacite	chalcopyrite	2.69	0.01
RB98-13	rhyodacite	chalcopyrite-bornite	2.63	0.01
RB98-19	rhyodacite	chalcopyrite-bornite	2.60	0.00
MP-677	rhyodacite	bornite	2.65	0.00
MP-713	rhyodacite	bornite	2.60	0.02
MP-718	rhyodacite	bornite	2.59	0.00
MP-856	rhyodacite	bornite	2.80	0.00
RB98-65	rhyodacite	bornite	2.56	0.00
RB98-66	rhyodacite	bornite	2.55	
RB98-67	rhyodacite	bornite	2.56	0.01
MP-664	rhyodacite	bornite-chalcocite	2.56	0.01
MP-746	rhyodacite	bornite-chalcocite	2.59	0.00
MP-778	rhyodacite	bornite-chalcocite	2.68	0.00
MP-782	rhyodacite	bornite-chalcocite	2.63	0.00
MP-864	rhyodacite	bornite-chalcocite	2.63	0.01
RB98-15	rhyodacite	bornite-chalcocite	2.64	0.00
RB98-56	rhyodacite	bornite-chalcocite	2.52	0.01
RB98-69	rhyodacite	bornite-chalcocite	2.53	
RB99-01	rhyodacite	bornite-chalcocite		0.02
RB99-02	rhyodacite	bornite-chalcocite		0.00
MP-737	rhyodacite	chalcocite	2.57	0.01
MP-754	rhyodacitic dyke	background pyrite-sphalerite-galena	2.63	0.01
MP-757	rhyodacitic dyke	background pyrite-sphalerite-galena	2.58	0.00
MP-846	rhyodacitic dyke	background pyrite	2.56	0.01
MP-701	rhyodacitic dyke	pyrite	2.76	0.14
MP-770	rhyodacitic dyke	pyrite	2.56	0.00
MP-839	rhyodacitic dyke	pyrite	2.67	0.00
MP-768	rhyodacitic dyke	pyrite-chalcopyrite	2.73	0.00
RB98-73	rhyodacitic dyke	pyrite-chalcopyrite		0.00
MP-764	rhyodacitic dyke	chalcopyrite	2.57	0.00
MP-855	volcanic sediment	background pyrite	2.58	0.00
Z619-95	volcanic sediment	background pyrite		0.02
MP-861	sandstone	background pyrite		0.00
MP-858	volcanic sediment	pyrite		0.00
MP-869	volcanic sediment	chalcopyrite		0.00
MP-817	volcanic sediment	bornite-chalcocite		0.01
MP-854	volcanic sediment	bornite-chalcocite	2.56	0.00
Z603-95	Veta Negra basalt	background		0.90
MP-851	Veta Negra basalt	bornite-chalcocite		0.00

6.- PHOTOGRAPHS OF Na - COBALTINITRITE – STAINED SAMPLES

- Samples listed by rock type and K_2O contents

Rhyodacitic Dyke K_2O : 7.75%
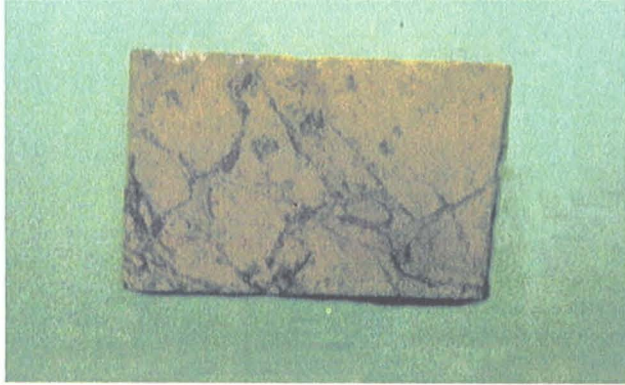
MP 770 pyrite zone, Valdivia Sur

Rhyodacite K_2O : 5.24%
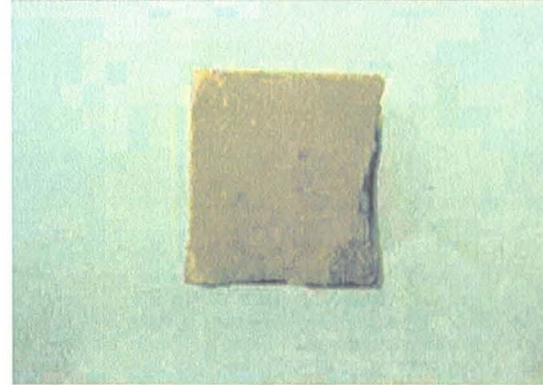
MP 848 pyrite background zone, Morro

Rhyodacite K_2O : 6.39%

MP 778 bornite-chalcocite zone, Valdivia Sur

Rhyodacite K_2O : 4.93%
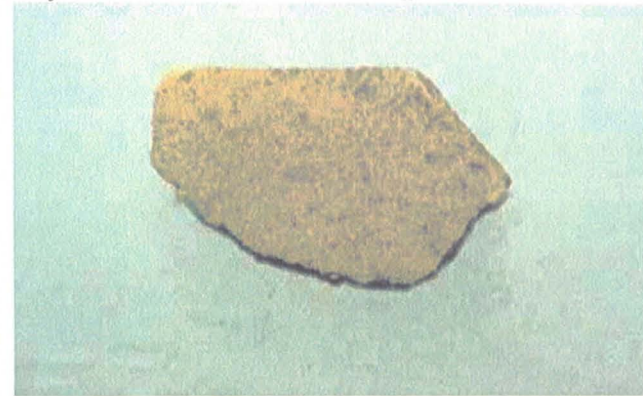
MP 864 bornite-chalcocite zone, Morro

Rhyodacitic Dyke   K₂O : 4.89%

MP 757 pyrite-sphalerite-galena background zone, Paso Riel

Rhyodacite   K₂O : 3.90%
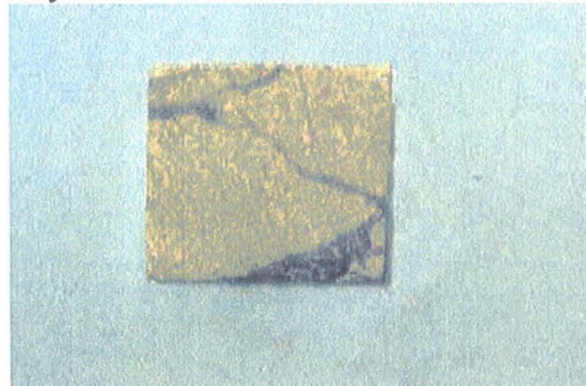
MP 775 chalcopyrite zone, Valdivia Sur

Rhyodacite   K₂O : 4.45%
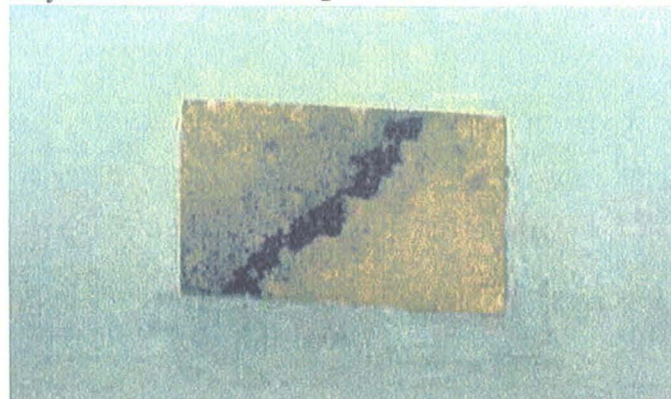
MP677 bornite zone, Osorno

Rhyodacitic Dyke   K₂O : 3.49%
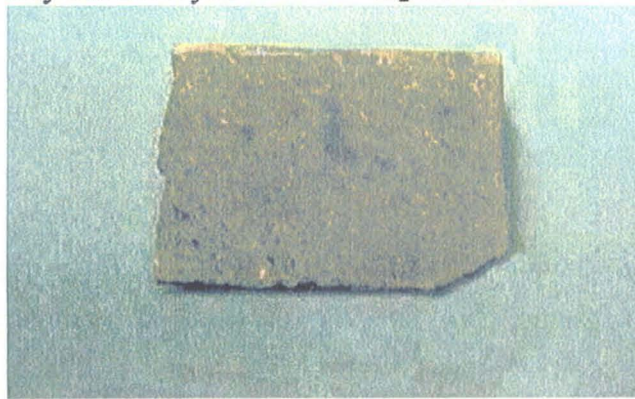
MP 846 pyrite background zone, Morro

Rhyodacite   K$_2$O : 3.16%

MP 667 bornite zone, Osorno

Rhyodacite   K$_2$O : 2.40%
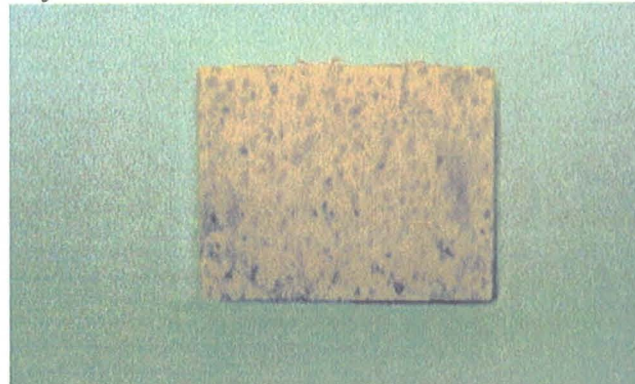
MP 782 bornite-chalcocite zone, Valdivia Sur

Rhyodacite   K$_2$O : 3.16%

RB98-61 background zone, Filo

Rhyodacite   K$_2$O : 2.37%

RB98-9 pyrite zone, Valdivia Sur

Rhyodacite   K$_2$O : 2.19%
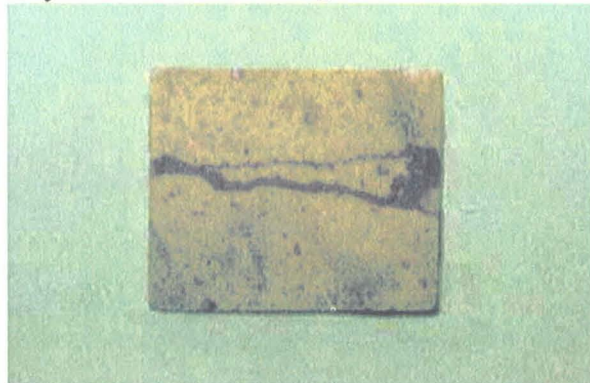
MP 701 pyrite zone, Osorno

Rhyodacite   K$_2$O : 1.72%

RB98-10 pyrite zone, Valdivia Sur

Rhyodacite   K$_2$O : 2.10%

RB98-10 pyrite zone, Valdivia Sur

Rhyodacite   K$_2$O : 0.68%

MP 713 bornite zone, Morro

Rhyodacitic Dyke   K$_2$O : 0.23%

MP 764 chalcopyrite zone, Valdivia Sur

Volcanic sediment   K$_2$O : 6.67%
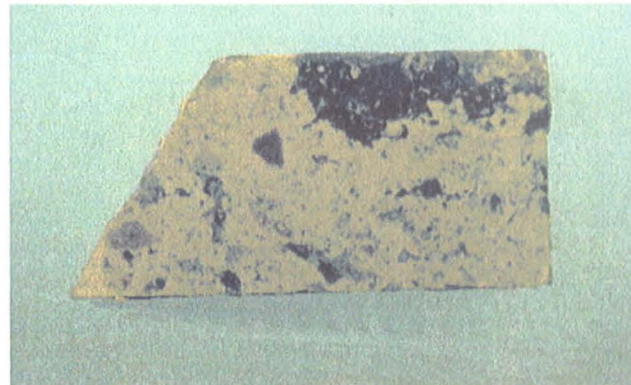
MP 855 pyrite background zone, Valdivia Sur

Rhyodacite   K$_2$O : <0.01%

RB98-15 bornite-chalcocite zone, Valdivia Sur

Volcanic sediment   K$_2$O : 0.30%
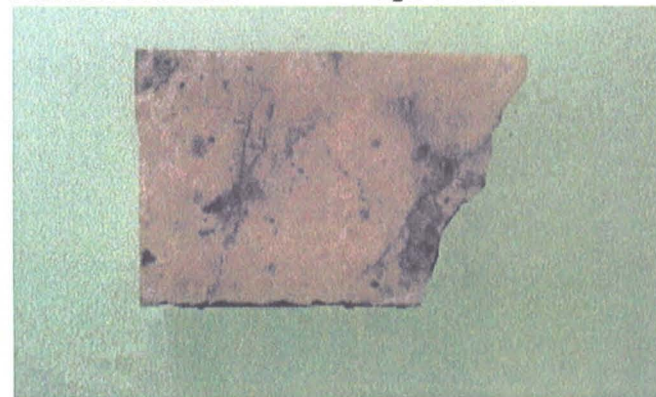
MP 854 bornite zone, Valdivia Sur

Basaltic Dyke K_2O : 6.31%

MP 772 chalcocite zone, Valdivia Sur

Fine Andesitic Dyke K_2O : 4.66%
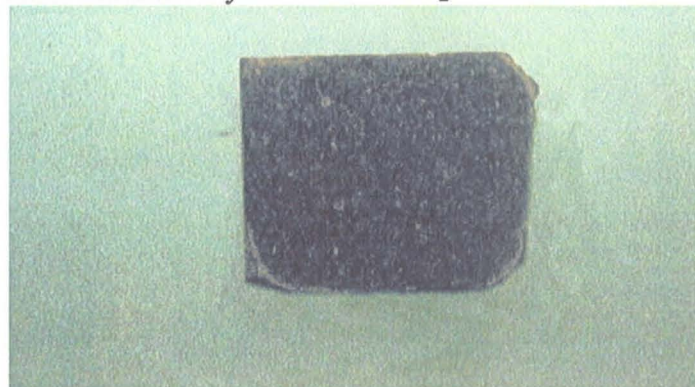
MP 866 background zone, Arauco

Veta Negra Basalt K_2O : 4.85%
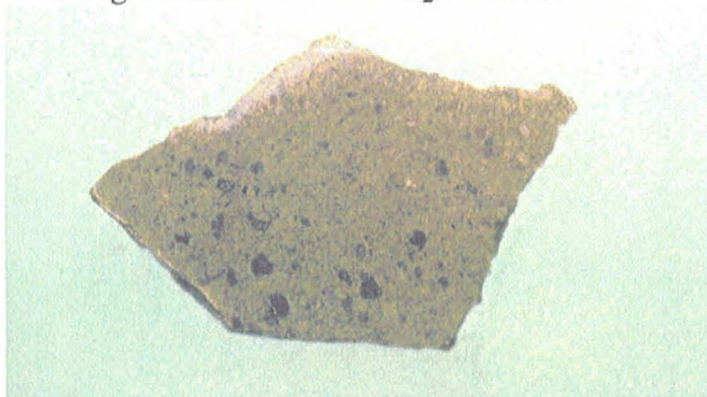
Z603-95 background zone, Filo

Basalt K_2O : 3.66%

MP 865 pyrite zone, Valdivia Sur

Basalt   K$_2$O : 2.19%

RB98-49 pyrite background zone, Filo

Basalt   K$_2$O : 1.47%

RB98-48 pyrite-chalcopyrite zone, Filo

Basalt   K$_2$O : 1.95%

RB98-31 pyrite-chalcopyrite zone, Valdivia Sur

Basalt   K$_2$O : 0.09%

MP 790 chalcopyrite-bornite zone, Filo

7.- COMPILATION OF PREVIOUS RELEVANT ANALYTICAL DATA

- 7.1.- Geochronological data.
- 7.2.- Fluid inclusion data.
- 7.3.- Isotopic data.
- 7.4.- Geochemical data.

Appendix 7.1.- Compilation of Geochronological Data from El Soldado

K/Ar Ages Sample	Rock Unit	Rock Type	Mineral	Age (Ma)	Error (Ma)	Relationship with Mineralization	Reference
Isol 1	Intrudes Upper Lo Prado	basaltic dyke	plagioclase	116	4	unmineralized, weakly altered	2
IS227-87	Upper Lo Prado	basalt	whole rock	113	4	unmineralized, weakly altered, distal to orebodies	1
SP-150	Upper Lo Prado	rhyodacitic dyke	whole rock	100	3	mineralized, altered	1
SP-485	Upper Lo Prado	volcanic breccia	whole rock	97	4	altered	1
ESI-11	Upper Lo Prado	vein	K-fd	97.2	2	with copper sulphides	1
S67-82	Upper Lo Prado	basalt	whole rock	96	5	mineralized, altered	1
RB 419	Ocoa M Veta Negra Fm.	andesite	whole rock	115	4	unmineralized, out of El Soldado	2
RB 419	Ocoa M Veta Negra Fm.	andesite	plagioclase	94	2	unmineralized, out of El Soldado	2
RB443	Ocoa M Veta Negra Fm.	andesite	whole rock	100	4	unmineralized, out of El Soldado	2
RB444	Ocoa M Veta Negra Fm.	andesite	whole rock	100	3	unmineralized, out of El Soldado	2
Rb/Sr Ages Sample	**Rock Unit**	**Rock Type**	**Mineral**	**Age (Ma)**	**Error (Ma)**	**Relationship with Mineralization**	**Reference**
SP383,SP326,SP220,SP4 85,SP507	Upper Lo Prado	rhyodacite, rhyodacitic dyke, breccia, basaltic dyke	whole rock	109	4	altered mineralized	1
Isol 6, 12,43,44,49, 56	Upper Lo Prado	rhyodacite, basalt	whole rock	105.9	1.6	unmineralized, weakly altered, distal to orebodies	2
$^{40}Ar/^{39}Ar$ Ages (2 steps)	**Rock Unit**	**Rock Type**	**Mineral**	**Total Gas Age (Ma)**	**Error Ma**		
Isol 8	Upper Lo Prado	rhyodacite	K-fd - albite	113.3		altered mineralized	2
Isol 20	Upper Lo Prado	vein in basalt	K-fd - albite	105.1		with copper sulphides	2
Isol 21	Upper Lo Prado	vein in basalt	K-fd - albite	103.5		with copper sulphides	2
Isol12	Upper Lo Prado	rhyodacite	K-fd - albite	109.4		unmineralized, weakly altered, distal to orebodies	2
Isol 39	Upper Lo Prado	dacitic porphyry	K-fd - albite	104.3		mineralized, La Isla Mine, 5 km south El Soldado	2
Isol 37	Upper Lo Prado	dacitic porphyry	K-fd - albite	99.3		mineralized, La Isla Mine, 5 km south El Soldado	2
Isol 50	Upper Lo Prado	vug in basalt	K-fd - albite	105.0		unmineralized, distal to orebodies	2
Isol 31	Veta Negra Fm	vug in basaltic andesite	K-fd - albite	101.1		unmineralized, distal to orebodies	2
Isol 28	Veta Negra Fm	vug in basaltic andesite	K-fd - albite	101.4		unmineralized, distal to orebodies	2
$^{40}Ar/^{39}Ar$ Ages (multiple steps)	**Rock Unit**	**Rock Type**	**Mineral**	**Plateau Age (Ma)**	**Error (Ma)**		
Isol 10	Upper Lo Prado	rhyodacitic dyke	K-fd - albite	131.8	3.1	altered, weakly mineralized	2
Isol 1	Intrudes Upper Lo prado	basaltic dyke	plagioclase	118.7	2.2	unmineralized, weakly altered, pre ore	2
isol 64	Intrudes Upper Lo prado	andesitic dyke	plagioclase	122.7	1.1	unmineralized, 5km south El soldado	2
Isol 51	Intrudes Upper Lo prado	gabbro	plagioclase	104.3	1.4	unmineralized, weakly altered	2
NW 127-2	Upper Lo Prado	rhyodacite	K-fd	112.0	2	K-fd in vein (late) with chalcopyrite (early)	3
NW 113	Upper Lo Prado	basalt	K-fd	109.5	1.2	K-fd not related to Cu sulphides	3
ES 165	Upper Lo Prado	rhyodacite	K-fd	109.4	1.2	umbiguos relationship with copper sulphides	3
NW 43	Upper Lo Prado	basalt	K-fd	106.1	1.1	K-fd in veins (early) with chalcopyrite (late)	3
NW 143	Upper Lo Prado	basalt	K-fd	105.3	1.1	K-fd (late) in pore with Cu sulphides (early)	3
NW 156	Upper Lo Prado	basalt	K-fd	104.8	1	K-fd in pore (late) with Cu sulphides (learly)	3
NW 159	Upper Lo Prado	basalt	K-fd	102.9	1.1	no copper sulphides related to K-fd vein	3
NW 48	Upper Lo Prado	rhyodacie	K-fd	102.5	2	K-fd included and crosscut by Cu sulphides	3
NW 66	Upper Lo Prado	vug in basalt	K-fd	101.0	1.5	K-fd filliing in vugs, not related to Cu Sulphides	3
NW 154	Upper Lo Prado	basalt	K-fd	100.5	1.5	K-fd crosscut by Cu sulphide veins	3

References: (1) Munizaga et al., 1988; (2) Boric & Munizaga, 1994; (3) Wilson, 1998a

Appendix 7.2.- Compilation of Fluid Inclusions Data from El Soldado Cu Deposit

Sample	Ore zone	Rock	Mineral	TH C	Salinity %	Observations	Area	Reference
mp557	py	rhyodacite	calcite	240-296	9.5-30.5		Arauco	3
mp555	py	rhyodacite	calcite	118-200	28.9-31.2		Arauco	3
mp552	py	sedimentary bx	calcite	169-280			Arauco	3
mp544	py	sedimentary bx	calcite	120-235			Arauco	3
mp439	py-(cp)	basalt	calcite	214-234	28-29(CaCl2)		Sta Clara	1
mp420	cp	rhyodacite	quartz	105-119	20(CaCl2)		Morro	1
mp420	cp	rhyodacite	quartz	128-141			Morro	1
mp420	cp	rhyodacite	quartz	204-234	22(CaCl2)		Morro	1
mp420	cp	rhyodacite	quartz	239-257			Morro	1
mp420	cp	rhyodacite	quartz	185-230	20-28(CaCl2)		Morro	1
mp420	cp	rhyodacite	calcite	167-170			Morro	1
mp420	cp	rhyodacite	calcite	148-208	25(CaCl2)		Morro	1
sva8/87	cp		calcite	200-300(355)		early veins ep-cal-cl-ab-cp	Osorno	2
mp422	cp-bn	rhyodacite	calcite	129-303	< 29 Ca Cl2		Morro	1
mp428	cp-bn	rhyodacite	calcite	106-145	17.2 NaCl (28CaCl2)		Arauco	1
s144/87	bn-cp	rhyodacite	calcite	118-158	3.4-16	bx,cal in filling	Osorno	2
sva8/87	bn-(cp)		calcite	102-149	28.6-29.6	late vein cal-ab-cl-bn-cc-cp	Osorno	2
mp430	bn	basalt	calcite	107-151		qz-cal-cl-bn	Block AB	1
mp431	bn	basalt	calcite	113-144		cal-cl-hem-bn-qz	California	1
mp424	bn-cc	basalt	quartz	110-174	31 (Na Cl)		Filo	1
Ex1	bn-cc	bx basalt	calcite	196-202			V.del Agua	1
Ex1	bn-cc	bx basalt	calcite	113-137			V.del Agua	1
sva7/87	bn-cc	bx rhyodacite	calcite	139-187	27-31	bx, bn-cc-cp-cal-ab	V.del Agua	2
s144/87	bn-cc	rhyodacite	calcite	136-244(330)	7.6-13.9	early fillings vugs	Osorno	2
Ex2	cc	bx basalt	calcite	194-204		thick cal vein	V.del Agua	1
1550	cc	basalt	quartz	138-182	23.3	open space in vugs	V.del Agua	2
mp439	py-(cp)	basalt	calcite	122-155	20-25(CaCl2)	late calcite vein	Sta Clara	1
mp431	bn	basalt	calcite	110-129		late barren calcite	California	1
Ex2	cc	bx basalt	calcite	105-124	29 (CaCl2)	late barren vein	V.del Agua	1
mp424	bn-cc	basalt	calcite	93-170	3.4-22.5 (NaCl)	late calcite vein	Filo	1
mp482	barren	basalt	calcite	98-142	low	late barren vein	Block 12	1
mp483	barren	basalt	calcite	82-104		late barren vein	Taller	1
Caqui 1	cc-bn	breccia	quartz	103-111	12.0-17.0	out of El Soldado	Caquicito	4

References: (1) Holmgren,1985; (2) Skewes, 1987a; (3) Skewes, 1987b; (4) Skewews, 1988.

py=pyrite, cp=chalcopyrite, bn=bornite, cc=chalcocite, cal=calcite; qz=quartz, ep=epidote, cl=chlorite, ab=albite, hem=hematite, bx breccia

Appendix 7.3.- Compilation of isotopic and reflectance data of El Soldado and Veta Negra Cu Deposits

I. δ^{34}S Data for Sulfides

Sample	Mineralogy	δ^{34} S		Mine Block	Ore Zone	Observations	References
D-1	chalcopyrite + pyrite	-5.2		Santa Clara	cp-py	orebody	1, 2
D-2	bornite	-1.5		Santa Clara	bn	orebody	1, 2
D-3	chalcopyrite	-0.3		Santa Clara	cp	orebody	1, 2
D-4	framboidal pyrite	28.0		Santa Clara	py	background zone, with bitumen and calcite	1, 2
D-5	pyrite in sediments	7.3		Santa Clara	py	in sediments Lower Lo Prado	1, 2
S233-87a	pyrite	6.2		Santa Clara	py	background zone, with bitumen and calcite	3
S233-87b	pyrite	9.4		Santa Clara	py	background zone, with bitumen and calcite	3
VL-01	chalcopyrite	-0.1		Lena	cp	calcite-sulphide vein	4
CM-01	chalcopyrite	0.9		Morro	cp	orebody	4
S9-91	chalcocite	-4.6		Filo	cc	orebody	4
T4	pyrite	-15.8		tunnel 4	py	Veta Negra deposit	4
T7	chalcocite	-31.7		tunnel 7	cc	Veta Negra deposit	4
VK19	chalcopyrite	-21.1		tunnel 7	cp	Veta Negra deposit	4

II. ^{87}Sr/^{86}Sr Ratios for Hydrothermal Calcite and for Calcite in Sedimentary Rocks

Sample	Mineral / Rock	^{87}Sr/^{86}Sr		Mine Block		Observations	
ESI-3	calcite	0.70578+-35		Arauco		associated with cp-bn	6
ESI-8	calcite	0.70475+-15		Arauco		amygdule with qz, ep	6
ESI-10	calcite	0.70520+-42		Arauco		late vein with ep, ab, K-fd, hem	6
ESI-11	calcite	0.70448+-10		Arauco		amygdule with qz, ep, ab, K-fd, hem, Cu sulphides	6
ESI-5	calcite	0.70441+-8		Valdivia Sur		bn-cc ore zone, core of orebodie	6
ESI-7	calcite	0.70447+-8		California		associated with cp-bn	6
ESI-2	calcite	0.70615+-53		external halo		associated with py-cp	6
ISOL59	calcareous sandstone	0.70710+-5		out of El Soldado		outcrop, access road to El Soldado	6
ISOL60	black limestone	0.70638+-5		out of El Soldado		outcrop, access road to El Soldado	6
ISOL66	sand limestone	0.70514+-8		out of El Soldado		outcrop, access road to El Soldado	6

III. ^{187}Re/^{188}Os Ratios for Pyrite

Sample	Mineral	^{187}Re/^{188}Os	(^{187}Os/^{188}Os)i		Location	
El Soldado	pyrite	1.72300	3.94977		El Soldado	7

Appendix 7.3.- Compilation of isotopic and reflectance data of El Soldado and Veta Negra Cu Deposits

IV. $\delta^{13}C$ and $\delta^{18}O$ for Hydrothermal Calcite and for Calcite in Sedimentary Rocks							
Sample	Mineral	$\delta^{13}C$	$\delta^{18}O$	Mine Block	Ore Zone	Observations	References
MZ-01	calcite	-10.8	12.8	Filo	py-cp	associated with bitumen	5
MZ-02	calcite	-10.3	13.1	Filo	py-cp	associated with bitumen	5
MZ-03	calcite	-16.3	12.7	Filo	py	associated with bitumen	5
MZ-04	calcite	-17.6	12.6	Filo	py-cp	associated with bitumen	5
MZ-05	calcite	-11.6	12.4	Filo	bn-cc	associated with bitumen	5
MZ-06	calcite	-8.7	13.5	Filo	bn-cc	associated with bitumen	5
MZ-07	calcite	-6.6	12.9	Filo	cc	associated with bitumen	5
MZ-08	calcite	-16.0	12.0	Filo	bn-cc	associated with bitumen	5
MZ-09	calcite	-13.4	12.5	Filo	bn-cp	associated with bitumen	5
MZ-11	calcite	-8.4	12.8	Filo	cp	associated with bitumen	5
MZ-12	calcite	-11.7	12.8	Filo	bn-cp	associated with bitumen	5
MZ-13	calcite	-14.6	12.7	Filo	bn-cc	associated with bitumen	5
S233	calcite	-10.6	12.3	Santa clara	background py	associated with bitumen	5
Z-106	calcite	-4.8	13.2	external halo	background py	sediments in Upper Lo prado	5
Z-106A	calcite	-3.2	12.9	external halo	background py	sediments in Upper Lo prado	5
ESI-8	calcite	-6.38	15.0	Arauco	cp-py	amygdule with qz, ep	6
ESI-10	calcite	-9.72	13.5	Arauco	cp-py	late vein with ep, ab, K-fd, hem	6
ESI-11	calcite	-9.53	12.9	Arauco	cc-bn-cp	amygdule with qz, ep, ab, K-fd, hem, Cu sulphides	6
ESI-5	calcite	-10.14	14.1	Valdivia Sur	bn-cc	core of orebodie	6
ESI-7	calcite	-5.98	12.5	California	cp-bn		6
ISOL66	sandy limestone	-1.5	12.8	out of El Soldado	unmineralized	outcrop, access road to El Soldado	6
MZ-15	calcite	-11.9	13.0	dril core	cp-bn	Veta Negra deposit	5
Z-100	calcite	-14.9	19.9	tunnel 5	bn-cc-cv	Veta Negra deposit	5
Z-101	calcite	-2.7	26.4	tunnel 7	bn-cc	Veta Negra deposit	5
Z102	calcite	-11.3	13.2	dril core	cp-bn-cc	Veta Negra deposit	5
Z-103	calcite	-13.7	24.0	tunnel 5	cc	Veta Negra deposit	5
Z-104	calcite	-11.9	14.6	dril core	py-cp-bn	Veta Negra deposit	5
Z-105	calcite	-12.5	12.9	dril core	bn-cc	Veta Negra deposit	5
Z-107	calcite	-13.0	13.5	tunnel 7	bn-cc	Veta Negra deposit	5

Appendix 7.3.- Compilation of isotopic and reflectance data of El Soldado and Veta Negra Cu Deposits

V. $\delta^{13}C$ and Reflectance Data for Bitumen							
Sample	Mineral	$\delta^{13}C$	BR_0	Mine Block	Ore Zone	Observations	References
MZ-01	bitumen	-29.2	4.29	Filo	py-cp	associated to ore	5
MZ-02	bitumen	-26.9		Filo	py-cp	associated to ore	5
MZ-03	bitumen	-28.1	4.26	Filo	py	associated to ore	5
MZ-04	bitumen	-30.8	4.22	Filo	py-cp	associated to ore	5
MZ-05	bitumen	-25.9	2.8	Filo	bn-cc	associated to ore	5
MZ-06	bitumen	-27.0	3.88	Filo	bn-cc	associated to ore	5
MZ-07	bitumen	-26.6	3.37	Filo	cc	associated to ore	5
MZ-08	bitumen	-29.9	4.13	Filo	bn-cc	associated to ore	5
MZ-09	bitumen	-29.6	4.2	Filo	bn-cp	associated to ore	5
MZ-10	bitumen	-29.9	3.66	Filo	bn-cc	associated to ore	5
MZ-11	bitumen	-30.1	4.36	Filo	cp	associated to ore	5
MZ-12	bitumen	-26.9	3.92	Filo	bn-cp	associated to ore	5
MZ-13	bitumen	-30.1		Filo	bn-cc	associated to ore	5
S233	bitumen	-22.0	3.2	Santa clara	background py		5
Z-106	bitumen	-28.9	2.77	external halo	background py	sediments in Upper Lo Prado	5
Z-106A	bitumen	-29.0		external halo	background py	sediments in Upper Lo Prado	5
MZ-15	bitumen	-21.5	2.47*	drill core	cp-bn	Veta Negra deposit	4, 5
Z-100	bitumen	-21.4	1.0*	tunnel 5	bn-cc-cv	Veta Negra deposit	4, 5
Z-101	bitumen	-26.3	2.57	tunnel 7	bn-cc	Veta Negra deposit	4, 5
Z102	bitumen	-23.4	1.26	drill core	cp-bn-cc	Veta Negra deposit	4, 5
Z-103	bitumen	-22.2	1.14*	tunnel 5	cc	Veta Negra deposit	4, 5
Z-104	bitumen	-22.7	1.03*	drill core	py-cp-bn	Veta Negra deposit	4, 5
Z-105	bitumen	-22.6	3.36	drill core	bn-cc	Veta Negra deposit	4, 5
Z-107	bitumen	-24.6	2.77	tunnel 7	bn-cc	Veta Negra deposit	4, 5

References: (1) Holmgren, 1987; (2) Klohn et al., 1990; (3) Westra, 1988b; (4) Villalobos 1995; (5) Zentilli et al 1997;
(6) Munizaga, 1992; (7) Ruiz et al., 1997.

Abbreviators: py:pyrite, cp:pyrite, bn:bornite, cc:chalcocite, cv:covellite, ab: albite, cal:calcite, ep: epidote, K-fd: potassic feldspar,
qz: quartz, hem: hematite

Appendix 7.4.- Compilation of Lithochemistry: Regional Data

Reference (*)	Rock (**)	Sample	SiO$_2$ %	TiO$_2$ %	AL$_2$O$_3$ %	FeOT %	MnO %	MgO %	CaO %	Na$_2$O %	K$_2$O %	P$_2$O$_5$ %	LOI %	Ba ppm	Co ppm	Cs ppm	Cu ppm	Hf ppm	Nb ppm	Ni ppm
(4)	Rd LP	sol 44	71.57	0.56	14.80	2.90	0.06	0.23	3.98	2.83	3.05	0.01	4.95	265	34	<10	<10			20
(4)	Rd LP	sol 59	74.76	0.34	12.87	1.31	0.11	0.34	4.90	1.30	4.08	traces	5.54	645	50	<10	<10			17
(4)	An LP	sol 46	59.81	0.61	16.76	6.69	0.22	3.82	6.78	3.27	2.04	0.01	2.23	509	50	32	43			40
(4)	Ban LP	sol 49	49.31	1.00	16.78	9.90	0.20	6.98	12.05	2.52	1.09	0.17	1.82	270	55	128	213			65
(4)	Ban LP	sol 52	49.45	0.97	20.67	8.83	0.28	5.59	9.67	3.25	1.18	0.12	2.68	341	54	53	<10			51
(4)	Ban LP	sol 53	51.30	0.91	19.56	8.87	0.25	5.53	8.77	3.47	1.21	0.13	3.15	334	36	43	<10			30
(4)	Ban LP	sol 47	55.64	0.83	16.73	8.32	0.31	4.63	8.58	3.27	1.49	0.20	1.72	385	62	48	140			46
(4)	Ban dk	sol 1	55.61	0.70	19.28	8.34	0.26	3.29	4.58	5.82	1.92	0.19	3.96	461	15	10	45			<10
(4)	Ban dk	sol 55	52.18	1.01	20.81	8.65	0.24	3.89	8.73	2.79	1.53	0.16	3.45	428	59	18	182			45
(4)	Ban VNp	sol 35	57.00	0.88	17.01	7.90	0.26	4.16	3.53	5.24	3.79	0.24	2.15	855	<10	47	<10			<10
(4)	Ban VNp	sol 37	54.73	0.84	17.38	7.67	0.30	4.76	6.75	3.91	3.50	0.16	2.06	534	<10	90	215			17
(4)	Ban VNp	sol 2	54.94	1.30	15.91	10.34	0.37	3.42	6.98	3.63	2.87	0.25	1.37	426	53	13	52			30
(4)	Ban VNo	sol 13	58.96	0.97	15.57	8.81	0.27	2.84	5.44	3.89	3.02	0.24	1.16	427	48	<10	<10			15
(4)	Ban VNo	sol 17	56.34	0.88	16.35	8.36	0.23	4.58	7.83	2.89	2.43	0.11	1.52	300	43	66	<10			28
(4)	Ban VNo	sol 28	57.30	0.84	17.36	7.68	0.17	3.71	7.08	3.11	2.61	0.13	1.64	332	48	37	<10			29
(4)	Ban VNo	sol 15	58.30	1.01	16.40	7.44	0.21	2.86	6.08	3.60	3.50	0.60	1.46	476	44	12	74			11
(4)	Ban VNo	sol 27	55.46	0.85	16.60	8.50	0.24	4.78	7.66	3.20	2.61	0.10	1.49	331	71	62	<10			34
(4)	Ban VNo	sol 30	56.56	0.95	16.97	8.10	0.22	3.60	6.79	3.11	3.40	0.29	1.50	488	20	41	30			20
(5)	Rd LP	sol 59	74.71	0.34	12.86	1.30	0.11	0.34	4.89	1.29	4.07	0.07	0.53	748	1			4.83	4.79	3
(5)	Ban LP	sol 52	49.43	0.97	20.66	8.83	0.28	5.59	9.66	3.25	1.18	0.15	6.09	386	86			2.06	1.18	32
(5)	Ban VN	BUS-19	51.91	0.88	19.99	9.25	0.18	3.38	8.08	3.77	2.35	0.21	3.81	434	22			2.03	1.48	7
(5)	Ban VN	BUS-35	53.39	0.98	18.17	9.30	0.31	3.99	8.28	2.86	2.44	0.28	5.79	609	22			4.10	2.56	47
(5)	Ban VN	CER-73	57.87	1.21	15.34	8.77	0.25	2.56	6.86	2.76	3.92	0.45	4.55	514	16			5.98	5.9	11

(*) (4) Levi 1985, writte communication; (5) Vergara et al, 1995

(**) Rd: rhyodacite Lo Prado Fm; Ban LP: basaltic andesite Lo Prado Fm; Ban dk: basaltic andesitic dyke; Ban VNp: basaltic andesite Purehue Member, Veta Negra Fm;

Ban Vno: basaltic andesite Ocoa Member, Veta Negra Fm; Ban VN basaltic andesite Veta Negra Fm

Appendix 7.4.- Compilation of Lithochemistry: Regional Data (continued)

Rock (**)	Sample	Rb ppm	Sr ppm	Ta ppm	Th ppm	U ppm	V ppm	Y ppm	Zr ppm	La ppm	Ce ppm	Nd ppm	Sm ppm	Eu ppm	Gd ppm	Dy ppm	Er ppm	Yb ppm	Lu ppm	^{87}Sr/^{86}Sr(i)
Rd LP	sol 44	84	48				<10	40	206											
Rd LP	sol 59	195	36				15	29	209											
An LP	sol 46	51	267				140	25	131	11.36	29.04	14.19	3.56	0.90	3.39	3.37	1.93	2.13	0.39	
Ban LP	sol 49	30	495				294	21	68	10.24	28.12	15.87	3.78	1.10	3.50	2.90	1.53	1.45	0.25	
Ban LP	sol 52	38	455				297	21	55											
Ban LP	sol 53	39	468				270	20	53											
Ban LP	sol 47	42	428				181	34	147											
Ban dk	sol 1	44	558				103	25	66											
Ban dk	sol 55	41	437				232	27	82											
Ban VNp	sol 35	132	307				252	26	108											
Ban VNp	sol 37	119	360				261	20	93	11.79	30.52	16.19	3.76	1.05	3.25	2.90	1.63	1.67	0.27	
Ban VNp	sol 2	95	349				317	36	102											
Ban VNo	sol 13	102	291				191	38	143											
Ban VNo	sol 17	93	303				224	28	120	13.22	33.67	18.08	4.48	1.12	4.52	4.31	2.43	2.53	0.37	
Ban VNo	sol 28	89	304				193	31	134											
Ban VNo	sol 15	145	308				142	49	220											
Ban VNo	sol 27	91	329				211	26	107	9.26	26.97	15.01	3.69	0.98	3.36	3.40	1.96	2.03	0.31	
Ban VNo	sol 30	128	381				222	30	152	17.74	44.93	23.56	5.46	1.25	4.59	4.04	2.29	2.35	0.38	
Rd LP	sol 59	92	58	0.44	9.2	2.42	17	26	186	10.8	20.6	11.3	2.74	0.81	2.61	3.63	2.35	2.66	0.46	0.70455
Ban LP	sol 52	44	528	0.10	1.6	0.43	364	15.8	43	7.7	26.2	16.7	3.45	1.20	3.12	2.89	1.61	1.81	0.19	0.70385
Ban VN	BUS-19	34	621	0.13	2.0	0.58	313	19	58	9.9	22.1	14.8	3.93	0.99	2.81	3.03	1.75	1.93	0.31	0.70378
Ban VN	BUS-35	57	694	0.21	4.7	1.36	334	29	113	14.6	33.6	20.5	4.93	1.38	4.57	4.76	2.67	3.09	0.44	0.70370
Ban VN	CER-73	83	429	0.45	7.0	1.96	200	34	206	19.2	44.8	24.4	6.36	1.26	5.10	5.18	2.90	3.27	0.44	0.70380

Appendix 7.4.- Compilation of Lithochemistry: Local Data

Reference (*)	Rock (**)	Sample	SiO2 %	TiO2 %	AL2O3 %	FeOT %	MnO %	MgO %	CaO %	Na2O %	K2O %	P2O5 %	LOI %	Cu ppm	Zr ppm
(2)	RdLP	RA-41	66.56	0.53	16.17	3.66	0.16	1.12	2.23	5.76	3.68	0.13		2237	153
(2)	RdLP	RA-42	68.32	0.41	13.19	4.68	0.10	0.32	4.40	4.86	3.61	0.12		1518	128
(2)	RdLP	RA-45	68.36	0.49	16.43	3.29	0.09	0.84	1.00	6.95	2.41	0.13		799	170
(2)	RdLP	RA-46	67.67	0.37	15.50	2.63	0.10	0.60	4.08	6.74	2.22	0.08		1917	136
(2)	RdLP	RA-47	66.46	0.40	16.06	2.71	0.15	0.59	4.89	5.42	3.23	0.09		1677	136
(2)	Rddk	RA-37	70.32	0.35	12.98	2.29	0.09	0.24	5.14	4.96	3.55	0.08		799	136
(2)	Rddk	RA-55	61.03	0.52	19.04	3.06	0.10	0.76	6.53	7.03	1.79	0.13		399	119
(2)	Rddk	RA-56	68.33	0.40	14.74	1.19	0.06	0.14	4.89	6.34	3.81	0.10		799	153
(2)	BanLP	RA-66	56.44	0.72	18.02	7.48	0.38	3.86	5.24	5.41	2.25	0.20		479	77
(2)	BanLP	RA-67	52.65	0.61	17.11	9.23	0.65	5.35	6.44	5.04	2.77	0.16		399	60
(2)	BanLP	RA-68	54.28	0.63	17.61	8.20	0.59	5.94	5.41	5.37	1.81	0.16		719	68
(2)	BanLP	RA-69	56.56	0.56	13.61	8.19	0.50	2.63	9.64	6.65	1.49	0.16		1518	60
(2)	Bandk	RA-57	56.21	0.81	17.65	7.53	0.40	3.88	6.00	4.36	2.97	0.19		799	68
(2)	Bandk	RA-58	54.17	0.72	20.91	7.55	0.33	3.74	6.24	3.76	2.39	0.18		320	68
(2)	Bandk	RA-59	54.07	0.72	19.84	7.62	0.29	3.78	6.73	3.60	3.17	0.19		240	68
(2)	Bandk	RA-59a	57.14	0.67	17.31	7.63	0.29	3.72	6.64	3.36	3.03	0.20		240	68
(2)	Bandk	RA-60	57.34	0.72	17.67	6.75	0.29	3.21	6.68	4.85	2.28	0.19		320	68
(2)	Bdk	RA-61	47.87	0.73	20.42	9.57	0.39	7.20	8.72	3.31	1.67	0.11		320	34
(2)	Bdk	RA-61a	50.79	0.67	18.09	9.70	0.40	7.10	8.42	3.07	1.64	0.12		320	34
(2)	Bdk	RA-62	48.52	0.82	19.95	9.60	0.51	7.68	7.05	3.97	1.76	0.14		320	34
(2)	Didk	RA-36	57.30	0.71	15.05	7.82	1.12	5.06	2.46	7.10	3.04	0.33			85
(2)	Didk	RA-71	55.70	0.54	19.11	7.37	0.36	2.64	6.15	6.25	1.71	0.17		719	43
(3)	RdLP	Average (7)	65.70	0.41	16.14	2.93	0.15	0.91	3.40	4.99	5.24	0.13	3.32		
(3)	Rddk	Average (5)	71.95	0.38	14.79	0.53	0.04	0.14	2.59	3.61	5.88	0.09	4.42		
(3)	BanLP	Average (3)	56.64	0.69	16.39	9.00	0.32	4.93	5.18	4.50	2.22	0.14	4.40		

(*) (2) Ahumada, 1985a; (3) Klohn et al,1990

(**) RdLP:rhyodacite Lo Prado Fm; Rddk:rhyodacitic dyke; BanLP:basaltic andesite, Lo Prado Fm;

Bandk:basaltic andesitic dyke; Bdk: basaltic dyke; Didk: microdioritic dyke;

APPENDIX 8 . RESUMÉ

RICARDO BORIC

Personal Data

Name: Ricardo Boric
Nationality: Chilean
Date and Place of Birth: 06/12/1956 - Punta Arenas, Chile
Marital Status: Married, three children
Address: 2730 Lota Avenue, Apt. 51, Providencia, Santiago, Chile
                             Tel: (562)2316814
                             E-mail: rboric@ctcinternet.cl

Education

Universidad de Chile: 1974-1979.

> Professional Geologist Degree (Geólogo)
> Thesis: "Geología de los Cuadrángulos Estación Colupito y Toco, Antofagasta II Región" (Translated Title: "Geology of the Colupito and Toco Station Quadrangles, Antofagasta, II Region".

Universidad de Chile: April-December1997

> Post Graduate Programme: Design and Evaluation of Projects

Dalhousie University: 1998 – October 2002

> Master of Science, Department of Earth Sciences
> Thesis: Geology, Mineral Zoning and Lithochemistry of the El Soldado Manto Type Copper Deposit, Chile. Supervisor Dr. Marcos Zentilli.

Professional experience

1980-1987: Geologist at the Economic Geology Department of the Chilean Mining and Geological Survey.

> Main work: Elaboration of geological and metallogenic charts; study of mining resources potential; ore deposits research; regional metallogenic analysis.

1987-1988: Geologist at Compañía Minera El Bronce de Petorca (gold mining company)

> Main work: Exploration and evaluation programs of ore reserves; geological and district-scale and regional metallogenic analyses.

1988-1997: Senior Geologist at Compañía Minera Disputada de Las Condes (Chilean branch of Exxon Mobil Coal and Mineral Company), assigned to El Soldado Mine.

> Main work: Geology of production; exploration programs, evaluation of mining reserves, quality control programs, research studies on geological, metallurgical and genetic models of El Soldado deposit.

1999-2001: Senior Geologist at Compañía Minera Disputada de Las Condes (Chilean branch of Exxon Mobil Coal and Mineral Company), El Soldado Mine.
Main work: Design, supervising, and management of exploration programs at the mine and at the El Soldado District. Exploration programs have included geological, geochemical, geophysics studies, and intensive drilling campaigns.

Research Activities

1991-1993: Co-investigator in the Fondecyt Project: "Isotopic characterization of the hydrothermal fluids: involvement in the genesis of strata-bound copper deposits of Chile" (Project N° 1240-91).

Selected Seminars and Courses

May, 1981: "Geochemical Exploration for Minerals", Japan International Cooperation Agency, Tokio, Japan.
October, 1984: "Stable Isotopes Geology", Dr. Baruch Spiro, Universidad de Chile, Santiago.
August, 1986: "Geology and Geochemistry of Silver and Gold Epithermal Deposits ", Dr. William Atkinson, Universidad de Chile, Santiago.
August, 1987: "Geological-Mining Exploration, Practical Aspects", Dr. David Lowell, Universidad de Chile, Santiago.
August, 1988: "Geological Principles Applied to Mining Prospection", Universidad de Chile, Santiago.
December, 1990: "Geostatistic Estimation of Reserves", Dr. Marcos Alfaro, Instituto de Ingenieros de Mina, Santiago.
August, 1992: "Advanced Methods of Exploration", Dr. William Chávez, Universidad Católica del Norte, Antofagasta.
May, 2001: "Lithogeochemical exploration for hydrothermal ore deposits using Pearce Element Ratio Analysis", Dr. Clifford Stanley, Santiago.
June, 2001: "Introductory course of ArcView", Vicente Alfaro, Geoinformaciones, Santiago.

Selected Publications

Boric, R.,1981, Cuadrángulos Estación Colupito y Toco, Región de Antofagasta (*Colupito and Toco Stations Quandrangles, Antofagasta Region*), Carta Geológica de Chile N° 49 y 50, Instituto de Investigaciones Geológicas.

Boric, R., 1985, Geología y Yacimientos Metálicos del Distrito Talcuna, Región de Coquimbo (*Geology and Metallic Deposits of the Talcuna District, Coquimbo Region*), Revista Geológica de Chile, N° 25-26 p.57-75.

Camus, F., Skewes, M.A., and Boric, R., 1986, El Distrito de Oro El Bronce y su Relación con la Caldera Morro Hediondo, Región de Valparaíso, Chile ("*El Bronce Gold District and its Relationship with the Morro Hediondo Caldera, Valparaíso Region, Chile*"), Revista Geológica de Chile N° 28-29, p. 95-101.

Maksaev, V., Boric R., Zentilli, M., and Reynolds, P.H., 1988, Significado metalogénico de dataciones K-Ar, ^{40}Ar/^{39}Ar y trazas de fisión de zonas mineralizadas en el norte de Chile (*Metallogenic significance of K-Ar, ^{40}Ar/^{39}Ar and fission track dating of mineralized zones in northern Chile*), V Congreso Geológico Chileno,1 p.B65-B86.

Boric, R., Díaz, F., and Maksaev, V., 1990. Geología y yacimientos metalíferos de la Región de Antofagasta ("*Geology and Metalliferous deposits of the Antofagasta Region*"). Servicio Nacional de Geología y Minería, Boletín N° 40, Santiago, 246 p. Maps.

Camus, F., Boric, R., Skewes, A., Castelli, J.C., Reichhard, E., Mestre, A. 1991, Geological, Structural and Fluid Inclusion Studies of El Bronce Epithermal Vein System, Petorca, Central Chile, Economic Geology, v.86, p.1317-1345.

Zentilli, M., Boric, R., Munizaga, F., and Graves, M.C., 1994. Petroleum involvement in the genesis of some strata-bound copper deposits of Chile. VII Congr. Geol. Chileno, Concepción, II, p.542-1546.

Boric, R. and Munizaga, F., 1994, Geocronología Ar-Ar y Rb-Sr del depósito estratoligado de cobre El Soldado, Chile central *("Ar-Ar and Rb-Sr geochronology of the El Soldado strata-bound copper deposit, central Chile)*, Comunicaciones, Universidad de Chile, v. 25-26, p.57-75.

Boric, R., 1995, Mineral zoning at El Soldado Copper deposit, Central Chile, (abstract). GSA Annual Meeting, New Orleans, Geological Society of America, Abstracts with Program.

Munizaga, F., Zentilli, M., Tassinari, C., Boric, R., Ramírez, R. and Reynolds, P.H., 1995. Geochronological and isotopic signatures of Mesozoic Stratabound "manto-type" copper deposits of Chile (abstract). GSA Annual Meeting, New Orleans, Geological Society of America, Abstracts with Program, 27, 6, A-410.

Boric, R., 1997, Nuevos antecedentes sobre el modelo genético del yacimiento de cobre El Soldado, Chile central, VIII Congr. Geol. Chileno, Antofagasta, p.862-866.

Zentilli, M., Munizaga, F., Graves, M. C., Boric. R., Wilson. N.S.F., Mukhopadhyay, P. K., and Snowdon, L.R., 1997, Hydrocarbon involvement in the genesis of ore

deposits: an example in Cretaceous strata-bound (manto type) copper deposits of central Chile, International Geology Review, Vol.39, p.1-21.

Boric, R. and Zentilli, M., 2001, Geology, mineral zoning and lithogeochemistry of hydrothermal alteration at the El Soldado manto type copper deposit, Chile. Abstracts Atlantic Geoscience Society Colloquium and Annual Meeting, Moncton New Brunswick, Atlantic Geology, v. 37, Abstract in press.

Zentilli, M., Heaman, L., Pop, N., and Boric, R., 2001. Evidence of Precambrian crust under the Coastal Cordillera of Chile: xenocrystic zircons in Cretaceous volcanic rocks. (Abstract published, not presented). III South American Symposium on Isotope Geology. Comunicaciones, Universidad de Chile.

Boric, R., Holmgren, C., Wilson, N.S.F. and Zentilli, M., 2002. The geology of the El Soldado Cu-(Ag) deposit, Central Chile. In M. Porter (ed.) Hydrothermal Iron-oxide copper-gold & related deposits: A global perspective, Volume 2, PGC Publishing, Adelaide, Australia, p.163-184.

Wilson, N.S.F., Zentilli, M., Reynolds, P.H. and Boric, R. $^{40}Ar/^{39}Ar$ Geochronology of K-feldspar from the El Soldado Manto-Type Copper Deposit, Chile (in press) Chemical Geology.

Collins, P.G., Boric, R., Wilson, N.S.F. and Zentilli, M. , 2002. Fixation of sulphur during framboidal pyrite development in a petroleum reservoir in Cretaceous volcanins in the Andes: implications for Cu metallogenesis. Atlantic Geoscience Society Symposium, February 9, Antigonish, Nova Scotia, Canada. In press in Atlantic Geology, v. 38.

Other Skills

Computer: familiar with the use of:
- MS Office (Word, Excel, Power Point, Outlook).
- GEMCOM software (geology and ore reserves estimation).
- Arcview (GIS) software
- Corel Draw, MINPET

Languages:
- Spanish as a native language; English.

Safety:
- Risk control and industrial safety courses; safe-driving courses; clean driving record.

Sports:
- Member of the basquetball team of Universidad de Chile (1975-1980).
- Active basquetball, soccer and tennis player.
-

Affiliations: Member of Colegio de Geólogos de Chile; Sociedad Geológica de Chile